

NATIONAL TECHNICAL UNIVERSITY OF ATHENS

SCHOOL OF CIVIL ENGINEERING

DEPARTMENT OF STRUCTURAL ENGINEERING

INSTITUTE OF STRUCTURAL ANALYSIS & ANTISEISMIC RESEARCH



**GEOMETRIC AND MATERIAL NONLINEAR
ANALYSIS OF BEAM-SOIL INTERACTION
SYSTEMS**

DOCTORAL DISSERTATION

for the title of Doctor of Philosophy in Engineer submitted in
the School of Civil Engineering, National Technical University of Athens

KAMPITSIS E. ANDREAS

Diploma in Civil Engineering N.T.U.A.

Master of Science in Civil Engineering N.T.U.A.

ATHENS 2014

ΕΘΝΙΚΟ ΜΕΤΣΟΒΙΟ ΠΟΛΥΤΕΧΝΕΙΟ

ΣΧΟΛΗ ΠΟΛΙΤΙΚΩΝ ΜΗΧΑΝΙΚΩΝ

ΤΟΜΕΑΣ ΔΟΜΟΣΤΑΤΙΚΗΣ

ΕΡΓΑΣΤΗΡΙΟ ΣΤΑΤΙΚΗΣ & ΑΝΤΙΣΕΙΣΜΙΚΩΝ ΕΡΕΥΝΩΝ



**ΓΕΩΜΕΤΡΙΚΑ ΜΗ ΓΡΑΜΜΙΚΗ ΚΑΙ ΑΝΕΛΑΣΤΙΚΗ
ΑΝΑΛΥΣΗ ΣΥΣΤΗΜΑΤΩΝ ΑΛΛΗΛΕΠΙΔΡΑΣΗΣ
ΔΟΚΟΥ-ΕΛΑΦΟΥΣ**

ΔΙΔΑΚΤΟΡΙΚΗ ΔΙΑΤΡΙΒΗ

για τον Επιστημονικό Τίτλο του Διδάκτορα Μηχανικού υποβληθείσα στη
Σχολή Πολιτικών Μηχανικών του Εθνικού Μετσόβιου Πολυτεχνείου

ΚΑΜΠΙΤΣΗΣ Ε. ΑΝΔΡΕΑΣ

Διπλωματούχος Πολιτικός Μηχανικός Ε.Μ.Π.

Μεταπτυχιακό Δίπλωμα Ειδίκευσης Ε.Μ.Π.

ΑΘΗΝΑ 2014



NATIONAL TECHNICAL UNIVERSITY OF ATHENS
SCHOOL OF CIVIL ENGINEERING
DEPARTMENT OF STRUCTURAL ENGINEERING
INSTITUTE OF STRUCTURAL ANALYSIS & ANTISEISMIC RESEARCH

GEOMETRIC AND MATERIAL NONLINEAR ANALYSIS OF BEAM–SOIL INTERACTION SYSTEMS

DOCTORAL DISSERTATION

for the title of Doctor of Philosophy in Engineer submitted in
the School of Civil Engineering, National Technical University of Athens

KAMPITSIS E. ANDREAS

M.Sc., Diploma in Civil Engineering N.T.U.A.

ADVISORY COMMITTEE:

- 1 Sapountzakis J. Evangelos,
Professor N.T.U.A. (Supervisor)
- 2 Gazetas George,
Professor N.T.U.A.
- 3 Koumousis K. Vlasis,
Professor N.T.U.A.

EXAMINATION COMMITTEE:

- 1 Sapountzakis J. Evangelos,
Professor N.T.U.A. (Supervisor)
- 2 Gazetas George,
Professor N.T.U.A.
- 3 Koumousis K. Vlasis,
Professor N.T.U.A.
- 4 Papadrakakis Manolis,
Professor N.T.U.A.
- 5 Gantes Charis,
Professor N.T.U.A.
- 6 Gerolymos Nikos,
Assistant Professor N.T.U.A.
- 7 Lagaros D. Nikos,
Assistant Professor N.T.U.A.

The research for this dissertation was conducted for the project *DARE: Soil-Foundation-Structure Systems Beyond Conventional Seismic “Failure” Thresholds: Application to New or Existing Structures and Monuments*, funded by the European Research Council (ERC) under its IDEAS-Advanced Grant program : ERC-2008-AdG: 228254-DARE.

Copyright © Kampitsis E. Andreas, 2014

All rights reserved.

To my parents...

If you would be a real seeker after truth it is necessary that at least once in your life you doubt, as far as possible, all things.

René Descartes

Acknowledgements

First and foremost, I would like to express my sincere gratitude to my teacher and advisor, Professor Evangelos Sapountzakis, for the exemplary guidance and constant encouragement throughout the course of this study. His continuous support, motivation and dedicated involvement in every step of the way extend beyond his academic role and for that I am deeply thankful.

I would also like express my most sincere gratitude to Professor George Gazetas and Professor Vlasis Koumousis for serving on my doctoral advisory committee. Their beneficial comments, as well as their illuminating lectures have contributed the most to the accomplishment of this dissertation and are highly appreciated. My sincere gratitude also goes to Professor Manolis Papadrakakis, Professor Charis Gantes, Assistant Professor Nikos Gerolymos and Assistant Professor Nikos Lagaros for serving on my doctoral examination committee and for their constructive comments which enriched this dissertation.

Special thanks are due to my officemates and fellow travellers to this PhD journey, Ioannis Dikaros, Vassilis Tsipiras, Ioannis Ntourakopoulos, Ioannis Tsiptsis, Marina-Myrto Manola and Savvas Triantafyllou for the constructive and stimulating discussions on research matters but mainly for their friendship and moral support. My sincere gratitude goes to Ms. Fani Kouvaki for being always supportive, while I would also like to thank Spyros Giannakos for the excellent collaboration and the exchange of ideas.

My sincere gratitude goes to my friends Kostas Adamakos, Angelos Vasilas, Dimitris Giannopoulos, Nikos Dais and to my Tennis Team, while special thanks are also due to my schoolmates Takaki, Giannis, Giorgos and Stathis for being next to me for nearly my entire life.

To the very special person of my life, my companion, I will always be grateful for her love, patience and support. Thank you for encouraging me and believing that limits are there only to be surpassed.

Most of all, I would like to thank my parents Evangelos and Xanthi. My deepest appreciation is expressed to them for being a constant source of inspiration. Their unconditional love, unwavering support and constant encouragement will follow me throughout my life.

I wish to express my appreciation to the Bodossaki Foundation for financially supporting my postgraduate studies. This support is greatly acknowledged.

This work has been conducted with financial support from the EU 7th Framework research project funded through the European Research Council's Programme "Ideas", Support for Frontier Research-Advanced Grant, under Contract number ERC-2008-AdG 228254-DARE.

Περίληψη

Διδακτορική Διατριβή του Καμπίτση Ε. Ανδρέα

ΓΕΩΜΕΤΡΙΚΑ ΜΗ ΓΡΑΜΜΙΚΗ ΚΑΙ ΑΝΕΛΑΣΤΙΚΗ ΑΝΑΛΥΣΗ ΣΥΣΤΗΜΑΤΩΝ ΑΛΛΗΛΕΠΙΔΡΑΣΗΣ ΔΟΚΟΥ-ΕΔΑΦΟΥΣ

Η παρούσα διδακτορική διατριβή αποτελεί συμβολή στη γεωμετρικά μη γραμμική και ανελαστική ανάλυση συστημάτων αλληλεπίδρασης δοκού – εδάφους. Συγκεκριμένα, διατυπώνονται καινοτόμες θεωρίες δοκού και αναπτύσσονται προηγμένες μεθοδολογίες για τη διερεύνηση και επίλυση προβλημάτων που συναντώνται στην επιστήμη του μηχανικού. Η παρούσα ερευνητική προσπάθεια στοχεύει επίσης στην απόκτηση νέων γνώσεων σχετικά με την επίδραση μη γραμμικών φαινομένων στην ολική απόκριση του συστήματος.

Για το σκοπό αυτό μελετάται και επιλύεται σειρά προβλημάτων μη γραμμικής ανάλυσης δοκού τυχούσας διπλά συμμετρικής διατομής, εδραζόμενης επί μη γραμμικού εδάφους. Η προσομοίωση του δομικού στοιχείου γίνεται με εφαρμογή της μονοδιάστατης θεωρίας δοκού, ενώ του εδαφικού μέσου υλοποιήθηκε με ποικίλους μη γραμμικούς ελατηριωτούς σχηματισμούς, όπου λαμβάνεται υπόψη και η μη γραμμικότητα διεπιφάνειας. Αρχικά, διερευνάται η γεωμετρικά μη γραμμική στατική και δυναμική ελαστική ανάλυση δοκών επί μη γραμμικού εδάφους, λαμβάνοντας υπόψη διατμητικές παραμορφώσεις. Εν συνεχεία, η έρευνα επεκτείνεται στην ανελαστική ανάλυση του προβλήματος, όπου τόσο το εδαφικό μέσο όσο και το δομικό στοιχείο ακολουθούν μη γραμμικούς ανελαστικούς νόμους. Τέλος, μελετάται η γεωμετρικά μη γραμμική και ανελαστική δυναμική απόκριση του συστήματος αλληλεπίδρασης δοκού – εδάφους.

Η γεωμετρική μη γραμμικότητα λαμβάνεται υπόψη στα εξεταζόμενα προβλήματα μέσω ολικής διατύπωσης Lagrange και της θεωρίας μεγάλων μετατοπίσεων - μικρών παραμορφώσεων, διατηρώντας τα τετράγωνα των κλίσεων των εγκάρσιων μετατοπίσεων στην έκφραση των ορθών παραμορφώσεων ως προς τη διαμήκη

διεύθυνση. Ως εκ τούτου τα προβλήματα αυτά δεν υπόκεινται στους περιορισμούς της γραμμικοποιημένης ανάλυσης δεύτερης τάξης (θεώρηση σταθερής αξονικής δύναμης). Η επιρροή των διατμητικών παραμορφώσεων λαμβάνεται υπόψη με τη βοήθεια της θεωρίας δοκού Timoshenko, η οποία συνυπολογίζει έμμεσα το φαινόμενο αυτό μέσω διορθωτικών συντελεστών διάτμησης. Στην παρούσα διατριβή οι συντελεστές αυτοί υπολογίζονται με εφαρμογή ενεργειακής μεθόδου. Οι πλαστικές παραμορφώσεις προσδιορίζονται μέσω προσομοιώματος κατανεμημένης πλαστικότητας (στοιχείο ινών) χρησιμοποιώντας τρισδιάστατες καταστατικές σχέσεις, ενώ η μαθηματική διατύπωση βασίζεται στη μέθοδο των μετατοπίσεων. Τα μονοδιάστατα και διδιάστατα προβλήματα συνοριακών τιμών και αρχικών συνοριακών τιμών που μορφώνονται επιλύονται αριθμητικά εφαρμόζοντας τη Μέθοδο Συνοριακών Στοιχείων, τη Μέθοδο Αναλογικής Εξίσωσης και την Πεδιακή Μέθοδο Συνοριακών Στοιχείων.

Βάσει των αναλυτικών και αριθμητικών διαδικασιών που αναπτύσσονται, μελετώνται αντιπροσωπευτικά αριθμητικά παραδείγματα ιδιαίτερου πρακτικού ενδιαφέροντος. Η ακρίβεια και αξιοπιστία των προτεινόμενων μεθόδων επιβεβαιώνονται με υπάρχουσες αναλυτικές και αριθμητικές λύσεις, πειραματικά αποτελέσματα καθώς και με προσομοιώματα στερεών και κελυφωτών πεπερασμένων στοιχείων.

Πίνακας Περιεχομένων Εκτενούς Περίληψης

I.	Εισαγωγή.....	<i>i</i>
II.	Γεωμετρικά Μη Γραμμική Ανάλυση Δοκών με Διατμητικές Παραμορφώσεις επί Μη Γραμμικού Εδάφους.....	<i>vi</i>
III.	Γεωμετρικά Μη Γραμμική Δυναμική Ανάλυση Δοκών με Διατμητικές Παραμορφώσεις επί Μη Γραμμικού Εδάφους.....	<i>xi</i>
IV.	Γεωμετρικά Μη Γραμμική και Ανελαστική Ανάλυση Δοκών με Διατμητικές Παραμορφώσεις επί Μη Γραμμικού Ανελαστικού Εδάφους.....	<i>xx</i>
V.	Γεωμετρικά Μη Γραμμική και Ανελαστική Δυναμική Ανάλυση Συστημάτων Αλληλεπίδρασης Δοκού – Εδάφους.....	<i>xxvii</i>
VI.	Συμπεράσματα.....	<i>xxiv</i>
VII.	Ιδέες για Μελλοντική Έρευνα.....	<i>xxvii</i>

Εκτενής Περίληψη

Γεωμετρικά Μη Γραμμική και Ανελαστική Ανάλυση Συστημάτων Αλληλεπίδρασης Δοκού – Εδάφους

I. Εισαγωγή

Η απόκριση συστημάτων αλληλεπίδρασης δοκού – εδάφους υπό στατική και δυναμική φόρτιση αποτελεί ένα πεδίο συνεχούς και εκτεταμένης έρευνας, τόσο στον τομέα της δομικής μηχανικής όσο και σε αυτόν της γεωτεχνικής μηχανικής. Σημαντικές ερευνητικές προσπάθειες έχουν πραγματοποιηθεί τα τελευταία χρόνια, με σκοπό να ενσωματωθεί η αποκτηθείσα γνώση στην ανάλυση και το σχεδιασμό των συστημάτων αυτών. Οι μέθοδοι μελέτης των συστημάτων αλληλεπίδρασης δοκού – εδάφους αξιολογούνται συνεχώς και βελτιώνονται λαμβάνοντας υπόψη ιστορικά στοιχεία, νέα πειραματικά δεδομένα και αποτελέσματα από μελέτες πεδίου, τα οποία καταδεικνύουν τη σημασία της ακριβούς ανάλυσης. Εντούτοις, η εγγενής πολυπλοκότητα του προβλήματος αλλά και οι αβεβαιότητες που σχετίζονται με την ίδια τη φύση του συστήματος καθιστούν ιδιαίτερα δύσκολη τόσο τη μαθηματική διατύπωση όσο και τη διαδικασία επίλυσης του.

Με την πάροδο των χρόνων, αρκετοί ερευνητές έχουν αναπτύξει και προτείνει πλήθος μεθόδων για τη μελέτη της περίπλοκης συμπεριφοράς των συστημάτων αλληλεπίδρασης δοκού – εδάφους. Οι μέθοδοι ανάλυσης μπορούν να ομαδοποιηθούν σε τρεις κυρίαρχες κατηγορίες. Στην πρώτη κατηγορία ανήκουν οι μέθοδοι που βασίζονται στη θεωρία δοκού επί ελατηριωτού εδάφους, στη δεύτερη κατηγορία οι μέθοδοι που βασίζονται στη θεωρία συνεχούς μέσου, ενώ τελευταία έχουν αναπτυχθεί οι μέθοδοι μακρο-στοιχείου.

Στα πλαίσια της πρώτης κατηγορίας (θεωρίας δοκού), το εδαφικό μέσο προσομοιώνεται από ελατηριωτούς σχηματισμούς, ενώ το δομικό μέλος προσομοιώνεται με ραβδωτά στοιχεία. Η μεθοδολογία αυτή έχει αποδειχθεί αποδοτική και ακριβής. Αντιθέτως, τα προσομοιώματα που βασίζονται στη θεωρία συνεχούς

μέσου επιδιώκουν να περιγράψουν την πραγματική συμπεριφορά του συστήματος μέσω της ρεαλιστικής προσομοίωσης του εδάφους αλλά και της κατασκευής. Στην περίπτωση της γραμμικά ελαστικής απόκρισης έχουν αναπτυχθεί αναλυτικές εκφράσεις, οι οποίες όμως, παρότι είναι ιδιαίτερα εύχρηστες, αγνοούν την πλαστικοποίηση του εδάφους και περιορίζονται στην παραδοχή μικρών παραμορφώσεων. Για να ληφθεί υπόψη η μη γραμμικότητα υλικού καθώς και η μη γραμμικότητα γεωμετρίας και διεπιφάνειας, έχουν αναπτυχθεί μη γραμμικά προσομοιώματα τρισδιάστατων πεπερασμένων στοιχείων, τα οποία όμως απαιτούν εξειδικευμένες μεθόδους βαθμονόμησης αλλά και μεγάλο υπολογιστικό κόστος. Τέλος, πρόσφατα έχει αναπτυχθεί η μέθοδος του μακρο-στοιχείου, η οποία επιδιώκει να περιγράψει τη συνολική συμπεριφορά του συστήματος μέσω μιας μακροσκοπικής προσομοίωσης.

Οι μέθοδοι που βασίζονται στη θεωρία δοκού, ίσως είναι οι πιο δημοφιλείς για την ανάλυση των συστημάτων αλληλεπίδρασης αλλά και γενικότερα για τη μελέτη φορέων που συναντώνται σε έργα πολιτικού μηχανικού. Αυτό οφείλεται στα σημαντικά πλεονεκτήματα της θεωρίας δοκού έναντι των προσομοιωμάτων τρισδιάστατης ελαστικότητας ή ελαστοπλαστικότητας. Τα κυριότερα πλεονεκτήματα της θεωρίας δοκού συνοψίζονται ακολούθως:

i. Ευκολία στην προσομοίωση και το χειρισμό.

Ο ανθρώπινος και υπολογιστικός χρόνος στη φάση προ-επεξεργασίας των δεδομένων εισόδου της ανάλυσης είναι σαφώς μειωμένος, σε σύγκριση με τα τρισδιάστατα προσομοιώματα, όπου παρά την ύπαρξη αυτόματων γεννητόρων διακριτοποίησης, η διαδικασία της προσομοίωσης και της διακριτοποίησης της κατασκευής είναι χρονικά δαπανηρή.

ii. Μικρό υπολογιστικό κόστος.

Ο υπολογιστικός χρόνος στη φάση αριθμητικής επίλυσης των εξισώσεων του προβλήματος είναι ελάχιστος συγκριτικά με τα χρονικά δαπανηρά τρισδιάστατα προσομοιώματα. Η διαφορά αυτή γίνεται πιο αισθητή στην περίπτωση δυναμικής ανάλυσης ή όπου λαμβάνεται υπόψη η επιρροή γεωμετρικής και υλικής μη γραμμικότητας, καθώς απαιτείται η επίλυση μη γραμμικών συστημάτων αλγεβρικών εξισώσεων.

iii. Άμεση επιβολή φορτίσεων και στηρίξεων.

Η επιβολή των εξωτερικών φορτίων καθώς και των στηρίξεων της κατασκευής γίνεται με απλό και άμεσο τρόπο, σε αντίθεση με τα προσομοιώματα τρισδιάστατων πεπερασμένων στοιχείων τα οποία απαιτούν εξειδικευμένες μεθοδολογίες.

iv. Ευκολία στη μελέτη επιρροής διαφόρων φαινομένων και στην αξιολόγηση των αποτελεσμάτων.

Με τη χρήση απλών και πιο σύνθετων θεωριών δοκού είναι δυνατή η γρήγορη αξιολόγηση της επιρροής διάφορων φαινομένων στη συνολική απόκριση της κατασκευής και ως εκ τούτου η γρήγορη λήψη αποφάσεων σε επίπεδο σχεδιασμού. Επιπλέον, υπολογίζονται άμεσα μονοδιάστατα κινηματικά και εντατικά μεγέθη, τα οποία προσφέρονται για γρήγορη αξιολόγηση. Αντιθέτως, τα αποτελέσματα τρισδιάστατων προσομοιωμάτων αποτελούν τριδιάστατες συναρτήσεις, οι οποίες εποπτεύονται και αξιολογούνται με δυσκολία. Εξάλλου, οι σύγχρονοι κανονισμοί που διέπουν την ανάλυση και το σχεδιασμό έργων πολιτικού μηχανικού συνήθως είναι διατυπωμένοι με βάση τη λογική των εντατικών μεγεθών.

v. Ευκολία στην εκτέλεση παραμετρικών αναλύσεων.

Η θεωρία δοκού προσφέρεται στις περιπτώσεις παραμετρικών αναλύσεων και βελτιστοποίησης ραβδωτών κατασκευών. Αντιθέτως, τα τρισδιάστατα πεπερασμένα στοιχεία απαιτούν τη χρήση πολλαπλών προσομοιωμάτων.

vi. Ευκολία στην άμεση παρομοίωση περίπλοκων κατασκευών.

Σε πολλές περιπτώσεις η διερεύνηση δύσκολων πρακτικών προβλημάτων της επιστήμης του μηχανικού απαιτεί αρχικά τη μελέτη απλών προσομοιωμάτων (όπου δεν είναι επιθυμητή η ανάλυση τοπικών φαινομένων). Ο προσδιορισμός της ποιοτικής συμπεριφοράς της κατασκευής μπορεί να γίνει ευκολότερα εφαρμόζοντας τη θεωρία δοκού, συγκριτικά με τις τρισδιάστατες εξισώσεις της Μηχανικής Συνεχούς Μέσου.

vii. Αποτελεσματικότητα στη μελέτη κατασκευών από δοκούς λεπτότοιχης διατομής.

Αντιμετωπίζονται επιτυχώς τα προβλήματα του μεμβρανικού (membrane-locking) και διατμητικού (shear-locking) κλειδώματος.

viii. Αποτελεσματικός χειρισμός της στρέβλωσης της διατομής.

Αντιμετωπίζεται επιτυχώς το πρόβλημα της στρέβλωσης της διατομής, το οποίο αδυνατούν να περιγράψουν τα κελυφωτά πεπερασμένα στοιχεία (midline models - shell finite elements).

Αξίζει βέβαια να επισημανθεί ότι ο γενικός χαρακτήρας και η μεγάλη αξιοπιστία των προσομοιωμάτων τρισδιάστατων πεπερασμένων στοιχείων τα καθιστούν πολύ χρήσιμο εργαλείο στα χέρια του μηχανικού ή του ερευνητή, ο οποίος επιθυμεί να προσδιορίσει την αξιοπιστία των αποτελεσμάτων που λαμβάνει από άλλες αριθμητικές μεθόδους.

Κύριος στόχος της παρούσας διδακτορικής διατριβής είναι η διατύπωση καινοτόμων θεωριών δοκού και η ανάπτυξη προηγμένων μεθόδων για την επίλυση του προβλήματος αλληλεπίδρασης δοκού – εδάφους, καθώς και η απόκτηση νέων γνώσεων σχετικά με την επίδραση μη γραμμικών φαινομένων. Για το σκοπό αυτό μελετάται και επιλύεται σειρά προβλημάτων μη γραμμικής ανάλυσης δοκού τυχούσας διπλά συμμετρικής διατομής, εδραζόμενης επί μη γραμμικού εδάφους. Η προσομοίωση του δομικού στοιχείου γίνεται με εφαρμογή της μονοδιάστατης θεωρίας δοκού, ενώ του εδαφικού μέσου υλοποιήθηκε με ποικίλους μη γραμμικούς ελατηριωτούς σχηματισμούς, όπου λαμβάνεται υπόψη και η μη γραμμικότητα διεπιφάνειας. Αρχικά, διερευνάται η γεωμετρικά μη γραμμική στατική και δυναμική ελαστική ανάλυση δοκών επί μη γραμμικού εδάφους, λαμβάνοντας υπόψη διατμητικές παραμορφώσεις. Εν συνεχεία, η έρευνα επεκτείνεται στην ανελαστική ανάλυση του προβλήματος, όπου τόσο το εδαφικό μέσο όσο και το δομικό στοιχείο ακολουθούν μη γραμμικούς ανελαστικούς νόμους. Τέλος, μελετάται η γεωμετρικά μη γραμμική και ανελαστική δυναμική απόκριση του συστήματος αλληλεπίδρασης δοκού – εδάφους. Η διατύπωση και επίλυση των εξεταζόμενων προβλημάτων είναι πλήρης, συστηματική, πρωτότυπη και συμβάλλει στην ρεαλιστικότερη προσέγγισή τους. Βάσει των αναλυτικών και αριθμητικών διαδικασιών που αναπτύσσονται στην εργασία αυτή συντάχθηκε πλήθος προγραμμάτων ηλεκτρονικού υπολογιστή, με τη βοήθεια των οποίων μελετήθηκαν αντιπροσωπευτικά αριθμητικά παραδείγματα ιδιαίτερου πρακτικού ενδιαφέροντος, τα οποία καταδεικνύουν την αποτελεσματικότητα και το εύρος εφαρμογής των προτεινόμενων μεθόδων. Η ακρίβεια και αξιοπιστία των ληφθέντων αποτελεσμάτων επιβεβαιώνεται με υπάρχουσες αναλυτικές και αριθμητικές λύσεις, πειραματικά αποτελέσματα, καθώς και με προσομοιώματα στερεών (εξαεδρικών) και κελυφωτών

(τετραπλευρικών) πεπερασμένων στοιχείων. Από την ανάλυση, υπολογίζονται όλα τα εντατικά, παραμορφωσιακά και κινηματικά μεγέθη του κάθε προβλήματος.

Η έρευνα που παρουσιάζεται στη διατριβή αυτή είναι πρωτοποριακή και πρωτότυπη. Τα κύρια στοιχεία πρωτοτυπίας συνοψίζονται στα ακόλουθα.

- i. Για πρώτη φορά στη διεθνή βιβλιογραφία, παρουσιάζεται ολοκληρωμένα η μαθηματική διατύπωση και επίλυση του δυναμικού προβλήματος της γεωμετρικά μη γραμμικής ανελαστικής ανάλυσης συστήματος αλληλεπίδρασης δοκού – εδάφους, όπου το εδαφικό μέσο αλλά και το δομικό στοιχείο ακολουθούν μη γραμμικούς ανελαστικούς νόμους.
- ii. Στα εξεταζόμενα προβλήματα, η μη γραμμικότητα υλικού αντιμετωπίζεται μέσω προσομοιώματος κατανεμημένης πλαστικότητας (στοιχείο ινών) χρησιμοποιώντας τρισδιάστατες καταστατικές σχέσεις, ενώ η μαθηματική διατύπωση βασίζεται στη μέθοδο των μετατοπίσεων.
- iii. Το προτεινόμενο προσομοίωμα λαμβάνει υπόψη τη γεωμετρική μη γραμμικότητα διατηρώντας τα τετράγωνα των κλίσεων των εγκάρσιων μετατοπίσεων στην έκφραση των ορθών παραμορφώσεων ως προς τη διαμήκη διεύθυνση, αποφεύγοντας με αυτόν τον τρόπο τους περιορισμούς της γραμμικοποιημένης ανάλυσης δεύτερης τάξης (θεώρηση σταθερής αξονικής δύναμης). Για το σκοπό αυτό υιοθετείται η συνολική διατύπωση Lagrange (θεωρία μετρίως μεγάλων παραμορφώσεων).
- iv. Η επιρροή της διατμητικής παραμόρφωσης λαμβάνεται υπόψη με τη βοήθεια των συντελεστών διατμητικής παραμόρφωσης της θεωρίας δοκού Timoshenko, η οποία συνυπολογίζει έμμεσα το φαινόμενο αυτό μέσω διορθωτικών συντελεστών διάτμησης. Στην παρούσα διατριβή οι συντελεστές αυτοί υπολογίζονται με εφαρμογή ενεργειακής μεθόδου.
- v. Το προτεινόμενο μαθηματικό προσομοίωμα συνυπολογίζει τα πεπλεγμένα φαινόμενα των καμπτικών και διατμητικών παραμορφώσεων κατά μήκος της δοκού καθώς και τις αναπτυσσόμενες διατμητικές δυνάμεις από το αξονικό φορτίο. Επιπλέον, η δοκός υποβάλλεται σε τυχούσα συγκεντρωμένη ή κατανεμημένη αξονική και καμπτική φόρτιση, ενώ τα άκρα της υπόκεινται στις πλέον γενικές συνοριακές συνθήκες συμπεριλαμβανομένης και της ελαστικής στήριξης.
- vi. Η προσομοίωση του εδαφικού μέσου υλοποιήθηκε με ποικίλους μη γραμμικούς ελατηριωτούς σχηματισμούς, όπου λαμβάνεται υπόψη και η μη γραμμικότητα διεπιφάνειας.

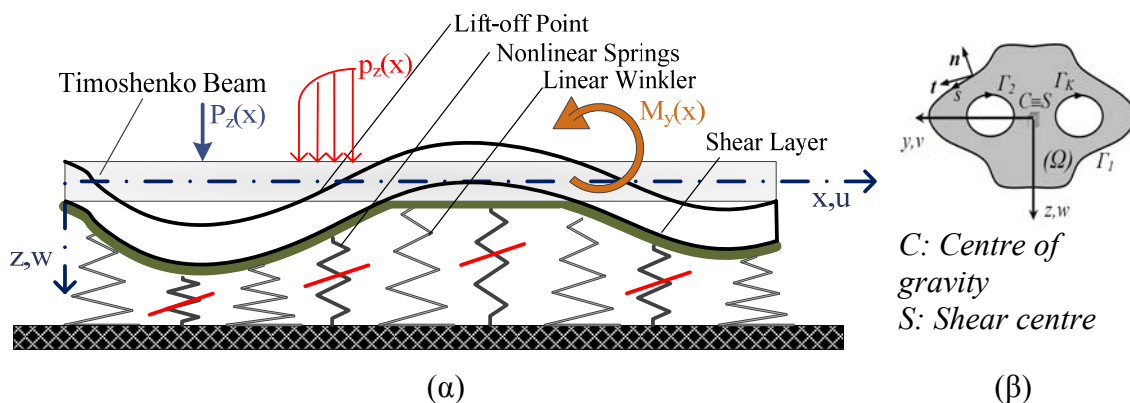
vii. Τα εξεταζόμενα προβλήματα επιλύονται αριθμητικά με τη βοήθεια συνοριακών ολοκληρωτικών εξισώσεων (Μέθοδος Συνοριακών Στοιχείων, Αναλογικής Εξίσωσης και Πεδιακή Μέθοδος Συνοριακών Στοιχείων), μέσω καινοτόμων αλγορίθμων σε υπολογιστικό περιβάλλον.

Τέλος, αξίζει να αναφερθεί ότι από την παρούσα ερευνητική προσπάθεια προέκυψαν δημοσιεύσεις σε έγκριτα επιστημονικά περιοδικά διεθνούς κυκλοφορίας, σε πρακτικά διεθνών και εθνικών συνεδρίων καθώς και κεφάλαια σε βιβλία που εκδόθηκαν από διεθνείς εκδοτικούς οίκους.

II. Γεωμετρικά Μη Γραμμική Ανάλυση Δοκών με Διατμητικές Παραμορφώσεις επί Μη Γραμμικού Εδάφους

Στην παρούσα διδακτορική διατριβή παρουσιάζεται η γεωμετρικά μη γραμμική ανάλυση δοκού διπλά συμμετρικής διατομής, επί μη γραμμικού τριπαραμετρικού ελαστικού εδάφους. Η δοκός υποβάλλεται σε τυχούσα συγκεντρωμένη ή κατανεμημένη καμπτική φόρτιση καθώς και σε τυχόν αξονικό φορτίο, ενώ τα άκρα της υπόκεινται στις πλέον γενικές συνοριακές συνθήκες συμπεριλαμβανομένης και της ελαστικής στήριξης. Η γεωμετρική μη γραμμικότητα λαμβάνεται υπόψη σε ολική διατύπωση Lagrange μέσω της θεωρίας μεγάλων μετατοπίσεων - μικρών παραμορφώσεων. Η επιρροή των διατμητικών παραμορφώσεων λαμβάνεται υπόψη με τη βοήθεια της θεωρίας δοκού Timoshenko, η οποία συνυπολογίζει έμμεσα το φαινόμενο αυτό μέσω διορθωτικών συντελεστών διάτμησης. Στην παρούσα διατριβή οι συντελεστές αυτοί υπολογίζονται με εφαρμογή ενεργειακής μεθόδου. Το εδαφικό προσομοίωμα χαρακτηρίζεται από γραμμικά και μη γραμμικά ελατήρια τύπου Winkler και από ελατήρια τύπου Pasternak, ενώ επίσης έχει προσομοιωθεί η αδυναμία ανάληψης εφελκυστικών τάσεων (tensionless foundation models). Σύμφωνα με την προτεινόμενη μέθοδο μορφώνονται με τη βοήθεια της θεωρίας ελαστικότητας πέντε προβλήματα συνοριακών τιμών. Συγκεκριμένα, μορφώνονται τρία μονοδιάστατα πρόβλημα συνοριακών τιμών αναφορικά με την αξονική και τις εγκάρσιες μετατοπίσεις, που επιλύονται με τη βοήθεια της Μεθόδου Αναλογικής Εξίσωσης, σε συνδυασμό με την υβριδική μέθοδο Powell για την επίλυση μη γραμμικών συστημάτων αλγεβρικών εξισώσεων, καθώς και δύο διδιάστατα προβλήματα συνοριακών τιμών αναφορικά με τις ταστικές συναρτήσεις που αναφέρονται στους συντελεστές διάτμησης, τα οποία επιλύονται με τη βοήθεια “αμιγούς” Μεθόδου Συνοριακών Στοιχείων.

Για τη μαθηματική διατύπωση του προβλήματος, εξετάζεται ευθύγραμμη πρισματική δοκός μήκους l (Σχ. 1), σταθερής τυχούσας διπλά συμμετρικής διατομής που αποτελείται από ομογενές, ισότροπο και γραμμικά ελαστικό υλικό με μέτρο ελαστικότητας E , μέτρο διάτμησης G και λόγο Poisson ν , το οποίο καταλαμβάνει περιοχή Ω του επιπέδου yz και είναι απλά ή πολλαπλά συνεκτικό (υπάρχει η δυνατότητα να περιλαμβάνει οπές). Το σύνορο της διατομής του χωρίου Ω , είναι τμηματικά λείο, μπορεί δηλαδή να περιλαμβάνει πεπερασμένο αριθμό γωνιών και συμβολίζεται με $\Gamma = \bigcup_{j=1}^K \Gamma_j$ ($j = 1, 2, \dots, K$). Στο Σχ. 1, με $Cxyz$ συμβολίζεται το κύριο καμπτικό σύστημα αξόνων που διέρχεται από το κέντρο βάρους της διατομής C . Η δοκός θεωρείται μερικώς εδραζόμενη επί μη γραμμικού τριπαραμετρικού ελαστικού εδάφους. Λαμβάνοντας υπόψη τη μη γραμμική επαφή μεταξύ της δοκού και του εδαφικού μέσου (interface nonlinearity), η εδαφική αντίδραση επί της δοκού ενεργεί μόνο σε περίπτωση συμπίεσης των ελατηρίων και δίδεται για τις τρεις διευθύνσεις από τις ακόλουθες εκφράσεις



Σχ. 1. Πρισματική δοκός υποβαλλόμενη σε τυχούσα καμπτική και αξονική φόρτιση (α) με ομογενή διατομή τυχόντος διπλά συμμετρικού σχήματος (β).

$$p_{sx} = k_x u(x) \quad (1\alpha)$$

$$p_{sy} = \tilde{H}_y(x) \left(k_{Ly} v(x) + k_{NLy} v^3(x) - k_{Py} \frac{\partial^2 v(x)}{\partial x^2} \right) \quad (1\beta)$$

$$p_{sz} = \tilde{H}_z(x) \left(k_{Lz} w(x) + k_{NLz} w^3(x) - k_{Pz} \frac{\partial^2 w(x)}{\partial x^2} \right) \quad (1\gamma)$$

όπου $\tilde{H}_y(x)$, $\tilde{H}_z(x)$ είναι συναρτήσεις Heaviside μοναδιαίου βήματος.

Η δοκός υποβάλλεται σε συνδυασμό φορτίσεων από τυχόν συγκεντρωμένο ή/και κατανεμημένο αξονικό φορτίο $p_x = p_x(x)$ κατά μήκος του άξονα x , εγκάρσιο φορτίο $p_y = p_y(x)$, $p_z = p_z(x)$ κατά μήκος των αξόνων y και z , αντίστοιχα, καθώς και καμπτική φόρτιση $m_y = m_y(x)$, $m_z = m_z(x)$ κατά μήκος των αξόνων y και z , αντίστοιχα.

Το πεδίο μετατοπίσεων τυχαίου σημείου της διατομής λαμβάνοντας υπόψη τη διατμητική παραμόρφωση, προσδιορίζεται ως (Ramm & Hofmann 1995)

$$\bar{u}(x, y, z) = u(x) - y\theta_z(x) + z\theta_y(x) \quad (2\alpha)$$

$$\bar{v}(x, y, z) = v(x) \quad \bar{w}(x, y, z) = w(x) \quad (2\beta, \gamma)$$

όπου \bar{u} , \bar{v} , \bar{w} είναι η διαμήκης και οι εγκάρσιες συνιστώσες της μετατόπισης ενός τυχαίου σημείου ως προς το σύστημα αξόνων Cyz . Επίσης, $u = u(x)$, $v = v(x)$, $w = w(x)$ είναι η διαμήκης και οι εγκάρσιες μετατοπίσεις του κέντρου βάρους C , ενώ $\theta_y(x)$, $\theta_z(x)$ είναι οι γωνίες στροφής της διατομής λόγω της κάμψης, ως προς το κέντρο βάρους. Αξίζει να σημειωθεί ότι οι γωνίες στροφής της διατομής λόγω κάμψης δεν ταυτίζονται με τις παραγώγους των μετακινήσεων ($\theta_z \neq v'$, $\theta_y \neq w'$) λόγω διατμητικών παραμορφώσεων.

Θεωρώντας μικρές παραμορφώσεις και ότι το υλικό της δοκού είναι ομογενές, ισότροπο, συνεχές και γραμμικά ελαστικό, οι συνιστώσες του 2^{ου} τανυστή τάσης Piola-Kirchhoff δίδονται συναρτήσει των παραμορφώσεων Green από το γενικευμένο νόμο του Hooke. Εν συνεχεία, εφαρμόζοντας την ισορροπία δυνάμεων και ροπών του στοιχειώδους τμήματος της δοκού στην παραμορφωμένη διαμόρφωση ή εναλλακτικά την Αρχή Δυνατών Έργων σε ολική διατύπωση Lagrange προκύπτουν οι διαφορικές εξισώσεις που περιγράφουν την καθολική ισορροπία του συστήματος, οι οποίες εκφράζονται ως

$$-EA(u'' + w'w'' + v'v'') + k_{Lx}u = p_x \quad (3\alpha)$$

$$-(Nv')' - GA_y(v'' - \theta_z') + \tilde{H}_y(k_{Ly}v + k_{NLy}v^3 - k_{Py}v'') = p_y \quad (3\beta)$$

$$-(Nw')' - GA_z(w'' + \theta_y') + \tilde{H}_z(k_{Lz}w + k_{NLz}w^3 - k_{Pz}w'') = p_z \quad (3\gamma)$$

$$-EI_z\theta_z'' - GA_y(v' - \theta_z) = m_z \quad -EI_y\theta_y'' + GA_z(w' + \theta_y) = m_y \quad (3\delta,\epsilon)$$

όπου (') συμβολίζει την παράγωγο ως προς τη χωρική μεταβλητή x .

Συνδυάζοντας τις εξισώσεις (3β), (3δ) και (3γ), (3ε) για την απαλοιφή των γωνιών στροφής προκύπτουν οι τρεις διαφορικές εξισώσεις ισορροπίας της δοκού Timoshenko επί μη γραμμικού εδάφους υπό αξονική, εγκάρσια και καμπτική φόρτιση ως

$$-EA(u'' + w'w'' + v'v'') + k_{Lx}u = p_x \quad (4\alpha)$$

$$EI_z v'''' - (Nv')' + p_{sy} + \frac{EI_y}{GA_y} \left((Nw')''' - p_{sy}'' \right) = p_y - \frac{EI_y}{GA_z} p_y'' - m_z' \quad (4\beta)$$

$$EI_y w'''' - (Nw')' + p_{sz} + \frac{EI_y}{GA_z} \left((Nw')''' - p_{sz}'' \right) = p_z - \frac{EI_y}{GA_z} p_z'' + m_y' \quad (4\gamma)$$

Οι αντίστοιχες συνοριακές συνθήκες στα άκρα της δοκού $x = 0, l$ διατυπώνονται με την ακόλουθη γενική μορφή

$$a_1 u(x) + \alpha_2 N(x) = \alpha_3 \quad (5\alpha)$$

$$\beta_1 v(x) + \beta_2 V_y(x) = \beta_3 \quad \bar{\beta}_1 \theta_z(x) + \bar{\beta}_2 M_z(x) = \bar{\beta}_3 \quad (5\beta,\gamma)$$

$$\gamma_1 w(x) + \gamma_2 V_z(x) = \gamma_3 \quad \bar{\gamma}_1 \theta_y(x) + \bar{\gamma}_2 M_y(x) = \bar{\gamma}_3 \quad (5\delta,\epsilon)$$

όπου $\alpha_i, \beta_i, \bar{\beta}_i, \gamma_i, \bar{\gamma}_i$ ($i = 1, 2, 3$) είναι γνωστοί συντελεστές, ενώ τα εντατικά μεγέθη που αναπτύσσονται στη διατομή στην παραμορφωμένη κατάσταση και οι στροφές λόγω κάμψης δίδονται από τις ακόλουθες σχέσεις

$$V_y = -EI_z v'''' + Nv' - \frac{EI_z}{GA_y} \left[(Nv')'' + p_y' - p_{sy}' \right] - m_z \quad (6\alpha)$$

$$V_z = -EI_y w'''' + Nw' - \frac{EI_y}{GA_z} \left[(Nw')'' + p_z' - p_{sz}' \right] + m_y \quad (6\beta)$$

$$M_y = -EI_y w'' - \frac{EI_y}{GA_z} \left((Nw')' + p_z - p_{sz} \right) \quad M_z = EI_z v'' + \frac{EI_z}{GA_y} \left((Nv')' + p_y - p_{sy} \right) \quad (6\gamma, \delta)$$

$$\theta_y = -\frac{EI_y}{(GA_z)^2} \left((Nw'')' + p'_{sz} \right) - \frac{I}{GA_z} (EI_y w''' + GA_z w') \quad (6\epsilon)$$

$$\theta_z = \frac{EI_z}{(GA_y)^2} \left((Nv'')' - p'_{sy} \right) + \frac{I}{GA_y} (EI_z v''' + GA_y v') \quad (6\zeta)$$

Η αριθμητική επίλυση του πεπλεγμένου προβλήματος συνοριακών τιμών επιτυγχάνεται με τη βοήθεια της μεθόδου Αναλογικής Εξίσωσης (Katsikadelis 1994, 2002). Το διάστημα της δοκού $(0, l)$ διαιρείται σε L στοιχεία και η εφαρμογή της μεθόδου οδηγεί στη μόρφωση ενός μη γραμμικού συστήματος $3L + 20$ αλγεβρικών εξισώσεων, το οποίο εκφράζεται σε τυπική μορφή ως

$$(\mathbf{K} + \mathbf{K}^{nl}(\mathbf{d}))\mathbf{d} = \mathbf{p} \quad (7)$$

όπου \mathbf{K} το γενικευμένο γνωστό γραμμικό μητρώο στιβαρότητας, \mathbf{K}^{nl} το γενικευμένο γνωστό μη γραμμικό μητρώο στιβαρότητας, \mathbf{d} το γενικευμένο μητρώο στήλη άγνωστων ποσοτήτων και \mathbf{p} το γενικευμένο γνωστό μητρώο στήλη φόρτισης. Για την αριθμητική επίλυση του μη γραμμικού συστήματος αλγεβρικών εξισώσεων εφαρμόστηκε η υβριδική μέθοδος επίλυσης Powell (1977, 1985).

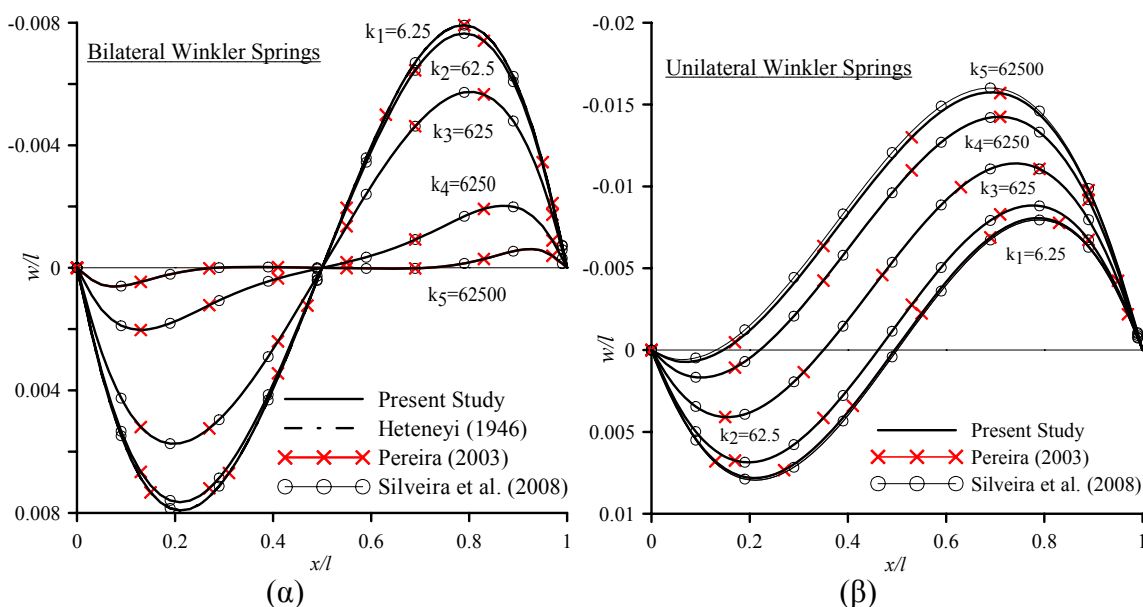
Με βάση την αναπτυχθείσα αναλυτική και αριθμητική διαδικασία, συντάχθηκε πρόγραμμα ηλεκτρονικού υπολογιστή σε υπολογιστικό περιβάλλον Fortran 90/95 με τη βοήθεια του οποίου μελετήθηκαν αντιπροσωπευτικά παραδείγματα με πρακτικό ενδιαφέρον, προκειμένου να διαπιστωθεί η αποτελεσματικότητα και το εύρος εφαρμογής της προτεινόμενης μεθόδου. Η ακρίβεια των αριθμητικών αποτελεσμάτων ελέγχεται, όπου είναι εφικτό, με υπάρχουσες αριθμητικές λύσεις και πειραματικά δεδομένα, ενώ παράλληλα διερευνάται η επιρροή της γεωμετρικής μη γραμμικότητας, της διατμητικής παραμόρφωσης καθώς και της εδαφικής προσομοίωσης στην απόκριση του συστήματος αλληλεπίδρασης δοκού – εδάφους.

Ως αντιπροσωπευτική αριθμητική εφαρμογή, μελετήθηκε αμφιέριστη δοκός επί ομογενούς ελαστικού εδάφους. Η δοκός έχει μήκος $l = 5m$ και καμπτική δυσκαμψία $EI = 10^3 kNm^2$ ενώ υποβάλλεται σε συγκεντρωμένες καμπτικές ροπές στα άκρα $M_l =$

$M_2 = -100kNm$. Στο Σχ. 2, παρουσιάζονται οι εγκάρσιες μετακινήσεις κατά μήκος της δοκού αγνοώντας (Σχ.2α) ή λαμβάνοντας υπόψη (Σχ.2β) τη μη γραμμικότητα διεπιφάνειας, για διάφορες τιμές της εδαφικής δυσκαμψίας. Στο ίδιο σχήμα παρουσιάζονται επίσης τα αντίστοιχα αποτελέσματα τόσο από την αναλυτική λύση (Hetenyi 1946) όσο και από λύσεις βασισμένες σε αριθμητικές μεθόδους (Pereira 2003, Silveira et al. 2008). Από τη σύγκριση των αποτελεσμάτων επιβεβαιώνεται η ακρίβεια της προτεινόμενης μεθόδου και διαπιστώνεται η σημασία της μη γραμμικότητας διεπιφάνειας.

III. Γεωμετρικά Μη Γραμμική Δυναμική Ανάλυση Δοκών με Διατμητικές Παραμορφώσεις επί Μη Γραμμικού Εδάφους

Στη συνέχεια διερευνάται και επιλύεται το δυναμικό πρόβλημα της γεωμετρικά μη γραμμικής ανάλυσης δοκού διπλά συμμετρικής διατομής, επί μη γραμμικού τριπαραμετρικού ελαστικού εδάφους με ξώδη απόσβεση. Η δοκός υποβάλλεται σε τυχούσα συγκεντρωμένη ή κατανομημένη δυναμική καμπτική φόρτιση καθώς και σε τυχόν χρονικά μεταβαλλόμενο αξονικό φορτίο, ενώ τα άκρα της υπόκεινται στις πλέον γενικές συνοριακές συνθήκες συμπεριλαμβανομένης και της ελαστικής στήριξης.



Σχ. 2. Εγκάρσια μετακίνηση της δοκού για διάφορες τιμές της εδαφικής δυσκαμψίας αγνοώντας (α) ή λαμβάνοντας υπόψη (β) τη μη γραμμικότητα διεπιφάνειας.

Η γεωμετρική μη γραμμικότητα και η επιρροή των διατμητικών παραμορφώσεων λαμβάνεται υπόψη ομοίως με τη περίπτωση στατικής ανάλυσης. Το εδαφικό προσομοίωμα χαρακτηρίζεται από γραμμικά και μη γραμμικά ελατήρια τύπου Winkler, από ελατήρια τύπου Pasternak και το συντελεστή απόσβεσης, ενώ επίσης έχει προσομοιωθεί η αδυναμία ανάληψης εφελκυστικών τάσεων (tensionless foundation models). Σύμφωνα με την προτεινόμενη μέθοδο μορφώνονται με τη βοήθεια της θεωρίας ελαστικότητας πέντε προβλήματα συνοριακών τιμών. Συγκεκριμένα, μορφώνονται τρία μονοδιάστατα πρόβλημα συνοριακών τιμών αναφορικά με την αξονική και τις εγκάρσιες μετατοπίσεις, που επιλύονται με τη βοήθεια της Μεθόδου Αναλογικής Εξίσωσης, σε συνδυασμό με τη μέθοδο Petzold–Gear για την επίλυση μη γραμμικών συστημάτων διαφορικών-αλγεβρικών εξισώσεων, καθώς και δύο διδιάστατα προβλήματα συνοριακών τιμών αναφορικά με τις τασικές συναρτήσεις που αναφέρονται στους συντελεστές διάτμησης, τα οποία επιλύονται με τη βοήθεια “αμιγούς” Μεθόδου Συνοριακών Στοιχείων.

Για τη μαθηματική διατύπωση του προβλήματος, εξετάζεται ευθύγραμμη πρισματική δοκός με γεωμετρικά χαρακτηριστικά όμοια με αυτά της προηγούμενης παραγράφου, ενώ επιπλέον ορίζεται και η πυκνότητα της δοκού ρ . Η εδαφική αντίδραση επί της δοκού δίδεται για τις τρεις διευθύνσεις από τις ακόλουθες εκφράσεις

$$p_{sx} = k_{Lx}u(x,t) \quad (8\alpha)$$

$$p_{sy}(x,t) = \tilde{H}(x,t)p_{rey}(x,t) \quad p_{sz}(x,t) = \tilde{H}(x,t)p_{rez}(x,t) \quad (8\beta,\gamma)$$

όπου

$$p_{rey}(x,t) = k_{Ly}v(x,t) + k_{NLy}v^3(x,t) - k_{Py} \frac{\partial^2 v(x,t)}{\partial x^2} + c_y \frac{\partial v(x,t)}{\partial t} \quad (9\alpha)$$

$$p_{rez}(x,t) = k_{Lz}w(x,t) + k_{NLz}w^3(x,t) - k_{Pz} \frac{\partial^2 w(x,t)}{\partial x^2} + c_z \frac{\partial w(x,t)}{\partial t} \quad (9\beta)$$

Η δοκός υποβάλλεται σε συνδυασμό φορτίσεων από τυχόν συγκεντρωμένο ή κατανεμημένο δυναμικό αξονικό φορτίο $p_x(x,t)$ κατά μήκος του άξονα x , χρονικά εξαρτώμενο εγκάρσιο φορτίο $p_y(x,t)$, $p_z(x,t)$ κατά μήκος των αξόνων y και z ,

αντίστοιχα, καθώς και καμπτική φόρτιση $m_y(x,t)$, $m_z(x,t)$ κατά μήκος των αξόνων y και z , αντίστοιχα. Μέσω της παρούσας διατύπωσης μπορεί να περιγραφεί οποιαδήποτε δυναμική φόρτιση συμπεριλαμβανομένων των κρουστικών πηληγμάτων, των κινούμενων φορτίων ή μαζών, καθώς και των σεισμικών φορτίσεων.

Το πεδίο μετατοπίσεων τυχαίου σημείου της διατομής λαμβάνοντας υπόψη τη διατμητική παραμόρφωση, προσδιορίζεται ως (Ramm & Hofmann 1995)

$$\bar{u}(x, y, z, t) = u(x, t) - y\theta_z(x, t) + z\theta_y(x, t) \quad (10\alpha)$$

$$\bar{v}(x, t) = v(x, t) \quad \bar{w}(x, t) = w(x, t) \quad (10\beta, \gamma)$$

Θεωρώντας μικρές παραμορφώσεις και ότι το υλικό της δοκού είναι ομογενές, ισότροπο, συνεχές και γραμμικά ελαστικό, οι συνιστώσες του 2^{ου} τανυστή τάσης Piola-Kirchhoff δίδονται συναρτήσει των παραμορφώσεων Green από το γενικευμένο νόμο του Hooke. Εν συνεχεία, εφαρμόζοντας την αρχή του Hamilton σε ολική διατύπωση Lagrange προκύπτουν οι κυρίαρχες διαφορικές εξισώσεις καθολικής δυναμικής ισορροπίας του συστήματος, οι οποίες εκφράζονται ως

$$\rho A \ddot{u} - EA(u'' + w'w'' + v'v'') + k_x u = p_x \quad (11\alpha)$$

$$\rho A \ddot{v} - (Nv')' - GA_y(v'' - \theta_z') + p_{sy} = p_y \quad \rho I_z \ddot{\theta}_z - EI_z \theta_z'' - GA_y(v' - \theta_z) = m_z \quad (11\beta, \gamma)$$

$$\rho A \ddot{w} - (Nw')' - GA_z(w'' + \theta_y') + p_{sz} = p_z \quad \rho I_y \ddot{\theta}_y - EI_y \theta_y'' + GA_z(w' + \theta_y) = m_y \quad (11\delta, \epsilon)$$

όπου (\cdot) συμβολίζει την παράγωγο ως προς τη χρονική μεταβλητή t .

Συνδυάζοντας τις εξισώσεις (11β,γ) και (11δ,ε) για την απαλοιφή των γωνιών στροφής και αγνοώντας τις παραγώγους τέταρτης τάξεως ως προς το χρόνο t , προκύπτουν οι τρεις διαφορικές εξισώσεις ισορροπίας της δοκού Timoshenko επί μη γραμμικού εδάφους υπό αξονική, εγκάρσια και καμπτική φόρτιση ως

$$\rho A \ddot{u} - EA(u'' + w'w'' + v'v'') + k_x u = p_x \quad (12\alpha)$$

$$\begin{aligned} & \rho A \ddot{v} + EI_z v'''' - (Nv')' + p_{sy} + \frac{EI_z}{GA_y} \left[(Nv)''' - \rho A \frac{\partial^2 \dot{v}}{\partial x^2} - p_{sy}'' + p_y'' \right] - \\ & - \rho I_z \frac{\partial^2 \dot{v}}{\partial x^2} - \frac{\rho I_z}{GA_y} \left[\frac{\partial^2 (Nv)'}{\partial t^2} - \rho A \ddot{v}' - \ddot{p}_{sy} + \ddot{p}_y \right] = p_y - m_z' \end{aligned} \quad (12\beta)$$

$$\begin{aligned} & \rho A \ddot{w} + EI_y w'''' - (Nw')' + p_{sz} + \frac{EI_y}{GA_z} \left[(Nw)''' - \rho A \frac{\partial^2 \dot{w}}{\partial x^2} - p_{sz}'' + p_z'' \right] - \\ & - \rho I_y \frac{\partial^2 \dot{w}}{\partial x^2} - \frac{\rho I_y}{GA_z} \left[\frac{\partial^2 (Nw)'}{\partial t^2} - \rho A \ddot{w}' - \ddot{p}_{sz} + \ddot{p}_z \right] = p_z + m_y' \end{aligned} \quad (12\gamma)$$

Οι αντίστοιχες χρονικά μεταβαλλόμενες συνοριακές συνθήκες στα άκρα της δοκού $x = 0, l$ διατυπώνονται με την ακόλουθη γενική μορφή

$$a_1 u(x, t) + \alpha_2 N(x, t) = \alpha_3 \quad (13\alpha)$$

$$\beta_1 v(x, t) + \beta_2 V_y(x, t) = \beta_3 \quad \bar{\beta}_1 \theta_z(x, t) + \bar{\beta}_2 M_z(x, t) = \bar{\beta}_3 \quad (13\beta, \gamma)$$

$$\gamma_1 w(x, t) + \gamma_2 V_z(x, t) = \gamma_3 \quad \bar{\gamma}_1 \theta_y(x, t) + \bar{\gamma}_2 M_y(x, t) = \bar{\gamma}_3 \quad (13\delta, \epsilon)$$

Ενώ από την εφαρμογή της αρχής του Hamilton προκύπτουν και οι αντίστοιχες αρχικές συνθήκες ($x \in (0, l)$) στις οποίες υπόκεινται η δοκός

$$u(x, 0) = \bar{u}_0(x) \quad \dot{u}(x, 0) = \dot{\bar{u}}_0(x) \quad (14\alpha, \beta)$$

$$v(x, 0) = \bar{v}_0(x) \quad \dot{v}(x, 0) = \dot{\bar{v}}_0(x) \quad w(x, 0) = \bar{w}_0(x) \quad \dot{w}(x, 0) = \dot{\bar{w}}_0(x) \quad (14\gamma-\zeta)$$

Τα εντατικά μεγέθη που αναπτύσσονται στη διατομή στην παραμορφωμένη κατάσταση και οι στροφές λόγω κάμψης δίδονται από τις ακόλουθες σχέσεις

$$V_y = Nv' - EI_z v''' - \frac{EI_z}{GA_y} \left[(Nv)'' - \rho A \frac{\partial \dot{v}}{\partial x} + p_y' - p_{sy}' \right] + \rho I_z \ddot{\theta}_z \quad (15\alpha)$$

$$V_z = Nw' - EI_y w''' - \frac{EI_y}{GA_z} \left[(Nw)'' - \rho A \frac{\partial \dot{w}}{\partial x} + p_z' - p_{sz}' \right] - \rho I_y \ddot{\theta}_y \quad (15\beta)$$

$$M_z = EI_z v'' + \frac{EI_z}{GA_y} \left[(Nv)' - \rho A \dot{v} + p_y - p_{sy} \right] \quad (15\gamma)$$

$$M_y = -EI_y w'' - \frac{EI_y}{GA_z} \left[(Nw')' - \rho A \dot{w} + p_z - p_{sz} \right] \quad (15\delta)$$

$$\theta_y = \frac{EI_y}{G^2 A_z^2} \left(\rho A \frac{\partial \dot{w}}{\partial x} - (Nw)'' - p'_z + p'_{sy} \right) - \frac{l}{GA_z} (EI_y w''' + \rho I_y \ddot{\theta}_y + GA_z w') \quad (15\epsilon)$$

$$\theta_z = \frac{EI_z}{G^2 A_y^2} \left((Nv)'' - \rho A \frac{\partial \dot{v}}{\partial x} + p'_y - p'_{sz} \right) + \frac{l}{GA_y} (EI_z v''' - \rho I_z \ddot{\theta}_z + GA_y v') \quad (15\zeta)$$

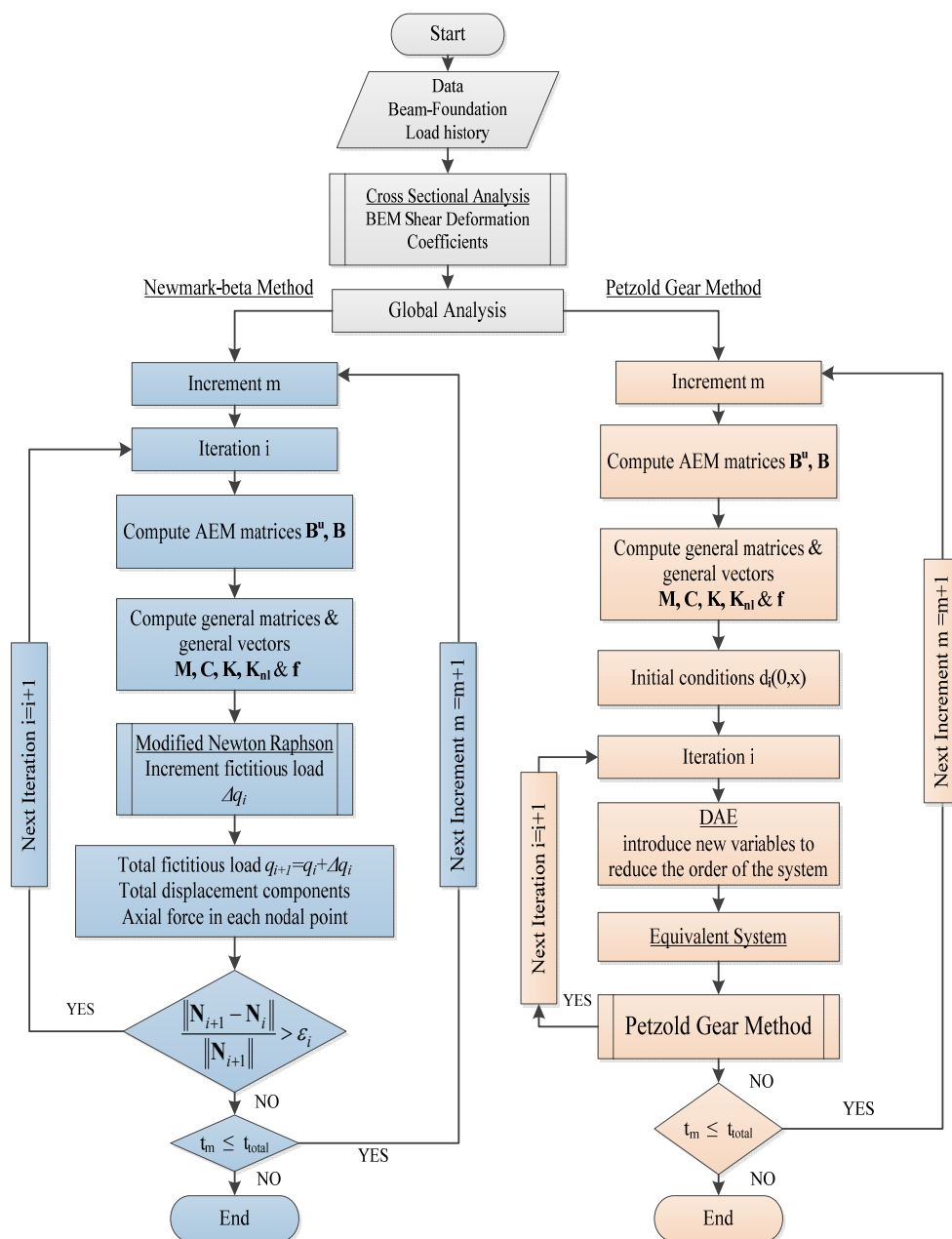
Η αριθμητική επίλυση του πεπλεγμένου προβλήματος αρχικών τιμών επιτυγχάνεται με τη βοήθεια της μεθόδου Αναλογικής Εξίσωσης (Katsikadelis 1994, 2002). Το διάστημα της δοκού $(0, l)$ διαιρείται σε L στοιχεία και η εφαρμογή της μεθόδου οδηγεί στη μόρφωση ενός μη γραμμικού συστήματος $3L + 20$ διαφορικών-αλγεβρικών εξισώσεων (DAE) ως προς $3L + 20$ αγνώστους, το οποίο μπορεί να εκφραστεί σε τυπική μορφή και ως

$$\mathbf{M}\ddot{\mathbf{d}} + \mathbf{C}\dot{\mathbf{d}} + \mathbf{K}\mathbf{d} + \mathbf{f}^{\text{nl}} = \mathbf{f} \quad (16)$$

όπου \mathbf{M} το γενικευμένο μητρώο μάζας, \mathbf{C} το γενικευμένο μητρώο απόσβεσης, \mathbf{K} το γενικευμένο μητρώο στιβαρότητας, \mathbf{f}^{nl} το γενικευμένο μη γραμμικό μητρώο στιβαρότητας και \mathbf{f} το γενικευμένο μητρώο στήλη φόρτισης. Για την αριθμητική επίλυση του μη γραμμικού συστήματος διαφορικών-αλγεβρικών εξισώσεων μπορεί να εφαρμοστεί είτε μια εκ των Newmark-beta μεθόδων σε συνδυασμό με μια μη γραμμική επαναληπτική διαδικασία (Newton Raphson, Modified Newton Raphson, Arc-Length), είτε να χρησιμοποιηθεί η μέθοδος Petzold-Gear αφού εισαχθούν ισάριθμες νέες μεταβλητές ώστε να μειωθεί η τάξη του προβλήματος αρχικών τιμών ($ind = 1$). Εναλλακτικά το πρόβλημα που μορφώνεται από τις εξισώσεις (11) και (13,14) επιλύθηκε με τη μέθοδο Πεδιακών Συνοριακών Στοιχείων (Domain-BEM). Στο Σχ. 3, παρουσιάζεται το διάγραμμα ροής του μη γραμμικού επαναληπτικού αλγορίθμου επίλυσης του προβλήματος.

Με βάση την αναπτυχθείσα αναλυτική και αριθμητική διαδικασία, συντάχθηκε πρόγραμμα ηλεκτρονικού υπολογιστή σε υπολογιστικό περιβάλλον Fortran 90/95 με τη βοήθεια του οποίου μελετήθηκαν αντιπροσωπευτικά παραδείγματα με πρακτικό ενδιαφέρον, προκειμένου να διαπιστωθεί η αποτελεσματικότητα και το εύρος εφαρμογής της προτεινόμενης μεθόδου. Η ακρίβεια των αριθμητικών αποτελεσμάτων

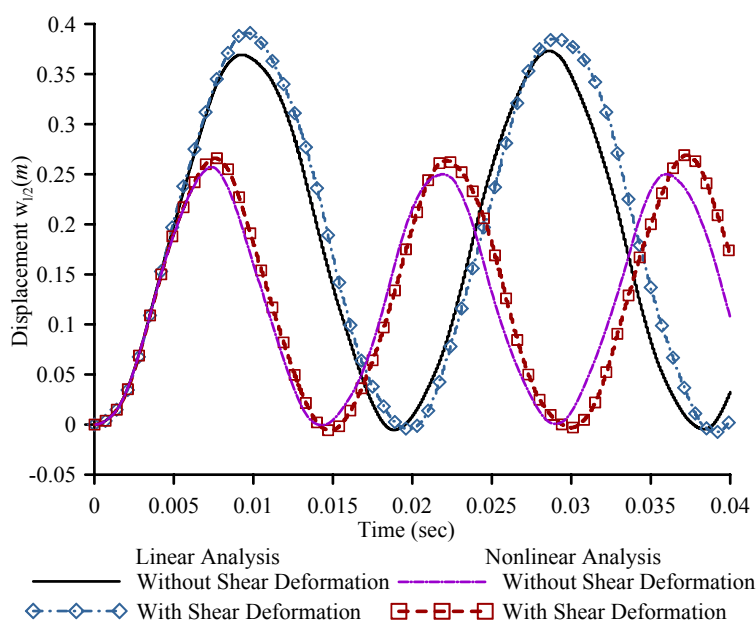
ελέγχεται, όπου είναι εφικτό, με υπάρχουσες αναλυτικές και αριθμητικές λύσεις, ενώ παράλληλα διερευνάται η επιρροή της γεωμετρικής μη γραμμικότητας, της διατμητικής παραμόρφωσης καθώς και της εδαφικής προσομοίωσης στη δυναμική απόκριση του συστήματος αλληλεπίδρασης δοκού – εδάφους. Επιπλέον, προκειμένου να διερευνηθεί η αξιοπιστία της προτεινόμενης μεθοδολογίας, τα ληφθέντα αριθμητικά αποτελέσματα συγκρίνονται με αυτά που προκύπτουν από προσομοιώματα στερεών (εξαεδρικών) και κελυφωτών (τετραπλευρικών) πεπερασμένων στοιχείων.



Σχ. 3. Διάγραμμα ροής του επαναληπτικού αλγορίθμου του προβλήματος ελαστικής δυναμικής απόκρισης συστήματος αλληλεπίδρασης δοκού – εδάφους.

Ως αντιπροσωπευτική αριθμητική εφαρμογή, μελετήθηκε αμφίπακτη δοκός μήκους $l = 4.9m$, κοίλης ορθογωνικής διατομής ($E = 210GPa$, $\nu = 0.3$, $\rho = 7.85tn/m^3$) η οποία εδράζεται επί ελαστικού εδάφους. Στο Σχ. 4 παρουσιάζεται η χρονοϊστορία της εγκάρσιας μετατόπισης $w(l/2)$ του κέντρου βάρους της μεσαίας διατομής της δοκού που προκύπτει με εφαρμογή γραμμικής ή μη γραμμικής ανάλυσης λαμβάνοντας υπόψη ή αγνοώντας τη διατμητική παραμόρφωση.

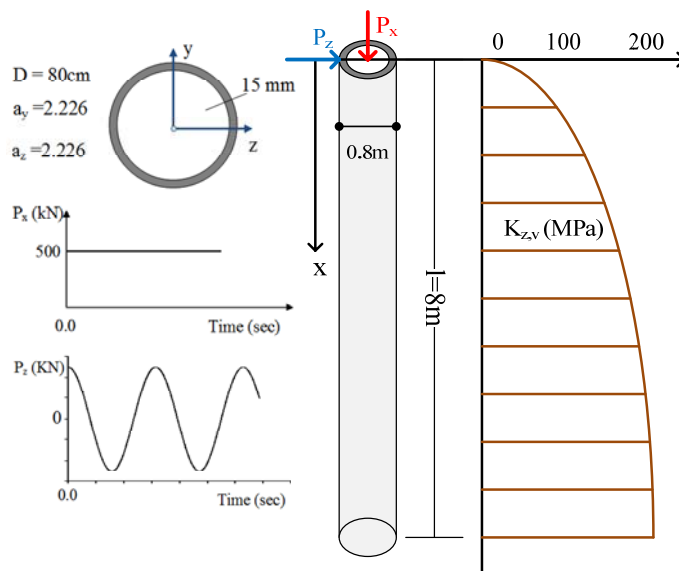
Παρατηρείται ότι, λόγω δέσμμευσης της αξονικής μετακίνησης στα δύο άκρα της δοκού, αναπτύσσονται σημαντικές εφελκυστικές δυνάμεις οι οποίες απομειώνουν τα βέλη και το χρόνο ταλάντωσης που προκαλεί η εξωτερική φόρτιση. Αντίθετα, το φαινόμενο της διατμητικής παραμόρφωσης προκαλεί αύξηση τόσο στις μετατοπίσεις όσο και στο χρόνο ταλάντωσης του πρώτου κύκλου κίνησης της δοκού.



Σχ. 4. Χρονοϊστορία μετακίνησης του κέντρου βάρους της μεσαίας διατομής της δοκού επί ελαστικού εδάφους $k_z = 645kPa$.

Επιπλέον, προκειμένου να διερευνηθεί η επιρροή της γεωμετρικής μη γραμμικότητας καθώς και της διατμητικής παραμόρφωσης, μελετήθηκε πάσσαλος μήκους $l = 8m$, κοίλης κυκλικής διατομής ($E = 210GPa$, $\nu = 0.3$, $\rho = 7.85tn/m^3$). Τα γεωμετρικά χαρακτηριστικά της διατομής, η δυσκαμψία του εδαφικού μέσου καθώς και η φόρτιση της κεφαλής του πασσάλου απεικονίζονται στο Σχ. 5. Μελετάται η κατάσταση πρωτεύοντος συντονισμού του πασσάλου κατά την οποία ασκείται

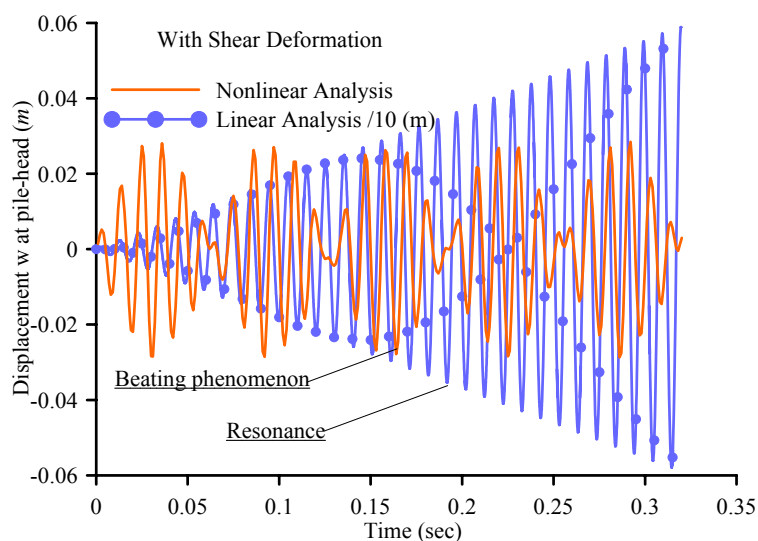
εξωτερικά επιβαλλόμενη συγκεντρωμένη ημιτονοειδής εγκάρσια φόρτιση στο κέντρο βάρους της κεφαλής του πασσάλου.



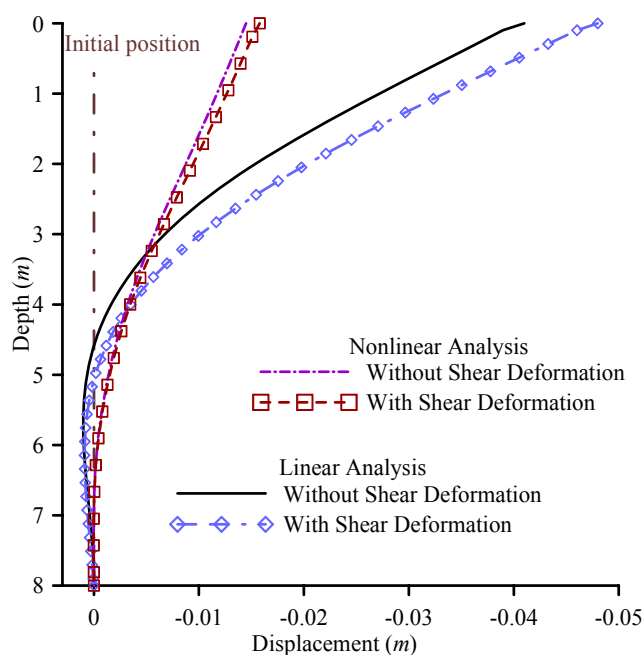
Σχ.5. Πάσσαλος κοίλης κυκλικής διατομής εμπηγνύομενος σε ανομοιογενές έδαφος.

Στο Σχ. 6 παρουσιάζεται η χρονοϊστορία της εγκάρσιας μετατόπισης $w(l/2)$ του κέντρου βάρους της κεφαλής του πασσάλου που προκύπτει με εφαρμογή γραμμικής ή μη γραμμικής ανάλυσης λαμβάνοντας υπόψη τη διατμητική παραμόρφωση. Όπως αναμενόταν, μόνο στη γραμμική ανάλυση η εγκάρσια μετατόπιση αυξάνεται με το χρόνο (συντονισμός). Το διακρότημα που παρατηρείται στη χρονική απόκριση της μη γραμμικής ανάλυσης μπορεί να εξηγηθεί από το γεγονός ότι οι μεγάλες εγκάρσιες μετατοπίσεις αυξάνουν τη θεμελιώδη ιδιοσυχνότητα του πασσάλου. Συνεπώς, προκαλείται αποσυντονισμός μεταξύ της χρονικά μεταβαλλόμενης θεμελιώδους ιδιοσυχνότητας και της σταθερής διεγείρουσας συχνότητας του εξωτερικού φορτίου. Αφού η μετατόπιση λαμβάνει τη μέγιστη τιμή της, το εύρος της ταλάντωσης μειώνεται με αποτέλεσμα να προκαλείται και πάλι συντονισμός λόγω αντιστροφής του προαναφερθέντος μηχανισμού.

Επιπρόσθετα, στο Σχ. 7 παρουσιάζεται η εγκάρσια μετατόπιση κατά μήκος του πασσάλου τη χρονική στιγμή $t = 0.04 \text{ sec}$ που προκύπτει με εφαρμογή γραμμικής ή μη γραμμικής ανάλυσης λαμβάνοντας υπόψη ή αγνοώντας τη διατμητική παραμόρφωση. Από το σχήμα διαπιστώνεται ότι η επιρροή τόσο της γεωμετρικής μη γραμμικότητας όσο και της διατμητικής παραμόρφωσης είναι σημαντική και πρέπει να λαμβάνεται υπόψη στη δυναμική ανάλυση.



Σχ. 6. Χρονοϊστορία εγκάρσια μετατόπισης της κεφαλής του πασσάλου.



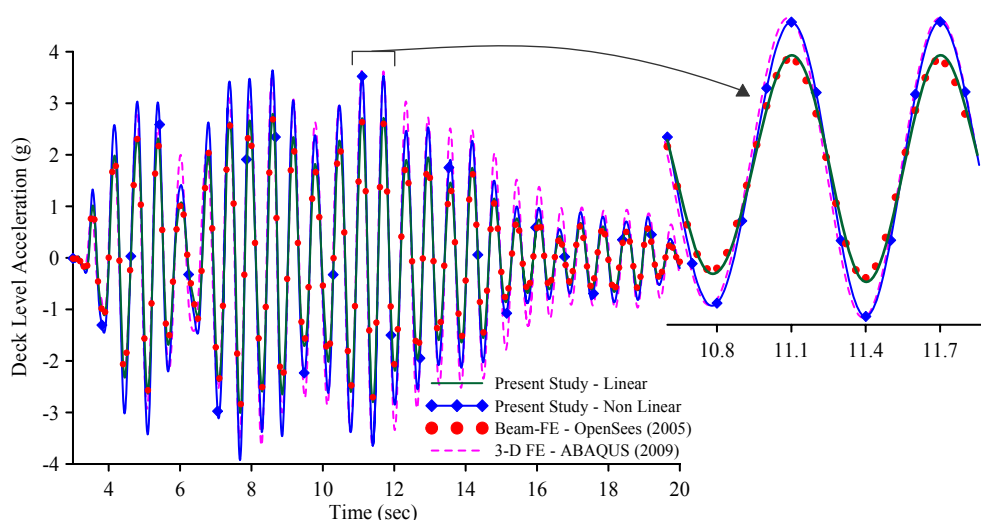
Σχ. 7. Εγκάρσια μετατόπιση κατά μήκος του πασσάλου τη χρονική στιγμή $t = 0.04 \text{ sec}$.

Εν συνεχεία, έχοντας επαληθεύσει την αξιοπιστία της μεθόδου, το προτεινόμενο προσομοίωμα δοκού εφαρμόστηκε στη μελέτη δυναμικής απόκρισης συστήματος εδάφους-πασσάλου-κατασκευής (soil-pile-structure interaction) υπό τρεις εξεταζόμενες σεισμικές διεγέρσεις. Συγκεκριμένα μελετήθηκαν τα επιταχυνσιογραφήματα του σεισμού του Αιγίου (1995), της Λευκάδας (2003) καθώς και του Kobe, Ιαπωνία (1995).

Η ανάλυση του συστήματος επιτυγχάνεται σε δύο διαδοχικά στάδια. Αρχικά πραγματοποιείται ανελαστική μη γραμμική ανάλυση της απόκρισης του εδαφικού

σηματισμού αμελώντας την παρουσία της θεμελίωσης και στη συνέχεια δυναμική ανάλυση του συστήματος εδάφους-πασσάλου-κατασκευής, λαμβάνοντας υπόψη τη γεωμετρική μη γραμμικότητα, τη διατμητική παραμόρφωση καθώς και την κινηματική και αδρανειακή αλληλεπίδραση. Για την προσομοίωση της μη γραμμικής ανελαστικής συμπεριφοράς του εδαφικού σχηματισμού χρησιμοποιήθηκε μια υβριδική διάταξη ελατηρίων και αποσβεστήρων.

Στο Σχ. 8 παρουσιάζεται η χρονοϊστορία επιτάχυνσης της κεφαλής του πασσάλου με βάση τα αποτελέσματα που ελήφθησαν από την εφαρμογή της προτεινόμενης μεθόδου. Στο ίδιο σχήμα παρουσιάζονται επίσης τα αποτελέσματα που προέκυψαν από τη λεπτομερή προσομοίωση του συστήματος σε τρισδιάστατο προσομοίωμα πεπερασμένων στοιχείων. Παρατηρείται ότι τα αποτελέσματα παρουσιάζουν άριστη σύγκλιση.



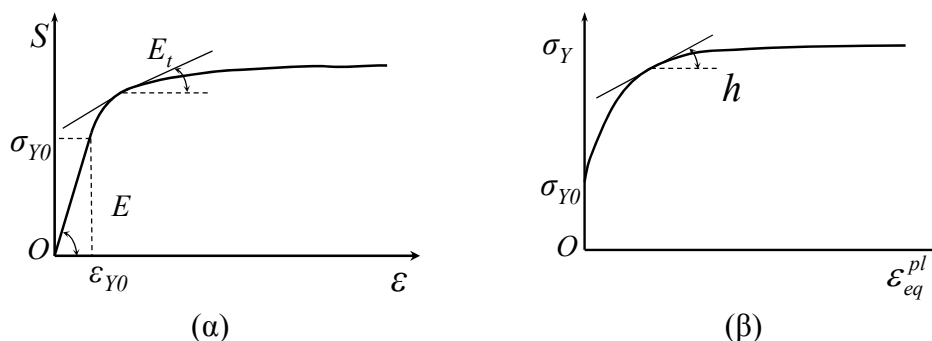
Σχ. 8. Χρονοϊστορία επιτάχυνσης της κεφαλής του πασσάλου για το σειсмоγράφημα της Λευκάδας (2003).

IV. Γεωμετρικά Μη Γραμμική και Ανελαστική Ανάλυση Δοκών με Διατμητικές Παραμορφώσεις επί Μη Γραμμικού Ανελαστικού Εδάφους

Στη συνέχεια διερευνάται και επιλύεται το στατικό πρόβλημα της γεωμετρικά μη γραμμικής ανελαστικής ανάλυσης δοκού διπλά συμμετρικής διατομής, επί μη γραμμικού ανελαστικού εδάφους. Το υλικό της δοκού είναι ελαστοπλαστικό με ισότροπη κράτυνση. Η δοκός υποβάλλεται σε τυχούσα συγκεντρωμένη ή κατανεμημένη καμπτική φόρτιση καθώς και σε τυχόν αξονικό φορτίο, ενώ τα άκρα της υπόκεινται στις

πλέον γενικές συνοριακές συνθήκες. Η γεωμετρική μη γραμμικότητα και η επιρροή των διατμητικών παραμορφώσεων λαμβάνεται υπόψη ομοίως με την περίπτωση της ελαστικής ανάλυσης. Το εδαφικό προσομοίωμα χαρακτηρίζεται από μη γραμμικά ελατήρια τύπου Winkler και από ελατήρια τύπου Pasternak, ενώ επίσης έχει προσομοιωθεί η αδυναμία ανάληψης εφελκυστικών τάσεων (tensionless foundation models). Οι πλαστικές παραμορφώσεις προσδιορίζονται μέσω προσομοιώματος κατανεμημένης πλαστικότητας (distributed plasticity model), γνωστό και ως προσομοίωμα ινών (fibre model) χρησιμοποιώντας τρισδιάστατες καταστατικές σχέσεις (J2 plasticity). Οι σχέσεις αυτές ολοκληρώνονται με τη βοήθεια αποδοτικής επαναληπτικής μεθόδου. Σύμφωνα με την προτεινόμενη μέθοδο μορφώνονται με τη βοήθεια των θεωριών ελαστικότητας και ελαστοπλαστικότητας πέντε προβλήματα συνοριακών τιμών. Πιο συγκεκριμένα, μορφώνονται δύο διδιάστατα προβλήματα συνοριακών τιμών αναφορικά με τις τασικές συναρτήσεις που αναφέρονται στους συντελεστές διάτμησης, τα οποία επιλύονται με τη βοήθεια “αμιγούς” Μεθόδου Συνοριακών Στοιχείων. Επίσης, μορφώνονται τρία μονοδιάστατα προβλήματα συνοριακών τιμών αναφορικά με την αξονική και τις εγκάρσιες μετατοπίσεις, που επιλύονται με τη βοήθεια της Πεδιακής Μεθόδου Συνοριακών Στοιχείων, σε συνδυασμό με την υβριδική μέθοδο Powell για την επίλυση μη γραμμικών συστημάτων αλγεβρικών εξισώσεων. Η επίλυση του προβλήματος αυτού πραγματοποιείται στα πλαίσια προσαυξητικού - επαναληπτικού αλγορίθμου που βασίζεται στη μέθοδο του ελέγχου φορτίου. Με την προτεινόμενη αριθμητική μέθοδο αντιμετωπίζεται επιτυχώς το πρόβλημα του «διατμητικού κλειδώματος».

Για τη μαθηματική διατύπωση του προβλήματος, εξετάζεται ευθύγραμμη πρισματική δοκός μήκους l , διατομής τυχόντος διπλά συμμετρικού σχήματος αποτελούμενη από συνεχές, ελαστοπλαστικό υλικό με ισότροπη κράτυνση, με μέτρο κράτυνσης h και εφαπτομενικό μέτρο ελαστοπλαστικότητας E_t (Σχ. 9) χωρίς να εμφανίζει βλάβη κατά την πλαστικοποίησή του, με μέτρο ελαστικότητας E , μέτρο διάτμησης G και τάση διαρροής σ_{Y0} , το οποίο καταλαμβάνει την περιοχή Ω του επιπέδου yz . Το σύνορο της διατομής του χωρίου Ω , είναι τμηματικά λείο, μπορεί δηλαδή να περιλαμβάνει πεπερασμένο αριθμό γωνιών και συμβολίζεται με $\Gamma = \bigcup_{j=0}^K \Gamma_j$ ($j = 1, 2, \dots, K$). Η δοκός θεωρείται μερικώς εδραζόμενη επί μη γραμμικού ανελαστικού εδάφους τύπου Pasternak, ενώ λαμβάνεται επίσης υπόψη η μη γραμμική επαφή μεταξύ της δοκού και του εδαφικού μέσου (interface nonlinearity).



Σχ. 9. Σχέση ορθών τάσεων - παραμορφώσεων (α) και σχέση τάσης διαρροής - ισοδύναμης πλαστικής παραμόρφωσης (β).

Υιοθετώντας το πεδίο μετατοπίσεων τυχαίου σημείου της διατομής λαμβάνοντας υπόψη τη διατμητική παραμόρφωση (εξ. 2) και θεωρώντας μικρές παραμορφώσεις, οι συνιστώσες του 2^{ου} τανυστή τάσης Piola-Kirchhoff δίδονται συναρτήσει των παραμορφώσεων και πλαστικών παραμορφώσεων Green ως

$$S_{xx} = E \left[\frac{du(x)}{dx} - y \frac{d\theta_z(x)}{dx} + z \frac{d\theta_y(x)}{dx} + \frac{1}{2} \left(\left(\frac{dv(x)}{dx} \right)^2 + \left(\frac{dw(x)}{dx} \right)^2 \right) - \varepsilon_{xx}^{pl} \right] \quad (17\alpha)$$

$$S_{xy} = G \left[\frac{dv(x)}{dx} - \theta_z(x) - \gamma_{xy}^{pl} \right] \quad S_{xz} = G \left[\frac{dw(x)}{dx} + \theta_y(x) - \gamma_{xz}^{pl} \right] \quad (17\beta,\gamma)$$

όπου με τον εκθέτη pl συμβολίζεται το πλαστικό μέρος των συνιστωσών του τανυστή παραμόρφωσης. Ως κριτήριο διαρροής χρησιμοποιείται η συνάρτηση von Mises (yield function, J2 plasticity)

$$\Phi_{vM} = \frac{\sqrt{S_{xx}^2 + 3(S_{xy}^2 + S_{xz}^2)}}{\sigma_Y(\varepsilon_{eq}^{pl})} - I \leq 0 \quad (18)$$

όπου (ε_{eq}^{pl}) είναι η ολική ισοδύναμη πλαστική παραμόρφωση (total equivalent plastic strain).

Αντικαθιστώντας τις εκφράσεις των τάσεων συναρτήσει των κινηματικών μεγεθών στους ορισμούς των εντατικών μεγεθών προκύπτουν οι ακόλουθες εκφράσεις

$$N = EA \left[u' + \frac{I}{2} (v'^2 + w'^2) \right] \underbrace{-E \int_{\Omega} \varepsilon_{xx}^{pl} dA}_{N^{pl}} = EA \left[u' + \frac{I}{2} (v'^2 + w'^2) \right] + N^{pl} \quad (19\alpha)$$

$$Q_z = GA_z (w'(x) + \theta_y(x)) \underbrace{-G \int_{A_z} \gamma_{xz}^{pl} dA}_{Q_z^{pl}} = GA_z (w'(x) + \theta_y(x)) + Q_z^{pl} \quad (19\beta)$$

$$Q_y = GA_y (v'(x) - \theta_z(x)) \underbrace{-G \int_{A_y} \gamma_{xy}^{pl} dA}_{Q_y^{pl}} = GA_y (v'(x) - \theta_z(x)) + Q_y^{pl} \quad (19\gamma)$$

$$M_y = EI_y \theta_y' \underbrace{-E \int_{\Omega} z \varepsilon_{xx}^{pl} dA}_{M_y^{pl}} = EI_y \theta_y' + M_y^{pl} \quad (19\delta)$$

$$M_z = EI_z \theta_z' \underbrace{-E \int_{\Omega} y \varepsilon_{xx}^{pl} dA}_{M_z^{pl}} = EI_z \theta_z' + M_z^{pl} \quad (19\epsilon)$$

όπου με N^{pl} , Q_z^{pl} , Q_y^{pl} , M_z^{pl} και M_y^{pl} συμβολίζεται το πλαστικό μέρος των αντιστοιχών εντατικών μεγεθών. Εν συνεχεία, εφαρμόζοντας την Αρχή Δυνατών Έργων σε ολική διατύπωση Lagrange προκύπτουν οι διαφορικές εξισώσεις που περιγράφουν την καθολική ισορροπία του συστήματος, οι οποίες εκφράζονται ως

$$EA(u'' + v'v'' + w'w'') + \frac{\partial N^{pl}}{\partial x} = -p_x \quad (20\alpha)$$

$$EA \left[\left(u' + \frac{I}{2} (v'^2 + w'^2) \right) v' \right]' + \frac{d(N^{pl} v')}{dx} + GA_y (v' - \theta_z)' + \frac{\partial Q_y^{pl}}{\partial x} - p_{sy} = -p_y \quad (20\beta)$$

$$EA \left[\left(u' + \frac{I}{2} (v'^2 + w'^2) \right) w' \right]' + \frac{d(N^{pl} w')}{dx} + GA_z (w' + \theta_y)' + \frac{\partial Q_z^{pl}}{\partial x} - p_{sz} = -p_z \quad (20\gamma)$$

$$EI_y \theta_y'' + \frac{dM_y^{pl}}{dx} - GA_z (w' + \theta_y) - Q_z^{pl} = -m_y \quad (20\delta)$$

$$EI_z \theta_z'' + \frac{dM_z^{pl}}{dx} + GA_y (v' - \theta_z) + Q_y^{pl} = -m_z \quad (20\epsilon)$$

Εναλλακτικά οι παραπάνω εξισώσεις γράφονται σε όρους εντατικών μεγεθών ως

$$\frac{d(N^{el} + N^{pl})}{dx} = -p_x \Rightarrow \frac{dN}{dx} = -p_x \quad (21\alpha)$$

$$-\frac{d(Nv')}{dx} - \frac{dQ_y}{dx} + p_{sy} = p_y \quad -\frac{d(Nw')}{dx} - \frac{dQ_z}{dx} + p_{sz} = p_z \quad (21\beta,\gamma)$$

$$\frac{dM_y}{dx} - Q_z = -m_y \quad \frac{dM_z}{dx} + Q_y = -m_z \quad (21\delta,\epsilon)$$

Από την εφαρμογή της Αρχής Δυνατών Έργων επίσης προκύπτουν οι αντίστοιχες συνοριακές συνθήκες στα άκρα της δοκού $x=0, l$ οι οποίες διατυπώνονται με την ακόλουθη γενική μορφή

$$a_1\mu(x) + a_2N_b(x) = a_3 \quad (22\alpha)$$

$$\beta_1v(x) + \beta_2V_{by}(x) = \beta_3 \quad \bar{\beta}_1\theta_z(x) + \bar{\beta}_2M_{bz}(x) = \bar{\beta}_3 \quad (22\beta,\gamma)$$

$$\gamma_1w(x) + \gamma_2V_{bz}(x) = \gamma_3 \quad \bar{\gamma}_1\theta_y(x) + \bar{\gamma}_2M_{by}(x) = \bar{\gamma}_3 \quad (22\delta,\epsilon)$$

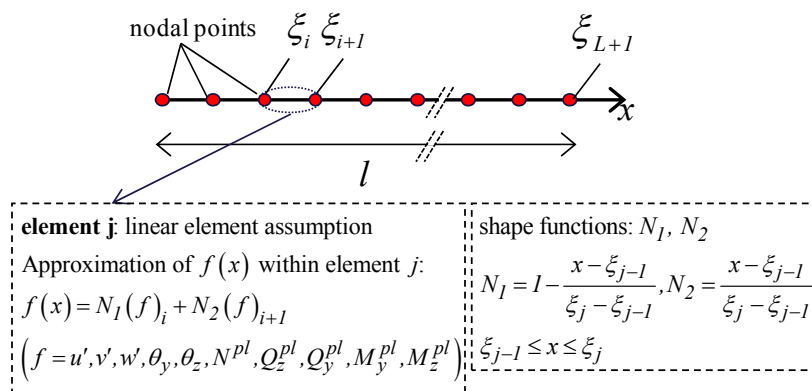
όπου V_{by} , V_{bz} είναι οι ολικές τέμνουσες και M_{by} , M_{bz} οι ολικές ροπές, και δίνονται από τις ακόλουθες σχέσεις

$$V_{by} = EA \left[u' + \frac{I}{2}(v'^2 + w'^2) \right] v' + N^{pl}v' + GA_y(v' - \theta_z) + Q_y^{pl} \quad (23\alpha)$$

$$V_{bz} = EA \left[u' + \frac{I}{2}(v'^2 + w'^2) \right] w' + N^{pl}w' + GA_z(w' + \theta_y) + Q_z^{pl} \quad (23\beta)$$

$$M_{by} = EI_y\theta'_y + M_y^{pl} \quad M_{bz} = EI_z\theta'_z + M_z^{pl} \quad (23\gamma,\delta)$$

Η αριθμητική επίλυση του πεπλεγμένου προβλήματος συνοριακών τιμών επιτυγχάνεται με τη βοήθεια της Πεδιακής Μεθόδου Συνοριακών Στοιχείων. Το διάστημα της δοκού $(0, l)$ διαιρείται σε L γραμμικά στοιχεία (Σχ. 10) και η εφαρμογή της μεθόδου οδηγεί στη μόρφωση ενός μη γραμμικού συστήματος $7L + 23$ αλγεβρικών εξισώσεων, το οποίο εκφράζεται σε τυπική μορφή ως

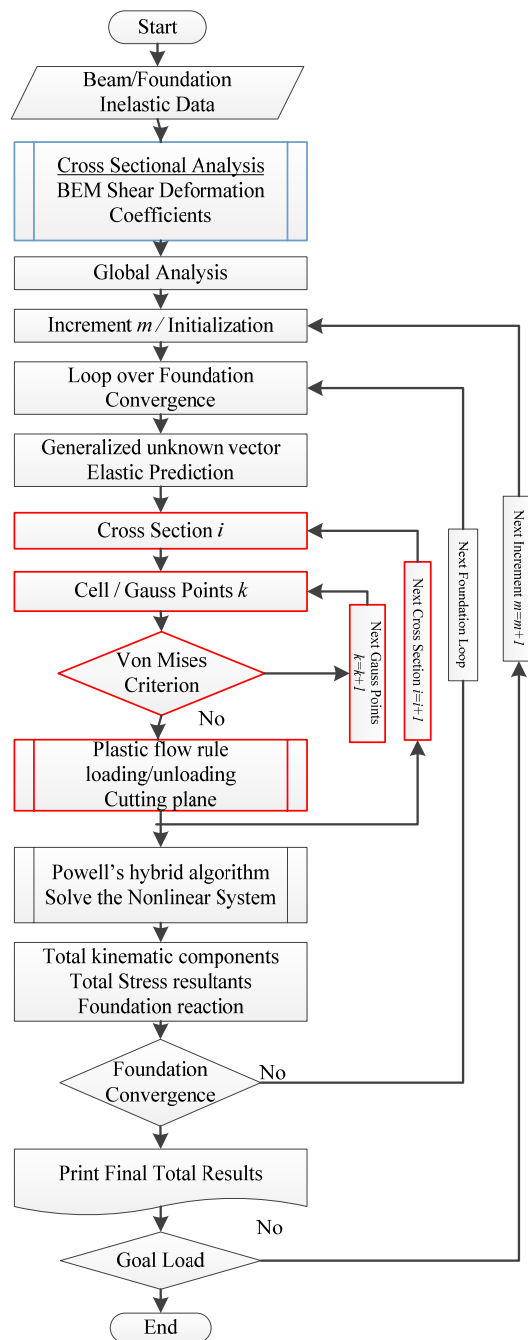


Σχ. 10. Διακριτοποίηση της δοκού σε γραμμικά στοιχεία.

$$[K(d)]\{d\} = \{b_{ext}\} + \{b_{pl}(d)\} \tag{24}$$

όπου $\{d\}$ το γενικευμένο μητρώο στήλη άγνωστων ποσοτήτων, $[K]$ το γενικευμένο μητρώο στιβαρότητας, $\{b_{pl}\}$ το γενικευμένο πλαστικό μητρώο στήλη και $\{b_{ext}\}$ το γενικευμένο γνωστό μητρώο στήλη φόρτισης. Για την αριθμητική επίλυση του μη γραμμικού συστήματος αλγεβρικών εξισώσεων εφαρμόστηκε η υβριδική μέθοδος επίλυσης Powell (1977, 1985). Στο Σχ. 11, παρουσιάζεται το διάγραμμα ροής του μη γραμμικού προσαυξητικού - επαναληπτικού αλγορίθμου επίλυσης του προβλήματος.

Με βάση την αναπτυχθείσα αναλυτική και αριθμητική διαδικασία, συντάχθηκε πρόγραμμα ηλεκτρονικού υπολογιστή σε υπολογιστικό περιβάλλον Fortran 90/95 με τη βοήθεια του οποίου μελετήθηκαν αντιπροσωπευτικά παραδείγματα με πρακτικό ενδιαφέρον, προκειμένου να διαπιστωθεί η αποτελεσματικότητα και το εύρος εφαρμογής της προτεινόμενης μεθόδου. Η ακρίβεια των αριθμητικών αποτελεσμάτων ελέγχεται, όπου είναι εφικτό, με υπάρχουσες αριθμητικές λύσεις και πειραματικά δεδομένα, ενώ παράλληλα διερευνάται η επιρροή της μη γραμμικότητας υλικού και γεωμετρίας, της διατμητικής παραμόρφωσης καθώς και της εδαφικής προσομοίωσης στην ανελαστική απόκριση του συστήματος αλληλεπίδρασης δοκού – εδάφους. Επιπλέον, προκειμένου να διερευνηθεί η αξιοπιστία της προτεινόμενης μεθοδολογίας, τα ληφθέντα αριθμητικά αποτελέσματα συγκρίνονται με αυτά που προκύπτουν από προσομοιώματα στερεών (εξαεδρικών) και κελυφωτών (τετραπλευρικών) πεπερασμένων στοιχείων.



Σχ. 11. Διάγραμμα ροής του προσανζητικού - επαναληπτικού αλγορίθμου για την ανελαστική απόκριση συστήματος αλληλεπίδρασης δοκού – εδάφους.

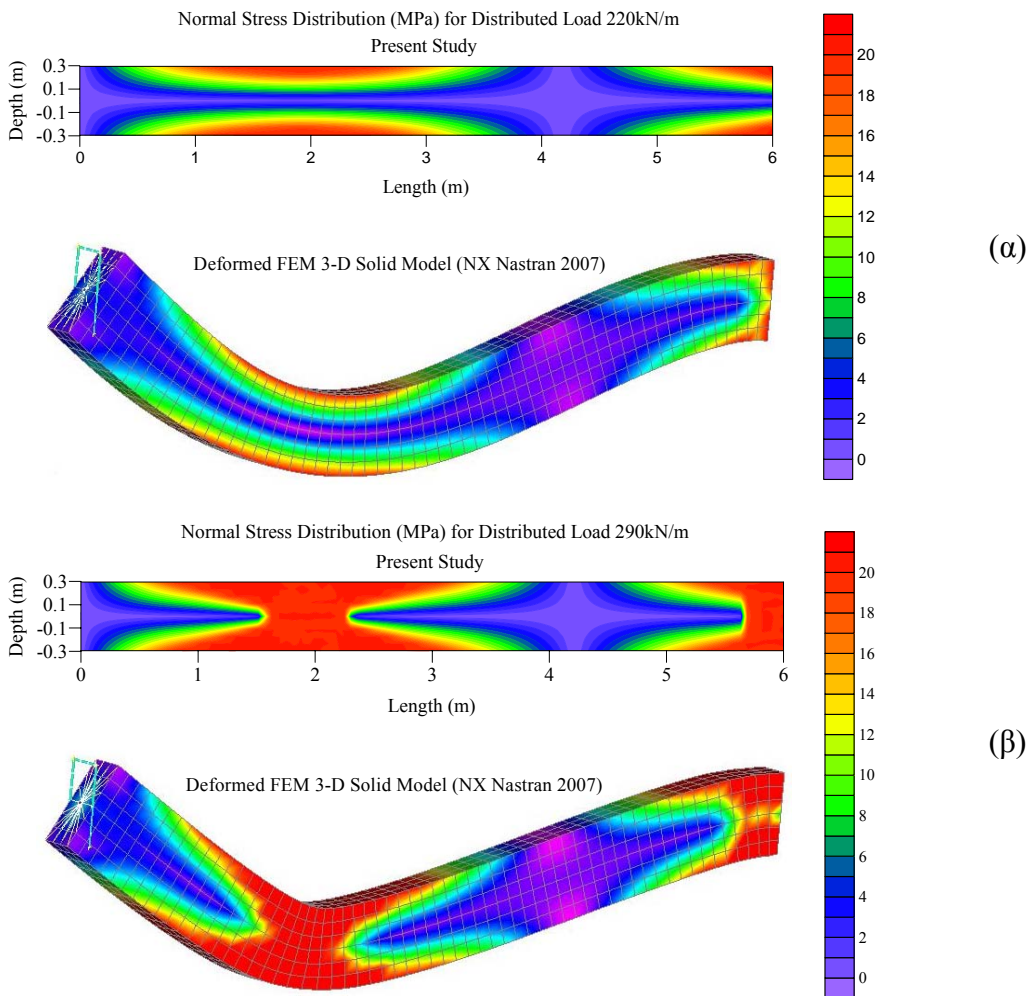
Ως αντιπροσωπευτική αριθμητική εφαρμογή, μελετήθηκε μονόπακτη δοκός μήκους $l = 6m$, συμπαγούς ορθογωνικής διατομής $60 \times 30cm^2$ ($E = 32318.4MPa$, $\sigma_{Y0} = 20MN/m^2$) η οποία εδράζεται επί μη γραμμικού ανελαστικού εδάφους και καταπονείται από ομοιόμορφα κατανεμημένο φορτίο στο τμήμα $0 \leq x \leq 3m$.

Στο Σχ. 12 παρουσιάζεται η κατανομή των ορθών τάσεων κατά μήκος της δοκού για διάφορα στάδια φόρτισης, με βάση τα αποτελέσματα που ελήφθησαν από την εφαρμογή της προτεινόμενης μεθόδου. Στο ίδιο σχήμα παρουσιάζονται επίσης τα αποτελέσματα που προέκυψαν από τη λεπτομερή προσομοίωση του συστήματος σε τρισδιάστατο προσομοίωμα πεπερασμένων στοιχείων. Παρατηρείται ότι τα αποτελέσματα παρουσιάζουν άριστη σύγκλιση.

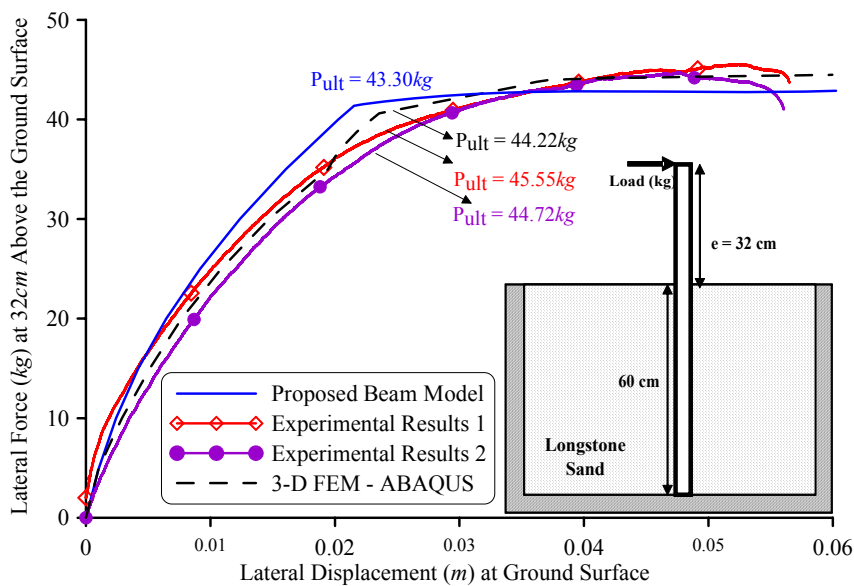
Έχοντας επαληθεύσει την αξιοπιστία της μεθόδου, το προτεινόμενο προσομοίωμα δοκού εφαρμόστηκε για την εκτενή σύγκριση με μία σειρά πειραμάτων μονοτονικός φορτιζομένων μεμονωμένων πασσάλων σε ξηρή άμμο υπό ροπή και οριζόντια δύναμη έως την αστοχία (Push-Over Tests) τα οποία διεξήχθησαν στο Εργαστήριο Δυναμικής / Εδαφομηχανικής του Εθνικού Μετσόβιου Πολυτεχνείου. Στο Σχ. 13 παρουσιάζονται τα αποτελέσματα που ελήφθησαν από την εφαρμογή της προτεινόμενης μεθόδου και συγκρίνονται με αυτά που προκύπτουν από την πειραματική διαδικασία καθώς και από τη λεπτομερή προσομοίωση σε τρισδιάστατο προσομοίωμα πεπερασμένων στοιχείων. Παρατηρείται ότι τα αποτελέσματα παρουσιάζουν πολύ καλή σύγκλιση.

V. Γεωμετρικά Μη Γραμμική και Ανελαστική Δυναμική Ανάλυση Συστημάτων Αλληλεπίδρασης Δοκού – Εδάφους

Στη συνέχεια διερευνάται και επιλύεται το δυναμικό πρόβλημα της γεωμετρικά μη γραμμικής ανελαστικής ανάλυσης δοκού διπλά συμμετρικής διατομής, επί μη γραμμικού ανελαστικού ελαστικού εδάφους. Η δοκός υποβάλλεται σε συνδυασμό φορτίσεων από τυχόν συγκεντρωμένο ή κατανεμημένο δυναμικό αξονικό και εγκάρσιο φορτίο (όμοια με την παράγραφο III), ενώ υπόκειται στις πλέον γενικές χρονικά εξαρτώμενες συνοριακές συνθήκες. Η γεωμετρική μη γραμμικότητα λαμβάνεται υπόψη σε ολική διατύπωση Lagrange μέσω της θεωρίας μεγάλων μετατοπίσεων - μικρών παραμορφώσεων. Το υστερητικό προσομοίωμα τύπου Bouc-Wen υιοθετείται για να περιγράψει την ανελαστική συμπεριφορά των εδαφικών ελατηρίων. Οι πλαστικές παραμορφώσεις προσδιορίζονται μέσω προσομοιώματος κατανεμημένης πλαστικότητας (distributed plasticity model), γνωστό και ως προσομοίωμα ινών (fibre model) χρησιμοποιώντας το υστερητικό προσομοίωμα τύπου Sivaselvan and Reinhorn. Οι σχέσεις αυτές ολοκληρώνονται με τη βοήθεια αποδοτικής - επαναληπτικής μεθόδου.



Σχ. 12. Κατανομή των ορθών τάσεων κατά μήκος της δοκού για διάφορα στάδια φόρτισης.



Σχ. 13. Καμπύλη φορτίου-μετατόπισης στην κεφαλή του πασσάλου.

Σύμφωνα με την προτεινόμενη μέθοδο μορφώνονται με τη βοήθεια της θεωρίας ελαστοπλαστικότητας τρία μονοδιάστατα προβλήματα συνοριακών τιμών αναφορικά με την αξονική και τις εγκάρσιες μετατοπίσεις, που επιλύονται με τη βοήθεια της Μεθόδου Αναλογικής Εξίσωσης, σε συνδυασμό με την μέθοδο Petzold–Gear για την επίλυση μη γραμμικών συστημάτων διαφορικών-αλγεβρικών εξισώσεων.

Για τη μαθηματική διατύπωση του προβλήματος, εξετάζεται ευθύγραμμη πρισματική δοκός με γεωμετρικά χαρακτηριστικά όμοια με αυτά της προηγούμενης παραγράφου. Η εδαφική αντίδραση επί της δοκού δίδεται από τις υστερητικές εκφράσεις δύναμης-μετατόπισης τύπου Bouc-Wen, ως

$$p_{sy} = a_{sy}k_y v + (1 - a_{sy})k_y z_{sy}^h \quad \text{και} \quad p_{sz} = a_{sz}k_z w + (1 - a_{sz})k_z z_{sz}^h \quad (25)$$

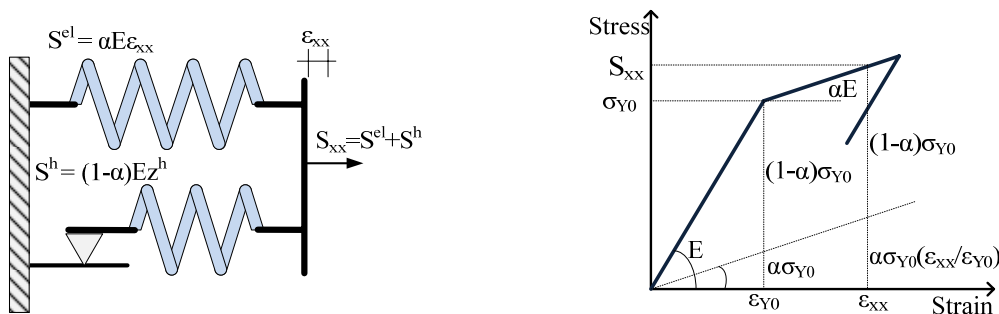
όπου p_{sy}, p_{sz} είναι οι δυνάμεις των ελατηρίων, k_y, k_z είναι η αρχική δυσκαμψία, a_{sy}, a_{sz} είναι οι λόγοι της μετελαστικής προς την ελαστική δυσκαμψία και z_{sy}^h, z_{sz}^h είναι το υστερητικό τμήμα της πραγματικής μετατόπισης στις y και z διευθύνσεις, αντίστοιχα και προσδιορίζονται από τις υστερητικές εξισώσεις Bouc-Wen, ως

$$\dot{z}_{sy}^h(z_{sy}^h, \dot{v}) = \left(1 - \left| \frac{z_{sy}^h}{z_{sy}^h - Yield} \right|^n \left(\beta + \gamma \text{sign}(z_{sy}^h \dot{v}) \right) \right) \dot{v} \quad (26\alpha)$$

$$\dot{z}_{sz}^h(z_{sz}^h, \dot{w}) = \left(1 - \left| \frac{z_{sz}^h}{z_{sz}^h - Yield} \right|^n \left(\beta + \gamma \text{sign}(z_{sz}^h \dot{w}) \right) \right) \dot{w} \quad (26\beta)$$

Η δοκός υποβάλλεται σε συνδυασμό φορτίσεων από τυχόν συγκεντρωμένο ή κατανομημένο δυναμικό αξονικό φορτίο $p_x(x, t)$, χρονικά εξαρτώμενο εγκάρσιο φορτίο $p_y(x, t)$, $p_z(x, t)$ καθώς και καμπτική φόρτιση $m_y(x, t)$, $m_z(x, t)$.

Υιοθετώντας το πεδίο μετατοπίσεων τυχαίου σημείου της διατομής (εξ. 10) αγνοώντας τη διατμητική παραμόρφωση (θεωρία δοκού Euler-Bernoulli), θεωρώντας μικρές παραμορφώσεις και χρησιμοποιώντας το φαινομενολογικό προσομοίωμα των Sivaselvan and Reinhorn (2003), η συνιστώσα του 2^{ου} τανυστή τάσης Piola-Kirchhoff δίδεται συναρτήσει της παραμόρφωσης Green και της υστερητικής παραμορφώσεων ως (Σχ. 14)



Σχ. 14. Υστερητικό προσομοίωμα Bouc-Wen (α) σχέση ορθής τάσης παραμόρφωσης (β).

$$S_{xx} = \alpha S_{xx}^{el} + (1-\alpha) S^h = \alpha E \varepsilon_{xx} + (1-\alpha) E z^h \quad (27)$$

όπου S_{xx}^{el} , S^h είναι το ελαστικό και το υστερητικό μέρος της τάσης, αντίστοιχα. Το υστερητικό μέρος εξελίσσεται στο χρόνο σύμφωνα με την υστερητική εξίσωση Bouc-Wen (Casciati 1995), ως

$$\dot{S}^h(z^h, \dot{\varepsilon}_{xx}) = E z^h = E(1-h_1 h_2) \dot{\varepsilon}_{xx} \quad (28)$$

με
$$h_1 = \left\| \Phi(S^h) + I \right\|^n \quad \text{και} \quad h_2 = \beta + \gamma \operatorname{sign}(S^h \dot{\varepsilon}_{xx}) \quad (29)$$

όπου $\Phi = \Phi_{vM} = S_{xx}^2 / \sigma_Y^2 (\varepsilon_{eq}^{pl}) - I \leq 0$ είναι μια απλοποιημένη έκφραση της συνάρτησης von Mises και αποτελεί το κριτήριο διαρροής.

Αντικαθιστώντας τις εκφράσεις των τάσεων συναρτήσει των κινηματικών μεγεθών στους ορισμούς των εντατικών μεγεθών προκύπτουν οι ακόλουθες εκφράσεις

$$N = \alpha EA \left[u' + \frac{1}{2} (v'^2 + w'^2) \right] + (1-\alpha) \int_{\Omega} S^h d\Omega = \alpha N^{el} + (1-\alpha) N^h \quad (30\alpha)$$

$$M_y = -\alpha EI_y w'' + (1-\alpha) \int_{\Omega} S^h z d\Omega = \alpha M_y^{el} + (1-\alpha) M_y^h \quad (30\beta)$$

$$M_z = \alpha EI_z v'' - (1-\alpha) \int_{\Omega} S^h y d\Omega = \alpha M_z^{el} - (1-\alpha) M_z^h \quad (30\gamma)$$

όπου με N^h , M_z^h και M_y^h συμβολίζεται το υστερητικό μέρος των αντιστοιχών εντατικών μεγεθών. Εν συνεχεία, εφαρμόζοντας την Αρχή Δυνατών Έργων σε ολική

διατύπωση Lagrange προκύπτουν οι διαφορικές εξισώσεις που περιγράφουν την καθολική ισορροπία του συστήματος, οι οποίες εκφράζονται ως

$$\rho A \ddot{u} - \alpha EA(u'' + v'v'' + w'w'') - \frac{(1-a)\partial N^h}{\partial x} = p_x(x,t) \quad (31\alpha)$$

$$\begin{aligned} \rho A \ddot{v} + aEI_z v'''' - (1-a)\frac{\partial^2 M_z^h}{\partial x^2} - aEA \left[\left(u'v' + \frac{1}{2}v'^3 + \frac{1}{2}w'^2v' \right)' \right] - \\ - (1-a)\frac{\partial(N^h v')}{\partial x} + p_{sy}(x,t) = p_y(x,t) - m'_z(x,t) \end{aligned} \quad (32\beta)$$

$$\begin{aligned} \rho A \ddot{w} + aEI_y w'''' - (1-a)\frac{\partial^2 M_y^h}{\partial x^2} - aEA \left[\left(u'w' + \frac{1}{2}w'^3 + \frac{1}{2}v'^2w' \right)' \right] - \\ - (1-a)\frac{\partial(N^h w')}{\partial x} + p_{sz}(x,t) = p_z(x,t) + m'_y(x,t) \end{aligned} \quad (32\gamma)$$

Εναλλακτικά οι παραπάνω εξισώσεις γράφονται σε όρους εντατικών μεγεθών ως

$$\rho A \ddot{u} - \left[\alpha \frac{\partial N^{el}}{\partial x} + (1-a)\frac{\partial N^h}{\partial x} \right] = p_x \quad (33\alpha)$$

$$\rho A \ddot{v} + aEI_z v'''' - (1-a)\frac{\partial^2 M_z^h}{\partial x^2} - a\frac{\partial(N^{el}v')}{\partial x} - (1-a)\frac{\partial(N^h v')}{\partial x} + p_{sy} = p_y - m'_z \quad (33\beta)$$

$$\rho A \ddot{w} + aEI_y w'''' - (1-a)\frac{\partial^2 M_y^h}{\partial x^2} - a\frac{\partial(N^{el}w')}{\partial x} - (1-a)\frac{\partial(N^h w')}{\partial x} + p_{sz} = p_z + m'_y \quad (33\gamma)$$

Από την εφαρμογή της Αρχής Δυνατών Έργων επίσης προκύπτουν οι αντίστοιχες συνοριακές συνθήκες στα άκρα της δοκού $x=0,l$ οι οποίες διατυπώνονται με την ακόλουθη γενική μορφή

$$\alpha_1 u(x,t) + \alpha_2 N_b(x,t) = \alpha_3 \quad (34\alpha)$$

$$\beta_1 v(x,t) + \beta_2 V_{by}(x,t) = \beta_3 \quad \bar{\beta}_1 \frac{\partial v}{\partial x}(x,t) + \bar{\beta}_2 M_{bz}(x,t) = \bar{\beta}_3 \quad (34\beta,\gamma)$$

$$\gamma_1 w(x,t) + \gamma_2 V_{bz}(x,t) = \gamma_3 \quad \bar{\gamma}_1 \frac{\partial w}{\partial x}(x,t) + \bar{\gamma}_2 M_{by}(x,t) = \bar{\gamma}_3 \quad (34\delta,\epsilon)$$

όπου V_{by} , V_{bz} είναι οι ολικές τέμνουσες και M_{by} , M_{bz} οι ολικές ροπές και δίνονται από τις ακόλουθες σχέσεις

$$V_{by} = aEA \left[u' + \frac{I}{2} (v'^2 + w'^2) \right] v' + (1-a) N^h v' - aEI_z v'' + (1-a) \frac{\partial M_z^h}{\partial x} \quad (35\alpha)$$

$$V_{bz} = aEA \left[u' + \frac{I}{2} (v'^2 + w'^2) \right] w' + (1-a) N^h w' - aEI_y w'' + (1-a) \frac{\partial M_y^h}{\partial x} \quad (35\beta)$$

$$M_{by} = -aEI_y w'' + (1-a) M_y^h \quad M_{bz} = EI_z v'' - (1-a) M_z^h \quad (35\gamma, \delta)$$

καθώς και οι αντίστοιχες αρχικές συνθήκες ($x \in (0, l)$) στις οποίες υπόκεινται η δοκός

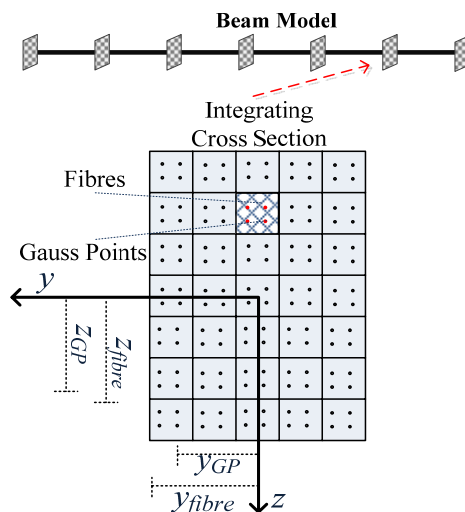
$$u(x, 0) = \bar{u}_0(x) \quad \dot{u}(x, 0) = \dot{\bar{u}}_0(x) \quad (36\alpha, \beta)$$

$$v(x, 0) = \bar{v}_0(x) \quad \dot{v}(x, 0) = \dot{\bar{v}}_0(x) \quad w(x, 0) = \bar{w}_0(x) \quad \dot{w}(x, 0) = \dot{\bar{w}}_0(x) \quad (36\gamma-\zeta)$$

Η αριθμητική επίλυση του πεπλεγμένου προβλήματος αρχικών τιμών επιτυγχάνεται με τη βοήθεια της μεθόδου Αναλογικής Εξίσωσης (Katsikadelis 1994, 2002). Το διάστημα της δοκού $(0, l)$ διαιρείται σε L στοιχεία (Σχ. 15) και η εφαρμογή της μεθόδου οδηγεί στη μόνωση ενός μη γραμμικού συστήματος $3L + 20$ διαφορικών-αλγεβρικών εξισώσεων (DAE) ως προς $3L + 20$ αγνώστους, το οποίο μπορεί να εκφραστεί σε τυπική μορφή και ως

$$\mathbf{M}\ddot{\mathbf{d}} + \mathbf{K}\mathbf{d} + \mathbf{P}^h = \mathbf{f} \quad (37)$$

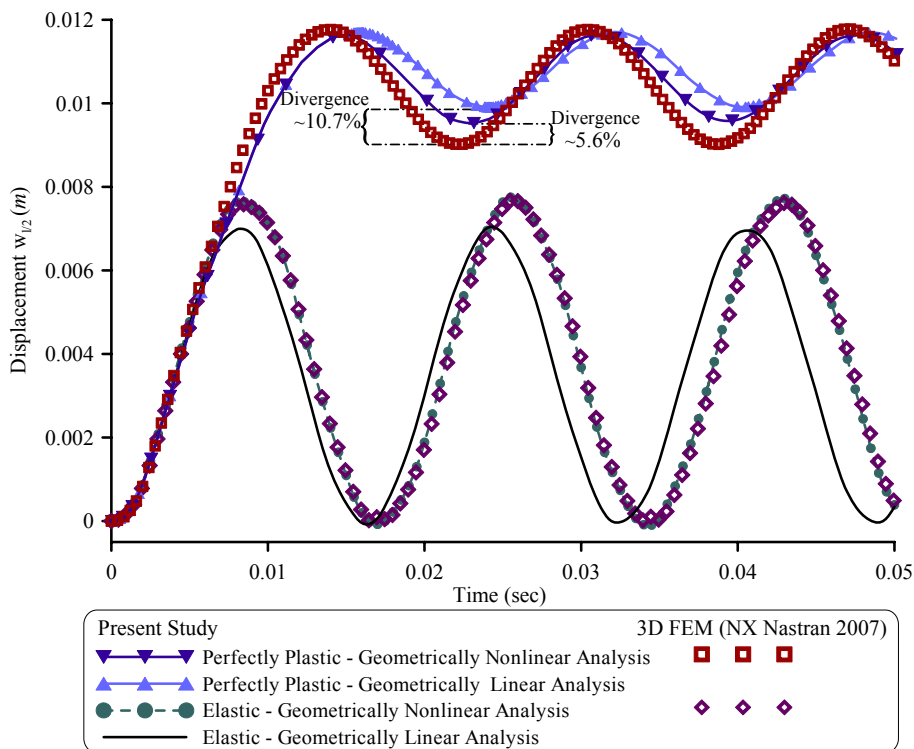
όπου \mathbf{P}^h είναι το γενικευμένο υστερητικό μητρώο. Το σύστημα εξισώσεων (37) μαζί με τις υστερητικές εξισώσεις Bouc-Wen επιλύεται αριθμητικά. Για την αριθμητική επίλυση του μη γραμμικού συστήματος διαφορικών-αλγεβρικών εξισώσεων εφαρμόστηκε η μέθοδος Petzold–Gear αφού εισήχθησαν ισάριθμες νέες μεταβλητές (State-Space formulation) ώστε να μειωθεί η τάξη του προβλήματος αρχικών τιμών ($ind = l$).



Σχ. 15. Διακριτοποίηση της δοκού σε στοιχεία και των διατομών ολοκλήρωσης σε κελιά και σημεία Gauss (στοιχείο ινών).

Με βάση την αναπτυχθείσα αναλυτική και αριθμητική διαδικασία, συντάχθηκε πρόγραμμα ηλεκτρονικού υπολογιστή σε υπολογιστικό περιβάλλον Fortran 90/95 με τη βοήθεια του οποίου μελετήθηκαν αντιπροσωπευτικά παραδείγματα με πρακτικό ενδιαφέρον, προκειμένου να διαπιστωθεί η αποτελεσματικότητα και το εύρος εφαρμογής της προτεινόμενης μεθόδου. Η ακρίβεια των αριθμητικών αποτελεσμάτων ελέγχεται, όπου είναι εφικτό, με υπάρχουσες αναλυτικές και αριθμητικές λύσεις, ενώ παράλληλα διερευνάται η επιρροή της μη γραμμικότητας υλικού και γεωμετρίας, καθώς και της εδαφικής προσομοίωσης στη δυναμική ανελαστική απόκριση του συστήματος αλληλεπίδρασης δοκού – εδάφους. Επιπλέον, προκειμένου να διερευνηθεί η αξιοπιστία της προτεινόμενης μεθοδολογίας, τα ληφθέντα αριθμητικά αποτελέσματα συγκρίνονται με αυτά που προκύπτουν από προσομοιώματα στερεών (εξαεδρικών) και κελυφωτών (τετραπλευρικών) πεπερασμένων στοιχείων.

Ως αντιπροσωπευτική αριθμητική εφαρμογή, μελετήθηκε αμφίπακτη δοκός μήκους $l = 6\text{ m}$, συμπαγούς ορθογωνικής διατομής $60 \times 30\text{ cm}^2$ ($E = 32318.4\text{ MPa}$, $\sigma_{Y0} = 20\text{ MN/m}^2$, $\rho = 2.5\text{ tn/m}^3$) η οποία εδράζεται επί μη γραμμικού ανελαστικού εδάφους και καταπονείται από ομοιόμορφα κατανεμημένο φορτίο. Στο Σχ. 16 παρουσιάζεται η ιστορία της εγκάρσιας μετατόπισης $w(l/2)$ του κέντρου βάρους της μεσαίας διατομής της δοκού που προκύπτει με εφαρμογή γεωμετρικά γραμμικής ή μη γραμμικής ανάλυσης λαμβάνοντας υπόψη ή αγνοώντας τη μη γραμμικότητα υλικού. Στο ίδιο σχήμα παρουσιάζονται επίσης τα αντίστοιχα αποτελέσματα που ελήφθησαν από λεπτομερές προσομοίωμα τρισδιάστατων πεπερασμένων στοιχείων.



Σχ. 16. Χρονοϊστορία της εγκάρσιας μετατόπισης του κέντρου βάρους της μεσαίας διατομής της δοκού.

Τέλος, στο Σχ.17 παρουσιάζεται η κατανομή των ορθών τάσεων κατά μήκος της δοκού για διάφορες χρονικές στιγμές φόρτισης, με βάση τα αποτελέσματα που ελήφθησαν από την εφαρμογή της προτεινόμενης μεθόδου. Στο ίδιο σχήμα παρουσιάζονται επίσης τα αποτελέσματα που προέκυψαν από τη λεπτομερή προσομοίωση του συστήματος σε τρισδιάστατο προσομοίωμα πεπερασμένων στοιχείων. Από την πολύ καλή σύγκλιση των αποτελεσμάτων επιβεβαιώνονται η ακρίβεια και η αξιοπιστία της προτεινόμενης μεθόδου καθώς επίσης και η αποτελεσματικότητα και αποδοτικότητα της στην περίπτωση της γεωμετρικά μη γραμμικής και ανελαστικής δυναμικής ανάλυσης συστημάτων αλληλεπίδρασης δοκού – εδάφους.

VI. Συμπεράσματα

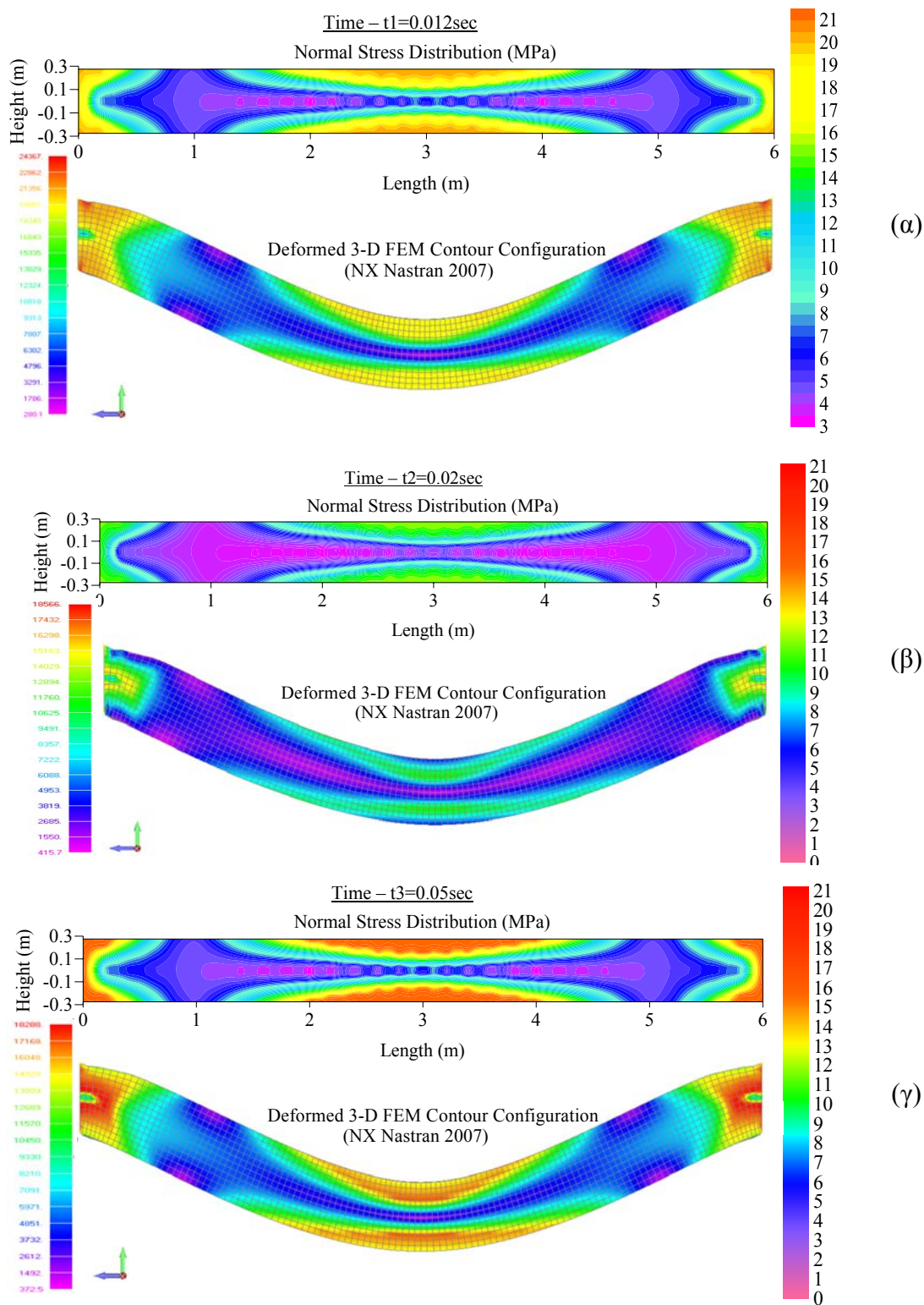
Στην παρούσα διδακτορική διατριβή διερευνάται και επιλύεται σειρά προβλημάτων που αφορούν στην ανάλυση συστημάτων αλληλεπίδρασης δοκού – εδάφους. Τα προβλήματα αυτά είναι τα ακόλουθα.

- Η γεωμετρικά μη γραμμική στατική ανάλυση δοκών με διατμητικές παραμορφώσεις επί μη γραμμικού εδάφους.
- Η γεωμετρικά μη γραμμική δυναμική ανάλυση δοκών με διατμητικές παραμορφώσεις επί μη γραμμικού εδάφους.
- Η γεωμετρικά μη γραμμική και ανελαστική στατική ανάλυση δοκών με διατμητικές παραμορφώσεις επί μη γραμμικού ανελαστικού εδάφους.
- Η γεωμετρικά μη γραμμική και ανελαστική δυναμική ανάλυση συστημάτων αλληλεπίδρασης δοκού – εδάφους.

Η επίλυση των εξεταζόμενων προβλημάτων βασίζεται στη διατύπωση καινοτόμων θεωριών δοκού. Τα προκύπτοντα μονοδιάστατα και διδιάστατα προβλήματα συνοριακών τιμών και αρχικών συνοριακών τιμών επιλύονται αριθμητικά εφαρμόζοντας τη Μέθοδο Συνοριακών Στοιχείων, τη Μέθοδο Αναλογικής Εξίσωσης και την Πεδιακή Μέθοδο Συνοριακών Στοιχείων. Τα κύρια συμπεράσματα της διατριβής συνοψίζονται στα ακόλουθα.

- i. Η ακρίβεια και η αξιοπιστία της προτεινόμενης μεθόδου επιβεβαιώνονται με υπάρχοντα αναλυτικά, αριθμητικά και πειραματικά αποτελέσματα καθώς και με αποτελέσματα στερεών (εξαεδρικών) και κελυφωτών (τετραπλευρικών) πεπερασμένων στοιχείων από εμπορικό λογισμικό.
- ii. Η αποτελεσματικότητα και αποδοτικότητα που παρουσιάζει η αναπτυχθείσα μέθοδος αξιολογείται μέσω σύγκρισης με λεπτομερή προσομοιώματα τρισδιάστατων πεπερασμένων στοιχείων. Η άριστη συμφωνία των αποτελεσμάτων και ο σαφώς μειωμένος απαιτούμενος υπολογιστικός χρόνος καταδεικνύουν τον πλεονεκτικό χαρακτήρα της μονοδιάστατης θεωρίας δοκού, σε όρους υπολογιστικού κόστους, αξιοπιστίας και μοντελοποίησης.
- iii. Η ανάπτυξη πλαστικών παραμορφώσεων μειώνει την καμπτική δυσκαμψία και τελικά οδηγεί στην πλαστική κατάρρευση όταν αγνοείται η γεωμετρική μη γραμμικότητα.
- iv. Το προτεινόμενο προσομοίωμα κατανεμημένης πλαστικότητας (στοιχείο ινών) αποδεικνύεται ιδιαίτερα αποτελεσματικό καθώς αποτυπώνει με ακρίβεια τόσο την αρχική διαρροή όσο και το (τελικό) φορτίο κατάρρευσης, ενώ παράλληλα ορίζει σαφώς την κατανομή των τάσεων στις περιοχές ανάπτυξης πλαστικών παραμορφώσεων. Το στοιχείο ινών αποτελεί κατάλληλο υπολογιστικό εργαλείο για

την αξιολόγηση της φέρουσας ικανότητας μελών κατασκευής, ξεπερνώντας τους περιορισμούς των στοιχείων συγκεντρωμένης πλαστικότητας.



Σχ. 17. Κατανομή των ορθών τάσεων κατά μήκος της δοκού για διάφορες χρονικές στιγμές φόρτισης.

- v. Η επιρροή της γεωμετρικής μη γραμμικότητας παρουσιάζεται μέσα από τη σημαντική απόκλιση μεταξύ των αποτελεσμάτων των θεωριών μικρών ή μεγάλων μετατοπίσεων, τόσο στη στατική όσο και στη δυναμική ανάλυση.
- vi. Η γεωμετρική μη γραμμικότητα φράσσει τα κινηματικά μεγέθη ελαστικών δοκών που υπόκεινται σε πρωτεύοντα συντονισμό. Η απόκριση τόσο των κινηματικών όσο και των εντατικών μεγεθών παρουσιάζει χαρακτηριστικά διακροτήματος. Ακόμα, οι μεγάλες μετατοπίσεις επηρεάζουν αισθητά και σύνθετα τη θεμελιώδη ιδιοσυχνότητα του συστήματος.
- vii. Η αλληλεπίδραση αξονικής-τέμνουσας-ροπής αποδεικνύεται καθοριστική στην περίπτωση ανελαστικής ανάλυσης.
- viii. Οι διατμητικές παραμορφώσεις μειώνουν την καμπτική δυσκαμψία καθώς και την ιδιοσυχνότητα του συστήματος, ενώ επηρεάζουν ουσιωδώς τα εντατικά και τασικά μεγέθη. Επίσης, αντιμετωπίζεται επιτυχώς το πρόβλημα του διατμητικού κλειδώματος.
- ix. Καταδεικνύεται η σημαντική επιρροή της προσομοίωσης του εδαφικού μέσου στην απόκριση του συστήματος αλληλεπίδρασης. Η μη γραμμικότητα του εδαφικού υλικού και της διεπιφάνειας δοκού – εδάφους επηρεάζουν καθοριστικά τη συμπεριφορά του συστήματος.
- x. Η προτεινόμενη μέθοδος προσφέρει τα πλεονεκτήματα της Μεθόδου Συνοριακών Στοιχείων (δεν χρησιμοποιείται παράγωγος συναρτήσεων σχήματος), ενώ η απαιτούμενη ακρίβεια επιτυγχάνεται με μικρό αριθμό στοιχείων.

VII. Ιδέες για Μελλοντική Έρευνα

Πιθανές κατευθύνσεις μελλοντικής έρευνας, με σημαντικό επιστημονικό και πρακτικό ενδιαφέρον, συνοψίζονται ακολούθως.

- i. Επέκταση της γεωμετρικά μη γραμμικής ανελαστικής δυναμικής ανάλυσης συστημάτων αλληλεπίδρασης δοκού – εδάφους, ώστε να λαμβάνεται υπόψη η διατμητική παραμόρφωση (J_2 plasticity).
- ii. Ενσωμάτωση συναρτήσεων στρέβλωσης για τον ακριβή υπολογισμό της κατανομής των διατμητικών τάσεων στη διατομή ελέγχου.
- iii. Περαιτέρω γενίκευση του προτεινόμενου προσομοιώματος μέσω της ενσωμάτωσης κινηματικής κράτυνσης.

- iv. Εφαρμογή της προτεινόμενης μεθοδολογίας για την ανάπτυξη στοιχείου δοκού.
- v. Εμπλουτισμός του στοιχείου ώστε να αντιμετωπίζεται η περίπτωση στρεπτοκαμπτικής ανάλυσης σύμμικτης δοκού.
- vi. Περαιτέρω γενίκευση του εδαφικού προσομοιώματος με τη χρήση εξελιγμένων θεωριών.

Abstract

Ph.D. Dissertation by Kampitsis E. Andreas

Geometric and Material Nonlinear Analysis of Beam–Soil Interaction Systems

In this Ph.D. dissertation the geometric and material nonlinear analysis of beam-soil interaction systems is investigated. More specifically, the geometrically nonlinear static and dynamic analysis of shear deformable beams supported on nonlinear foundation is presented. Subsequently, the study is further extended to account for material nonlinearity in static response, where both the structural member and the soil medium are assumed to be inelastic. Finally the attention is drawn to the dynamic time domain analysis of beam-soil interaction systems taking into account geometric and material nonlinearities.

The geometrical nonlinearity is taken into consideration through the Total Lagrangian formulation and the large displacements - small strains assumption. Shear deformation effect is taken into account using the Timoshenko beam theory, evaluating the shear deformation coefficients by using an energy approach. The material nonlinearity is treated through a displacement based formulation taking into account inelastic redistribution along the beam axis. Inelastic deformations are modelled through a distributed plasticity (fibre) model exploiting three dimensional material constitutive laws. The nonlinear half-space is approximated by nonlinear spring configurations, where interface nonlinearity is also taken into consideration.

The obtained boundary value and initial boundary value problems are numerically solved employing the Boundary Element Method, the Analog Equation Method and the Domain Boundary Element Method. On the basis of the developed analytical and numerical procedures, representative examples are studied. The accuracy and reliability of the proposed method are confirmed through existing numerical and experimental results, as well as through results obtained from solid and shell Finite Element analyses.

Table of Contents

CHAPTER 1: INTRODUCTION	1
1.1 Introduction and Motivation	1
1.2 Brief Literature Review and Novelities of the Dissertation	6
1.3 Outline of the Dissertation	10
CHAPTER 2: GEOMETRICALLY NONLINEAR STATIC ANALYSIS OF SHEAR DEFORMABLE BEAMS ON NONLINEAR FOUNDATION	15
2.1 Introduction	15
2.2 Statement of the Problem	19
2.2.1 Displacements, Strains & Stresses	20
2.2.2 Stress Resultants, Equations of Equilibrium, Boundary Conditions	24
2.3 Integral Representations – Numerical Solution	28
2.3.1 Axial $u(x)$ and transverse displacements $v(x), w(x)$	29
2.4 Numerical Examples	38
2.4.1 Example 1 – <i>Linear Analysis of Simply Supported Beam on Elastic Foundation</i>	38
2.4.2 Example 2 – <i>Nonlinear Analysis of Clamped Beam on Elastic Foundation</i>	43
2.4.3 Example 3 – <i>Experimental Validation of Pile–Foundation Systems</i>	47
2.4.4 Example 4 – <i>Beam on 3-Parameter Foundation</i>	49
2.4.5 Example 5 – <i>Axially Loaded Cantilever Beam on Pasternak Foundation</i>	51
2.4.6 Example 6 – <i>Free-Free Beam on 3-Parameter Foundation</i>	52

2.4.7 Example 7 – Pinned Beam on 3-Parameter Foundation: Unbonded Contact	54
2.5 Concluding Remarks	55
CHAPTER 3: GEOMETRICALLY NONLINEAR DYNAMIC ANALYSIS OF SHEAR DEFORMABLE BEAMS ON NONLINEAR FOUNDATION	59
3.1 Introduction	59
3.2 Statement of the Problem	66
3.2.1 Displacements, Strains & Stresses	68
3.2.2 Stress Resultants, Governing Equations of Motion, Boundary and Initial Conditions	71
3.3 Integral Representations – Numerical Solution	76
3.3.1 Axial $u(x)$ and transverse displacements $v(x), w(x)$	77
3.4 Alternative D-BEM Numerical Solution	86
3.4.1 Displacements $u(x,t), v(x,t), w(x,t)$ and rotations $\theta_y(x,t), \theta_z(x,t)$	87
3.5 Numerical Examples	92
3.5.1 Example 1 – <i>Linear Analysis of Simply Supported Beam on Pasternak Foundation</i>	92
3.5.2 Example 2 – <i>Nonlinear Analysis of Hollow Rectangular Beam on Winkler Foundation</i>	96
3.5.3 Example 3 – <i>Partially Embedded Pile in Winker Foundation</i>	98
3.5.4 Example 4 – <i>Fully Embedded Hollow Circular Pile in Non-constant Stiffness Soil</i>	101
3.5.5 Example 5 – <i>Clamped Beam on Nonlinear Three-Parameter Viscoelastic Foundation. Resonance and Damping Effects</i>	103
3.5.6 Example 6 – <i>Partially Embedded Column-Pile in Nonlinear Three-Parameter Viscoelastic Foundation</i>	108
3.5.7 Example 7 – <i>Timoshenko-Rayleigh Beam on Viscoelastic Pasternak Foundation under Concentrated Moving Load</i>	111
3.5.8 Example 8 – <i>UIC60 Rail Track on 3-Parameter Viscoelastic Foundation</i>	115
3.5.9 Example 9 – <i>HEA320 on Winkler Foundation under Axial Loading</i>	118

	<i>and Concentrated Moving Harmonic Force</i>	
3.5.10	Example 10 – <i>HEM 240 on 3-Parameter Viscoelastic Foundation under Axial Loading and Distributed Moving Harmonic Force</i>	120
3.5.11	Example 11 – <i>Extensive Case Study</i>	122
3.6	Concluding Remarks	140
CHAPTER 4:	GEOMETRICALLY NONLINEAR INELASTIC ANALYSIS OF SHEAR DEFORMABLE BEAMS ON INELASTIC FOUNDATION	143
4.1	Introduction	143
4.2	Statement of the Problem	147
4.2.1	Displacements, Strains & Stresses	149
4.2.2	Stress Resultants, Equations of Equilibrium and Boundary Conditions	153
4.3	Numerical Solution	157
4.3.1	Integral Representations for the Axial and Transverse Displacements u, v, w and Rotations θ_y, θ_z	157
4.3.2	Incremental–Iterative Solution Algorithms / Fibre Approach	163
4.3.2.1	Incremental–Iterative Solution based on Powell Hybrid Algorithm	163
4.3.2.2	Incremental–Iterative Solution based on Initial Stress Criterion	168
4.4	Numerical Examples	172
4.4.1	Example 1 – <i>Elastic Analysis of Free-Free Beam on Pasternak Foundation</i>	173
4.4.2	Example 2 – <i>Inelastic Analysis of Simply Supported Beam on Winkler Foundation</i>	176
4.4.3	Example 3 – <i>Inelastic Analysis of Simply Supported Beam on Nonlinear Pasternak Foundation</i>	178
4.4.4	Example 4 – <i>Beam on Nonlinear Foundation under Cyclic Loading</i>	181
4.4.5	Example 5 – <i>I-Beam on Nonlinear Foundation</i>	186
4.4.6	Example 6 – <i>I-Beam on Nonlinear Foundation under Cyclic Loading</i>	188
4.4.7	Example 7 – <i>Mono-Symmetric I Beam on Nonlinear Foundation under Cyclic Loading</i>	190

4.4.8	Example 8 – <i>Cantilever under Axial & Transverse Loading</i>	191
4.4.9	Example 9 – <i>Shear collapse of I-Beam on Inelastic Foundation</i>	194
4.4.10	Example 10 – <i>Influence of Geometrical Nonlinearity in Inelastic Analysis</i>	200
4.4.11	Case Study – <i>Pile-Foundation System: Numerical and Experimental Validation</i>	203
4.5	Concluding Remarks	212
CHAPTER 5: GEOMETRICALLY NONLINEAR DYNAMIC INELASTIC ANALYSIS OF BEAM-SOIL INTERACTION SYSTEMS		215
5.1	Introduction	215
5.2	Statement of the Problem	221
5.2.1	Displacements, Strains & Stresses	223
5.2.2	Stress Resultants, Equations of Equilibrium and Boundary Conditions	228
5.3	Numerical Solution	233
5.3.1	Axial $u(x,t)$ and Transverse Displacements $v(x,t), w(x,t)$	234
5.3.2	Dynamic Incremental–Iterative Solution Algorithm	241
5.3.2.1	State-Space Formulation / Fibre Approach	241
5.4	Numerical Examples	244
5.4.1	Example 1 – <i>Dynamic Inelastic Analysis of Cantilever Beam</i>	244
5.4.2	Example 2 – <i>Dynamic Inelastic Analysis of Clamped Beam on Foundation</i>	247
5.4.3	Example 3 – <i>I-Beam on Nonlinear Foundation</i>	256
5.5	Concluding Remarks	261
CHAPTER 6: CONCLUSIONS AND FUTURE RESEARCH		263
6.1	Concluding Remarks	263
6.2	Future Research	266

APPENDIX A1: AEM FOR ORDINARY DIFFERENTIAL EQUATIONS OF THE 2nd AND 4th ORDER	267
A1.1 Introduction	267
A1.2 Main Concepts of the Analog Equation Method	269
A1.3 AEM for Ordinary Differential Equations of the 2 nd Order	270
A1.3.1 Integral Representation – Numerical Solution	270
A1.3.2 Evaluation of Integrals	277
A1.4 AEM for Ordinary Differential Equations of the 4 th Order	278
A1.4.1 Integral Representation – Numerical Solution	278
A1.4.2 Evaluation of Integrals	288
APPENDIX A2: DOMAIN BEM FOR ORDINARY DIFFERENTIAL EQUATIONS OF THE 2nd ORDER	291
A2.1 Introduction	291
A2.2 Main Concepts of the Domain – Boundary Element Method	292
A2.3 Classical Domain Integration	293
A2.4 Approximation of the Field Function	295
APPENDIX A3: SHEAR CENTRE – SHEAR DEFORMATION COEFFICIENTS	297
A3.1 Introduction	297
A3.2 Statement of the Problem	304
REFERENCES	315

Chapter 1

Introduction

1.1 Introduction and Motivation

The main scope of structural analysis is to determine the stress and kinematical components of a physical structure subjected to external and self loading. Since the geometry of the structure, as well as the loading and boundary conditions are explicitly specified it is rather straightforward to determine a numerical model and analyse the response of the structure employing any available method.

In general, however, most of the physical structures are in direct contact with the supporting soil medium. Due to this contact, neither the structural nor the soil response are independent of each other when subjected to external forces, such as earthquake excitation, wind loading, etc. The phenomenon during which the motion of the soil medium influences the response of the structure and vice versa, is known as Soil-Structure Interaction.

In the special case where a light structure is founded on relatively stiff soil (e.g. rock) the motion of the base during a seismic event is practically independent from the superstructure and thus the soil-structure interaction can be neglected and the analysis can be restricted to the above ground structure. On the other hand, in case of heavily loaded structures or relatively soft soils, the effect of this interaction becomes prominent. It is thus not permissible to analyse the structure without accounting for the interaction with the surrounding soil.

The response of soil-structure interaction systems under static or dynamic loading is an area of extensive research activity in structural and geotechnical engineering. In recent years, significant research efforts have indicated that neglecting the soil-structure interaction may lead to unsafe design. Since the beneficial as well as the detrimental effects of this interaction are well documented, there is a significant attempt being carried out towards incorporating the latest acquired knowledge and methodologies in the analysis and design of these systems. The thorough understanding of the beam-soil

interaction mechanics is the key aspect of any developed methodology and is prerequisite in order to conduct precise analysis, without jeopardizing accuracy and thus safety. Currently, the methods of studying soil-structure interaction are continuously evaluated and improved since evidence from case histories, new experimental data and field studies have indicated the importance of a rigorous and precise analysis. To this end, all possible causes of nonlinearities should be taken into account. The nonlinearities with the most profound influence on the response of a soil-structure system originate from the inherent nonlinear stress-strain behaviour of the materials (material nonlinearity) as well as from the significant variations of the geometrical configuration during dynamic loading (geometrical nonlinearity).

Currently, modern design codes and the existing regulations indicate that the beam-soil interaction systems, such as piles and deep embedded foundations, have to be designed to behave elastically for every type of loading. More specifically, Eurocode-8 (EC-8, Part 2, § 5.8) explicitly states that “...*foundations shall not be intentionally used as sources of hysteretic energy dissipation and therefore shall, as far as practicable, be designed to remain undamaged under the design seismic action*”. This restriction, however, is most likely to be violated in a real case scenario, whereas significant research efforts have substantiate the beneficial character of permitting nonlinearities and inelasticity to occur at the beam-soil interaction system.

Furthermore, in order to design cost-effective structures following the performance or displacement based design the realistic estimation of the maximum displacements is essential. Towards this direction and having in mind the magnitude of the arising axial forces due to self weight, dead and environmental loadings the geometrical nonlinearity has also to be incorporated in the analysis. This effect alters the flexural rigidity of the structure and leads to different behaviour from that of small displacement assumption. Moreover, contemporary advancements in material science have facilitated the intensive use of materials having relatively high transverse shear modulus; thereby the error incurred from the ignorance of shear deformation effect may be substantial. Therefore, the Timoshenko beam theory has to be employed in such problems. As it is well documented, this effect leads to increased displacements, compared to the Euler-Bernoulli approach, and can have even greater influence in the dynamic time domain response. In any case, if the lateral loading is significant, the shear deformation effect can be proved crucial in both the elastic and inelastic regime.

Over the years, many researchers have developed and validated various methods for the study of the intricate behaviour of the beam-soil interaction systems. Nevertheless,

due to the significant difficulties of the problem there are many areas yet to be investigated. These difficulties are attributed not only to the inherent complexity of the problem involving both the structural and the geotechnical engineering, but also to the uncertainties related to the nature of the problem such as interaction effects, material nonlinearity and soil properties. These methods can be grouped into three major categories namely; the beam based formulations, the continuum mechanics approaches and the lately developed macro-element methods.

Within the context of beam approach, the supporting soil is approximated by a series of uncoupled springs while the structural components are modelled as beam elements. This approach was first introduced by Winkler (1867), therefore is known as Beam-on-Winkler-Foundation, and since then it has been adopted by a vast amount of investigators and engineers leading to analytical and numerical solutions. On the contrary, the continuum mechanics models take explicitly into account the physics of the problem through the realistic simulation. As long as the response of the continuum remains linear elastic, analytical solutions have been proposed (Poulos 1971, Veletsos & Verbic 1973), while several authors have developed closed forms and have presented parametric studies. Based on the same concept, the three dimensional finite element and the boundary element methods have also been employed. Nevertheless, linear models ignore the soil inelasticity and are limited to the small-strain assumption and steady-state dynamic problems. Thus, in order to take into consideration the inevitable soil nonlinearity as well as the interaction effects, the nonlinear continuum finite element models have been utilized. Although accurate, these models require sophisticated calibration and excessive computational time. Finally, a relatively new trend, not only in structural but also in geotechnical engineering, is the concept of macro-modelling. The macro-element methods allow the macroscopic simulation of the behaviour of the structure or the soil and it can be perceived as an advanced finite element.

Among the above mentioned, maybe the most attractive approach to both scientists and engineers for the interaction analysis as well as for the study of various beam-like structures is the one-dimensional beam model, due to its significant advantages over refined approaches. The major advantages of any beam model are listed below:

i. Simplicity in handling and reduced modelling effort.

More specifically, as far as the pre-processing procedure is concerned, the geometry simulation and the mesh of a beam model are straightforward and rather easily imported into any numerical code. On the contrary the implementation of a

three-dimensional or even two-dimensional model requires extensive effort, even though over the years many mesh generators have been developed.

ii. Reduced computational cost.

The computational time required for the numerical analysis of the boundary or initial value problem, is exponentially related to the amount of unknowns. The number of elements and subsequently of unknowns in three dimensional models is significantly larger than those of a beam model. This difference can be even greater if mesh refinement is required. The advantage of time performance becomes even more apparent in case of dynamic analysis. Modern design codes like the European standard for the Design of Structures for Earthquake Resistance (EN 1998, EC-8), the ASCE standard for the Seismic Rehabilitation of Existing Buildings (ASCE 2007) as well as the Greek norm for the Seismic Retrofit of Existing Buildings (Retrofitting 2013) are based on concepts such as the displacement based design and the performance based design for the estimation of structural integrity (Priestley 2007, Fardis 2010). This implies that in order to evaluate the necessary design quantities, a vast amount of nonlinear dynamic analyses are required. Specifically, Eurocode-8 (EN 1998, EC-8) states that *“The number of the accelerograms to be used shall be such as to give a stable statistical measure (mean and variance) of the response quantities of interest. The amplitude and the frequency content of the accelerograms shall be chosen such that their use results in an overall level of reliability commensurate with that implied by the use of the elastic response spectrum”*. Therefore, the required analysis time as well as the amount of input/output data needed for the design process becomes crucial.

iii. Straightforward modelling of external loading and supports.

The imposition of the external loads and the support implementation is direct and easily applied, contrary to the cumbersome solid models. Especially in case of beam-soil interaction systems the simulation of the soil medium and the interaction phenomena are extremely complicated employing continuum models. The implementation of such models in numerical codes presumes the use and calibration of quite advanced and complicated constitutive laws, making it a challenging and extremely time-consuming task. Furthermore, the free-field boundaries have to be accurately handled in order to avoid radiation damping. The investigation and calibration of several types of boundaries, like dashpots or multi-

point constrains, is essential in order to yield precise results, while the compatibility of the degrees of freedom at the coinciding nodes for different element types has also to be ensured.

iv. Convenience in isolation of structural phenomena and results interpretation.

Contrary to the reduced oversight of the three dimensional models, beam formulations provide the capability to assess the influence of each separate phenomenon to the overall response. Moreover, quantities such as rotation, warping parameter, stress resultants etc. are also evaluated in contrast to solid model which yields only displacements and stress components.

v. Convenience in performing parametric analyses.

In order to draw design guidelines parametric analyses are often performed. Thus a formulation capable of performing multiple analyses is required, unlike the solid modelling which often requires the setup of multiple models.

vi. Straightforward discretization of a complex structure.

Complex structures often require detailed simulation and thus the finite element mesh might be dense. This results in increased number of nodes and subsequently degrees of freedom (unknowns) leading to severe or unrealistic computational time.

vii. Effective handling of structures including thin-walled members.

Shear-locking and membrane-locking phenomena can be successfully addressed.

viii. Effective handling of warping phenomena.

The use of shell elements cannot give accurate results since warping of the walls of a cross section cannot be taken into account (midline models), while on the contrary the beam elements can successfully address these effects.

Having all this in mind, the development of a reliable and efficient computational tool based on the beam formulation, capable of performing beam-soil interaction analysis accounting for geometric, material and other key nonlinear effects is considered essential.

1.2 Brief Literature Review and Novelities of the Dissertation

Over the past decades, many researchers have employed the *Beam-on-Winkler-Foundation* model to study various problems related to both structural and geotechnical fields. Through these studies, the beam based model has been proved a powerful computational tool capable of analyzing in detail the beam–soil interaction systems. Both static and dynamic response can be studied through this model which retains the advantages of simplicity and time performance, while the obtained results are of good accuracy compared against more rigorous numerical schemes. In the following, a brief literature review is presented, while for each topic a detailed and extensive investigation of the bibliography is presented at the introduction section of the corresponding chapter.

Originally proposed by Winkler (1867), this approach has been used to solve a wide range of interaction problems. In this model the soil behaviour is represented as an array of closely spaced, mutually independent, linear elastic springs, while the structural element is modelled as a beam-column element. These springs are assumed to provide resistance in direct proportion to the deflection of the beam. This assumption, however, does not represent realistically the mechanical behaviour of the soil, thus nonlinear springs have been developed, where the shape of the load-deformation relationships is described by empirical p - y curves following non-proportional laws between the soil resistance per unit pile length p and the lateral displacement y . Numerous investigators have proposed recommendations for the estimation of the p - y curves (Matlock 1970, Reese et al. 1974, O'Neill & Murchison 1983, Georgiadis 1983, Ashour & Norris 2000, Reese & Van Impe 2001, Dahlberg 2002) based on results of high accuracy instrumented tests, while in the case of dynamic loading the spring configurations are enriched with appropriate dashpots accounting for the energy dissipation due to radiation damping. Furthermore, the original Winkler approach is also restricted to non-cohesive soil media due to its inability to take into account the continuity or cohesion of the soil (interaction between adjacent springs). To overcome this limitation, several alternative spring configuration schemes have been proposed, such as the Filonenko–Borodich, Pasternak, Vlasov or Hetenyi models among others.

The static linear elastic response of beam-soil interaction systems has been extensively investigated employing the beam-on-Winkler-foundation model (Hetenyi 1946), while the tensionless (unilateral) character of the subgrade reaction has also been introduced in the analysis (Sharma & Dasgupta 1975, Kaschiev & Mikhajlov 1995, Zhang & Murphy 2004, Avramidis & Morfidis 2006, Maheshwari 2007, Zhang 2008,

Ma et al. 2009a,b, Tullini & Tralli 2010). On the contrary, the geometrically nonlinear static analysis has received little attention in the literature (Silveira et al. 2008, Tsiatas 2010).

The dynamic analysis of these systems has also been extensively investigated (Wolf 1985). Analytical solutions of problems involving beam vibration of simple geometry and boundary conditions have received a good amount of attention in the literature (Krylov 1905, Timoshenko 1911, Rades 1972, Wang & Stephens 1977, Choros & Adams 1979, Morgan & Sinha 1983), while the linear vibrations of beams on foundation traversed by moving loading have also been studied (Inglis 1934, Lowan 1935, Weitsman 1971, Kolousek 1973, Fryba 1999). When the beam displacements are small, a wide range of linear dynamic analysis tools can be used and several authors have implemented the beam-on-Winkler-foundation model in order to investigate various phenomena (Kuczma & Switka 1990, Huang & Zou 1994, Thambiratnam & Zhuge 1996, Matsunaga 1999, Sun 2001, Chen et al. 2001, Sun 2001a,b, 2002, Coskun 2003, Chen et al. 2004, Kargarnovin & Younesian 2004, 2005, 2009, Muscolino & Palmeri 2007, Ying et al. 2008, Zehsaz et al. 2009, Millan & Dominguez 2009, Dimitrova 2010, Ansari et al. 2010, Chen & Chen 2011). As the beam displacements become larger, the induced geometric nonlinearities result in effects that are not observed in linear systems. Contrary to the good amount of attention in the literature concerning the linear dynamic analysis, very little work has been done on the corresponding nonlinear problem (Lewandowski 1989, Chang & Liu 1996, Chen et al. 2001, Kim & Cho 2006, Arboleda-Monsalve et al. 2007).

The beam approach has also been widely employed in studies regarding seismic excitations. In these cases, the analysis is performed in two different stages. At first a site response analysis is conducted for the seismic motion of the shear wave propagation on the free-field considering that it is uncoupled from the structures motion. Subsequently, employing the motions from the obtained excitation derived from the first stage, the analysis of the beam-soil system is carried out. One of the key phenomena in seismic analysis is the kinematic and inertial interaction. Modern seismic codes like Eurocode 8 (EN 1998, EC-8) recommend accounting for both inertial and kinematic soil-structure interaction effects. Specifically, EC-8, Part-5 states that piles and piers shall be designed to resist both *inertial forces* from the superstructure and *kinematic forces* arising from the deformation of the surrounding soil due to the passage of seismic waves. In order to address these effects, the beam-on-Winkler-foundation model has been successfully adopted by several authors producing results of remarkable accuracy

compared to rigorous numerical schemes (Boulanger et al. 1999, Nikolaou et al. 2001, Hutchinson et al. 2004, Gerolymos et al. 2009, Castelli & Maugeri 2009, Dezi et al. 2010, Sica et al. 2011, Anoyatis et al. 2013). Though this approach ignores the shear transfer between layers of soil as well as the interface and three-dimensional interaction, it has been preferred by many researchers due to its efficiency and simplicity.

Although the beam-soil analysis accounting for the nonlinear behaviour of the soil due to high strain level has been studied extensively, only few works have encountered the inelastic behaviour of both the beam and the foundation elements. According to this approach, the beam stress-strain and the foundation load-displacement relations are assumed to follow nonlinear inelastic constitutive laws. Consequently, such models are not easily formulated due to the complexity of the problem. Nevertheless, in order to conduct precise analysis and design cost-effective structures the realistic estimation of the systems response is essential. Towards this direction, many researchers have resorted to the use of refined finite element models in order to account for the material nonlinearity. Nevertheless, this solution is not recommended in engineering practice due to the inherent modelling and analysis problems. In an attempt to bridge the gap between the widely used beam formulations and the computationally expensive solid/shell finite element simulations, just a few static inelastic beam-on-Winkler foundation models have been developed (Budek et al. 2000, Ayoub 2003, Mullapudi & Ayoub 2010a). Following the same trend, even less has been done in the dynamic inelastic analysis of beam-soil interaction systems (Hutchinson et al. 2004, Gerolymos and Gazetas 2005, Mullapudi and Ayoub 2010b,c). It is worth noting that in most of these studies, the interaction system has been addressed as an assembly of finite elements rather than formulating a uniform solution strategy, while the statement of the problem is limited to the equations for the static response. Nevertheless, it is pointed out that a continuously growing demand, among the structural and geotechnical engineering communities, is observed towards incorporating geometrical and material nonlinearities into the analysis and design procedures. To this end, even though the basic understanding of beam-soil interaction system behaviour is acquired, there are still many areas to be thoroughly investigated.

The prime objective of this dissertation is to develop advanced methods and a reliable and efficient computational tool based on the beam formulation for the static and dynamic analysis of beam-soil interaction systems taking into consideration several nonlinear mechanisms. The motivation towards that scope is justified from the intention of gaining the accuracy of more rigorous models (i.e. shell/solid FE) while retaining the

simplicity of a beam formulation. In addition, the acquisition of knowledge regarding the influence of various key nonlinear phenomena consists also a main objective of the present dissertation.

The research work presented herein is considered original and its essential features and novel aspects are summarized as follows

- i. To the author's knowledge, for the first time in literature the geometrically nonlinear dynamic response of beam-soil interaction systems where both the beam and the foundation elements are assumed to be inelastic is investigated through the beam-on-Winkler-foundation approach.
- ii. For the problem at hand, the material nonlinearity is addressed through a distributed plasticity (fibre) approach, while the formulation is a displacement based one taking into account inelastic redistribution along the beam axis.
- iii. The proposed beam model accounts for the geometrical nonlinearity by retaining the square of the slope in the strain–displacement relations, avoiding in this way the inaccuracies arising from a linearized second-order analysis. For that purpose the total Lagrange formulation (intermediate non-linear theory) has been adopted.
- iv. Shear deformation effect is taken into account on the geometrically nonlinear elastic and static inelastic analysis (explicit axial-shear-flexure interaction). Especially in the static inelastic case, the developed formulation adopts a J2 three-dimensional plasticity law (von Mises) to assess the inelastic beam-foundation system response.
- v. The proposed model accounts for the coupling effect of bending and shear deformations along the member as well as shear forces along the span induced by the applied axial loading. Moreover, the beam is subjected to arbitrary external loading and is supported by the most general time dependent boundary conditions.
- vi. The nonlinear half-space is approximated by various nonlinear spring configurations. Interface nonlinearity is also taken under consideration using tensionless spring properties.
- vii. To the author's knowledge, a boundary element approach (BEM, AEM or D-BEM) has not yet been used for the solution of the problem at hand. The developed procedure retains most of the advantages of a BEM solution, since it does not require shape functions for the kinematical components; hence the minimum number of elements can be employed, while the accuracy of function derivatives is not compromised.

1.3 Outline of the Dissertation

This doctoral dissertation is organized in six chapters and three appendices. The structure of each chapter comprises the literature review of the corresponding problem “*State of the Art*”, the statement of the problem, the numerical solution, the representative numerical examples and finally the obtained concluding remarks. In the final chapter, the main conclusions drawn in this dissertation are summarized while directions for further research are proposed. The appendices include information necessary to understand the content of the main chapters of the dissertation.

In this research work the geometrical nonlinearity is taken into account through the Total Lagrangian formulation by retaining the square of the slope in the strain-displacement relations, avoiding in this way the inaccuracies arising from a linearized second-order analysis. In order to do so, the large displacements – small strains assumption (Armenakas 2006) is employed. Moreover, the material nonlinearity is treated through a displacement based formulation taking into account inelastic redistribution along the beam axis while a distributed plasticity (fibre) approach has been employed. On the basis of the analytical and numerical procedures presented in the each chapter a number of computer programs have been written using third and fourth generation high level languages, programming packages as well as symbolic languages. Representative examples of great practical interest have been studied to demonstrate the efficiency and the range of applications of the developed method. The accuracy and reliability of the obtained results have been verified by comparison with analytical solutions and experimental data as well as with the results obtained from shell (quadrilateral) or solid (hexahedral) finite element models.

In **Chapter 2**, the geometrically nonlinear static analysis of shear deformable beams partially supported on nonlinear three-parameter tensionless foundation, is presented. The beam is of arbitrary doubly symmetric simply or multiply connected constant cross-section and is subjected to the combined action of arbitrarily distributed or concentrated transverse loading and bending moments in both directions as well as to axial loading. The geometrical nonlinearity is taken into account through the Total Lagrangian formulation and the large displacements – small strains assumption. The beam is subjected to general boundary conditions while, to account for shear deformation effect the concept of shear deformation coefficients is used. The mechanical behaviour of the soil is taken into consideration by means of a refined spring configuration consisting of three independent parameters. In detail, foundation model is characterized by the linear

elastic Winkler spring element providing resistance in direct proportion to the displacement of the beam, the second shear layer parameter capturing the continuity or cohesion of the soil enabling interaction between adjacent springs and the nonlinear parameter describing the hardening/softening characteristics of the foundation. According to the proposed method, five boundary value problems are formulated. More specifically, two boundary value problems are formulated with respect to stress functions for the evaluation of the shear deformation coefficients and solved employing a pure Boundary Element Method, that is only boundary discretization is used. Moreover, three boundary value problems are formulated with respect to the transverse and axial displacements solved using the Analog Equation Method. Application of the boundary element technique yields a system of nonlinear equations from which the transverse and axial displacements are computed either by an iterative process or by employing the modified Powell's hybrid algorithm. The increase of the stiffness rigidity due to the geometrical nonlinearity is observed and the influence of the shear deformation effect is quantified. Furthermore, the significant impact of the soil characteristics as well as the tensionless character to the beam-foundation response is investigated.

In *Chapter 3*, the geometrically nonlinear dynamic analysis of shear deformable beams partially supported on nonlinear tensionless viscoelastic foundation, is presented. The beam is of arbitrary doubly symmetric simply or multiply connected constant cross-section and is subjected to the combined action of arbitrarily distributed or concentrated transverse loading and bending moments in both directions as well as to axial loading. This dynamic loading represents the most general case, which includes impact loading, transverse moving loading, seismic excitation, beam–soil interaction, etc. The geometrical nonlinearity is taken into account through the Total Lagrangian formulation and the large displacements – small strains assumption. The beam is subjected to general boundary conditions while, to account for shear deformation effect the concept of shear deformation coefficients is used. The mechanical behaviour of the soil is approached by two alternative formulations. Firstly, a refined spring configuration consisting of four independent parameters is employed. In detail, foundation model is characterized by the linear elastic Winkler spring element providing resistance in direct proportion to the displacement of the beam, the second shear layer parameter capturing the continuity or cohesion of the soil enabling interaction between adjacent springs, the nonlinear parameter describing the hardening/softening characteristics of the foundation and finally the viscous damping parameter. Alternatively, the soil nonlinearity is taken

into consideration by means of a hybrid spring configuration consisting of a nonlinear (p - y) spring connected in series to an elastic spring–damper model. The nonlinear spring captures the near–field plastification of the soil while the spring–damper system (Kelvin–Voigt element) represents the far–field viscoelastic character of the soil. According to the proposed method, five boundary value problems are formulated. More specifically, two boundary value problems are formulated with respect to stress functions for the evaluation of the shear deformation coefficients and solved employing a pure Boundary Element Method, that is only boundary discretization is used. Moreover, three initial boundary value problems are formulated with respect to the transverse and axial displacements solved using the Analog Equation Method. Application of the boundary element technique yields a system of nonlinear differential-algebraic equations from which the transverse and axial displacements are computed either by employing a Newmark-delta method or the Petzold-Gear backward differentiation formula. It is concluded that the large displacements change radically the dynamic response of the beam-foundation system influencing the natural frequencies while the significant affect of the shear deformations and the foundation modelling is verified. Subsequently, an extensive case study is carried out on a pile–column–deck system of a bridge subjected to earthquake excitations, providing insight to several phenomena.

In *Chapter 4*, the geometrically nonlinear (J2) inelastic analysis of shear deformable beams partially supported on inelastic tensionless Pasternak foundation, is presented. The beam is of arbitrary doubly symmetric simply or multiply connected constant cross-section and is subjected to the combined action of arbitrarily distributed or concentrated transverse loading and bending moments in both directions as well as to axial loading. The geometrical nonlinearity is taken into account through the Total Lagrangian formulation and the large displacements – small strains assumption. The beam is subjected to general boundary conditions while, to account for shear deformation effect the concept of shear deformation coefficients is used. The mechanical behaviour of the soil is taken into consideration by means of a two-parameter spring configuration consisting of two independent parameters. In detail, foundation model is characterized by the linear elastic Winkler spring element providing resistance in direct proportion to the displacement of the beam and the Pasternak shear layer parameter capturing the continuity or cohesion of the soil enabling interaction between adjacent springs. A displacement based formulation is developed and inelastic redistribution is modelled through a distributed plasticity (fibre) approach

exploiting three dimensional material constitutive laws and numerical integration over the cross sections. An incremental–iterative solution strategy along with an efficient iterative process is employed. According to the proposed method, a set of boundary value problems is formulated. More specifically, two boundary value problems are formulated with respect to stress functions for the evaluation of the shear deformation coefficients and solved employing a pure Boundary Element Method, that is only boundary discretization is used. Moreover, a boundary value problem is formulated with respect to the axial and transverse displacements and to the angles of rotation due to bending, solved using the domain Boundary Element Method. Application of the boundary element technique yields a system of nonlinear equations from which the unknowns of the problem are computed either by an iterative process or by employing the modified Powell’s hybrid algorithm. The influence of both the large displacements and the shear deformations to the plastic strain distribution is verified while the affect of the soil inelasticity is presented.

In *Chapter 5*, the geometrically nonlinear inelastic analysis of Euler-Bernoulli beams of arbitrary doubly symmetric simply or multiply connected constant cross-section, resting on inelastic Winkler foundation. The beam is subjected to the combined action of arbitrarily distributed or concentrated transverse dynamic loading and bending moments in both directions as well as to axial loading, while its edges are subjected to the most general boundary conditions. A hysteretic Bouc-Wen force-displacement model is employed in order to describe the inelastic behaviour of the Winkler springs. A displacement based formulation is developed and inelastic redistribution is modelled through a distributed plasticity (fibre) approach. A uniaxial hysteretic law is considered for the evolution of the plastic part of the normal stress following a phenomenological hysteresis model. Numerical integration over the cross sections is performed in order to resolve the hysteric parts of the stress resultants. Three boundary value problems are formulated with respect to the transverse and axial displacements and solved using the Analog Equation Method. Application of the boundary element technique yields a system of nonlinear Differential-Algebraic Equations which are written in state-space form and together with the hysteretic evolution equations are solved iteratively using the Petzold-Gear backward differentiation formula. It is concluded that the large displacements change radically the dynamic characteristics of the beam-foundation system. Furthermore, the influence of the plastic strain distribution is verified while the affect of the soil inelasticity is presented.

In *Chapter6*, the main conclusions drawn in this dissertation are summarized and the key advantages and novelties of the current formulation are highlighted. Moreover, directions for further research are suggested.

This doctoral dissertation contains also three appendices. In the first **Appendix A1**, the main principles of the Analog Equation Method in its general form are presented, in case of one-dimensional boundary value problems described by ordinary differential equations of the second and forth order, under the most general boundary conditions. In the second **Appendix A2**, the main principles of the Domain Boundary Element Method are presented, in case of one-dimensional boundary value problems described by ordinary differential equations of the second order. Finally, in the last **Appendix A3**, the solution for the general transverse shear loading problem in beams of arbitrary simply or multiply connected constant cross section is briefly presented while the shear deformation coefficients are established using pure Boundary Element Method. Finally, the references sited within the dissertation are presented in alphabetic order.

Finally, it is worth mentioning that the outcome of the conducted research activity presented in this doctoral dissertation has been published in international journals, in national and international conferences and in books published by international publishing companies. These publications are cited at the introduction section of the corresponding chapter.

Chapter 2

Geometrically Nonlinear Static Analysis of Shear Deformable Beams on Nonlinear Foundation

2.1 Introduction

In most investigations concerning *Beam-Foundation Systems* the assumption is made that, bodies are in full contact (beam and subgrade are bonded to each other) and consequently compressive as well as tensile reactions are developed. These bilateral foundation models were probably motivated more by the desire of mathematical simplicity rather than by physical reality. However, for most foundation materials, the admission of tensile stresses across the interface separating the beam from the foundation is not realistic. In order to address this issue, tensionless foundation models were proposed in which regions of no contact develop beneath the beam. These regions are not known in advance and the change of the transverse displacement sign provides the condition for the determination of the contact length.

Moreover, according to the modelling of the mechanical behaviour of the subsoil and the soil-foundation interaction, the earliest, most famous and most frequently adopted mechanical model is the Winkler elastic foundation (Hetenyi 1946). In this model the supporting soil behaviour is approximated by a series of closely spaced, mutually independent, linear elastic vertical spring elements, providing resistance in direct proportion to the deflection of the beam. However, the application of this model is restricted to non-cohesive soil media due to its inability to take into account the continuity or cohesion of the soil (interaction between adjacent springs). To overcome this weakness, a second parameter is introduced such as Filonenko–Borodich, Pasternak or Hetenyi models (Pasternak 1954), to account for the interaction among the linear elastic springs (Fig.2.1). The induction of this second parameter brings the modelling of the soil behaviour closer to reality but its response is still not as complicated as the elastic continuum model. This fact resulted in the development of more sophisticated models comprising three independent parameters for the description of the soil behaviour. More specifically, since in practice the support structure may be highly nonlinear due to the

foundation hardening characteristics (e.g. ballast and rail-pad), the inclusion of a third parameter associated with the cubic nonlinearity of the deflection was verified experimentally by Dahlberg (2002). Besides, this formulation renders the arising mechanical model capable of distributing stresses correctly (Kargarnovin et al. 2005).

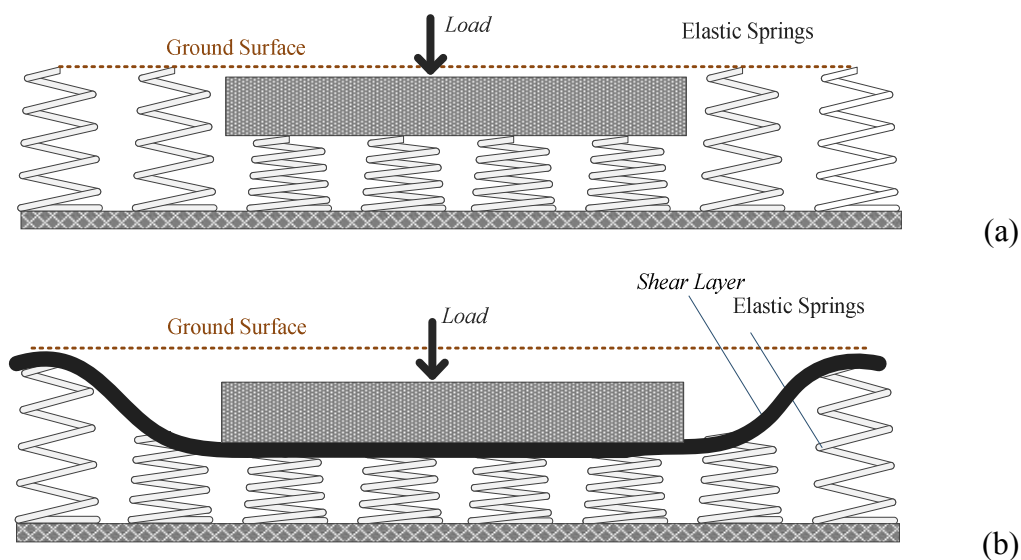


Fig. 2.1. Displacement of Winkler (a) and Pasternak (b) foundation models.

Furthermore, the study of nonlinear effects on the analysis of structural elements is essential in civil engineering applications, wherein weight saving is of paramount importance. This nonlinearity results from retaining the square of the slope in the strain–displacement relations (intermediate non-linear theory), avoiding in this way the inaccuracies arising from a linearized second–order analysis. Moreover, due to the intensive use of materials having relatively high transverse shear modulus, the error incurred from the ignorance of the effect of shear deformation may be substantial, particularly in the case of heavy lateral loading.

Over the past thirty years, many researchers have developed and validated various methods for performing analysis of beams partially supported on Winkler foundation but only few took into account the realistic tensionless character of the subgrade reaction. To begin with, Sharma and Dasgupta (1975) employed an iteration method using Green’s functions for the analysis of uniformly loaded Bernoulli beams, followed by Kaschiev and Mikhajlov (1995), who presented a finite element solution for beams subjected to arbitrary loading. Later, Zhang and Murphy (2004) presented for the same problem an analytical/numerical solution making no assumption about either the contact area or the kinematics associated with the transverse deflection of the beam. Avramidis

and Morfidis (2006) analyzed the bending problem of a Timoshenko beam on a Kerr-type three-parameter elastic foundation carrying out comparisons between one, two or three-parameter foundation models. Maheshwari (2007) employed the finite difference method with the help of appropriate boundary and continuity conditions for the analysis of beams on tensionless reinforced granular fill-soil system, while Ma et al. (2009a,b) used the transfer displacement function method (TDFM) to analyze the response of an infinite beam resting on a tensionless elastic foundation subjected to arbitrarily complex transverse loads. Zhang (2008) analyzed a beam resting on a tensionless Reissner foundation and demonstrated the improvements of the Reissner foundation model compared to the Winkler one, while Ying et al. (2008) presented exact solutions for bending and free vibration of functionally graded beams resting on a Winkler–Pasternak elastic foundation based on the two-dimensional theory of elasticity. Finally, Tullini and Tralli (2010) presented a finite element solution for the static analysis of a foundation Timoshenko beam resting on elastic half-plane by employing locking-free Hermite polynomials. Nevertheless, in all of the aforementioned research efforts only a geometrically linear analysis is performed.

As the deflections become larger, the induced *geometric nonlinearities* result in effects that are not observed in linear systems. Recently, Silveira et al. (2008) presented a nonlinear analysis of Bernoulli structural elements under unilateral contact constraints employing a Ritz type approach, while Tsiatas (2010) suggested a boundary integral equation solution to the nonlinear problem of non-uniform Bernoulli beams resting on a nonlinear triparametric elastic foundation. In these research efforts, the shear deformation effect is ignored.

In this chapter, a Boundary Element Method (BEM) is developed for the geometrically nonlinear analysis of shear deformable beams of arbitrary doubly symmetric simply or multiply connected constant cross-section, partially supported on nonlinear three-parameter tensionless foundation, undergoing moderate large deflections under general boundary conditions. The beam is subjected to the combined action of arbitrarily distributed or concentrated transverse loading and bending moments in both directions as well as to axial loading. To account for shear deformations, the concept of shear deformation coefficients is used. Five boundary value problems are formulated with respect to the transverse displacements, to the axial displacement and to two stress functions and solved using the Analog Equation Method (Katsikadelis 2002), a BE based method. Application of the boundary element technique yields a system of nonlinear equations from which the transverse and axial displacements are computed by

an iterative process. The evaluation of the shear deformation coefficients is accomplished from the aforementioned stress functions using only boundary integration.

Numerical examples of great practical interest are worked out to demonstrate the efficiency and the accuracy of the developed method through comparison with literature and FEM results, as well as its range of applications. In these examples, the effects arising in the nonlinear response of beams on nonlinear foundation are illustrated. The essential features and novel aspects of the present formulation compared with previous ones are summarized as follows.

- i. The proposed beam model accounts for the geometrical nonlinearity by retaining the square of the slope in the strain–displacement relations. For that purpose the Total Lagrangian formulation (intermediate non-linear theory) has been adopted.
- ii. Shear deformation effect is taken into account on the geometrically nonlinear analysis of beams on nonlinear foundation.
- iii. The proposed model takes into account the coupling effects of bending and shear deformations along the member as well as the shear forces along the span induced by the applied axial loading.
- iv. The shear deformation coefficients are evaluated using an energy approach, instead of Timoshenko’s (Timoshenko & Goodier 1984) and Cowper’s (1966) definitions, for which several authors (Schramm et al. 1994, 1997) have pointed out that one obtains unsatisfactory results or definitions given by other researchers (Stephen 1980, Hutchinson 2001) for which these factors take negative values.
- v. The beam is supported by the most general boundary conditions including elastic support or restraint, while it is subjected to arbitrary loading.
- vi. The nonlinear half-space is approximated by a nonlinear three-parameter tensionless foundation. The proposed method can also handle the case of negative foundation nonlinearity.
- vii. The proposed method employs a BEM approach while a small number of nodal points are required to achieve high accuracy.
- viii. The use of BEM permits the effective computation of derivatives of the field functions (e.g. stresses, stress resultants) which is very important during the nonlinear response of beam-foundation systems.

Finally, it is worth mentioning that the outcome of the conducted research activity presented in this chapter of the doctoral dissertation has been published in international journals (Sapountzakis & Kampitsis 2010a, 2011a) and in international conferences (Sapountzakis & Kampitsis 2010e).

2.2 Statement of the Problem

Let us consider a prismatic beam of length l (Fig.2.2), of constant arbitrary doubly symmetric cross-section of area A . The homogeneous isotropic and linear elastic material of the beam cross-section, with modulus of elasticity E , Poisson's ratio ν and shear modulus G ($G = E / (2(1 + \nu))$) occupies the two-dimensional multiply connected region Ω of the y, z plane and is bounded by the Γ_j ($j = 1, 2, \dots, K$) boundary curves, which are piecewise smooth, i.e. they may have a finite number of corners.

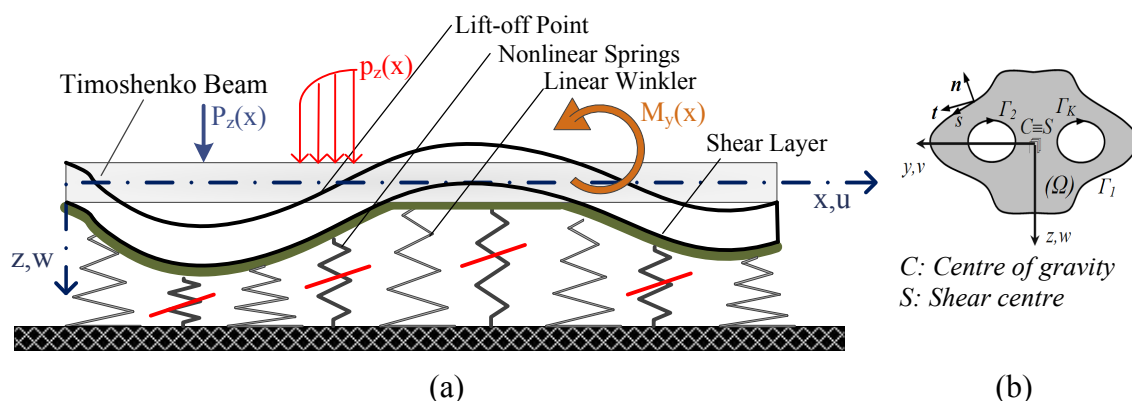


Fig. 2.2. x - z plane of prismatic beam under axial-flexural loading (a) with arbitrary doubly symmetric cross-section (b).

In Fig.2.2b Cyz is the principal bending coordinate system through the cross-section's centroid. The beam is partially supported on an elastic nonlinear tensionless three-parameter soil. The foundation model is characterized by the linear Winkler moduli k_{Lx} , k_{Ly} , k_{Lz} , the nonlinear Winkler moduli k_{NLy} , k_{NLz} and the Pasternak (shear) foundation moduli k_{Py} , k_{Pz} for the directions y , z , respectively. Having in mind that for the longitudinal direction the reaction is a bilateral one exhibiting both compressive and tensile tractions, while for the transverse directions is a unilateral one

(accounting for the unbonded contact between beam and subgrade), the interaction pressure at the interface can be written as

$$p_{sx} = k_x u(x) \quad (2.1a)$$

$$p_{sy} = \tilde{H}_y(x) \left(k_{Ly} v(x) + k_{NLy} v^3(x) - k_{Py} \frac{\partial^2 v(x)}{\partial x^2} \right) \quad (2.1b)$$

$$p_{sz} = \tilde{H}_z(x) \left(k_{Lz} w(x) + k_{NLz} w^3(x) - k_{Pz} \frac{\partial^2 w(x)}{\partial x^2} \right) \quad (2.1c)$$

where $\tilde{H}_y(x)$, $\tilde{H}_z(x)$ are the Heaviside unit step functions defined as

$$\tilde{H}_y(x) = \begin{cases} 1 & \text{if } \left(k_{Ly} v(x) + k_{NLy} v^3(x) - k_{Py} \frac{\partial^2 v(x)}{\partial x^2} \right) > 0 \\ 0 & \text{if } \left(k_{Ly} v(x) + k_{NLy} v^3(x) - k_{Py} \frac{\partial^2 v(x)}{\partial x^2} \right) \leq 0 \end{cases} \quad (2.2a)$$

$$\tilde{H}_z(x) = \begin{cases} 1 & \text{if } \left(k_{Lz} w(x) + k_{NLz} w^3(x) - k_{Pz} \frac{\partial^2 w(x)}{\partial x^2} \right) > 0 \\ 0 & \text{if } \left(k_{Lz} w(x) + k_{NLz} w^3(x) - k_{Pz} \frac{\partial^2 w(x)}{\partial x^2} \right) \leq 0 \end{cases} \quad (2.2b)$$

The beam is subjected to the combined action of the arbitrarily distributed or concentrated axial loading $p_x = p_x(x)$, transverse loading $p_y = p_y(x)$, $p_z = p_z(x)$ and bending moments $m_y = m_y(x)$, $m_z = m_z(x)$ acting along y , z directions, respectively (Fig.2.2a).

2.2.1 Displacements, Strains & Stresses

Under the action of the aforementioned loading, the displacement field of the beam taking into account shear deformation effect is given as (Ramm & Hofmann 1995)

$$\bar{u}(x, y, z) = u(x) - y\theta_z(x) + z\theta_y(x) \quad (2.3a)$$

$$\bar{v}(x, y, z) = v(x) \quad \bar{w}(x, y, z) = w(x) \quad (2.3b,c)$$

where \bar{u} , \bar{v} , \bar{w} are the axial and transverse beam displacement components with respect to the Cyz system of axes; $u(x)$, $v(x)$, $w(x)$ are the corresponding components of the centroid C and $\theta_y(x)$, $\theta_z(x)$ are the angles of rotation due to bending of the cross-section with respect to its centroid (Fig.2.3). It is worth here noting that since the additional angle of rotation of the cross-section due to shear deformation is taken into account, the one due to bending is not equal to the derivative of the deflection (i.e. $\theta_z \neq v'$, $\theta_y \neq w'$).

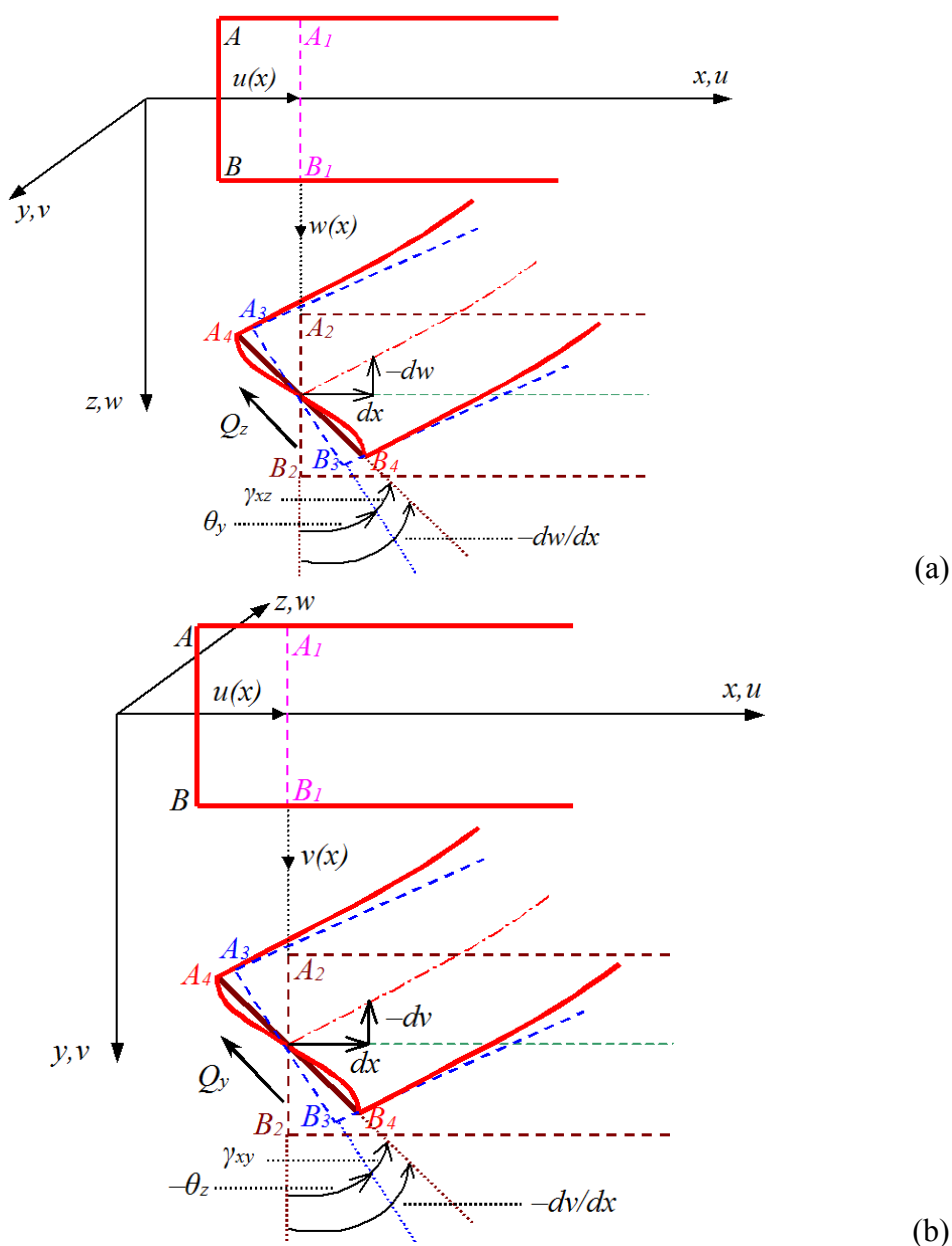


Fig. 2.3. Displacement field according to xz (a) and xy (b) planes of shear deformable Timoshenko beam.

Employing the strain-displacement relations of the three-dimensional elasticity the components of the Green-Lagrange strain are defined as

$$\varepsilon_{xx} = \frac{\partial \bar{u}}{\partial x} + \frac{1}{2} \left[\left(\frac{\partial \bar{u}}{\partial x} \right)^2 + \left(\frac{\partial \bar{v}}{\partial x} \right)^2 + \left(\frac{\partial \bar{w}}{\partial x} \right)^2 \right] \quad (2.4a)$$

$$\varepsilon_{yy} = \frac{\partial \bar{v}}{\partial y} + \frac{1}{2} \left[\left(\frac{\partial \bar{u}}{\partial y} \right)^2 + \left(\frac{\partial \bar{v}}{\partial y} \right)^2 + \left(\frac{\partial \bar{w}}{\partial y} \right)^2 \right] \quad (2.4b)$$

$$\varepsilon_{zz} = \frac{\partial \bar{u}}{\partial z} + \frac{1}{2} \left[\left(\frac{\partial \bar{u}}{\partial z} \right)^2 + \left(\frac{\partial \bar{v}}{\partial z} \right)^2 + \left(\frac{\partial \bar{w}}{\partial z} \right)^2 \right] \quad (2.4c)$$

$$\gamma_{xy} = \left(\frac{\partial \bar{v}}{\partial x} + \frac{\partial \bar{u}}{\partial y} \right) + \left(\frac{\partial \bar{u}}{\partial x} \frac{\partial \bar{u}}{\partial y} + \frac{\partial \bar{v}}{\partial x} \frac{\partial \bar{v}}{\partial y} + \frac{\partial \bar{w}}{\partial x} \frac{\partial \bar{w}}{\partial y} \right) \quad (2.4d)$$

$$\gamma_{xz} = \left(\frac{\partial \bar{w}}{\partial x} + \frac{\partial \bar{u}}{\partial z} \right) + \left(\frac{\partial \bar{u}}{\partial x} \frac{\partial \bar{u}}{\partial z} + \frac{\partial \bar{v}}{\partial x} \frac{\partial \bar{v}}{\partial z} + \frac{\partial \bar{w}}{\partial x} \frac{\partial \bar{w}}{\partial z} \right) \quad (2.4e)$$

$$\gamma_{yz} = \left(\frac{\partial \bar{w}}{\partial y} + \frac{\partial \bar{v}}{\partial z} \right) + \left(\frac{\partial \bar{u}}{\partial y} \frac{\partial \bar{u}}{\partial z} + \frac{\partial \bar{v}}{\partial y} \frac{\partial \bar{v}}{\partial z} + \frac{\partial \bar{w}}{\partial y} \frac{\partial \bar{w}}{\partial z} \right) \quad (2.4f)$$

Moreover, assuming relatively small centroidal axial displacement and moderate large transverse displacements (Ramm & Hofmann 1995, Rothert & Gensichen 1987, Brush & Almroth 1975) while strains remain small, the following strain components can be easily obtained

$$\varepsilon_{xx} = \frac{\partial \bar{u}}{\partial x} + \frac{1}{2} \left[\left(\frac{\partial \bar{v}}{\partial x} \right)^2 + \left(\frac{\partial \bar{w}}{\partial x} \right)^2 \right] \quad (2.5a)$$

$$\gamma_{xz} = \frac{\partial \bar{w}}{\partial x} + \frac{\partial \bar{u}}{\partial z} + \left(\frac{\partial \bar{v}}{\partial x} \frac{\partial \bar{v}}{\partial z} + \frac{\partial \bar{w}}{\partial x} \frac{\partial \bar{w}}{\partial z} \right) \quad (2.5b)$$

$$\gamma_{xy} = \frac{\partial \bar{v}}{\partial x} + \frac{\partial \bar{u}}{\partial y} + \left(\frac{\partial \bar{v}}{\partial x} \frac{\partial \bar{v}}{\partial y} + \frac{\partial \bar{w}}{\partial x} \frac{\partial \bar{w}}{\partial y} \right) \quad (2.5c)$$

$$\varepsilon_{yy} = \varepsilon_{zz} = \gamma_{yz} = 0 \quad (2.5d,e,f)$$

where it has been assumed that for moderate displacements $(\partial\bar{u}/\partial x)^2 \ll \partial\bar{u}/\partial x$, $(\partial\bar{u}/\partial x)(\partial\bar{u}/\partial z) \ll (\partial\bar{w}/\partial x) + (\partial\bar{u}/\partial z)$, $(\partial\bar{u}/\partial x)(\partial\bar{u}/\partial y) \ll (\partial\bar{v}/\partial x) + (\partial\bar{u}/\partial y)$. Substituting the displacement components (2.3) to the strain-displacement relations (2.5), the strain components can be written as

$$\varepsilon_{xx}(x, y, z) = \frac{du}{dx} + z \frac{d\theta_y}{dx} - y \frac{d\theta_z}{dx} + \frac{1}{2} \left(\frac{dv^2}{dx} + \frac{dw^2}{dx} \right) \quad (2.6a)$$

$$\gamma_{xy} = \frac{dv}{dx} - \theta_z \quad \gamma_{xz} = \frac{dw}{dx} + \theta_y \quad (2.6b,c)$$

where γ_{xy} , γ_{xz} are the additional angles of rotation of the cross-section due to shear deformation. It is worth noting what in the well known Euler-Bernoulli beam theory these shear deformations are neglected, thus

$$\theta_z = \frac{dv}{dx} \quad \theta_y = -\frac{dw}{dx} \quad (2.7b,c)$$

Considering strains to be small and assuming an isotropic and homogeneous material, the non vanishing work conjugate stress components of the second Piola-Kirchhoff stress tensor are defined in terms of the strain ones as

$$\begin{Bmatrix} S_{xx} \\ S_{xy} \\ S_{xz} \end{Bmatrix} = \begin{bmatrix} E & 0 & 0 \\ 0 & G & 0 \\ 0 & 0 & G \end{bmatrix} \begin{Bmatrix} \varepsilon_{xx} \\ \gamma_{xy} \\ \gamma_{xz} \end{Bmatrix} \quad (2.8)$$

or employing the strain-displacement relations (2.6) as

$$S_{xx} = E \left[\frac{du}{dx} + z \frac{d\theta_y}{dx} - y \frac{d\theta_z}{dx} + \frac{1}{2} \left(\frac{dv^2}{dx} + \frac{dw^2}{dx} \right) \right] \quad (2.9a)$$

$$S_{xy} = G \left(\frac{dv}{dx} - \theta_z \right) \quad S_{xz} = G \left(\frac{dw}{dx} + \theta_y \right) \quad (2.9b,c)$$

2.2.2 Stress Resultants, Equations of Equilibrium, Boundary Conditions

The equations of equilibrium and the boundary conditions of the beam-foundation system are derived employing the equilibrium method. It is mentioned that any energy principle (e.g. total potential energy) could also be implemented providing the same results. To this end, let's consider an infinitesimal beam element of length dx at its deformed configuration as this is depicted in Fig. 2.4.

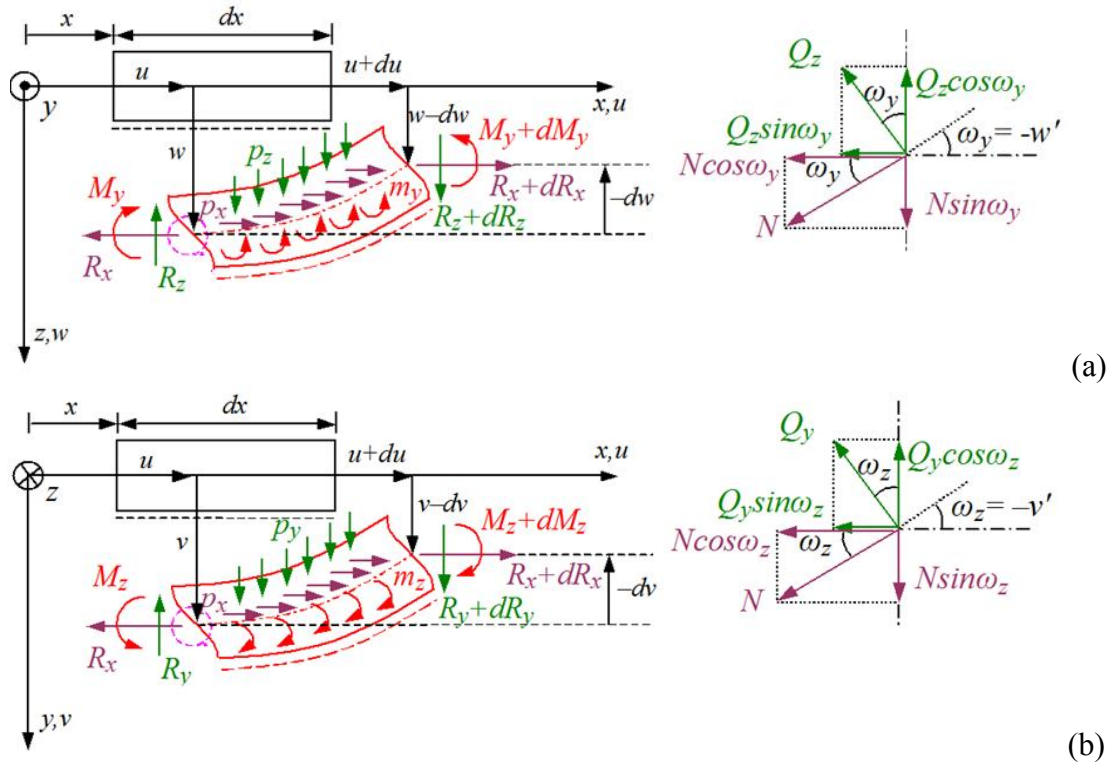


Fig. 2.4. Infinitesimal beam element of length dx at its deformed configuration under equilibrium according to xz (a) and xy (b) planes.

Moreover, the angles of rotation are assumed to be small, thus the following relations hold

$$\cos \omega_z \approx 1 \quad \sin \omega_z \approx \omega_z \quad \cos \omega_y \approx 1 \quad \sin \omega_y \approx \omega_y \quad (2.10a-d)$$

Consequently, the horizontal force R_x and the vertical forces V_y, V_z can be written in term of the axial N and the shear Q_y, Q_z forces, as (Fig. 2.4)

$$R_x = N + Q_y \omega_z + Q_z \omega_y \quad (2.11a)$$

$$V_y = Q_y - N \omega_z \quad V_z = Q_z - N \omega_y \quad (2.11b,c)$$

while the angles of rotation ω_y, ω_z are defined as

$$\omega_y = -\frac{dw}{dx} \quad \omega_z = -\frac{dv}{dx} \quad (2.12a,b)$$

Substituting eqns. (2.12a,b) to eqns. (2.11) yields

$$R_x = N + Q_y v' + Q_z w' \quad (2.11a)$$

$$V_y = Q_y - N v' \quad V_z = Q_z - N w' \quad (2.11b,c)$$

where (') denotes differentiation with respect to x , while the second and third term of the right hand side of eqn. (2.11a) express the influence of the shear forces to the horizontal one. Nevertheless, as $Q_y v', Q_z w' \ll N$ (Rothert & Gensichen 1987, Ramm & Hofmann 1995) the horizontal force is equated to the axial one, thus $R_x = N$.

Subsequently, equating the external loads with the internal reaction, the equations of equilibrium are written as

$$\frac{dN}{dx} - k_x u + p_x = 0 \quad (2.12a)$$

$$\frac{dQ_y}{dx} - p_{sy} + p_y = 0 \quad \frac{dQ_z}{dx} - p_{sz} + p_z = 0 \quad (2.12b,c)$$

$$\frac{dM_y}{dx} - Q_z + m_y = 0 \quad \frac{dM_z}{dx} + Q_y + m_z = 0 \quad (2.12d,e)$$

while the axial N and the shear Q_y, Q_z forces as well as the bending moments M_y, M_z of the beam in the deformed configuration are defined as

$$N = \int_{\Omega} S_{xx} d\Omega \quad (2.13a)$$

$$Q_y = \int_{A_y} S_{xy} d\Omega \quad Q_z = \int_{A_z} S_{xz} d\Omega \quad (2.13b,c)$$

$$M_y = \int_{\Omega} S_{xx} z d\Omega \quad M_z = -\int_{\Omega} S_{xx} y d\Omega \quad (2.13d,e)$$

After employing both the strain components of eqns. (2.6) and the stress-strain constitutive relations (2.9) for an isotropic and homogeneous material, eqns. (2.13) are written as

$$N = EA \left[u' + \frac{I}{2} (v'^2 + w'^2) \right] \quad (2.14a)$$

$$Q_y = GA_y \gamma_{xy} \quad Q_z = GA_z \gamma_{xz} \quad (2.14b,c)$$

$$M_y = EI_y \theta_y' \quad M_z = EI_z \theta_z' \quad (2.14c,d)$$

where A is the cross section area, while I_y , I_z are the moments of inertia with respect to the principle bending axes given as

$$A = \int_{\Omega} d\Omega \quad (2.15a)$$

$$I_y = \int_{\Omega} z^2 d\Omega \quad I_z = \int_{\Omega} y^2 d\Omega \quad (2.15b,c)$$

and GA_y , GA_z are its shear rigidities of the Timoshenko's beam theory, where

$$A_z = \kappa_z A = \frac{I}{a_z} A \quad A_y = \kappa_y A = \frac{I}{a_y} A \quad (2.16a,b)$$

are the shear areas with respect to y , z axes, respectively with κ_y , κ_z the shear correction factors and a_y , a_z the shear deformation coefficients (Appendix A3).

Substituting the stress resultants of eqns. (2.14) and the strain resultants of eqns. (2.6) in the equilibrium eqns. (2.12) the differential equations of equilibrium are written as

$$-EA(u'' + w'w'' + v'v'') + k_{Lx}u = p_x \quad (2.17a)$$

$$-(Nv')' - GA_y(v'' - \theta_z') + \tilde{H}_y(k_{Ly}v + k_{NLy}v^3 - k_{Py}v'') = p_y \quad (2.17b)$$

$$-(Nw')' - GA_z(w'' + \theta_y') + \tilde{H}_z(k_{Lz}w + k_{NLz}w^3 - k_{Pz}w'') = p_z \quad (2.17c)$$

$$-EI_z\theta_z'' - GA_y(v' - \theta_z) = m_z \quad -EI_y\theta_y'' + GA_z(w' + \theta_y) = m_y \quad (2.17d,e)$$

Combining eqns. (2.17b,d) and (2.17c,e), the governing differential equations with respect only to the displacement components u , v , w of a geometrically nonlinear Timoshenko beam, partially supported on a nonlinear three-parameter tensionless foundation, subjected to the combined action of axial and transverse loading are obtained as

$$-EA(u'' + w'w'' + v'v'') + k_{Lx}u = p_x \quad (2.18a)$$

$$EI_z v'''' - (Nv')' + p_{sy} + \frac{EI_y}{GA_y} \left((Nw')''' - p_{sy}'' \right) = p_y - \frac{EI_y}{GA_z} p_z'' - m_z' \quad (2.18b)$$

$$EI_y w'''' - (Nw')' + p_{sz} + \frac{EI_y}{GA_z} \left((Nw')''' - p_{sz}'' \right) = p_z - \frac{EI_y}{GA_z} p_z'' + m_y' \quad (2.18c)$$

These equations are also subjected to the pertinent boundary conditions of the problem at hand, which are given as

$$a_1 u(x) + \alpha_2 N(x) = \alpha_3 \quad (2.19a)$$

$$\beta_1 v(x) + \beta_2 V_y(x) = \beta_3 \quad \bar{\beta}_1 \theta_z(x) + \bar{\beta}_2 M_z(x) = \bar{\beta}_3 \quad (2.19b,c)$$

$$\gamma_1 w(x) + \gamma_2 V_z(x) = \gamma_3 \quad \bar{\gamma}_1 \theta_y(x) + \bar{\gamma}_2 M_y(x) = \bar{\gamma}_3 \quad (2.19d,e)$$

at the beam ends $x = 0, l$. In eqns. (2.19b-e) the vertical reactions V_y , V_z , the bending moments M_y , M_z and the angles of rotation due to bending θ_y , θ_z are given as

$$V_y = -EI_z v'''' + Nv' - \frac{EI_z}{GA_y} \left[(Nv')'' + p_y' - p_{sy}' \right] - m_z \quad (2.20a)$$

$$V_z = -EI_y w'''' + Nw' - \frac{EI_y}{GA_z} \left[(Nw')'' + p_z' - p_{sz}' \right] + m_y \quad (2.20b)$$

$$M_y = -EI_y w'' - \frac{EI_y}{GA_z} \left((Nw')' + p_z - p_{sz} \right) \quad (2.21a)$$

$$M_z = EI_z v'' + \frac{EI_z}{GA_y} \left((Nv')' + p_y - p_{sy} \right) \quad (2.21b)$$

$$\theta_y = -\frac{EI_y}{(GA_z)^2} \left((Nw')'' + p'_{sz} \right) - \frac{I}{GA_z} (EI_y w''' + GA_z w') \quad (2.22a)$$

$$\theta_z = \frac{EI_z}{(GA_y)^2} \left((Nv')'' - p'_{sy} \right) + \frac{I}{GA_y} (EI_z v''' + GA_y v') \quad (2.22b)$$

Finally, $\alpha_j, \beta_j, \bar{\beta}_j, \gamma_j, \bar{\gamma}_j$ ($j=1,2,3$) are functions specified at the beam ends $x=0, l$. Eqns. (2.19) describe the most general boundary conditions associated with the problem at hand and can include elastic support or restraint. It is apparent that all types of the conventional boundary conditions (clamped, simply supported, free or guided edge) can be derived from these equations by specifying appropriately these functions (e.g. for a clamped edge it is $\alpha_1 = \beta_1 = \gamma_1 = 1$, $\bar{\beta}_1 = \bar{\gamma}_1 = 1$, $\alpha_2 = \alpha_3 = \beta_2 = \beta_3 = \gamma_2 = \gamma_3 = \bar{\beta}_2 = \bar{\beta}_3 = \bar{\gamma}_2 = \bar{\gamma}_3 = 0$).

The solution of the boundary value problem given from eqns. (2.18) subjected to the boundary conditions (3.19) describes the axial-flexural response accounting for the geometrical nonlinearity (large displacements) of a Timoshenko beam, supported on a nonlinear three-parameter tensionless foundation. The evaluation of the shear deformation coefficients a_y, a_z corresponding to the principal centroidal system of axes C_{yz} , are established equating the approximate formula of the shear strain energy per unit length with the exact one as described in Appendix A3.

2.3 Integral Representations – Numerical Solution

According to the precedent analysis, the nonlinear axial-flexural analysis of a Timoshenko beam, partially supported on a nonlinear three-parameter tensionless foundation, undergoing moderate large deflections reduces in establishing the displacement components $u(x)$ and $v(x)$, $w(x)$ having continuous derivatives up to the second and up to the fourth order with respect to x , respectively. Moreover, these displacement components must satisfy the coupled governing differential equations (2.178) inside the beam and the boundary conditions (2.19) at the beam ends $x=0, l$. The differential equations of equilibrium are solved using the Analog Equation Method (Katsikadelis 1994, 2002) as it is described in Appendix A1.

2.3.1 Axial $u(x)$ and transverse displacements $v(x), w(x)$

According to this method, let $u(x)$, $v(x)$ and $w(x)$ be the sought solution of the aforementioned boundary value problem. Setting as $u_1(x) = u(x)$, $u_2(x) = v(x)$, $u_3(x) = w(x)$ and differentiating with respect to x these functions two and four times, respectively yields

$$\frac{\partial^2 u_i}{\partial x^2} = q_i(x,t) \quad \frac{\partial^4 u_i}{\partial x^4} = q_i(x,t) \quad (i=2,3) \quad (2.23)$$

Eqns. (2.23) are called analog equations and indicate that the solution of eqns. (2.18) can be established by solving eqns. (2.23) under the same boundary conditions (2.19), provided that the fictitious load distributions $q_i(x,t)$ ($i=1,2,3$) are first established. Following the procedure as described in Appendix A1, the integral representations of the displacement components u_i ($i=1,2,3$) obtained by eqn. (A1.8, A1.36) and their first derivatives with respect to x obtained by eqn. (A1.22, A1.43), when applied to the beam ends $(0,l)$, together with the boundary conditions (2.19) are employed to express the unknown boundary quantities $u_i(\zeta,t)$, $u_{i,x}(\zeta,t)$, $u_{i,xx}(\zeta,t)$ and $u_{i,xxx}(\zeta,t)$ ($\zeta=0,l$) in terms of the fictitious loads q_i ($i=1,2,3$). In order to accomplish this numerical formulation, the interval $(0,l)$ is divided into L elements, on which $q_i(x,t)$ is assumed to vary according to certain law (constant, linear, parabolic etc). The constant element assumption is employed here as the numerical implementation becomes very simple and the obtained results are of high accuracy.

Employing the aforementioned procedure, the following set of 20 nonlinear algebraic equations is obtained

$$\begin{bmatrix} \mathbf{T}_{11} & \mathbf{0} & \mathbf{0} \\ \mathbf{0} & \mathbf{T}_{22} & \mathbf{0} \\ \mathbf{0} & \mathbf{0} & \mathbf{T}_{33} \end{bmatrix} \begin{Bmatrix} \mathbf{d}_1 \\ \mathbf{d}_2 \\ \mathbf{d}_3 \end{Bmatrix} + \begin{Bmatrix} \mathbf{D}_1^{\text{nl}} \\ \mathbf{D}_2^{\text{nl}} \\ \mathbf{D}_3^{\text{nl}} \end{Bmatrix} = \begin{Bmatrix} \mathbf{a}_3 \\ \mathbf{b}_3 \\ \mathbf{c}_3 \end{Bmatrix} \quad (2.24)$$

with

$$\mathbf{T}_{11} = \begin{bmatrix} \mathbf{F}_1^u & \mathbf{E}_{11}^u & \mathbf{E}_{12}^u \\ \mathbf{0} & \mathbf{D}_{12}^u & \mathbf{D}_{22}^u \end{bmatrix} \quad (2.25a)$$

$$\mathbf{T}_{22} = \begin{bmatrix} \mathbf{F}_1 & \mathbf{E}_{11} & \mathbf{E}_{12} & \mathbf{E}_{13} & \mathbf{E}_{14} \\ \mathbf{F}_2 & \mathbf{0} & \mathbf{E}_{22} & \mathbf{E}_{23} & \mathbf{E}_{24} \\ \mathbf{0} & \mathbf{D}_{11} & \mathbf{D}_{12} & \mathbf{D}_{13} & \mathbf{D}_{14} \\ \mathbf{0} & \mathbf{D}_{21} & \mathbf{D}_{22} & \mathbf{D}_{23} & \mathbf{D}_{24} \end{bmatrix} \quad \mathbf{T}_{33} = \begin{bmatrix} \mathbf{F}_1 & \mathbf{E}_{11} & \mathbf{E}_{12} & \mathbf{E}_{13} & \mathbf{E}_{14} \\ \mathbf{F}_2 & \mathbf{0} & \mathbf{E}_{22} & \mathbf{E}_{23} & \mathbf{E}_{24} \\ \mathbf{0} & \mathbf{G}_{11} & \mathbf{G}_{12} & \mathbf{G}_{13} & \mathbf{G}_{14} \\ \mathbf{0} & \mathbf{G}_{21} & \mathbf{G}_{22} & \mathbf{G}_{23} & \mathbf{G}_{24} \end{bmatrix} \quad (2.25b,c)$$

where $\mathbf{E}_{11}^u, \mathbf{E}_{12}^u, \mathbf{E}_{11} - \mathbf{E}_{48}$ are rectangular 2×2 known coefficient matrices resulting from the values of the kernels $\mathcal{A}_j(r)$ ($j=1, 2, 3, 4$) at the beam ends and $\mathbf{F}_1^u, \mathbf{F}_1, \mathbf{F}_2$ are $2 \times L$ rectangular known matrices originating from the integration of the kernels along the axis of the beam, as defined in Appendix A1. Moreover, $\mathbf{D}_{11} - \mathbf{D}_{24}$ and $\mathbf{G}_{11} - \mathbf{G}_{24}$ are 2×2 known square matrices including the values of the functions $a_j, \beta_j, \bar{\beta}_j, \gamma_j, \bar{\gamma}_j$ ($j=1, 2$) of eqns.(2.19), while $\mathbf{D}_1^{nl}, \mathbf{a}_3$ and $\mathbf{D}_2^{nl}, \mathbf{D}_3^{nl}, \mathbf{b}_3, \mathbf{c}_3$ are 4×1 and 8×1 , respectively known column matrices including the boundary values of the functions $a_3, \beta_3, \bar{\beta}_3, \gamma_3, \bar{\gamma}_3$ of eqns. (2.19). Furthermore, $\mathbf{d}_1 - \mathbf{d}_3$ are the generalized unknown vectors including the L unknown nodal values of the fictitious loads $q_i = \{q_1^i, q_2^i, \dots, q_L^i\}^T$ ($i=1,2,3$) and the vectors including the unknown boundary values of the respective boundary quantities. More specifically, the expressions of the matrices of eqn. (2.25) are given as

$$\mathbf{D}_{12}^u = \begin{bmatrix} \alpha_1^0 & 0 \\ 0 & \alpha_1^l \end{bmatrix} \quad \mathbf{D}_{22}^u = \begin{bmatrix} \alpha_2^0 EA & 0 \\ 0 & \alpha_2^l EA \end{bmatrix} \quad (2.26a,b)$$

$$\mathbf{D}_1^{nl} = \frac{1}{2} EA \left\{ \begin{array}{c} [0] \\ \alpha_2^0 [\hat{u}_{2,x}(0) + \hat{u}_{3,x}(0)]^2 \\ \alpha_2^l [\hat{u}_{2,x}(l) + \hat{u}_{3,x}(l)]^2 \end{array} \right\} \quad \mathbf{a}_3 = \left\{ \begin{array}{c} [0] \\ \alpha_3^0 \\ \alpha_3^l \end{array} \right\} \quad (2.26c,d)$$

$$\mathbf{D}_{11} = \begin{bmatrix} \beta_1^0 & 0 \\ 0 & \beta_1^l \end{bmatrix} \quad \mathbf{D}_{12} = \begin{bmatrix} \beta_2^0 \left(N(0) + \frac{EI_z}{GA_y} \tilde{H}_y k_{Ly} \right) & 0 \\ 0 & \beta_2^l \left(N(l) + \frac{EI_z}{GA_y} \tilde{H}_y k_{Ly} \right) \end{bmatrix} \quad (2.27a,b)$$

$$\mathbf{D}_{13} = -\frac{2EI_z}{GA_y} \begin{bmatrix} \beta_2^0 N'(0) & 0 \\ 0 & \beta_2^l N'(l) \end{bmatrix} \quad \mathbf{D}_{14} = -EI_z \begin{bmatrix} \beta_2^0 \left(1 + \frac{1}{GA_y} (N(0) + \tilde{H}_y k_{Py}) \right) & 0 \\ 0 & \beta_2^l \left(1 + \frac{1}{GA_y} (N(l) + \tilde{H}_y k_{Py}) \right) \end{bmatrix} \quad (2.27c,d)$$

$$\mathbf{D}_{21} = -\bar{\beta}_2^0 \frac{EI_z}{GA_y} \begin{bmatrix} \tilde{H}_y k_{Ly} & 0 \\ 0 & \tilde{H}_y k_{Ly} \end{bmatrix} \quad (2.27e)$$

$$\mathbf{D}_{22} = \begin{bmatrix} \bar{\beta}_1^0 \left(1 - \frac{EI_z}{(GA_y)^2} \tilde{H}_y k_{Ly} \right) + \bar{\beta}_2^0 \frac{EI_z}{GA_y} N'(0) & 0 \\ 0 & \bar{\beta}_1^l \left(1 - \frac{EI_z}{(GA_y)^2} \tilde{H}_y k_{Ly} \right) + \bar{\beta}_2^l \frac{EI_z}{GA_y} N'(l) \end{bmatrix} \quad (2.27f)$$

$$\mathbf{D}_{23} = EI_z \begin{bmatrix} \bar{\beta}_2^0 \left(1 + \frac{1}{GA_y} N(0) - \frac{1}{GA_y} \tilde{H}_y k_P \right) + \bar{\beta}_1^0 \frac{2}{(GA_y)^2} N'(0) & 0 \\ 0 & \bar{\beta}_2^l \left(1 + \frac{1}{GA_y} N(l) - \frac{1}{GA_y} \tilde{H}_y k_P \right) + \bar{\beta}_1^l \frac{2}{(GA_y)^2} N'(l) \end{bmatrix} \quad (2.27g)$$

$$\mathbf{D}_{24} = \frac{EI_z}{GA_y} \begin{bmatrix} \bar{\beta}_1^0 \left(1 + \frac{1}{GA_y} (N(0) + \tilde{H}_y k_P) \right) & 0 \\ 0 & \bar{\beta}_1^l \left(1 + \frac{1}{GA_y} (N(l) + \tilde{H}_y k_P) \right) \end{bmatrix} \quad (2.27h)$$

$$\mathbf{D}_2^{\text{nl}} = -\frac{EI_z}{GA_y} \left\{ \begin{array}{c} [0] \\ -\beta_2^0 \tilde{H}_y k_{NLy} 3\hat{u}_2^2(0) \hat{u}_{2,x}(0) \\ -\beta_2^l \tilde{H}_y k_{NLy} 3\hat{u}_2^2(l) \hat{u}_{2,x}(l) \\ [0] \\ \bar{\beta}_1^0 \frac{3}{GA_y} \tilde{H}_y k_{NLy} \hat{u}_2^2(0) \hat{u}_{2,x}(0) + \bar{\beta}_2^0 \tilde{H}_y k_{NLy} \hat{u}_2^3(0) \\ \bar{\beta}_1^l \frac{3}{GA_y} \tilde{H}_y k_{NLy} \hat{u}_2^2(l) \hat{u}_{2,x}(l) + \bar{\beta}_2^l \tilde{H}_y k_{NLy} \hat{u}_2^3(l) \end{array} \right\} \quad (2.27i)$$

$$\mathbf{b}_3 = \left\{ \begin{array}{c} [0] \\ \beta_3^0 + \beta_2^0 \frac{EI_z}{GA_y} p'_y(0) \\ \beta_3^l + \beta_2^l \frac{EI_z}{GA_y} p'_y(l) \\ [0] \\ \bar{\beta}_3^0 - \frac{EI_z}{GA_y} \left(\frac{\bar{\beta}_1^0}{GA_y} p'_y(0) - \bar{\beta}_2^0 p_y(0) \right) \\ \bar{\beta}_3^l - \frac{EI_z}{GA_y} \left(\frac{\bar{\beta}_1^l}{GA_y} p'_y(l) - \bar{\beta}_2^l p_y(l) \right) \end{array} \right\} \quad (2.27j)$$

$$\mathbf{G}_{11} = \begin{bmatrix} \gamma_1^0 & 0 \\ 0 & \gamma_1^l \end{bmatrix} \quad \mathbf{G}_{12} = \begin{bmatrix} \gamma_2^0 \left(N(0) + \frac{EI_y}{GA_z} \tilde{H}_z k_{Lz} \right) & 0 \\ 0 & \gamma_2^l \left(N(l) + \frac{EI_y}{GA_z} \tilde{H}_z k_{Lz} \right) \end{bmatrix} \quad (2.28a,b)$$

$$\mathbf{G}_{13} = -\frac{2EI_y}{GA_z} \begin{bmatrix} \gamma_2^0 N'(0) & 0 \\ 0 & \gamma_2^l N'(l) \end{bmatrix} \quad \mathbf{G}_{14} = -EI_y \begin{bmatrix} \gamma_2^0 \left(1 + \frac{I}{GA_z} (N(0) + \tilde{H}_z k_{Pz}) \right) & 0 \\ 0 & \gamma_2^l \left(1 + \frac{I}{GA_z} (N(l) + \tilde{H}_z k_{Pz}) \right) \end{bmatrix} \quad (2.28c,d)$$

$$\mathbf{G}_{21} = -\bar{\gamma}_2^0 \frac{EI_y}{GA_z} \begin{bmatrix} \tilde{H}_z k_{Lz} & 0 \\ 0 & \tilde{H}_z k_{Lz} \end{bmatrix} \quad (2.28e)$$

$$\mathbf{G}_{22} = - \begin{bmatrix} \bar{\gamma}_1^0 \left(1 - \frac{EI_y}{(GA_z)^2} \tilde{H}_z k_{Lz} \right) + \bar{\gamma}_2^0 \frac{EI_y}{GA_z} N'(0) & 0 \\ 0 & \bar{\gamma}_1^l \left(1 - \frac{EI_y}{(GA_z)^2} \tilde{H}_z k_{Lz} \right) + \bar{\gamma}_2^l \frac{EI_y}{GA_z} N'(l) \end{bmatrix} \quad (2.28f)$$

$$\mathbf{G}_{23} = EI_y \begin{bmatrix} \bar{\gamma}_2^0 \left(1 + \frac{1}{GA_z} N(0) - \frac{1}{GA_z} \tilde{H}_z k_P \right) + \bar{\gamma}_1^0 \frac{2}{(GA_z)^2} N'(0) & 0 \\ 0 & \bar{\gamma}_2^l \left(1 + \frac{1}{GA_z} N(l) - \frac{1}{GA_z} \tilde{H}_z k_P \right) + \bar{\gamma}_1^l \frac{2}{(GA_z)^2} N'(l) \end{bmatrix} \quad (2.28g)$$

$$\mathbf{G}_{24} = \frac{EI_y}{GA_z} \begin{bmatrix} \bar{\gamma}_1^0 \left(1 + \frac{1}{GA_z} (N(0) + \tilde{H}_z k_P) \right) & 0 \\ 0 & \bar{\gamma}_1^l \left(1 + \frac{1}{GA_z} (N(l) + \tilde{H}_z k_P) \right) \end{bmatrix} \quad (2.28h)$$

$$\mathbf{D}_3^{\text{nl}} = \frac{EI_y}{GA_z} \left\{ \begin{array}{c} [0] \\ \gamma_2^0 \tilde{H}_z k_{NLz} 3\hat{u}_3^2(0) \hat{u}_{3,x}(0) \\ \gamma_2^l \tilde{H}_z k_{NLz} 3\hat{u}_3^2(l) \hat{u}_{3,x}(l) \\ [0] \\ \bar{\gamma}_1^0 \frac{3}{GA_z} \tilde{H}_z k_{NLz} \hat{u}_3^2(0) \hat{u}_{3,x}(0) + \bar{\gamma}_2^0 \tilde{H}_z k_{NLz} \hat{u}_3^3(0) \\ \bar{\gamma}_1^l \frac{3}{GA_z} \tilde{H}_z k_{NLz} \hat{u}_3^2(l) \hat{u}_{3,x}(l) + \bar{\gamma}_2^l \tilde{H}_z k_{NLz} \hat{u}_3^3(l) \end{array} \right\} \quad (2.28i)$$

$$\mathbf{c}_3 = \left\{ \begin{array}{c} [0] \\ \gamma_3^0 - \gamma_2^0 \frac{EI_y}{GA_z} p'_z(0) \\ \gamma_3^l - \gamma_2^l \frac{EI_y}{GA_z} p'_z(l) \\ [0] \\ \bar{\gamma}_3^0 + \frac{EI_y}{GA_z} \left(\frac{\bar{\gamma}_1^0}{GA_z} p'_z(0) - \bar{\gamma}_2^0 p_z(0) \right) \\ \bar{\gamma}_3^l + \frac{EI_y}{GA_z} \left(\frac{\bar{\gamma}_1^l}{GA_z} p'_z(l) - \bar{\gamma}_2^l p_z(l) \right) \end{array} \right\} \quad (2.28j)$$

$$\mathbf{d}_1 = \begin{Bmatrix} \mathbf{q}_1 \\ \hat{\mathbf{u}}_1 \\ \hat{\mathbf{u}}_{1,x} \end{Bmatrix} \quad \mathbf{d}_2 = \begin{Bmatrix} \mathbf{q}_2 \\ \hat{\mathbf{u}}_2 \\ \hat{\mathbf{u}}_{2,x} \\ \hat{\mathbf{u}}_{2,xx} \\ \hat{\mathbf{u}}_{2,xxx} \end{Bmatrix} \quad \mathbf{d}_3 = \begin{Bmatrix} \mathbf{q}_3 \\ \hat{\mathbf{u}}_3 \\ \hat{\mathbf{u}}_{3,x} \\ \hat{\mathbf{u}}_{3,xx} \\ \hat{\mathbf{u}}_{3,xxx} \end{Bmatrix} \quad (2.29)$$

where the boundary values of the displacement components u_i ($i=1,2,3$) and their derivatives with respect to x are written in matrix form as

$$\hat{\mathbf{u}}_i = \{u_i(0,t) \quad u_i(l,t)\}^T \quad (i=1,2,3) \quad (2.30a)$$

$$\hat{\mathbf{u}}_{i,x} = \left\{ \frac{\partial u_i(0,t)}{\partial x} \quad \frac{\partial u_i(l,t)}{\partial x} \right\}^T \quad (i=1,2,3) \quad (2.30b)$$

$$\hat{\mathbf{u}}_{i,xx} = \left\{ \frac{\partial^2 u_i(0,t)}{\partial x^2} \quad \frac{\partial^2 u_i(l,t)}{\partial x^2} \right\}^T \quad (i=2,3) \quad (2.30c)$$

$$\hat{\mathbf{u}}_{i,xxx} = \left\{ \frac{\partial^3 u_i(0,t)}{\partial x^3} \quad \frac{\partial^3 u_i(l,t)}{\partial x^3} \right\}^T \quad (i=2,3) \quad (2.30d)$$

Thereafter, the discretization of the integral representations of the displacement components u_i ($i=1,2,3$) and their derivatives with respect to x , and the application to the L collocation nodal points yields

$$\mathbf{u}_1 = \mathbf{A}_1^0 \mathbf{q}_1 + \mathbf{C}_0 \hat{\mathbf{u}}_1 + \mathbf{C}_1 \hat{\mathbf{u}}_{1,x} \quad (2.31a)$$

$$\mathbf{u}_{1,x} = \mathbf{A}_1^1 \mathbf{q}_1 + \mathbf{C}_0 \hat{\mathbf{u}}_{1,x} \quad \mathbf{u}_{1,xx} = \mathbf{q}_1 \quad (2.31b,c)$$

$$\mathbf{u}_2 = \mathbf{A}_2^0 \mathbf{q}_2 + \mathbf{C}_0 \hat{\mathbf{u}}_2 + \mathbf{C}'_1 \hat{\mathbf{u}}_{2,x} + \mathbf{C}_2 \hat{\mathbf{u}}_{2,xx} + \mathbf{C}_3 \hat{\mathbf{u}}_{2,xxx} \quad (2.32a)$$

$$\mathbf{u}_{2,x} = \mathbf{A}_2^1 \mathbf{q}_2 + \mathbf{C}_0 \hat{\mathbf{u}}_{2,x} + \mathbf{C}'_1 \hat{\mathbf{u}}_{2,xx} + \mathbf{C}_2 \hat{\mathbf{u}}_{2,xxx} \quad (2.32b)$$

$$\mathbf{u}_{2,xx} = \mathbf{A}_2^2 \mathbf{q}_2 + \mathbf{C}_0 \hat{\mathbf{u}}_{2,xx} + \mathbf{C}'_1 \hat{\mathbf{u}}_{2,xxx} \quad (2.32c)$$

$$\mathbf{u}_{2,xxx} = \mathbf{A}_2^3 \mathbf{q}_2 + \mathbf{C}_0 \hat{\mathbf{u}}_{2,xxx} \quad \mathbf{u}_{2,xxxx} = \mathbf{q}_2 \quad (2.32d,e)$$

$$\mathbf{u}_3 = \mathbf{A}_3^0 \mathbf{q}_3 + \mathbf{C}_0 \hat{\mathbf{u}}_3 + \mathbf{C}'_1 \hat{\mathbf{u}}_{3,x} + \mathbf{C}_2 \hat{\mathbf{u}}_{3,xx} + \mathbf{C}_3 \hat{\mathbf{u}}_{3,xxx} \quad (2.33a)$$

$$\mathbf{u}_{3,x} = \mathbf{A}_3^1 \mathbf{q}_3 + \mathbf{C}_0 \hat{\mathbf{u}}_{3,x} + \mathbf{C}'_1 \hat{\mathbf{u}}_{3,xx} + \mathbf{C}_2 \hat{\mathbf{u}}_{3,xxx} \quad (2.33b)$$

$$\mathbf{u}_{3,xx} = \mathbf{A}_3^2 \mathbf{q}_3 + \mathbf{C}_0 \hat{\mathbf{u}}_{3,xx} + \mathbf{C}'_1 \hat{\mathbf{u}}_{3,xxx} \quad (2.33c)$$

$$\mathbf{u}_{3,xxx} = \mathbf{A}_3^3 \mathbf{q}_3 + \mathbf{C}_0 \hat{\mathbf{u}}_{3,xxx} \quad \mathbf{u}_{3,xxxx} = \mathbf{q}_3 \quad (2.33d,e)$$

where \mathbf{A}_1^i , \mathbf{A}_2^j , \mathbf{A}_3^j ($i=0,1$), ($j=0,1,2,3$) are $L \times L$ known matrices; \mathbf{C}_0 , \mathbf{C}_1 , \mathbf{C}'_1 , \mathbf{C}_2 , \mathbf{C}_3 are $L \times 2$ known matrices and \mathbf{u}_i , $\mathbf{u}_{i,x}$, $\mathbf{u}_{i,xx}$, $\mathbf{u}_{i,xxx}$, $\mathbf{u}_{i,xxxx}$ are vectors including the values of $u_i(x,t)$ and their derivatives at the L nodal points. These equations can be assembled in a more convenient matrix form as

$$\mathbf{u}_1 = \mathbf{B}'' \mathbf{d}_1 \quad \mathbf{u}_{1,x} = \mathbf{B}''_{,x} \mathbf{d}_1 \quad (2.34a,b)$$

$$\mathbf{u}_2 = \mathbf{B} \mathbf{d}_2 \quad \mathbf{u}_{2,x} = \mathbf{B}_{,x} \mathbf{d}_2 \quad \mathbf{u}_{2,xx} = \mathbf{B}_{,xx} \mathbf{d}_2 \quad \mathbf{u}_{2,xxx} = \mathbf{B}_{,xxx} \mathbf{d}_2 \quad (2.35a-d)$$

$$\mathbf{u}_3 = \mathbf{B} \mathbf{d}_3 \quad \mathbf{u}_{3,x} = \mathbf{B}_{,x} \mathbf{d}_3 \quad \mathbf{u}_{3,xx} = \mathbf{B}_{,xx} \mathbf{d}_3 \quad \mathbf{u}_{3,xxx} = \mathbf{B}_{,xxx} \mathbf{d}_3 \quad (2.36a-d)$$

where \mathbf{B}'' , \mathbf{B} and their derivatives are $L \times (L+4)$ and $L \times (L+8)$ known matrices, respectively arising from \mathbf{A}'' , \mathbf{A} , \mathbf{C}'' , \mathbf{C} and their derivatives as presented in Appendix A1.

In conventional BEM, the load vectors \mathbf{q}_i are known and eqns. (2.34-2.36) are used to evaluate $u_i(x,t)$ and their derivatives at the L nodal points. This, however, cannot be applied here since \mathbf{q}_i are unknown. Thus, $3L$ additional equations are required in order to permit the establishment of \mathbf{q}_i . Therefore, the final step of AEM is implemented by applying the differential equations of equilibrium (2.18) to the L collocation points. Employing eqns. (2.34-2.36) leads to the formulation of the following set of $3 \times L$ nonlinear equations of equilibrium

$$\mathbf{K} \mathbf{d} + \mathbf{f}^{\text{nl}} = \mathbf{f} \Leftrightarrow \mathbf{K} \begin{Bmatrix} \mathbf{d}_1 \\ \mathbf{d}_2 \\ \mathbf{d}_3 \end{Bmatrix} + \mathbf{f}^{\text{nl}}(\mathbf{B}'' , \mathbf{B}, \mathbf{d}_1, \mathbf{d}_2, \mathbf{d}_3) = \begin{Bmatrix} \mathbf{f}_1 \\ \mathbf{f}_2 \\ \mathbf{f}_3 \end{Bmatrix} \quad (2.37)$$

where \mathbf{f}^{nl} is a nonlinear generalized stiffness vector and \mathbf{K} , \mathbf{f} are generalized stiffness matrices and force vector respectively, defined as

$$\mathbf{K}_1 = -[\mathbf{EA}]_{dg,L} + [\mathbf{K}_x \mathbf{B}^u]_{dg} \quad \mathbf{f}_1 = \mathbf{p}_x \quad (2.38a-b)$$

$$\mathbf{f}_1^{nl} = \mathbf{EA} \left[[\mathbf{B}_{,xx} \mathbf{d}_2]_{dg} [\mathbf{B}_{,x} \mathbf{d}_2] + [\mathbf{B}_{,xx} \mathbf{d}_3]_{dg} [\mathbf{B}_{,x} \mathbf{d}_3] \right] \quad (2.38c)$$

$$\begin{aligned} \mathbf{K}_2 = & [\mathbf{EI}_z]_{dg,L} - \mathbf{N}_x \mathbf{B}_{,x} - \mathbf{NB}_{,xx} + \mathbf{K}_{Ly}^{dg} \mathbf{B} - + \frac{EI_z}{GA_y} \left(3\mathbf{N}_x \mathbf{B}_{,xxx} + \mathbf{N} - \mathbf{K}_{Ly}^{dg} \mathbf{B}_{,xx} \right) - \\ & - \mathbf{K}_{Py}^{dg} \mathbf{B}_{,xx} - \frac{EI_z}{GA_y} \left(\mathbf{K}_{Ly}^{dg} \mathbf{B}_{,xx} - \mathbf{K}_{Py}^{dg} \right) \end{aligned} \quad (2.39a)$$

$$\mathbf{f}_2^{nl} = \mathbf{K}_{NLy}^{dg} (\mathbf{d}_2)^3 - \frac{EI_z}{GA_y} \left(\mathbf{K}_{NLy}^{dg} (\mathbf{B}_{,xx} \mathbf{d}_2)^3 \right) \quad \mathbf{f}_2 = \mathbf{p}_y - \mathbf{m}_{z,x} - \frac{EI_z}{GA_y} (\mathbf{p}_{y,xx}) \quad (2.39b,c)$$

$$\begin{aligned} \mathbf{K}_3 = & [\mathbf{EI}_y]_{dg,L} - \mathbf{N}_x \mathbf{B}_{,x} - \mathbf{NB}_{,xx} + \mathbf{K}_{Lz}^{dg} \mathbf{B} + \frac{EI_y}{GA_z} \left(3\mathbf{N}_x \mathbf{B}_{,xxx} + \mathbf{N} - \mathbf{K}_{Lz}^{dg} \mathbf{B}_{,xx} \right) - \\ & - \mathbf{K}_{Pz}^{dg} \mathbf{B}_{,xx} - \frac{EI_y}{GA_z} \left(\mathbf{K}_{Lz}^{dg} \mathbf{B}_{,xx} - \mathbf{K}_{Pz}^{dg} \right) \end{aligned} \quad (2.40a)$$

$$\mathbf{f}_3^{nl} = \mathbf{K}_{NLz}^{dg} (\mathbf{d}_3)^3 - \frac{EI_y}{GA_z} \left(\mathbf{K}_{NLz}^{dg} (\mathbf{B}_{,xx} \mathbf{d}_3)^3 \right) \quad \mathbf{f}_3 = \mathbf{p}_z + \mathbf{m}_{y,x} - \frac{EI_y}{GA_z} (\mathbf{p}_{z,xx}) \quad (2.40b,c)$$

where \mathbf{N} , $\mathbf{N}_{,x}$ are $L \times L$ diagonal matrices containing the values of the axial force and its derivatives with respect to x , respectively, at the L nodal points, \mathbf{p}_y , $\mathbf{p}_{y,xx}$, \mathbf{p}_z , $\mathbf{p}_{z,xx}$, $\mathbf{m}_{y,x}$ and $\mathbf{m}_{z,x}$ are $L \times 1$ vectors containing the values of the external loading and its derivatives at these points, while \mathbf{K}_{Li}^{dg} , \mathbf{K}_{NLi}^{dg} and \mathbf{K}_{Pi}^{dg} ($i = y, z$) are diagonal matrices whose diagonal elements represent the values of the corresponding foundation parameter at each nodal point. Moreover, substituting eqns. (2.34) in eqn. (2.14a), the discretized counterpart of the axial force at the neutral axis of the beam is given as

$$\mathbf{N} = EA (\mathbf{B}_{,x}^u \mathbf{d}_1) + \frac{I}{2} EA \left[[\mathbf{B}_{,xx} \mathbf{d}_2]_{dg} [\mathbf{B}_{,x} \mathbf{d}_2] + [\mathbf{B}_{,xx} \mathbf{d}_3]_{dg} [\mathbf{B}_{,x} \mathbf{d}_3] \right] \quad (2.41)$$

The above equations (2.37), together with eqns. (2.24) constitute a system of $3L + 20$ nonlinear algebraic equations which can be solved using any efficient solver. Within the framework of this doctoral dissertation two approaches have been performed. Firstly, the solution of this system was accomplished iteratively by

employing iterative numerical methods, such as the two term acceleration method (Isaacson & Keller 1966) and secondly, by using the modified Powell algorithm (Powell 1977, 1985). A step-by-step algorithmic approach of the numerical implementation is summarized in a flowchart form in Fig. 2.5.

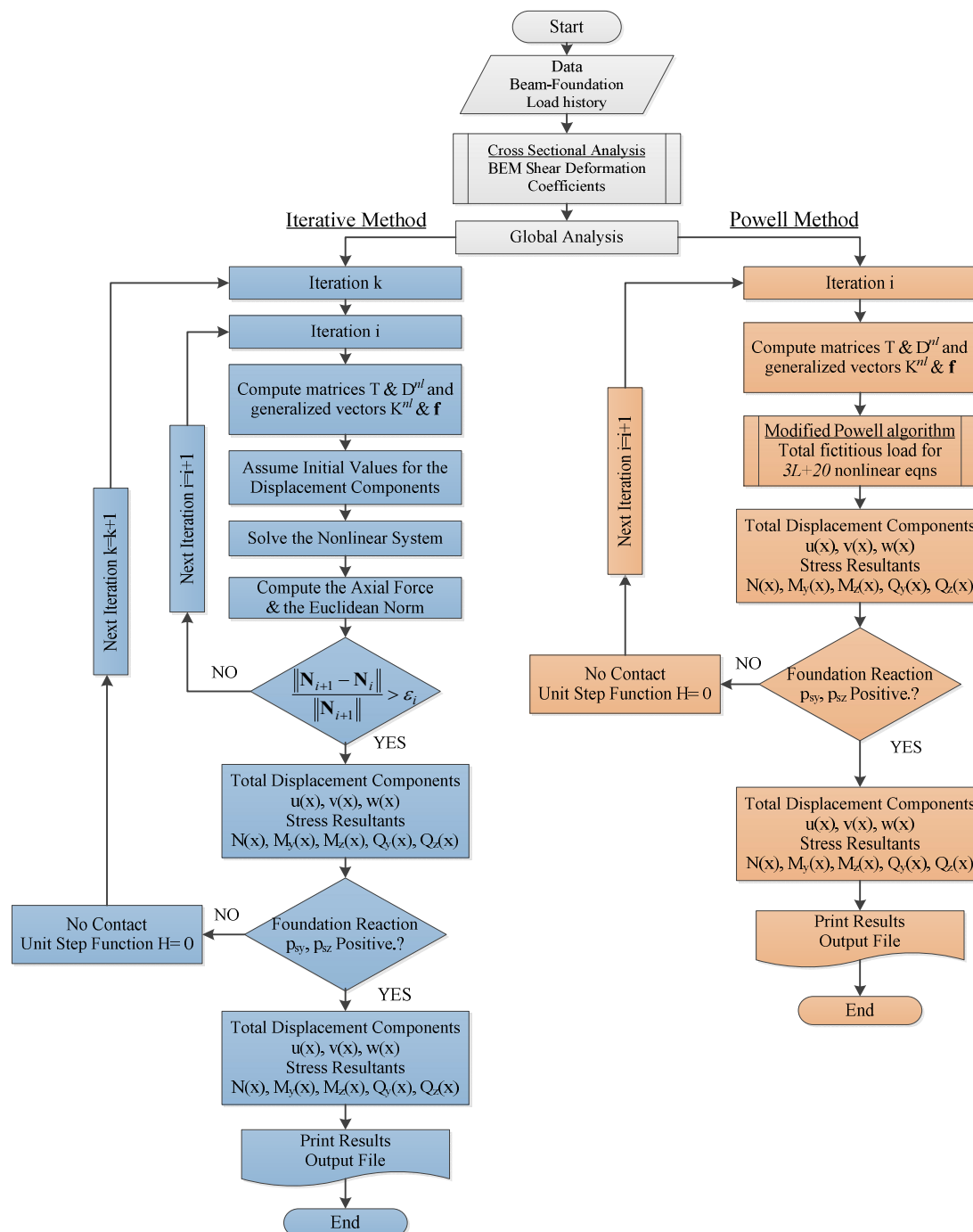


Fig. 2.5. Flowchart of the numerical implementation.

2.4 Numerical Examples

On the basis of the analytical and numerical procedures presented in the previous sections concerning the geometrically nonlinear analysis of shear deformable beams on nonlinear foundation, a computer program has been written using High Level 3G Fortran 90/95. Representative examples have been studied to demonstrate the efficiency, wherever possible the accuracy and the range of applications of the developed method.

2.4.1 Example 1 – Linear Analysis of Simply Supported Beam on Elastic Foundation

In the first example, for comparison reasons a linear analysis of a simply supported beam has been studied for three different load and geometry cases. Although displacements are considered small the problem is strongly nonlinear as the contact length is unknown. A beam of length $l = 5\text{ m}$ and flexural stiffness $EI = 10^3$ subjected to concentrated moments $M_1 = M_2 = -10^2\text{ kNm}$ at its ends, resting on a homogeneous elastic foundation with modulus of subgrade reaction k_z , as shown in Fig. 2.6 (case i), has been studied.

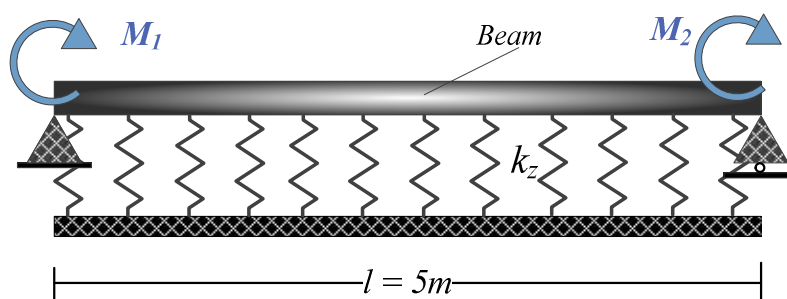


Fig. 2.6. Prismatic beam on elastic foundation subjected to concentrated moments at its ends (case i).

The present example was first investigated by Hetenyi (1946) who presented an analytical solution, according to which the midpoint deflection is evaluated by the following expression

$$w(l/2) = \frac{4M_1\lambda^2}{k_z} \frac{\sinh\left(\frac{\lambda l}{2}\right)\sin\left(\frac{\lambda l}{2}\right)}{\cosh(\lambda l) + \cos(\lambda l)} \quad \text{where} \quad \lambda = \sqrt[4]{k_z/4EI} \quad (2.41)$$

Lately, Pereira (2003) presented a FEM solution for the problem at hand, while Silveira et al. (2008) presented a nonlinear formulation employing a Ritz type approach. In Figs. 2.7a,b the beam deflections for the cases of conventional bilateral and unilateral (tensionless) Winkler springs, respectively are presented as compared with those obtained from analytical (Hetenyi 1946), FEM (Pereira 2003) and Ritz type (Silveira et al. 2008) solutions for various values of the dimensionless foundation parameter $k = k_z l^4 / EI$. Moreover, in Table 2.1 the extreme values of the beam deflection and of the soil reaction are presented for both cases of bilateral and unilateral foundation and for various values of the aforementioned parameter k . From these figures and table the accuracy of the obtained results is remarkable, while the influence of both the foundation stiffness and the unilateral character of the soil reaction are easily verified. Moreover, the discrepancy in the deflections between the bilateral and the unilateral foundation model especially for a stiff soil is underlined.

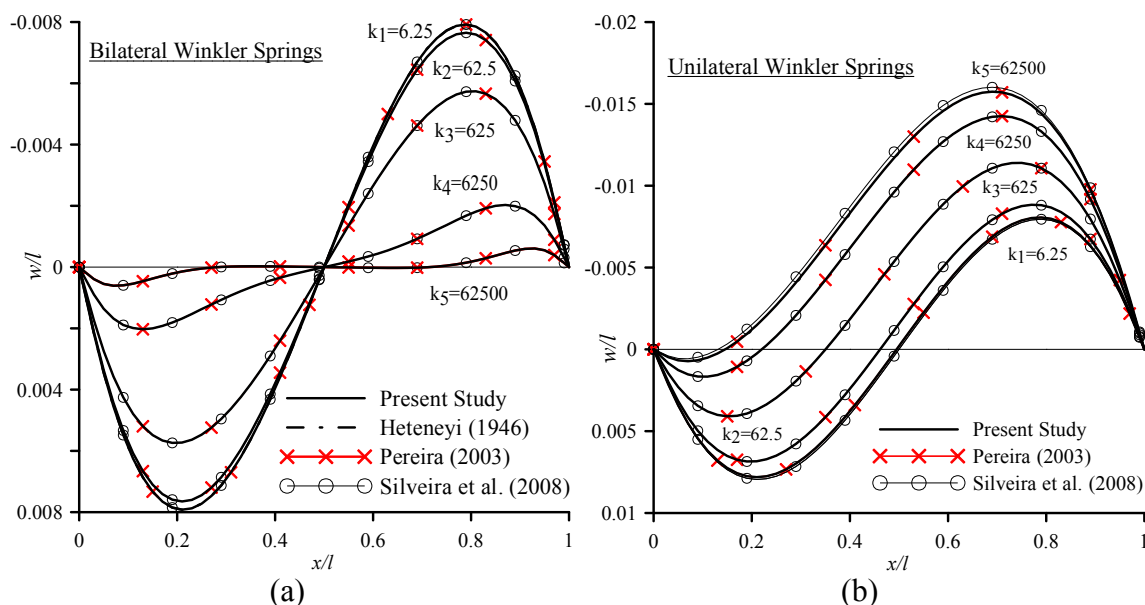


Fig. 2.7. Deflection for various values of the soil parameter k , of the beam of example 1 (case i) resting on a bilateral (a) and unilateral (b) elastic foundation.

As a variant of this example, the beam of length $l = 10m$ subjected to concentrated moments $M_1 = -M_2 = 10^2 kNm$ at its ends and a concentrated force $P(l/2) = 150kN$ at the midpoint of the beam, as this is shown in Fig. 2.8 (case ii), has also been studied. In Figs. 2.9a,b the beam deflections for the cases of conventional bilateral and unilateral Winkler springs, respectively are presented as compared with those obtained from

analytical (Hetenyi 1946), FEM (Pereira 2003) and Ritz type (Silveira et al. 2008) solutions for various values of the parameter k , while in Table 2.2 the extreme values of the beam deflection and of the soil reaction are presented for both cases of bilateral and unilateral foundation reaction, leading to the same conclusions drawn from the previous beam case.

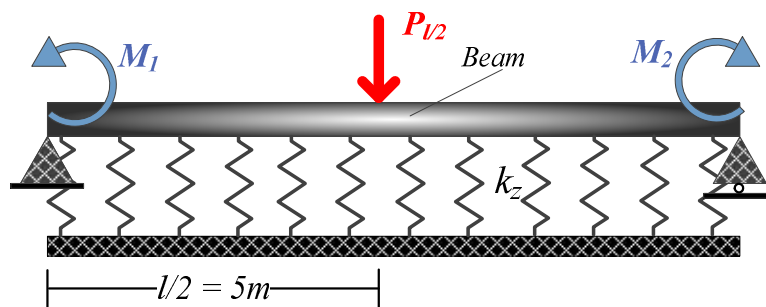


Fig. 2.8. Prismatic beam on elastic foundation subjected to concentrated moments at its ends and force at its midpoint (case ii).

Table 2.1. Extreme values of the deflections ($\times 10^{-2}$) and the foundation reaction of the beam of example 2.1 (case i).

k	Bilateral Winkler			Unilateral Winkler		
	Min w	Max w	$p_{sz}l^3/EI$	Min w	Max w	$p_{sz}l^3/EI$
6.25	-3.960	3.960	0.049	-4.030	3.905	0.048
62.5	-3.826	3.826	0.478	-4.418	3.425	0.428
625	-2.869	2.869	3.586	-5.697	2.046	2.557
6250	-1.015	1.015	12.688	-7.125	0.833	10.415
62500	-0.304	0.304	37.965	-8.008	0.287	35.854

Finally, as a second variant of this example, the beam of Fig. 2.8 subjected to concentrated moments $M_1 = -M_2 = -10^2 \text{ kNm}$ at its ends and a concentrated force $P(l/2) = -50 \text{ kN}$ at its midpoint, has also been studied (case iii). In Fig. 2.10 the deflections of the beam resting on a tensionless subgrade are presented as compared with those obtained from FEM (Pereira 2003) and Ritz type (Silveira et al. 2008)

solutions for various values of the dimensionless foundation parameter k . Moreover, in Fig. 2.11 the deflections of the beam ignoring the foundation reaction or resting either on unilateral or bilateral subgrade ($k = 10^4$), are presented as compared with those obtained from a Ritz type solution (Silveira et al. 2008) demonstrating once again the paramount importance of the tensionless character of Winkler foundation. Finally, in Table 2.3 the extreme values of the beam deflection and of the soil reaction are presented for both cases of bilateral and unilateral foundation reaction, leading to the conclusions already drawn and noting the significant influence of the unilateral character of the soil reaction in both the deflections and the soil reaction especially in the case of a stiff soil.

Table 2.2. Extreme values of the deflections (cm) and the foundation reaction of the beam of example 2.1 (case ii).

k	Bilateral Winkler			Unilateral Winkler		
	Min w	Max w	$p_{sz}l^3/EI$	Min w	Max w	$p_{sz}l^3/EI$
10^2	0	9.671	9.670	0	9.671	9.671
10^3	-0.239	2.341	23.41	-0.255	2.326	23.26
10^4	-0.326	0.549	54.90	-0.778	0.490	49.04
10^5	-0.095	0.0941	94.06	-0.9139	0.104	104.36

Table 2.3. Extreme values of the deflections (cm) and the foundation reaction of the beam of example 1 (case iii).

k	Bilateral Winkler			Unilateral Winkler		
	Min w	Max w	$p_{sz}l^3/EI$	Min w	Max w	$p_{sz}l^3/EI$
10^2	-0.248	0.661	0.66	0	1.286	1.28
10^3	-0.197	0.318	3.18	-0.41	0.609	6.09
10^4	-0.031	0.095	9.53	-1.266	0.239	23.95
10^5	-0.006	0.026	26.09	-1.789	0.082	81.47
10^6	0	0.005	54.05	-2.070	0.023	231.4

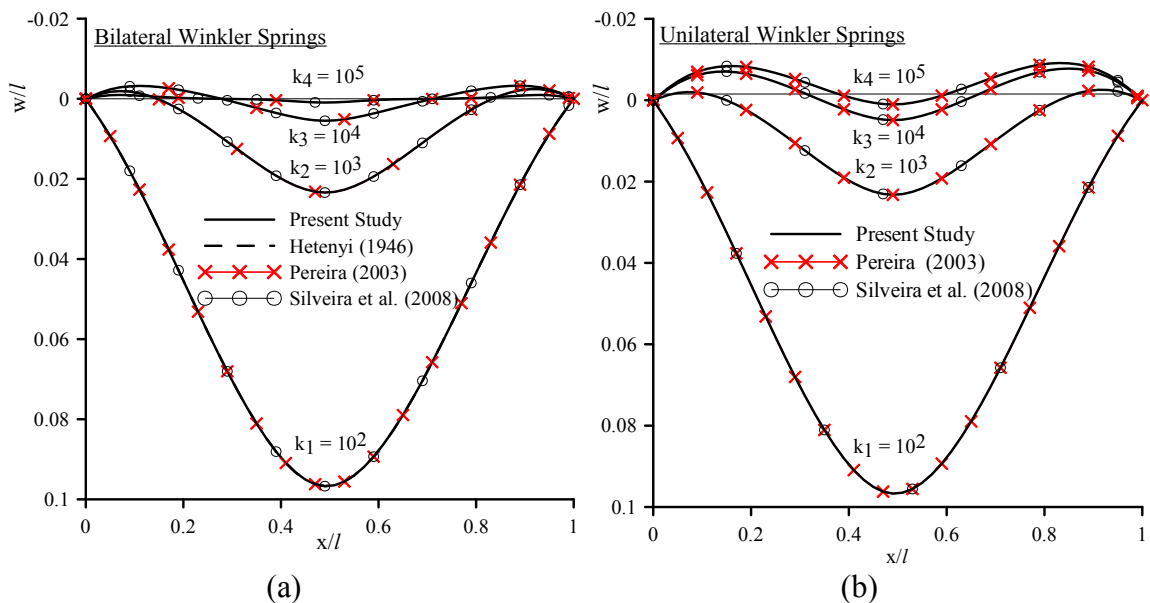


Fig. 2.9. Deflection of the beam of example 1 (case ii) resting on a bilateral (a) and unilateral (b) elastic foundation for various values of the parameter k .

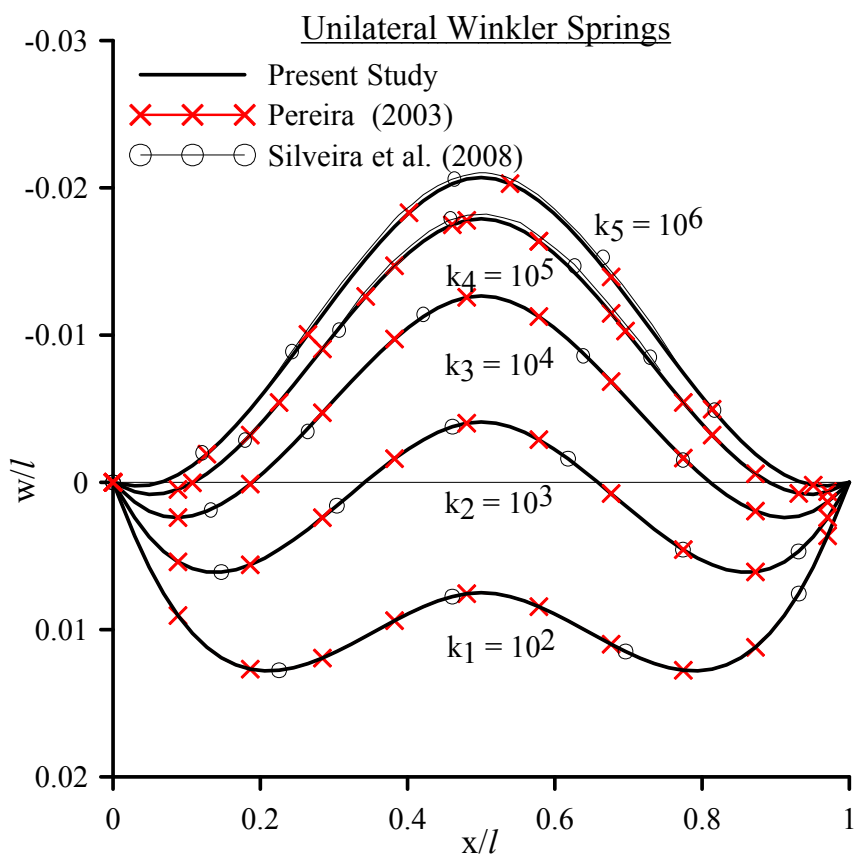


Fig. 2.10. Deflection of the beam of example 1 (case iii) resting on a unilateral elastic foundation for various values of the soil parameter k .

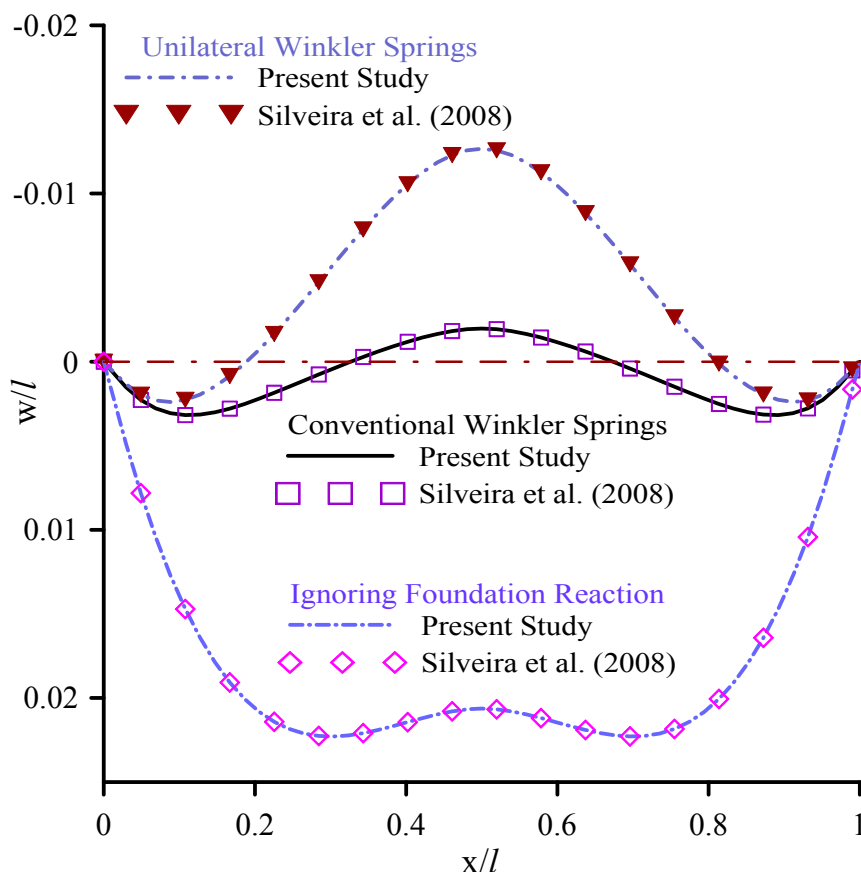


Fig. 2.11. Deflection of the beam of example 1 (case iii) ignoring the foundation reaction or resting either on unilateral or bilateral foundation $k = 10^4$.

2.4.2 Example 2 – Nonlinear Analysis of Clamped Beam on Elastic Foundation

In order to illustrate the importance of the nonlinear analysis and the influence of the shear deformation effect, a clamped beam of length $l = 5m$, having a hollow rectangular cross section ($E = 210 GPa$, $\nu = 0.3$, $a_z = 3.664$, $a_y = 1.766$) resting on homogeneous (either bilateral or unilateral) elastic foundation of stiffness k_z , as shown in Fig. 2.12, is examined.

In Fig. 2.13 the deflection curves along the beam resting on a tensionless foundation with $k_z = 50kN/m^2$ and subjected to a uniformly distributed load $p_z = 100kN/m$ (case i) are presented performing either linear or nonlinear analysis and taking into account or ignoring shear deformation effect. From this figure, the influence of the nonlinearity to the performed analysis is remarked, while the discrepancy of the obtained results due to the shear deformation effect justifies its importance even in thin

walled sections. Moreover, in Table 2.4 the deflections and the bending moments at the beam's midpoint and ends, respectively are presented performing either linear or nonlinear analysis and taking into account or ignoring shear deformation effect. Finally, in Fig. 2.14 the deflection curves of the beam resting on a tensionless foundation are presented for various values of the modulus k_z of the subgrade reaction, performing nonlinear analysis taking into account shear deformation effect and demonstrating the importance of the soil stiffness in the obtained results.

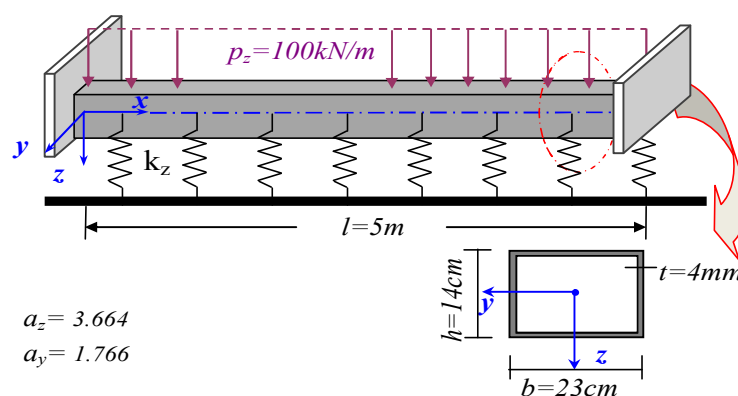


Fig. 2.12. Clamped beam of hollow rectangular cross section subjected to uniformly distributed load p_z (case i).

To illustrate the importance of the tensionless character of the subgrade reaction, the same beam subjected to a concentrated moment $M_y = -100kNm$ at its midpoint (case ii) is also studied. In Figs. 2.15(a,b) the deflection curves of the beam resting on a tensionless foundation and the foundation reaction are presented, respectively for various values of the subgrade reaction modulus k_z , performing nonlinear analysis and taking into account shear deformation effect. Additionally, in Table 2.5 the extreme values of the displacements and the soil reaction are presented for both cases of bilateral and unilateral soil reaction for various values of the modulus k_z performing a geometrical nonlinear analysis and taking into account shear deformation effect. From the aforementioned figure and table, it is concluded that the unilateral character of the foundation is of paramount importance and the error occurred from the ignorance of this behaviour is considerable.

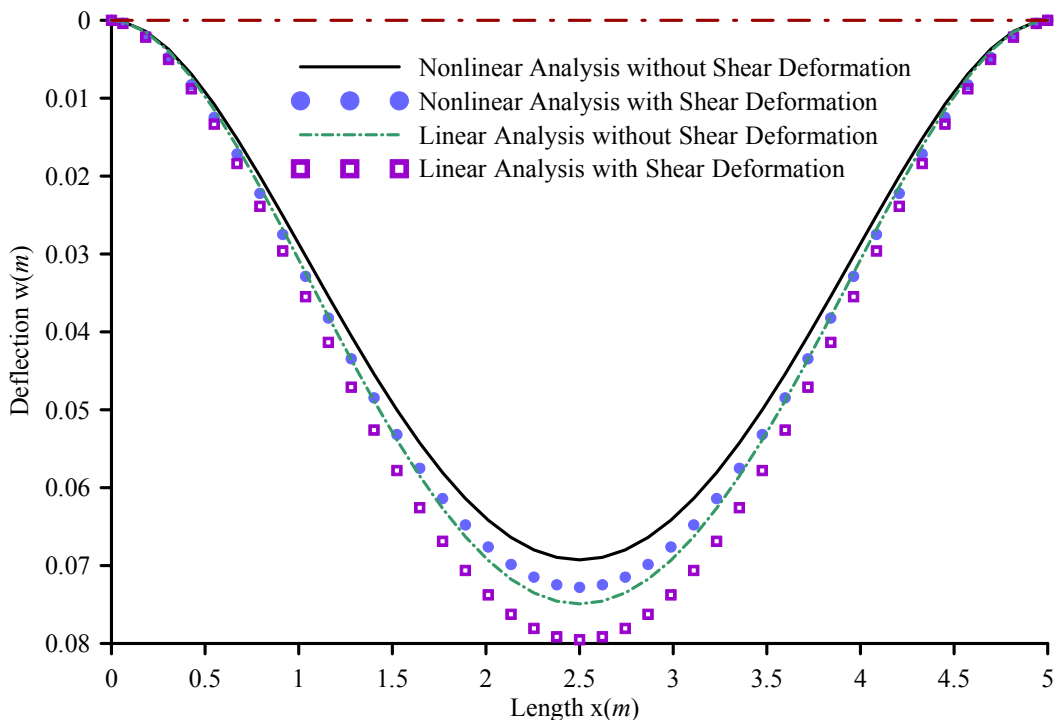


Fig. 2.13. Deflection along the beam of example 2 (case i), for soil stiffness $k_z = 50 \text{ kN} / \text{m}^2$.

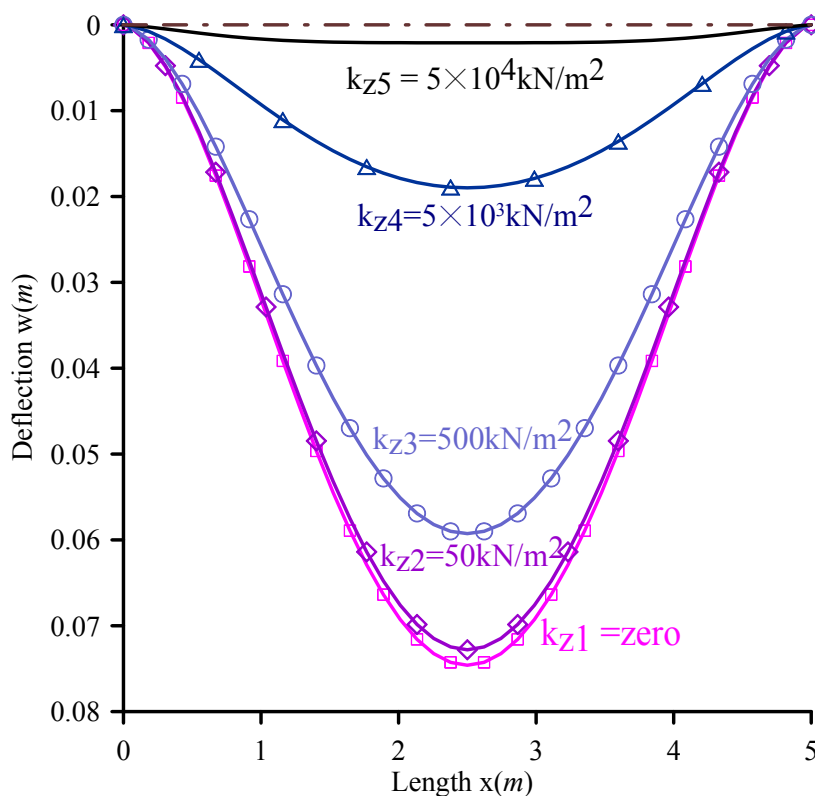


Fig. 2.14. Deflection along the beam of example 2 (case i), for various values of the subgrade reaction modulus k_z .

Table 2.4. Deflection (cm) and Moment (kNm) at the midpoint and the ends of the clamped beam, respectively of example 2 (case i), for $k_z = 50 \text{ kN/m}^2$.

Analysis	Without Shear Deformation		With Shear Deformation	
	Linear	Nonlinear	Linear	Nonlinear
$w(l/2)$	7.49	6.93	7.95	7.28
$M_y(0,l)$	-202.98	-192.85	-199.31	-187.54

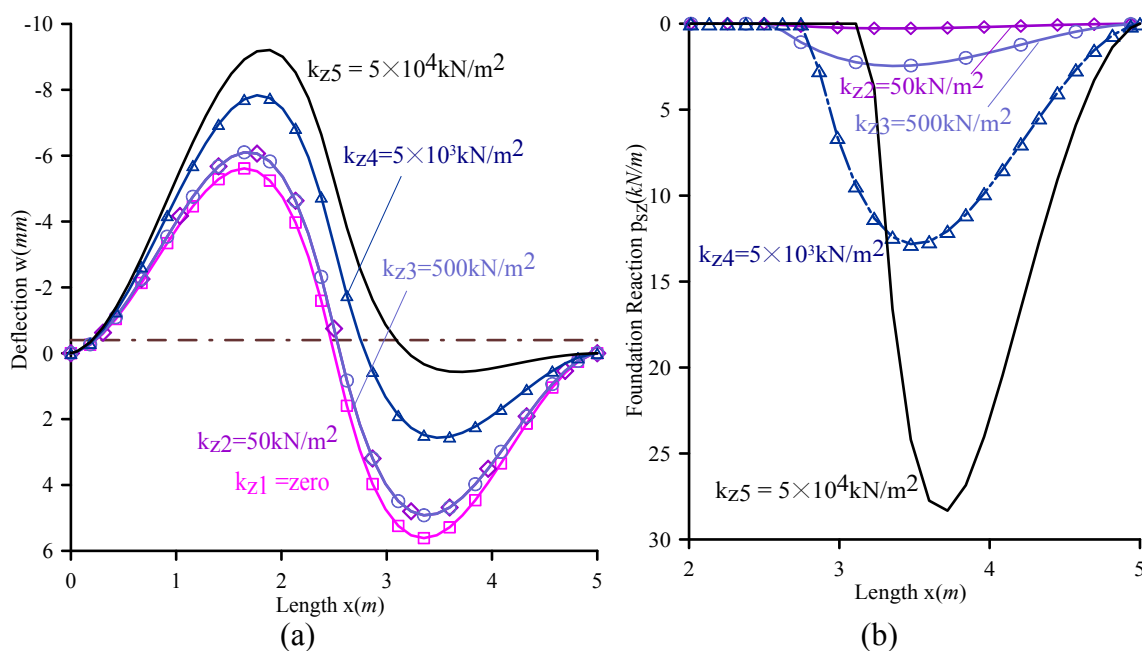


Fig. 2.15. Deflection curves of the beam (a) and foundation reaction (b) of example 2 (case ii) for various values of tensionless subgrade reaction k_z .

Table 2.5. Extreme values of the deflections (mm) and the foundation reaction (kN/m) of the beam of example 2 (case ii).

k_z (kN/m^2)	Bilateral Winkler			Unilateral Winkler		
	Min w	Max w	Max p_{sz}	Min w	Max w	Max p_{sz}
50	-5.59	5.59	0.279	-5.67	5.53	0.276
5×10^2	-5.39	5.39	2.694	-6.10	4.92	2.459
5×10^3	-4.01	4.01	20.007	-7.84	2.56	12.822
5×10^4	-1.45	1.45	72.675	-9.21	0.57	28.327

2.4.3 Example 3 – Experimental Validation of Pile–Foundation Systems

In this example, the accuracy of the developed formulation for the elastic analysis of pile–foundation systems is validated against experimental data and other numerical formulations available in literature.

Under this scope, a single pile (*i*) of length $l = 4.65m$, diameter $d = 0.3573m$ and modulus of elasticity $E_p = 20GPa$ driven into clay soil with $E_s = 9233kN / m^2$ and Poisson's ratio $\nu_s = 0.3$ (measured experimentally, taking the mean over the first three meters), is studied. The pile is subjected to concentrated horizontal force $P_z = 60kN$ and to bending moment $M_y = 69kNm$ at its head. In Fig. 2.16 the displacement curve along the pile is presented as compared with the experimental measurements obtained by Kerisel and Adam(1967) and those from a BEM-FEM coupling formulation presented by Filho et al. (2005).

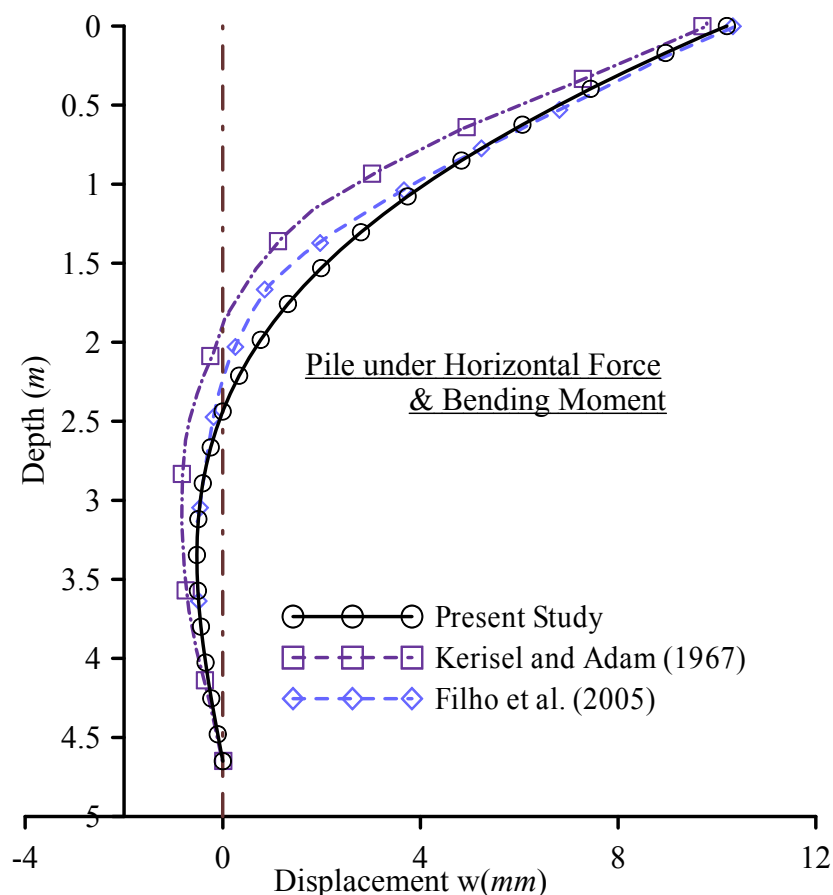


Fig. 2.16. Displacement along the pile (*i*) of example 3.

Moreover, a pile (ii) of length $l = 6.096\text{m}$ ($d = 60.96\text{cm}$, $E_p = 21.11\text{GPa}$) driven into clay soil ($E_s = 1\%E_p$, $\nu_s = 0.2$) under tip loading ($P_z = 181.6\text{kN}$, $M_y = -95.826\text{kNm}$), has also been studied. In Figs. 2.17a,b the displacement curves along the pile are presented as compared with those obtained from Vallabhan and Sivakumar (1986) and from a BEM-FEM coupling formulation presented by Filho et al. (2005). Additionally, in Fig 2.17b the settlement $u(x)$ due to axial force $P_x = 726.4\text{kN}$ is depicted, as compared with literature (Vallabhan & Sivakumar 1986, Ferro & Venturini 1992, Filho et al. 2005).

Finally, a pile (iii) of length $l = 12.2\text{m}$ ($d = 61\text{cm}$, $E_p = 20.67\text{GPa}$) driven into London clay ($E_s = 72.4\text{MN/m}^2$, $\nu_s = 0.5$) under vertical loading $P_x = 1.1\text{MN}$, has been examined. The predicted settlement at the tip of the pile is evaluated from the current formulation at $u = 0.285\text{cm}$ while the experimentally measured one (Whitaker & Cooke 1966) is $u^{\text{ex}} = 0.284\text{cm}$, giving a divergence of only 0.35%. From these comparisons a very good agreement can be verified between the experimental data, the other numerical formulations and the proposed model.

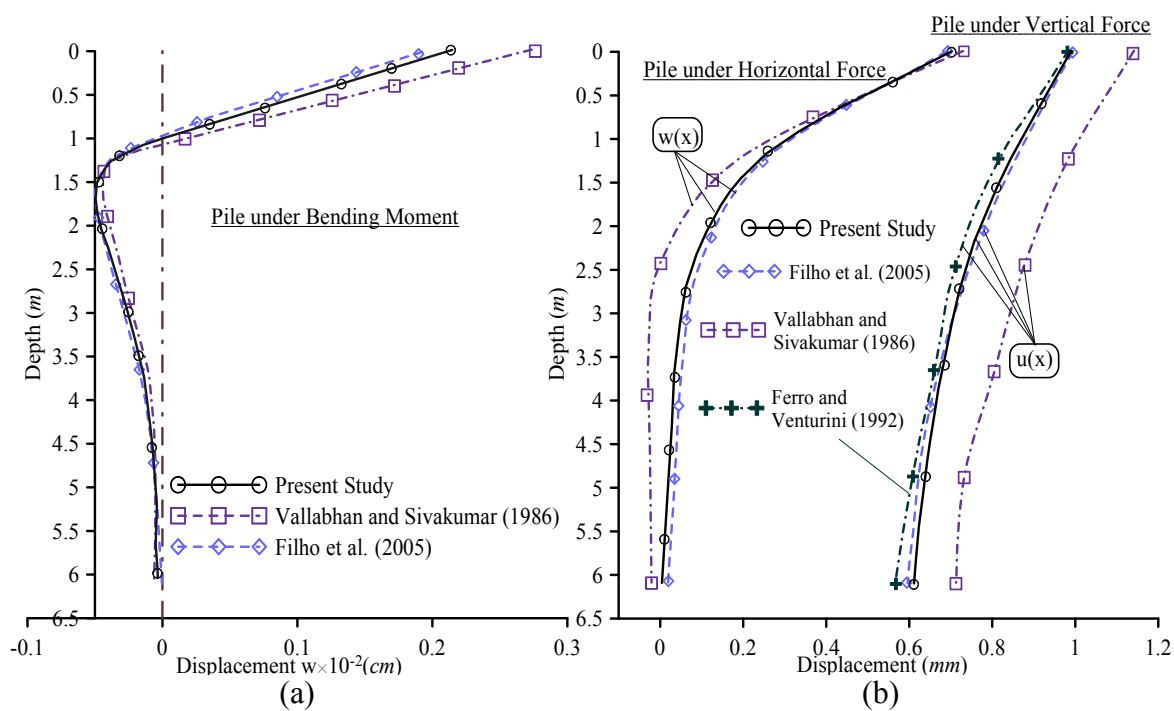


Fig. 2.17. Displacement along the pile (ii) of example 3.

2.4.4 Example 4 – Beam on 3-Parameter Foundation

In order to illustrate the influence of the soil modelling to the beam-foundation system response, a beam of length $l = 3\text{m}$ ($E = 2.9 \times 10^6 \text{kN/m}^2$, $A = 0.02\text{m}^2$, $I_y = 6.67 \times 10^{-5} \text{m}^4$, $a_z = 1.2$) resting on a three-parameter foundation, has been studied. The beam is subjected to a uniformly distributed load $p_z = 500 \text{kN/m}$, while three types of boundary conditions have been examined; namely (i) hinged- hinged, (ii) hinged-fixed and (iii) fixed-fixed.

In Tables 2.6-2.8 the central beam deflection for various values of the foundation parameters are presented taking into account or ignoring shear deformation effect as compared with those obtained from a BEM solution ignoring this effect (Tsiatas 2010), for the aforementioned cases of boundary conditions, respectively. Moreover, in Fig. 2.18 the deflection curve along the clamped beam resting on a three-parameter nonlinear foundation with $k_{Lz} = 1000 \text{kN/m}^2$, $k_{NLz} = 1000 \text{kN/m}^4$ and $k_{pz} = 1000 \text{kN}$ is presented performing either a linear or a nonlinear analysis and taking into account or ignoring shear deformation effect. From this figure, the influence of geometrical nonlinearity to the performed analysis is remarked.

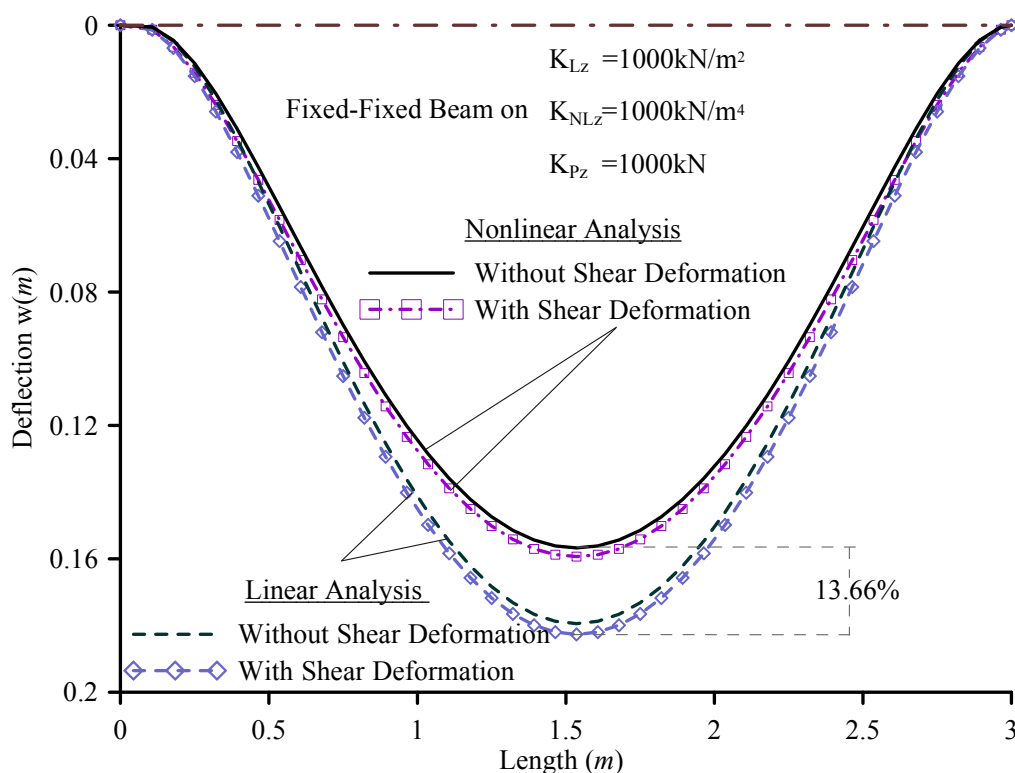


Fig. 2.18. Deflection along the fixed-fixed beam of example 4.

Table 2.6. Deflections (m) at the midpoint of the hinged-hinged beam of example 4.

k_{Lz} (kN/m ²)	k_{NLz} (kN/m ⁴)	k_{Pz} (kN)	With Shear Deformation	Without Shear Deformation	Tsiatas (2010)
0	0	0	0.31189	0.31259	0.31272
1000	0	0	0.25452	0.25537	0.25546
0	1000	0	0.30742	0.30812	0.30825
0	0	1000	0.25086	0.25172	0.25176
1000	1000	0	0.25168	0.25253	0.25262
1000	0	1000	0.20057	0.20152	0.20154
0	1000	1000	0.24820	0.24906	0.24909
1000	1000	1000	0.19912	0.20005	0.20009

Table 2.7. Deflections (m) at the midpoint of the hinged-fixed beam of example 4.

k_{Lz} (kN/m ²)	k_{NLz} (kN/m ⁴)	k_{Pz} (kN)	With Shear Deformation	Without Shear Deformation	Tsiatas (2010)
0	0	0	0.28398	0.28184	0.28207
1000	0	0	0.23144	0.23022	0.23038
0	1000	0	0.28052	0.27849	0.27871
0	0	1000	0.22395	0.22222	0.22242
1000	1000	0	0.22933	0.22816	0.22832
1000	0	1000	0.17989	0.17894	0.17910
0	1000	1000	0.22204	0.22038	0.22058
1000	1000	1000	0.17889	0.17796	0.17812

Table 2.8. Deflections (m) at the midpoint of the fixed-fixed beam of example 4.

k_{Lz} (kN/m ²)	k_{NLz} (kN/m ⁴)	k_{Pz} (kN)	With Shear Deformation	Without Shear Deformation	Tsiatas (2010)
0	0	0	0.25747	0.25292	0.25324
1000	0	0	0.20956	0.20651	0.20675
0	1000	0	0.25492	0.25054	0.25086
0	0	1000	0.19759	0.19359	0.19390
1000	1000	0	0.20807	0.20511	0.20533
1000	0	1000	0.15997	0.15757	0.15757
0	1000	1000	0.19633	0.19242	0.19274
1000	1000	1000	0.15932	0.15673	0.15696

2.4.5 Example 5 – Axially Loaded Cantilever Beam on Pasternak Foundation

In order to illustrate the influence of axial loading to the response of beam-foundation systems, a cantilever beam of length $l = 1.0\text{ m}$, ($E = 21 \times 10^7 \text{ kN/m}^2$, $\nu = 0.3$, $A = 2.9 \times 10^{-3} \text{ m}^2$, $I_y = 5.124 \times 10^{-6} \text{ m}^4$, $a_z = 4.513$) resting on a Pasternak type foundation of stiffness $k_{Lz} = 2000 \text{ kN/m}^2$, $k_{Pz} = 1000 \text{ kN}$, is examined. The beam is subjected to a uniformly distributed axial compressive $p_x = 100 \text{ kN/m}$ and transverse $p_z = 200 \text{ kN/m}$ loading as well as to a concentrated compressive axial force at its end $P_x(l) = 200 \text{ kN}$.

In Fig.2.19 the deflection curves of the beam are presented performing either a linear or a nonlinear analysis and taking into account or ignoring shear deformation effect. From this figure, the influence of the shear deformation effect to the performed analysis is remarked. Moreover, in Table 2.9 the deflections and the bending moments at the ends $x = l$ and $x = 0$, respectively of the beam are presented for both of the aforementioned cases of analysis and taking into account or ignoring shear deformation effect. From the above analysis, it is easily concluded that the geometrically nonlinear analysis and the shear deformation effect are of paramount importance.

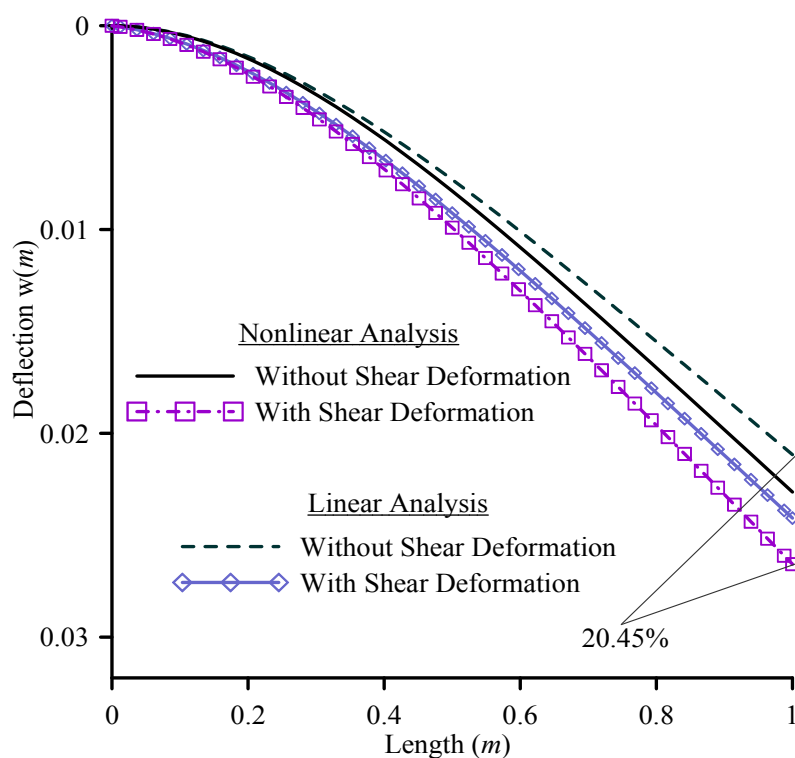


Fig. 2.19. Deflection curves along the cantilever beam of example 5.

Table 2.9. Deflection (cm) and bending moment (kNm) at the ends $x=l$ and $x=0$, respectively of the beam of example 5.

Analysis	Without Shear Deformation		With Shear Deformation	
	Linear	Nonlinear	Linear	Nonlinear
$w(l)$	2.10	2.29	2.42	2.64
$M_y(0)$	-94.53	-99.96	-96.64	-102.9

2.4.6 Example 6 – Free-Free Beam on 3-Parameter Foundation

To demonstrate the range of applications of the proposed method, a free-free beam resting on a three-parameter foundation ($k_{Lz} = 35 \text{ MN/m}^2$, $k_{NLz} = \pm 3.5 \times 10^6 \text{ MN/m}^4$, $k_{Pz} = 35 \text{ MN}$), is examined. The beam of length $l = 6.0 \text{ m}$ ($E = 29 \times 10^6 \text{ kN/m}^2$, $\nu = 0.2$, $A = 0.135 \text{ m}^2$, $I_y = 1.013 \cdot 10^{-3} \text{ m}^4$, $a_z = 1.2$) is subjected to a concentrated axial force at its ends $P_x(0) = -P_x(l) = 600 \text{ kN}$ and to a concentrated transverse force at its midpoint $P_z(l/2) = 100 \text{ kN}$.

In Figs. 2.20, 2.21 the deflection curves of the Timoshenko beam performing nonlinear analysis are presented, for different types of foundation modelling taking into account or ignoring the tensionless character of the soil, respectively. Moreover, in Table 2.10 the deflections at the free ends and the bending moments at the midpoint of the beam are presented performing either a linear or a nonlinear analysis and taking into account or ignoring shear deformation effect.

In Table 2.11 the extreme values of the deflection and the foundation reaction of the Timoshenko beam performing a nonlinear analysis are presented, for different types of foundation modelling taking into account or ignoring the tensionless character of the soil. Finally, in Fig. 2.22 the displacement $w(l/2)$ versus the applied load $P_z(l/2)$ is presented for various types of foundation modelling illustrating the hardening and softening effect of the nonlinear foundation. The significant influence of the unilateral soil reaction to the deflections and the importance of the modelling of the subgrade to the response of the beam are once again verified.

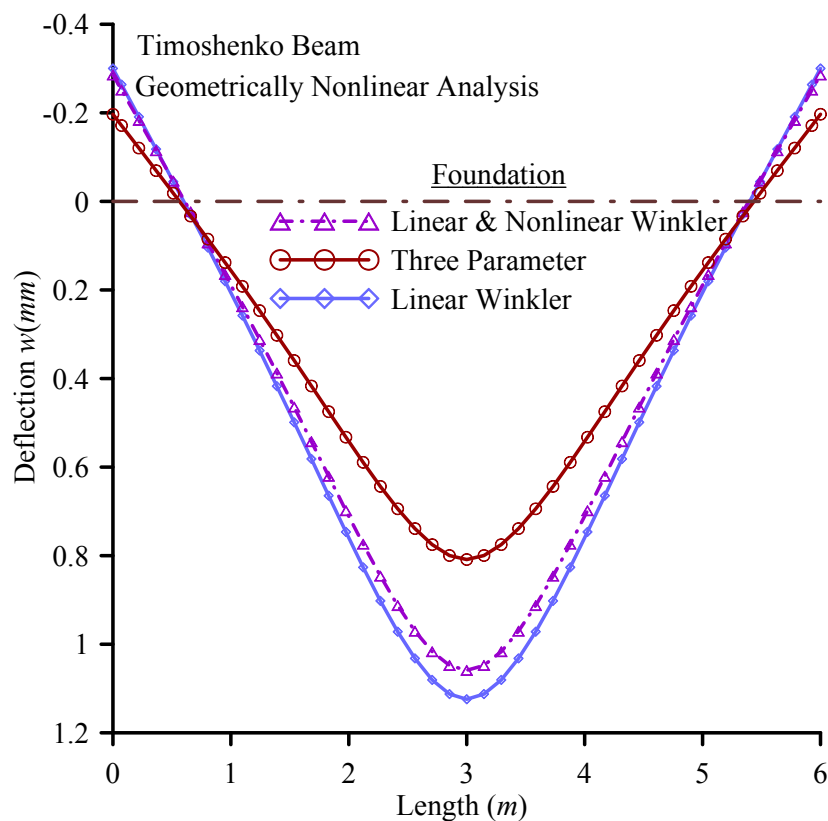


Fig. 2.20. Deflection along the free beam of example 6, for unilateral foundation.

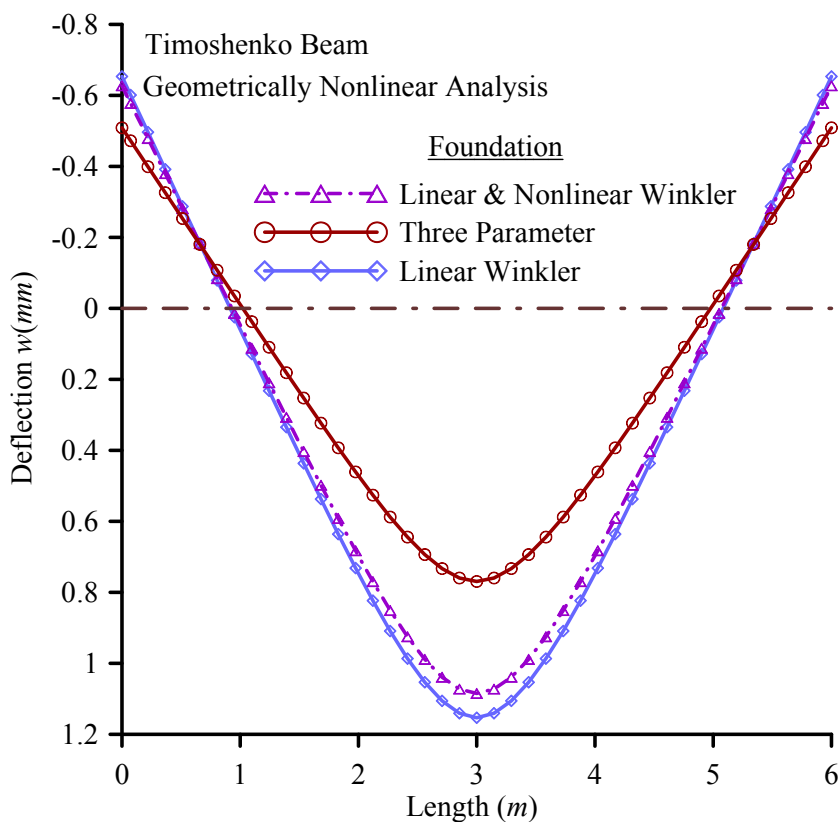


Fig. 2.21. Deflection along the free beam of example 6, for bilateral foundation.

Table 2.10. Deflection ($\times 10^{-4} m$) at $x = 0$ and bending moment (kNm) at $x = l / 2$ of the beam of example 6, resting on a three-parameter foundation.

Analysis	Without Shear Deformation		With Shear Deformation	
	Linear	Nonlinear	Linear	Nonlinear
$w(0)$	-4.60	-5.23	-4.46	-5.09
$M_y(l / 2)$	23.0	23.5	23.8	24.2

Table 2.11. Extreme values of the deflections ($\times 10^{-4} m$) and the foundation reactions (kN / m) of the beam of example 6.

	Bilateral Winkler			Unilateral Winkler		
	Min w	Max w	Max p_{sz}	Min w	Max w	Max p_{sz}
Linear Winkler	-3.00	11.2	39.4	-6.53	11.5	40.4
Nonlinear & Linear Winkler	-2.86	10.6	41.2	-6.27	10.8	42.4
Three-Parameter (Positive)	-1.97	8.09	61.1	-5.09	7.69	61.6
Three-Parameter (Negative)	-2.07	8.56	64.0	-5.23	8.06	63.9

2.4.7 Example 7 – Pinned Beam on 3-Parameter Foundation: Unbonded Contact

Finally, in order to demonstrate the importance of the unbonded contact between the structural elements and the supporting subgrade, a pinned-pinned beam of length $l = 5m$ ($E = 210GPa$, $\nu = 0.3$, $A = 86.82 \times 10^{-4} m^2$, $I_y = 10.45 \times 10^{-5} m^4$, $a_y = 1.462$, $a_z = 4.668$) resting on a three-parameter foundation reacting according to the following relation, is examined.

$$p_{sz} (MN / m) = \gamma \left(U_w \left(5w + 5w^3 - \frac{\partial^2 w}{\partial x^2} \right) \right) \quad (2.42)$$

where γ is a scale factor. The beam is subjected to a concentrated bending moment $M_y = 100kNm$ at its midpoint.

In Figs. 2.23a,b the deflection curves of the beam and the foundation reaction performing nonlinear analysis and taking into account shear deformation effect are presented, respectively, for either bilateral or unilateral soil reaction and for two values of the factor γ . It is worth noting that the zero values of the soil reaction curve of Fig. 2.23b denote the detachment of the beam. Finally, in Table 2.12 the extreme values of the aforementioned quantities are given for both cases of bilateral and unilateral soil reaction and for various values of the factor γ . From the aforementioned figures and table, it is concluded that the unilateral character of the foundation is of paramount importance and cannot be ignored.

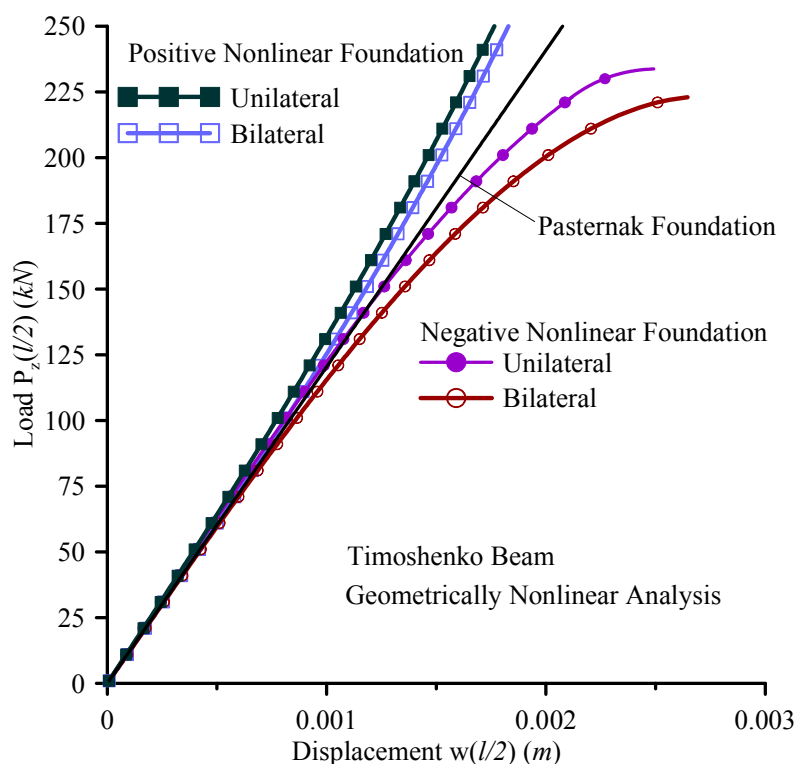


Fig. 2.22. Midpoint displacement vs. applied load of the free beam of example 6.

2.5 Concluding Remarks

In this chapter, a Boundary Element Method is developed for the geometrically nonlinear analysis of shear deformable beams of arbitrary doubly symmetric simply or multiply connected constant cross-section, partially supported on nonlinear three-

parameter tensionless foundation, undergoing moderate large deflections under general boundary conditions. The beam is subjected to the combined action of arbitrarily distributed or concentrated transverse loading and bending moments in both directions as well as to axial loading. The main conclusions that can be drawn from this investigation are

- i. The proposed beam formulation is capable of yielding results of high accuracy, as verified by comparing with analytical, semi-analytical, FEM and experimental results, with minimum computational cost, providing a simple, reliable and efficient computational tool for the static analysis of beam-foundation systems.

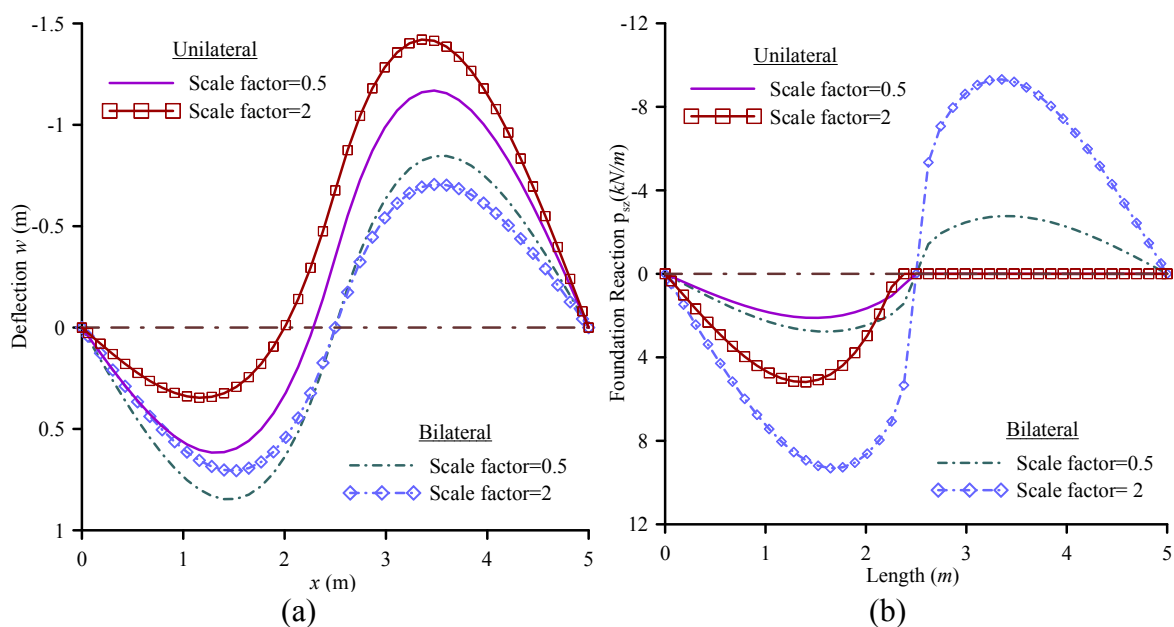


Fig. 2.23. Deflection curves (a) and foundation reactions (b) of the beam of example 7.

Table 2.12. Extreme values of the displacements (mm) and the foundation reactions (kN / m) of the beam of example 7.

(γ)	Bilateral Contact			Unilateral Contact		
	Min w	Max w	Max p_{sz}	Min w	Max w	Max p_{sz}
0.5	-0.846	0.846	2.76	-1.17	0.617	2.11
1.0	-0.793	0.793	5.20	-1.30	0.475	3.38
1.5	-0.747	0.747	7.37	-1.38	0.394	4.33
2.0	-0.706	0.706	9.31	-1.42	0.346	5.18

- ii. The influence of geometrical nonlinearity is illustrated through the significant discrepancy between the results of the linear and the nonlinear analyses.
- iii. The proposed model takes into account the coupling effects of bending and shear deformations along the member as well as the shear forces along the span induced by the applied axial loading.
- iv. In some cases, the effect of shear deformation is significant, especially for low beam slenderness values.
- v. The inclusion of both the coupling effect of the linear elastic springs and the nonlinear character of the subgrade reaction influences the response of the beam and makes the modelling of the mechanical behaviour of the subsoil more realistic and effective.
- vi. The significant influence of the unilateral character of the foundation in both the deflections and the soil reaction, especially in the case of a stiff soil is demonstrated.
- vii. The lift up of the beam caused by the tensionless character of the foundation is observed, leading to significantly different response compared to the bilateral one.
- viii. The developed procedure retains most of the advantages of a BEM solution while requiring a small number of nodal points to achieve high accuracy.
- ix. The use of BEM enables the accurate calculation of the stress resultants which are very important during both the analysis and the design of beam-foundation systems.

Geometrically Nonlinear Dynamic Analysis of Shear Deformable Beams on Nonlinear Foundation

3.1 Introduction

Many problems related to *Soil–Structure–Interaction* can be modelled by means of a beam or beam-column on/in nonlinear foundation. This model is commonly employed in the analysis of practical applications like spread footing, continuously supported pipelines and strip foundations. Also, the vibration analysis of beams on nonlinear foundations traversed by moving loads is of great interest in the area of high-speed transportation or rocket-sledge technology. Moreover, the seismic response of column-pile systems under transient earthquake excitation is an area of extensive active research, since pile foundation is widely used to support superstructures such as bridges, wind-turbines and offshore platforms.

Over the past thirty years, many researchers have developed and validated various methods for the study of *Dynamic Beam–Soil–Interaction*. Moreover, evidence from case histories (Mizuno 1987, Makris & Gazetas 1996, Matsui 1996, Tokimatsu 1996, Gazetas & Mylonakis 1998) as well as from experimental investigations (Chau et al. 2009, Manna & Baidya 2010) and field studies (Novak 1976, Burr et al. 1997, Blaney & O’Neill 1989, Han & Novak 1988, Han 1989, Marsafawi et al. 1992, Nikolaou et al. 2001) have indicated the importance of a rigorous and precise dynamic analysis, since damages due to interaction may occur during a seismic excitation.

Besides, having in mind the magnitude of the arising axial forces due to self weight, dead and environmental loading and the importance of weight saving in engineering structures, the study of nonlinear effects on the analysis of supporting structural elements becomes essential. This nonlinearity results from retaining the square of the slope in the strain–displacement relations (intermediate nonlinear theory), avoiding in this way the inaccuracies arising from a linearized second–order analysis. Moreover, due to the intensive use of materials having relatively high shear modulus, the error in the beam analysis incurred from the ignorance of the effect of shear deformation may be

substantial, particularly in the case of heavy lateral loading. All of the above concepts constitute the motive for the development of an advanced beam model capable of performing rigorous beam–soil kinematic and inertial interaction analysis accounting for the effects induced by geometrical nonlinearity, rotary inertia and shear deformation.

The *Beam on Nonlinear Foundation* model is a powerful tool capable of analyzing in detail the *Beam–Soil–Interaction* and has been adopted by several authors producing results of remarkable accuracy compared to rigorous numerical schemes. Both the geometrical nonlinearities and the interaction effects (Kavvadas & Gazetas 1993, Mylonakis et al. 1997, Mylonakis 2001) can be studied through a beam model which retains the advantage of time performance and deriving directly perceptible quantities, while the obtained results are in remarkable agreement with more sophisticated models (i.e. two/three dimensional finite element analysis) (Nikolaou et al. 2001, Maiorano et al. 2009, Dezi et al. 2010, Thavaraj et al. 2010, Di Laora et al. 2013).

When the beam displacements are small, a wide range of *linear analysis tools*, such as modal analysis, can be used and some analytical results are possible. Analytical solutions of problems involving beam vibrations of simple geometry and boundary conditions have received a good amount of attention in the literature, with pioneer the works of Krylov (1905) and later the one of Timoshenko (1911) who determined the dynamic stresses in beam structures. Furthermore, contributions concerning the linear transverse vibrations of simply supported beams traversed by a constant force moving at a constant velocity were presented by Inglis (1934), Lowan (1935) and later on by Kolousek (1973) and Fryba (1999). In these approaches the results are usually expressed as an infinite sum of normal modes, obtaining the contribution of each mode by the method of integral transformation. Moreover, Hetenyi (1966) studied the elementary Euler-Bernoulli beam on elastic Winkler foundation, while Weitsman (1971) presented an Euler-Bernoulli beam subjected to a concentrated load moving with constant speed resting on a tensionless foundation, relating the load amplitudes that bring the beam to the verge of separation from the foundation with the velocity of motion. Rades (1972) presented the steady-state response of a finite rigid beam resting on a foundation defined by one inertial and three elastic parameters in the assumption of a permanent and smooth contact between beam and foundation considering only uncoupled modes. Wang and Stephens (1977) studied the natural vibrations of a Timoshenko beam on a Pasternak-type foundation showing the effects of rotary inertia, shear deformation and foundation constants of the beam employing general analytic solutions for simple cases of boundary conditions. Choros and Adams (1979)

investigated the steady-state deformation of an infinite beam on a tensionless undamped elastic foundation under a single moving force, while Morgan and Sinha (1983) investigated the stability of Beck's column supported by three different viscoelastic foundations, namely the standard linear soil, the Maxwell and the Kelvin-Voigt one, performing an exact dynamic analysis for each foundation model. Nevertheless, due to the simplifying assumptions made to all of the above contributions, it must be stressed that the results obtained correspond only to an estimate of the structural response.

Since then, important development has been achieved regarding more rigorous *linear dynamic analysis of beams on nonlinear foundation*. To begin with, Kuczma and Switka (1990) presented a solution algorithm for the analysis of unilateral, frictionless contact between a beam and a viscoelastic foundation. The problem was formulated in the form of a variational inequality, from which after space discretization by the finite element method, a linear complementary problem was derived. Later, Huang and Zou (1994) analysed the dynamic response of an elastic beam on a linear viscoelastic Winkler foundation, impacted by a moving body at a low velocity, while Thambiratnam and Zhuge (1996) studied the dynamic analysis of beams on elastic foundation subjected to moving point loads employing the finite element method and modelling the foundation by springs of variable stiffness. Matsunaga (1999) employing the method of power series expansion presented the natural frequencies and buckling stresses of a deep beam-column on a two-parameter elastic foundations taking into account the effect of shear deformation, depth change and rotary inertia. De Rosa (1995) and El-Mously (1999) derived explicit formulae for the fundamental natural frequencies of finite Timoshenko-beams mounted on finite Pasternak foundation. Sun (2001) employed the Fourier transform to solve the problem of steady-state response of a beam on a viscoelastic foundation subjected to a harmonic line load. Boulanger et al. (1999) developed a beam formulation for analyzing seismic soil-pile-structure interaction and evaluated it against the results of a series of dynamic centrifuge model tests. Sensitivity of the results to dynamic p - y model parameters and site response calculations were also examined, while Nikolaou et al. (2001) implemented a beam model for piles in homogeneous and layered soils illustrating that the magnitude of kinematic moments depends mainly on the stiffness contrast between the soil layers, the pile-soil stiffness contrast, the excitation frequency, and the number of excitation cycles. Chen et al. (2001) established the dynamic stiffness matrix of an infinite or semi-infinite Timoshenko beam on a Winkler viscoelastic foundation subjected to a harmonic moving load, followed by Sun (2001a,b, 2002) who proposed a closed-form

displacement responses of beam-type structures subjected to moving line or concentrated loads after obtaining a Green's function of the beam on elastic or viscoelastic foundation by means of Fourier transform. Coskun (2003) studied the response of an elastic beam on a two-dimensional tensionless Pasternak foundation subjected to a central concentrated harmonic load using trigonometric-hyperbolic functions, while Chen et al. (2004) proposed a mixed formulation combining the state-space and the differential quadrature methods, for the bending and free vibration analysis of arbitrarily thick beams resting on a Pasternak elastic foundation. Hutchinson et al. (2004) used nonlinear dynamic analyses to evaluate the inelastic seismic response of bridge and viaduct structures supported on extended pile shafts. For the nonlinear dynamic soil–pile interaction analyses the beam on nonlinear foundation model was employed. The results focused on the influence of the ground motion characteristics and the variations in structural configurations on the performance measures which evaluated the inelastic seismic response of the structures examined. Kargarnovin and Younesian (2004, 2005) presented the response of an infinite length Timoshenko beam of uniform cross-section, supported by either a generalized Pasternak-type or a nonlinear viscoelastic foundation and subjected to arbitrarily distributed harmonic moving loading and employing either complex Fourier transformation in conjunction with the residue and convolution integral theorems or a straightforward technique using Lindstedt–Poincare perturbation method in conjunction with a Fourier integral transformation. Muscolino and Palmeri (2007) studied the response of beams resting on viscoelastically damped foundation under moving single–degree–of–freedom (SDoF) oscillators through a novel state-space formulation, in which a number of internal variables is introduced with the aim of representing the frequency-dependent behaviour of the viscoelastic foundation. Ying et al. (2008) derived an exact solution for bending and free vibration analysis of functionally graded beams resting on a Winkler–Pasternak elastic foundation based on the two-dimensional theory of elasticity and employing the state space method. Lately, Zehsaz et al. (2009) studied the dynamics of railway, as a Timoshenko beam of limited length, lying on a Pasternak viscoelastic foundation, subjected to moving load employing the modal superposition method, while Calim (2009) presented the dynamic behaviour of Timoshenko beams on Pasternak-type viscoelastic foundation subjected to time-dependent loading, employing the complementary functions method. Millan and Dominguez (2009) developed a simplified model for the analysis of the dynamic response of structures on piles and pile groups in viscoelastic or poroelastic soils under time harmonic excitation using a

coupled boundary element–finite element model able to take into account dynamic pile–soil–pile interaction in a rigorous manner. Younesian and Kargarnovin (2009) presented the dynamic response of infinite beams supported by random viscoelastic Pasternak foundation subjected to harmonic moving loads, employing the first order perturbation theory and calculating appropriate Green’s functions. Gerolymos et al. (2009) employed nonlinear distributed Winkler-type springs and dashpots to investigate the soil-pile-bridge system interaction to seismic loading with emphasis on structural nonlinearity. The analyses focused on the influence of various parameters such as soil compliance and pile yielding on the local and global ductility demands and the maximum drift ratio. Castelli and Maugeri (2009) developed a simplified pseudostatic approach based on the p - y soil reaction in order to evaluate the internal response of piles under earthquake loading, verifying the obtained results with experimental and numerical ones. Dezi et al. (2010) performed a parametric kinematic seismic interaction analysis of single piles embedded in soil deposit focusing on the bending moments induced by the transient motion by employing an Euler–Bernoulli beam embedded in a layered Winkler–type medium. Dimitrovova (2010) presented the transverse vibrations induced by a load moving at a constant speed along a finite or an infinite beam resting on a piecewise homogeneous viscoelastic foundation employing the normal-mode analysis and paying attention to the amplification of the vibrations arising from a foundation discontinuity. Ansari et. al. (2010) studied the vibration of a finite Euler–Bernoulli beam, supported by non-linear viscoelastic foundation and traversed by a moving load employing the Galerkin method, while the solution for different harmonics is obtained using the Multiple Scales Method. Chen and Chen (2011) studied the effect of damping on the multiple steady state deformations of an infinite beam resting on a tensionless Winkler-type foundation subjected to a point load moving with a sub- critical speed. Sica et al. (2011) highlighted the severity of kinematic pile bending through a parametric study of the dynamic response of piles to seismic loading based on a properly calibrated a beam model where the pile was modelled though an Euler–Bernoulli beam embedded in soil consisting of two homogeneous viscoelastic layers of sharply different stiffness and subjected to vertically propagating seismic S waves. Recently, Anoyatis et al. (2013) employed a beam model for investigating the behaviour of kinematically stressed piles for different boundary conditions at the head and tip deriving new closed-form analytical solutions.

As the beam displacements become larger, the induced *geometric nonlinearities* result in effects that are not observed in linear systems. Contrary to the good amount of

attention in the literature concerning the linear dynamic analysis of beam supported on nonlinear foundation, very little work has been done on the corresponding nonlinear problem. Lewandowski (1989) studied the nonlinear free vibration analysis of multispan beams on elastic supports, employing the dynamic finite element method, neglecting the horizontally and rotary inertia forces and considering the beams as distributed mass systems. Moreover, Chang and Liu (1996) performed the deterministic and random vibration nonlinear analysis of a beam on an elastic foundation subjected to a moving load employing the Galerkin method in conjunction with the finite element method, while the nonlinear system of differential equation has been solved by the implicit direct integration method. Rotary inertia and shear deformations are neglected, while the effects of longitudinal deflections and inertia have been considered so that the coupled equations of longitudinal and transverse deflections can be derived based on Euler-Bernoulli hypothesis. Chen et al. (2001) performing a geometrically nonlinear analysis with constant axial force presented the dynamic stiffness matrix of an infinite Timoshenko beam on viscoelastic foundation subjected to a harmonic moving load and determined the critical velocities and the resonant frequencies. Kim and Cho (2006) presented the vibration and buckling of an infinite beam-column under constant axial force, resting on an elastic foundation and subjected to moving loads of either constant or harmonically varying amplitude with a constant advance velocity, taking into account shear deformation effect. Finally, Arboleda-Monsalve et al. (2007) presented a Timoshenko beam resting on a two-parameter elastic foundation with generalized end conditions. The proposed model includes the frequency effects on the stiffness matrix and load vector as well as the coupling effects of bending and shear deformations along the member and the shear forces along the span induced by the applied axial load as the beam deforms according to the ‘modified shear equation’ proposed by Timoshenko.

In this chapter, a Boundary Element Method (BEM) is developed for the geometrically nonlinear response of shear deformable beams of simply or multiply connected constant cross-section, partially supported on nonlinear three-parameter tensionless viscoelastic foundation, undergoing moderate large displacements under general boundary conditions. The beam is subjected to the combined action of arbitrarily distributed or concentrated transverse loading and bending moments in both directions as well as to axial loading. This dynamic loading represents the most general case, which includes impact loading, transverse moving loading, seismic excitation, beam–soil interaction, etc. To account for shear deformations, the concept of shear deformation coefficients is used. Five boundary value problems are formulated with

respect to the transverse displacements, to the axial displacement and to two stress functions and solved using the Analog Equation Method (Katsikadelis 2002), a BE based method. Application of the boundary element technique yields a system of nonlinear Differential-Algebraic Equations (DAE), which is solved iteratively using the Petzold-Gear backward differentiation formula (Brenan et al. 1989), a linear multistep method for differential equations coupled to algebraic equations. The evaluation of the shear deformation coefficient is accomplished from the aforementioned stress function using only boundary integration.

Numerical examples of great practical interest are worked out to demonstrate the efficiency and the accuracy of the developed method through comparison with literature and FEM results, as well as its range of applications. In these examples, the effects arising in the nonlinear dynamic analysis of beams on nonlinear foundation are illustrated. Subsequently, an extensive case study is carried out on a pile–column–deck system of a bridge, founded in two cohesive layers of sharply different stiffness and subjected in various earthquake excitations, providing insight to several phenomena. The essential features and novel aspects of the present formulation compared with previous ones are summarized as follows.

- i. The proposed beam model accounts for the geometrical non-linearity by retaining the square of the slope in the strain–displacement relations. For that purpose the Total Lagrangian formulation (intermediate non-linear theory) has been adopted.
- ii. Shear deformation effect and rotary inertia are taken into account in the nonlinear dynamic analysis of beams on nonlinear foundation.
- iii. The proposed model accounts for the coupling effect of bending and shear deformations along the member as well as shear forces along the span induced by the applied axial loading.
- iv. The shear deformation coefficients are evaluated using an energy approach, instead of Timoshenko's (Timoshenko & Goodier 1984) and Cowper's (1966) definitions, for which several authors (Schramm et al. 1994, 1997) have pointed out that one obtains unsatisfactory results or definitions given by other researchers (Stephen 1980, Hutchinson 2001) for which these factors take negative values.
- v. The beam is subjected to arbitrary external loading and is supported by the most general boundary conditions including elastic support or restraint, while its cross

section is an arbitrary doubly symmetric one, unless it is mentioned otherwise (i.e. mono symmetric cross sections).

- vi. The nonlinear half-space is approximated by a tensionless three-parameter viscoelastic foundation.
- vii. Soil nonlinearity can also be taken under consideration by means of a hybrid spring configuration consisting of a nonlinear (p - y) spring for the near-field plastification, connected in series to a Kelvin–Voigt element representing the far-field viscoelastic character of the soil.
- viii. In cases of earthquake excitations the site seismic response is obtained through one dimensional shear wave propagation analysis.
- ix. The proposed model employs a BEM approach, while a small number of nodal points are required to achieve high accuracy.
- x. The use of BEM permits the effective computation of derivatives of the field functions (e.g. stresses, stress resultants) which is very important during the dynamic analysis of beams.

Finally, it is worth mentioning that the outcome of the conducted research activity presented in this chapter of the doctoral dissertation has been published in international journals (Sapountzakis & Kampitsis 2010b, 2011b, 2013a,b, Kampitsis et al. 2013a, Sapountzakis et al. 2014), in national and international conferences (Sapountzakis & Kampitsis 2009a,b, Sapountzakis et al. 2010, Sapountzakis & Kampitsis 2010c,d, 2011c,d, 2012c, Sapountzakis et al. 2013, Kampitsis et al. 2013b) and in books published by international publishing companies (Sapountzakis & Kampitsis 2010f, 2013e).

3.2 Statement of the Problem

Let us consider a prismatic beam of length l (Fig. 3.1a), of constant arbitrary doubly symmetric cross-section of area A . The homogeneous isotropic and linearly elastic material of the beam cross-section, with modulus of elasticity E , shear modulus G and Poisson's ratio ν occupies the two dimensional multiply connected region Ω of the y,z plane and is bounded by the Γ_j ($j = 1, 2, \dots, K$) boundary curves, which are piecewise smooth, i.e. they may have a finite number of corners. In Fig. 3.1b C_{yz} is the

principal bending coordinate system through the cross section's centroid. The beam is partially supported on a nonlinear tensionless three-parameter viscoelastic soil. The foundation model is characterized by the linear Winkler moduli k_{Lx} , k_{Ly} , k_{Lz} , the nonlinear Winkler moduli k_{NLy} , k_{NLz} the Pasternak (shear) foundation moduli k_{Py} , k_{Pz} and the damping coefficients c_y , c_z corresponding to the directions y , z respectively. Having in mind that for the longitudinal direction the reaction is a bilateral one exhibiting both compressive and tensile tractions, while for the transverse directions is a unilateral one (accounting for the unbonded contact between beam and subgrade), the interaction pressure at the interface can be written as

$$p_{sx} = k_{Lx}u(x,t) \quad (3.1a)$$

$$p_{sy}(x,t) = \tilde{H}(x,t)p_{rey}(x,t) \quad p_{sz}(x,t) = \tilde{H}(x,t)p_{rez}(x,t) \quad (3.1b,c)$$

where

$$p_{rey}(x,t) = k_{Ly}v(x,t) + k_{NLy}v^3(x,t) - k_{Py}\frac{\partial^2 v(x,t)}{\partial x^2} + c_y\frac{\partial v(x,t)}{\partial t} \quad (3.2a)$$

$$p_{rez}(x,t) = k_{Lz}w(x,t) + k_{NLz}w^3(x,t) - k_{Pz}\frac{\partial^2 w(x,t)}{\partial x^2} + c_z\frac{\partial w(x,t)}{\partial t} \quad (3.2b)$$

with $\tilde{H}_y(x,t)$, $\tilde{H}_z(x,t)$ being the Heaviside unit step functions defined as

$$\tilde{H}_y(x,t) = \begin{cases} 1 & \text{if } p_{rez}(x,t) > 0 \\ 0 & \text{if } p_{rez}(x,t) \leq 0 \end{cases} \quad \tilde{H}_z(x,t) = \begin{cases} 1 & \text{if } p_{rey}(x,t) > 0 \\ 0 & \text{if } p_{rey}(x,t) \leq 0 \end{cases} \quad (3.3a,b)$$

The foundation reaction p_{rey} , p_{rez} of eqns. (3.2a,b) takes into account the nonlinear behaviour of the soil (e.g. ballast and rail-bed) as proposed by Dahlberg (2002) who demonstrated that the employed nonlinear three-parameter model captures accurately the hardening behaviour of the foundation whereas the equivalent linear fails, yielding in considerable differences in the beam-foundation system response. Later, Wu and Thompson (2004) presented a similar nonlinear model and studied the problem of wheel/track impact employing the finite element method. Moreover, for real sample of

the hardening behaviour of the foundation one can refer to (Iwnicky 2007) where detailed field measurement results are presented.

The beam is subjected to the combined action of the arbitrarily distributed or concentrated time dependent axial loading $p_x = p_x(x,t)$, transverse loading $p_y = p_y(x,t)$, $p_z = p_z(x,t)$ acting in the y , z directions, respectively and bending moments $m_y = m_y(x,t)$, $m_z = m_z(x,t)$ along y , z axes, respectively (Fig. 3.1a).

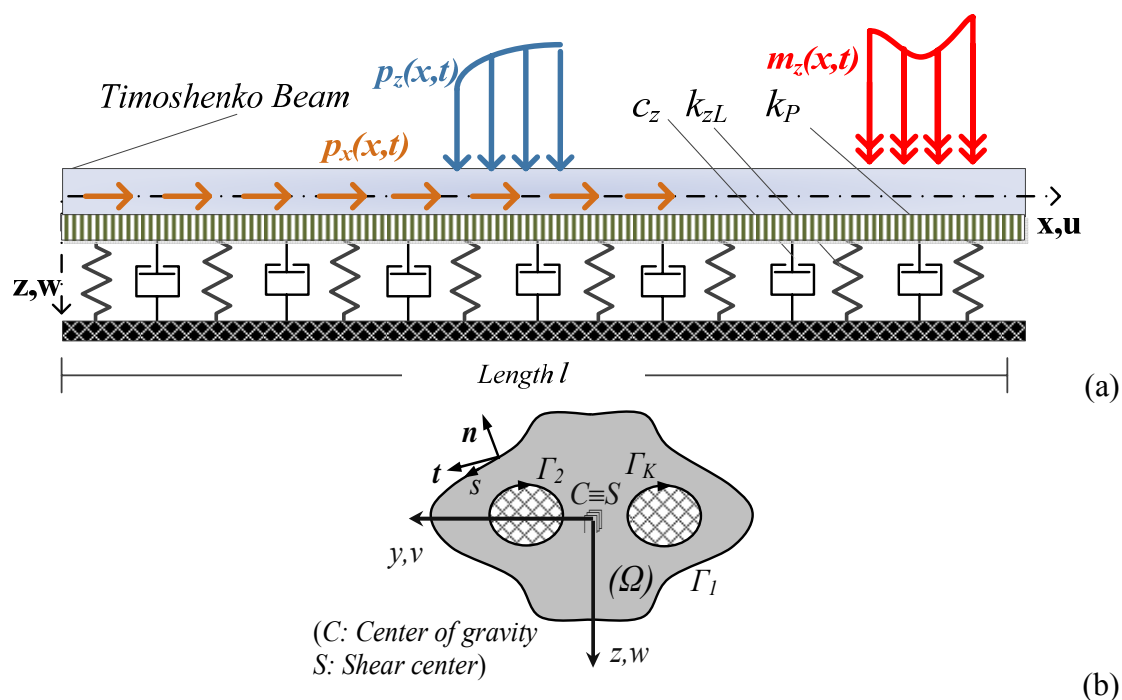


Fig.3.1. x - z plane of prismatic beam under axial-flexural loading (a) with arbitrary doubly symmetric cross-section (b).

3.2.1 Displacements, Strains & Stresses

Under the action of the aforementioned loading, the displacement field of the beam taking into account shear deformation effect is given as (Ramm & Hofmann 1995)

$$\bar{u}(x, y, z, t) = u(x, t) - y\theta_z(x, t) + z\theta_y(x, t) \quad (3.4a)$$

$$\bar{v}(x, t) = v(x, t) \quad \bar{w}(x, t) = w(x, t) \quad (3.4b,c)$$

where \bar{u} , \bar{v} , \bar{w} are the axial and transverse beam displacement components with respect to the Cyz system of axes; $u(x,t)$, $v(x,t)$, $w(x,t)$ are the corresponding components of the centroid C and $\theta_y(x,t)$, $\theta_z(x,t)$ are the angles of rotation due to bending of the cross-section with respect to its centroid. It is worth here noting that since the additional angle of rotation of the cross-section due to shear deformation is taken into account, the one due to bending is not equal to the derivative of the displacements (i.e. $\theta_z \neq v'$, $\theta_y \neq w'$).

Employing the strain-displacement relations of the three-dimensional elasticity the components of the Green-Lagrange strain are defined as

$$\varepsilon_{xx} = \frac{\partial \bar{u}}{\partial x} + \frac{1}{2} \left[\left(\frac{\partial \bar{u}}{\partial x} \right)^2 + \left(\frac{\partial \bar{v}}{\partial x} \right)^2 + \left(\frac{\partial \bar{w}}{\partial x} \right)^2 \right] \quad (3.5a)$$

$$\varepsilon_{yy} = \frac{\partial \bar{v}}{\partial y} + \frac{1}{2} \left[\left(\frac{\partial \bar{u}}{\partial y} \right)^2 + \left(\frac{\partial \bar{v}}{\partial y} \right)^2 + \left(\frac{\partial \bar{w}}{\partial y} \right)^2 \right] \quad (3.5b)$$

$$\varepsilon_{zz} = \frac{\partial \bar{w}}{\partial z} + \frac{1}{2} \left[\left(\frac{\partial \bar{u}}{\partial z} \right)^2 + \left(\frac{\partial \bar{v}}{\partial z} \right)^2 + \left(\frac{\partial \bar{w}}{\partial z} \right)^2 \right] \quad (3.5c)$$

$$\gamma_{xy} = \left(\frac{\partial \bar{v}}{\partial x} + \frac{\partial \bar{u}}{\partial y} \right) + \left(\frac{\partial \bar{u}}{\partial x} \frac{\partial \bar{u}}{\partial y} + \frac{\partial \bar{v}}{\partial x} \frac{\partial \bar{v}}{\partial y} + \frac{\partial \bar{w}}{\partial x} \frac{\partial \bar{w}}{\partial y} \right) \quad (3.5d)$$

$$\gamma_{xz} = \left(\frac{\partial \bar{w}}{\partial x} + \frac{\partial \bar{u}}{\partial z} \right) + \left(\frac{\partial \bar{u}}{\partial x} \frac{\partial \bar{u}}{\partial z} + \frac{\partial \bar{v}}{\partial x} \frac{\partial \bar{v}}{\partial z} + \frac{\partial \bar{w}}{\partial x} \frac{\partial \bar{w}}{\partial z} \right) \quad (3.5e)$$

$$\gamma_{yz} = \left(\frac{\partial \bar{w}}{\partial y} + \frac{\partial \bar{v}}{\partial z} \right) + \left(\frac{\partial \bar{u}}{\partial y} \frac{\partial \bar{u}}{\partial z} + \frac{\partial \bar{v}}{\partial y} \frac{\partial \bar{v}}{\partial z} + \frac{\partial \bar{w}}{\partial y} \frac{\partial \bar{w}}{\partial z} \right) \quad (3.5f)$$

Moreover, assuming relatively small centroidal axial displacement and moderate large transverse displacements (Ramm & Hofmann 1995, Rothert & Gensichen 1987, Brush & Almroth 1975) while strains remain small, the following strain components can be easily obtained

$$\varepsilon_{xx} = \frac{\partial \bar{u}}{\partial x} + \frac{1}{2} \left[\left(\frac{\partial \bar{v}}{\partial x} \right)^2 + \left(\frac{\partial \bar{w}}{\partial x} \right)^2 \right] \quad (3.6a)$$

$$\gamma_{xz} = \frac{\partial \bar{w}}{\partial x} + \frac{\partial \bar{u}}{\partial z} + \left(\frac{\partial \bar{v}}{\partial x} \frac{\partial \bar{v}}{\partial z} + \frac{\partial \bar{w}}{\partial x} \frac{\partial \bar{w}}{\partial z} \right) \quad (3.6b)$$

$$\gamma_{xy} = \frac{\partial \bar{v}}{\partial x} + \frac{\partial \bar{u}}{\partial y} + \left(\frac{\partial \bar{v}}{\partial x} \frac{\partial \bar{v}}{\partial y} + \frac{\partial \bar{w}}{\partial x} \frac{\partial \bar{w}}{\partial y} \right) \quad (3.6c)$$

$$\varepsilon_{yy} = \varepsilon_{zz} = \gamma_{yz} = 0 \quad (3.6d,e,f)$$

where it has been assumed that for moderate displacements $\left(\frac{\partial \bar{u}}{\partial x}\right)^2 \ll \frac{\partial \bar{u}}{\partial x}$, $\left(\frac{\partial \bar{u}}{\partial x}\right)\left(\frac{\partial \bar{u}}{\partial z}\right) \ll \left(\frac{\partial \bar{w}}{\partial x}\right) + \left(\frac{\partial \bar{u}}{\partial z}\right)$, $\left(\frac{\partial \bar{u}}{\partial x}\right)\left(\frac{\partial \bar{u}}{\partial y}\right) \ll \left(\frac{\partial \bar{v}}{\partial x}\right) + \left(\frac{\partial \bar{u}}{\partial y}\right)$. Substituting the displacement components (3.4) to the strain-displacement relations (3.6), the strain components can be written as

$$\varepsilon_{xx}(x, y, z, t) = u' + z\theta_y' - y\theta_z' + \frac{I}{2}(v'^2 + w'^2) \quad (3.7a)$$

$$\gamma_{xy} = v' - \theta_z \quad \gamma_{xz} = w' + \theta_y \quad (3.7b,c)$$

where (') denotes differentiation with respect to x and γ_{xy} , γ_{xz} are the additional angles of rotation of the cross-section due to shear deformation.

Considering strains to be small and assuming an isotropic and homogeneous material, the non vanishing work conjugate stress components of the second Piola–Kirchhoff stress tensor are defined in terms of the strain ones as

$$\begin{Bmatrix} S_{xx} \\ S_{xy} \\ S_{xz} \end{Bmatrix} = \begin{bmatrix} E & 0 & 0 \\ 0 & G & 0 \\ 0 & 0 & G \end{bmatrix} \begin{Bmatrix} \varepsilon_{xx} \\ \gamma_{xy} \\ \gamma_{xz} \end{Bmatrix} \quad (3.8)$$

or employing the strain-displacement relations (3.7) as

$$S_{xx} = E \left[u' + z\theta_y' - y\theta_z' + \frac{I}{2}(v'^2 + w'^2) \right] \quad (3.9a)$$

$$S_{xy} = G(v' - \theta_z) \quad S_{xz} = G(w' + \theta_y) \quad (3.9b,c)$$

3.2.2 Stress Resultants, Governing Equations of Motion, Boundary and Initial Conditions

The governing equations of motion and the boundary conditions of the beam-foundation system subjected to nonlinear vibrations are obtained employing Hamilton's principle in the total Lagrange formulation, neglecting body forces, defined as

$$\delta \int_{t_1}^{t_2} (U_{\text{int}} + U_b - K - W_{\text{ext}}) dt = 0 \quad (3.10)$$

where $\delta(\cdot)$ denotes variation of quantities, t_1, t_2 are the initial and the final times of two sequential configurations, while U_{int} is the strain energy of the beam due to normal and shear stress, U_b is the strain energy of the elastic boundary conditions and K, W_{ext} are the kinetic energy and the external load work, respectively given as

$$\delta U_{\text{int}} = \int_V (S_{xx} \delta \varepsilon_{xx} + S_{xy} \delta \gamma_{xy} + S_{xz} \delta \gamma_{xz}) dV \quad (3.11a)$$

$$\delta U_b = \delta \left(\frac{1}{2} \sum_b \left(k_u^b u_b^2 + k_w^b w_b^2 + k_{\theta_y}^b \theta_{yb}^2 + k_v^b v_b^2 + k_{\theta_z}^b \theta_{zb}^2 \right) \right) \quad (3.11b)$$

$$\begin{aligned} \delta W_{\text{ext}} = & \int_L \left(p_x \delta u + p_y \delta v - \delta (W_{p_{sy}}) + m_y \delta \theta_y + p_z \delta w - \delta (W_{p_{sz}}) + m_z \delta \theta_z \right) dx + \\ & + \sum_b^{0,1} \left(N_x^b \delta u_b + V_y^b \delta v_b + M_z^b \delta \theta_{zb} + V_z^b \delta w_b + M_y^b \delta \theta_{yb} \right) \end{aligned} \quad (3.11c)$$

$$\delta K = \frac{1}{2} \int_V \rho \left(\delta \dot{u}^2 + \delta \dot{v}^2 + \delta \dot{w}^2 \right) dV \quad (3.11d)$$

where $(\dot{\cdot})$ denotes differentiation with respect to time t , $k_j^b, (j = u, v, w, \theta_y, \theta_z)$ are the translational and rotational springs and $N_x^b, V_z^b, V_y^b, M_y^b$ and M_z^b are the externally applied forces and moments at the boundaries, V is the initial volume of the beam in the undeformed configuration, while the variations of strains are expressed in terms of displacements as

$$\delta\varepsilon_{xx} = \delta(u') + z\delta(\theta_y') - y\delta(\theta_z') + \frac{I}{2}\delta(v'^2 + w'^2) = \quad (3.12a)$$

$$= \delta(u') + z\delta(\theta_y') - y\delta(\theta_z') + v'\delta(v') + w'\delta(w')$$

$$\delta\gamma_{xy} = \delta(v') - \delta(\theta_z') \quad \delta\gamma_{xz} = \delta(w') + \delta(\theta_y') \quad (3.12b,c)$$

Substituting the expressions of the stress components (3.9) into the stress resultants of the beam defined as

$$N = \int_{\Omega} S_{xx} d\Omega \quad (3.13a)$$

$$Q_y = \int_{A_y} S_{xy} d\Omega \quad Q_z = \int_{A_z} S_{xz} d\Omega \quad (3.13b,c)$$

$$M_y = \int_{\Omega} S_{xx} z d\Omega \quad M_z = -\int_{\Omega} S_{xx} y d\Omega \quad (3.13d,e)$$

the following equation are obtained

$$N = EA \left[u' + \frac{I}{2}(v'^2 + w'^2) \right] \quad (3.14a)$$

$$Q_y = GA_y \gamma_{xy} \quad Q_z = GA_z \gamma_{xz} \quad (3.14b,c)$$

$$M_y = EI_y \theta_y' \quad M_z = EI_z \theta_z' \quad (3.14d,e)$$

where N is the axial force, Q_y, Q_z are the shear forces and M_y, M_z are the bending moments, A is the cross section area while I_y, I_z the moments of inertia with respect to the principle bending axes given as

$$A = \int_{\Omega} d\Omega \quad (3.1a)$$

$$I_y = \int_{\Omega} z^2 d\Omega \quad I_z = \int_{\Omega} y^2 d\Omega \quad (3.15b,c)$$

and GA_y, GA_z are its shear rigidities of the Timoshenko's beam theory, where

$$A_z = \kappa_z A = \frac{I}{a_z} A \quad A_y = \kappa_y A = \frac{I}{a_y} A \quad (3.16a,b)$$

are the shear areas with respect to y , z axes, respectively with κ_y , κ_z the shear correction factors and a_y , a_z the shear deformation coefficients (Appendix A3).

Hamilton's principle requires that this first-order variation is zero for all possible perturbations, thus exploiting the stress-displacement eqns. (3.9), the relations describing the displacement field (3.4) and after conducting algebraic manipulations the D' Alembert's equilibrium equations, expressed as a function of the stress resultants acting on the cross section of the beam in the deformed configuration are derived as

$$\rho A \ddot{u} - EA(u'' + w'w'' + v'v'') + k_x u = p_x \quad (3.17a)$$

$$\rho A \ddot{v} - (Nv')' - GA_y(v'' - \theta_z') + p_{sy} = p_y \quad (3.17b)$$

$$\rho I_z \ddot{\theta}_z - EI_z \theta_z'' - GA_y(v' - \theta_z) = m_z \quad (3.17c)$$

$$\rho A \ddot{w} - (Nw')' - GA_z(w'' + \theta_y') + p_{sz} = p_z \quad (3.17d)$$

$$\rho I_y \ddot{\theta}_y - EI_y \theta_y'' + GA_z(w' + \theta_y) = m_y \quad (3.17e)$$

Eqns. (3.13) constitute the governing coupled differential equations of a Timoshenko-Rayleigh beam, supported on a tensionless nonlinear three-parameter viscoelastic foundation, subjected to nonlinear vibrations due to the combined action of arbitrarily distributed or concentrated transverse loading as well as to axial loading, accounting for the effects of geometrical nonlinearity, rotary inertia and shear deformation. The motivation to use this particular formulation is justified from the intention of gaining the advantages of a more rigorous model while retaining the simplicity of a beam approach. As it is well known (Antes et al. 2004), Timoshenko-Rayleigh's beam theory gives more reliable results than Euler-Bernoulli's one, especially at higher frequencies, thus beam-structures under arbitrary dynamic excitations (i.e. earthquake, moving load) should be analyzed on the basis of this refined approach. Moreover, it has been proved that the magnitude of the maximum displacement of a Timoshenko beam is larger than that of an Euler-Bernoulli one, while the magnitude of the bending moments differs as well (Younesian & Kargarnovin 2009, Sapountzakis & Kampitsis 2011).

Subsequently, by combining equations (3.17b,c) and (3.17d,e) in order to eliminate the angles of rotation due to bending $\theta_y(x,t)$, $\theta_z(x,t)$, the following differential equations with respect to u , v , w are derived as

$$\rho A \ddot{u} - EA(u'' + w'w'' + v'v'') + k_x u = p_x \quad (3.18a)$$

$$\begin{aligned} \rho A \ddot{v} + EI_z v'''' - (Nv')' + p_{sy} + \frac{EI_z}{GA_y} \left((Nv')''' - \rho A \frac{\partial^2 \ddot{v}}{\partial x^2} - p_{sy}'' + p_y'' \right) - \\ - \rho I_z \frac{\partial^2 \ddot{v}}{\partial x^2} - \frac{\rho I_z}{GA_y} \left(\frac{\partial^2 (Nv')'}{\partial t^2} - \rho A \ddot{v} - \ddot{p}_{sy} + \ddot{p}_y \right) = p_y - m_z' \end{aligned} \quad (3.18b)$$

$$\begin{aligned} \rho A \ddot{w} + EI_y w'''' - (Nw')' + p_{sz} + \frac{EI_y}{GA_z} \left((Nw')''' - \rho A \frac{\partial^2 \ddot{w}}{\partial x^2} - p_{sz}'' + p_z'' \right) - \\ - \rho I_y \frac{\partial^2 \ddot{w}}{\partial x^2} - \frac{\rho I_y}{GA_z} \left(\frac{\partial^2 (Nw')'}{\partial t^2} - \rho A \ddot{w} - \ddot{p}_{sz} + \ddot{p}_z \right) = p_z + m_y' \end{aligned} \quad (3.18c)$$

The above combined equations are easily simplified by crossing out the nonlinear terms and the components regarding the shear deformation effect, leading to the well known second order equation with respect to the axial and fourth order equation with respect to the transverse directions.

The governing equations of motion are also subjected to the time dependent boundary conditions derived also by the Hamilton's principle as

$$\left[EA \left(u' + \frac{I}{2}(v' + w') \right) \right]_0 + N_x^0 \delta u(0) = 0 \xrightarrow{\text{eqn.(3.14a)}} [N(0) + N_x^0] \delta u(0) = 0 \quad (3.19a)$$

$$\left[EA \left(u' + \frac{I}{2}(v' + w') \right) \right]_l - N_x^l \delta u(l) = 0 \xrightarrow{\text{eqn.(3.14a)}} [N(l) - N_x^l] \delta u(l) = 0 \quad (3.19b)$$

$$\left[EA \left(u'v' + \frac{I}{2}v'^3 + \frac{I}{2}v'w'^2 \right) \right]_0 + GA_y (v' - \theta_z')|_0 + V_y^0 \delta v(0) = 0 \quad (3.19c)$$

$$\left[EA \left(u'v' + \frac{I}{2}v'^3 + \frac{I}{2}v'w'^2 \right) \right]_l + GA_y (v' - \theta_z')|_l - V_y^l \delta v(l) = 0 \quad (3.19d)$$

$$\left[EA \left(u'w' + \frac{I}{2} v'^2 w' + \frac{I}{2} w'^3 \right) \Big|_0 + GA_z (w' + \theta'_y) \Big|_0 + V_z^0 \right] \delta w(0) = 0 \quad (3.19e)$$

$$\left[EA \left(u'w' + \frac{I}{2} v'^2 w' + \frac{I}{2} w'^3 \right) \Big|_l + GA_z (w' + \theta'_y) \Big|_l - V_z^l \right] \delta w(l) = 0 \quad (3.19f)$$

$$\left[EI_y \theta'_y \Big|_0 + M_y^0 \right] \delta \theta_y(0) = 0 \xrightarrow{\text{eqn.(3.14d)}} \left[M_y(0) + M_y^0 \right] \delta \theta_y(0) = 0 \quad (3.19g)$$

$$\left[EI_y \theta'_y \Big|_l - M_y^l \right] \delta \theta_y(l) = 0 \xrightarrow{\text{eqn.(3.14d)}} \left[M_y(l) - M_y^0 \right] \delta \theta_y(l) = 0 \quad (3.19h)$$

$$\left[EI_z \theta'_z \Big|_0 + M_z^0 \right] \delta \theta_z(0) = 0 \xrightarrow{\text{eqn.(3.14e)}} \left[M_z(0) + M_z^0 \right] \delta \theta_z(0) = 0 \quad (3.19i)$$

$$\left[EI_z \theta'_z \Big|_l - M_z^l \right] \delta \theta_z(l) = 0 \xrightarrow{\text{eqn.(3.14e)}} \left[M_z(l) - M_z^0 \right] \delta \theta_z(l) = 0 \quad (3.19j)$$

which can be written in a more convenient form as

$$a_1 u(x,t) + \alpha_2 N(x,t) = \alpha_3 \quad (3.20a)$$

$$\beta_1 v(x,t) + \beta_2 V_y(x,t) = \beta_3 \quad \bar{\beta}_1 \theta_z(x,t) + \bar{\beta}_2 M_z(x,t) = \bar{\beta}_3 \quad (3.20b,c)$$

$$\gamma_1 w(x,t) + \gamma_2 V_z(x,t) = \gamma_3 \quad \bar{\gamma}_1 \theta_y(x,t) + \bar{\gamma}_2 M_y(x,t) = \bar{\gamma}_3 \quad (3.20d,e)$$

at the beam ends $x = 0, l$, together with the initial conditions

$$u(x,0) = \bar{u}_0(x) \quad \dot{u}(x,0) = \dot{\bar{u}}_0(x) \quad (3.21a,b)$$

$$v(x,0) = \bar{v}_0(x) \quad \dot{v}(x,0) = \dot{\bar{v}}_0(x) \quad (3.21c,d)$$

$$w(x,0) = \bar{w}_0(x) \quad \dot{w}(x,0) = \dot{\bar{w}}_0(x) \quad (3.21e,f)$$

where $\bar{u}_0(x)$, $\bar{v}_0(x)$, $\bar{w}_0(x)$, $\dot{\bar{u}}_0(x)$, $\dot{\bar{v}}_0(x)$ and $\dot{\bar{w}}_0(x)$ are prescribed functions. In the boundary eqns. (3.20b-e) V_y , V_z and M_z , M_y are the reactions and bending moments with respect to y , z , respectively, which together with the angles of rotation due to bending θ_y , θ_z are given by the following relations

$$V_y = Nv' - EI_z v''' - \frac{EI_z}{GA_y} \left[(Nv')'' - \rho A \frac{\partial \dot{v}}{\partial x} + p_y' - p'_{sy} \right] + \rho I_z \ddot{\theta}_z \quad (3.22a)$$

$$V_z = Nw' - EI_y w''' - \frac{EI_y}{GA_z} \left[(Nw')'' - \rho A \frac{\partial \ddot{w}}{\partial x} + p_z' - p_{sz}' \right] - \rho I_y \ddot{\theta}_y \quad (3.22b)$$

$$M_z = EI_z v'' + \frac{EI_z}{GA_y} \left[(Nv')' - \rho A \dot{v} + p_y - p_{sy} \right] \quad (3.22c)$$

$$M_y = -EI_y w'' - \frac{EI_y}{GA_z} \left[(Nw')' - \rho A \dot{w} + p_z - p_{sz} \right] \quad (3.22d)$$

$$\theta_y = \frac{EI_y}{G^2 A_z^2} \left(\rho A \frac{\partial \ddot{w}}{\partial x} - (Nw')'' - p_z' + p_{sy}' \right) - \frac{I}{GA_z} (EI_y w''' + \rho I_y \ddot{\theta}_y + GA_z w') \quad (3.22e)$$

$$\theta_z = \frac{EI_z}{G^2 A_y^2} \left((Nv')'' - \rho A \frac{\partial \dot{v}}{\partial x} + p_y' - p_{sz}' \right) + \frac{I}{GA_y} (EI_z v''' - \rho I_z \ddot{\theta}_z + GA_y v') \quad (3.22f)$$

Finally, $\alpha_k, \beta_k, \bar{\beta}_k, \gamma_k, \bar{\gamma}_k$ ($k = 1, 2, 3$) are functions specified at the beam ends $x = 0, l$. Eqns.(3.20) describe the most general nonlinear boundary conditions associated with the problem at hand and can include elastic support or restraint. It is apparent that all types of the conventional boundary conditions (clamped, simply supported, free or guided edge) can be derived from these equations by specifying appropriately these functions (e.g. for a clamped edge it is $\alpha_1 = \beta_1 = \gamma_1 = 1$, $\bar{\beta}_1 = \bar{\gamma}_1 = 1$, $\alpha_2 = \alpha_3 = \beta_2 = \beta_3 = \gamma_2 = \gamma_3 = \bar{\beta}_2 = \bar{\beta}_3 = \bar{\gamma}_2 = \bar{\gamma}_3 = 0$).

The solution of the initial boundary value problem given from eqns. (3.17) or from the combined eqns.(3.18), subjected to the boundary conditions (3.20) and the initial conditions (3.21), describes the axial-flexural dynamic response accounting for the geometrical nonlinearity (large displacements) of a Timoshenko-Rayleigh beam, supported on a tensionless nonlinear three-parameter viscoelastic foundation. The evaluation of the shear deformation coefficients a_y, a_z corresponding to the principal centroidal system of axes Cyz , are established equating the approximate formula of the shear strain energy per unit length with the exact one as described in Appendix A3.

3.3 Integral Representations – Numerical Solution

According to the precedent analysis, the nonlinear axial-flexural dynamic analysis of Timoshenko-Rayleigh beams, supported on a tensionless nonlinear three-parameter viscoelastic foundation, undergoing moderate large displacements reduces in

establishing the displacement components $u(x,t)$ and $v(x,t)$, $w(x,t)$ having continuous derivatives up to the second order and up to the fourth order with respect to x , respectively, and also having derivatives up to the second order with respect to t (ignoring the inertia terms of the fourth order (Thomson 1981)). These displacement components must satisfy the coupled governing differential equations (3.18) inside the beam, the boundary conditions (3.20) at the beam ends $x = 0, l$ and the initial conditions (3.21). Eqns. (3.18) are solved using the Analog Equation Method (Katsikadelis 1994, 2002) as it is described in Appendix A1.

3.3.1 Axial $u(x,t)$ and Transverse Displacements $v(x,t), w(x,t)$

According to this method, let $u(x,t)$, $v(x,t)$ and $w(x,t)$ be the sought solution of the aforementioned initial value problem. Setting as $u_1(x,t) = u(x,t)$, $u_2(x,t) = v(x,t)$, $u_3(x,t) = w(x,t)$ and differentiating with respect to x these functions two and four times, respectively yields

$$\frac{\partial^2 u_i}{\partial x^2} = q_i(x,t) \quad \frac{\partial^4 u_i}{\partial x^4} = q_i(x,t) \quad (i = 2, 3) \quad (3.23)$$

Eqns. (3.23) are quasi-static that is the time variable appears as a parameter. They indicate that the solution of eqns. (3.18) can be established by solving eqns. (3.23) under the same boundary conditions (3.20), provided that the fictitious load distributions $q_i(x,t)$ ($i = 1, 2, 3$) are first established. Following the procedure as described in Appendix A1, the integral representations of the displacement components u_i ($i = 1, 2, 3$) obtained by eqn. (A1.8, A1.36) and their first derivatives with respect to x obtained by eqn. (A1.22, A1.43), when applied to the beam ends $(0, l)$, together with the boundary conditions (3.20) are employed to express the unknown boundary quantities $u_i(\zeta, t)$, $u_{i,x}(\zeta, t)$, $u_{i,xx}(\zeta, t)$ and $u_{i,xxx}(\zeta, t)$ ($\zeta = 0, l$) in terms of the fictitious loads q_i ($i = 1, 2, 3$). In order to accomplish this numerical formulation, the interval $(0, l)$ is divided into L elements, on which $q_i(x,t)$ is assumed to vary according to certain law (constant, linear, parabolic etc). The constant element

assumption is employed here as the numerical implementation becomes very simple and the obtained results are of high accuracy.

Employing the aforementioned procedure, the following set of 20 nonlinear algebraic equations is obtained

$$\begin{bmatrix} \mathbf{T}_{11} & \mathbf{0} & \mathbf{0} \\ \mathbf{0} & \mathbf{T}_{22} & \mathbf{0} \\ \mathbf{0} & \mathbf{0} & \mathbf{T}_{33} \end{bmatrix} \begin{Bmatrix} \mathbf{d}_1 \\ \mathbf{d}_2 \\ \mathbf{d}_3 \end{Bmatrix} + \begin{Bmatrix} \mathbf{D}_1^{\text{nl}} \\ \mathbf{D}_2^{\text{nl}} \\ \mathbf{D}_3^{\text{nl}} \end{Bmatrix} = \begin{Bmatrix} \mathbf{a}_3 \\ \mathbf{b}_3 \\ \mathbf{c}_3 \end{Bmatrix} \quad (3.24)$$

with

$$\mathbf{T}_{11} = \begin{bmatrix} \mathbf{F}_1^{\text{u}} & \mathbf{E}_{11}^{\text{u}} & \mathbf{E}_{12}^{\text{u}} \\ \mathbf{0} & \mathbf{D}_{12}^{\text{u}} & \mathbf{D}_{22}^{\text{u}} \end{bmatrix} \quad (3.25a)$$

$$\mathbf{T}_{22} = \begin{bmatrix} \mathbf{F}_1 & \mathbf{E}_{11} & \mathbf{E}_{12} & \mathbf{E}_{13} & \mathbf{E}_{14} \\ \mathbf{F}_2 & \mathbf{0} & \mathbf{E}_{22} & \mathbf{E}_{23} & \mathbf{E}_{24} \\ \mathbf{0} & \mathbf{D}_{11} & \mathbf{D}_{12} & \mathbf{D}_{13} & \mathbf{D}_{14} \\ \mathbf{0} & \mathbf{D}_{21} & \mathbf{D}_{22} & \mathbf{D}_{23} & \mathbf{D}_{24} \end{bmatrix} \quad \mathbf{T}_{33} = \begin{bmatrix} \mathbf{F}_1 & \mathbf{E}_{11} & \mathbf{E}_{12} & \mathbf{E}_{13} & \mathbf{E}_{14} \\ \mathbf{F}_2 & \mathbf{0} & \mathbf{E}_{22} & \mathbf{E}_{23} & \mathbf{E}_{24} \\ \mathbf{0} & \mathbf{G}_{11} & \mathbf{G}_{12} & \mathbf{G}_{13} & \mathbf{G}_{14} \\ \mathbf{0} & \mathbf{G}_{21} & \mathbf{G}_{22} & \mathbf{G}_{23} & \mathbf{G}_{24} \end{bmatrix} \quad (3.25b,c)$$

where $\mathbf{E}_{11}^{\text{u}}, \mathbf{E}_{12}^{\text{u}}, \mathbf{E}_{11} - \mathbf{E}_{48}$ are rectangular 2×2 known coefficient matrices resulting from the values of the kernels $A_j(r)$ ($j = 1, 2, 3, 4$) at the beam ends and $\mathbf{F}_1^{\text{u}}, \mathbf{F}_1, \mathbf{F}_2$ are $2 \times L$ rectangular known matrices originating from the integration of the kernels along the axis of the beam, as defined in Appendix A1. Moreover, $\mathbf{D}_{11} - \mathbf{D}_{24}$ and $\mathbf{G}_{11} - \mathbf{G}_{24}$ are 2×2 known square, time dependent matrices including the values of the functions $a_j, \beta_j, \bar{\beta}_j, \gamma_j, \bar{\gamma}_j$ ($j = 1, 2$) of eqns.(3.20), while $\mathbf{D}_1^{\text{nl}}, \mathbf{a}_3$ and $\mathbf{D}_2^{\text{nl}}, \mathbf{D}_3^{\text{nl}}, \mathbf{b}_3, \mathbf{c}_3$ are 4×1 and 8×1 , respectively known, in general time dependent, column matrices including the boundary values of the functions $a_3, \beta_3, \bar{\beta}_3, \gamma_3, \bar{\gamma}_3$ of eqns. (3.20). Furthermore, $\mathbf{d}_1 - \mathbf{d}_3$ are the generalized unknown vectors including the L unknown time dependent nodal values of the fictitious loads $q_i = \{q_1^i, q_2^i, \dots, q_L^i\}^T$ ($i = 1, 2, 3$) and the vectors including the unknown time dependent boundary values of the respective boundary quantities. More specifically, the expressions of the matrices of eqn. (3.25) are given as

$$\mathbf{D}_{12}^u = \begin{bmatrix} \alpha_1^0 & 0 \\ 0 & \alpha_1^l \end{bmatrix} \quad \mathbf{D}_{22}^u = \begin{bmatrix} \alpha_2^0 EA & 0 \\ 0 & \alpha_2^l EA \end{bmatrix} \quad (3.26a,b)$$

$$\mathbf{D}_1^{nl} = \frac{1}{2} EA \begin{Bmatrix} [0] \\ \alpha_2^0 [\hat{u}_{2,x}(0) + \hat{u}_{3,x}(0)]^2 \\ \alpha_2^l [\hat{u}_{2,x}(l) + \hat{u}_{3,x}(l)]^2 \end{Bmatrix} \quad \mathbf{a}_3 = \begin{Bmatrix} [0] \\ \alpha_3^0 \\ \alpha_3^l \end{Bmatrix} \quad (3.26c,d)$$

$$\mathbf{D}_{11} = \begin{bmatrix} \beta_1^0 & 0 \\ 0 & \beta_1^l \end{bmatrix} \quad \mathbf{D}_{12} = \begin{bmatrix} \beta_2^0 \left(N(0) + \frac{EI_z}{GA_y} \tilde{H}_y k_{Ly} \right) & 0 \\ 0 & \beta_2^l \left(N(l) + \frac{EI_z}{GA_y} \tilde{H}_y k_{Ly} \right) \end{bmatrix} \quad (3.27a,b)$$

$$\mathbf{D}_{13} = -\frac{2EI_z}{GA_y} \begin{bmatrix} \beta_2^0 N'(0) & 0 \\ 0 & \beta_2^l N'(l) \end{bmatrix} \quad \mathbf{D}_{14} = -EI_z \begin{bmatrix} \beta_2^0 \left(1 + \frac{1}{GA_y} (N(0) + \tilde{H}_y k_{Py}) \right) & 0 \\ 0 & \beta_2^l \left(1 + \frac{1}{GA_y} (N(l) + \tilde{H}_y k_{Py}) \right) \end{bmatrix} \quad (3.27c,d)$$

$$\mathbf{D}_{21} = -\bar{\beta}_2^0 \frac{EI_z}{GA_y} \begin{bmatrix} \tilde{H}_y k_{Ly} & 0 \\ 0 & \tilde{H}_y k_{Ly} \end{bmatrix} \quad (3.27e)$$

$$\mathbf{D}_{22} = \begin{bmatrix} \bar{\beta}_1^0 \left(1 - \frac{EI_z}{(GA_y)^2} \tilde{H}_y k_{Ly} \right) + \bar{\beta}_2^0 \frac{EI_z}{GA_y} N'(0) & 0 \\ 0 & \bar{\beta}_1^l \left(1 - \frac{EI_z}{(GA_y)^2} \tilde{H}_y k_{Ly} \right) + \bar{\beta}_2^l \frac{EI_z}{GA_y} N'(l) \end{bmatrix} \quad (3.27f)$$

$$\mathbf{D}_{23} = EI_z \begin{bmatrix} \bar{\beta}_2^0 \left(1 + \frac{1}{GA_y} N(0) - \frac{1}{GA_y} \tilde{H}_y k_P \right) + \bar{\beta}_1^0 \frac{2}{(GA_y)^2} N'(0) & 0 \\ 0 & \bar{\beta}_2^l \left(1 + \frac{1}{GA_y} N(l) - \frac{1}{GA_y} \tilde{H}_y k_P \right) + \bar{\beta}_1^l \frac{2}{(GA_y)^2} N'(l) \end{bmatrix} \quad (3.27g)$$

$$\mathbf{D}_{24} = \frac{EI_z}{GA_y} \begin{bmatrix} \bar{\beta}_1^0 \left(1 + \frac{I}{GA_y} (N(0) + \tilde{H}_y k_P) \right) & 0 \\ 0 & \bar{\beta}_1^l \left(1 + \frac{I}{GA_y} (N(l) + \tilde{H}_y k_P) \right) \end{bmatrix} \quad (3.27h)$$

$$\mathbf{D}_2^{\text{nl}} = -\frac{EI_z}{AG_y} \left\{ \begin{array}{c} [0] \\ -\beta_2^0 \tilde{H}_y k_{NLy} 3\hat{u}_2^2(0) \hat{u}_{2,x}(0) \\ -\beta_2^l \tilde{H}_y k_{NLy} 3\hat{u}_2^2(l) \hat{u}_{2,x}(l) \\ [0] \\ \bar{\beta}_1^0 \frac{3}{AG_y} \tilde{H}_y k_{NLy} \hat{u}_2^2(0) \hat{u}_{2,x}(0) + \bar{\beta}_2^0 \tilde{H}_y k_{NLy} \hat{u}_2^3(0) \\ \bar{\beta}_1^l \frac{3}{AG_y} \tilde{H}_y k_{NLy} \hat{u}_2^2(l) \hat{u}_{2,x}(l) + \bar{\beta}_2^l \tilde{H}_y k_{NLy} \hat{u}_2^3(l) \end{array} \right\} \quad (3.27i)$$

$$\mathbf{b}_3 = \left\{ \begin{array}{c} [0] \\ \beta_3^0 + \beta_2^0 \frac{EI_z}{AG_y} p'_y(0) \\ \beta_3^l + \beta_2^l \frac{EI_z}{AG_y} p'_y(l) \\ [0] \\ \bar{\beta}_3^0 - \frac{EI_z}{AG_y} \left(\frac{\bar{\beta}_1^0}{AG_y} p'_y(0) - \bar{\beta}_2^0 p_y(0) \right) \\ \bar{\beta}_3^l - \frac{EI_z}{AG_y} \left(\frac{\bar{\beta}_1^l}{AG_y} p'_y(l) - \bar{\beta}_2^l p_y(l) \right) \end{array} \right\} \quad (3.27j)$$

$$\mathbf{G}_{11} = \begin{bmatrix} \gamma_1^0 & 0 \\ 0 & \gamma_1^l \end{bmatrix} \quad \mathbf{G}_{12} = \begin{bmatrix} \gamma_2^0 \left(N(0) + \frac{EI_y}{GA_z} \tilde{H}_z k_{Lz} \right) & 0 \\ 0 & \gamma_2^l \left(N(l) + \frac{EI_y}{GA_z} \tilde{H}_z k_{Lz} \right) \end{bmatrix} \quad (3.28a,b)$$

$$\mathbf{G}_{13} = -\frac{2EI_y}{GA_z} \begin{bmatrix} \gamma_2^0 N'(0) & 0 \\ 0 & \gamma_2^l N'(l) \end{bmatrix} \quad \mathbf{G}_{14} = -EI_y \begin{bmatrix} \gamma_2^0 \left(1 + \frac{I}{GA_z} (N(0) + \tilde{H}_z k_{Pz}) \right) & 0 \\ 0 & \gamma_2^l \left(1 + \frac{I}{GA_z} (N(l) + \tilde{H}_z k_{Pz}) \right) \end{bmatrix} \quad (3.28c,d)$$

$$\mathbf{G}_{21} = -\bar{\gamma}_2^0 \frac{EI_y}{GA_z} \begin{bmatrix} \tilde{H}_z k_{Lz} & 0 \\ 0 & \tilde{H}_z k_{Lz} \end{bmatrix} \quad (3.28e)$$

$$\mathbf{G}_{22} = - \begin{bmatrix} \bar{\gamma}_1^0 \left(1 - \frac{EI_y}{(GA_z)^2} \tilde{H}_z k_{Lz} \right) + \bar{\gamma}_2^0 \frac{EI_y}{GA_z} N'(0) & 0 \\ 0 & \bar{\gamma}_1^l \left(1 - \frac{EI_y}{(GA_z)^2} \tilde{H}_z k_{Lz} \right) + \bar{\gamma}_2^l \frac{EI_y}{GA_z} N'(l) \end{bmatrix} \quad (3.28f)$$

$$\mathbf{G}_{23} = EI_y \begin{bmatrix} \bar{\gamma}_2^0 \left(1 + \frac{I}{GA_z} N(0) - \frac{I}{GA_z} \tilde{H}_z k_P \right) + \bar{\gamma}_1^0 \frac{2}{(GA_z)^2} N'(0) & 0 \\ 0 & \bar{\gamma}_2^l \left(1 + \frac{I}{GA_z} N(l) - \frac{I}{GA_z} \tilde{H}_z k_P \right) + \bar{\gamma}_1^l \frac{2}{(GA_z)^2} N'(l) \end{bmatrix} \quad (3.28g)$$

$$\mathbf{G}_{24} = \frac{EI_y}{GA_z} \begin{bmatrix} \bar{\gamma}_1^0 \left(1 + \frac{I}{GA_z} (N(0) + \tilde{H}_z k_P) \right) & 0 \\ 0 & \bar{\gamma}_1^l \left(1 + \frac{I}{GA_z} (N(l) + \tilde{H}_z k_P) \right) \end{bmatrix} \quad (3.28h)$$

$$\mathbf{D}_3^{\text{nl}} = \frac{EI_y}{AG_z} \left\{ \begin{array}{c} [0] \\ \gamma_2^0 \tilde{H}_z k_{NLz} 3\hat{u}_3^2(0) \hat{u}_{3,x}(0) \\ \gamma_2^l \tilde{H}_z k_{NLz} 3\hat{u}_3^2(l) \hat{u}_{3,x}(l) \\ [0] \\ \bar{\gamma}_1^0 \frac{3}{AG_z} \tilde{H}_z k_{NLz} \hat{u}_3^2(0) \hat{u}_{3,x}(0) + \bar{\gamma}_2^0 \tilde{H}_z k_{NLz} \hat{u}_3^3(0) \\ \bar{\gamma}_1^l \frac{3}{AG_z} \tilde{H}_z k_{NLz} \hat{u}_3^2(l) \hat{u}_{3,x}(l) + \bar{\gamma}_2^l \tilde{H}_z k_{NLz} \hat{u}_3^3(l) \end{array} \right\} \quad (3.28i)$$

$$\mathbf{c}_3 = \left\{ \begin{array}{c} [0] \\ \gamma_3^0 - \gamma_2^0 \frac{EI_y}{AG_z} p'_z(0) \\ \gamma_3^l - \gamma_2^l \frac{EI_y}{AG_z} p'_z(l) \\ [0] \\ \bar{\gamma}_3^0 + \frac{EI_y}{AG_z} \left(\frac{\bar{\gamma}_1^0}{AG_z} p'_z(0) - \bar{\gamma}_2^0 p_z(0) \right) \\ \bar{\gamma}_3^l + \frac{EI_y}{AG_z} \left(\frac{\bar{\gamma}_1^l}{AG_z} p'_z(l) - \bar{\gamma}_2^l p_z(l) \right) \end{array} \right\} \quad (3.28j)$$

$$\mathbf{d}_1 = \begin{Bmatrix} \mathbf{q}_1 \\ \hat{\mathbf{u}}_1 \\ \hat{\mathbf{u}}_{1,x} \end{Bmatrix} \quad \mathbf{d}_2 = \begin{Bmatrix} \mathbf{q}_2 \\ \hat{\mathbf{u}}_2 \\ \hat{\mathbf{u}}_{2,x} \\ \hat{\mathbf{u}}_{2,xx} \\ \hat{\mathbf{u}}_{2,xxx} \end{Bmatrix} \quad \mathbf{d}_3 = \begin{Bmatrix} \mathbf{q}_3 \\ \hat{\mathbf{u}}_3 \\ \hat{\mathbf{u}}_{3,x} \\ \hat{\mathbf{u}}_{3,xx} \\ \hat{\mathbf{u}}_{3,xxx} \end{Bmatrix} \quad (3.29)$$

where the boundary values of the displacement components u_i ($i=1,2,3$) and their derivatives with respect to x are written in matrix form as

$$\hat{\mathbf{u}}_i = \{u_i(0,t) \quad u_i(l,t)\}^T \quad (i=1,2,3) \quad (3.30a)$$

$$\hat{\mathbf{u}}_{i,x} = \left\{ \frac{\partial u_i(0,t)}{\partial x} \quad \frac{\partial u_i(l,t)}{\partial x} \right\}^T \quad (i=1,2,3) \quad (3.30b)$$

$$\hat{\mathbf{u}}_{i,xx} = \left\{ \frac{\partial^2 u_i(0,t)}{\partial x^2} \quad \frac{\partial^2 u_i(l,t)}{\partial x^2} \right\}^T \quad (i=2,3) \quad (3.30c)$$

$$\hat{\mathbf{u}}_{i,xxx} = \left\{ \frac{\partial^3 u_i(0,t)}{\partial x^3} \quad \frac{\partial^3 u_i(l,t)}{\partial x^3} \right\}^T \quad (i=2,3) \quad (3.30d)$$

Thereafter, the discretization of the integral representations of the displacement components u_i ($i=1,2,3$) and their derivatives with respect to x , and the application to the L collocation nodal points yields

$$\mathbf{u}_1 = \mathbf{A}_1^0 \mathbf{q}_1 + \mathbf{C}_0 \hat{\mathbf{u}}_1 + \mathbf{C}_1 \hat{\mathbf{u}}_{1,x} \quad (3.31a)$$

$$\mathbf{u}_{1,x} = \mathbf{A}_1^1 \mathbf{q}_1 + \mathbf{C}_0 \hat{\mathbf{u}}_{1,x} \quad \mathbf{u}_{1,xx} = \mathbf{q}_1 \quad (3.31b,c)$$

$$\mathbf{u}_2 = \mathbf{A}_2^0 \mathbf{q}_2 + \mathbf{C}_0 \hat{\mathbf{u}}_2 + \mathbf{C}'_1 \hat{\mathbf{u}}_{2,x} + \mathbf{C}_2 \hat{\mathbf{u}}_{2,xx} + \mathbf{C}_3 \hat{\mathbf{u}}_{2,xxx} \quad (3.32a)$$

$$\mathbf{u}_{2,x} = \mathbf{A}_2^1 \mathbf{q}_2 + \mathbf{C}_0 \hat{\mathbf{u}}_{2,x} + \mathbf{C}'_1 \hat{\mathbf{u}}_{2,xx} + \mathbf{C}_2 \hat{\mathbf{u}}_{2,xxx} \quad (3.32b)$$

$$\mathbf{u}_{2,xx} = \mathbf{A}_2^2 \mathbf{q}_2 + \mathbf{C}_0 \hat{\mathbf{u}}_{2,xx} + \mathbf{C}'_1 \hat{\mathbf{u}}_{2,xxx} \quad (3.32c)$$

$$\mathbf{u}_{2,xxx} = \mathbf{A}_2^3 \mathbf{q}_2 + \mathbf{C}_0 \hat{\mathbf{u}}_{2,xxx} \quad \mathbf{u}_{2,xxxx} = \mathbf{q}_2 \quad (3.32d,e)$$

$$\mathbf{u}_3 = \mathbf{A}_3^0 \mathbf{q}_3 + \mathbf{C}_0 \hat{\mathbf{u}}_3 + \mathbf{C}'_1 \hat{\mathbf{u}}_{3,x} + \mathbf{C}_2 \hat{\mathbf{u}}_{3,xx} + \mathbf{C}_3 \hat{\mathbf{u}}_{3,xxx} \quad (3.33a)$$

$$\mathbf{u}_{3,x} = \mathbf{A}_3^1 \mathbf{q}_3 + \mathbf{C}_0 \hat{\mathbf{u}}_{3,x} + \mathbf{C}'_1 \hat{\mathbf{u}}_{3,xx} + \mathbf{C}_2 \hat{\mathbf{u}}_{3,xxx} \quad (3.33b)$$

$$\mathbf{u}_{3,xx} = \mathbf{A}_3^2 \mathbf{q}_3 + \mathbf{C}_0 \hat{\mathbf{u}}_{3,xx} + \mathbf{C}'_1 \hat{\mathbf{u}}_{3,xxx} \quad (3.33c)$$

$$\mathbf{u}_{3,xxx} = \mathbf{A}_3^3 \mathbf{q}_3 + \mathbf{C}_0 \hat{\mathbf{u}}_{3,xxx} \quad \mathbf{u}_{3,xxxx} = \mathbf{q}_3 \quad (3.33d,e)$$

where \mathbf{A}_1^i , \mathbf{A}_2^j , \mathbf{A}_3^j ($i = 0,1$), ($j = 0,1,2,3$) are $L \times L$ known matrices; \mathbf{C}_0 , \mathbf{C}_1 , \mathbf{C}'_1 , \mathbf{C}_2 , \mathbf{C}_3 are $L \times 2$ known matrices and \mathbf{u}_i , $\mathbf{u}_{i,x}$, $\mathbf{u}_{i,xx}$, $\mathbf{u}_{i,xxx}$, $\mathbf{u}_{i,xxxx}$ are time dependent vectors including the values of $u_i(x,t)$ and their derivatives at the L nodal points. These equations can be assembled in a more convenient matrix form as

$$\mathbf{u}_1 = \mathbf{B}'' \mathbf{d}_1 \quad \mathbf{u}_{1,x} = \mathbf{B}_{,x}'' \mathbf{d}_1 \quad (3.34a,b)$$

$$\mathbf{u}_2 = \mathbf{B} \mathbf{d}_2 \quad \mathbf{u}_{2,x} = \mathbf{B}_{,x} \mathbf{d}_2 \quad \mathbf{u}_{2,xx} = \mathbf{B}_{,xx} \mathbf{d}_2 \quad \mathbf{u}_{2,xxx} = \mathbf{B}_{,xxx} \mathbf{d}_2 \quad (3.35a-d)$$

$$\mathbf{u}_3 = \mathbf{B} \mathbf{d}_3 \quad \mathbf{u}_{3,x} = \mathbf{B}_{,x} \mathbf{d}_3 \quad \mathbf{u}_{3,xx} = \mathbf{B}_{,xx} \mathbf{d}_3 \quad \mathbf{u}_{3,xxx} = \mathbf{B}_{,xxx} \mathbf{d}_3 \quad (3.36a-d)$$

where \mathbf{B}'' , \mathbf{B} and their derivatives are $L \times (L+4)$ and $L \times (L+8)$ known matrices, respectively arising from \mathbf{A}'' , \mathbf{A} , \mathbf{C}'' , \mathbf{C} and their derivatives as presented in Appendix A1.

In conventional BEM, the load vectors \mathbf{q}_i are known and eqns. (3.34-3.36) are used to evaluate $u_i(x,t)$ and their derivatives at the L nodal points. This, however, cannot be applied here since \mathbf{q}_i are unknown. Thus, $3L$ additional equations are required in order to permit the establishment of \mathbf{q}_i . Therefore, the final step of AEM is implemented by applying the governing equations of motion (3.18) to the L collocation points, after ignoring the inertia terms of the fourth order arising from coupling of shear deformations and rotary inertia (Thomson 1981), and employing eqns. (3.34-3.36) leads to the formulation of the following set of $3 \times L$ semi-discretized nonlinear equations of motion

$$\mathbf{M}\ddot{\mathbf{d}} + \mathbf{C}\dot{\mathbf{d}} + \mathbf{K}\mathbf{d} + \mathbf{f}^{nl} = \mathbf{f} \Rightarrow$$

$$\mathbf{M} \begin{Bmatrix} \ddot{\mathbf{d}}_1 \\ \ddot{\mathbf{d}}_2 \\ \ddot{\mathbf{d}}_3 \end{Bmatrix} + \mathbf{C} \begin{Bmatrix} \dot{\mathbf{d}}_1 \\ \dot{\mathbf{d}}_2 \\ \dot{\mathbf{d}}_3 \end{Bmatrix} + \mathbf{K} \begin{Bmatrix} \mathbf{d}_1 \\ \mathbf{d}_2 \\ \mathbf{d}_3 \end{Bmatrix} + \mathbf{f}^{nl}(\mathbf{B}^u, \mathbf{B}, \mathbf{d}_1, \mathbf{d}_2, \mathbf{d}_3) = \mathbf{f} \quad (3.37)$$

where \mathbf{f}^{nl} is a nonlinear generalized stiffness vector and $\mathbf{M}, \mathbf{C}, \mathbf{K}, \mathbf{f}$ are generalized mass, damping, stiffness matrices and force vector respectively, defined as

$$\mathbf{M}_1 = \rho A \mathbf{B}^u \quad \mathbf{K}_1 = -[\mathbf{EA}]_{dg,L} + [\mathbf{K}_x \mathbf{B}^u]_{dg} \quad \mathbf{f}_1 = \mathbf{p}_x \quad (3.38a-c)$$

$$\mathbf{f}_1^{nl} = \mathbf{EA} \left[[\mathbf{B}_{,xx} \mathbf{d}_2]_{dg}, [\mathbf{B}_{,x} \mathbf{d}_2] + [\mathbf{B}_{,xx} \mathbf{d}_3]_{dg}, [\mathbf{B}_{,x} \mathbf{d}_3] \right] \quad (3.38d)$$

$$\mathbf{M}_2 = \rho A \mathbf{B} - \rho I_z \left(1 + \frac{Ea_y}{G} \right) \mathbf{B}_{,xx} - \frac{\rho I_z}{GA_y} \left(\mathbf{N}_x \mathbf{B}_{,x} + [\mathbf{N} + \mathbf{K}_{Py}^{dg}] \mathbf{B}_{,xx} - \mathbf{K}_{Ly}^{dg} \mathbf{B} \right) \quad (3.39a)$$

$$\mathbf{C}_2 = \mathbf{C}_y^{dg} \mathbf{B} - \frac{EI_z}{GA_y} \mathbf{C}_y^{dg} \mathbf{B}_{,xx} - \frac{2\rho I_z}{GA_y} (\mathbf{N}_{xt} \mathbf{B}_{,x} + \mathbf{N}_t \mathbf{B}_{,xx}) \quad (3.39b)$$

$$\mathbf{K}_2 = [\mathbf{EI}_z]_{dg,L} - \mathbf{N}_x \mathbf{B}_{,x} - \mathbf{N} \mathbf{B}_{,xx} + \frac{EI_z}{GA_y} \left(3\mathbf{N}_x \mathbf{B}_{,xxx} + \mathbf{N} - \mathbf{K}_{Ly}^{dg} \mathbf{B}_{,xx} \right) -$$

$$- \frac{\rho I_z}{GA_y} (\mathbf{N}_{xtt} \mathbf{B}_{,x} + \mathbf{N}_{tt} \mathbf{B}_{,xx}) + \mathbf{K}_{Ly}^{dg} \mathbf{B} - \mathbf{K}_{Py}^{dg} \mathbf{B}_{,xx} - \frac{EI_z}{GA_y} (\mathbf{K}_{Ly}^{dg} \mathbf{B}_{,xx} - \mathbf{K}_{Py}^{dg}) \quad (3.39c)$$

$$\mathbf{f}_2^{nl} = \mathbf{K}_{NLy}^{dg} (\mathbf{d}_2)^3 - \frac{EI_z}{GA_y} \left(\mathbf{K}_{NLy}^{dg} (\mathbf{B}_{,xx} \mathbf{d}_2)^3 \right) - \frac{\rho I_z}{GA_y} (\mathbf{B} \mathbf{d}_2)^3 \quad (3.39d)$$

$$\mathbf{f}_2 = \mathbf{p}_y - \mathbf{m}_{z,x} - \frac{EI_z}{GA_y} (\mathbf{p}_{y,xx}) + \frac{\rho I_z}{GA_y} \mathbf{p}_{y,tt} \quad (3.39e)$$

$$\mathbf{M}_3 = \rho A \mathbf{B} - \rho I_y \left(1 + \frac{Ea_z}{G} \right) \mathbf{B}_{,xx} - \frac{\rho I_y}{GA_z} \left(\mathbf{N}_x \mathbf{B}_{,x} + [\mathbf{N} + \mathbf{K}_{Pz}^{dg}] \mathbf{B}_{,xx} - \mathbf{K}_{Lz}^{dg} \mathbf{B} \right) \quad (3.40a)$$

$$\mathbf{C}_3 = \mathbf{C}_z^{dg} \mathbf{B} - \frac{EI_y}{GA_z} \mathbf{C}_z^{dg} \mathbf{B}_{,xx} - \frac{2\rho I_y}{GA_z} (\mathbf{N}_{xt} \mathbf{B}_{,x} + \mathbf{N}_t \mathbf{B}_{,xx}) \quad (3.40b)$$

$$\mathbf{K}_3 = \left[\mathbf{EI}_y \right]_{dg,L} - \mathbf{N}_x \mathbf{B}_{,x} - \mathbf{NB}_{,xx} + \frac{EI_y}{GA_z} \left(3\mathbf{N}_x \mathbf{B}_{,xxx} + \mathbf{N} - \mathbf{K}_{Lz}^{dg} \mathbf{B}_{,xx} \right) - \frac{\rho I_y}{GA_z} \left(\mathbf{N}_{xtt} \mathbf{B}_{,x} + \mathbf{N}_{tt} \mathbf{B}_{,xx} \right) + \mathbf{K}_{Lz}^{dg} \mathbf{B} - \mathbf{K}_{Pz}^{dg} \mathbf{B}_{,xx} - \frac{EI_y}{GA_z} \left(\mathbf{K}_{Lz}^{dg} \mathbf{B}_{,xx} - \mathbf{K}_{Pz}^{dg} \right) \quad (3.40c)$$

$$\mathbf{f}_3^{nl} = \mathbf{K}_{NLz}^{dg} (\mathbf{d}_3)^3 - \frac{EI_y}{GA_z} \left(\mathbf{K}_{NLz}^{dg} (\mathbf{B}_{,xx} \mathbf{d}_3)^3 \right) - \frac{\rho I_y}{GA_z} (\mathbf{B} \mathbf{d}_3)^3 \quad (3.40d)$$

$$\mathbf{f}_3 = \mathbf{p}_z + \mathbf{m}_{y,x} - \frac{EI_y}{GA_z} (\mathbf{p}_{z,xx}) + \frac{\rho I_y}{GA_z} \mathbf{p}_{z,tt} \quad (3.40e)$$

where \mathbf{N} , \mathbf{N}_{km} ($k, m = x, t$) are $L \times L$ diagonal matrices containing the values of the axial force and its derivatives with respect to k and m parameters at the L nodal points, \mathbf{p}_y , $\mathbf{p}_{y,xx}$, $\mathbf{p}_{y,tt}$, \mathbf{p}_z , $\mathbf{p}_{z,xx}$, $\mathbf{p}_{z,tt}$, $\mathbf{m}_{y,x}$ and $\mathbf{m}_{z,x}$ are $L \times 1$ vectors containing the values of the external loading and its derivatives at these points, while \mathbf{K}_{Li}^{dg} , \mathbf{K}_{NLi}^{dg} , \mathbf{K}_{Pi}^{dg} and \mathbf{C}_i^{dg} ($i = y, z$) are diagonal matrices whose diagonal elements represent the values of the corresponding foundation parameter at each nodal point. Moreover, substituting eqns. (3.34) in eqn. (3.14a), the discretized counterpart of the axial force at the neutral axis of the beam is given as

$$\mathbf{N} = EA (\mathbf{B}_{,x}^u \mathbf{d}_1) + \frac{I}{2} EA \left[\left[\mathbf{B}_{,xx} \mathbf{d}_2 \right]_{dg} \left[\mathbf{B}_{,x} \mathbf{d}_2 \right] + \left[\mathbf{B}_{,xx} \mathbf{d}_3 \right]_{dg} \left[\mathbf{B}_{,x} \mathbf{d}_3 \right] \right] \quad (3.41)$$

Subsequently, the initial conditions of the problem are formulated in discretized form by substituting eqns. (3.34) in eqns. (3.21) yielding the following $3L$ linear equations with respect to the generalized displacements \mathbf{d}_1 , \mathbf{d}_2 , \mathbf{d}_3 and the generalized velocities $\dot{\mathbf{d}}_1$, $\dot{\mathbf{d}}_2$, $\dot{\mathbf{d}}_3$ for $t = 0$ as

$$\mathbf{B}^u \mathbf{d}_1(0) = \bar{\mathbf{u}}_0 \quad \mathbf{B}^u \dot{\mathbf{d}}_1(0) = \dot{\bar{\mathbf{u}}}_0 \quad (3.42a,b)$$

$$\mathbf{B} \mathbf{d}_2(0) = \bar{\mathbf{v}}_0 \quad \mathbf{B} \dot{\mathbf{d}}_2(0) = \dot{\bar{\mathbf{v}}}_0 \quad (3.42c,d)$$

$$\mathbf{B} \mathbf{d}_3(0) = \bar{\mathbf{w}}_0 \quad \mathbf{B} \dot{\mathbf{d}}_3(0) = \dot{\bar{\mathbf{w}}}_0 \quad (3.42e,f)$$

The above equations (4.42a,c,e), together with eqns. (3.24) written for $t = 0$, form a set of $3L + 20$ nonlinear algebraic equations which are solved to establish the initial

conditions $\mathbf{d}_1(0)$, $\mathbf{d}_2(0)$, $\mathbf{d}_3(0)$ while similarly equations (3.42b,d,f) together with 12 equations resulting after differentiating eqns. (3.24) with respect to time and writing them for $t=0$, form a set of $3L+20$ linear algebraic equations from which the initial conditions $\dot{\mathbf{d}}_1(0)$, $\dot{\mathbf{d}}_2(0)$, $\dot{\mathbf{d}}_3(0)$ are established.

The aforementioned initial conditions along with eqns. (3.24), (3.37) form an initial value problem of Differential-Algebraic Equations (DAE), which can be solved using any efficient solver. Within the framework of this doctoral dissertation two approaches have been performed. Firstly, the solution of this system was accomplished iteratively by employing the Newmark Average Acceleration Method in combination with the modified Newton Raphson Method (Chang 2004, Isaacson & Keller 1966) and secondly, the Petzold Gear Method was used (Brenan et al. 1989) after introducing new variables to reduce the order of the system (Bazant & Cedolin 1991) and after differentiating (3.24) with respect to time to obtain an equivalent system with a value of system index $\text{ind}=1$. A step-by-step algorithmic approach of the numerical implementation is summarized in a flowchart form in Fig. 3.2.

3.4 Alternative D-BEM Numerical Solution

Alternatively, the nonlinear axial-flexural dynamic analysis of Timoshenko-Rayleigh beams supported on a tensionless nonlinear three-parameter viscoelastic foundation undergoing moderate large displacements, can be numerically solved employing the domain boundary element method, as described in Appendix A2. According to the formulation presented in section 3.2, the problem reduces in establishing either both the displacement and rotational components following the system of eqns. (3.17) or only the displacement components following the combined system of eqns. (3.18). Herein, the first approach is employed in order to alleviate any inaccuracies introduced from the combination of the differential equations into a single field equation representing Timoshenko dynamics (Bhaskar 2009). To this end, the components $u(x,t)$, $v(x,t)$, $w(x,t)$, $\theta_y(x,t)$ and $\theta_z(x,t)$ are assumed to have continuous derivatives up to the second order with respect to both space x and time t variables. These components must satisfy the governing differential equations (3.17) inside the beam, the boundary conditions (3.20) at the beam ends $x=0,l$ and the initial conditions (3.21).

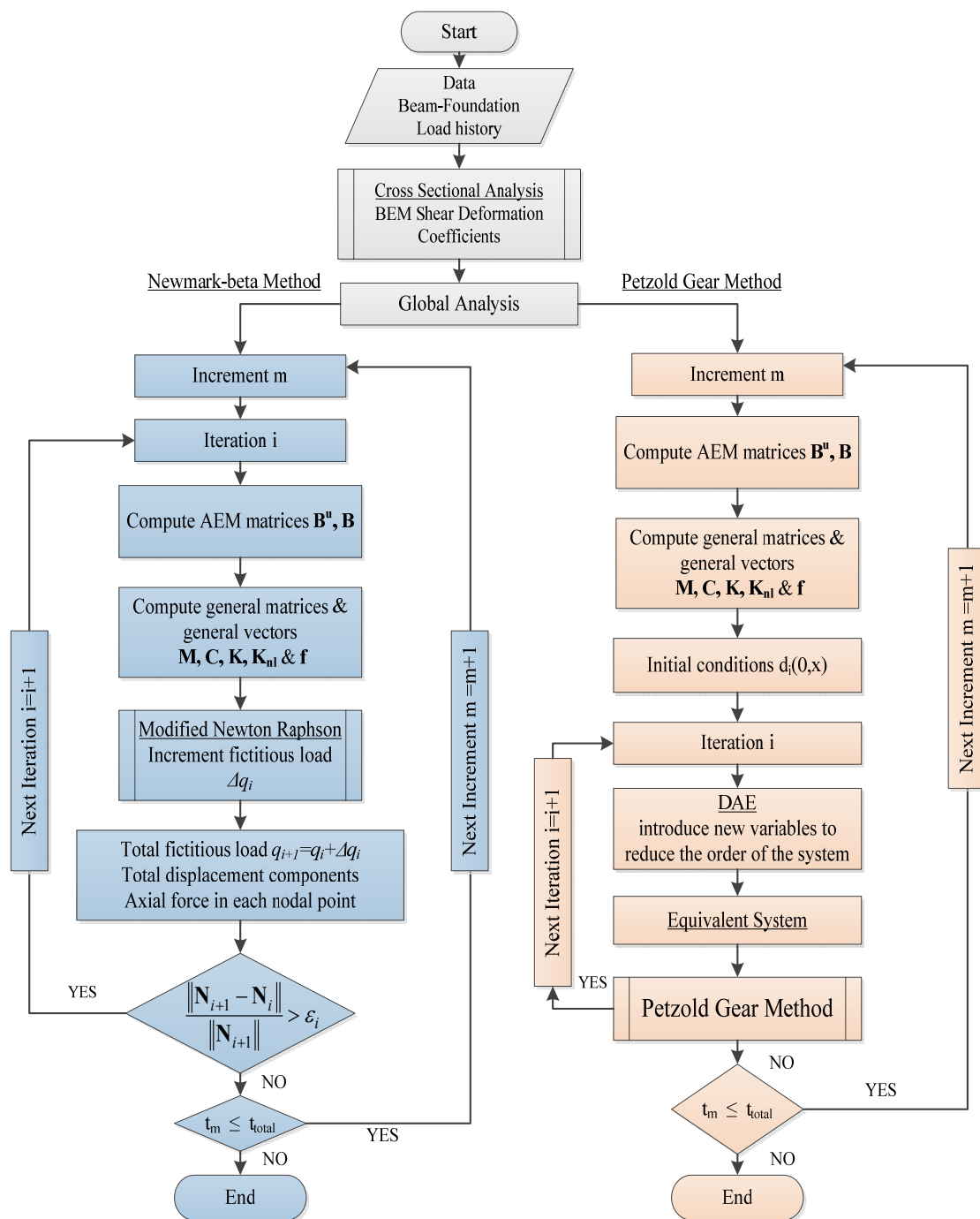


Fig.3.2. Flowchart of the numerical implementation.

3.4.1 Displacements $u(x,t)$, $v(x,t)$, $w(x,t)$ and rotations $\theta_y(x,t)$, $\theta_z(x,t)$

According to this method, let $u_1 = u(x,t)$, $u_2(x,t) = v(x,t)$, $u_3(x,t) = w(x,t)$, $u_4(x,t) = \theta_y(x,t)$ and $u_5(x,t) = \theta_z(x,t)$ be the sought solution of the problem at hand.

The solution of the second order differential equations $d^2u_i / dx^2 = q''$, ($i = 1, 2, \dots, 5$) and ($q = u, v, w, \theta_y, \theta_z$) are given in the well known integral form as

$$u_i(\xi, t) = \int_0^l \frac{\partial^2 u_i}{\partial x^2} \Lambda_2^u dx - \left[\Lambda_2^u \frac{\partial u_i}{\partial x} - \Lambda_1^u u_i \right]_0^l \quad (i = 1, 2, \dots, 5) \quad (3.43)$$

where the kernels $\Lambda_j^u(r)$, ($j = 1, 2$) are as defined in Appendix A1. Since EA , GA_z , GA_y , EI_y and EI_z are independent of x , eqns. (3.43) can be written as

$$EAu_1(\xi, t) = \int_0^l \left[EA \frac{\partial^2 u_1}{\partial x^2} \right] \Lambda_2^u dx - EA \left[\Lambda_2^u \frac{\partial u_1}{\partial x} - \Lambda_1^u u_1 \right]_0^l \quad (3.44a)$$

$$GA_y u_2(\xi, t) = \int_0^l \left[GA_y \frac{\partial^2 u_2}{\partial x^2} \right] \Lambda_2^u dx - GA_y \left[\Lambda_2^u \frac{\partial u_2}{\partial x} - \Lambda_1^u u_2 \right]_0^l \quad (3.44b)$$

$$GA_z u_3(\xi, t) = \int_0^l \left[GA_z \frac{\partial^2 u_3}{\partial x^2} \right] \Lambda_2^u dx - GA_z \left[\Lambda_2^u \frac{\partial u_3}{\partial x} - \Lambda_1^u u_3 \right]_0^l \quad (3.44c)$$

$$EI_y u_4(\xi, t) = \int_0^l \left[EI_y \frac{\partial^2 u_4}{\partial x^2} \right] \Lambda_2^u dx - EI_y \left[\Lambda_2^u \frac{\partial u_4}{\partial x} - \Lambda_1^u u_4 \right]_0^l \quad (3.44d)$$

$$EI_z u_5(\xi, t) = \int_0^l \left[EI_z \frac{\partial^2 u_5}{\partial x^2} \right] \Lambda_2^u dx - EI_z \left[\Lambda_2^u \frac{\partial u_5}{\partial x} - \Lambda_1^u u_5 \right]_0^l \quad (3.44e)$$

Solving eqns. (3.18a-e) with respect to EAu'' , $GA_y v''$, $GA_z w''$, $EI_y \theta_y''$ and $EI_z \theta_z''$ and substituting the result into eqns. (3.44a-e), respectively, the following integral representations are obtained

$$EAu_1 = \int_0^l \left[\rho A \ddot{u}_1 - EA(u_2'' u_2'' + u_3'' u_3'') + k_x u_1 - p_x \right] \Lambda_2^u dx - EA \left[\Lambda_2^u \frac{\partial u_1}{\partial x} - \Lambda_1^u u_1 \right]_0^l \quad (3.45a)$$

$$GA_y u_2 = \int_0^l \left[\rho A \ddot{u}_2 - (Nu_2')' - GA_y u_2' + p_{sy} - p_y \right] \Lambda_2^u dx - GA_y \left[\Lambda_2^u \frac{\partial u_2}{\partial x} - \Lambda_1^u u_2 \right]_0^l \quad (3.45b)$$

$$GA_z u_3 = \int_0^l \left[\rho A \ddot{u}_3 - (Nu'_3)' + GA_z u'_4 + p_{sz} - p_z \right] A_2^u dx - GA_z \left[A_2^u \frac{\partial u_3}{\partial x} - A_1^u u_3 \right]_0^l \quad (3.45c)$$

$$EI_y u_4 = \int_0^l \left[\rho I_z \ddot{u}_4 + GA_z (u'_3 + u_4) - m_y \right] A_2^u dx - EI_y \left[A_2^u \frac{\partial u_4}{\partial x} - A_1^u u_4 \right]_0^l \quad (3.45d)$$

$$EI_z u_5 = \int_0^l \left[\rho I_y \ddot{u}_5 - GA_y (u'_2 - u_5) - m_z \right] A_2^u dx - EI_z \left[A_2^u \frac{\partial u_5}{\partial x} - A_1^u u_5 \right]_0^l \quad (3.45e)$$

After carrying out several integrations by parts the above equations can be written as

$$\begin{aligned} EA u_1 = & \int_0^l \rho A \ddot{u}_1 A_2^u dx - \frac{I}{2} \int_0^l EA \left(\frac{du_2}{dx} \right)^2 A_1^u dx - \frac{I}{2} \int_0^l EA \left(\frac{du_3}{dx} \right)^2 A_1^u dx + \\ & + \int_0^l k_x u_1 A_2^u dx - \int_0^l p_x A_2^u dx + \frac{EA}{2} A_2^u \left[\left(\frac{du_2}{dx} \right)^2 + \left(\frac{du_3}{dx} \right)^2 \right]_0^l - \\ & - EA \left[A_2^u \frac{\partial u_1}{\partial x} - A_1^u u_1 \right]_0^l \end{aligned} \quad (3.46a)$$

$$\begin{aligned} GA_y u_2 = & \rho A \int_0^l \ddot{u}_2 A_2^u dx - Nu_2 + GA_y \int_0^l u_5 A_1^u dx + \int_0^l p_{sy} A_2^u dx - \int_0^l p_y A_2^u dx + \\ & + \left[Nu'_2 A_2^u \right]_0^l - \left[Nu_2 A_1^u \right]_0^l - GA_y \left[u_2 A_2^u \right]_0^l - GA_y \left[A_2^u \frac{\partial u_2}{\partial x} - A_1^u u_2 \right]_0^l \end{aligned} \quad (3.46b)$$

$$\begin{aligned} GA_z u_3 = & \rho A \int_0^l \ddot{u}_3 A_2^u dx - Nu_3 + GA_z \int_0^l u_4 A_1^u dx + \int_0^l p_{sz} A_2^u dx - \int_0^l p_z A_2^u dx + \\ & + \left[Nu'_3 A_2^u \right]_0^l - \left[Nu_3 A_1^u \right]_0^l - GA_z \left[u_3 A_2^u \right]_0^l - GA_z \left[A_2^u \frac{\partial u_3}{\partial x} - A_1^u u_3 \right]_0^l \end{aligned} \quad (3.46c)$$

$$\begin{aligned} EI_y u_4 = & \rho I_z \int_0^l \ddot{u}_4 A_2^u dx + GA_z \int_0^l u_4 A_2^u dx - GA_z \int_0^l u_3 A_1^u dx - \int_0^l m_y A_2^u dx + \\ & + GA_z \left[u'_3 A_2^u \right]_0^l - EI_y \left[A_2^u \frac{\partial u_4}{\partial x} - A_1^u u_4 \right]_0^l \end{aligned} \quad (3.46d)$$

$$\begin{aligned} EI_z u_5 = & \rho I_y \int_0^l \ddot{u}_5 A_2^u dx + GA_y \int_0^l u_5 A_2^u dx + GA_y \int_0^l u_2 A_1^u dx - \int_0^l m_z A_2^u dx - \\ & - GA_y \left[u'_2 A_2^u \right]_0^l - EI_z \left[A_2^u \frac{\partial u_5}{\partial x} - A_1^u u_5 \right]_0^l \end{aligned} \quad (3.46e)$$

Numerical methods requiring domain approximation of unknown quantities exhibit “locking” effects when Timoshenko theory is applied to cases where the Euler–Bernoulli theory could also be used ($u_4 \approx u'_2, u_5 \approx u'_3$) (Crisfield 1991, Zienkiewicz & Taylor 2005). Since domain approximation is also required in the present numerical technique, locking effects are alleviated by employing linear interpolation scheme for the longitudinal displacement and a linked interpolation scheme for the transverse displacement and the rotation due to bending. More specifically, the beam interval $(0, l)$ is divided into L elements in each of which $u_i (i = 1, \dots, 5)$ are assumed to vary according to the abovementioned law and a Gauss integration scheme is implemented assuming K integration points. Thus the displacement quantities of the beam can be written as a function of the nodal displacements

$$u_1 = N_1 u_1^i + N_2 u_1^j \quad (3.47a)$$

$$u_2 = N_1 u_2^i + N_2 u_2^j + N_3 (u_4^i - u_4^j) \quad u_3 = N_1 u_3^i + N_2 u_3^j + N_3 (u_5^i - u_5^j) \quad (3.47b,c)$$

$$u_4 = N_1 u_4^i + N_2 u_4^j \quad u_5 = N_1 u_5^i + N_2 u_5^j \quad (3.47d,e)$$

where $N_1 = \frac{l}{2}(1 - \xi)$, $N_2 = \frac{l}{2}(1 + \xi)$ and $N_3 = -\frac{L_e}{8}(1 - \xi^2)$. By applying this interpolation scheme into eqns. (3.46) and performing mathematical manipulations the governing equations of the problem have been brought into a convenient form to establish a numerical computation of the unknown quantities. Applying eqns. (3.46) to the L collocation points and employing eqns. (3.47), $5L \times K$ nonlinear equations of motion are formulated as

$$[\mathbf{M}] \begin{Bmatrix} \ddot{\mathbf{u}}_1 \\ \ddot{\mathbf{u}}_2 \\ \ddot{\mathbf{u}}_3 \\ \ddot{\mathbf{u}}_4 \\ \ddot{\mathbf{u}}_5 \end{Bmatrix} + [\mathbf{C}] \begin{Bmatrix} \dot{\mathbf{u}}_1 \\ \dot{\mathbf{u}}_2 \\ \dot{\mathbf{u}}_3 \\ \dot{\mathbf{u}}_4 \\ \dot{\mathbf{u}}_5 \end{Bmatrix} + [\mathbf{K}] \begin{Bmatrix} \mathbf{u}_1 \\ \mathbf{u}_2 \\ \mathbf{u}_3 \\ \mathbf{u}_4 \\ \mathbf{u}_5 \end{Bmatrix} + \{\mathbf{f}\}^{\text{nl}}(\mathbf{u}_1, \mathbf{u}_2, \mathbf{u}_3, \mathbf{u}_4, \mathbf{u}_5) = \{\mathbf{f}\} \quad (3.48)$$

where $\mathbf{M}, \mathbf{C}, \mathbf{K}, \mathbf{f}$ are generalized mass, damping, stiffness matrices and force vector, respectively and \mathbf{f}^{nl} is a nonlinear generalized stiffness vector. The boundary integral

equations (BIEs) at the interval of the beam, together with the boundary conditions (3.20) at the beam ends $x=0,l$ and the initial conditions (3.21) form a set of $5L \times K + 10$ nonlinear algebraic equations with respect to the unknowns of the problem at hand. The aforementioned initial boundary value problem consisting of differential-algebraic equations (DAE) can be solved using any efficient solver. In this study, the Petzold Gear Method was used (Brenan et al. 1989) after introducing new variables to reduce the order of the system (Bazant & Cedolin 1991) to obtain an equivalent system with a value of system index $\text{ind}=1$. Having solved the initial value problem, the derivatives of each quantity and subsequently the stress resultants can be easily calculated at every point of the interval $(0,l)$ by employing the boundary integral equations derived by differentiating eqns. (3.46) with respect to x . A step-by-step algorithmic approach of the numerical implementation is summarized in a flowchart form in Fig. 3.3.

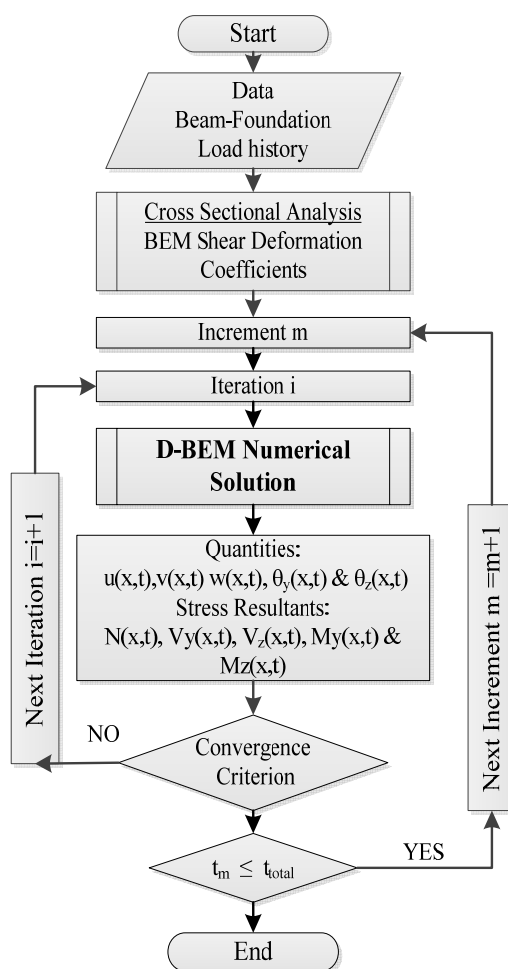


Fig.3.3. Flowchart of the D-BEM numerical implementation.

3.5 Numerical Examples

On the basis of the analytical and numerical procedures presented in the previous sections concerning the geometrically nonlinear dynamic analysis of shear deformable beams on nonlinear foundation, a computer program has been written using High Level 3G Fortran 90/95. Representative examples have been studied to demonstrate the efficiency, wherever possible the accuracy and the range of applications of the developed method. In all the examples treated, the results have been obtained using $L = 21$ nodal points (longitudinal discretization), 400 boundary elements (cross section discretization) and a time step of $\Delta t = 1.0 \mu sec$, unless it is stated otherwise.

3.5.1 Example 1 – Linear Analysis of Simply Supported Beam on Pasternak Foundation

In the first example, for comparison purposes the linear dynamic analysis of a simply supported beam of length $l = 6.096 m$ ($E = 24.82 GPa$, $\rho = 3387 Kg / m^3$, $\nu = 0.3$, $I = 143.9 \times 10^{-5} m^4$) resting on a homogeneous viscoelastic Pasternak (either bilateral or unilateral) foundation with modulus of subgrade reaction $k_{Lz} = 16.55 MN / m^2$, $k_{pz} = 16.55 MN$, as shown in Fig.3.4a is examined. The beam is subjected to a triangular impulsive load of amplitude $P_{l/2} = 100 kN$ at its midpoint (Fig. 3.4b).

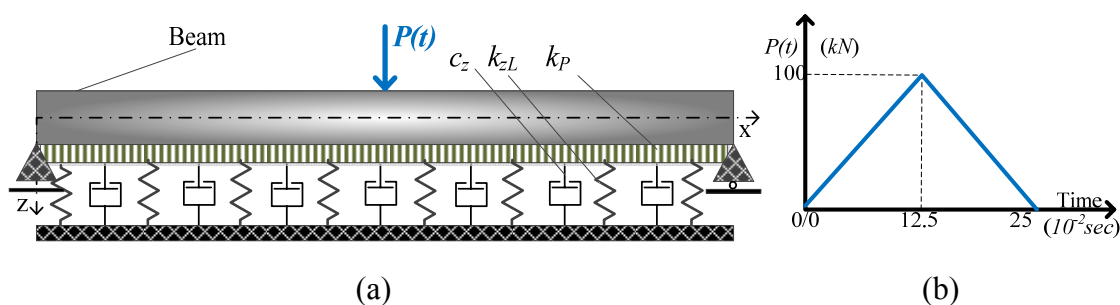


Fig. 3.4. Simply supported beam on viscoelastic Pasternak foundation (a) subjected to a triangular impulsive load (b).

The free vibrations case of this example has been analyzed by Timoshenko et al. (1974), Lai et al. (1992), Thambiratnam and Zhuge (1996) and Friswell et al. (2007) assuming Winkler foundation, while the forced vibrations one by Calim (2009). In Table 3.1, the evaluated first five natural frequencies of the beam resting on the bilateral elastic Winkler foundation are presented as compared with those obtained from

literature. In Figs. 3.5, 3.6a,b the time history of the transverse displacement $w(l/2)$ at the beam's midpoint, of the bending moment $M_y(l/2)$ at the same point and of the shear force $Q_z(l)$ at the right supported end, respectively are presented either for bilateral or unilateral Winkler elastic foundation model and compared with those obtained from a complementary functions method and a FEM solution (Calim 2009) demonstrating the accuracy of the results of the proposed method. Moreover, in Table 3.2 the extreme values of the displacement w and of the soil reaction p_{sz} at the beam's midpoint are also presented for both cases of bilateral and unilateral soil reaction.

Table 3.1. First five natural frequencies (Hz) of the beam of example 1.

Analysis / Modes	1	2	3	4	5
Timoshenko et al. (1974)	32.9032	56.8135	112.908	–	–
Lai et al (1992)	32.9049	56.8220	111.973	–	–
Thambiratnam & Zhuge (1996)	32.9033	56.8193	111.961	–	–
Friswell et al.(2007)	32.8980	56.8080	111.900	193.760	–
Calim (2009) - CFM	32.8633	56.5972	110.759	189.939	222.078
ANSYS FEM (Calim 2009)	32.8624	56.5891	110.739	189.901	222.043
Present Study	32.7946	56.5476	110.722	189.489	222.077

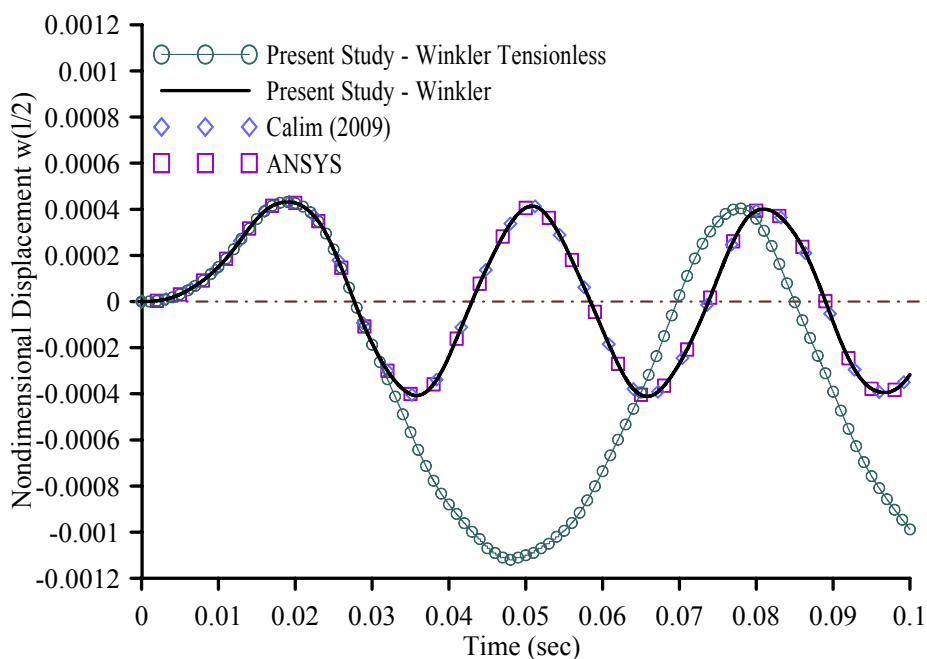


Fig. 3.5. Midpoint displacement time history of the beam of example 1.

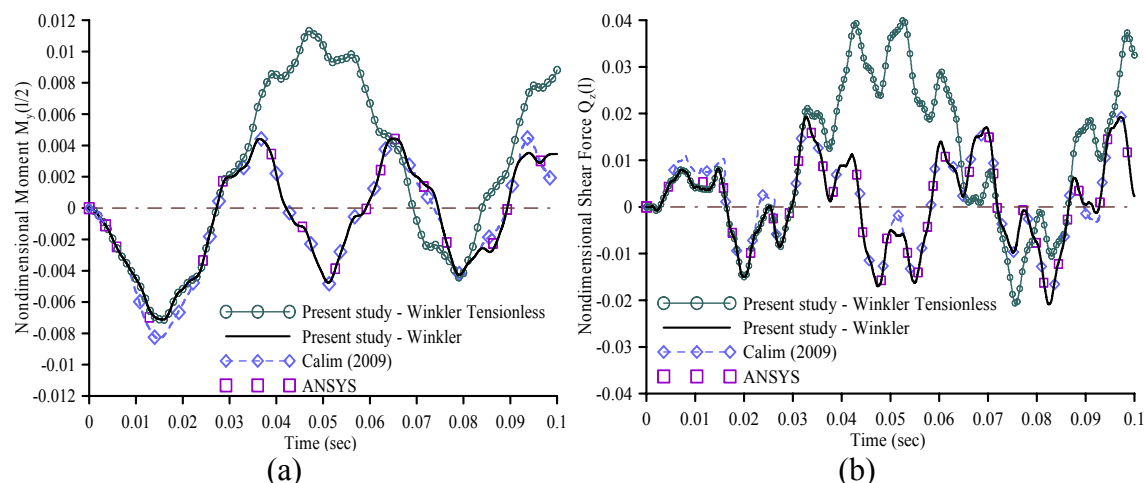


Fig. 3.6. Time history of the midpoint bending moment (a) and of the shear force at the right supported end (b) of the beam of example 1.

Table 3.2. Extreme values of the midpoint displacement w and foundation reaction p_{sz} of the beam of example 1.

Midpoint ($l/2$)	Winkler		Tensionless Winkler	
	w (mm)	p_{sz} (kN)	w (mm)	p_{sz} (kN)
Max	2.63	43.6	2.63	43.6
Min	-2.50	-41.5	-6.80	0.00

Additionally, in Figs. 3.7a,b the time histories of the transverse displacement $w(l/2)$ and the bending moment $M_y(l/2)$ at the beam's midpoint are presented for various values of the damping coefficient c_z (kNs/m^2). In this figure the corresponding curves obtained from the solution of the same beam resting on a Pasternak-type viscoelastic foundation are also presented employing the complementary functions method in order to calculate the element dynamic stiffness matrix in the Laplace domain (Calim 2009). The Pasternak-type viscoelastic foundation is characterized by the Winkler spring constant which is multiplied by the displacement, the visco-compressibility coefficient which is multiplied by the derivative of the displacement with respect to time, the Pasternak spring constant which is multiplied by the rotation and the viscosity coefficient which is multiplied by the derivative of the bending rotation with respect to time. Comparing the obtained results and those from literature the accuracy of the proposed method is verified. The small discrepancies between the

proposed results and those obtained from literature are attributed to the additional viscosity term of the Pasternak-type model that causes smaller amplitudes and less damping time. Moreover, in Table 3.3 the extreme values of the displacement $w(l/2)$ and the bending moment $M_y(l/2)$ at the beam-column's midpoint and of the shear force $Q_z(l)$ at its right supported end are also presented for various values of the damping coefficient and for both Pasternak-type and Winkler-type foundations.

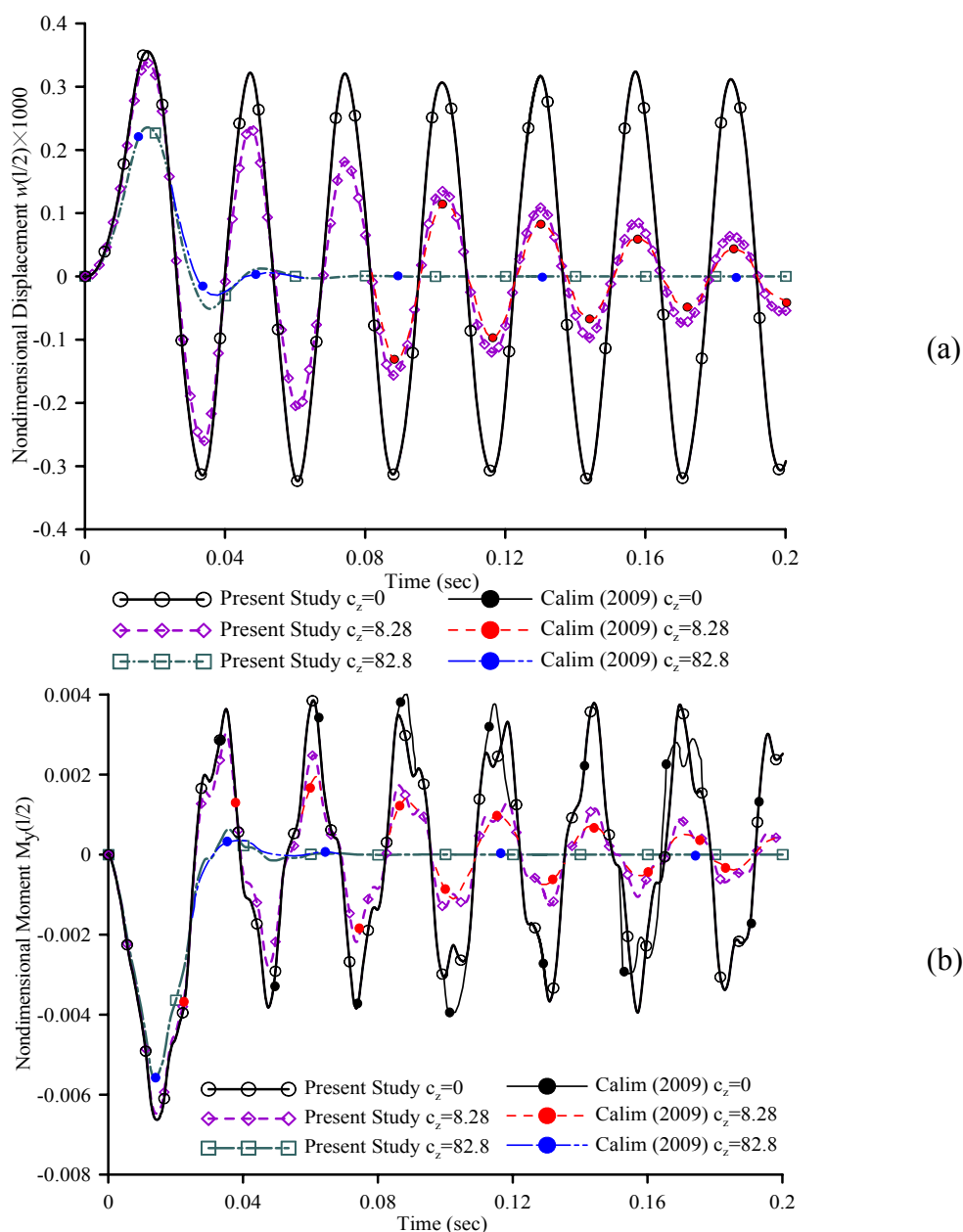


Fig. 3.7. Midpoint time history of the displacement (a) and bending moment (b) of the beam for various values of the damping coefficient of example 1.

Table 3.3. Extreme values of the displacement w (mm), bending moment M_y (kN/m) and shear force Q_z (kN) of the beam of example 1.

	Pasternak			Winkler		
	$w(l/2)$	$M_y(l/2)$	$Q_z(l)$	$w(l/2)$	$M_y(l/2)$	$Q_z(l)$
Max values						
$c_z = 0$	2.17	22.6	16.7	2.63	27.6	21.3
$c_z = 1.655$	2.15	20.7	16.4	2.60	25.9	19.0
$c_z = 8.28$	2.06	17.8	14.2	2.48	22.1	16.2
$c_z = 16.55$	1.96	14.9	11.9	2.34	18.1	13.3
$c_z = 82.8$	1.44	3.74	7.51	1.65	3.56	9.68
Min values						
$c_z = 0$	-1.97	-38.9	-16.4	-2.51	-43.4	-21.1
$c_z = 1.655$	-1.85	-38.7	-14.3	-2.38	-43.1	-18.6
$c_z = 8.28$	-1.59	-37.9	-11.3	-2.02	-4.21	-13.9
$c_z = 16.55$	-1.33	-37.1	-9.62	-1.65	-4.10	-1.26
$c_z = 82.8$	-0.31	-3.27	-5.33	-0.31	-3.57	-6.62

3.5.2 Example 2 – Nonlinear Analysis of Hollow Rectangular Beam on Winkler Foundation

In order to illustrate the importance of the nonlinear analysis and the influence of the shear deformation effect in flexural vibrations, a clamped beam of length $l = 4.90\text{m}$, having a hollow rectangular cross section ($E = 210\text{GPa}$, $\nu = 0.3$, $a_z = 3.664$, $a_y = 1.766$, $\rho = 7.85\text{tn/m}^3$) resting on a homogeneous (either bilateral or unilateral) elastic foundation of stiffness k_z , as this is shown in Fig. 3.8 is examined.

In Figs. 3.9a,b the displacement curves $w(x,t)$ along the beam subjected to a suddenly applied consecrated bending moment $M_y = 200\text{kNm}$ at its midpoint are presented at the time instant $t = 1.6 \times 10^{-2}\text{sec}$ for various values of the stiffness k_z for the cases of bilateral and unilateral soil reaction, respectively. The influence of both the foundation stiffness parameter k_z and the unilateral character of the soil reaction are easily verified. Moreover, in Fig. 3.10 the time history of the central transverse

displacement $w(l/2)$ and in Table 3.4 the maximum central displacement $w_{max}(m)$ and the period $T_z(sec)$ of the first cycle of motion of the beam additionally subjected to a uniformly distributed load $p_z = 350 kN/m$ (Fig. 3.8) are presented for a unilateral subgrade model with $k_z = 645 kPa$, performing either linear or nonlinear analysis and taking into account or ignoring both shear deformation effect and rotary inertia. From the obtained results, the discrepancy between the linear and the nonlinear analysis is not negligible and should not be ignored, while the significant influence of the shear deformation effect increasing both central transverse displacement and the obtained period of the first cycle of motion is remarked in both linear and nonlinear analysis.

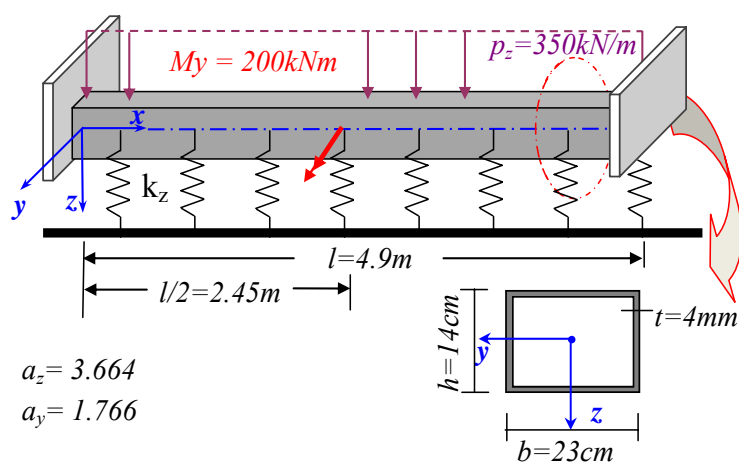


Fig. 3.8. Clamped beam of hollow rectangular cross section subjected to concentrated bending moment M_y and uniformly distributed load p_z .

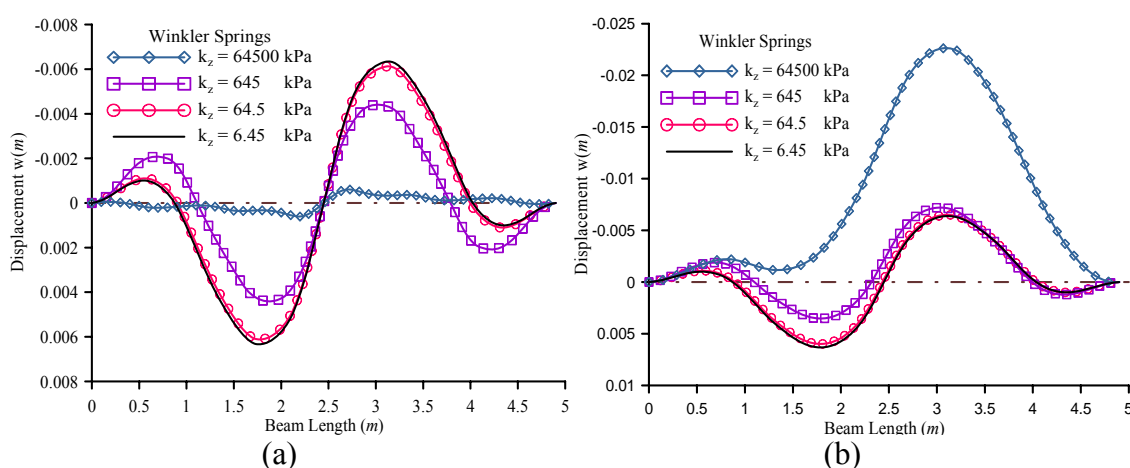


Fig. 3.9. Displacement along the beam of example 2, for various stiffness k_z values of the bilateral (a) and unilateral (b) Winkler springs.

Table 3.4. Maximum central displacement w_{max} (m) and period T_z (sec) of the first cycle of motion of the clamped beam of example 2.

Analysis	Without Shear Deformation		With Shear Deformation	
	Linear	Nonlinear	Linear	Nonlinear
w_{max}	0.3729	0.2572	0.3914	0.2688
T_z	0.01890	0.01482	0.01973	0.01607

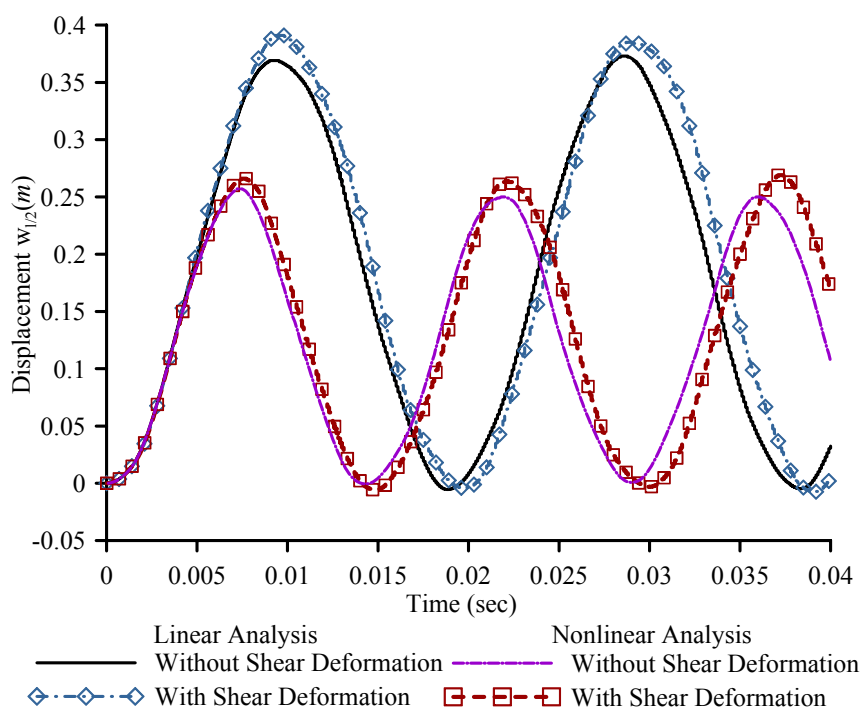


Fig. 3.10. Time history of the central displacement of the beam of example 2, for a unilateral subgrade model with $k_z = 645.0$ kPa.

3.5.3 Example 3 – Partially Embedded Pile in Winker Foundation

In the third example, a partially embedded pile in a homogeneous elastic Winker foundation with spring stiffness $k_z = k_y = 85.0$ MN/m², of total length $l = 15.0$ m ($l_{free} = 6.20$ m, $l_{embed} = 8.80$ m), of circular cross section of diameter $D = 1.0$ m ($E = 29$ GPa, $A = 0.785$ m², $\nu = 0.2$, $I_y = I_z = 0.049$ m⁴, $a_y = a_z = 1,172$), as this is shown in Fig. 3.11 has been studied. According to its boundary conditions, the pile end

at the elastic foundation is clamped, while the other end is free according to its displacements and blocked according to its rotations. The pile is subjected to a suddenly applied concentrated axial load $P_x(0,t)=1.0MN$, ($t \geq 0.0$) and to a uniformly distributed transverse load $p_y(t)=500kN/m$, ($t \geq 0.0$) acting to the free part of the length of the pile.

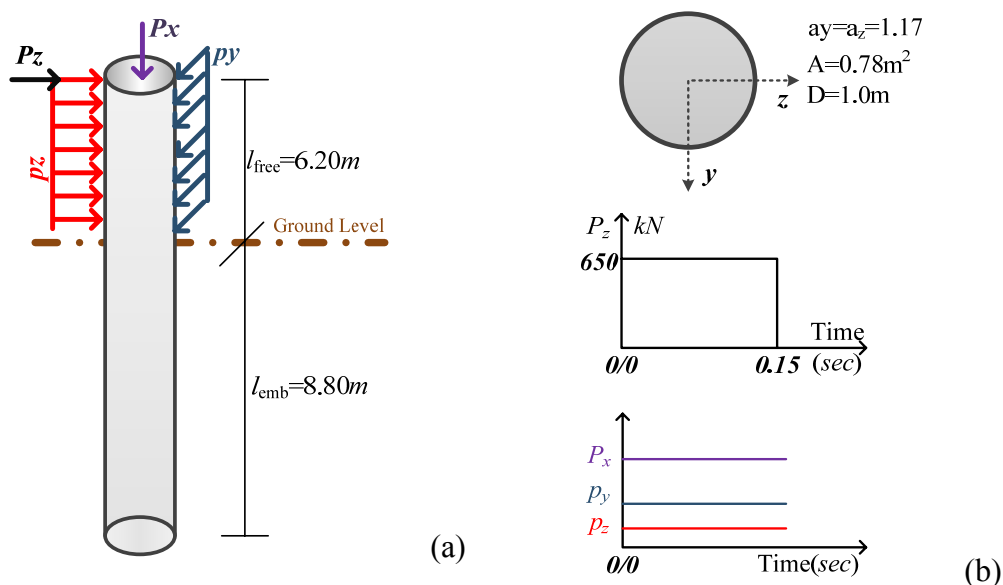


Fig. 3.11. Pile of circular cross section in axial-flexural loading subjected to rectangular impulsive concentrated load P_z , concentrated axial load P_x and to uniformly distributed loading p_y , p_z .

In Figs. 3.12a,b the time history of the head displacement v_{top} of the pile and the displacement v along the pile at the time instant $t=7.0 \cdot 10^{-2}sec$ are presented, respectively performing either linear or nonlinear analysis, taking into account or ignoring both rotary inertia and shear deformation effect. Moreover, in Table 3.5 the maximum value of the head displacement v_{max} and the period T_y of the first-cycle of motion are presented for the aforementioned cases.

Moreover, the examined pile in addition to the aforementioned loading is also subjected to a uniformly distributed load $p_z=100kN/m$ at its free length and to a suddenly applied concentrated load $P_z(t)=650kN$, $t \in [0,0.15]$ acting at its top, as shown in Fig. 3.11. In Fig. 3.13 the time history of the head displacement of the pile w_{top} performing either linear or nonlinear analysis is presented taking into account or

ignoring shear deformation effect. Finally, in Table 3.6 the maximum values of the head displacements v_{max} , w_{max} and the periods T_y, T_z of the first cycle are presented for the same cases of analysis. It is worth noting that the minor discrepancy of the head displacement v_{max} between Tables 3.5, 3.6 is due to the coupling effect of the transverse displacements in y, z directions in the nonlinear analysis.

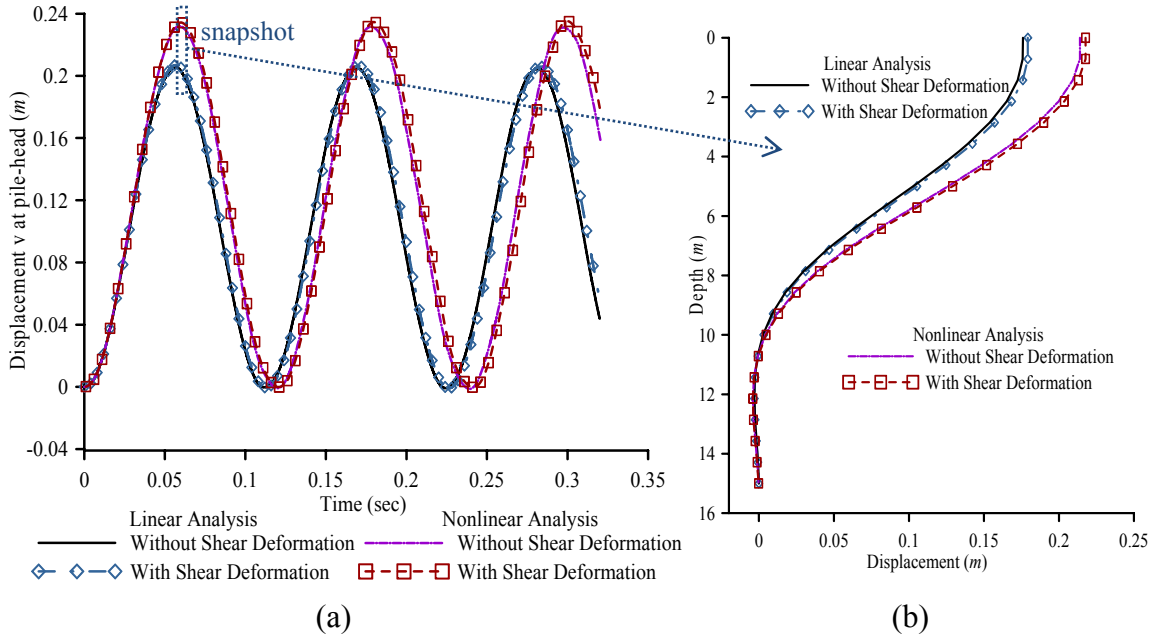


Fig.3.12. Head displacement time history (a) and displacement v at 7×10^{-2} sec time instant along the pile (b) of example 3.

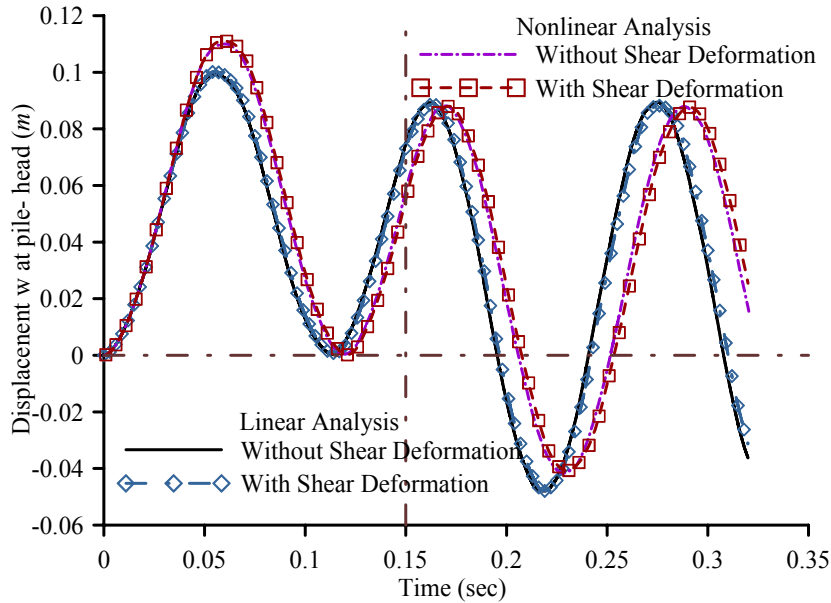


Fig. 3.13. Head displacement time history w_{top} of the pile of example 3.

Table 3.5. Maximum head displacement and period of the first cycle of motion of the pile of example 3.

Analysis	Without Shear Deformation		With Shear Deformation	
	Linear	Nonlinear	Linear	Nonlinear
$v_{max} (m)$	0.2699	0.2321	0.2699	0.2353
T_y	0.1105	0.1180	0.111	0.1201

Table 3.6. Maximum head displacements and periods of the first cycle of the pile of example 3.

Analysis	Without Shear Deformation		With Shear Deformation	
	Linear	Nonlinear	Linear	Nonlinear
$v_{max} (m)$	0.2054	0.2320	0.2070	0.2351
$w_{max} (m)$	0.0992	0.1109	0.1002	0.1111
$T_y (sec)$	0.1105	0.1172	0.1111	0.1192
$T_z (sec)$	0.1133	0.1189	0.1143	0.1215

3.5.4 Example 4 – Fully Embedded Hollow Circular Pile in Non-constant Stiffness Soil

In this example, a fully embedded in stiff cohesive soil with non constant stiffness free head pile of length $l=8.0 m$ of a hollow circular cross section ($E=210 GPa$, $\rho=7.85 tn/m^3$, $\alpha_y=a_z=2.226$, $\nu=0.3$), as shown in Fig. 3.14 is examined. The pile is subjected to a concentrated axial $P_x(t)=500 kN$, ($t \geq 0.0$) and transverse loading $P_z(t)=750 \cos(\omega_{f,lin}t) kN$ acting at the tip, where $\omega_{f,lin}=614.329 rad/sec$ is the first natural frequency of the pile-soil system.

In Figs. 3.15, 3.16 the time history of the pile head displacement w_{top} and the displacement w along the pile at the time instant $t=0.04 sec$ are presented, respectively, performing either linear or nonlinear analysis and taking into account or ignoring both rotary inertia and shear deformation effect. The discrepancy between linear and nonlinear analysis is remarkable, while in the resonance case the beating phenomenon observed in the nonlinear response (Fig. 3.15) is explained from the fact that large head displacements increase the beam's fundamental natural frequency ω_f

(by increasing the stiffness of the beam), thereby causing a detuning of ω_f with the frequency of the external loading. Since the head displacement reaches its maximum value, the amplitude of displacements decreases, leading to the reversal of the previously mentioned effects.

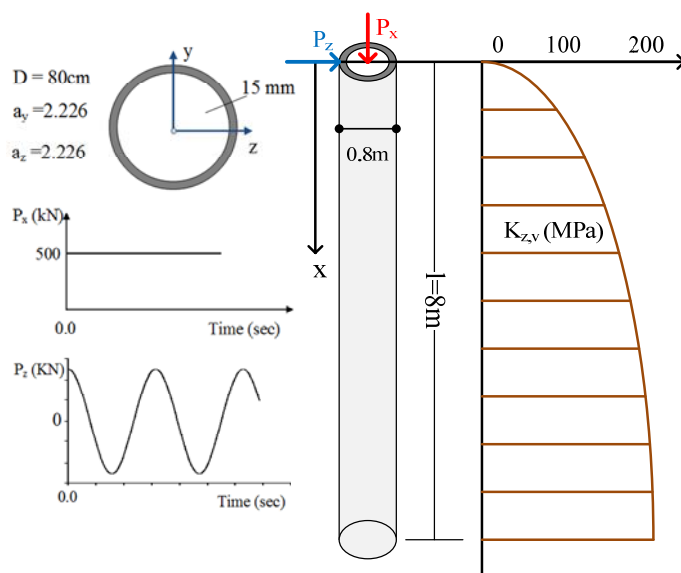


Fig. 3.14. Hollow circular pile embedded in non constant stiffness soil subjected to concentrated axial P_x and transverse P_z head loading.

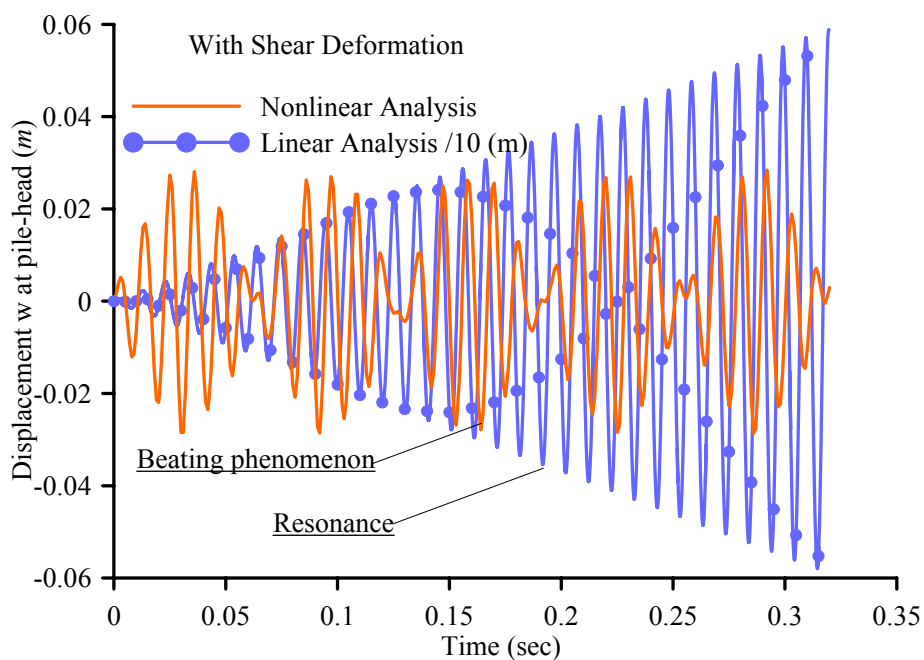


Fig. 3.15. Head displacement time history w_{top} of the pile of example 4 (for graphic purposes displacements obtained from linear analysis are divided by 10).

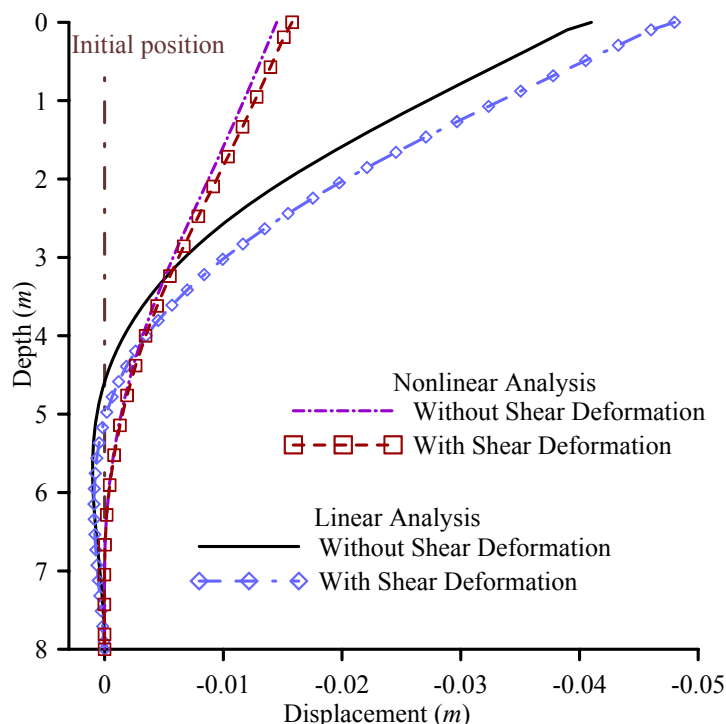


Fig. 3.16. Displacement at time instant $t = 0.04$ sec along the pile of example 4.

3.5.5 Example 5 – Clamped Beam on Nonlinear Three-Parameter Viscoelastic Foundation. Resonance and Damping Effects

In order to illustrate the importance of both the nonlinear analysis and the shear deformation effects in flexural vibrations, a clamped beam of length $l = 2m$, having a hollow rectangular cross section $0.15 \times 0.10 \times 0.01 m$ ($E = 210 GPa$, $\nu = 0.3$, $a_z = 3.263$, $a_y = 1.778$, $\rho = 7.85 tn/m^3$) is examined. The beam is resting on a Winkler viscoelastic foundation with modulus of subgrade reaction $k_{Lz} = 2MPa$, damping coefficient $c = 4.8kNs / m^2$ and is subjected to a uniformly distributed transverse load $p_z(x, t) = 1000kN / m$. For the validation of the proposed numerical method, the obtained result have been compared with a FEM solution (NX-Nastran 2007) obtained by implementing 41 Beam elements and a 3-D FEM solution (NX-Nastran 2007) obtained by employing 4600 Solid Hexahedral (brick) elements (Fig. 3.17).

In Fig. 3.18 the time history of the beam's midpoint displacement $w(l/2)$ free of foundation support performing either linear or nonlinear analysis and taking into account or ignoring both shear deformation effect and rotary inertia is presented as

compared with those obtained from the aforementioned FEM models, while in Fig. 3.19 the same results are presented assuming the beam on Winkler viscoelastic foundation. Moreover, in Table 3.7 the maximum values of the displacement of the Timoshenko beam taking into account or ignoring the damping effect are presented as compared with the FEM models for different values of the distributed load. The accuracy of the proposed method is verified for both linear and nonlinear analysis.

As a variant of the above example, the examined beam is resting on a nonlinear viscoelastic c_z (kNs / m^2) three-parameter foundation with moduli $k_{Lz} = 20MPa$, $k_{NLz} = 20MN / m^4$, $k_{pz} = 10MN$. Two cases of loading are examined namely; (*load case i*) a transverse concentrated load $P_z(l/2, t) = 100 \sin(\omega_{f,lin} t) kN$ acting at its midpoint, where $\omega_{f,lin} = 1345.7 rad / sec$ is the fundamental frequency of the linear beam-soil system and (*load case ii*) an orthogonal impulsive load of amplitude $p_z = 200kN / m$.

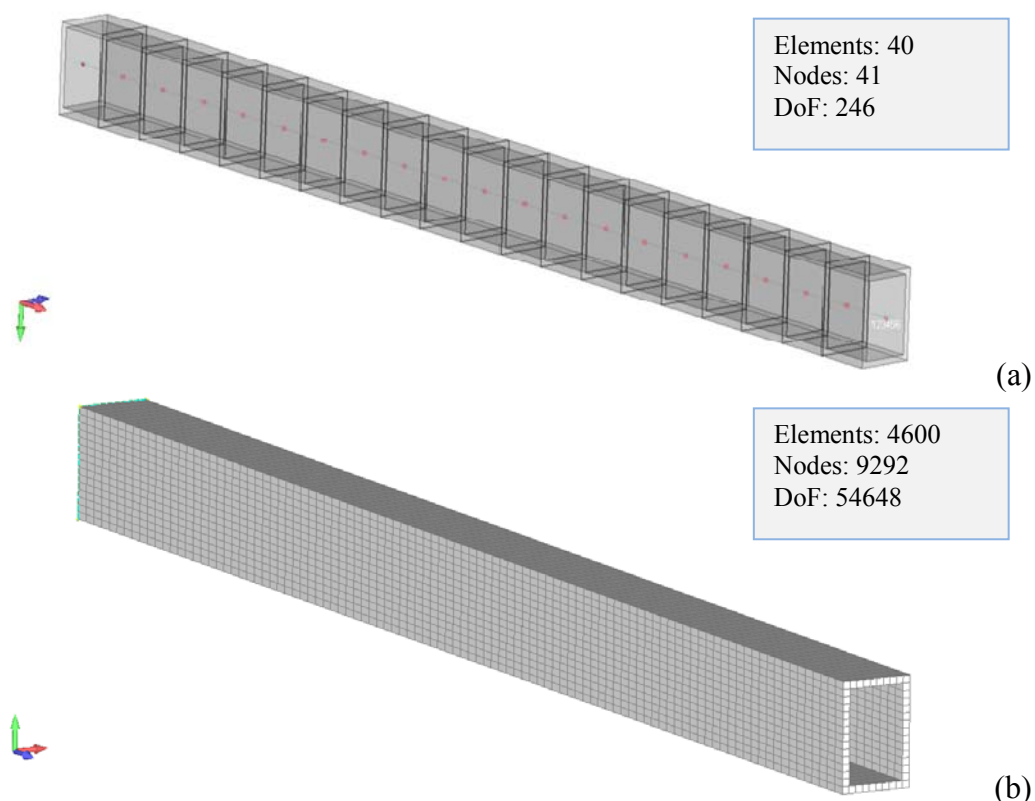


Fig. 3.17. Clamped beam implemented in NX-Nastran (2007) with Beam Elements (a) and Solid Hexahedral (brick) Elements (b)

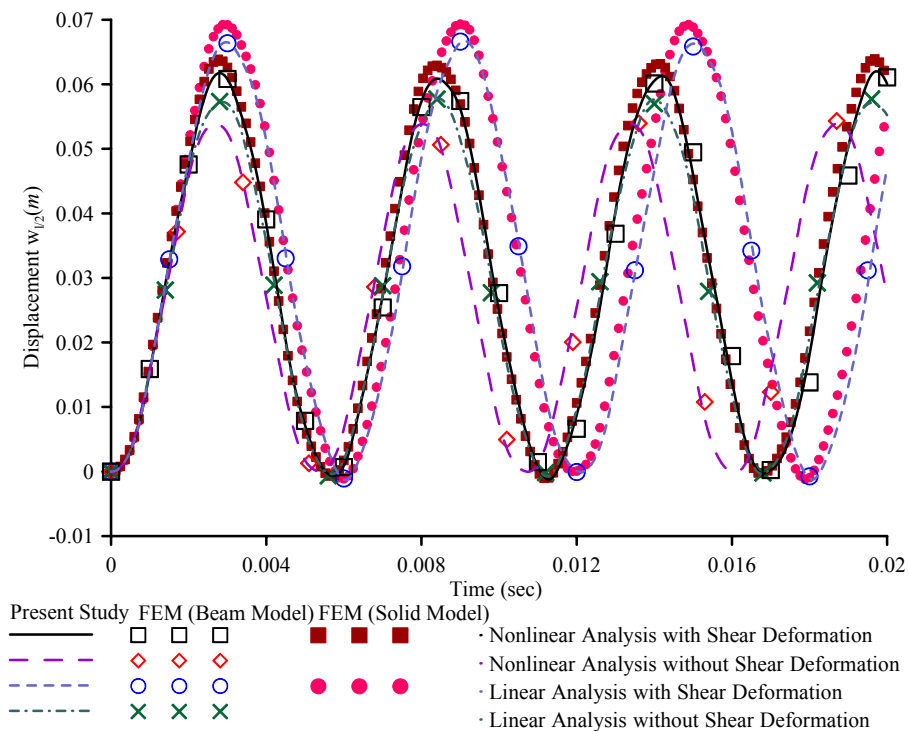


Fig. 3.18. Midpoint displacement time history $w(l/2)$ of the beam of example 5, free of foundation support.

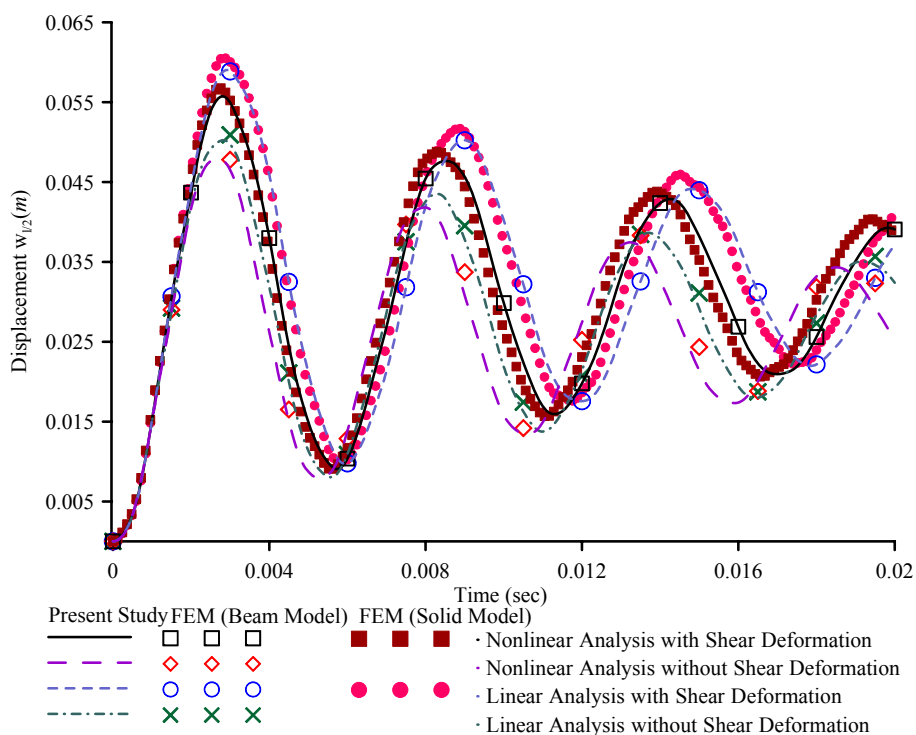


Fig. 3.19. Midpoint displacement time history $w(l/2)$ of the beam of example 5, resting on Winkler viscoelastic foundation.

Table 3.7. Maximum displacement of the clamped Timoshenko beam on Winkler viscoelastic foundation of example 5, for different loading values.

w_{max} (cm)	Present Study		FEM (Beam Model)		FEM (Solid Model)	
	Linear	Nonlinear	Linear	Nonlinear	Linear	Nonlinear
p_z (kN/m)	No Damping ($c = 0$)					
1000	6.370	5.936	6.349	5.949	6.623	6.078
2000	12.741	10.431	12.699	10.462	13.245	10.567
3000	19.111	13.841	19.048	13.813	19.868	13.981
	With Damping ($c = 4.8kNs / m^2$)					
1000	5.784	5.440	5.772	5.466	6.011	5.6801
2000	11.576	9.732	11.543	9.771	12.021	9.905
3000	17.354	13.063	17.315	13.038	18.031	13.127

In Fig. 3.20a the time history of the beam's midpoint displacement $w(l/2)$ resting on a linear Winkler foundation ($k_{Lz} = 20MPa$, $k_{NLz} = k_{Pz} = 0$) is presented ignoring or accounting for geometrical nonlinearity, while in Fig. 3.20b the time history of the beam's midpoint displacement resting on a three-parameter foundation performing a nonlinear analysis is presented taking into account or ignoring both shear deformation effect and rotary inertia.

According to Fig. 3.20a the beating phenomenon is observed in the nonlinear response contrary to the resonance occurred in the linear one. This is explained from the fact that large displacements increase the beam's fundamental natural frequency ω_f (by increasing the stiffness of the beam), thereby causing a detuning of ω_f with the frequency of the external loading ($\omega_{f,lin}$). Since the displacement reaches its maximum value, the displacement amplitude decreases, leading to the reversal of the previously mentioned effects. In Table 3.8 the maximum displacements of the midpoint $w(l/2)$ performing either a linear or a nonlinear analysis and taking into account or ignoring both shear deformation effect and rotary inertia are presented for different types of foundation reaction. From this figure and table the intense influence of these effects is remarked.

Finally, in Fig.3.21 the time history of the beam's midpoint displacement $w(l/2)$ performing nonlinear analysis and taking into account both shear deformation effect and rotary inertia is presented for various values of the damping coefficient c_z , while in Table 3.9 the maximum values of the displacement w_{max} and the period T_z of the first cycle of motion are presented for all the cases of analysis for $c_z = 0$.

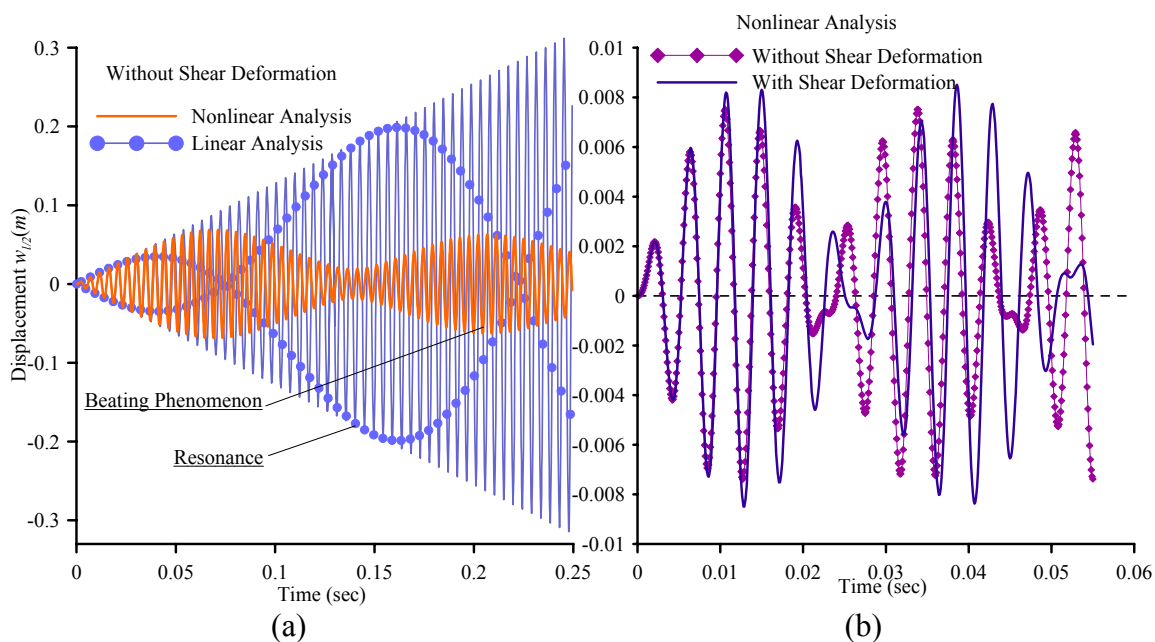


Fig. 3.20. Midpoint displacement time history $w(l/2)$ of the beam of example 5 resting on Winkler (a) or 3-parameter foundation (b) (load case i).

Table 3.8. Maximum displacement of the beam of example 5 for different types of foundation reaction (load case i).

w_{max} (mm)	Without Shear Deformation		With Shear Deformation	
	Linear	Nonlinear	Linear	Nonlinear
Linear Winkler	Resonance- ∞	68.827	–	–
Pasternak	7.729	7.511	9.178	8.507
Linear & Nonlinear Winkler	11.866	10.932	14.468	12.678
Three-Parameter	7.512	7.495	8.922	8.305

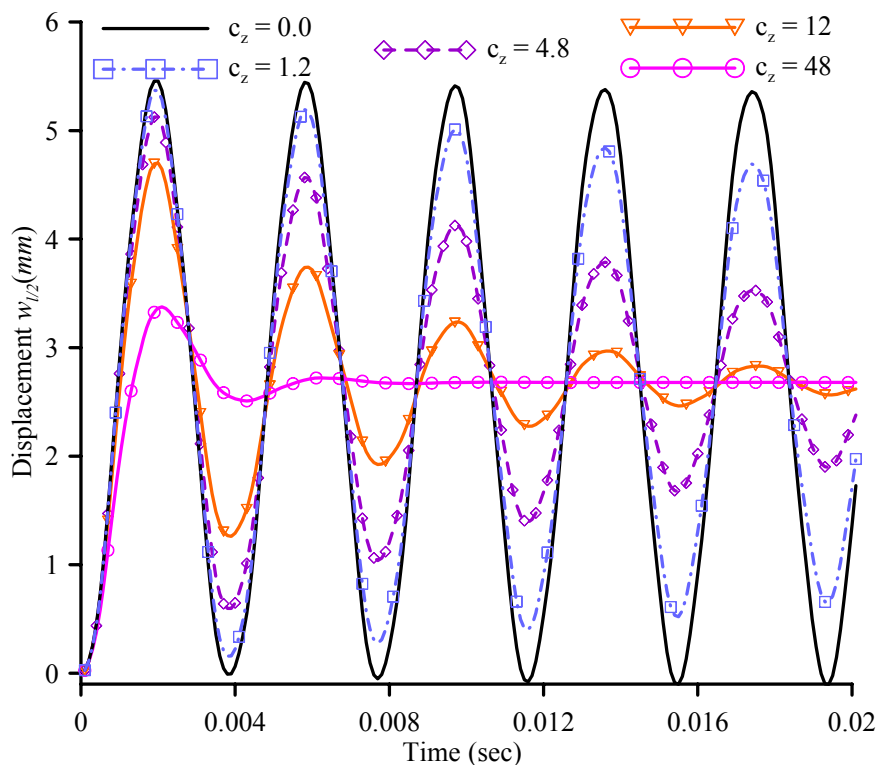


Fig. 3.21. Midpoint displacement time history $w(l/2)$ of the beam of example 5, resting on a 3-parameter viscoelastic foundation (load case ii).

Table 3.9. Maximum displacement and period of the first cycle of motion of the beam of example 5 (load case ii).

Analysis	Without Shear Deformation		With Shear Deformation	
	Linear	Nonlinear	Linear	Nonlinear
w_{max} (mm)	6.12	5.46	6.41	5.73
T_z (ms)	4.01	3.81	4.14	3.95

3.5.6 Example 6 – Partially Embedded Column-Pile in Nonlinear Three-Parameter Viscoelastic Foundation

In this example, a partially embedded column-pile of total length $l = 10m$ ($l_{free} = 3.0m$, $l_{embed} = 7m$) of circular cross section of diameter $D = 0.5m$ ($E = 29GPa$, $\nu = 0.2$, $A = 0.196m^2$, $I_y = I_z = 3.066 \times 10^{-3}m^4$) is studied. The foundation model is characterized by the linear Winkler modulus $k_L = 17.4MN / m^2$, the nonlinear Winkler

one $k_{NL} = 17.4GN / m^4$, the Pasternak (shear) modulus $k_p = 8.7MN$ and the damping coefficient $c = 12kNs / m^2$. According to its boundary conditions, the embedded column-pile end is free, while the other end is free according to its displacements and blocked according to its rotations. The column-pile is subjected to a concentrated compressive axial load $P_x(0,t) = 1.5MN$, ($t \geq 0.0$) and to a concentrated transverse force $P_z(0,t) = 1MN$, ($t \geq 0.0$) acting at its top.

In Fig. 3.22a,b the time histories of the head displacement w_{top} of the column-pile embedded in a Winkler type foundation are presented for two values of the damping coefficient ($c = 0$ or $12kNs / m^2$) respectively, taking into account the rotary inertia and the shear deformation effect, performing either a linear or a nonlinear analysis. The obtained results are also compared with those from a FEM solution (NX Nastran 2007) employing the Beam Element formulation. Moreover, in Fig. 3.23 the time histories of the head displacement w_{top} of the column-pile for various models of the mechanical behaviour of the subsoil are presented performing a nonlinear analysis and taking into account the rotary inertia and shear deformation effect, while in Table 3.10 the maximum values of the head displacement w_{max} and the periods T_z of the first-cycle of motion are presented for the aforementioned cases of analysis. Finally, in Fig. 3.24 the static deflection curves of the column-pile performing either a linear or a nonlinear static analysis for various foundation models are presented, taking into account the shear deformation effect. The influence of the nonlinear Winkler and Pasternak (shear) moduli on the response of the beam-column is observed.

Finally, in order to demonstrate the coupling effect of the transverse displacements in both directions in the nonlinear analysis, the examined column-pile additionally to the already described loading is also subjected to a concentrated transverse force $P_y(0,t) = 2MN$, acting also at its top. In Table 3.11 the maximum values of the head transverse displacements w_{max} , v_{max} are presented performing either a linear or a nonlinear analysis for the aforementioned foundation models. The difference in the elements of the first columns of Tables 3.10, 3.11 is due to the coupling effect of the transverse displacements.

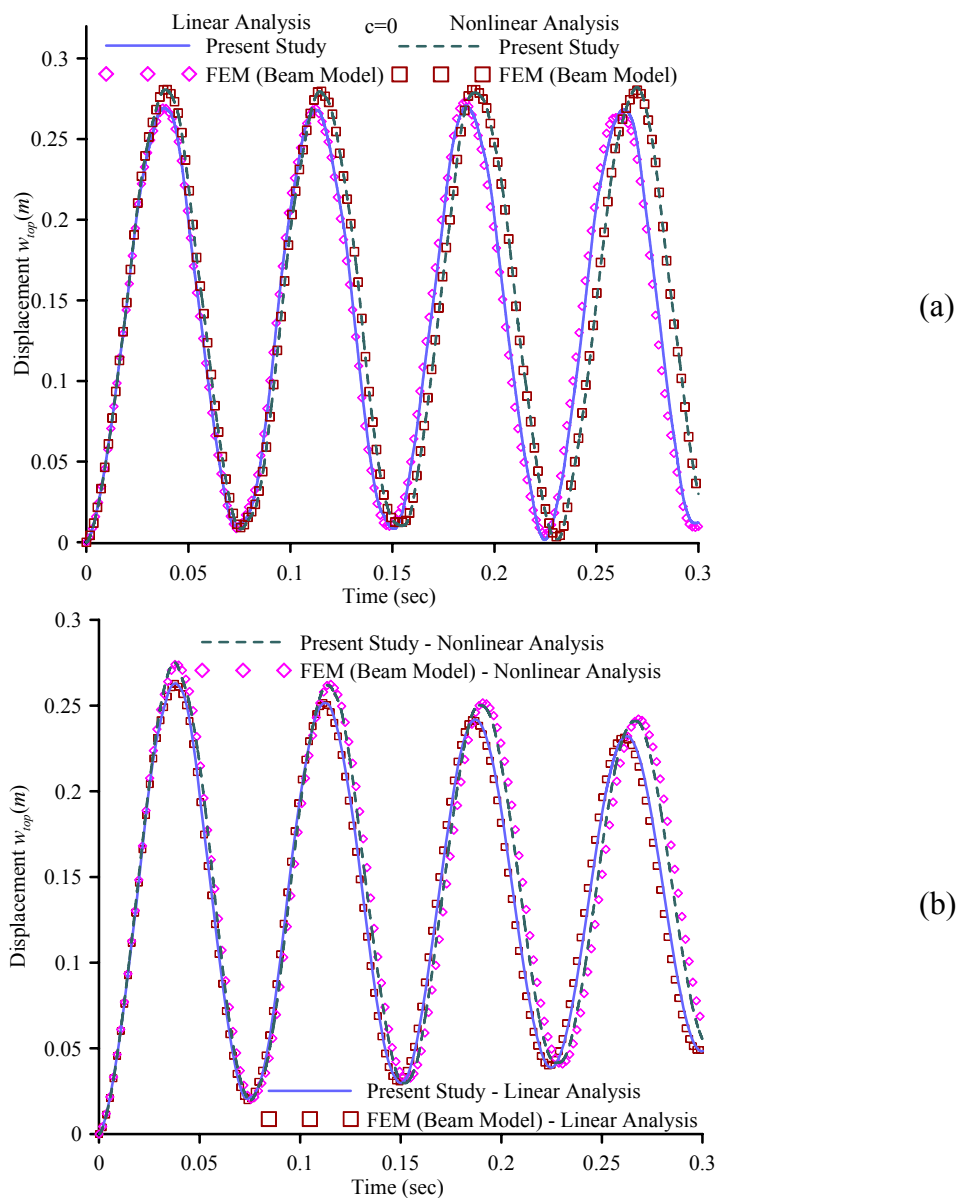


Fig. 3.22. Head displacement time history of the column-pile of example 6, for undamped (a) and damped (b) case.

Table 3.10. Maximum head displacement and period of the first cycle of motion of the column-pile of example 6.

Analysis / $\times 10^{-2}$	Nonlinear		Linear	
	w_{top} (m)	T_z (sec)	w_{top} (m)	T_z (sec)
Linear Winkler	29.662	8.10	26.956	7.28
Pasternak	31.224	8.23	28.228	7.85
Linear & Nonlinear Winkler	20.900	5.80	19.843	5.32
Three-Parameter	21.059	5.92	19.941	5.66

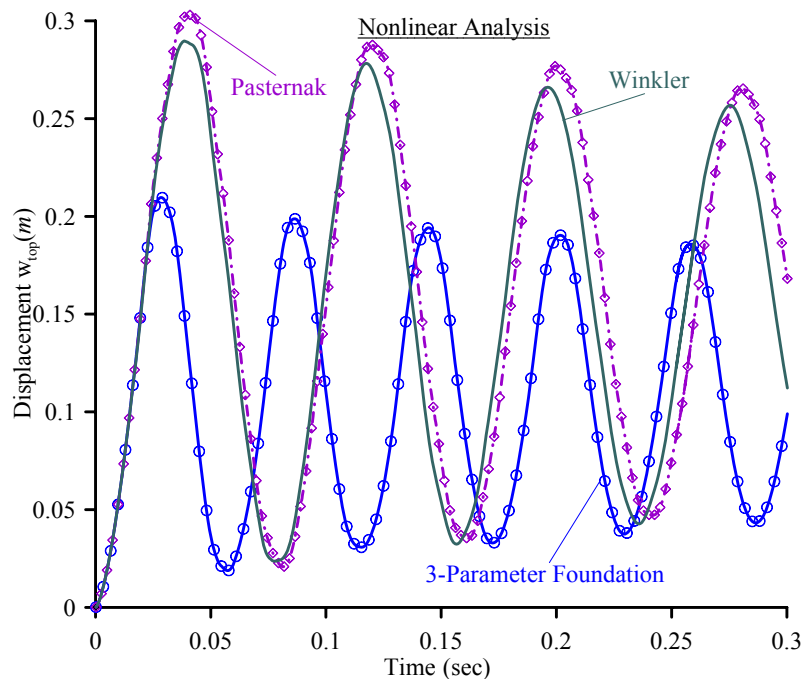


Fig. 3.23. Head displacement time history of the column-pile of example 6, for various foundation models.

Table 3.11. Maximum head transverse displacements of the column-pile of example 6.

Analysis / $\times 10^{-2}$ (m)	Nonlinear		Linear	
	w_{max}	v_{max}	w_{max}	v_{max}
Linear Winkler	29.671	59.343	26.956	53.912
Pasternak	31.231	62.463	28.228	56.456
Linear & Nonlinear Winkler	20.909	41.819	19.843	39.686
Three-Parameter	21.062	42.123	19.941	39.882

3.5.7 Example 7 – Timoshenko-Rayleigh Beam on Viscoelastic Pasternak Foundation under Concentrated Moving Load

For comparison purposes, in this example the linear dynamic analysis of a simply supported steel Timoshenko beam free of foundation support is examined. The material and geometric constants are given in Table 3.12. The beam is subjected to a concentrated moving load with constant velocity, $p_z(x,t) = P\delta(x-Vt)$, $P = 700N$, $V = 12km/h$ (δ is the Dirac's delta function). In Table 3.13, the maximum displacements of the midpoint of the beam for various internal nodal points'

discretization schemes are presented; illustrating that convergence is achieved for a small number of nodal points. In Fig. 3.25, the time history of the displacement w at the beam's midpoint is presented for various internal nodal points' discretization schemes as compared with the one obtained from a modal superposition method (Zehsaz et al. 2009) demonstrating the accuracy of the proposed method.

Table 3.12. Geometric constants of the beam of example 7.

$l(m)$	10	$I_y(m^4)$	1.04×10^{-6}	$\rho(kg/m^3)$	7040
$E(GPa)$	207	$A(m^2)$	10^{-3}	a_z	1.2

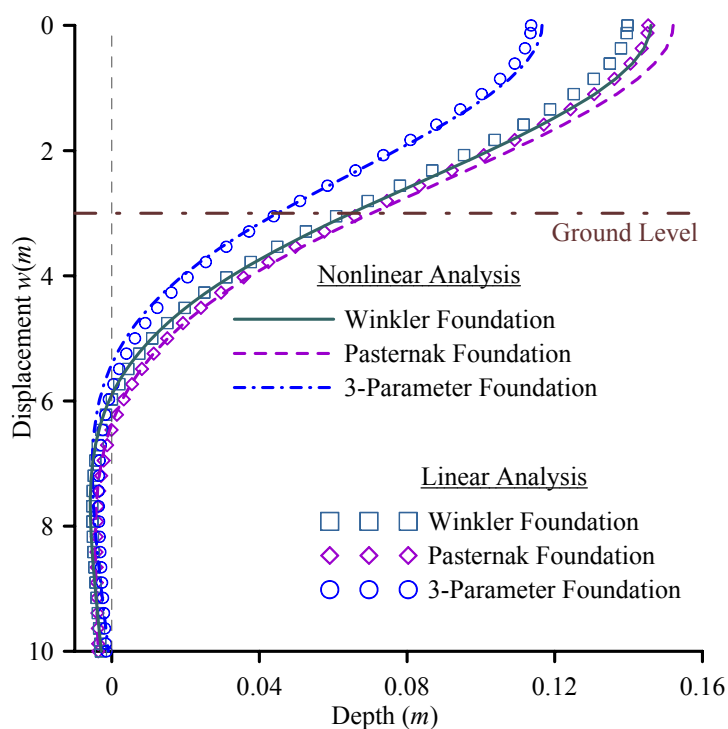


Fig. 3.24. Static deflection of the column-pile of example 6, for various foundation models.

Table 3.13. Maximum displacements of the beam of example 7 and divergence values for various discretization schemes.

Nodal Points	11	17	21	27	31	37	41
$w_{\max}(cm)$	6.9578	6.9636	7.0158	7.0167	7.0617	7.0967	7.0968
Divergence (%)	1.96	1.88	1.14	1.13	0.5	0.001	-

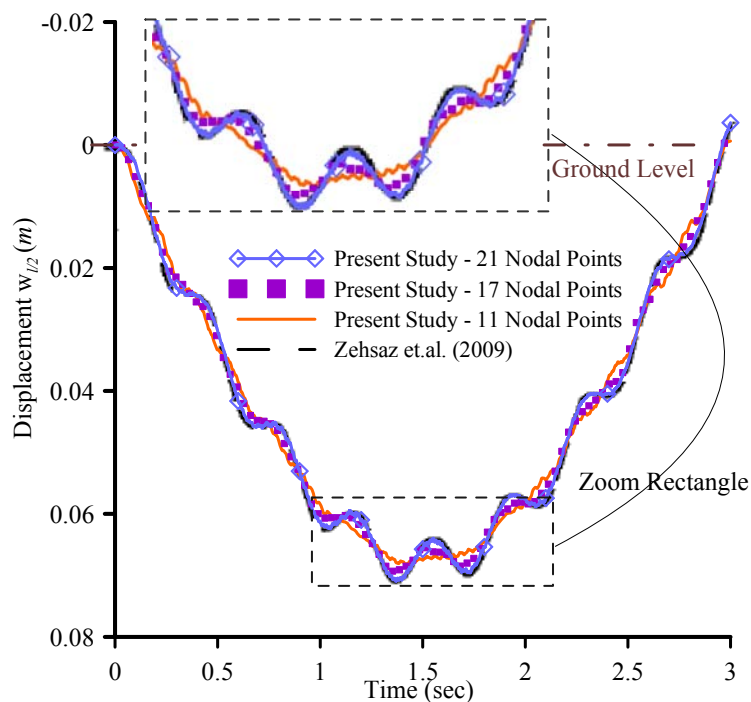


Fig. 3.25. Midpoint displacement time history of the beam of example 7.

As a variant of this example, a simply supported Timoshenko-Rayleigh beam subjected to a concentrated moving load with constant velocity, $p_z(x,t) = P\delta(x-Vt)$, having the material, geometric and loading constants given in Table 3.14 and resting on a Pasternak viscoelastic foundation is considered.

Table 3.14. Geometric, foundation and loading constants of the beam of example 7.

$l(m)$	10	$I_y(m^4)$	39.5×10^{-6}	$\rho(kg/m^3)$	7820
$E(GPa)$	207	$A(m^2)$	86.13×10^{-4}	a_z	1.176
ν	0.3	$k_L(MPa)$	20	$k_P(kN)$	69
$c(kNs/m^2)$	138	$P(kN)$	144	$V(km/h)$	60

In Fig. 3.26 the time history of the bending moment $M_y(l/2,t)$ at the beam's midpoint is presented for various internal nodal points' and time discretization schemes, while in Figs. 3.27a,b the displacement $w(x,0.3)$ and the bending moment $M_y(x,0.3)$ at the time instant $t=0.3s$ along the beam axis, respectively are also given. In these figures the corresponding curves obtained from the solution of the same beam resting on

a Pasternak-type viscoelastic foundation (using a viscous shear layer) are also presented employing the modal superposition method considering the first ten modes (Zehsaz et al. 2009). From these figures, it is easily verified that due to the high value of the damping coefficient, the response of the beam approaches to zero after passage of the moving load. Moreover, the bed influence limiting the effect of the moving load to the nearby points is remarked.

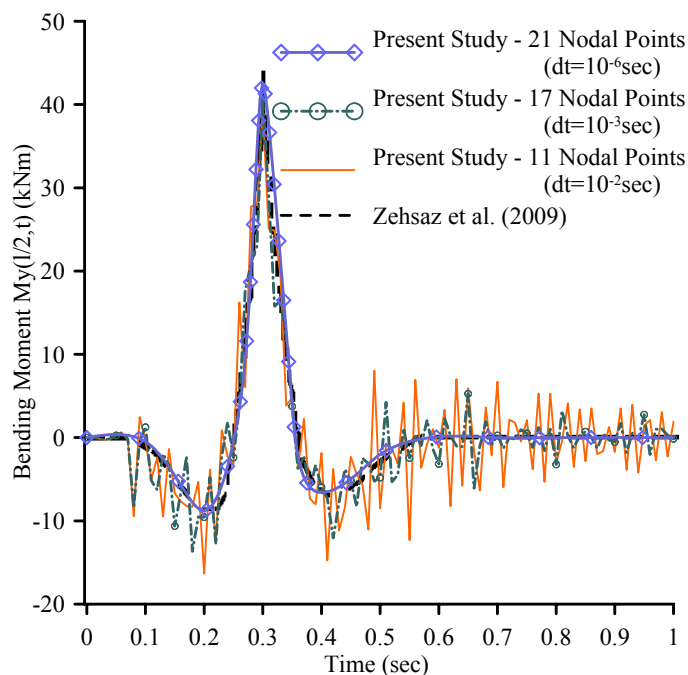


Fig. 3.26. Midpoint time history of the bending moment of the beam of example 7.

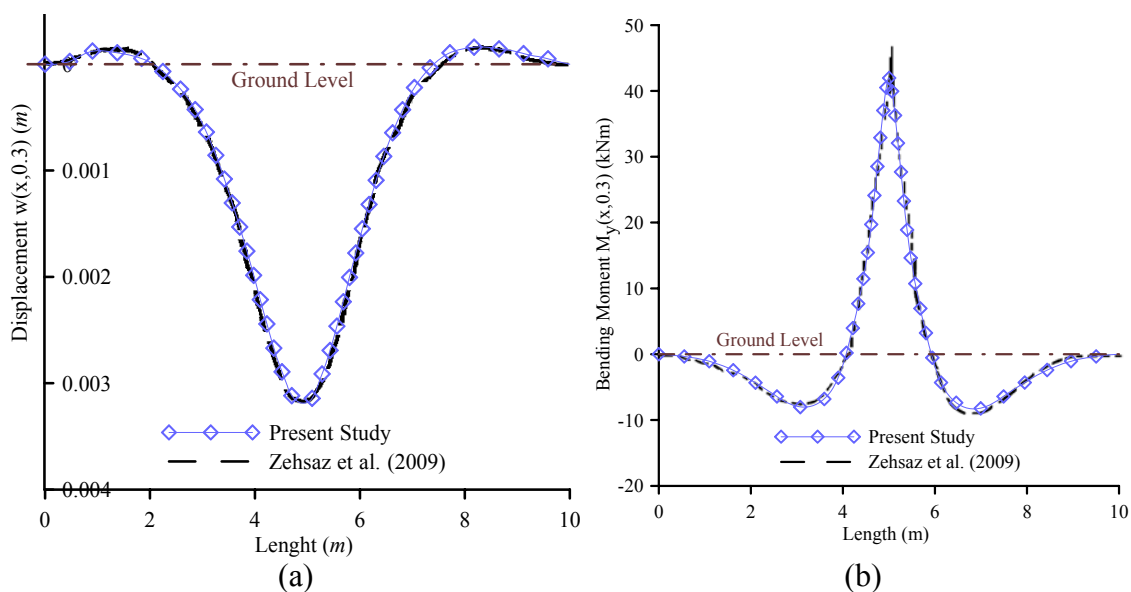


Fig. 3.27. Displacement (a) and bending moment (b) along the beam axis at the time instant $t = 0.3s$ of the beam of example 7.

Finally, in Table 3.15 the absolute maximum displacement w_{\max} as well as the maximum displacement $w(l/2)_{\max}$ and bending moment $M(l/2)_{y\max}$ at the midpoint of the beam are presented for various values of the velocity for both Pasternak and Winkler foundations, taking into account shear deformation effect. From this table the negligible, in this example, decrease of the transverse displacements and the bending moments arising from the shear foundation layer are remarked.

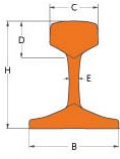
Table 3.15. Absolute maximum displacement and maximum midpoint displacement (mm) and bending moment (kNm) of the beam of example 7, taking into account shear deformation effect.

V (km/h)	Pasternak			Winkler		
	w_{\max}	$w(l/2)_{\max}$	$M(l/2)_{y\max}$	w_{\max}	$w(l/2)_{\max}$	$M(l/2)_{y\max}$
0	3.318	3.171	38.37	3.327	3.185	38.43
10	3.335	3.189	39.91	3.346	3.200	40.92
60	3.345	3.202	41.17	3.350	3.209	41.24
100	3.466	3.281	41.89	3.473	3.285	42.40
120	3.522	3.363	45.99	3.531	3.369	46.17
150	3.649	3.465	48.01	3.657	3.471	48.19

3.5.8 Example 8 – UIC60 Rail Track on 3-Parameter Viscoelastic Foundation

In order to illustrate the importance of the geometrically nonlinear analysis, a simply supported UIC60 rail track, resting on a three-parameter viscoelastic bilateral foundation is examined. The geometric, foundation and loading constants of the track, are given in Table 3.16.

Table 3.16. Geometric, foundation and loading constants of the UIC60 rail track (Dahlberg 2002, Kargarnovin et al. 2005) of example 8.

	l (m)	10	I_y (m ⁴)	30.55×10^{-6}	ρ (kg / m ³)	7850
	E (GPa)	210	A (m ²)	76.86×10^{-4}	a_z	2.68
	G (GPa)	77	k_L (MPa)	35	k_P (kN)	200
	k_{NL} (MN / m ⁴)	4×10^8	c (kNs / m ²)	145	P (kN)	100

The track is subjected to a concentrated moving harmonic load $p_z(x,t) = P\delta(x-Vt)\sin(\Omega t)$, where P, Ω are the amplitude and the frequency of the harmonic load, respectively and δ is the Dirac's delta function. Moreover, the track is subjected to an either tensile or compressive distributed axial load $p_x(x,t) = \pm 2500(kN/m)$.

In Fig. 3.28 the time history and the extreme values of the central displacement $w(l/2,t)$ of the track resting on the viscoelastic Winkler foundation and subjected to a concentrated harmonic load at its midpoint ($V = 0m/s, \Omega = 100rad/s$) is presented, performing either a small or a large deflection analysis and taking into account both rotary inertia and shear deformation effect.

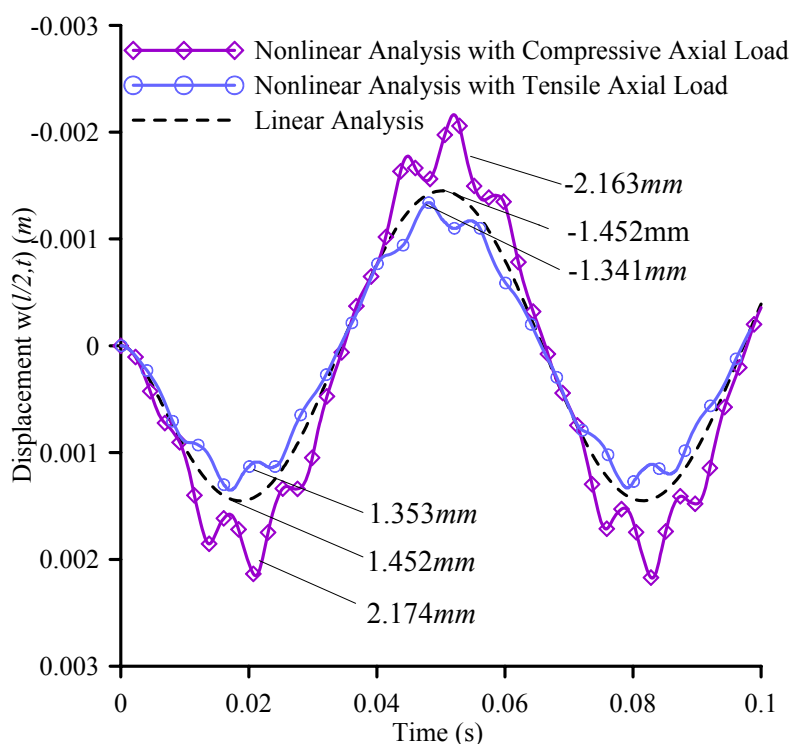


Fig. 3.28. Midpoint time history and extreme values of the displacement of the track of example 8.

To illustrate the significant effect of the load frequency, in Table 3.17 the maximum midpoint displacement $w(l/2,t)$ of the track resting on the nonlinear three-parameter bilateral viscoelastic foundation, subjected to a harmonic moving load with constant velocity $V = 100m/s$ are presented for various values of the excitation frequency Ω , performing either small or large deflection analysis (for both cases of tensile or compressive axial load). Moreover, in Table 3.18 the maximum displacements

and bending moments of the track are presented for different types of bilateral viscoelastic foundation reaction, for $\Omega = 400 \text{ rad/s}$, $V = 100 \text{ m/s}$, while in Fig. 3.29 the displacement $w(x, 0.055)$ along the track axis at the time instant $t = 0.055 \text{ s}$ as well as their maximum values are also presented for both small and large deflection analysis for viscoelastic Winkler and three-parameter foundation. From the obtained results, it is concluded that the discrepancy between the geometrically linear and nonlinear analysis is not negligible and should not be ignored, while the influence of the shear deformation effect (increasing the transverse displacements and decreasing the bending moments) in both of the aforementioned analyses is observed. This latter influence is more pronounced as the length of the track becomes smaller.

Table 3.17. Maximum midpoint displacement $w(l/2)_{\max}$ (mm) of the track of example 8, for various values of the excitation frequency Ω .

$w(l/2)_{\max}$ $\Omega(\text{rad / s})/\text{Analysis}$	Linear	Nonlinear Tensile Load	Nonlinear Compressive Load
1.0	0.0715	0.0607	0.1009
5.0	0.2699	0.2338	0.3374
10	0.3999	0.3626	0.4693
50	0.4609	0.4445	0.5147
100	0.5690	0.5448	0.6272
200	0.5150	0.4724	0.5745
400	0.5782	0.5257	0.6589

Table 3.18. Maximum displacement w_{\max} and bending moments $M_{y\max}$ of the track of example 8, for different types of foundation reaction.

w_{\max} (mm) $M_{y\max}$ (kNm)	Without Shear Deformation		With Shear Deformation	
	Linear	Nonlinear	Linear	Nonlinear
<i>Linear Winkler</i>	0.9879	1.4336	0.9973	1.4436
	15.449	22.869	15.285	22.805
<i>Pasternak</i>	0.9861	1.4235	0.9937	1.4452
	15.942	22.779	15.255	22.735
<i>Linear & Nonlinear Winkler</i>	0.5788	0.6859	0.5923	0.6992
	12.906	15.917	12.161	15.916
<i>Three-Parameter</i>	0.5783	0.6851	0.5820	0.6893
	12.887	15.886	12.148	15.880

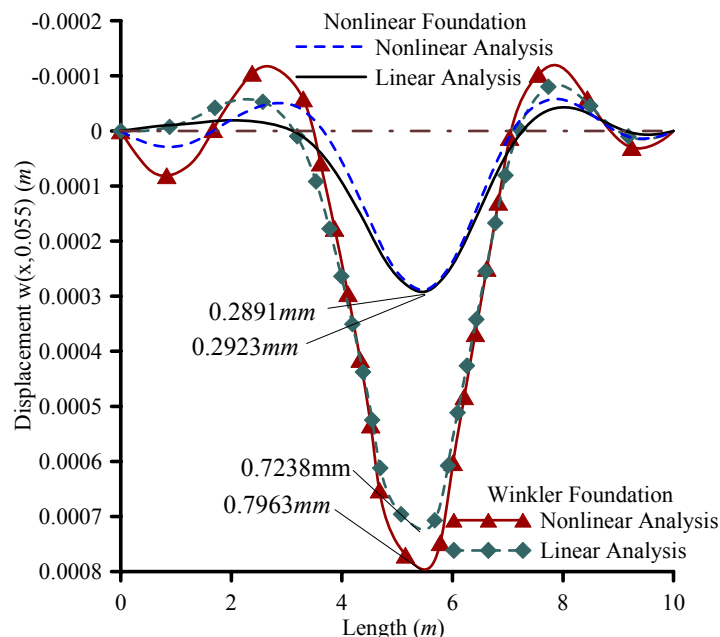


Fig. 3.29. Displacement at the time instant $t = 0.055s$ and their maximum values of the beam of example 8.

3.5.9 Example 9 – HEA320 on Winkler Foundation under Axial Loading and Concentrated Moving Harmonic Force

In this example, a clamped-pinned HEA320 beam of length $l = 6.5\text{ m}$ ($E = 210\text{ GPa}$, $\nu = 0.3$, $a_y = 1.475$, $a_z = 4.512$, $\rho = 7.85\text{ tn/m}^3$) resting on a constant stiffness soil of $k_z = 1.2\text{ MPa}$, as shown in Fig. 3.30, is considered. The beam is subjected to a uniformly distributed axial loading $p_x(t) = 500\text{ kN}$, ($t \geq 0.0$) and to a transverse concentrated moving harmonic load $P_z(t) = 10\delta(x - Vt)\sin(\Omega t)\text{ MN}$ with constant velocity of $V = 65\text{ m/s}$, and excitation frequency $\Omega = 100\text{ rad/sec}$.

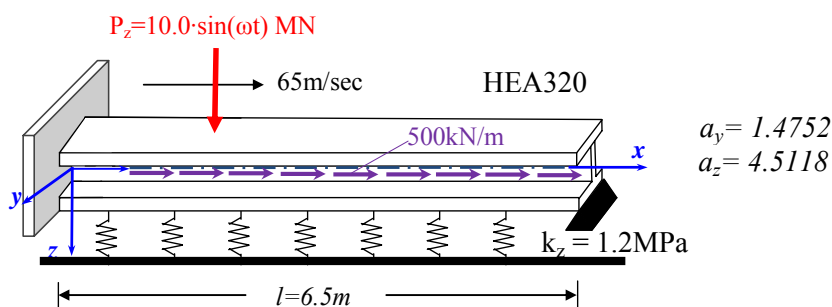


Fig.3.30. Beam under axial-flexural loading on constant stiffness soil.

In Fig. 3.31a the time history of the central transverse displacement $w(l/2)$ of the beam, performing either linear or nonlinear analysis, taking into account or ignoring both rotary inertia and shear deformation effect is presented, while in Fig. 3.31b the displacement curves w at the time instant $t = 0.05\text{sec}$ are also presented either for conventional Winkler or for tensionless Winkler soil performing nonlinear analysis and taking into account or ignoring shear deformation effect. Moreover, in Table 3.19 the extreme displacements w_{max} , w_{min} and in Fig. 3.32 the effect of the frequency ω of the concentrated moving load to the maximum displacement w_{max} are presented for all of the aforementioned cases.

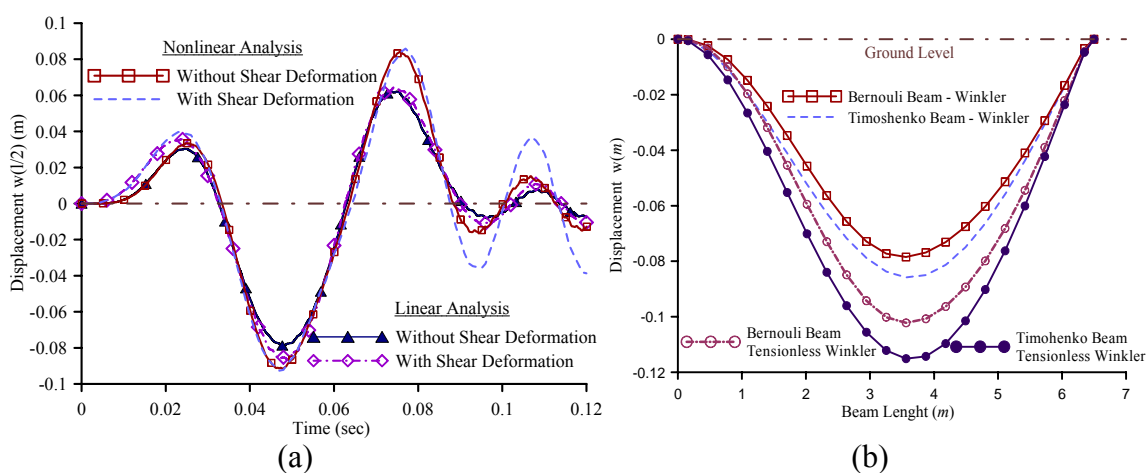


Fig. 31. Central displacement time history (a) and displacement curves at time instant $t = 0.05\text{sec}$ (b) of the beam of example 9.

Table 3.19. Extreme values of the displacement of the beam of example 9.

Analysis		Winkler			
		Without Shear Deformation		With Shear Deformation	
$\times 10^{-2}$ (m)		Linear	Nonlinear	Linear	Nonlinear
w_{max}		6.21	8.43	6.45	8.58
w_{min}		-7.87	-9.15	-8.17	-9.26
Analysis		Tensionless Winkler			
		Without Shear Deformation		With Shear Deformation	
$\times 10^{-2}$ (m)		Linear	Nonlinear	Linear	Nonlinear
w_{max}		5.92	6.84	6.67	6.98
w_{min}		-10.18	-10.96	-11.46	12.34

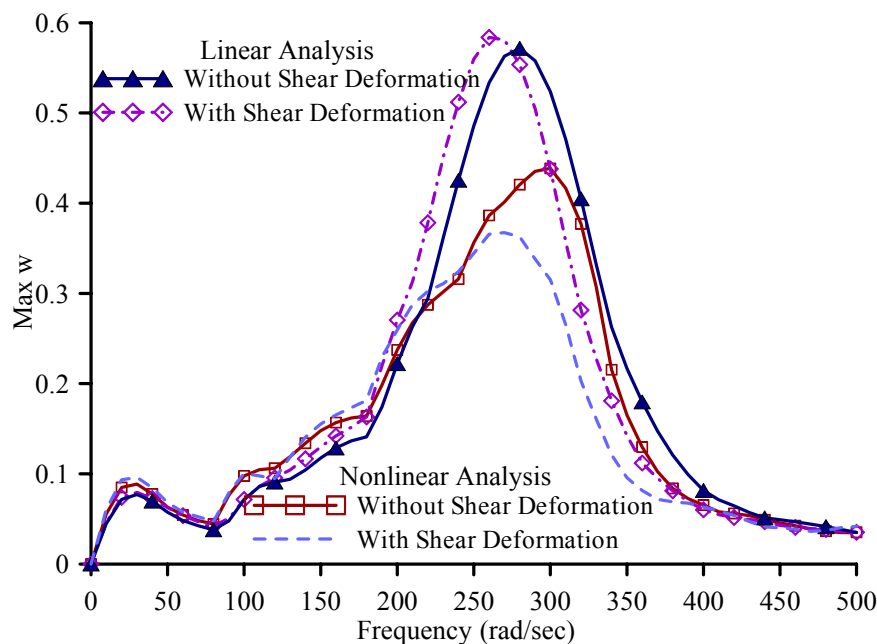


Fig.3.32. Frequency effect to the maximum displacement of the beam of example 9.

3.5.10 Example 10 – HEM 240 on 3-Parameter Viscoelastic Foundation under Axial Loading and Distributed Moving Harmonic Force

To demonstrate the range of applications of the developed method, in this example, a clamped-slide supported HEM 240 beam of length $l=8m$ ($E=210GPa$, $\nu=0.3$, $a_z=4.344$, $\rho=7.85tn/m^3$) has been studied. The foundation model is characterized by the linear Winkler modulus $k_L=1.5MN/m^2$, the nonlinear Winkler one $k_{NL}=1.5GN/m^4$, the Pasternak (shear) modulus $k_p=400kN$ and the damping coefficient $c(kNs/m^2)$. The beam is subjected to a uniformly distributed axial loading $p_x(x,t)=-1000kN/m$ and to a moving harmonic line load $p_z(x,t)$ of length $2a$ defined as

$$p_z(x,t) = P \frac{H(a^2 - s^2)}{2a} \cos(\Omega t) \quad (3.xx)$$

where P, Ω are the amplitude and the frequency of the harmonic load, H is the Heaviside step function and s is given as $s = (x + a) - Vt$. It is considered that $P = 200kN$, $\Omega = 100rad / s$ and $a = 0.381m$.

In Fig. 3.33a the midpoint displacement time history $w(l/2, t)$ of the beam subjected to the aforementioned load ($c = 15kNs / m^2$, $V = 0m / s$) for the time period $t \in [0, 0.03]$ sec is presented, performing either small or large displacement analysis, taking into account rotary inertia, shear deformation effect and the tensionless character of the foundation, demonstrating the discrepancy between the conventional and the tensionless foundation, while in Fig. 3.33b the midpoint displacement time history $w(l/2, t)$ of the beam subjected to the aforementioned load ($c = 15kNs / m^2$, $V = 80m / s$) is also presented, performing either small or large deflection analysis and taking into account both shear deformation effect and rotary inertia. Moreover, in Table 3.20 the maximum values of the displacement $w(x, t)$ of the beam resting on either nonlinear or tensionless nonlinear three-parameter foundation are presented for various values of the damping coefficient c , performing both small and large deflection analysis and taking into account or ignoring shear deformation effect and rotary inertia. From the results obtained the influence of the damping coefficient is illustrated and the importance of large deflection analysis is verified.

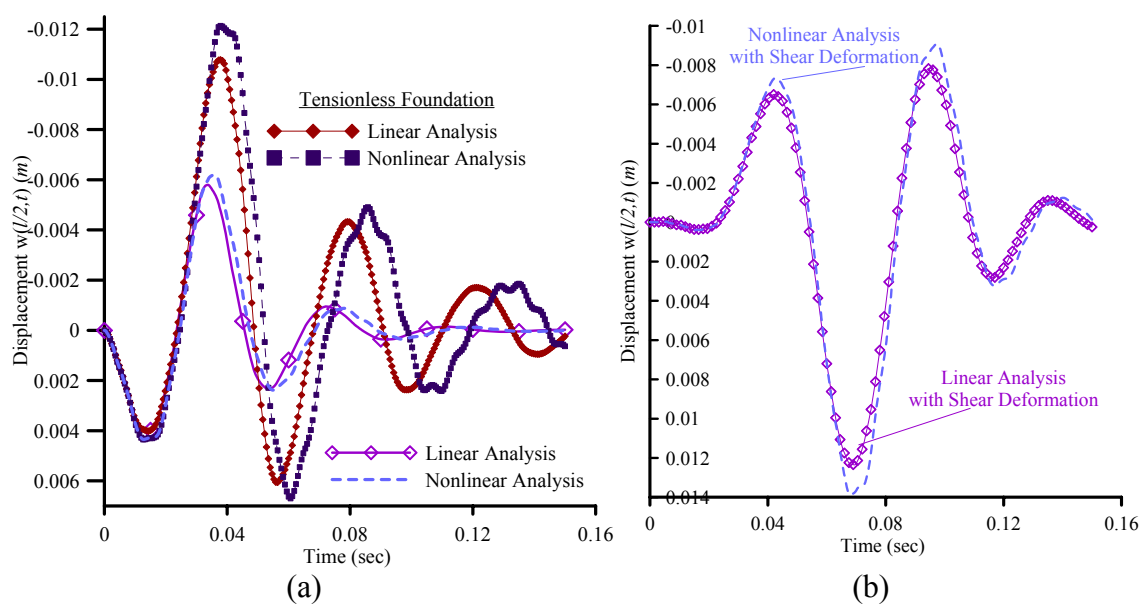


Fig. 3.33. Midpoint displacement time history of the beam of example 10 for $c = 15kNs / m^2$, $V = 0m / s$ (a) and $V = 80m / s$ (b).

Table 3.20. Maximum displacement w_{max} (cm) of the beam of example 10.

Analysis	Nonlinear Foundation			
	Without Shear Deformation		With Shear Deformation	
w_{max}	Linear	Nonlinear	Linear	Nonlinear
$c = 0$	1.985	2.373	2.019	2.448
$c = 5$	1.678	1.966	1.715	2.023
$c = 10$	1.471	1.681	1.487	1.713
$c = 15$	1.323	1.472	1.335	1.484
$c = 20$	1.197	1.305	1.210	1.314
$c = 40$	0.8579	0.924	0.861	0.925

Analysis	Nonlinear Tensionless Foundation			
	Without Shear Deformation		With Shear Deformation	
w_{max}	Linear	Nonlinear	Linear	Nonlinear
$c = 0$	2.473	3.094	2.568	3.376
$c = 5$	2.169	2.544	2.254	2.651
$c = 10$	1.925	2.251	2.001	2.352
$c = 15$	1.726	2.014	1.794	2.104
$c = 20$	1.561	1.819	1.619	1.896
$c = 40$	1.128	1.298	1.165	1.343

3.5.11. Example 11 – Extensive Case Study

The main purpose of this final example is to investigate the accuracy of the advanced beam model developed in the previous sections under the concept of an extensive case study concerning soil–pile–structure kinematic and inertial interaction, as well as to demonstrate its efficiency and advantages compared to other commonly used beam or solid models.

Within this context, a column-pile monolithically connected to a bridge deck, embedded in two layers of cohesive soil and excited by seismic motion (Fig.3.34), has been studied. The concentrated mass at the centre of the deck is $M_{top} = 60\text{tons}$, the height of the pier is $H = 10\text{m}$, the embedment length of the pile is $L = 30\text{m}$, and the diameter of the column-pile equals to $d = 1.5\text{m}$. The column-pile is assumed to be linear elastic, while the idealized soil profile from the Agios Stefanos bay depicted in

Fig. 3.34 was used for the ground response analyses. More specifically, a soft to medium normally consolidated clay sets on top of a stiff clay. The bedrock is encountered at -50m and is assumed to be rigid. The soft clay has a thickness of 18m and a plasticity index $PI(\%) = 35$. The second layer is 32m thick and has constant undrained shear strength of 100kPa . The maximum shear modulus was calculated by the empirical equations of Seed and Idriss (1970).

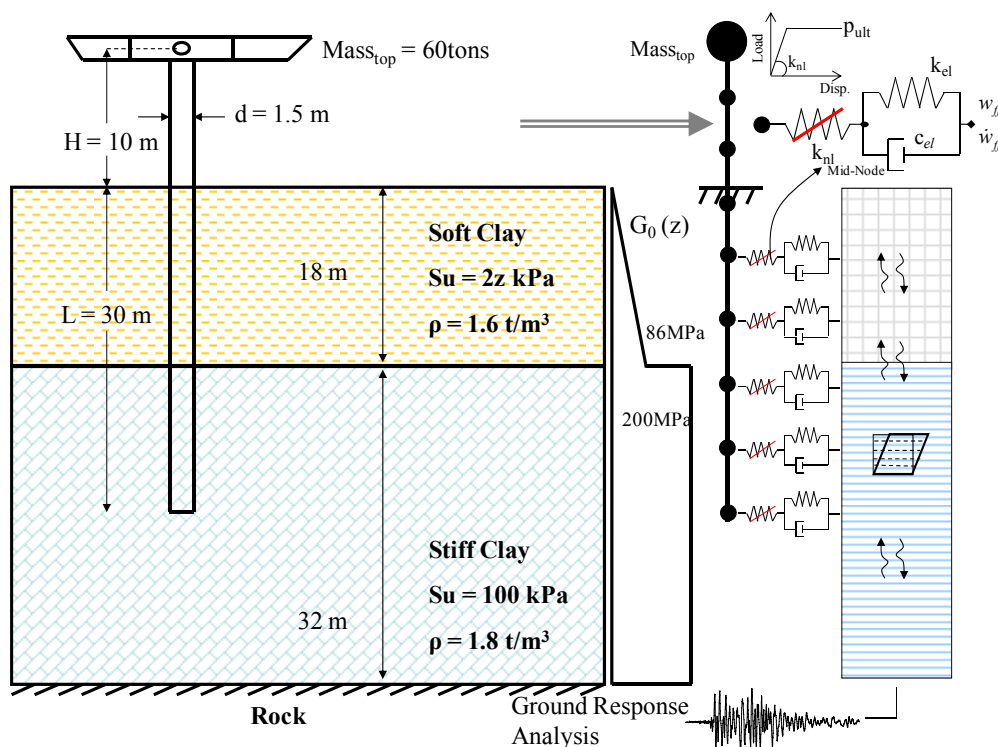


Fig. 3.34. Column-pile monolithically connected to bridge deck embedded in two layers of cohesive soil and the adopted beam model.

The layered soil profile is simulated by a Winkler type hybrid spring configuration. As proposed by Wang et al. (1998), the soil is separated into two zones, namely a far-field zone implemented by Kelvin-Voigt element (k_{el}, c_{el}) and a near-field one represented by hysteretic element (k_{nl}) . More specifically, the adopted hybrid model consists of a nonlinear spring connected in series to a dashpot-elastic spring parallel configuration. The free extremities of the configuration are excited by the free-field (w_{ff}, \dot{w}_{ff}) displacement and velocities time histories obtained at each depth from the free-field seismic response analysis (Fig.3.34). The equilibrium of forces at the mid-node of the spring configuration results in an additional equation

$$k_{el}(w_{mnode} - w_{ff}) + c_{el}(\dot{w}_{mnode} - \dot{w}_{ff}) = k_{nl}(w - w_{mnode}) \quad (3.49)$$

where, w_{ff} , \dot{w}_{ff} and w_{mnode} , \dot{w}_{mnode} correspond to the free-field and mid-node displacement and velocity, respectively. Eqn. (3.49) together with the equilibrium equations of motion (3.17) constitute the governing coupled differential equations of a Timoshenko column-pile embedded in a layered nonlinear Winkler-type soil profile accounting for the kinematic and inertial soil–pile–structure interaction and for the effects of geometrical nonlinearity, rotary inertia and shear deformation.

The calibration of the spring and dashpot coefficients of the examined hybrid spring configuration is based on the methodology presented by Giannakos (2013). The lateral soil reaction against a deflecting pile is expressed as the sum of a hysteretic elastic–perfectly plastic and a visco–plastic component, according to the lumped parameter model, as depicted in Fig.3.34. In this way, the frequency–dependent characteristics of the subgrade reaction are realistically captured through a series–parallel assembly of frequency–independent springs and dashpots. In the elastic regime, the small–amplitude frequency–dependent spring and dashpot coefficients for the lateral soil reaction are approximated by

$$k_x = Re\left(\frac{p_z}{w}\right) \approx \frac{k_{el} + \frac{k_{el}^2}{k_{nl}} + \frac{(\omega c_{el})^2}{k_{nl}}}{\left(1 + \frac{k_{el}}{k_{nl}}\right)^2 + \left(\frac{\omega c_{el}}{k_{nl}}\right)^2} \quad (3.50a)$$

$$c_x = Im\left(\frac{p_z}{\omega w}\right) \approx \frac{c_{el}}{\left(1 + \frac{k_{el}}{k_{nl}}\right)^2 + \left(\frac{\omega c_{el}}{k_{nl}}\right)^2} \quad (3.50b)$$

in which ω is the circular frequency. In the above equations, k_{nl} denotes the stiffness of the elastic branch of the nonlinear spring. The parameters k_{el} , c_{el} and k_{nl} are appropriately calibrated through an optimization procedure to match the stiffness and dashpot coefficients (Fig. 3.35) proposed by Makris and Gazetas (1992)

$$k_x = 1.2E_s \quad \text{and} \quad c_x = 6a_0^{-1/4} \rho_s V_s d \quad (3.51a,b)$$

in which E_s , V_s and ρ_s are the Young's modulus, shear wave velocity and mass density of the supporting soil, and α_0 is a dimensionless frequency parameter defined as $\alpha_0 = \omega d/V_s$.

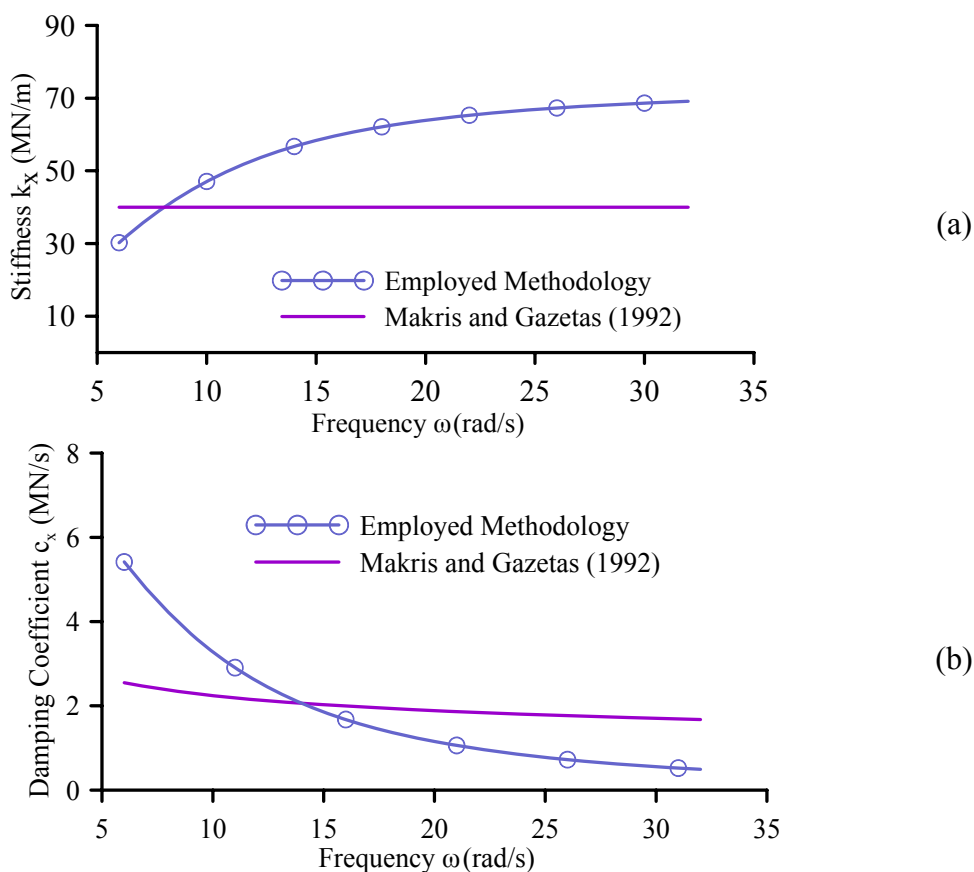


Fig. 3.35. Calibration of stiffness k_x (a) and damping coefficient c_x (b) for the examined configuration.

Having calibrated the stiffness k_x and dashpot coefficient c_x according to Eqns. (3.51), plastic behaviour is then introduced by imposing a threshold value for the reaction force of spring k_{nl} equal to the ultimate soil resistance per unit length of the pile (p_{ult}) as determined by Matlock (1970) and Reese et al. (1975) at near surface (top layer) and at greater depths (bottom layer), respectively. The architecture of the proposed assembly of springs and dashpots is such that the maximum transmissible force on to the pile is limited to the ultimate resistance of the nonlinear spring. When the force (per unit length of the pile) of the nonlinear spring reaches its threshold value

(p_{ult}), the corresponding tangential spring stiffness becomes zero. Thus, the arranged in-parallel spring and dashpot unit is deactivated and the radiation damping vanishes.

The influence of shaking on the seismic response is investigated by selecting three well known acceleration records as seismic excitations:

- i) the record from Aegion earthquake (1995)
- ii) the record from Lefkada earthquake (2003)
- iii) the JMA record from Kobe earthquake (1995)

The first two records were chosen as two strong motions of the seismic environment of Greece, with one and many cycles, respectively. JMA record is used to investigate the dynamic response of the soil-pile-structure system to a quite unfavourable incident. All the records were first scaled to a Peak Ground Acceleration (PGA) of $0.5g$ and $0.8g$ at the ground surface. The acceleration time histories at the surface scaled to $a_g = 0.5g$ and the corresponding elastic response spectra for $\xi = 5\%$ damping are presented in Figs. 3.36, 3.37, respectively.

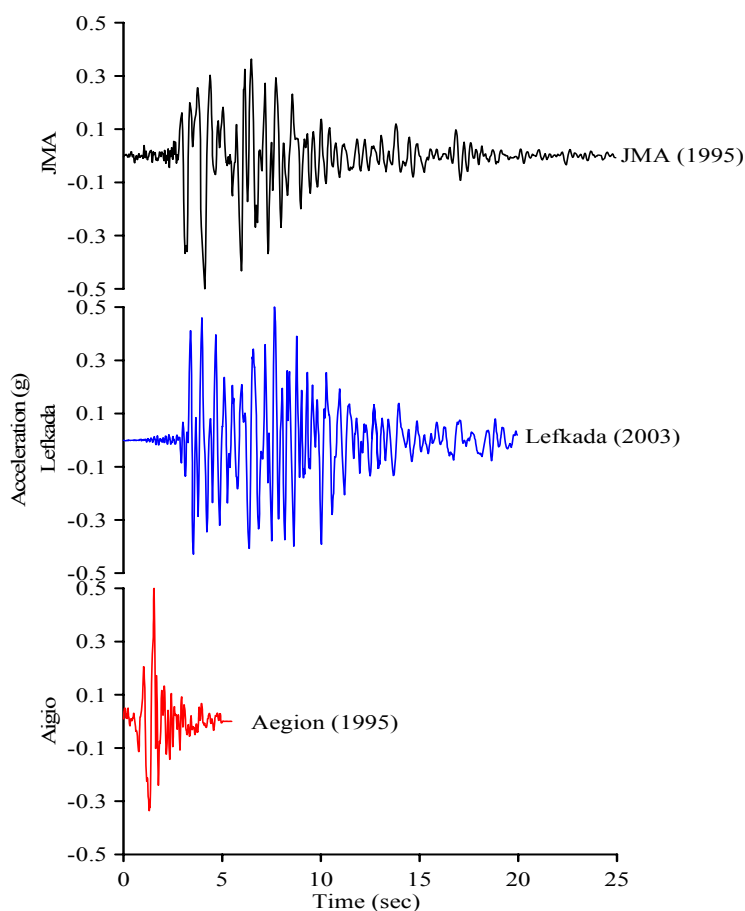


Fig. 3.36. Excitation motion accelerograms scaled to $a_g = 0.5g$.

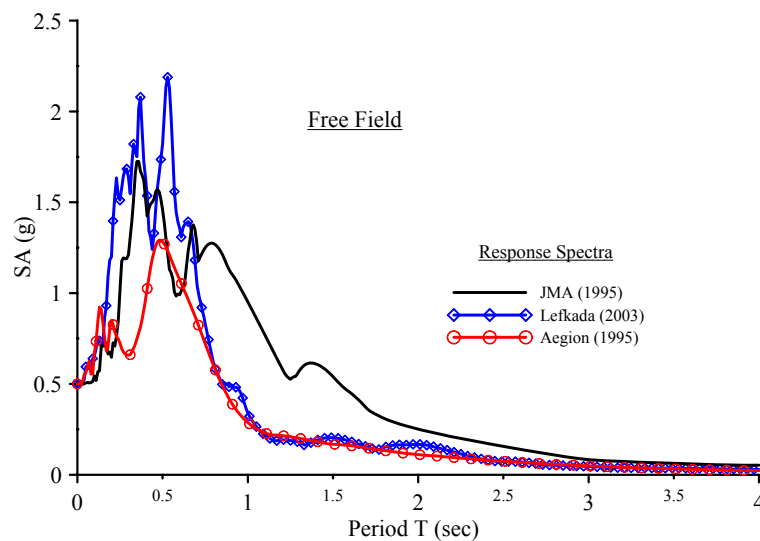


Fig. 3.37. Corresponding response spectra of the scaled motions ($a_g = 0.5g$).

Then, through deconvolution analyses conducted with SHAKE91 (1991), the bedrock motion as well as the motion at various depths along the pile were estimated. Both elastic and inelastic soil response are investigated. For the elastic soil, the response of the soil–pile–structure system is investigated further with two different methods; namely a simplified Beam–FE model employing the OpenSees code (2005), and a rigorous fully 3–D continuum FE scheme materialized in the ABAQUS (2009) code. For the inelastic soil response, the proposed model is verified only against the Beam–FE solution due to the fact that soil response in the 3–D continuum FEM strongly depends on the adopted soil constitutive model.

In the Beam–Finite Element formulation (Giannakos 2013), two different stages of analysis are required. At first, the analysis of the seismic site response without the presence of the structure is performed with the use of the computer program SHAKE91 (1991). Thereinafter, employing the obtained excitation motions derived from the first stage, the analysis of the soil–pile–structure system is carried out with the use of a Beam–FE model using the code OpenSees (2005). In the first stage, the seismic site response analysis considers the soil profile as a one-dimensional system of homogeneous visco–elastic sub-layers of infinite horizontal extend. The response of this system is calculated using the wave equation and the assumption of vertically propagating shear waves. An equivalent linear method models the nonlinear variation of soil shear modulus and damping as a function of shear strain. Curves of shear modulus reduction G and damping ratio ξ increase with shear strain γ developed by Ishibashi and Zhang (1993) were used in the case of the nonlinear site response analysis. In the

second stage, the column-pile is discretized into linear elastic beam elements of $1m$ length. The mass of the deck is simulated as a concentrated mass at the top node of the pile–column, while the distributed mass of the extended pile is simulated by lumped masses on the beam–element nodes. The free extremities of the spring configuration are excited by the displacement time histories obtained at each depth from the free–field seismic response analysis. Rayleigh damping which represents material damping was taken equal to $\xi=5\%$ in order to avoid spurious oscillations at very small deformations.

On the contrary, in the fully 3-D Finite Element Model (Giannakos 2013) the calculations of the site response and the soil–pile–structure interaction are performed in a fully coupled manner with the Finite Element Code ABAQUS (2009). The pile–column is modelled with 3–D beam elements placed at its centre and connected with appropriate kinematic restraints with the nodes at the perimeter of the pile in order to model the complete geometry of the pile as depicted in Fig. 3.38b. The solid elements inside the perimeter of the pile have no stiffness. In this way, each pile section behaves as a rigid disc, i.e. rotation is allowed on the condition that the disc remains always perpendicular to the beam axis, but stretching cannot occur. The pile–column and the soil behaviour are assumed to be elastic, while P- δ effects (linearized 2nd order analysis) are also taken into account. The soil is modelled with 8-node brick elements. The vertical length of the elements is identical to the beam model in order to avoid mesh sensitivity differences. Appropriate kinematic constraints are imposed to the lateral edges of the model, allowing it to move as the free–field. The acceleration time histories derived from the site response analysis with SHAKE91 at $30m$ depth were used as the input excitation motion in the fully 3–D FE model. Rayleigh damping of the soil elements was taken equal to the equivalent damping from the dampers of the Beam–FE model in order to avoid spurious oscillations at very small deformations. Due to symmetry, only half of the problem was analyzed, as depicted in Fig. 3.38a, significantly reducing computational demands leading to approximately 15,000 elements for each analysis.

In order to construct a rigorous and precise fully 3–D FE model, the free-field boundaries had to be investigated first by two different types of boundaries; namely i) 3 dashpots (one in each direction) on each node on the boundaries of the 3–D model were employed, while the soil motion at each depth from the free-field seismic response analysis was imposed on every node on the boundaries and ii) appropriate kinematic constraints were used, imposed to the lateral edges of the model, allowing it to move as

the free-field, namely Multi-Point Constrains (MPC) boundaries, and the soil motion at 30m depth from the free-field seismic response analysis was imposed only on the nodes of the bottom boundaries of the model. The comparison of the acceleration, displacement and rotation time histories at the deck level with both the boundary types studied for the JMA record scaled at $a_g = 0.5g$, yield identical results. This behaviour was expected since the effective period of the soil was $T_{efsoil} = 0.45s$ from Fast Fourier Transform Analysis, while the effective period of the soil-foundation-structure system was $T_{efsys} = 0.63s$, as shown in Fig. 3.39 and thus no radiation of waves from the system to the soil takes place (Veletsos & Wei 1971). Hence, the MPC boundaries were selected for all of the analyses conducted similarly to Zafeirakos and Gerolymos (2013).

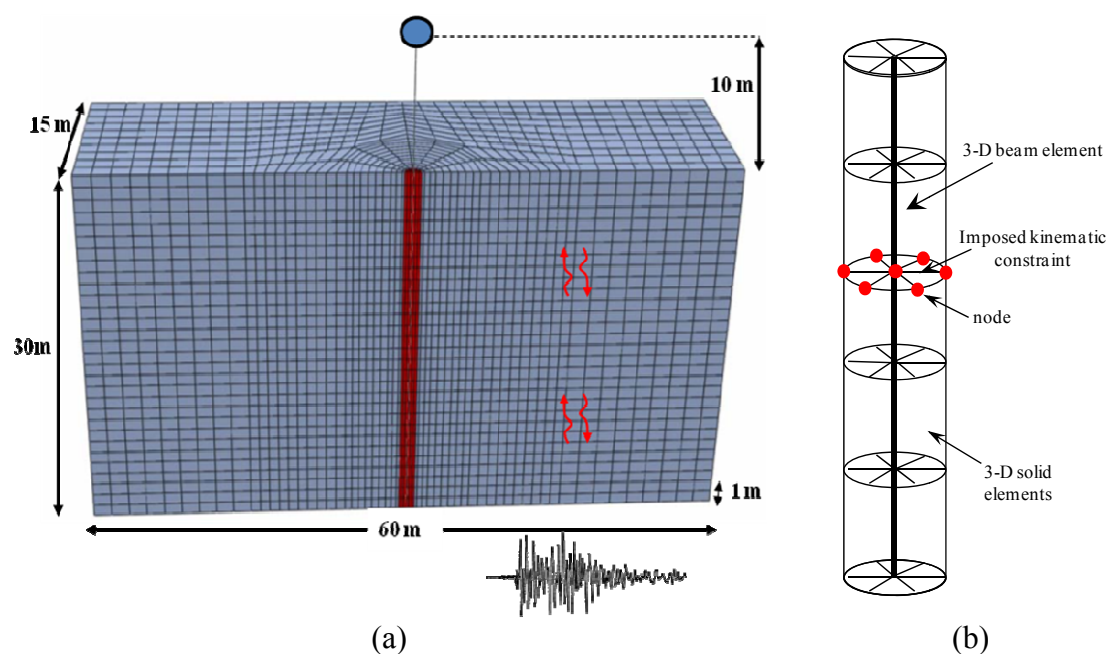


Fig. 3.38. Fully 3-D FE modelling of the investigated problem (a) and modelling of the pile (b).

An additional factor that had to be investigated in order to perform the 3-D analysis was the damping of the soil elements. Rayleigh damping of $\xi=5\%$ was initially selected for the soil elements of the 3-D FE model. It was found that this resulted in an overestimation of the computed acceleration, displacement and rotation time histories in comparison to the Beam-FE model. Indeed, the existence of a cut-off frequency for radiation damping holds true when the source of radiation is attributed to the so-called inertial interaction effect, referring to the response of the pile-structure system to

excitation by D'Alambert forces. There is also a second source of radiation. That is the kinematically driven radiation damping due to the interaction of the pile with the surrounding soil, driven by the free-field response. To capture in a crude but simple way the effect of the latter source of radiation damping, the parameters of the Rayleigh damping for the soil elements were calibrated to match the equivalent damping from the dampers of the Beam-FE model at a frequency which equals the fundamental frequency of the soil $\xi = \omega C/2K$, where ω is the soil frequency, C is the damping coefficient of the damper, and K is the spring stiffness, leading to improvement of the response of the 3-D FE model in comparison to the beam model. Alternatively, the matching could have been done at the predominant frequency of the excitation as well, leading to a similar response Saitoh (2012). The main disadvantage of the second approximation lies on the estimation of the predominant excitation frequency which varies with depth and is different for different seismic motions.

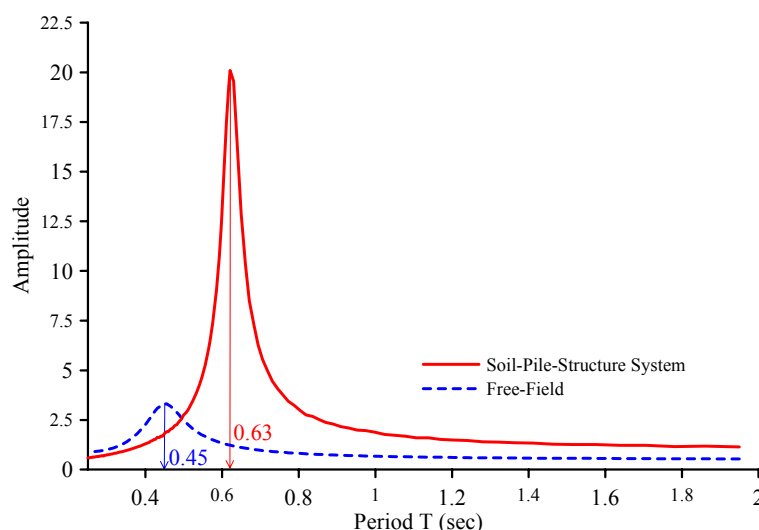


Fig. 3.39. Fast Fourier Transform Analysis for the free-field and Soil-Pile-Structure system response.

The numerical results obtained by the proposed advanced beam model using a set of 6 excitation motions, have been compared against both FE models. More specifically, in Figs. 3.40a-c the acceleration time histories at the bridge deck level $\ddot{w}(H,t)$ corresponding to the Lefkada, JMA and Aegion excitation motions scaled to $a_g = 0.8g$, are presented, respectively. In these figures the geometrically linear and nonlinear analysis of the proposed model, taking into account both rotary inertia and shear deformation effect are compared with the Beam-FE and the fully 3-D FE models. From

the obtained results it is observed that the proposed nonlinear formulation can capture accurately the response of the solid model accounting for P- δ effect, while the linear case predicts identical acceleration time histories with the Beam-FE model. From the conducted investigation, it is deduced that instead of executing time-expensive 3-D analyses for the soil-pile-bridge system, the proposed beam model can be employed providing minimum calculation effort while retaining high precision in the obtained results. Under the scope of efficiency, it is worth noting that as the two approaches have fundamental differences (i.e. 101 elements for the proposed model instead of approximately 15,000 elements for the solid one), the difference between the computational time required for the analyses is significant. Indicatively, it is mentioned that the sophisticated solid model required approximately 2.5h to 5.5h for the Aegion and JMA excitation, respectively (even though half of the system is concerned), while the proposed one required from 25sec to 70sec for the same excitations.

Moreover, in Fig. 3.41 the corresponding ($\xi = 5\%$) response spectra are also presented. As expected, the response spectra of the 3-D FE model produce higher peak acceleration values, due to the fact that the damping in this model is less than in the beam models, as stated before. Nevertheless, the response spectra from both approaches produce the maximum acceleration values at the same periods.

Similarly, Figs. 3.42-3.47 illustrate the displacement time histories at the deck level $w(H,t)$ and pile head (ground surface) level $w(L,t)$ corresponding to the Lefkada, JMA and Aegion excitation motions, respectively for the same cases of analysis, while in Figs. 3.48-3.50 the rotation time histories at the deck level $\theta_y(H,t)$ are also presented. Once again the proposed nonlinear formulation captures well the response of the 3-D FE model while response for the linear analysis and the Beam-FE model are identical. As in the case of the acceleration time histories, the peak displacement and rotation values calculated with the solid model are higher than those from the linear Beam-FE analysis.

What is of great interest is the case of Aegion (1995) (Figs. 3.46, 3.47), where a great difference in the response of the system is observed, even though the acceleration time histories are similar. In order to justify the difference between the 3-D analysis and both the proposed model and the one implemented in the Finite Element code OpenSees (2005), a Beam-FE model was also created in the Finite Element code ABAQUS (2009) which provides a graphical interface. The results obtained from that model lead to similar displacement time histories as the rest of the beam models.

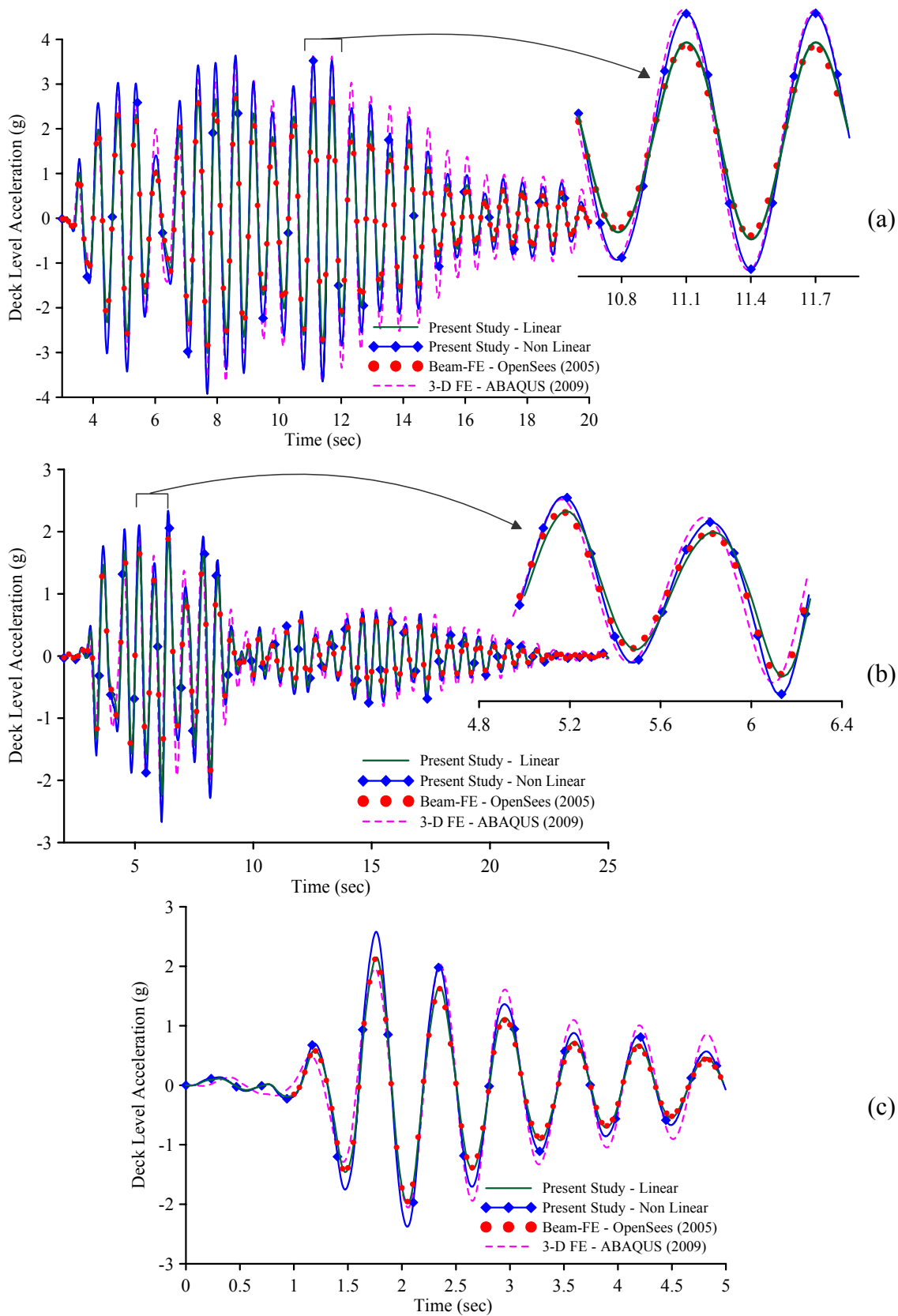


Fig. 3.40. Acceleration time history of the deck level for Lefkada(a), JMA(b) and Aegion (c) excitation.

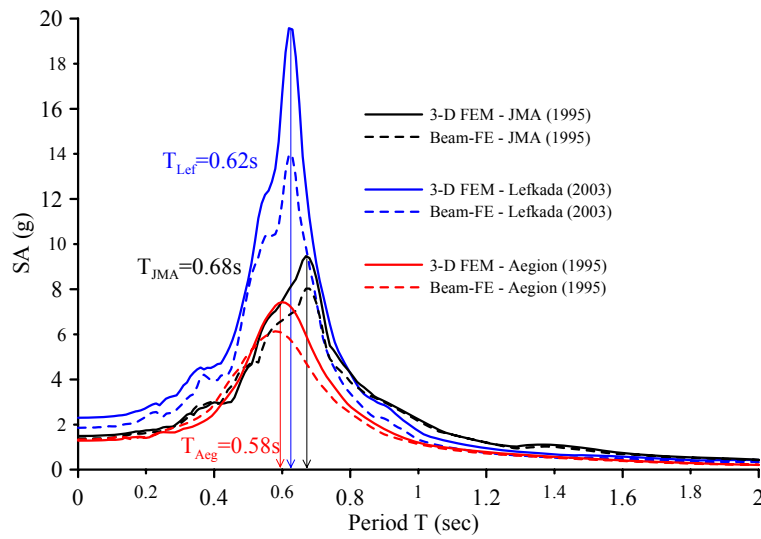


Fig. 3.41. Comparison between the response spectra ($\zeta=5\%$) at the deck level.

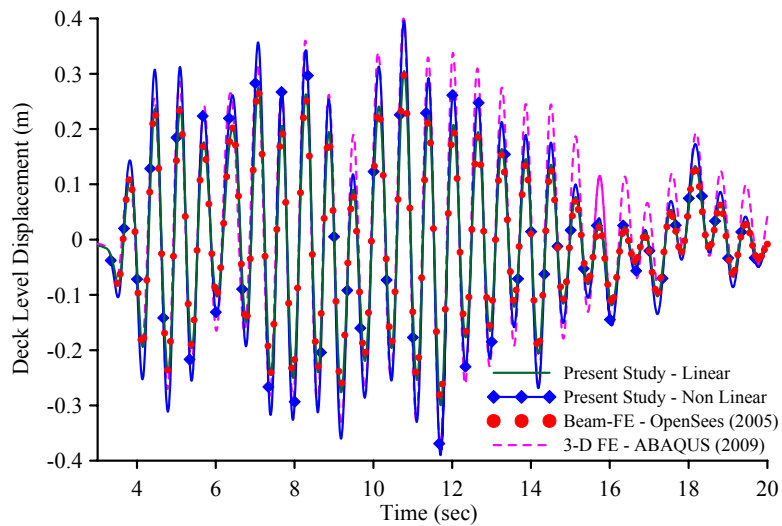


Fig. 3.42. Displacement time history of the deck level for Lefkada excitation.

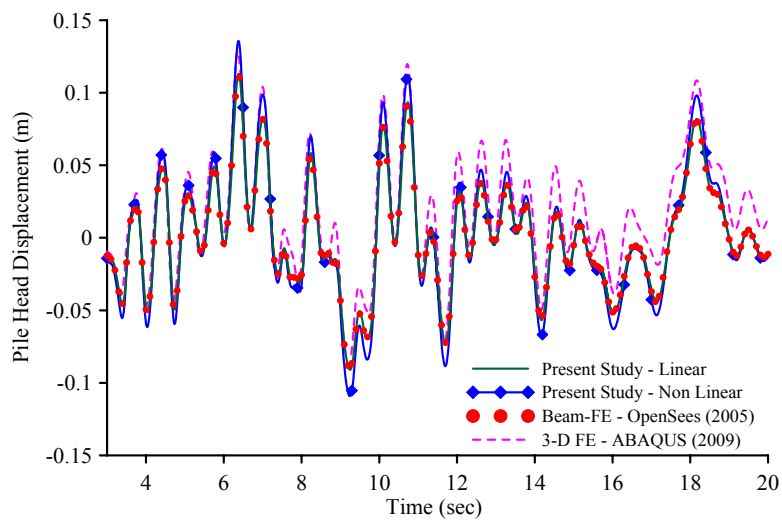


Fig. 3.43. Displacement time history of the pile head for Lefkada excitation.

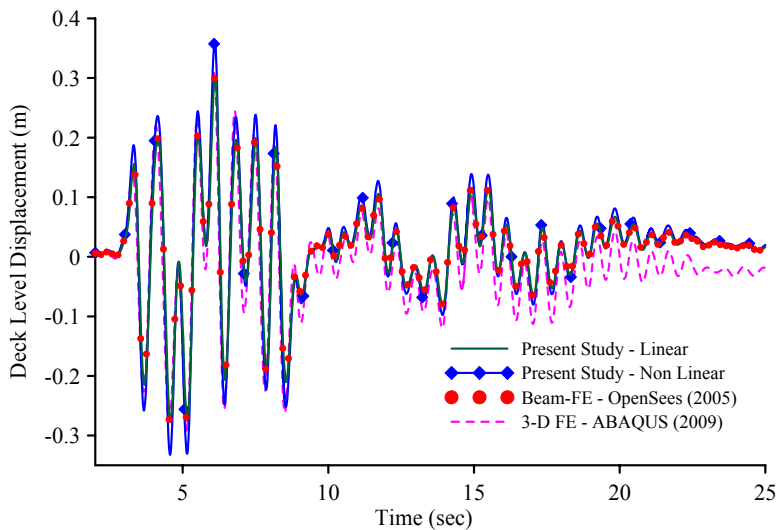


Fig. 3.44. Displacement time history of the deck level for JMA excitation.

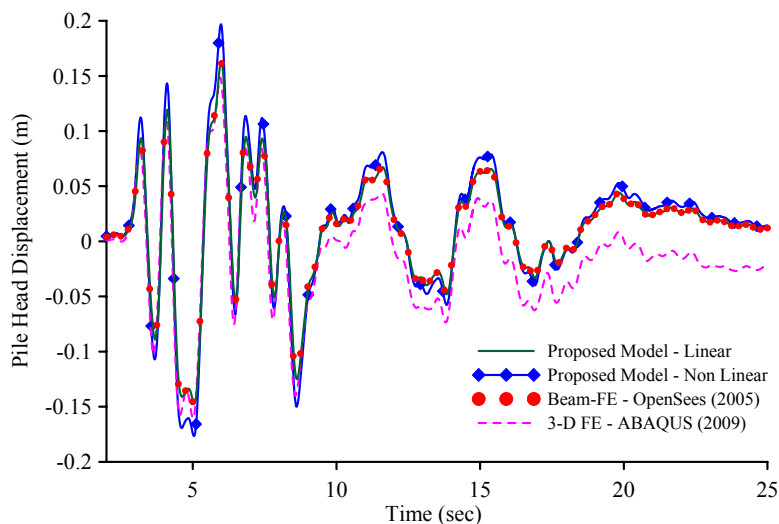


Fig. 3.45. Displacement time history of the pile head for JMA excitation.

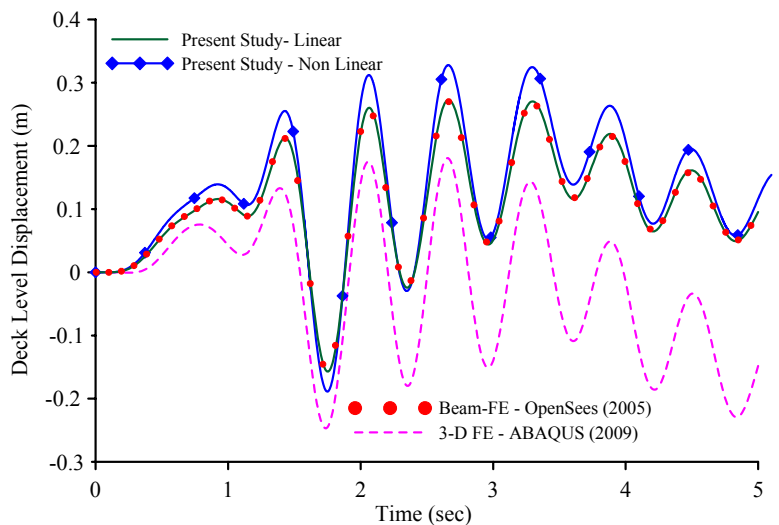


Fig. 3.46. Displacement time history of the deck level for Aegion excitation.

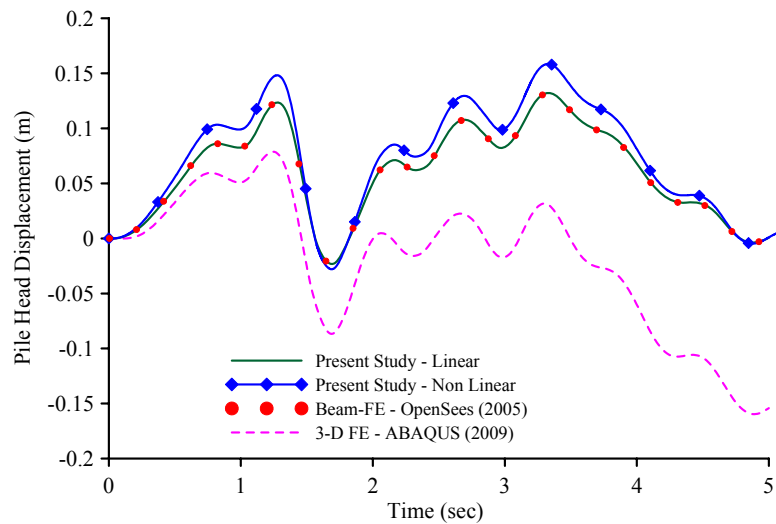


Fig. 3.47. Displacement time history of the pile head for Aegion excitation.

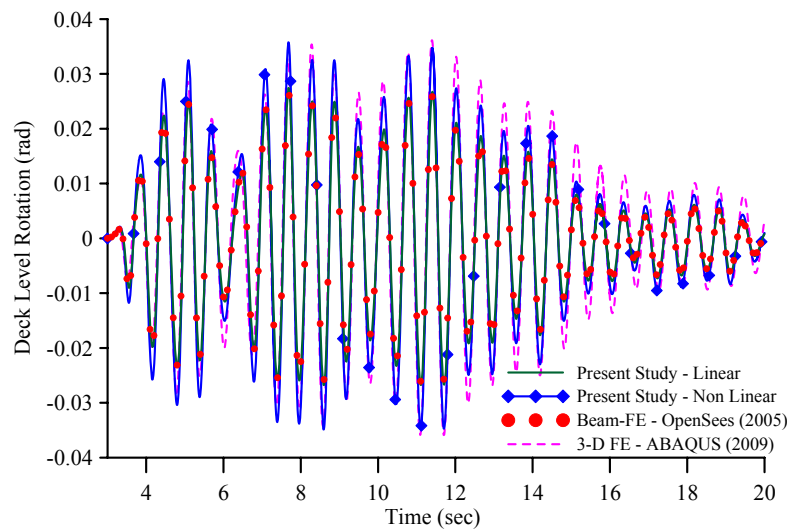


Fig. 3.48. Rotation time history of the deck level for Lefkada excitation.

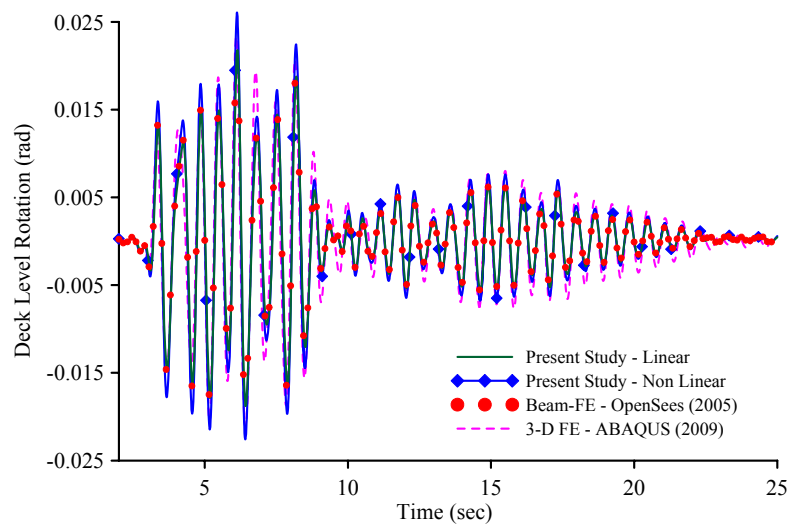


Fig. 3.49. Rotation time history of the deck level for JMA excitation.

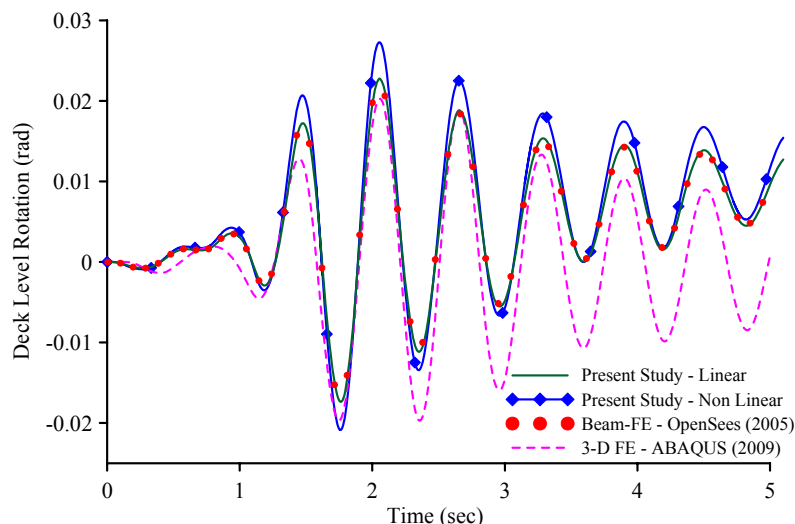


Fig. 3.50. Rotation time history of the deck level for Aegion excitation.

The difference in the displacement time histories is attributed to the sequence of significant pulses of the Aegion (1995) record. The response of the deck calculated by all the beam models (Fig. 3.46) exhibits greater displacement at the first peak displacement (positive direction) than that estimated by the 3–D FE model. As the deck starts to move towards the opposite direction, it does not pass far from its initial position in the beam model, while it moves greater towards the negative direction in the solid one. By the end of second positive peak displacement, the deck moves even further towards the positive direction in both models. The distance covered until the second negative peak displacement is smaller than the previous stages. Thus, in the 3–D FE the deck moves to the left, while in the beam models the deck remains to the right side. As the distance covered among each peak displacement value decreases, the deck oscillates in the side that was before until the end of the oscillation. This phenomenon becomes also evident from the rotation time history (Fig. 3.50). The difference in the responses becomes greater as the peak ground acceleration increases from 0.5 to 0.8 g. However, this is a unique case, since analyses with other records that contain asymmetric loading (e.g. Lefkada 1973) showed no differences in the response of the system. Fig. 3.51 illustrates snapshots of the deformed column-pile for the Aegion (1995) excitation scaled to $a_g = 0.5g$ at the time instants $t_a = 1.75s$, $t_b = 2.65s$, $t_c = 3.6s$ and $t_d = 4.5s$ in comparison to the undeformed state (scaling factor 50) from the solid and the beam models in FE code ABAQUS, verifying the aforementioned justification.

Moreover, Figs. 3.52-3.54 illustrate the displacement time histories at the deck level $w(H,t)$ corresponding to the Lefkada, JMA and Aegion excitation motions,

respectively taking into account or ignoring soil material nonlinearity. In Figs. 3.55a-c the bending moment envelopes of the column-pile corresponding to the Lefkada, JMA and Aegion excitation motions, respectively, are presented performing either a linear or a nonlinear analysis of the proposed model, compared with the Beam-FE and the fully 3-D FE models. Both the results from the elastic and the inelastic soil response are illustrated. In general, the agreement between the computed curves is quite satisfactory.

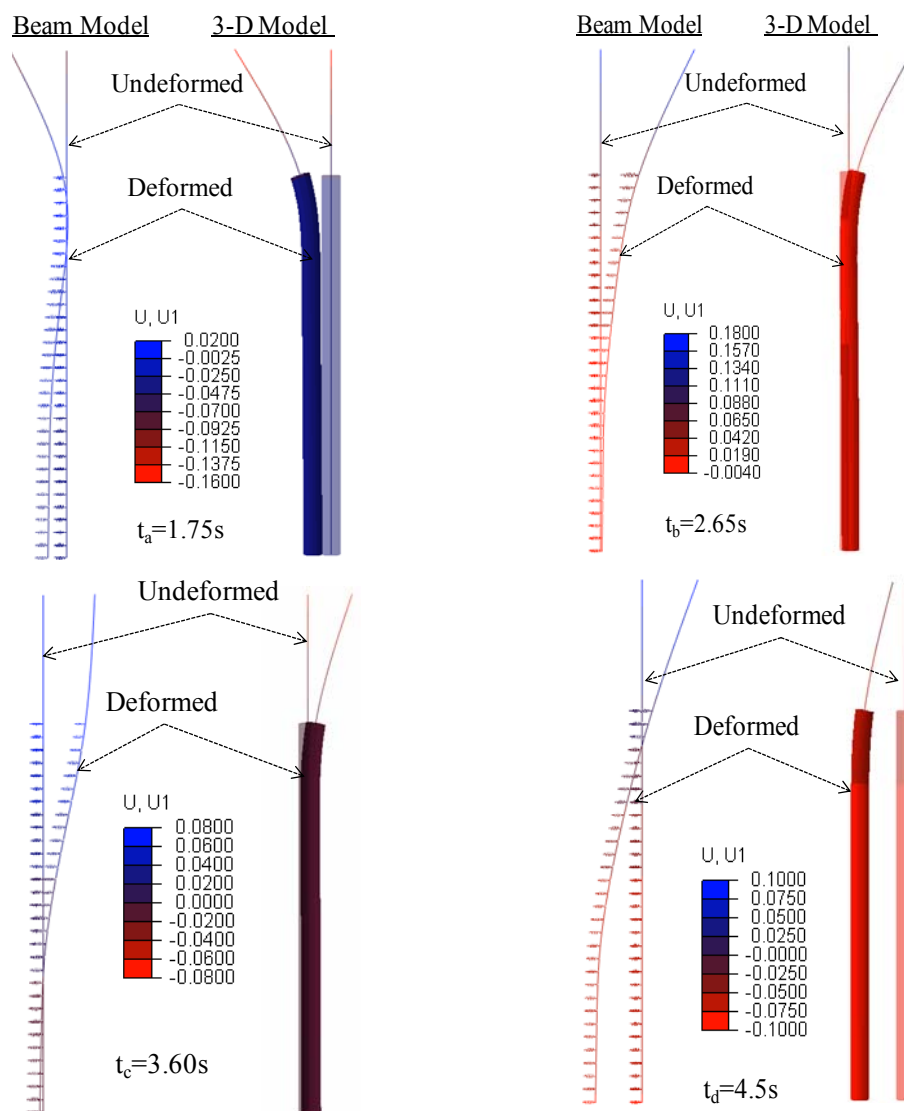


Fig. 3.51. Snapshots of the deformed column-pile for the Aegion (1995) excitation scaled to $a_g = 0.5g$ at the time instants $t_a = 1.75s$, $t_b = 2.65s$, $t_c = 3.6s$ and $t_d = 4.5s$ in comparison to the undeformed state (scaling factor 50) from the 3-D FE model and the Beam-FE model ABAQUS.

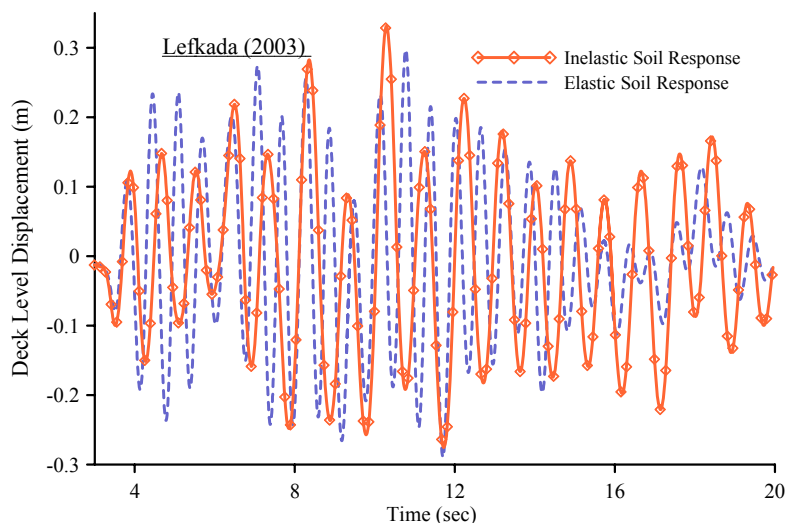


Fig. 3.52. Displacement time history of the deck level for Lefkada excitation.

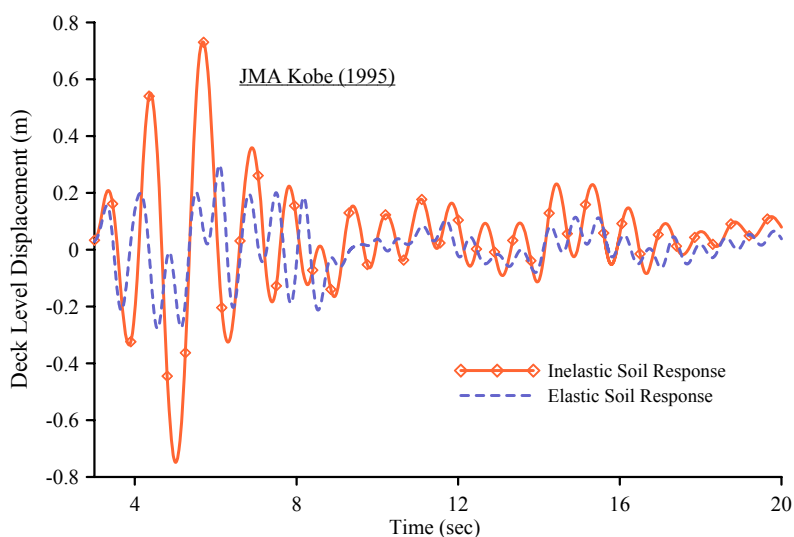


Fig. 3.53. Displacement time history of the deck level for JMA excitation.

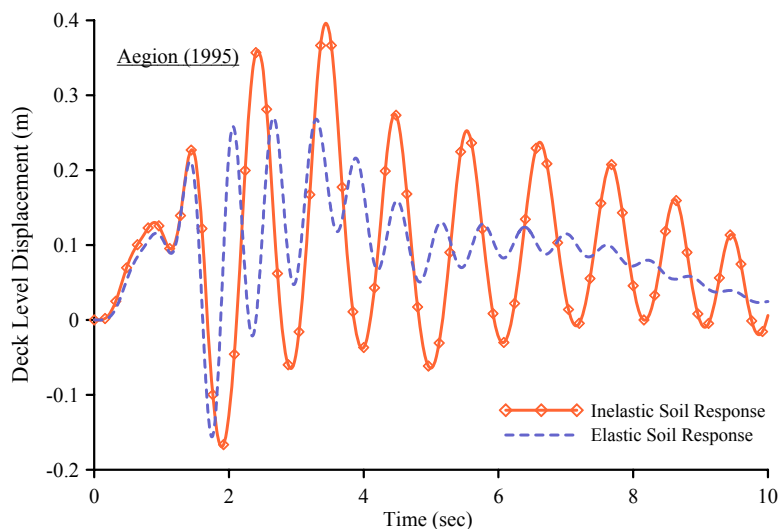


Fig. 3.54. Displacement time history of the deck level for Aegion excitation.

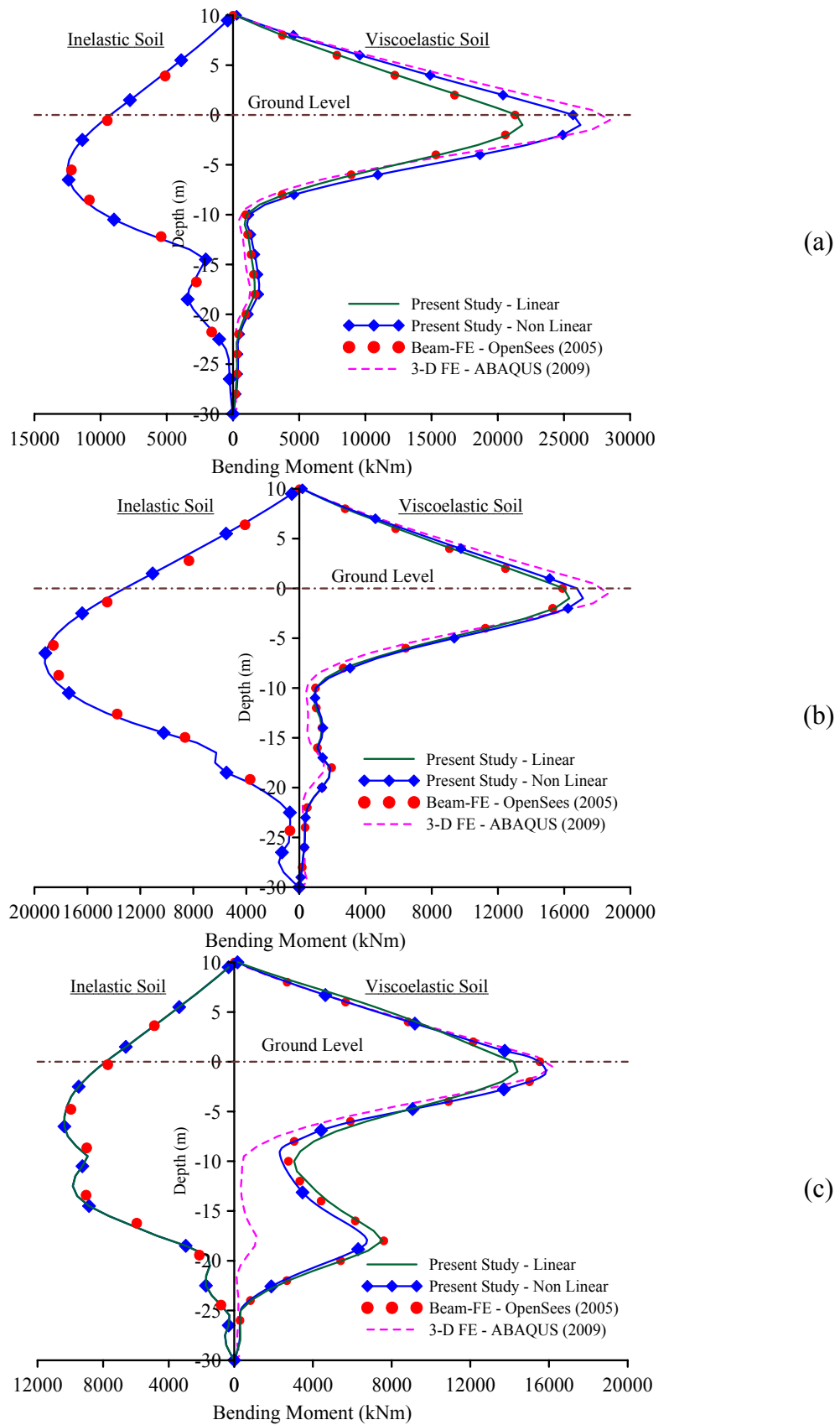


Fig. 3.55. Maximum bending moment distribution for Lefkada (a), JMA (b) and Aegion (c) excitation.

Finally, in Table 3.21 the maximum values of the bending moment along with their location are presented for different cases of analysis for all the excitation motions. From these figures and table it is concluded that the proposed geometrically nonlinear formulation captures accurately the calculated response according to the other methods of analysis used, while all the models predict similar shapes of the moment distribution and the increase of the bending moment at the interface of the two soil layers. The models also predict the same depth of the maximum bending moment as well as the shift of the maximum bending moment at a higher depth as the peak ground acceleration increases for the case of the inelastic soil response. The increased bending moment predicted by the proposed nonlinear analysis and the 3–D FE model is attributed to the higher predicted acceleration values at the deck level.

3.6 Concluding Remarks

In this chapter, a Boundary Element Method is developed for the geometrically nonlinear response of shear deformable beams of simply or multiply connected constant cross-section, partially supported on nonlinear three-parameter tensionless viscoelastic foundation, undergoing moderate large displacements under general boundary conditions. The beam is subjected to the combined action of arbitrarily distributed or concentrated transverse loading and bending moments in both directions as well as to axial loading. The main conclusions that can be drawn from this investigation are

- i. The proposed beam formulation is capable of yielding results of high accuracy, as verified by comparing with 2D/3D FEM models and experimental results, with minimum computational cost, providing a simple, reliable and efficient computational tool.
- ii. In the examined examples, the influence of geometrical nonlinearity is illustrated through
 - The significant discrepancy between the results of the linear and the nonlinear analyses.
 - The remarkable discrepancy in the response of a beam-foundation system in the resonance case.
 - The increase or decrease of the stiffness rigidity.
 - The affect on the natural frequencies.

- iii. The coupling effect of the transverse displacements in both directions in the nonlinear analysis influences these displacements

Table 3.21. Maximum values of the bending moment for elastic soil M_{el} and inelastic soil M_{pl} (MPa) and their location (m) from the ground level.

Excitation	Analysis / Model	Elastic Soil		Inelastic Soil	
		M_{el}	Location	M_{pl}	Location
<i>Lefkada</i> (2003) $a_g = 0.5g$	Present Study–Linear	13.68	-1.0	7.19	-4.5
	Present Study–Non Linear	17.01	-1.0	7.16	-4.5
	Beam FE–OpenSees (2005)	13.58	-1.0	7.18	-4.5
	3–D FE Abaqus (2009)	17.80	-0.5	–	–
<i>Lefkada</i> (2003) $a_g = 0.8g$	Present Study–Linear	21.87	-1.0	12.75	-5.5
	Present Study–Non Linear	27.66	-1.0	12.52	-5.5
	Beam FE–OpenSees (2005)	21.72	-1.0	12.60	-5.5
	3–D FE Abaqus (2009)	28.48	-0.5	–	–
<i>JMA</i> (1995) $a_g = 0.5g$	Present Study–Linear	10.27	-1.0	12.58	-6.5
	Present Study–Non Linear	11.02	-1.0	12.70	-6.5
	Beam FE–OpenSees (2005)	10.13	-1.0	12.55	-6.5
	3–D FE Abaqus (2009)	11.67	-0.5	–	–
<i>JMA</i> (1995) $a_g = 0.8g$	Present Study–Linear	16.31	-1.0	19.18	-7.5
	Present Study–Non Linear	17.14	-1.0	19.20	-7.5
	Beam FE–OpenSees (2005)	16.21	-1.0	19.16	-7.5
	3–D FE Abaqus (2009)	18.67	-0.5	–	–
<i>Aegion</i> (1995) $a_g = 0.5g$	Present Study–Linear	9.94	-1.0	6.75	-4.5
	Present Study–Non Linear	10.00	-1.0	6.72	-4.5
	Beam FE–OpenSees (2005)	9.93	-1.0	6.74	-4.5
	3–D FE Abaqus (2009)	10.11	-0.5	–	–
<i>Aegion</i> (1995) $a_g = 0.8g$	Present Study–Linear	14.40	-1.0	10.26	-5.5
	Present Study–Non Linear	15.86	-1.0	10.36	-6.5
	Beam FE–OpenSees (2005)	15.89	-1.0	10.30	-5.5
	3–D FE Abaqus (2009)	16.18	-0.5	–	–

- iv. In some cases, the effect of shear deformation is significant, especially for low beam slenderness values, increasing both the maximum transverse displacements and the calculated periods of the first cycle of motion, in both small and large deflection analyses.
- v. The superiority of the presented Timoshenko beam formulation over Euler-Bernoulli elements is also verified by yielding results closer to rigorous FEM model.
- vi. Shear-locking has been successfully avoided.
- vii. The proposed model takes into account both kinematic and inertial interaction to the geometrical nonlinear dynamic response of a column-pile embedded in a layered soil profile.
- viii. The soil nonlinearity can be easily treated by means of a hybrid spring configuration consisting of a nonlinear (p - y) spring connected in series to an elastic Kelvin–Voigt element.
- ix. The lift up of the beam caused by the tensionless character of the foundation is observed, leading to magnification of the consequences of the dynamic response.
- x. The response of the beam is strongly influenced by the linear and nonlinear parameters of the foundation reaction.
- xi. The damping coefficient is of paramount importance for beams on viscoelastic foundations, as it reduces the vibration amplitude and the consequences of the dynamic response
- xii. The imposed dynamic loading (e.g. sequence of significant pulses of the Aegion (1995) record) could influence the response of the beam-foundation system according to the implemented model.

Geometrically Nonlinear Inelastic Analysis of Shear Deformable Beams on Inelastic Foundation

4.1. Introduction

In design of civil engineering structures (e.g. bridges, wind-turbines, offshore platforms, etc.) the analysis of beam–foundation systems is most often encountered. In order to conduct precise analysis, without jeopardizing accuracy and thus safety, the thorough understanding of the mechanics of the beam–foundation system is required. Currently, these systems are designed to behave elastically for every type of loading (EC8 2004), however recent research efforts (Gerolymos et al. 2009, Chiou et al. 2012) have investigated the beneficial character of permitting plastification to occur at the beam–foundation system.

Moreover, design of beams and engineering structures based on elastic analysis are most likely to be extremely conservative not only due to significant difference between initial yield and full plastification in a cross section, but also due to the unaccounted, yet significant, strength reserves that are mobilized in redundant members after inelastic redistribution takes place. Thus, material nonlinearity is important for investigating the ultimate strength of a beam that resists bending loading, while distributed plasticity models are acknowledged in the literature (Teh & Clarke 1999, Nukala & White 2004, Saritas & Filippou 2009) to capture more rigorously material nonlinearities than cross sectional stress resultant approaches (Attalla et al. 1994) or lumped plasticity idealizations (Orbison et al. 1982, Ngo-Huu et al. 2007). Furthermore, the cost-effective design of infrastructures requires the realistic estimation of the beam–foundation system response, accounting for all sources of nonlinearities; namely nonlinear stress–strain behaviour of the structural member and the soil (material nonlinearity) along with the geometrical nonlinearity. Moreover, the contemporary advancements in material science have facilitated the intensive use of materials having relatively high transverse shear modulus; thereby the error incurred from the ignorance of shear deformation effect may be substantial, particularly in the case of significant lateral loading.

Over the years, the beam-foundation interaction has been an area of extensive research activity and various methods have been developed in order to study the complex behaviour of the system, from the material level to the interaction between structural and foundation elements. These methods can be grouped into three major categories; namely the limit equilibrium (Broms 1964a, 1964b, 1965), the beam-on-Winkler-foundation (Winkler 1867, Filonenko-Borodich 1940, Hetenyi 1946, Pasternak 1954, Vlasov 1966) and those based on the continuum mechanics. Among them, the most commonly employed in engineering practice is the beam approach due to the significant advantages over the other methods, such as the simplicity in formulation and modelling together with the high level of accuracy with minor computational cost.

Within this framework, several researches have employed the concept of *Elastic Beam on Nonlinear Foundation*. In this formulation, the foundation load-displacement relation is assumed to follow a nonlinear law while the beam remains elastic throughout the analysis. The load-displacement relationships are described by empirical p - y curves (Brown & Shie 1990,91, Laman et al. 1999, Kim & Jeong 2011) where the spring stiffness value is variable, allowing consideration of a non-proportional relationship between the soil resistance per unit pile length p and the lateral displacement y . To this end, Sharma and Dasgupta (1975) employed an iteration method using Green's functions for the analysis of uniformly loaded axially constrained hinged beams assuming an exponential load-displacement foundation reaction law. Beaufait and Hoadley (1980) approximated the nonlinear load-displacement relationship of the Winkler foundation with a bilinear curve and utilized the midpoint difference method to analyze the beam coupled with the weighted averages scheme to estimate the spring stiffness for each iteration, followed by Yankelevsky et al. (1989) who presented an iterative procedure based on the exact stiffness matrix for the beam on Winkler foundation by approximating the load-displacement curve by three to five regions rather than two. Kaliszky and Logo (1994) adopted the extremum principle to analyze a nonlinear elastic beam on nonlinear elastic foundation. Both the beam and the Winkler springs were assumed to follow a bilinear material model while the beam was subdivided into series of rigid bars and the deformation was concentrated in the hinges and spring elements. El Naggar and Novak (1996) used a Winkler model employing a hyperbolic stress strain relationship to evaluate the lateral response of piles, while Wang et al. (1998) employed the same method to predict results of centrifuge model tests of single piles in a soft clay soil profile. Lately, Sapountzakis and Kampitsis (2011a) studied the nonlinear static analysis of shear deformable beam-columns partially

supported on tensionless three parameter foundation, undergoing moderate large deflections under general boundary conditions. In general, this method is the most commonly used in engineering practice. Its popularity derives from the simplicity and the adequate accuracy while the main drawback of the method is that it neglects the soil continuity. In order to overcome this disadvantage several researchers have adopted the *three-dimensional continuum* model, where nonlinear behaviour of the ground can be taken into consideration employing various constitutive laws. Although the continuum approach is a powerful and rigorous way of simulating the whole system accounting for various three-dimensional interaction effects and the nonlinear behaviour of soil, it is not widely implemented, besides research purposes, as it is intractable, mathematically complex and the computational and modelling effort required is extremely time consuming.

Although the nonlinear behaviour of the soil due to high strain level has been studied extensively (Brown & Shie 1991, Laman et al. 1999, Kim & Jeong 2011) only few studies have encountered the inelastic behaviour of both the beam and the foundation elements. According to this, the beam stress-strain and the foundation load-displacement relations are assumed to follow nonlinear inelastic constitutive laws. Consequently, such models are not easily formulated due to the complexity of the problem. To start with, Budek et al. (2000) investigated the inelastic response of a reinforced concrete pile in cohesionless soil while Ayoub (2003) presented an inelastic finite element formulation capable of capturing the nonlinear behaviour of both the beam and the foundation. The element is derived from a two-field mixed formulation with independent approximation of forces and displacements and compared with the displacement based formulation. Mullapudi and Ayoub (2010a) expanded this research in inelastic analysis of beams resting on two-parameter foundation where the values for the parameters are derived through an iterative technique that is based on an assumption of plane strain conditions for the soil medium.

In this chapter, a Boundary Element Method (BEM) is developed for the geometrically nonlinear inelastic analysis of Timoshenko beams of arbitrary doubly symmetric simply or multiply connected constant cross-section, resting on inelastic tensionless two-parameter foundation. The beam is subjected to the combined action of arbitrarily distributed or concentrated transverse loading and bending moments in both directions as well as to axial loading, while its edges are subjected to the most general boundary conditions. To account for shear deformations, the concept of shear deformation coefficients is used. A displacement based formulation is developed and

inelastic redistribution is modelled through a distributed plasticity (fibre) approach exploiting three dimensional material constitutive laws and numerical integration over the cross sections. An incremental–iterative solution strategy along with an efficient iterative process are employed (Ortiz & Simo 1986), while the arising boundary value problem is solved employing the boundary element method (Katsikadelis 2002).

Numerical examples are worked out confirming the accuracy and the computational efficiency of the proposed beam formulation through comparison with literature and FEM results. In these examples, the significant influence of the geometrical nonlinearity and the shear deformation effect in the response of a beam-foundations system are also illustrated. Subsequently, the proposed formulation is validated against a series of Laboratory Pushover tests on vertical single piles embedded in dry sand under different load paths to failure in M–Q space conducted in the Laboratory of Soil Mechanics/Dynamics in NTUA by Gerolymos (2012) and Giannakos (2013). The obtained results are also compared to those obtained from a fully 3D Nonlinear Finite Element (FE) simulation implemented in the finite element code ABAQUS (Dassault 2009). The essential features and novel aspects of the present formulation compared with previous ones are summarized as follows.

- i. The proposed beam model accounts for the geometrical nonlinearity by retaining the square of the slope in the strain–displacement relations, avoiding in this way the inaccuracies arising from a linearized second-order analysis. For that purpose the total Lagrange formulation (intermediate non-linear theory) has been adopted.
- ii. Shear deformation effect is taken into account on the geometrically nonlinear inelastic analysis of beams on nonlinear foundation (explicit axial-shear-flexure interaction).
- iii. The formulation presented adopts a J2 three-dimensional plasticity law (von Mises) to assess the inelastic beam-foundation system response.
- iv. The formulation is a displacement based one taking into account inelastic redistribution along the beam axis.
- v. A distributed plasticity (fibre) approach has been employed.
- vi. The inelasticity of the soil medium is taken into account, employing an inelastic spring foundation model.
- vii. The tensionless character of the foundation is also taken into consideration.

- viii. An incremental-iterative solution strategy is adopted to restore global equilibrium of the system.
- ix. The shear deformation coefficients are evaluated using an energy approach, instead of Timoshenko's (Timoshenko & Goodier 1984) and Cowper's (1966) definitions, for which several authors (Schramm et al. 1994, 1997) have pointed out that one obtains unsatisfactory results or definitions given by other researchers (Stephen 1980, Hutchinson 2001) for which these factors take negative values.
- x. The beam is supported by the most general nonlinear boundary conditions.
- xi. The use of BEM permits the effective computation of derivatives of the field functions (e.g. stresses, stress resultants) which is very important during the nonlinear inelastic response of beam-foundation systems.
- xii. To the author's knowledge, a BEM approach has not yet been used for the solution of the aforementioned problem, while the developed procedure retains most of the advantages of a BEM solution even though domain discretization is required.

Finally, it is worth mentioning that the outcome of the conducted research activity presented in this chapter of the doctoral dissertation has been published in international journals (Sapountzakis & Kampitsis 2012a, 2013c, Kampitsis et al. 2014), and in international conferences (Sapountzakis & Kampitsis 2011e, 2012b, 2013d).

4.2 Statement of the Problem

Let us consider a prismatic beam of length l (Fig. 4.1) with an arbitrarily shaped doubly symmetric constant cross section, occupying the two dimensional multiply connected region Ω of the y, z plane bounded by the Γ_j ($j = 1, 2, \dots, K$) boundary curves, which are piecewise smooth, i.e. they may have a finite number of corners. In Fig. 4.1, C_{yz} is the principal bending coordinate system through the cross section's centroid. The normal stress-strain relationship for the material is assumed to be elastic-plastic-strain hardening with initial modulus of elasticity E , shear modulus G , post-yield modulus of elasticity E_t , yield stress σ_{Y0} , and yield strain ε_{Y0} . The beam is partially supported on inelastic tensionless two-parameter foundation. According to the Pasternak hypothesis, the foundation reaction is expressed as

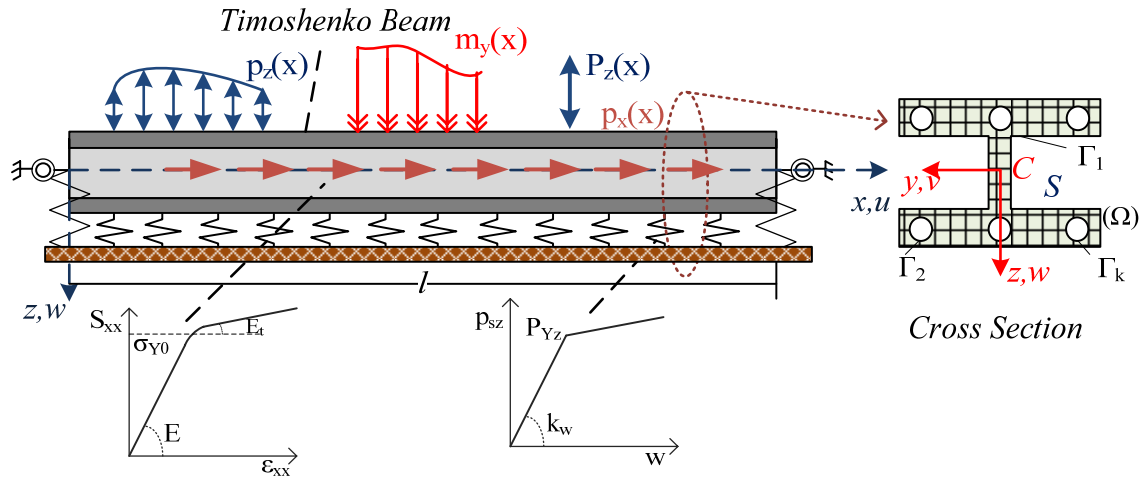


Fig. 4.1. x - z plane of prismatic beam resting on inelastic foundation under axial-flexural loading.

$$p_{sy} = p_{Wy} - \frac{d(p_{Py})}{dx} \quad p_{sz} = p_{Wz} - \frac{d(p_{Pz})}{dx} \quad (4.1a,b)$$

with Winkler and Pasternak reactions related to the transverse displacements and their derivatives as

$$p_{Wy} = \begin{cases} k_{Wy}v \\ 0 \end{cases} \quad \text{and} \quad p_{Py} = \begin{cases} k_{Py} \frac{dv}{dx} & \text{if } p_{sy} > 0 \\ 0 & \text{if } p_{sy} \leq 0 \end{cases} \quad (4.2a)$$

$$p_{Wz} = \begin{cases} k_{Wz}w \\ 0 \end{cases} \quad \text{and} \quad p_{Pz} = \begin{cases} k_{Pz} \frac{dw}{dx} & \text{if } p_{sz} > 0 \\ 0 & \text{if } p_{sz} \leq 0 \end{cases} \quad (4.2b)$$

The nonlinear Winkler and Pasternak inelastic functions depend on the initial stiffnesses $k_{Ly}, k_{Py}, k_{Lz}, k_{Pz}$, yielding loads P_y^Y, P_z^Y , and hardening moduli k_{yt}, k_{zt} according to y and z axes, respectively.

The beam is subjected to the combined action of the arbitrarily distributed or concentrated axial loading $p_x = p_x(x)$, transverse loading $p_y = p_y(x)$, $p_z = p_z(x)$ and bending moments $m_y = m_y(x)$, $m_z = m_z(x)$ acting along y, z directions, respectively (Fig.4.1).

4.2.1 Displacements, Strains & Stresses

Under the action of the aforementioned loading, the displacement field of the beam taking into account shear deformation effect is given as (Ramm & Hofmann 1995)

$$\bar{u}(x, y, z) = u(x) - y\theta_z(x) + z\theta_y(x) \quad (4.3a)$$

$$\bar{v}(x) = v(x) \quad \bar{w}(x) = w(x) \quad (4.3b,c)$$

where \bar{u} , \bar{v} , \bar{w} are the axial and transverse beam displacement components with respect to the Cyz system of axes; $u(x)$, $v(x)$, $w(x)$ are the corresponding components of the centroid C and $\theta_y(x)$, $\theta_z(x)$ are the angles of rotation due to bending of the cross-section with respect to its centroid. It is worth noting that since the additional angle of rotation of the cross-section due to shear deformation is taken into account, the angle of rotation due to bending is not equal to the derivative of the displacement (i.e. $\theta_y \neq w'$, $\theta_z \neq v'$).

Employing the strain-displacement relations of the three-dimensional elasticity for moderate large displacements (Ramm & Hofmann 1995, Rothert & Gensichen 1987, Brush & Almroth 1975) while strains remain small, the following strain components can be easily obtained

$$\varepsilon_{xx} = \frac{\partial \bar{u}}{\partial x} + \frac{I}{2} \left[\left(\frac{\partial \bar{v}}{\partial x} \right)^2 + \left(\frac{\partial \bar{w}}{\partial x} \right)^2 \right] \quad (4.4a)$$

$$\gamma_{xz} = \frac{\partial \bar{w}}{\partial x} + \frac{\partial \bar{u}}{\partial z} + \left(\frac{\partial \bar{v}}{\partial x} \frac{\partial \bar{v}}{\partial z} + \frac{\partial \bar{w}}{\partial x} \frac{\partial \bar{w}}{\partial z} \right) \quad \gamma_{xy} = \frac{\partial \bar{v}}{\partial x} + \frac{\partial \bar{u}}{\partial y} + \left(\frac{\partial \bar{v}}{\partial x} \frac{\partial \bar{v}}{\partial y} + \frac{\partial \bar{w}}{\partial x} \frac{\partial \bar{w}}{\partial y} \right) \quad (4.4b,c)$$

$$\varepsilon_{yy} = \varepsilon_{zz} = \gamma_{yz} = 0 \quad (4.4d)$$

Substituting the displacement components of eqn. (4.3) to the nonlinear strain-displacement relations of the Green-Lagrange strain tensor and exploiting the assumptions of moderate large displacements $((\partial \bar{u}/\partial x)^2 \ll \partial \bar{u}/\partial x$, $(\partial \bar{u}/\partial x)(\partial \bar{u}/\partial z) \ll (\partial \bar{u}/\partial x) + (\partial \bar{u}/\partial z)$, $(\partial \bar{u}/\partial z)(\partial \bar{u}/\partial y) \ll (\partial \bar{u}/\partial z) + (\partial \bar{u}/\partial y)$) the non vanishing (total) strain components are obtained as

$$\varepsilon_{xx}(x, y, z) = \frac{du(x)}{dx} - y \frac{d\theta_z(x)}{dx} + z \frac{d\theta_y(x)}{dx} + \frac{1}{2} \left[\left(\frac{dv(x)}{dx} \right)^2 + \left(\frac{dw(x)}{dx} \right)^2 \right] \quad (4.5a)$$

$$\gamma_{xy}(x) = \frac{dv(x)}{dx} - \theta_z(x) \quad \gamma_{xz}(x) = \frac{dw(x)}{dx} + \theta_y(x) \quad (4.5b,c)$$

It is worth noting what in the well known Euler-Bernoulli beam theory these shear deformations are neglected, thus

$$\theta_z = \frac{dv}{dx} \quad \theta_y = -\frac{dw}{dx} \quad (4.6b,c)$$

Considering strains to be small, employing the work conjugate second Piola–Kirchhoff stress tensor (Crisfield 1991), assuming an isotropic and homogeneous material without exhibiting any damage during its plastification and neglecting the vanishing S_{yy} , S_{zz} , S_{yz} components, the stress rates are defined in terms of the strain ones as

$$\begin{Bmatrix} dS_{xx} \\ dS_{xy} \\ dS_{xz} \end{Bmatrix} = \begin{bmatrix} E^* & & \\ & G & \\ & & G \end{bmatrix} \begin{Bmatrix} d\varepsilon_{xx}^{el} \\ d\gamma_{xy}^{el} \\ d\gamma_{xz}^{el} \end{Bmatrix} \quad (4.7)$$

where $d(\cdot)$ denotes infinitesimal incremental quantities over time (rates), the superscript el denotes the elastic part of the strain component and $E^* = E(1-\nu)/[(1+\nu)(1-2\nu)]$. If the plane stress hypothesis is undertaken then $E^* = E/(1-\nu^2)$ holds, while E is frequently considered instead of E^* ($E^* \approx E$) in beam formulations (Vlasov 1963, Armenakas 2006). This last consideration has been followed throughout the paper, while any other reasonable expression of E^* could also be used without any difficulty in many beam formulations.

As long as the material remains elastic or elastic unloading occurs

$$\{d\varepsilon_{xx} \quad d\gamma_{xy} \quad d\gamma_{xz}\}^T = \{d\varepsilon_{xx}^{el} \quad d\gamma_{xy}^{el} \quad d\gamma_{xz}^{el}\}^T \quad (4.8)$$

the stress rates are given with respect to the total strain ones occupying the Hooke's law (eqn. (4.7)), while when plastic flow occurs

$$\left\{ d\varepsilon_{xx} \quad d\gamma_{xy} \quad d\gamma_{xz} \right\}^T = \left\{ d\varepsilon_{xx}^{el} \quad d\gamma_{xy}^{el} \quad d\gamma_{xz}^{el} \right\}^T + \left\{ d\varepsilon_{xx}^{pl} \quad d\gamma_{xy}^{pl} \quad d\gamma_{xz}^{pl} \right\}^T \quad (4.9)$$

the stress rates are given with respect to the total and plastic strain ones through eqns. (4.7) and (4.9) as

$$\begin{Bmatrix} dS_{xx} \\ dS_{xy} \\ dS_{xz} \end{Bmatrix} = \begin{bmatrix} E & & \\ & G & \\ & & G \end{bmatrix} \begin{Bmatrix} d\varepsilon_{xx} - d\varepsilon_{xx}^{pl} \\ d\gamma_{xy} - d\gamma_{xy}^{pl} \\ d\gamma_{xz} - d\gamma_{xz}^{pl} \end{Bmatrix} \quad (4.10)$$

where the superscript *pl* denotes the plastic part of the strain component. The von Mises yield criterion (J2 plasticity), an associated flow rule and an isotropic hardening rule for the material are considered (Crisfield 1991), permitting the determination of the plastic strain components. The yield condition is described with the expression

$$\Phi_{vM} = \frac{\sqrt{S_{xx}^2 + 3(S_{xy}^2 + S_{xz}^2)}}{\sigma_Y(\varepsilon_{eq}^{pl})} - I \leq 0 \quad (4.11)$$

where σ_Y is the yield stress of the material and ε_{eq}^{pl} is the equivalent plastic strain, the rate of which is defined in (Crisfield 1991) and is equal to $d\varepsilon_{eq}^{pl} = d\lambda$ with $d\lambda$ being the proportionality facto. Moreover, the plastic modulus h is defined as $h = d\sigma_Y / d\varepsilon_{eq}^{pl}$ or $d\sigma_Y = hd\lambda$ and can be estimated from a tension test as $h = E_t E / (E - E_t)$ (Fig. 4.2).

According to the associated flow rule the plastic strain rates are given as

$$\left\{ d\varepsilon_{xx}^{pl} \quad d\gamma_{xy}^{pl} \quad d\gamma_{xz}^{pl} \right\}^T = d\lambda \left\{ \frac{\partial \Phi_{vM}}{\partial S_{xx}} \quad \frac{\partial \Phi_{vM}}{\partial S_{xy}} \quad \frac{\partial \Phi_{vM}}{\partial S_{xz}} \right\}^T \quad (4.12)$$



Fig. 4.2. Normal stress–strain (a) and yield stress – equivalent plastic strain (b) relationships.

Using the aforementioned relation linking the yield stress rate and the proportionality factor, eqns. (4.5), (4.7)-(4.11) and exploiting the plastic loading condition ($df = 0$), the stress rates - total strain rates relations are resolved as

$$\begin{Bmatrix} dS_{xx} \\ dS_{xy} \\ dS_{xz} \end{Bmatrix} = \frac{1}{c} \underbrace{\begin{bmatrix} c_{11} & & sym. \\ c_{21} & c_{22} & \\ c_{31} & c_{32} & c_{33} \end{bmatrix}}_{D^{elpl}} \begin{Bmatrix} d\varepsilon_{xx} \\ d\gamma_{xy} \\ d\gamma_{xz} \end{Bmatrix} \quad (4.13)$$

where D^{elpl} is the elastoplastic constitutive matrix with

$$c = hS_e^2 + ES_{xx}^2 + 9G(S_{xy}^2 + S_{xz}^2) \quad c_{11} = E \left[hS_e^2 + 9G(S_{xy}^2 + S_{xz}^2) \right] \quad (4.14a,b)$$

$$c_{21} = -3EGS_{xx}S_{xy} \quad c_{22} = G \left[hS_e^2 + ES_{xx}^2 + 9GS_{xz}^2 \right] \quad c_{31} = -3EGS_{xx}S_{xz} \quad (4.14c,d,e)$$

$$c_{32} = -9G^2S_{xy}S_{xz} \quad c_{33} = G \left[hS_e^2 + ES_{xx}^2 + 9GS_{xy}^2 \right] \quad S_e = \sqrt{S_{xx}^2 + 3(S_{xy}^2 + S_{xz}^2)} \quad (4.14f,g,h)$$

By setting $h = 0$ in the above relations, the constitutive matrix presented by Baba and Kajita (1982) is obtained, while if one of the shear stress components (along with the corresponding strain one) is dropped out, the constitutive relations presented by Chen and Trahair (1992) are also precisely recovered.

4.2.2 Stress Resultants, Equations of Equilibrium and Boundary Conditions

In order to establish the global equilibrium equations and the boundary conditions of the beam-foundation system, the principle of virtual work under a Total Lagrangian formulation neglecting body forces is employed as

$$\delta W_{int} = \delta W_{ext} \quad (4.15)$$

where $\delta(\cdot)$ denotes virtual quantities, W_{int} is the strain energy of the beam due to normal and shear stress and W_{ext} is the external load work, defined as

$$\delta W_{int} = \int_V (S_{xx} \delta \varepsilon_{xx} + S_{xy} \delta \gamma_{xy} + S_{xz} \delta \gamma_{xz}) dV \quad (4.16a)$$

$$\begin{aligned} \delta W_{ext} = & \int_l (p_x \delta u + p_y \delta v + m_y \delta \theta_y + p_z \delta w + m_z \delta \theta_z) dx - \int_l (p_{sy} \delta v + p_{sz} \delta w) dx \\ & + \sum_b^{0,1} (N_b \delta u + V_{by} \delta v + V_{bz} \delta w + M_{bz} \delta \theta_z + M_{by} \delta \theta_y) \end{aligned} \quad (4.16b)$$

where V is the volume and l is the length of the beam in the undeformed configuration, p_{sy} , p_{sz} are the foundation reaction according to y and z axes, respectively, while N_b , V_{by} , V_{bz} , M_{by} and M_{bz} are the externally applied forces and moments at the beam boundaries. Within this framework, the stress resultants of the beam are defined as

$$N = \int_{\Omega} S_{xx} d\Omega \quad (4.17a)$$

$$Q_y = \int_{A_y} S_{xy} d\Omega \quad Q_z = \int_{A_z} S_{xz} d\Omega \quad (4.17b,c)$$

$$M_y = \int_{\Omega} S_{xx} z d\Omega \quad M_z = - \int_{\Omega} S_{xx} y d\Omega \quad (4.17d,e)$$

where N , Q_y , Q_z correspond to the axial and shear forces and M_y , M_z correspond to the bending moments according to y and z axes, respectively. Subsequently, substituting the expressions of the stress components given from eqn. (4.10) and exploiting the strain-displacement relations (4.6), the stress resultants are obtained as

$$N = EA \left[u' + \frac{I}{2} (v'^2 + w'^2) \right] - \underbrace{E \int_{\Omega} \varepsilon_{xx}^{pl} dA}_{N^{pl}} = EA \left[u' + \frac{I}{2} (v'^2 + w'^2) \right] + N^{pl} \quad (4.18a)$$

$$Q_z = GA_z (w'(x) + \theta_y(x)) - \underbrace{G \int_{A_z} \gamma_{xz}^{pl} dA}_{Q_z^{pl}} = GA_z (w'(x) + \theta_y(x)) + Q_z^{pl} \quad (4.18b)$$

$$Q_y = GA_y (v'(x) - \theta_z(x)) - \underbrace{G \int_{A_y} \gamma_{xy}^{pl} dA}_{Q_y^{pl}} = GA_y (v'(x) - \theta_z(x)) + Q_y^{pl} \quad (4.18c)$$

$$M_y = EI_y \theta_y' - \underbrace{E \int_{\Omega} z \varepsilon_{xx}^{pl} dA}_{M_y^{pl}} = EI_y \theta_y' + M_y^{pl} \quad (4.18d)$$

$$M_z = EI_z \theta_z' - \underbrace{E \int_{\Omega} y \varepsilon_{xx}^{pl} dA}_{M_z^{pl}} = EI_z \theta_z' + M_z^{pl} \quad (4.18e)$$

where (\prime) denotes differentiation with respect to x , N^{pl} , Q_z^{pl} , Q_y^{pl} , M_z^{pl} and M_y^{pl} are the plastic parts of the corresponding stress resultants, A is the cross section area, I_y , I_z the moments of inertia with respect to the principle bending axes and GA_y , GA_z are its shear rigidities of the Timoshenko's beam theory, where

$$A_z = \kappa_z A = \frac{I}{a_z} A \quad A_y = \kappa_y A = \frac{I}{a_y} A \quad (4.19a,b)$$

are the shear areas with respect to y , z axes, respectively with κ_y , κ_z the shear correction factors and a_y , a_z the shear deformation coefficients. It is worth noting that these stress resultants refer to the directions of the infinitesimal elements of the cross section at its deformed configuration, since they have been defined with respect to the second Piola-Kirchhoff stress tensor.

After substituting eqns. (4.6) and (4.18) into eqn. (4.15) and conducting some algebraic manipulations, the global equilibrium equations of the beam-foundation system are obtained as

$$EA(u'' + v'v'' + w'w'') + \frac{\partial N^{pl}}{\partial x} = -p_x \quad (4.20a)$$

$$EA \left[\left(u' + \frac{1}{2}(v'^2 + w'^2) \right) v' \right]' + \frac{d(N^{pl}v')}{dx} + GA_y(v' - \theta_z)' + \frac{\partial Q_y^{pl}}{\partial x} - p_{sy} = -p_y \quad (4.20b)$$

$$EA \left[\left(u' + \frac{1}{2}(v'^2 + w'^2) \right) w' \right]' + \frac{d(N^{pl}w')}{dx} + GA_z(w' + \theta_y)' + \frac{\partial Q_z^{pl}}{\partial x} - p_{sz} = -p_z \quad (4.20c)$$

$$EI_y \theta_y'' + \frac{dM_y^{pl}}{dx} - GA_z(w' + \theta_y) - Q_z^{pl} = -m_y \quad (4.20d)$$

$$EI_z \theta_z'' + \frac{dM_z^{pl}}{dx} + GA_y(v' - \theta_z) + Q_y^{pl} = -m_z \quad (4.20e)$$

or in terms of the total stress resultants as

$$\frac{d(N^{el} + N^{pl})}{dx} = -p_x \Rightarrow \frac{dN}{dx} = -p_x \quad (4.21a)$$

$$-\frac{d(Nv')}{dx} - \frac{dQ_y}{dx} + p_{sy} = p_y \quad -\frac{d(Nw')}{dx} - \frac{dQ_z}{dx} + p_{sz} = p_z \quad (4.21b,c)$$

$$\frac{dM_y}{dx} - Q_z = -m_y \quad \frac{dM_z}{dx} + Q_y = -m_z \quad (4.21d,e)$$

Furthermore, the application of the principle of virtual work yields the corresponding boundary conditions as

$$a_1 u(x) + a_2 N_b(x) = a_3 \quad (4.22a)$$

$$\beta_1 v(x) + \beta_2 V_{by}(x) = \beta_3 \quad \bar{\beta}_1 \theta_z(x) + \bar{\beta}_2 M_{bz}(x) = \bar{\beta}_3 \quad (4.22b,c)$$

$$\gamma_1 w(x) + \gamma_2 V_{bz}(x) = \gamma_3 \quad \bar{\gamma}_1 \theta_y(x) + \bar{\gamma}_2 M_{by}(x) = \bar{\gamma}_3 \quad (4.22d,e)$$

at the beam ends $x=0, l$, where the total vertical reactions V_{by} , V_{bz} , and the total bending moments M_{by} , M_{bz} are given by the following relations

$$V_{by} = EA \left[u' + \frac{I}{2} (v'^2 + w'^2) \right] v' + N^{pl} v' + GA_y (v' - \theta_z) + Q_y^{pl} \quad (4.23a)$$

$$V_{bz} = EA \left[u' + \frac{I}{2} (v'^2 + w'^2) \right] w' + N^{pl} w' + GA_z (w' + \theta_y) + Q_z^{pl} \quad (4.23b)$$

$$M_{by} = EI_y \theta'_y + M_y^{pl} \quad M_{bz} = EI_z \theta'_z + M_z^{pl} \quad (4.23c,d)$$

Finally, $\alpha_j, \beta_j, \bar{\beta}_j, \gamma_j, \bar{\gamma}_j$ ($j = 1, 2, 3$) are functions specified at the beam ends $x = 0, l$. Eqns. (19) describe the most general boundary conditions associated with the problem at hand and can include elastic support or restraint. It is apparent that all types of the conventional boundary conditions (clamped, simply supported, free or guided edge) can be derived from these equations by specifying appropriately these functions (e.g. for a clamped edge it is $\alpha_1 = \beta_1 = \gamma_1 = 1$, $\bar{\beta}_1 = \bar{\gamma}_1 = 1$, $\alpha_2 = \alpha_3 = \beta_2 = \beta_3 = \gamma_2 = \gamma_3 = \bar{\beta}_2 = \bar{\beta}_3 = \bar{\gamma}_2 = \bar{\gamma}_3 = 0$). Dropping the plastic quantities of the global equilibrium equations, the boundary value problem of the examined problem is formulated.

The above equations of equilibrium and boundary conditions are easily simplified by crossing out the nonlinear terms corresponding to material non linearity, leading to the well known elastic formulation while, by crossing out the nonlinear terms corresponding to the geometrical nonlinearity and the components regarding the shear deformation effect, leads to the well known second order equation with respect to the axial and transverse directions.

The evaluation of the shear deformation coefficients a_y, a_z corresponding to the principal centroidal system of axes Cyz , are established equating the approximate formula of the shear strain energy per unit length with the exact one as described in Appendix A3 while, in the case of negligible shear deformations $a_z = a_y = 0$.

4.3 Numerical Solution

According to the precedent analysis, the geometrically nonlinear inelastic problem of Timoshenko beams supported on nonlinear inelastic soil, reduces to establishing the axial and transverse displacement components $u(x)$, $v(x)$, $w(x)$ as well as the

rotations due to bending $\theta_y(x)$, $\theta_z(x)$ having continuous derivatives up to the second order with respect to x and satisfying the boundary value problem described by the governing differential equation (4.20) along the beam and the boundary conditions (4.22) at the beam ends $x = 0, l$.

This boundary value problem is solved employing the BEM (Katsikadelis 2002), as this is developed in Appendix A2 for the solution of coupled second order differential equations, after modifying it as follows. The motivation to use this particular technique is justified from the intention to retain the advantages of a BEM solution over a domain approach, while using simple fundamental solutions and avoiding finite differences to the solution of the problem.

4.3.1. Integral Representations for the Axial and Transverse Displacements u, v, w and Rotations θ_y, θ_z

According to this method, let $u_1(x) = u(x)$, $u_2(x) = v(x)$, $u_3(x) = w(x)$, $u_4(x) = \theta_y(x)$ and $u_5(x) = \theta_z(x)$ be the sought solution of the problem. The solution of the second order differential equation $d^2u_i/dx^2 = q''$ ($i = 1, 2, \dots, 5$) and ($q = u, v, w, \theta_y, \theta_z$) is given in integral form as

$$u_i(\xi) = \int_0^l \frac{d^2u_i}{dx^2} u^* dx - \left[u^* \frac{du_i}{dx} - \frac{\partial u^*}{\partial x} u_i \right]_0^l \quad (i = 1, 2, \dots, 5) \quad (4.24)$$

where u^* is the fundamental solution given as $u^* = 0.5|r|$, with $r = x - \xi$, x, ξ points of the beam, as defined in Appendix A1. Since EA , GA_z, GA_y , EI_y and EI_z are independent of x , eqns. (4.24) can be written as

$$EAu_1(\xi) = \int_0^l \left[EA \frac{\partial^2 u_1}{\partial x^2} \right] A_2 dx - EA \left[A_2 \frac{\partial u_1}{\partial x} - A_1 u_1 \right]_0^l \quad (4.25a)$$

$$GA_y u_2(\xi) = \int_0^l \left[GA_y \frac{\partial^2 u_2}{\partial x^2} \right] A_2 dx - GA_y \left[A_2 \frac{\partial u_2}{\partial x} - A_1 u_2 \right]_0^l \quad (4.25b)$$

$$GA_z u_3(\xi) = \int_0^l \left[GA_z \frac{\partial^2 u_3}{\partial x^2} \right] \Lambda_2 dx - GA_z \left[\Lambda_2 \frac{\partial u_3}{\partial x} - \Lambda_1 u_3 \right]_0^l \quad (4.25c)$$

$$EI_y u_4(\xi) = \int_0^l \left[EI_y \frac{\partial^2 u_4}{\partial x^2} \right] \Lambda_2 dx - EI_y \left[\Lambda_2 \frac{\partial u_4}{\partial x} - \Lambda_1 u_4 \right]_0^l \quad (4.25d)$$

$$EI_z u_5(\xi) = \int_0^l \left[EI_z \frac{\partial^2 u_5}{\partial x^2} \right] \Lambda_2 dx - EI_z \left[\Lambda_2 \frac{\partial u_5}{\partial x} - \Lambda_1 u_5 \right]_0^l \quad (4.25e)$$

where the kernels $\Lambda_j(r) = \Lambda_j(x, \xi)$ ($j = 1, 2$) are given in eqns. (A1.9a,b). Solving the global equilibrium equations of the beam–foundation system (4.20a–e) with respect to EAu'' , $GA_y v''$, $GA_z w''$, $EI_y \theta_y''$ and $EI_z \theta_z''$ and substituting the result into eqns. (4.25a–e), respectively, the following integral representations are obtained

$$EAu_1(\xi) = \int_0^l \left(-p_x(x) - \frac{dN^{pl}}{dx} - EA \left(\frac{du_2}{dx} \frac{d^2 u_2}{dx^2} + \frac{du_3}{dx} \frac{d^2 u_3}{dx^2} \right) \right) \Lambda_2 dx - EA \left[\Lambda_2 \frac{du_1}{dx} - \Lambda_1 u_1 \right]_0^l \quad (4.26a)$$

$$GA_y u_2(\xi) = \int_0^l \left[-GA_y \frac{du_2}{dx} - EA \left(\frac{d^2 u_1}{dx^2} + \frac{du_2}{dx} \frac{d^2 u_2}{dx^2} + \frac{du_3}{dx} \frac{d^2 u_3}{dx^2} \right) \frac{du_2}{dx} - \frac{dN^{pl}}{dx} \frac{du_2}{dx} + p_{sy} \right] \Lambda_2 dx - \int_0^l \left[EA \left(\frac{du_1}{dx} + \frac{1}{2} \left(\left(\frac{du_2}{dx} \right)^2 + \left(\frac{du_3}{dx} \right)^2 \right) \right) \frac{d^2 u_2}{dx^2} + N^{pl} \frac{d^2 u_2}{dx^2} + \frac{\partial Q_z^{pl}}{\partial x} + p_y \right] \Lambda_2 dx - GA_y \left[\Lambda_2 \frac{du_2}{dx} - \Lambda_1 u_2 \right]_0^l \quad (4.26b)$$

$$GA_z u_3(\xi) = \int_0^l \left[-GA_z \frac{du_3}{dx} - EA \left(\frac{d^2 u_1}{dx^2} + \frac{du_2}{dx} \frac{d^2 u_2}{dx^2} + \frac{du_3}{dx} \frac{d^2 u_3}{dx^2} \right) \frac{du_3}{dx} - \frac{dN^{pl}}{dx} \frac{du_3}{dx} + p_{sz} \right] \Lambda_2 dx - \int_0^l \left[EA \left(\frac{du_1}{dx} + \frac{1}{2} \left(\left(\frac{du_2}{dx} \right)^2 + \left(\frac{du_3}{dx} \right)^2 \right) \right) \frac{d^2 u_3}{dx^2} + N^{pl} \frac{d^2 u_3}{dx^2} + \frac{\partial Q_z^{pl}}{\partial x} + p_z \right] \Lambda_2 dx - GA_z \left[\Lambda_2 \frac{du_3}{dx} - \Lambda_1 u_3 \right]_0^l \quad (4.26c)$$

$$EI_y u_4(\xi) = \int_0^l \left(GA_z \left(\frac{du_3}{dx} + u_4 \right) + Q_y^{pl} - \frac{\partial M_y^{pl}}{\partial x} - m_y \right) \Lambda_2 dx - EI_y \left[\Lambda_2 \frac{du_4}{dx} - \Lambda_1 u_4 \right]_0^l \quad (4.26d)$$

$$EI_z u_5(\xi) = \int_0^l \left(GA_y \left(\frac{du_2}{dx} - u_5 \right) + Q_z^{pl} - \frac{\partial M_z^{pl}}{\partial x} - m_z \right) \Lambda_2 dx - EI_z \left[\Lambda_2 \frac{du_5}{dx} - \Lambda_1 u_5 \right]_0^l \quad (4.26e)$$

After carrying out several integrations by parts, eqns. (4.26) yield

$$\begin{aligned} EAu_1(\xi) = & -\int_0^l p_x \Lambda_2 dx + \int_0^l N^{pl} \Lambda_1 dx + \frac{1}{2} EA \int_0^l \left[\left(\frac{du_2}{dx} \right)^2 + \left(\frac{du_3}{dx} \right)^2 \right] \Lambda_1 dx - \\ & - \left[\left(\frac{1}{2} EA \left[\left(\frac{du_2}{dx} \right)^2 + \left(\frac{du_3}{dx} \right)^2 \right] + N^{pl} \right) \Lambda_2 \right]_0^l - EA \left[\Lambda_2 \frac{du_1}{dx} - \Lambda_1 u_1 \right]_0^l \end{aligned} \quad (4.27a)$$

$$\begin{aligned} GA_y u_2(\xi) = & GA_y \int_0^l u_2 \Lambda_1 dx - \int_0^l p_y \Lambda_2 dx + EA \int_0^l \left(\frac{du_1}{dx} + \frac{1}{2} \left[\left(\frac{du_2}{dx} \right)^2 + \left(\frac{du_3}{dx} \right)^2 \right] \right) \frac{du_2}{dx} \Lambda_1 dx + \\ & + \int_0^l N^{pl} \frac{du_2}{dx} \Lambda_1 dx + \int_0^l Q_y^{pl} \Lambda_1 dx - \int_0^l p_{sy} \Lambda_2 dx + GA_y [u_2 \Lambda_1]_0^l - \\ & - \left[\left(EA \left(\frac{du_1}{dx} + \frac{1}{2} \left[\left(\frac{du_2}{dx} \right)^2 + \left(\frac{du_3}{dx} \right)^2 \right] \right) + N^{pl} \right) \frac{du_2}{dx} \Lambda_2 + \left(GA_y \left(\frac{du_2}{dx} + u_4 \right) + Q_y^{pl} \right) \Lambda_2 \right]_0^l \end{aligned} \quad (4.27b)$$

$$\begin{aligned} GA_z u_3(\xi) = & GA_z \int_0^l u_3 \Lambda_1 dx - \int_0^l p_z \Lambda_2 dx + EA \int_0^l \left(\frac{du_1}{dx} + \frac{1}{2} \left[\left(\frac{du_2}{dx} \right)^2 + \left(\frac{du_3}{dx} \right)^2 \right] \right) \frac{du_3}{dx} \Lambda_1 dx + \\ & + \int_0^l N^{pl} \frac{du_3}{dx} \Lambda_1 dx + \int_0^l Q_z^{pl} \Lambda_1 dx - \int_0^l p_{sz} \Lambda_2 dx + GA_z [u_3 \Lambda_1]_0^l - \\ & - \left[\left(EA \left(\frac{du_1}{dx} + \frac{1}{2} \left[\left(\frac{du_2}{dx} \right)^2 + \left(\frac{du_3}{dx} \right)^2 \right] \right) + N^{pl} \right) \frac{du_3}{dx} \Lambda_2 + \left(GA_z \left(\frac{du_2}{dx} - u_5 \right) + Q_z^{pl} \right) \Lambda_2 \right]_0^l \end{aligned} \quad (4.27c)$$

$$\begin{aligned} EI_y u_4(\xi) = & GA_z \int_0^l \left(\frac{du_3}{dx} + u_4 \right) \Lambda_2 dx + \int_0^l Q_z^{pl} \Lambda_2 dx + \int_0^l M_y^{pl} \Lambda_1 dx - \int_0^l m_y \Lambda_2 dx - \\ & - \left[M_y^{pl} \Lambda_2 \right]_0^l - EI_y \left[\Lambda_2 \frac{du_4}{dx} - \Lambda_1 u_4 \right]_0^l \end{aligned} \quad (4.27d)$$

$$\begin{aligned}
 EI_z u_5(\xi) = & GA_y \int_0^l \left(\frac{du_2}{dx} - u_5 \right) \Lambda_2 dx + \int_0^l Q_y^{pl} \Lambda_2 dx + \int_0^l M_z^{pl} \Lambda_1 dx - \int_0^l m_z \Lambda_2 dx - \\
 & - \left[M_z^{pl} \Lambda_2 \right]_0^l - EI_z \left[\Lambda_2 \frac{du_5}{dx} - \Lambda_1 u_5 \right]_0^l
 \end{aligned} \tag{4.27e}$$

while by assembling the boundary terms in a more convenient form the integral representations are written as

$$\begin{aligned}
 EA u_1(\xi) = & - \int_0^l p_x \Lambda_2 dx + \int_0^l N^{pl} \Lambda_1 dx + \frac{1}{2} EA \int_0^l \left[\left(\frac{du_2}{dx} \right)^2 + \left(\frac{du_3}{dx} \right)^2 \right] \Lambda_1 dx - \\
 & - \left[N \Lambda_2 - EA \Lambda_1 u_1 \right]_0^l
 \end{aligned} \tag{4.28a}$$

$$\begin{aligned}
 GA_y u_2(\xi) = & GA_y \int_0^l u_2 \Lambda_1 dx + EA \int_0^l \left(\frac{du_1}{dx} + \frac{1}{2} \left(\left(\frac{du_2}{dx} \right)^2 + \left(\frac{du_3}{dx} \right)^2 \right) \right) \frac{du_2}{dx} \Lambda_1 dx + \\
 & + \int_0^l N^{pl} \frac{du_2}{dx} \Lambda_1 dx + \int_0^l Q_y^{pl} \Lambda_1 dx - \int_0^l p_y \Lambda_2 dx - \int_0^l p_{sy} \Lambda_2 dx - \\
 & - \left[V_{by} \Lambda_2 - GA_y u_2 \Lambda_1 \right]_0^l
 \end{aligned} \tag{4.28b}$$

$$\begin{aligned}
 GA_z u_3(\xi) = & GA_z \int_0^l u_3 \Lambda_1 dx + EA \int_0^l \left(\frac{du_1}{dx} + \frac{1}{2} \left(\left(\frac{du_2}{dx} \right)^2 + \left(\frac{du_3}{dx} \right)^2 \right) \right) \frac{du_3}{dx} \Lambda_1 dx + \\
 & + \int_0^l N^{pl} \frac{du_3}{dx} \Lambda_1 dx + \int_0^l Q_z^{pl} \Lambda_1 dx - \int_0^l p_z \Lambda_2 dx - \int_0^l p_{sz} \Lambda_2 dx - \\
 & - \left[V_{bz} \Lambda_2 - GA_z u_3 \Lambda_1 \right]_0^l
 \end{aligned} \tag{4.28c}$$

$$\begin{aligned}
 EI_y u_4(\xi) = & GA_z \int_0^l \left(\frac{du_3}{dx} + u_4 \right) \Lambda_2 dx + \int_0^l Q_z^{pl} \Lambda_2 dx + \int_0^l M_y^{pl} \Lambda_1 dx - \int_0^l m_y \Lambda_2 dx \\
 & - \left[M_{by} \Lambda_2 - EI_y u_4 \Lambda_1 \right]_0^l
 \end{aligned} \tag{4.28d}$$

$$\begin{aligned}
 EI_z u_5(\xi) = & GA_y \int_0^l \left(\frac{du_2}{dx} - u_5 \right) \Lambda_2 dx + \int_0^l Q_y^{pl} \Lambda_2 dx + \int_0^l M_z^{pl} \Lambda_1 dx - \int_0^l m_z \Lambda_2 dx \\
 & - \left[M_{bz} \Lambda_2 - EI_z u_5 \Lambda_1 \right]_0^l
 \end{aligned} \tag{4.28e}$$

If shear deformation effects are negligible, then $u_5 \approx u'_2$ and $u_4 \approx u'_3$. In such cases, numerical methods requiring domain approximation of unknown quantities, such as FEM, exhibit “locking” effects, when Timoshenko theory is applied to cases where the Euler–Bernoulli theory could also be used (Zienkiewicz & Taylor 2005). Since domain approximation of unknown quantities is employed in the present numerical technique, locking effects are alleviated by employing the same order of approximation for u_4, u_5 and u'_2, u'_3 . In order to achieve explicit appearance of u'_2, u'_3 in eqns. (4.28b,c), respectively these integral representations are differentiated with respect to ξ , yielding

$$GA_y \frac{du_2(\xi)}{d\xi} = \int_0^l p_y A_I dx - GA_y u_2(\xi) - EA \left(u'_1(\xi) + \frac{1}{2} (u'^2_2(\xi) + u'^2_3(\xi)) \right) u'_2(\xi) - N^{pl} u'_2(\xi) - Q_y^{pl} + \int_0^l p_{sy} A_I dx + [V_{by} A_I]_0^l \quad (4.29a)$$

$$GA_z \frac{u_3(\xi)}{d\xi} = \int_0^l p_z A_I dx + GA_z u_3(\xi) + EA \left(u'_1(\xi) + \frac{1}{2} (u'^2_2(\xi) + u'^2_3(\xi)) \right) u'_3(\xi) - N^{pl} u'_3(\xi) - Q_z^{pl} + \int_0^l p_{sz} A_I dx + [V_{bz} A_I]_0^l \quad (4.29b)$$

Moreover, noting that plastic parts of the stress resultants depend on the derivatives of the displacement components, it is deduced that u'_1, u'_4, u'_5 must also be computed in order to resolve the total stress resultants (as well as strain components), thus the integral representations (4.28a,d,e) are differentiated with respect to ξ , yielding

$$EA \frac{du_1(\xi)}{d\xi} = \int_0^l p_x A_I dx - N^{pl}(\xi) - \frac{1}{2} EA (u'^2_2(\xi) + u'^2_3(\xi)) + [N A_I]_0^l \quad (4.30a)$$

$$EI_y \frac{du_4(\xi)}{d\xi} = \int_0^l m_y A_I dx - GA_z \int_0^l \left(\frac{du_3}{dx} + u_4 \right) A_I dx - \int_0^l Q_z^{pl} A_I dx - M_y^{pl} + [M_{by} A_I]_0^l \quad (4.30b)$$

$$EI_z \frac{du_5(\xi)}{d\xi} = \int_0^l m_z A_I dx - GA_z \int_0^l \left(\frac{du_2}{dx} - u_5 \right) A_I dx - \int_0^l Q_y^{pl} A_I dx - M_z^{pl} + [M_{bz} A_I]_0^l \quad (4.30c)$$

Thereafter it is deduced that eqns. (4.28d,e), (4.29a,b) and (4.30a-c) have been brought into a convenient form to establish a numerical computation of the unknown quantities. Thus, the interval $(0,l)$ is divided into L elements, on each of which the unknown quantities together with the plastic parts of the stress resultants are assumed to vary according to a certain law (constant, linear, parabolic etc). The linear element assumption is employed here (Fig. 4.3) as the numerical implementation is simple and the obtained results are very good. It is worth here noting that this technique does not require either differentiation of shape functions or finite differences application.

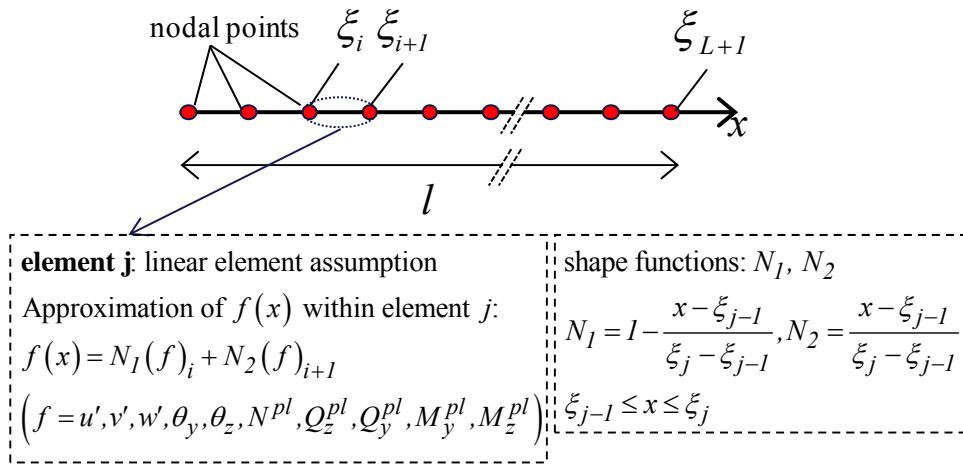


Fig.4.3. Discretization of the beam interval into linear elements, distribution of the nodal points and approximation of quantities.

Employing the aforementioned procedure and a collocation technique, a set of $7(L+1)$ algebraic equations is obtained. Six additional algebraic equations are obtained by applying the integral representation (4.28a-c) at the beam ends $\xi = 0, l$, while together the ten boundary conditions (eqns. (4.22)) yield a linear system of $7L+23$ simultaneous algebraic equations

$$[K(d)]\{d\} = \{b_{ext}\} + \{b_{pl}(d)\} \quad (4.31)$$

where $K(d)$ is a generalized elastic (geometrically) nonlinear stiffness matrix, $\{d\}$ is a $7L+23$ generalized unknown vector given as

$$\{d\}^T = \left\{ \begin{array}{cccccccc} u'_{1j} & u'_{2j} & u'_{3j} & u'_{4j} & u_{4j} & u'_{5j} & u_{5j} & u_{Li\dots} \\ \dots u_{2i} & u_{3i} & N_i & Q_{zi} & Q_{yi} & M_{yi} & M_{zi} & \end{array} \right\} \begin{pmatrix} j = 1, 2, \dots, L+1 \\ i = 1, L+1 \end{pmatrix} \quad (4.32)$$

while $\{b_{ext}\}$, $\{b_{pl}(d)\}$ are vectors representing all the terms related to the externally applied loading and the plastic parts of the stress resultants, respectively. Finally, after solving the system of eqns. (4.31), the integral representations (4.28a-c) can be employed in a post-processing step in order to obtain the axial and transverse displacement components $u_1 = u(x)$, $u_2 = v(x)$, $u_3 = w(x)$, respectively at any interior point ξ_i ($i = 1, 2, \dots, L+1$) of the beam.

4.3.2. Incremental–Iterative Solution Algorithms / Fibre Approach

In the framework of this doctoral thesis, two alternative approaches have been implemented for the incremental-iterative solution algorithm based on the fibre approach. The first one is based on the Powell's hybrid algorithm (Powell 1970a,b) while the second executes sequential iterations until an initial stress criterion is satisfied. In both incremental–iterative procedures, the loading history has to be known in order to establish the plastic strains thus; the first step is to determine the external load vector. To this end, load control (Crisfield 1991) over the incremental steps is used and load stations are chosen according to load history and convergence requirements.

4.3.2.1 Incremental–Iterative Solution based on Powell Hybrid Algorithm

In the first approach, at each load station the system of nonlinear equations (4.31) is numerically solved employing an iterative solution strategy. In the framework of this dissertation the modification of Powell's hybrid algorithm (Powell 1970a,b) has been used. This algorithm is a variation of Newton's method requiring the following quantities.

- a. The Jacobian matrix (More et al. 1980) of the nonlinear system which corresponds to the generalized stiffness matrix of the problem. This matrix is defined explicitly, avoiding this way any possible inaccuracy resulting from the finite differences approximation while, significantly improving the computational time.

- b. An initial guess of the solution $\{d_{init}\}$ (at each load station). The resolved vector $\{d\}$ of the previously converged load station is employed $\{d_{init}\} = \{d_{conv}\}$ while $\{d\} = \{0\}$ is used at the first load station.
- c. A tolerance parameter tol to perform the convergence criterion of the algorithm. In this study this parameter takes values of the range $tol = 10^{-7} \div 10^{-10}$.

The incremental steps of the algorithm are executed until the target load is fully undertaken from the beam–foundation inelastic system or convergence cannot be achieved. Thereafter, a number of monitoring cross sections is defined. It is assumed that the monitoring sections coincide with the $L + 1$ nodal points of the beam interval (Fig. 4.3).

The fibre approach is to be followed for the integrating the section internal forces and moments. Each section is divided into a number of triangular or quadrilateral cells and standard two-dimensional Gauss quadrature rules are employed in each cell to resolve the plastic parts of the stress resultants. If the same number of Gauss points is employed in every cell, then $N_{dof} = N_{cells} \times N_{Gauss}$ holds. Thus, the monitoring stations of each cross section coincide with the Gauss points of its cells, while exact patch between adjacent cells is not required.

At each load station, the system of nonlinear eqns. (4.31) is expressed without explicitly deriving its incremental form which is more extensive due to terms associated with geometrical nonlinearity. This is achieved by exploiting the values of the stresses S_{xx} , S_{xy} , S_{xz} the plastic parts of the strains ε_{eq}^{pl} , ε_{xx}^{pl} , γ_{xy}^{pl} , γ_{xz}^{pl} and the kinematic components u'_1 , u'_2 , u'_3 , u'_4 , u'_4 , u_5 , u'_5 of the previously converged load station at the current monitoring stations and adhering to the following steps.

- i. **Elastic prediction step:** At each monitoring station of the beam, evaluate the trial stress components as

$$S_{xx}^{Tr} = (S_{xx})_{conv} + E(\Delta u'_1) + Ez_{cell}(\Delta u'_4) - Ey_{cell}(\Delta u'_5) + E \frac{I}{2} [(\Delta u'_2) + (\Delta u'_3)]^2 \quad (4.33a)$$

$$S_{xy}^{Tr} = (S_{xy})_{conv} + \sqrt{k_y} (G(\Delta u'_2) - G(\Delta u'_4)) \quad (4.33b)$$

$$S_{xz}^{Tr} = \left(S_{xz}^{Tr} \right)_{conv} + \sqrt{k_z} \left(G(\Delta u'_3) + G(\Delta u'_5) \right) \quad (4.33c)$$

where $\Delta u'_i = (u'_i)_{cur} - (u'_i)_{conv}$ ($i = 1, 2, \dots, 5$) while, the subscript *cur* denotes the current value of a quantity that is iteratively updated through the algorithm and the subscript *conv* denotes the converged value of a quantity from a previous load station

- ii. **Yield criterion:** At each monitoring station of the beam the von Mises yield criterion is performed, employing eqn. (4.11) as

$$\Phi_{vM}^{Tr} = \frac{\sqrt{\left(S_{xx}^{Tr} \right)^2 + 3 \left(\left(S_{xy}^{Tr} \right)^2 + \left(S_{xz}^{Tr} \right)^2 \right)}}{\sigma_Y \left(\left(\varepsilon_{eq}^{pl} \right)_{conv} \right)} - 1 \quad (4.34)$$

- If $\Phi_{vM}^{Tr} \leq 0$ then yield criterion is satisfied and the stress state lies within the elastic domain. Thus, the trial state is the final admissible one, the incremental plastic strain components are zero and the total plastic strain components along with the equivalent plastic strain get the corresponding values of the previously converged load station.
 - If $\Phi_{vM}^{Tr} > 0$ then plastic flow occurs and return must be made to yield surface (plastic correction step). A local Newton–Raphson method is initiated to integrate the inelastic constitutive equations by employing the generalized cutting-plane algorithm (Ortiz & Simo 1986, Simo & Hughes 1998). The incremental plastic strain components along with the equivalent plastic strain are updated according to this algorithm by using a prescribed tolerance $tol_{cp} = 10^{-5}$ in its convergence criterion and subsequently the total plastic strain components are resolved by adding the corresponding incremental quantities to the ones of the previously converged load station.
- iii. At each monitoring cross section of the beam, plastic parts of the stress resultants are evaluate numerically employing the two-dimensional numerical integration scheme.

- iv. Employ the obtained plastic parts of the stress resultants to evaluate the vector $\{b_{pl}\}_{cur}$ of eqn. (4.31). Apart from elementary computations, this step requires the computation of line integrals along the beam interval (eqns. (4.28d,e), (4.29a,b) and (4.30a-c)) which is performed employing a semi-analytical scheme. It is worth noting here that the line integrals arising in the term $[K(d)]_{cur} \{d\}_{cur}$ of eqn. (4.31) (including the ones associated with geometrical nonlinearity) are also computed semi-analytically without any special difficulty.
- v. Since convergence is achieved then the foundation reaction is computed employing eqns. (4.1). The parameters are updated and the process described by steps (i)-(iv) is repeated until the foundation convergence criterion is achieved by using a prescribed tolerance of $tol_{found} = 10^{-10}$.
- vi. The increments of the external loading continue until the target load is fully undertaken from the beam-foundation inelastic system or convergence cannot be achieved, which means that the last additional increment cannot be undertaken (plastic collapse).

Finally, it is worth noting that the monitoring displacement components u , v and w at any interior point of the beam are updated after convergence in each increment by employing the integral representations (4.28a-c), respectively.

A step-by-step algorithmic approach of the nonlinear solution is presented in a flowchart form in Fig.4.4.

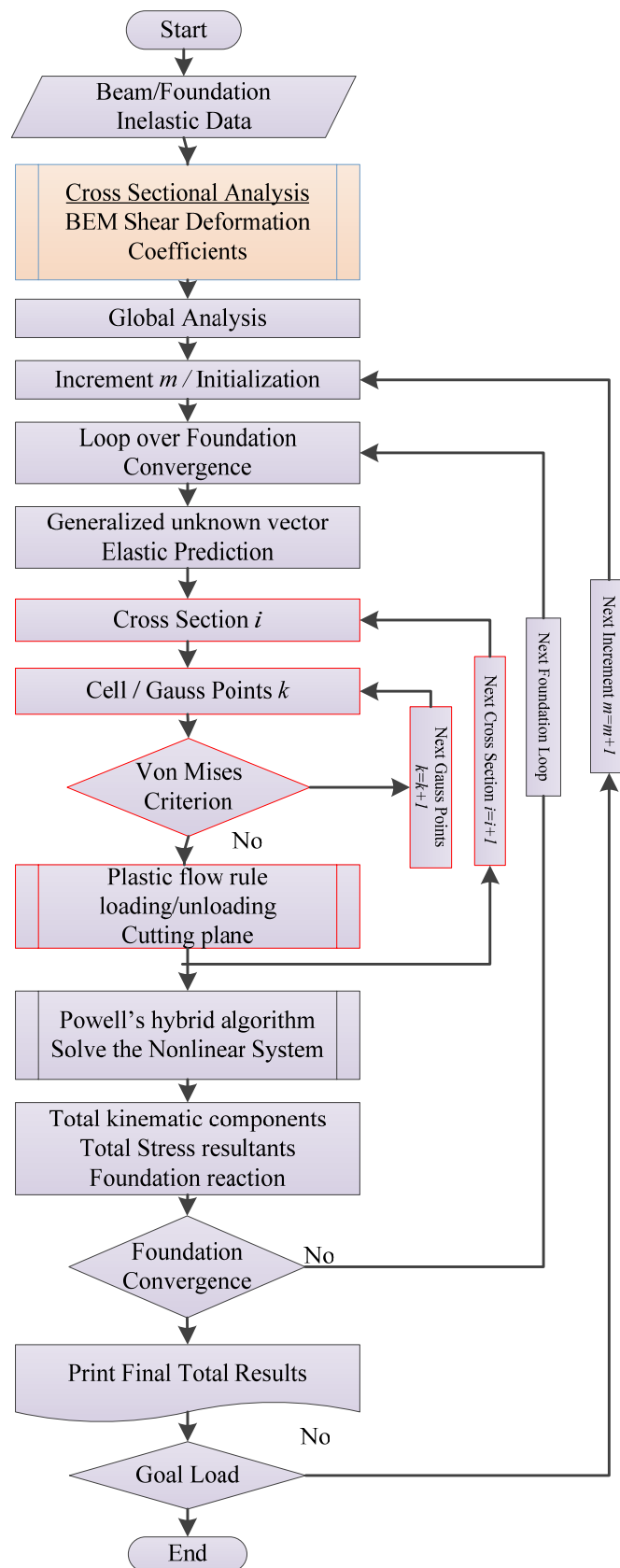


Fig. 4.4. Flowchart of the incremental-iterative solution algorithm on Powell Hybrid algorithm.

4.3.2.2 Incremental–Iterative Solution based on Initial Stress Criterion

In the second alternative approach, the incremental stress resultants are decomposed into elastic and plastic parts, as this is presented in eqns. (4.18). These quantities are computed through an iterative procedure since usually, changes between the plastic parts of incremental stress resultants of two successive iterations are not negligible due to the rate nature of the flow rule (Crisfield 1991). Thus, using the subscript m to denote the load step, the superscript l to denote the iterative cycle and the symbol $\Delta(\cdot)$ to denote incremental quantities, the l -th iteration of the m -th load step of the incremental–iterative solution algorithm can be described as follows

- i. Evaluation of the generalized iterative unknown vector $\{\Delta d\}_m^l$ from the solution of the nonlinear system of eqns. (4.31) having been written as

$$[K(d)]\{\Delta d\}_m^l = \{\Delta b_{ext}\}_m + \{\Delta b_{pl}\}_m^{l-1} \quad (4.35)$$

If $m = 1$ and $l = 1$, it is assumed that $\{\Delta b_{pl}\}_1^0 = \{0\}$. If $m > 1$ and $l = 1$, it is assumed that $\{\Delta b_{pl}\}_m^0 = \{0\}$ or $\{\Delta b_{pl}\}_m^0 = \{\Delta b_{pl}\}_{m-1}^n$, where n is the total number of iterations performed in the previous increment $m - 1$.

- ii. Evaluation of the incremental unknown derivatives by exploiting $\{\Delta d\}_m^l$.
- iii. **Elastic prediction step:** At each monitoring station k of the i -th cross section of the beam ($k = 1, 2, \dots, N_{dof}$, $i = 1, 2, \dots, L + 1$): Evaluation of the trial stress components as

$$\left(S_{xx}^{Tr}(\xi_i, z_k)\right)_m^l = \left(S_{xx}(\xi_i, z_k)\right)_m^0 + \left(\Delta S_{xx}^{Tr}(\xi_i, z_k)\right)_m^l \quad (4.36a)$$

$$S_{xy}^{Tr} = \left(S_{xy}(\xi_i, y_k, z_k)\right)_m^0 + \left(\Delta S_{xy}^{Tr}(\xi_i, y_k, z_k)\right)_m^l \quad (4.36b)$$

$$S_{xz}^{Tr} = \left(S_{xz}(\xi_i, y_k, z_k)\right)_m^0 + \left(\Delta S_{xz}^{Tr}(\xi_i, y_k, z_k)\right)_m^l \quad (4.36c)$$

where the incremental trial stress components are obtained as

$$\begin{aligned} \left(\Delta S_{xx}^{Tr}(\xi_i, y_k, z_k) \right)_m^l &= E \left[\Delta u_1'(\xi_i) + \Delta u_4'(\xi_i) z_k - \Delta u_5'(\xi_i) y_k \right]_m^l + \\ &+ \frac{E}{2} \left[\left(\Delta u_2'(\xi_i) + \Delta u_3'(\xi_i) \right)^2 \right]_m^l \end{aligned} \quad (4.37a)$$

$$\left(\Delta S_{xy}^{Tr}(\xi_i, y_k, z_k) \right)_m^l = G \sqrt{k_y} \left[\Delta u_2'(\xi_i) - \Delta u_4'(\xi_i) \right]_m^l \quad (4.37b)$$

$$\left(\Delta S_{xz}^{Tr}(\xi_i, y_k, z_k) \right)_m^l = G \sqrt{k_z} \left[\Delta u_3'(\xi_i) + \Delta u_5'(\xi_i) \right]_m^l \quad (4.37c)$$

iv. Perform the yield criterion at each monitoring station k of the i -th cross section of the beam ($k = 1, 2, \dots, N_{dof}$, $i = 1, 2, \dots, L + 1$) employing eqn. (4.34).

- If $\Phi_{vM}^{Tr} \leq 0$ then yield criterion is satisfied and the stress state lies within the elastic domain. Thus, the trial state is the final admissible one, the incremental plastic strain components are zero and the total plastic strain components along with the equivalent plastic strain get the corresponding values of the previously converged load station.

$$\left(\Delta \varepsilon_{xx}^{pl} \right)_m^l = \left(\Delta \gamma_{xy}^{pl} \right)_m^l = \left(\Delta \gamma_{xz}^{pl} \right)_m^l = 0 \quad (4.38a)$$

$$\left(\varepsilon_{eq}^{pl} \right)_m^l = \left(\varepsilon_{eq}^{pl} \right)_m^0 \quad (4.38b)$$

- If $\Phi_{vM}^{Tr} > 0$ then plastic flow occurs and return must be made to yield surface (plastic correction step). A local Newton–Raphson method is initiated to integrate the inelastic constitutive equations by employing the generalized cutting-plane algorithm (Ortiz & Simo 1986, Simo & Hughes 1998). The incremental plastic strain components along with the equivalent plastic strain are updated according to this algorithm by using a prescribed tolerance $tol_{cp} = 10^{-5}$ in its convergence criterion.
- v. For each cross section of the beam, the evaluation of the plastic parts of the stress resultants is performed by employing a two-dimensional numerical integration scheme. Similarly to the procedure presented in section 4.3.2.1, the fibre approach

is adopted. To this end, the cross sections are divided into a number of triangular or quadrilateral cells and standard two-dimensional Gauss quadrature rules are employed in each cell to approximate the domain integrals of eqns. (4.18). If the same number of Gauss points is employed in every cell, then $N_{dof} = N_{cells} \times N_{Gauss}$ holds. Thus, the monitoring stations of each cross section coincide with the Gauss points of its cells, while exact patch between adjacent cells is not required.

- vi. Employ the obtained plastic quantities from the previous step to evaluate the vector $\{\Delta b_{pl}\}_m^l$ related to plastic quantities as well as the plastic quantities required to perform step (ii) for the next iteration $l+1$. Apart from elementary computations, the current step also requires the computation of line integrals. A numerical integration scheme must be employed to resolve these integrals since plastic quantities are not known in the whole beam interval $(0, l)$. A semi-analytical scheme has been implemented, according to which the incremental plastic stress resultants vary on an element $(1, 2, \dots, L)$ of the beam interval following the same law that is used to approximate the problems unknowns. This leads to the integration of kernels being products of functions $A_i(r)$ and two-node linear shape functions, thus it is performed analytically without any difficulty.
- vii. Initial Stress Convergence. Convergence occurs if the Euclidian norm of the incremental plastic stress resultants reaches a value smaller than a predetermined tolerance. If convergence is achieved after n iterations then:
- For each monitoring station k of the i -th cross section of the beam ($k = 1, 2, \dots, N_{dof}$, $i = 1, 2, \dots, L+1$), the stress components along with the equivalent plastic strain are initialized for the next increment $m+1$ as

$$(S_{xx})_{m+1}^0 = (S_{xx})_m^n \quad (S_{xy})_{m+1}^0 = (S_{xy})_m^n \quad (S_{xz})_{m+1}^0 = (S_{xz})_m^n \quad (4.39a)$$

$$(\varepsilon_{eq}^{pl})_{m+1}^0 = (\varepsilon_{eq}^{pl})_m^n \quad (4.39b)$$

- Resolve the vector $\{\Delta b_{ext}\}_{m+1}$ related to externally applied loading as well as the terms related to the externally applied loading required to perform step (ii) for the next increment. Apart from elementary computations, the current step requires the computation of line integrals. Since the distributions of the external loads are usually prescribed in codes and regulations with simple analytical relations, these integrals are evaluated analytically, demonstrating the efficiency of the developed numerical procedure (e.g. concentrated loads may be treated using the Dirac function, without adhering to any simplifications).
- vii. Since convergence is achieved then the foundation reaction is computed employing eqns. (4.1). The parameters are updated and the process described by steps (i)-(vii) is repeated until the foundation convergence criterion is achieved by using a prescribed tolerance of $tol_{found} = 10^{-10}$.
- viii. The increments of the external loading continue until the target load is fully undertaken from the beam-foundation inelastic system or convergence cannot be achieved, which means that the last additional increment cannot be undertaken (plastic collapse).

Finally, it is worth noting that the monitoring displacement components u , v and w at any interior point of the beam are updated after convergence in each increment by employing the integral representations (4.28a-c), respectively.

A step-by-step algorithmic approach of the nonlinear solution is presented in a flowchart form in Fig.4.5.

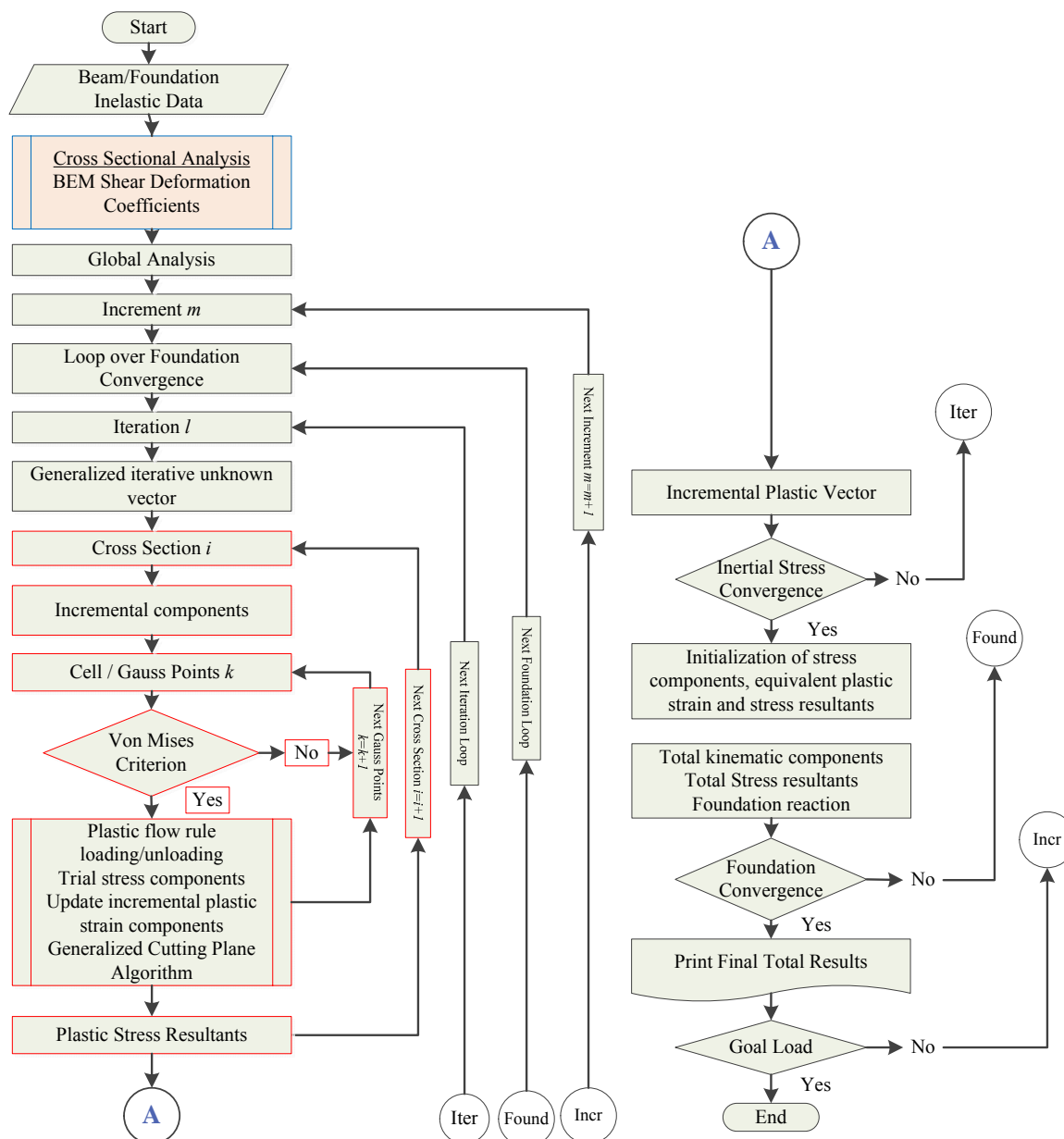


Fig. 4.5. Flowchart of the incremental–iterative solution algorithm based on the initial stress criterion

4.4 Numerical Examples

On the basis of the analytical and numerical procedures presented in the previous sections concerning the geometrically nonlinear inelastic analysis of shear deformable beams on nonlinear foundation, a computer program has been written using High Level 3G Fortran 90/95. Representative examples have been studied to demonstrate the efficiency, wherever possible the accuracy and the range of applications of the

developed method. Furthermore, the accuracy of the developed beam formulation is validated against a series of Laboratory Pushover tests on vertical single piles embedded in dry sand under different load paths to failure in $M-Q$ space conducted in the Laboratory of Soil Mechanics/Dynamics in NTUA.

4.4.1 Example 1 – Elastic Analysis of Free-Free Beam on Pasternak Foundation

For comparison purposes, in the first example the elastic analysis of a free-free beam of length $l = 5m$ resting on Pasternak elastic foundation subjected to a concentrated bending moment $M_y = 50kNm$ acting at its midpoint, as shown in Fig. 4.6 is examined.

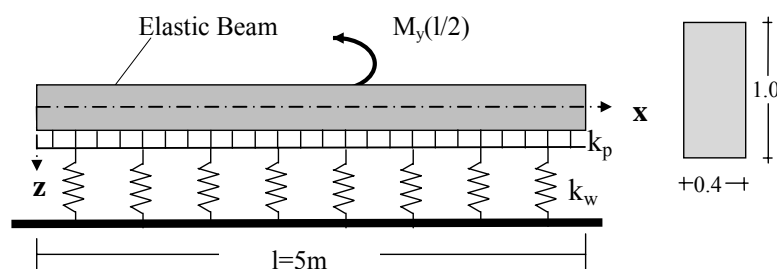


Fig. 4.6. Prismatic elastic beam on elastic two parameter foundation subjected to bending moment at its midpoint.

The beam is made out of timber with elastic modulus $E = 10.5GPa$, Poisson ratio $\nu = 0.25$ and has rectangular cross section of width $b = 0.4m$ and depth $h = 1.0m$. The elastic foundation is sandy clay with modulus of elasticity $E_s = 45.5MPa$ and Poisson ratio $\nu_s = 0.21$. The values of Winkler and Pasternak foundation parameters are evaluated as $k_w = 3.081MPa$ and $k_p = 12449kN$, respectively according to both Zhaohua and Cook (1983) and Mullapudi and Ayoub (2010) considering $\nu_s = 0.25$ and $\gamma = 1.0$. The present example was first studied by Shirima and Ginger (1990) who presented a complete solution of the stiffness matrix and nodal action vectors for a Timoshenko beam element resting on a two-parameter elastic foundation employing the displacement method. Later, Mullapudi and Ayoub (2010) solved the same problem deriving the values of the foundation parameters through an iterative technique that is based on the plain strain assumption for the soil medium, while the beam is discretized

into four mixed elements with cubic moment interpolation functions, assuming five integration points for each finite element.

In Table 4.1, the evaluated deflection at the beam's right end $w(l)$ and the midpoint rotation $w'(l/2)$ for both Winkler and Pasternak formulations are presented as compared with those obtained from the literature (the compared values have been extracted from a graph). Moreover, in Fig. 4.7 the bending moment distribution along the beam length is also presented as compared with available results from the literature for the aforementioned cases, demonstrating the accuracy of the proposed method in elastic analysis and noting that the bending moment is slightly underestimated if ignoring the Pasternak effects.

Table 4.1. Deflection (mm) and rotation (rad) of the beam of example 1.

	Winkler		Pasternak	
	Present Analysis	Mullapudi & Ayoub (2010)	Present Analysis	Mullapudi & Ayoub (2010)
Deflection $w(l)$	3.88	3.90	1.32	1.30
Rotation $w'(l/2) \times 10^{-3}$	1.599	1.600	0.5849	0.5850

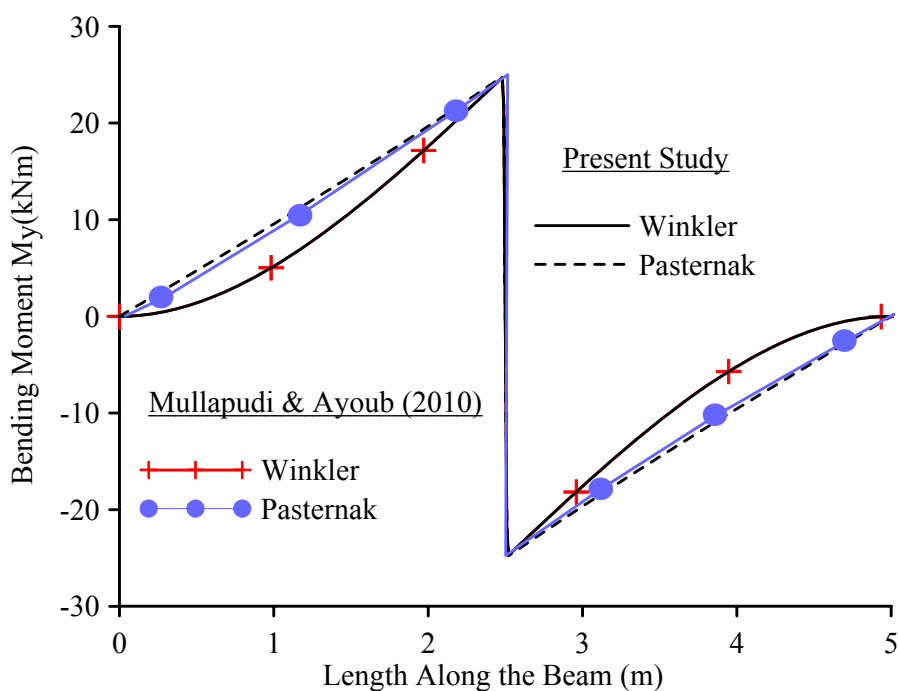


Fig. 4.7. Bending moment distribution $M_y(x)$ along the beam of example 1.

In order to demonstrate the effect of the unilateral character of the soil the same free-free elastic beam resting on tensionless Winkler foundation is analyzed, being subjected to a concentrated vertical force of $P(l/2) = 100kN$ and to a concentrated bending moment $M(l/2)$ acting at its midpoint. In Table 4.2 the deflection of both ends for various values of the applied moment, while in Fig. 4.8 the moment-rotation curve at the beam's midpoint are presented as compared (wherever possible) with those obtained from literature (Mullapudi & Ayoub 2010). A very good agreement is once again verified.

Table 4.2. Deflection (cm) at both ends of the beam of example 1, for tensionless Winkler foundation.

Present Analysis					
$M(kNm)$	20	50	100	150	168
$w(0)$	0.555	0.245	-0.180	-1.510	-2.633
$w(l)$	0.710	1.020	1.425	2.154	2.570
Mullapudi & Ayoub (2010) - $M=168kNm$					
	$w(0) = -2.490$		$w(l) = 2.450$		

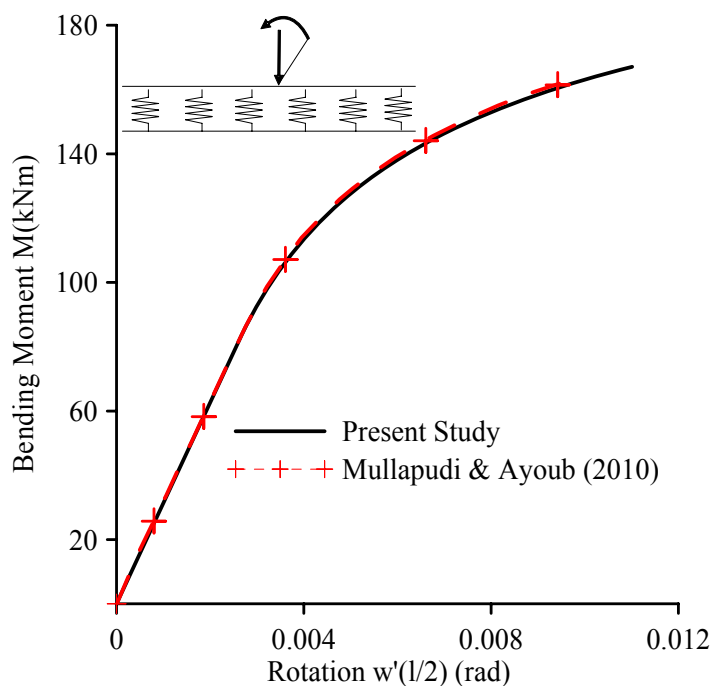


Fig. 4.8. Moment vs. rotation at the midpoint of the beam of example 1, for tensionless Winkler foundation.

4.4.2 Example 2 – Inelastic Analysis of Simply Supported Beam on Winkler Foundation

As a second example, also for comparison purposes, a simply supported beam of length $l = 300\text{in}$ and square cross section of side $d = 6.26\text{in}$ subjected to a monotonically increasing concentrated vertical load P at its midpoint has been studied. The material of the beam is assumed to follow an elastic–plastic behaviour with modulus of elasticity $E = 29000\text{ksi}$, yielding stress $\sigma_{Y0} = 30\text{ksi}$ and a strain hardening slope of 1.4% (tangent modulus $E_t = 406\text{ksi}$), while the Winkler foundation load-displacement relation is also considered to be elastic–plastic with initial stiffness equals to $k_w = 0.5\text{kip} / \text{in}^2$, yielding force $P_{wY} = 1.0\text{k} / \text{in}$ and hardening slope of 1.0% (tangent stiffness $k_{wt} = 5 \cdot 10^{-3}\text{kip} / \text{in}^2$). For the longitudinal discretization 20 linear elements have been employed, while the cross section has been discretized into 36 quadrilateral cells (6 fibres) and a 2×2 Gauss integration scheme has been used for each cell.

The present example has been studied by Ayoub (2003), developing both displacement and mixed-based finite element formulation capable of capturing the nonlinear behaviour of both the beam and the foundation. The beam's section has been discretized into 16 fibres, while for both the displacement and mixed models two different order of interpolation functions were used, employing a 6 element discretization. The results were compared with the converged solution obtained by a displacement-based model with fifth order polynomial and a mesh consisting of 32 elements.

In Table 4.3, the maximum deflections of the midpoint of the beam for various internal nodal points' discretization schemes are presented; illustrating that convergence is achieved for a small number of nodal points. The obtained values are compared for the same load stage $P_z = 160\text{kN}$ (the compared values have been extracted from a graph), with the one presented in Ayoub (2003). In Fig. 4.9, the load–displacement curve at the beam's midpoint is presented, as compared with those obtained from a FEM solution (Ayoub 2003) demonstrating a very good agreement. More specifically, the obtained curve is almost identical with the results of the mixed model with cubic moment function and the converged solution, which is assumed to describe the exact behaviour of the beam–foundation system, while the other models present a perceptible amount of error in the inelastic region.

Table 4.3. Maximum values of the deflection $w_{\max}(l/2)$ of the beam of example 2 and divergence values for various discretization schemes.

Nodal Points	6	11	17	20	Ayoub (2003)
Max Deflection (cm)	3.894	3.906	3.937	3.925	3.975
Divergence (%)	2.03	1.73	0.95	0.01	-

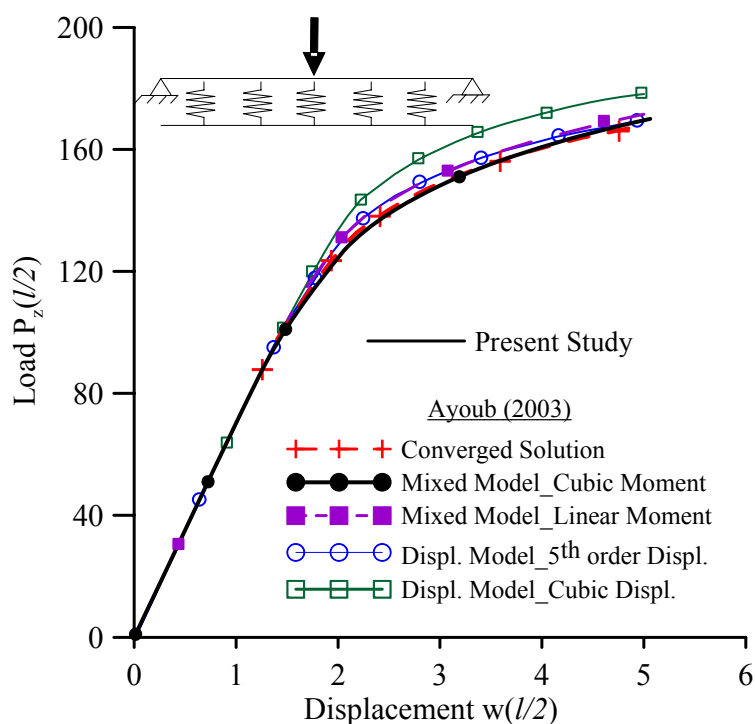


Fig. 4.9. Load–displacement curve at the midpoint of the beam of example 2.

In Fig. 4.10a,b the bending moment M_y and the displacement w curves along the beam length are presented as compared with those from the literature for the load stage producing deflection at the midspan equal to 5. As it can be observed, the corresponding curves of the present study capture the exact behaviour rather accurately and agree with the converged solution and the results of the mixed model with cubic moment interpolation function, while differ from the curves of the displacement model with cubic displacement function. Finally, in Table 4.4 the midpoint curvature $w''(l/2)$ and the foundation reaction p_s at $x=l/6$ are also presented and compared for the same load stage (the compared values have been extracted from a graph), verifying that the maximum values of the curvature and the soil reaction are accurately represented.

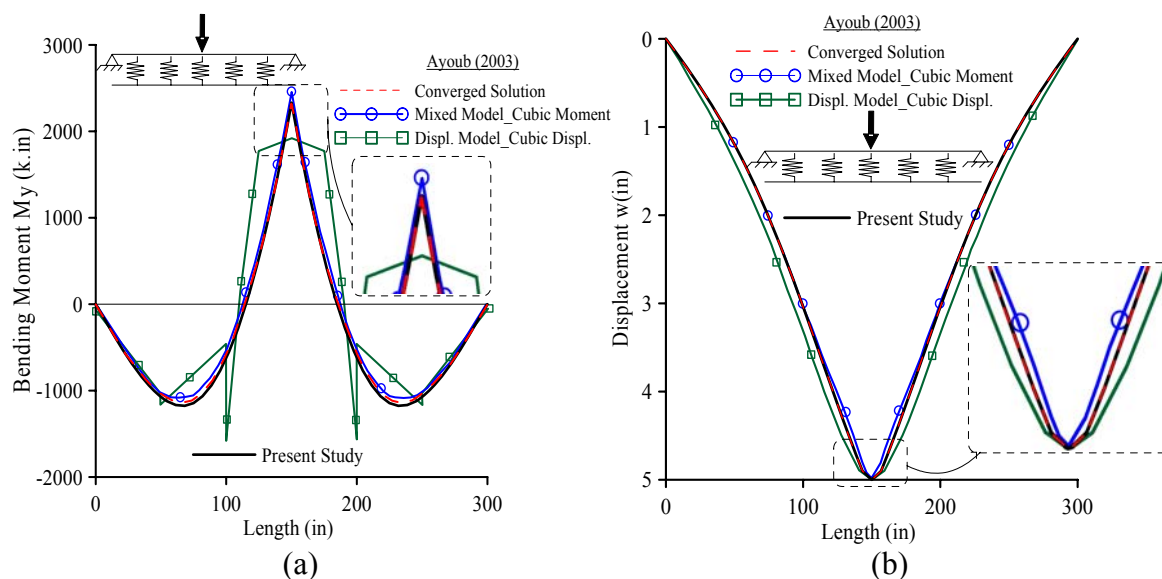


Fig. 4.10. Bending moment $M_y(x)$ and displacement $w(x)$ distribution along the beam of example 2.

Table 4.4. Curvature (1/in) and foundation reaction (k/in) of the beam of example 2.

Analysis	Present	Ayoub (2003)				
		Converged Solution	Mixed Model cubic moment	linear moment	5 th order	cubic
Curvature $w''(l/2) \times 10^{-3}$ (1/in)	9.98	10.66	11.85	9.95	4.91	2.26
Foundation Reaction $p_f(l/6)$ (k/in)	0.601	0.60	0.60	0.611	0.619	0.689

4.4.3 Example 3 – Inelastic Analysis of Simply Supported Beam on Nonlinear Pasternak Foundation

In order to demonstrate the range of applications of the developed method, in the third example a rectangular cross section ($h = 0.60m$, $b = 0.30m$) beam of length $l = 6.0m$, clamped at both ends has been studied, employing 20 linear longitudinal elements, 400 boundary elements, 72 quadrilateral cells (12 fibres) and a 3×3 Gauss integration scheme for each cell (cross sectional discretization). Two material cases have been analyzed, namely an elastic-perfectly plastic with $E = 32318.4MPa$, $\sigma_{Y0} = 20MN / m^2$

and $E_t = 0$ and an elastoplastic-strain hardening with $E_t = 650\text{MPa}$, while two load cases have been examined namely a concentrated load at $2l/3$ and a uniformly distributed one, both monotonically increasing.

In Figs. 4.11a,b the load-displacement curves at the load position are presented for the two load cases, as compared with a FEM solution (NX Nastran 2007) obtained by employing 60 beam elements and a 3-D FEM solution (NX Nastran 2007) obtained by employing 8250 solid (brick) elements. In the case of elastic-perfectly plastic material an additional curve is presented in Fig. 4.11a applying the Step by Step concentrated plasticity method. A good agreement between the results of the present method and the 3-D FEM solution is observed, especially in the elastoplastic-strain hardening case. Moreover, in Fig. 4.12 the normal stress distribution along the beam length is presented for different load stages for both load cases ($P(2l/3) = 610\text{kN}$, 780kN and 810kN corresponding to the occurrence of the plastic hinges).

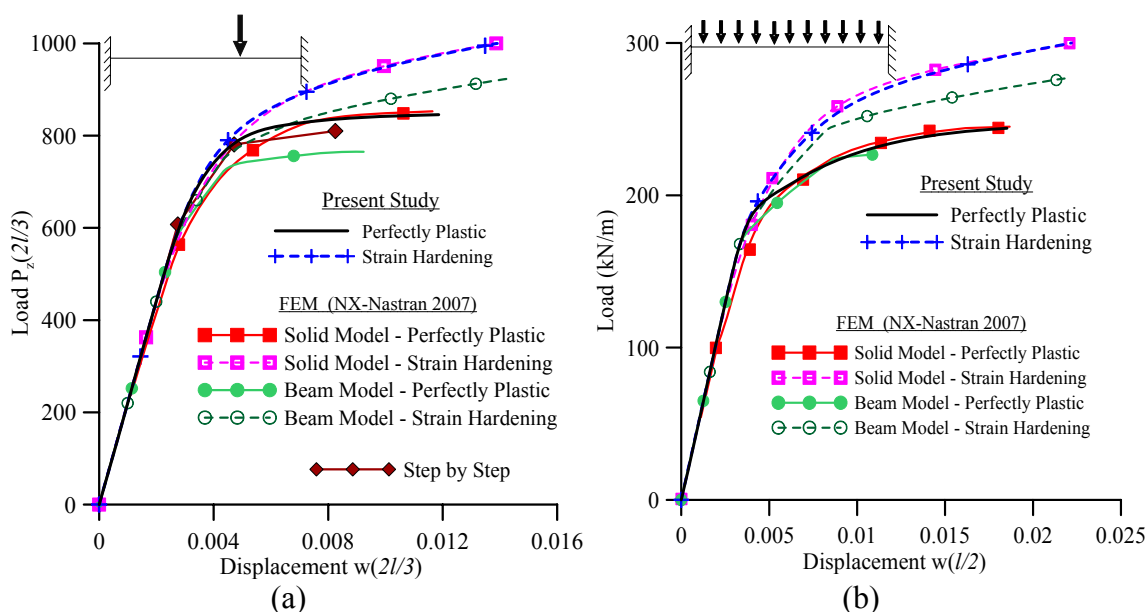


Fig. 4.11. Load–displacement curve of the beam of example 3, for concentrated (a) and uniformly distributed (b) load.

As a variant of this example, the same beam subjected to the same load cases resting on a tensionless Pasternak foundation is examined. The nonlinear load-displacement foundation reaction is characterized by the perfectly plastic Winkler part with initial stiffness $k_w = 20\text{MPa}$ and yielding force $P_{wY} = 60\text{kN} / m$ and the Pasternak part with stiffness $k_p = 5000\text{kN}$. In Figs. 4.13a,b the load-displacement curves are

presented for different types of beam and soil material properties and for both load cases, verifying the significant influence of the inelastic analysis to the soil-beam system response and the importance to the deflections of the subgrade modelling. Finally, in Table 4.5 the deflection of the midpoint of the beam $w(l/2)$ is presented in the case of a uniformly distributed load for both types of foundation modelling for various load stages taking into account or ignoring the beam’s material strain hardening slope. From this figure and table, it is easily concluded that the inelastic analysis and the soil nonlinearity are of paramount importance.

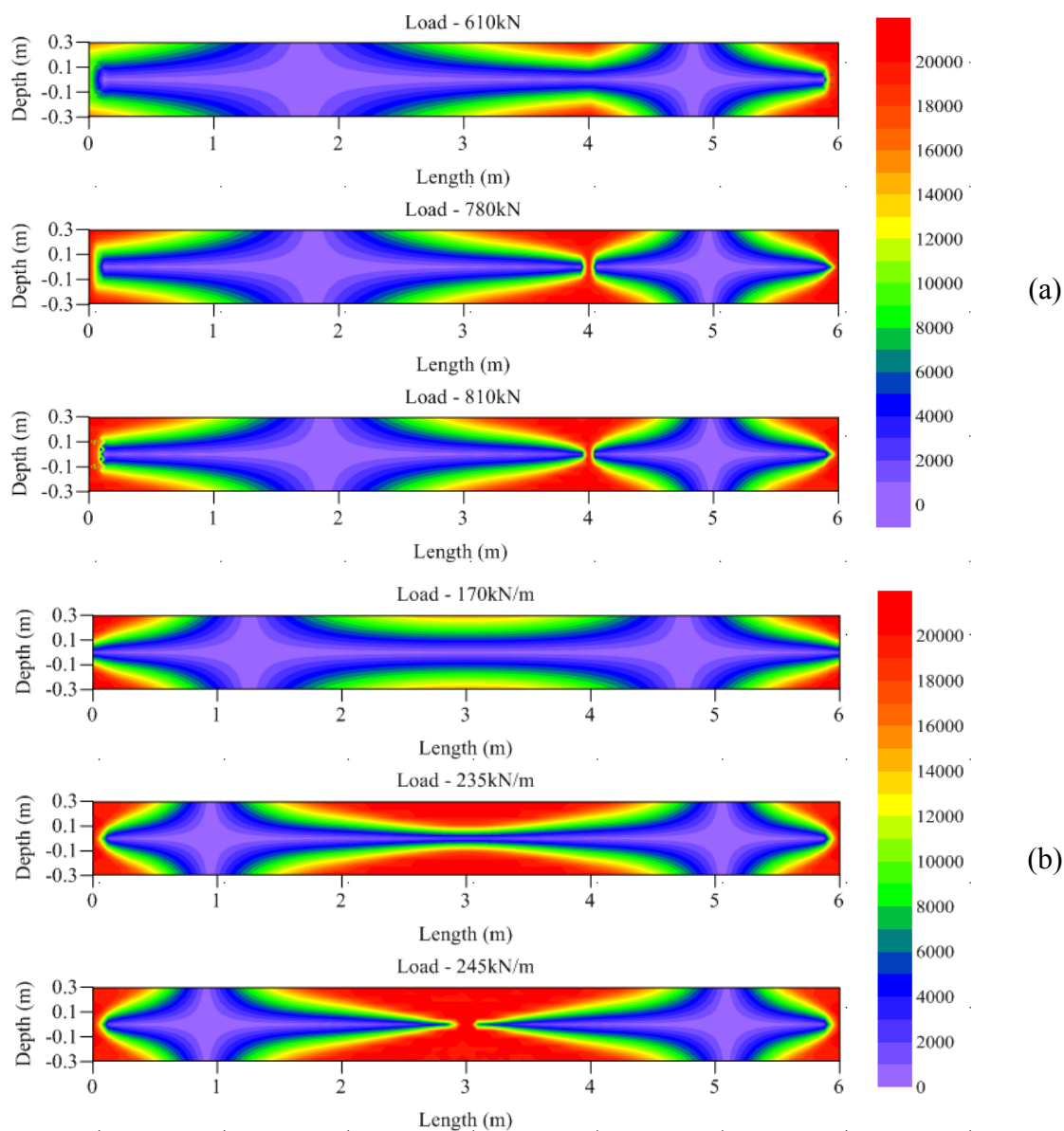


Fig. 4.12. Normal stress distribution along the beam length for different load stages and for concentrated (a) or uniformly distributed (b) load.

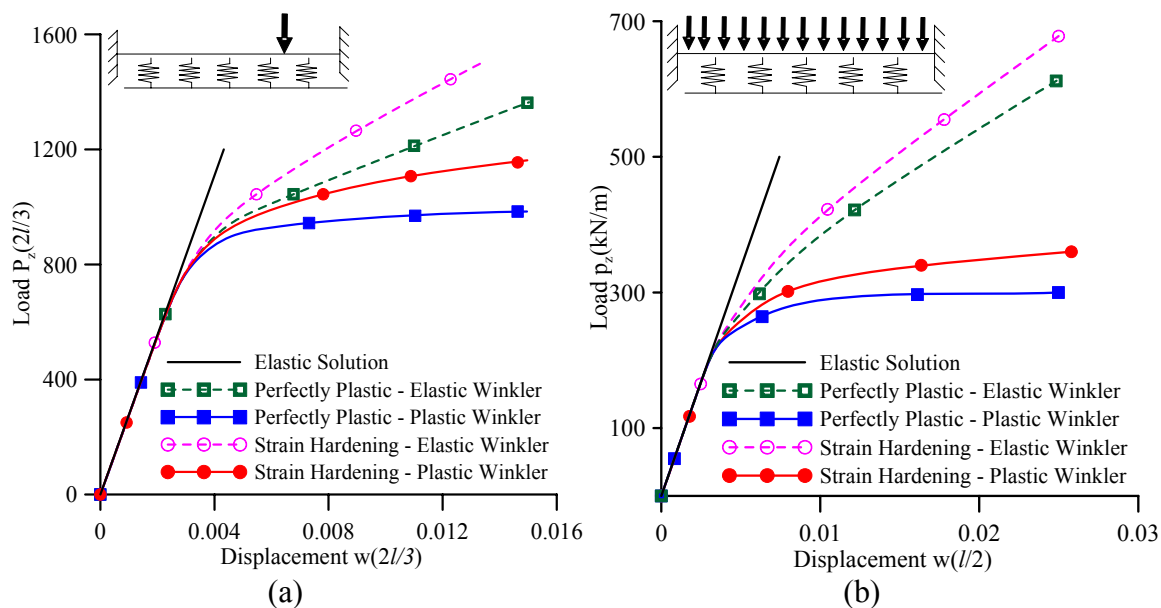


Fig. 4.13. Load–displacement curve of the beam of example 3 resting on nonlinear foundation, for concentrated (a) and uniformly distributed (b) load.

Table 4.5. Deflection (mm) of the midpoint of the beam of example 3, subjected to uniformly distributed loading (load step 2kN/m).

p_z/w	Perfectly Plastic $E_t = 0$			Strain Hardening $E_t = 650\text{MN}/\text{m}^2$		
	Elastic Winkler	Elastic Pasternak	Plastic Pasternak	Elastic Winkler	Elastic Pasternak	Plastic Pasternak
100	1.49	1.46	1.46	1.49	1.46	1.46
250	4.31	4.16	4.78	4.15	4.03	4.39
300	6.16	5.94	10.40	5.63	5.46	7.10
600	24.01	22.30	–	20.39	19.08	–

4.4.4 Example 4 – Beam on Nonlinear Foundation under Cyclic Loading

In this example, a pinned–fixed beam resting on an elastic–plastic Winkler foundation with initial stiffness $k_w = 20\text{MPa}$ and yielding force $P_{wY} = 100\text{kN}/\text{m}$ has been studied (Fig. 4.14a), employing 20 linear longitudinal elements, 400 boundary elements, 72 quadrilateral cells (12 fibres) and a 3×3 Gauss integration scheme for each cell (cross sectional discretization). The geometric properties of the beam are assumed equal to those of example 3, while it is subjected to a cyclic uniformly distributed loading

acting at $0 \leq x \leq 3.0\text{m}$, as presented in Figs. 4.14a,b. Two material cases have been analyzed, namely an elastic-perfectly plastic with $E = 32318.4\text{MPa}$, $\sigma_{Y0} = 20\text{MN} / \text{m}^2$ and $E_t = 0$ and an elastoplastic-strain hardening with $E_t = 650\text{MPa}$.

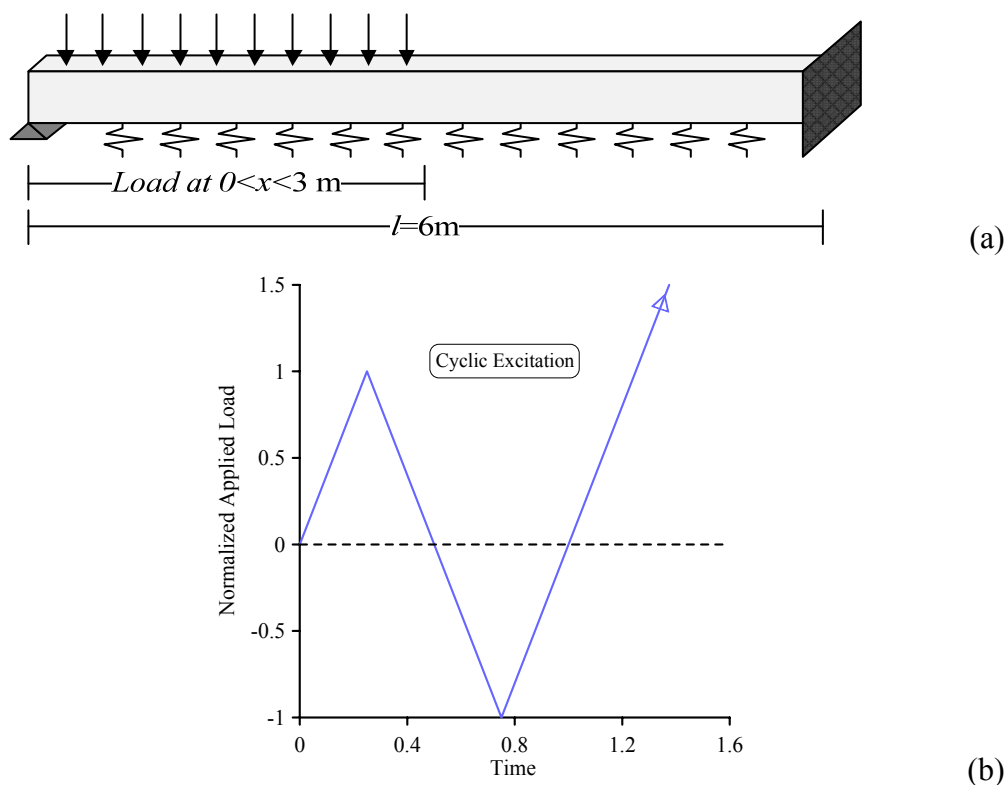


Fig. 4.14. Pinned-fixed beam resting on an elastic-plastic Winkler foundation (a) subjected to a uniformly distributed cyclic loading (b).

In Figs. 4.15a,b the load–displacement curves at the midpoint $w(l/2)$ of the beam are presented for different types of material properties, as compared with a 3-D FEM solution (NX Nastran 2007) employing 2561 solid elements, ignoring the foundation reaction. Furthermore, the load–displacement curves at the midpoint $w(l/2)$ of the beam on elastic-plastic Winkler foundation for different types of material properties are depicted in Figs. 4.16a,b, as compared with a FEM solution (NX Nastran 2007) obtained by employing 2561 solid elements and 81 nonlinear springs following the elastic-plastic law given above.

Moreover, in Fig. 4.17 the normal stress distribution along the beam's length is presented for different load stages, as compared with the corresponding deformed 3-D

FEM contour representation. From these figures a very good agreement between the results is observed verifying the accuracy and applicability of the proposed formulation.

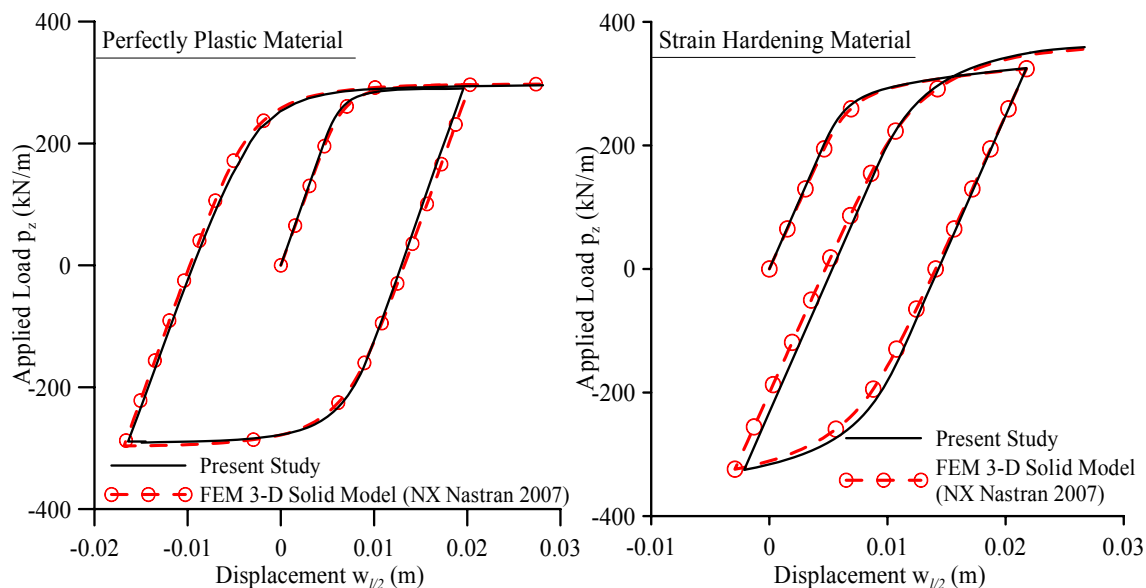


Fig. 4.15. Load–displacement curve at the midpoint of the beam of example 4, in case of elastic-perfectly plastic (a) and elastoplastic-strain hardening (b) material.

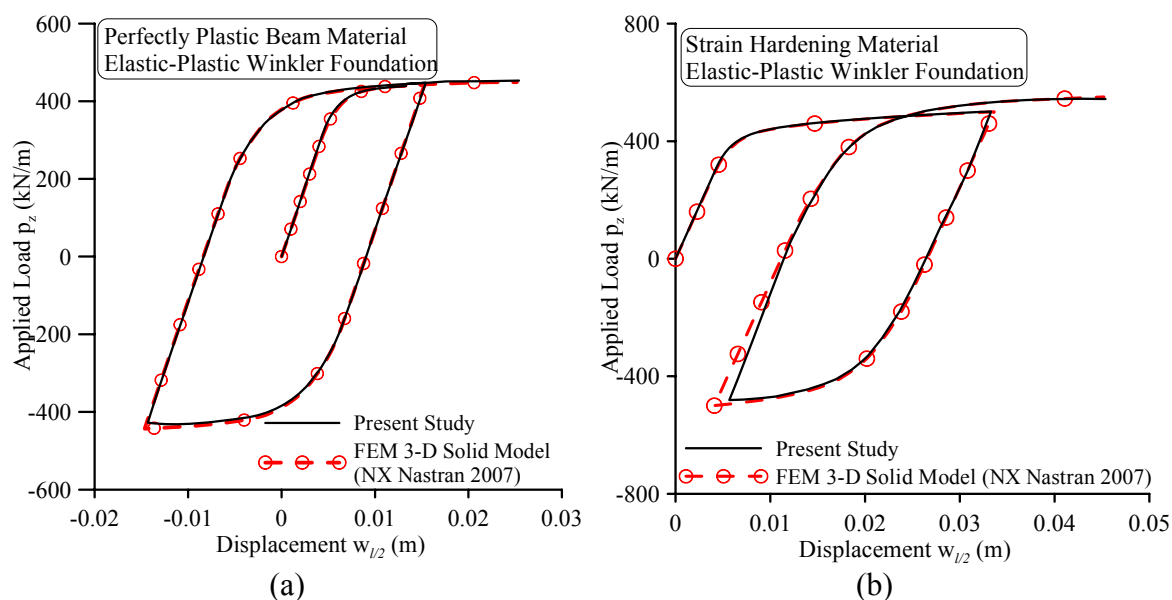


Fig. 4.16. Load–displacement curve at the midpoint of the beam on elastic-plastic Winkler foundation of example 4, in case of elastic-perfectly plastic (a) and elastoplastic-strain hardening (b) beam material.

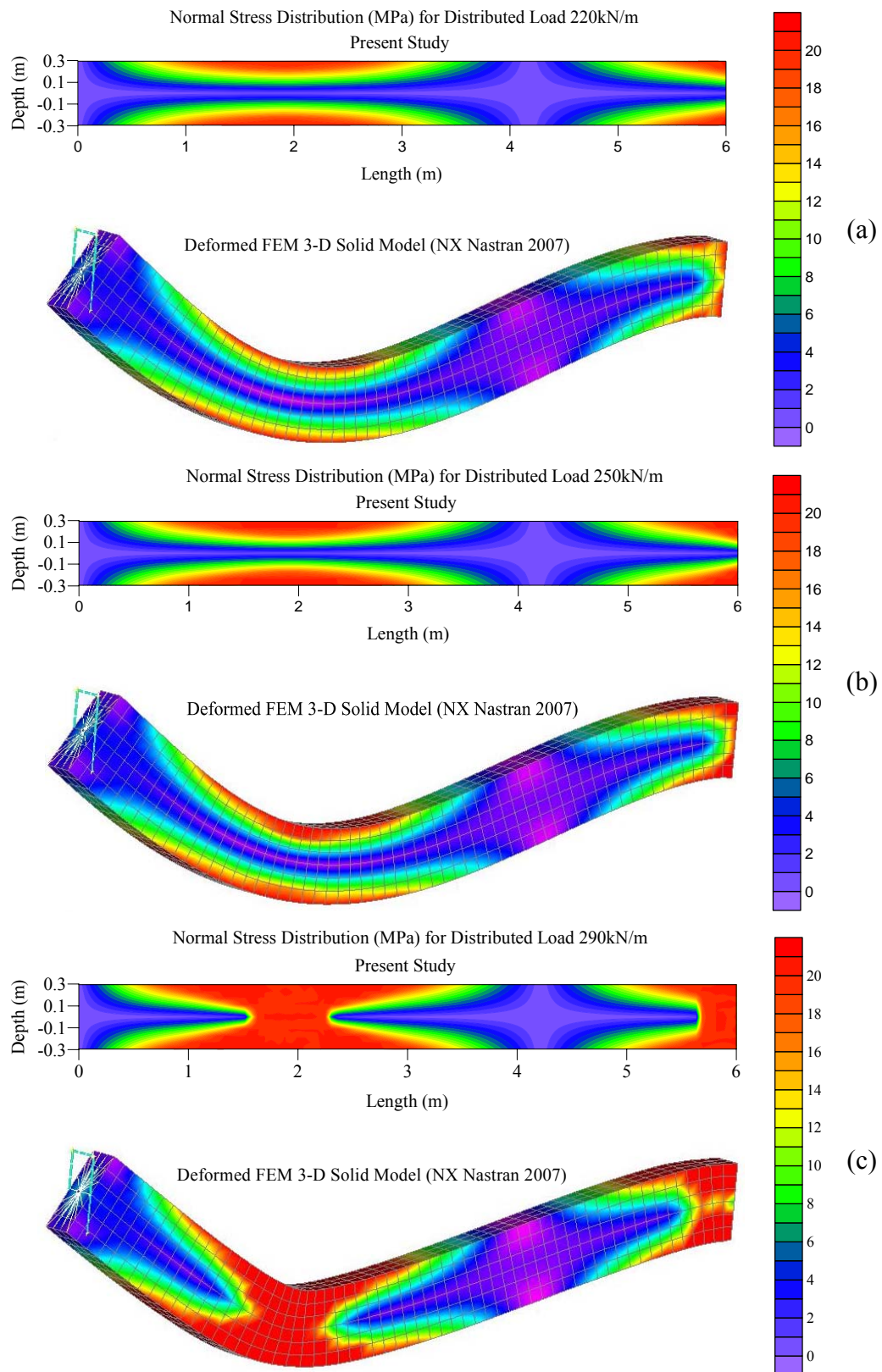


Fig. 4.17. Normal stress distribution along the beam's length for different load stages compared to the corresponding deformed 3-D FEM contour representation.

Finally, in Table 4.6 the maximum beam deflection w_{max} is presented for different load stages and material properties as compared with those obtained from two FEM models, namely the aforementioned 3-D solid one and a one dimensional model employing 120 beam and spring elements, observing the convergence between the proposed formulation and the solid simulation, as well as the inability of the FEM beam model to capture accurately the systems response. From these figures and table, the significant influence of the inelastic analysis to the beam-foundation response, as well as the reliability of the proposed method are verified.

Table 4.6. Maximum deflection w (cm) of the beam of example 4, for different types of beam and foundation material properties.

Elastic Winkler Foundation						
p_z/w_{max}	Perfectly Plastic $E_t = 0$			Strain Hardening $E_t = 650MN/m^2$		
	Present Study	FEM Solid Model	FEM Beam Model	Present Study	FEM Solid Model	FEM Beam Model
500	0.987	1.002	1.100	0.980	0.984	1.041
550	1.202	1.213	–	1.158	1.170	1.252
600	1.438	1.468	–	1.364	1.384	1.483
Perfectly Plastic Winkler Foundation						
p_z/w_{max}	Perfectly Plastic $E_t = 0$			Strain Hardening $E_t = 650MN/m^2$		
	Present Study	FEM Solid Model	FEM Beam Model	Present Study	FEM Solid Model	FEM Beam Model
350	0.567	0.589	0.576	0.566	0.585	0.586
400	0.767	0.780	0.758	0.756	0.769	0.811
440	1.657	1.659	–	1.199	1.215	2.128
Hardening ($k_{wt} = 1.0MPa$) Winkler Foundation						
p_z/w_{max}	Perfectly Plastic $E_t = 0$			Strain Hardening $E_t = 650MN/m^2$		
	Present Study	FEM Solid Model	FEM Beam Model	Present Study	FEM Solid Model	FEM Beam Model
400	0.750	0.773	0.810	0.743	0.766	0.789
450	1.663	1.632	–	1.254	1.285	1.938
500	5.689	5.651	–	2.618	2.678	3.876

4.4.5 Example 5 – I-Beam on Nonlinear Foundation

In this numerical application, an I-shaped cross section (total height $h = 0.3\text{ m}$, total width $b = 0.3\text{ m}$, flange width $t_f = 0.02\text{ m}$, web width $t_w = 0.01\text{ m}$) fixed-pinned beam ($E = 213.4\text{ GPa}$, $\sigma_{Y0} = 285\text{ MPa}$) of length $l = 8\text{ m}$ resting on an elastic-plastic Winkler foundation ($k_w = 25\text{ MPa}$, $P_{wY} = 100\text{ kN/m}$, $k_{wt} = 1.25\text{ MPa}$) has been studied, employing 32 linear longitudinal elements, 400 boundary elements, 43 quadrilateral cells (15 fibres) and a 3×3 Gauss integration scheme for each cell (cross sectional discretization). The computational model implemented in the proposed formulation is presented in Fig. 4.18a. The beam is subjected either to a concentrated load at position $x = 3\text{ m}$ from the fixed end or to a uniformly distributed one, both monotonically increasing.

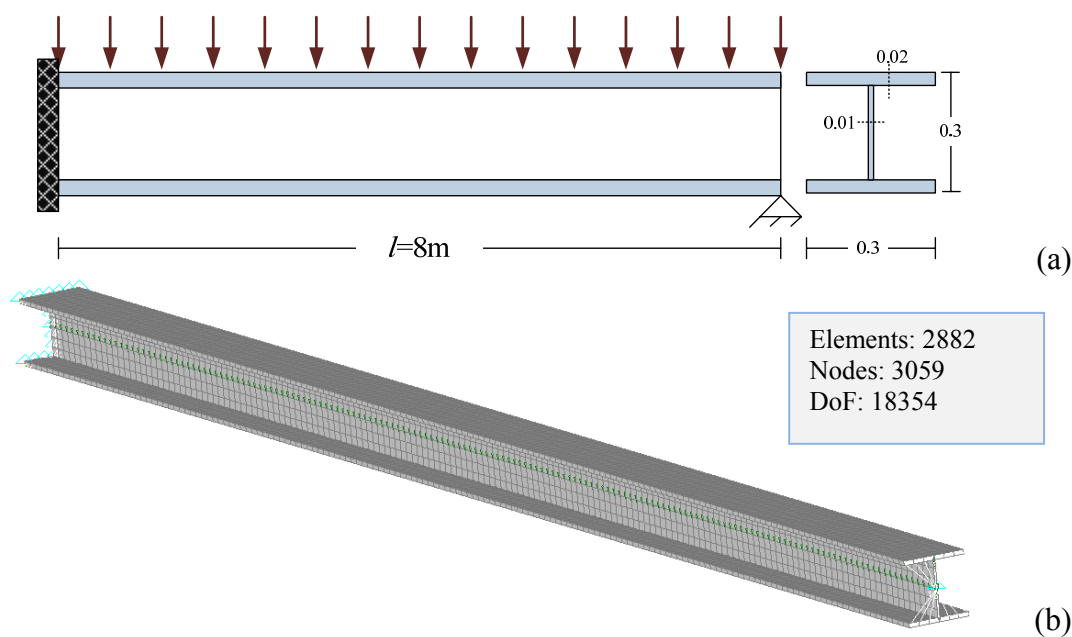


Fig. 4.18. Fixed pinned beam subjected to a uniformly distributed loading (a) and shell model implemented in NX Nastran (2007) (b).

In Figs. 4.19a,b the load-displacement curves are presented for different types of beam material properties ignoring the foundation reaction and for both load cases, as compared with a FEM solution (NX Nastran 2007) obtained by employing 2882 quadrilateral shell elements (Fig. 4.18b). Excellent agreement between the results is observed. In the same figures the normal stress distribution is also presented for several inelastic load levels illustrating the spread of plasticity along the cross section. Finally,

in Figs. 4.20a,b the load-displacement curves are presented for different types of beam and soil material properties and for both load cases, as compared with a FEM solution (NX Nastran 2007) obtained by employing 2882 quadrilateral shell elements for the I-shaped beam and assuming 161 nonlinear springs following the elastic-plastic law given above. From these figures, the significant influence of the inelastic analysis to the soil-beam system response and the accuracy of the proposed formulation are verified.

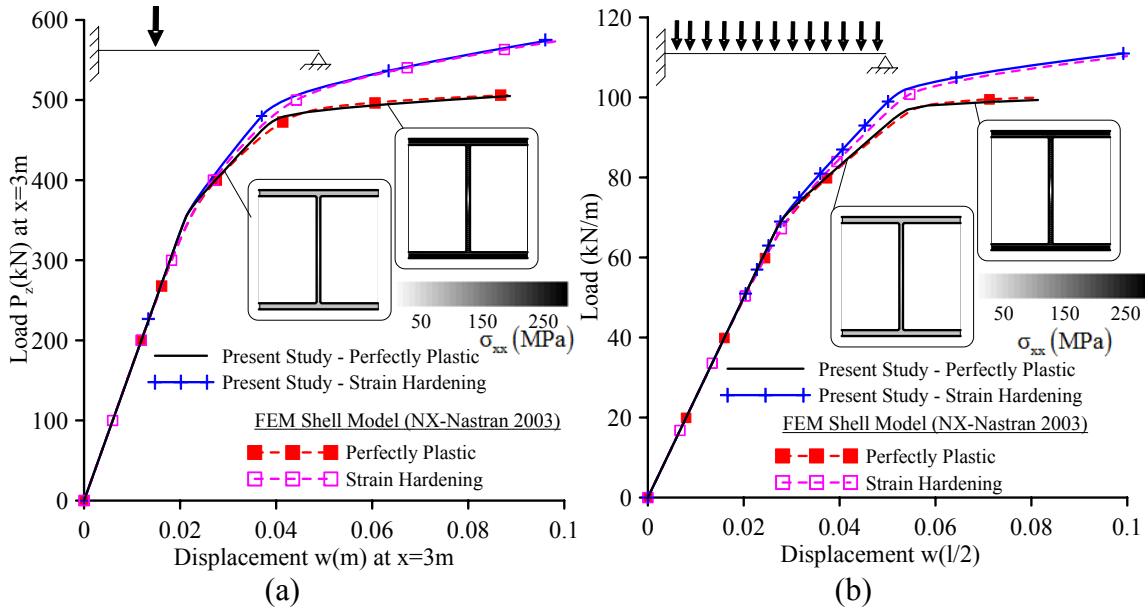


Fig. 4.19. Load–displacement curve of the beam of example 5, for concentrated (a) and uniformly distributed (b) load.

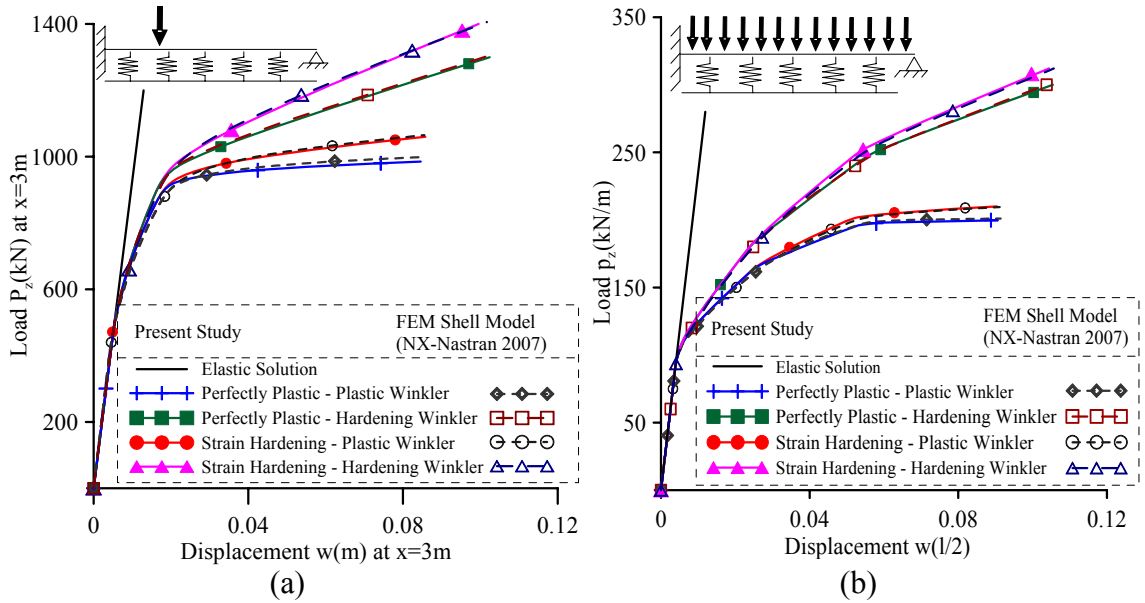


Fig. 4.20. Load–displacement curve of the beam of example 5 resting on nonlinear foundation, for concentrated (a) and uniformly distributed (b) load.

4.4.6 Example 6 – I-Beam on Nonlinear Foundation under Cyclic Loading

As an extension of the previous example, the same I-shaped cross has been analysed assuming two material cases; namely an elastic-perfectly plastic one with $E = 213.4\text{GPa}$, $\sigma_{Y0} = 285\text{MPa}$, $E_t = 0$ and an elastoplastic-strain hardening one with $E_t = 6000\text{MPa}$. The beam is subjected to uniformly distributed cyclic loading, as presented in Fig. 4.21.

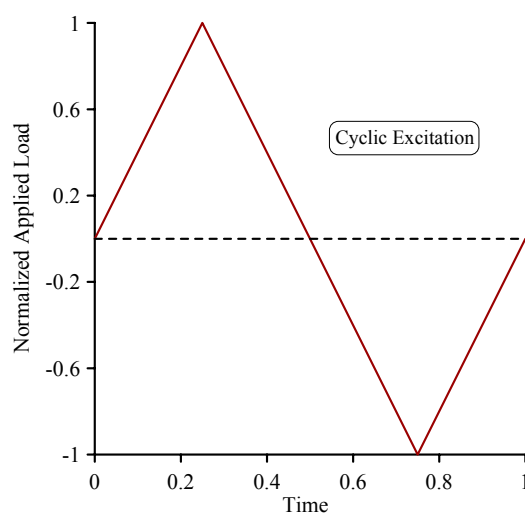


Fig. 4.21. Normalized cyclic excitation of example 6.

To demonstrate the convergence of the developed numerical procedure, in Table 4.7 pairs of applied transverse loading and displacement values at the midpoint of the beam are presented, for both cases of material properties, for three longitudinal discretization schemes. The first loading level of the table corresponds to an elastic behaviour, while the remaining ones refer to inelastic response. Moreover, in this table the ultimate transverse load p_z^u that can be undertaken by the beam (plastic collapse load) is also presented for the aforementioned longitudinal discretization schemes. Furthermore, in Figs. 4.22a,b the load–displacement curves are presented as compared with the FEM solution (NX Nastran 2007), taking into account or ignoring the material elastoplastic hardening. Excellent agreement between the obtained results and the shell finite element model is observed, illustrating once again the accuracy of the proposed method.

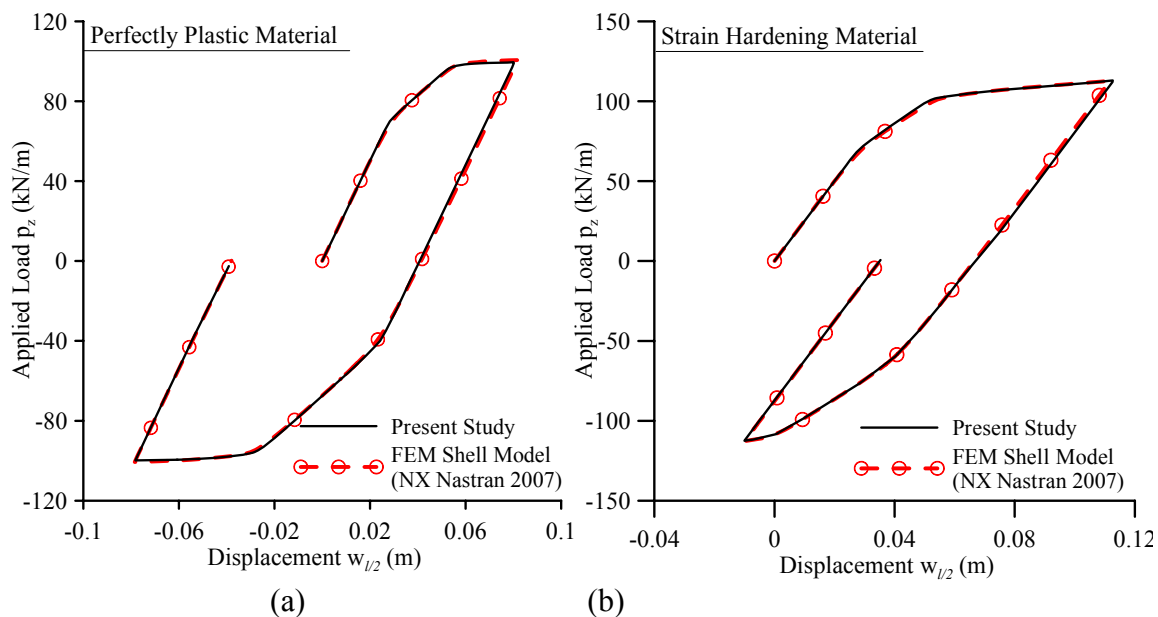


Fig. 4.22. Load–displacement curve at the midpoint of the beam of example 6, for elastic-perfectly plastic (a) and elastoplastic-strain hardening (b) material.

Table 4.7. Applied load versus displacement at $x=l/2$ along with ultimate transverse load p_z^u undertaken by the beam of example 6, for various longitudinal discretization schemes.

Material	Elastic-perfectly plastic			Elastoplastic-strain hardening		
Number of elements	15	30	40	15	30	40
p_z (kN/m)	$w_{l/2} \times 10^{-2}$ (m)					
65	2.597	2.598	2.598	2.597	2.598	2.598
80	3.688	3.719	3.721	3.405	3.518	3.522
90	4.653	4.665	4.671	4.180	4.236	4.288
95	5.020	5.150	5.164	4.598	4.674	4.682
	p_z^u (kN / m)					
	99.8	99.8	100	–		

4.4.7 Example 7 – Mono-Symmetric I Beam on Nonlinear Foundation under Cyclic Loading

As a special numerical example, a mono-symmetric I-shaped cross section of total height $h = 0.3m$, upper/lower flange width $b_f^{top} = 0.3m / b_f^{bot} = 0.4m$, thickness $t_f = 0.02m$, and web thickness $t_w = 0.01m$, clamped beam ($E = 213.4GPa$, $\sigma_{Y0} = 285MPa$) of length $l = 7m$ resting on an inelastic Winkler foundation ($k_w = 25MPa$, $P_{wY} = 100kN / m$, $k_{wt} = 2.5MPa$) has been studied, employing 32 linear longitudinal elements, 400 boundary elements, 43 quadrilateral cells (15 fibres) and a 3×3 Gauss integration scheme for each cell (cross sectional discretization). The beam is subjected to a cyclic concentrated load acting at $x = 2.5m$ from the left support.

In Fig. 4.23 the load–displacement curves at the loading point are presented for different types of beam and soil material properties in case of monotonically increasing concentrate load, verifying the significant influence of the inelastic analysis to the beam–foundation system response and the importance of the subgrade modelling to the beam deflections. Moreover, in Figs. 4.24a,b the load–displacement curves are presented accounting for or ignoring the beam’s and Winkler’s spring hardening slope, verifying the importance of the soil nonlinearity to the system’s cyclic response.

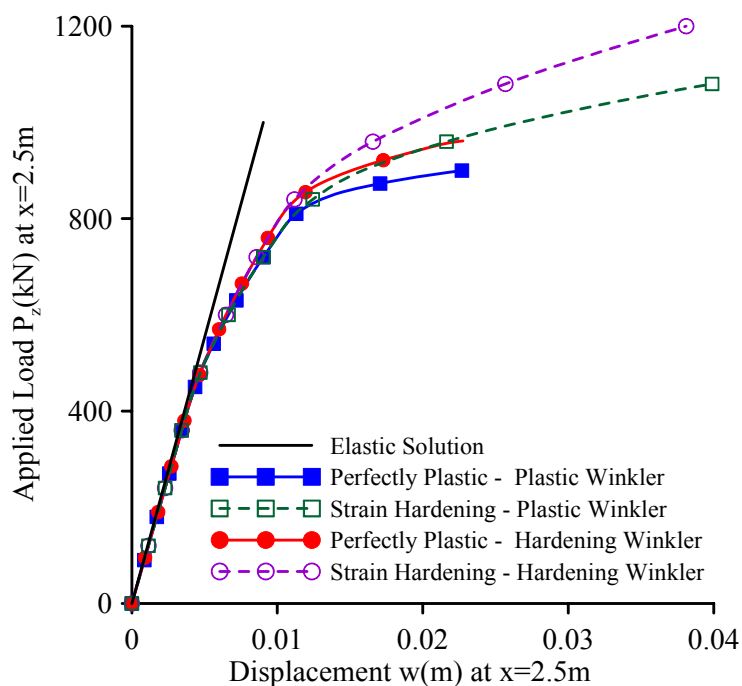


Fig. 4.23. Load–displacement curve at the loading point of the beam of example 7 resting on nonlinear foundation.

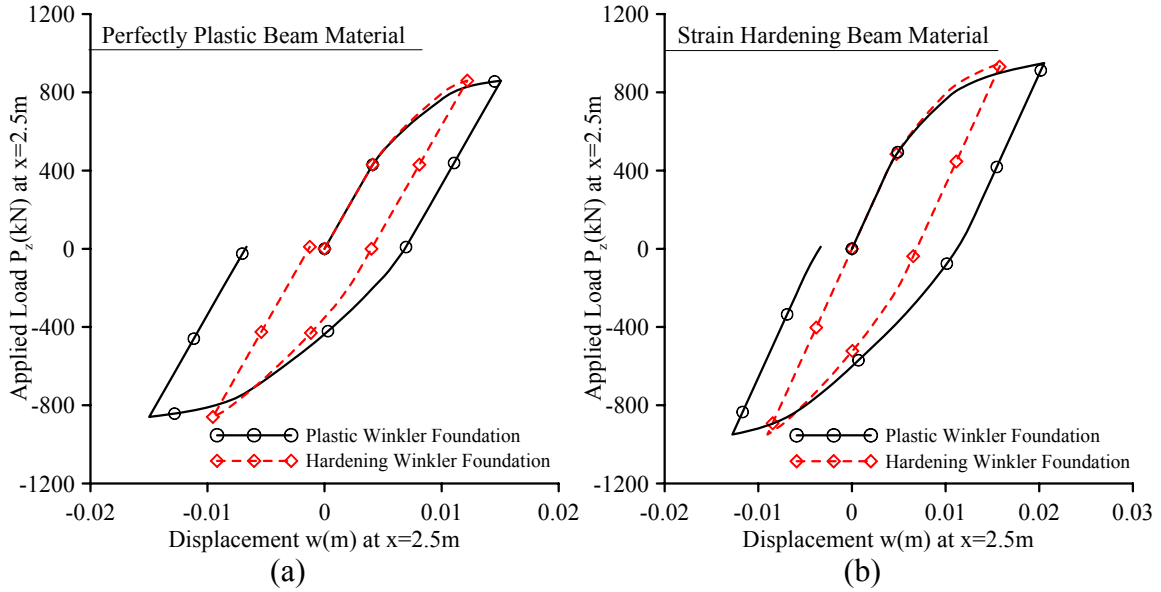


Fig. 4.24. Load–displacement curve at the loading point of the beam of example 7, in case of elastic–perfectly plastic (a) and elastoplastic–strain hardening (b) beam material.

4.4.8 Example 8 – Cantilever under Axial & Transverse Loading

For comparison purposes, in this example a cantilever beam of length $l = 2m$ under concentrated transverse and axial forces $P_z(l)$, $P_x(l)$, respectively acting at the tip, has been studied. The beam is made out of aluminium with modulus of elasticity $E = 69GPa$, shear modulus $G = 26GPa$ and yielding stress $\sigma_{Y0} = 275MPa$, with rectangular cross section of width $b = 0.02m$, height $h = 0.8m$ and shear correction factor $\alpha_z = 1.2$. The efficiency of the proposed formulation is illustrated through a convergence analysis performed in case of linear elastic response as compared with the exact solution for the tip displacement w_{exact} and rotation $\theta_{y exact}$ evaluated by the analytical expressions

$$w_{exact} = \frac{P_z l^3}{3EI_z} + \frac{P_z l}{GA_z} \quad (4.40a)$$

$$\theta_{y exact} = -\frac{P_z l^2}{2EI_z} \quad (4.40b)$$

In Fig. 4.25, the percentage error of the maximum tip displacement and rotation for various internal nodal points' discretization schemes is presented, while in Table 4.8 the converged values are compared with those obtained from the Reduced Integration Element (RIE) proposed by Reddy (1997). From the obtained results it is concluded that the shear locking has been successfully prevented and satisfactory accuracy is achieved (i.e. $error \leq 1\%$) with small number of nodal points, while it is noted that in order to achieve adequate accuracy with RIE several elements are required (Reddy 1997, Saritas and Filippou 2009).

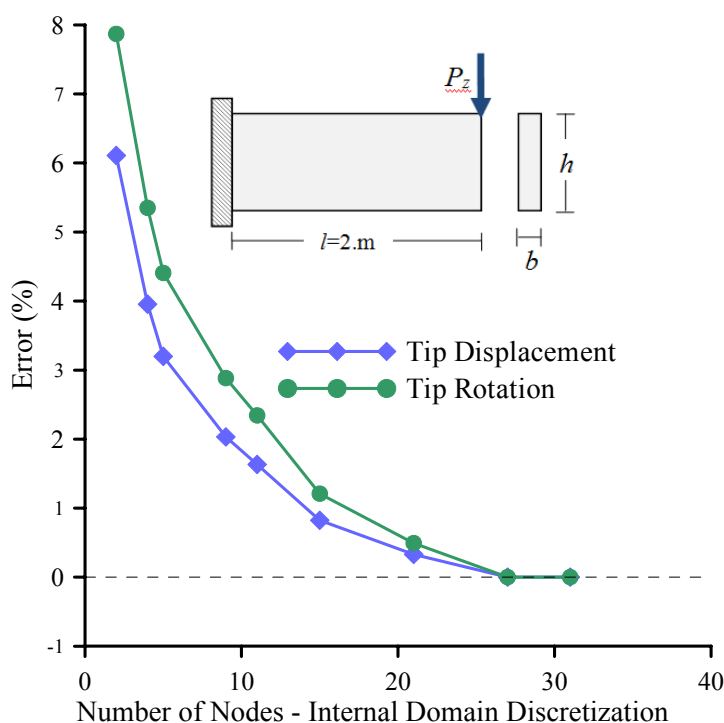


Fig. 4.25. Tip displacement and rotation error for different internal domain discretization schemes.

Table 4.8. Deflection (m) and rotation (rad) of the tip of the cantilever of example 8.

Load $P_z = 100kN$	$w_{tip} (10^{-3})$	Error(%) w	$\theta_{y\ tip} (10^{-3})$	Error(%) θ_y
Exact Solution	5.1059	-	-3.3967	-
Converged Solution (21Nodal Points)	5.0890	0.33	-3.3799	0.49
RIE Reddy (1997)	3.9737	22.17	-3.3967	0.00

Thereinafter, the geometrically nonlinear inelastic response of the cantilever is investigated taking into account the shear deformation effect (axial-shear-flexural interaction), employing 22 linear longitudinal elements, 40 quadrilateral cells and a 2×2 Gauss integration scheme for each cell. The influence of the normalized axial loading $n_x = P_x / P_{ult}$ on the nonlinear response of the beam is also investigated. The present example was first studied by Triantafyllou and Koumoussis (2011) who presented a hysteric Timoshenko beam element based on the lumped plasticity assumption, accounting for the interaction between axial, shear and bending, implementing the yield criterion proposed by Simo et al. (1984).

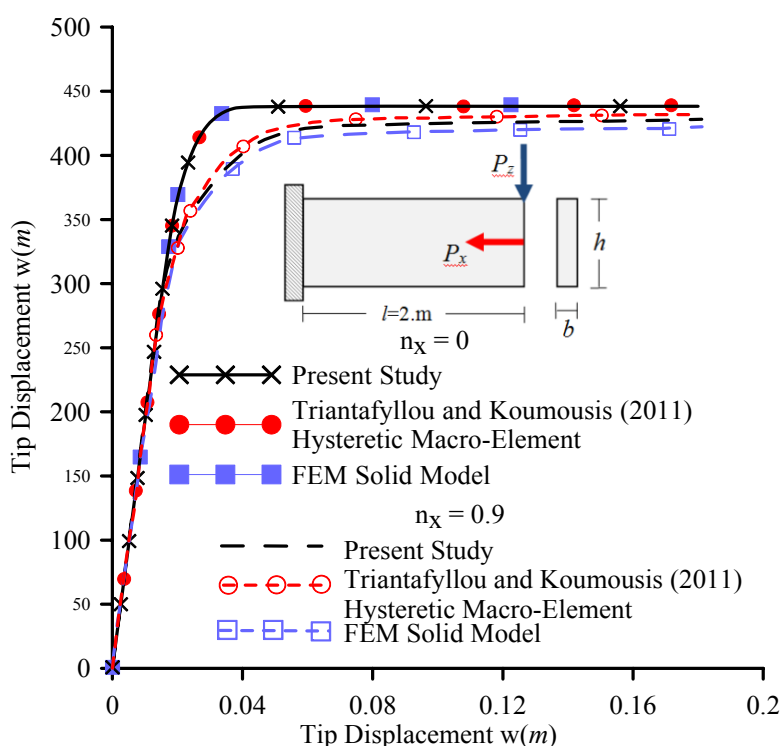


Fig. 4.26. Load–displacement curves at the tip of the cantilever beam of example 8.

In Fig. 4.26, the load–displacement curves at the cantilever’s tip are presented for two axial load cases; namely zero axial force and $n_x = 0.9$. The results obtained with the proposed formulation are compared with those from Triantafyllou and Koumoussis (2011) and from a 3-D FEM solution (NX Nastran 2007) by employing 640 solid (brick) elements. Excellent agreement between the results is observed in case of zero axial load while very good convergence is achieved for $n_x = 0.9$. Moreover, the ultimate load predicted from the proposed formulation for zero axial force

$(P_{z_{ult}}^{n_x=0} = 440.05kN)$ practically coincides with the value predicted from plasticity theory (Lubliner 2008) ($P_{z_{ult}} = 440kN$), while for $n_x = 0.9$ the calculated ultimate load ($P_{z_{ult}}^{n_x=0.9} = 422.7kN$) deviates from the FEM solution for less than 1.2%.

Finally, in Figs. 4.27a,b the von Mises stress distribution along the cantilever's length is presented for different load stages showing the spread of plasticity, while in Figs. 4.27c,d the normal and shear stress profile along the cross section at $x = 0.1m$ from the fixed end, are presented assuming either constant or a more accurate parabolic shear stress distribution as presented in (Saritas and Filippou 2009). From these figures, the flexural character of the plastification becomes apparent while it is evident that the influence of the shear stress profile is negligible, in this example.

4.4.9 Example 9 – Shear collapse of I-Beam on Inelastic Foundation

The influence of the geometrical nonlinearity and the shear deformation effect (axial-shear–flexure coupling) on the behaviour of the beam-foundation system is investigated in this example. For this purpose, an I-shaped cross section beam of length $l = 2m$, has been studied. The geometric properties of the selected cross section are presented in Table 4.8, while the beam's material is considered to be elastic-perfectly plastic with modulus of elasticity $E = 213.4GPa$, shear modulus $G = 82GPa$ and yielding stress $\sigma_{Y0} = 285MPa$. The beam is either clamped or fixed-pinned supported, leaning on a plastic Winkler foundation with initial stiffness of $k_z = 20MPa$ and yielding force $P_z^Y = 100KN/m$, while it is subjected to monotonically increasing uniformly distributed load. The beam is discretized with 22 linear longitudinal elements, 43 quadrilateral cells (12 layers in the web and 2 in each flange) and a 1×1 Gauss integration scheme for each cell.

Table 4.9. Geometric properties of the I-shaped cross section, of example 9.

Total height	$h = 0.3m$	Flange width	$t_f = 0.02m$
Total width	$b = 0.3m$	Web width	$t_w = 0.01m$
Moment of Inertia	$I_y = 25.0247 \times 10^{-5}m^4$	Shear Correction Factor	$a_z = 5.3897$

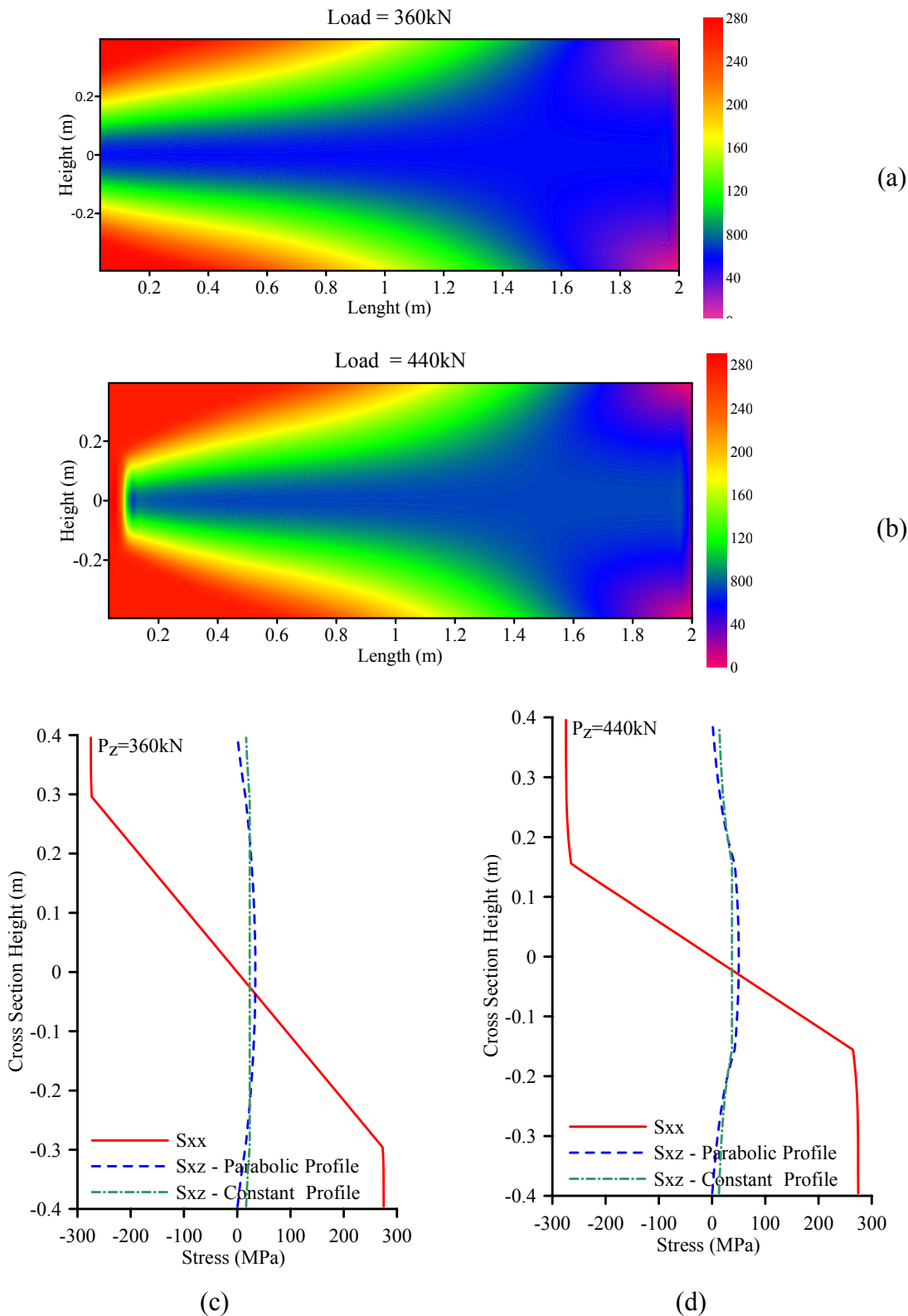


Fig. 4.27. Von Mises stress (MPa) distribution along length (a) and normal & shear stress (MPa) distribution along cross section (b) for different load stages.

In Figs. 4.28, 4.29 the load–displacement curves are presented, performing either geometric and material nonlinear (GMNL) analysis or material nonlinear (MNL) analysis ignoring the foundation reaction, for both the boundary condition cases. The results are compared with those obtained from a FEM model (NX Nastran 2007) implemented by employing 2400 quadrilateral shell elements. Excellent convergence between the results is observed. In the same figures the von Mises stress σ_{vM} distribution is also presented illustrating the plastification of the web, as well as the non-symmetry of the normal stresses due to the developed axial force. Additionally, the flexure-only response is presented in these figures. Since the beam yields in shear, the Euler-Bernoulli model fails to capture the nonlinear response and overestimates the collapse load of approximately 320% for the clamped and 256% for the fixed-pinned boundary conditions.

The main reason for that divergence is the inability of the flexure-only model to predict the exact collapse mechanism, as it ignores the development of the shear stresses. In more detail, Figs. 4.30a,b depicts the stress distribution along the length of the web for geometrically nonlinear and linear analysis, respectively indicating the shear character of the collapse mechanism. In the same figure the corresponding deformed shell FEM contour representations are also presented verifying the accuracy of the presented model. On the contrary, Fig. 4.30c show the von Mises stress distribution assuming a flexure-only model demonstrating the collapse mechanism due to bending, which require the formation of three plastic hinges instead of two in the axial-shear–flexure coupling model.

Moreover, under the scope of efficiency, it is worth noting that even though the two approaches have fundamental differences (i.e. 22 elements for the proposed model instead of 2400 elements for the shell one), the difference between the computational time required for the analyses is significant, while the obtained results have the same accuracy. Indicatively, it is mentioned that the refined shell model required approximately 30 min to 1.0 h depending on the analysis type and model parameters, while the proposed one required from 10 sec to 240 sec for the same type of analysis.

Finally, in Figs. 4.31, 4.32 the load–displacement curves of the beam–foundation system are presented, performing either geometrically nonlinear or linear inelastic analysis for both cases of boundary conditions, making evident the influence of the geometrical nonlinearity on the response of the system. Additionally, the flexure-only

response is presented in these figures, illustrating once again the importance of the shear deformation effect on the behaviour of the beam-foundation system.

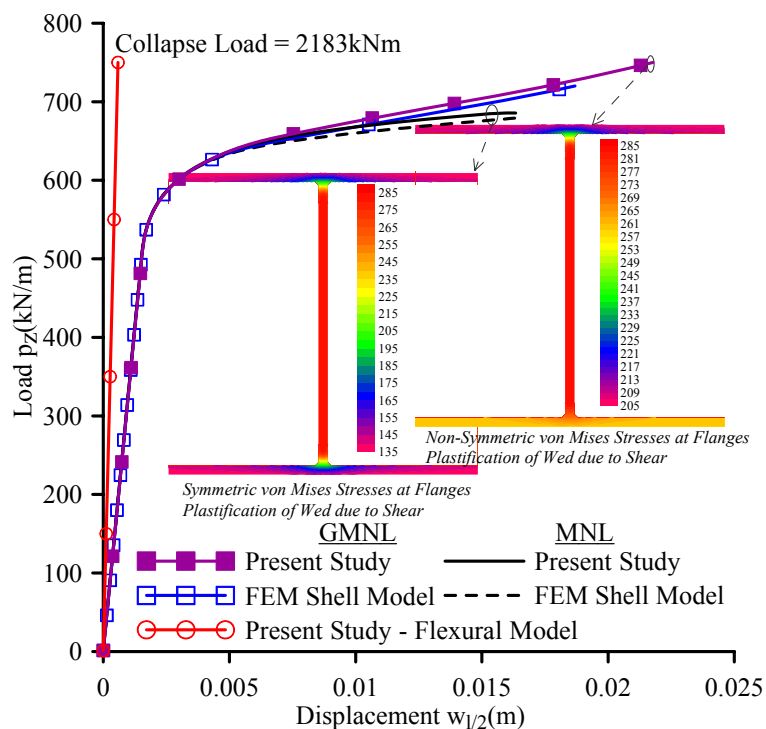


Fig. 4.28. Midpoint load–displacement curve of the clamped beam of example 9.

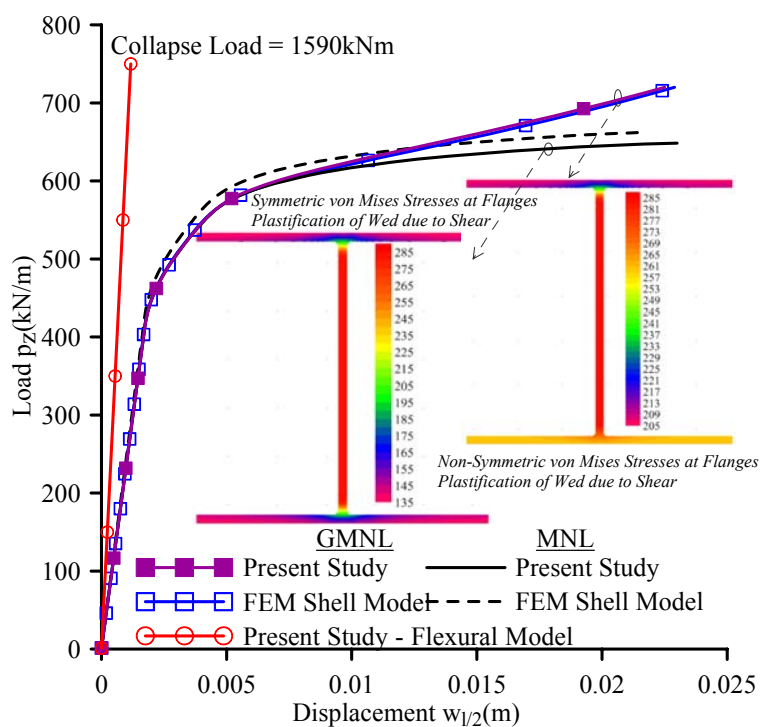


Fig. 4.29. Midpoint load–displacement curve of the fixed-pinned beam of example 9.

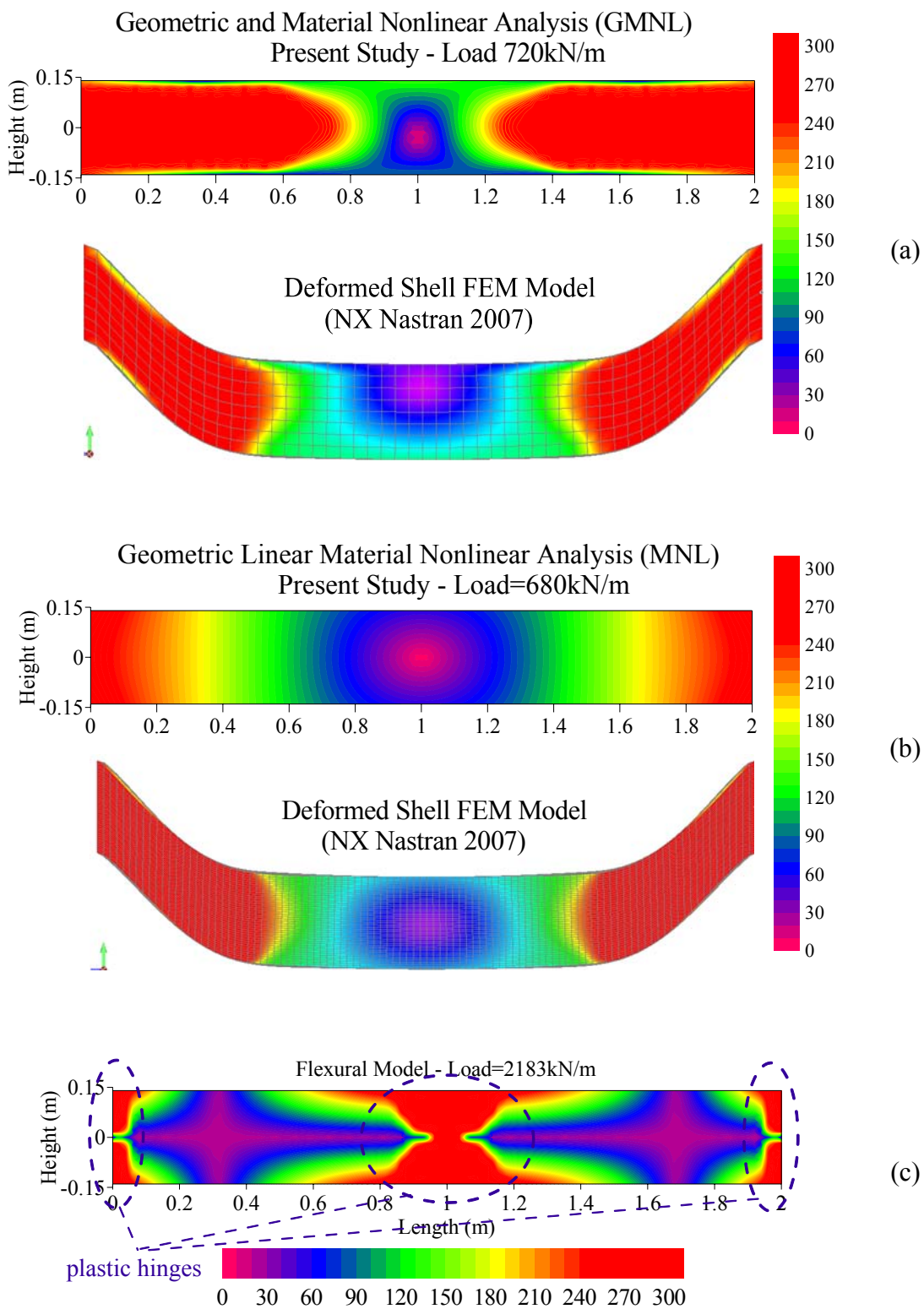


Fig. 4.30. Von Mises stress distribution contour diagrams along the length of the web for geometrically nonlinear (a) & linear (b) analysis as compared with the shell FEM model. Flexure-only model (c).

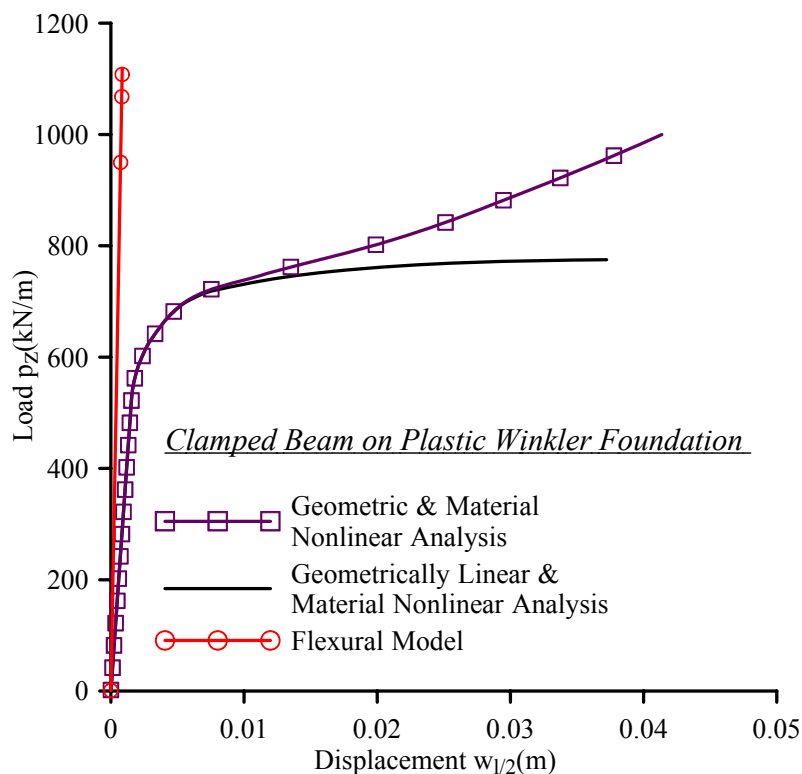


Fig. 4.31. Load–displacement curve at the midpoint of the clamped beam–foundation system of example 9.

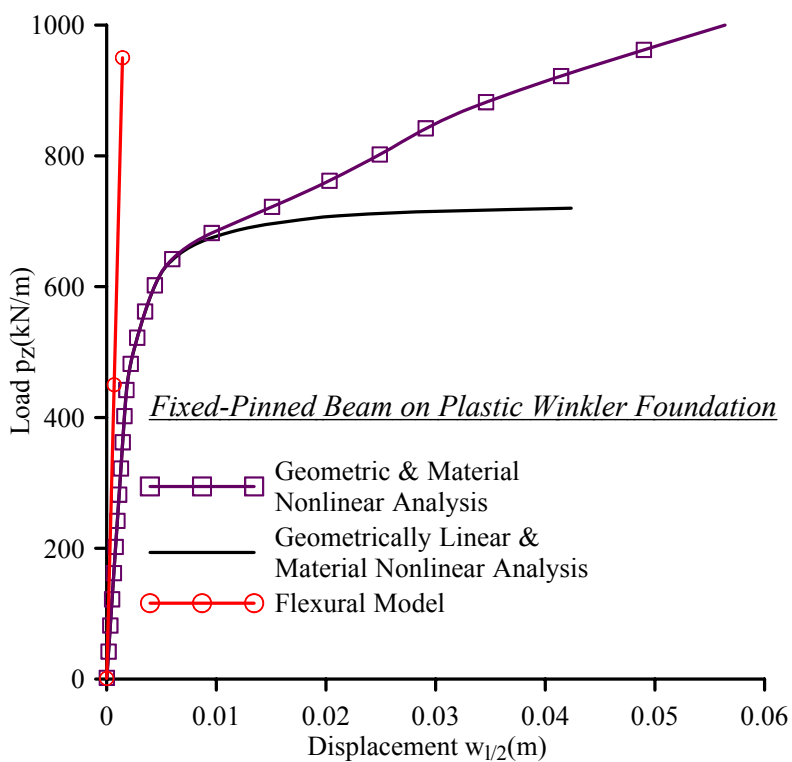


Fig. 4.32. Load–displacement curve at the midpoint of the fixed-pinned beam–foundation system of example 9.

4.4.10 Example 10 – Influence of Geometrical Nonlinearity in Inelastic Analysis

In order to demonstrate the influence of the geometrical nonlinearity even in case of no axial loading, in this example a rectangular cross section ($h = 0.40\text{m}$, $b = 0.20\text{m}$) clamped beam of length $l = 5.0\text{m}$, as shown in Fig. 4.33, has been studied. For the numerical implementation 15 linear longitudinal elements, 40 quadrilateral cells (10 fibres) and a 2×2 Gauss integration scheme have been employed. Two material cases have been analyzed; namely an elastic-perfectly plastic with modulus of elasticity $E = 20\text{GPa}$, shear modulus $G = 8.3\text{GPa}$ and yielding stress $\sigma_{Y0} = 100\text{MPa}$ and an elastoplastic-strain hardening with $E_t = 1\text{GPa}$. The beam is supported on a plastic Winkler foundation with initial stiffness of $k_z = 20\text{MPa}$ and yielding force $P_z^Y = 100\text{KN/m}$, while it is subjected to a monotonically increasing concentrated load at its midpoint.

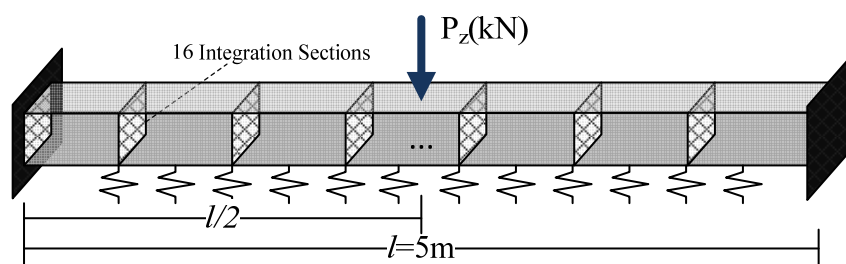


Fig. 4.33. Inelastic beam-foundation system subjected to monotonically increasing concentrated load.

The geometrically linear case with absence of foundation reaction has been studied by Papachristidis et al. (2010), who proposed a force-based (*FB*) 3D fiber beam element formulation accounting for the axial–shear–moment interaction. In Fig. 4.34 the load–displacement curve at the beam’s midpoint is presented as compared with those obtained from (Papachristidis et al. 2010) assuming both force and displacement based (*DB*) formulations for numerous integration sections and numerical integration schemes. The accuracy and efficiency of the proposed formulation are confirmed by the excellent agreement between the converged solution of Papachristidis et al. (2010) obtained by 2 *FB* elements with 8 integration sections and the one obtained from the conducted analysis assuming the same number of integration sections (i.e. 16). More specifically, from this figure it is concluded that the conventional displacement based elements of

equal length fail to capture accurately the collapse load. This shortcoming can be resolved by employing either more dense mesh or adaptively spaced elements. Contrary to the conventional *DB* elements, the *FB* are capable of describing the inelastic response of the beam with a single element per member. However the results may differ with respect to the number of integration sections and the numerical integration scheme (i.e. Gauss (G) and Gauss–Lobatto (G-L)).

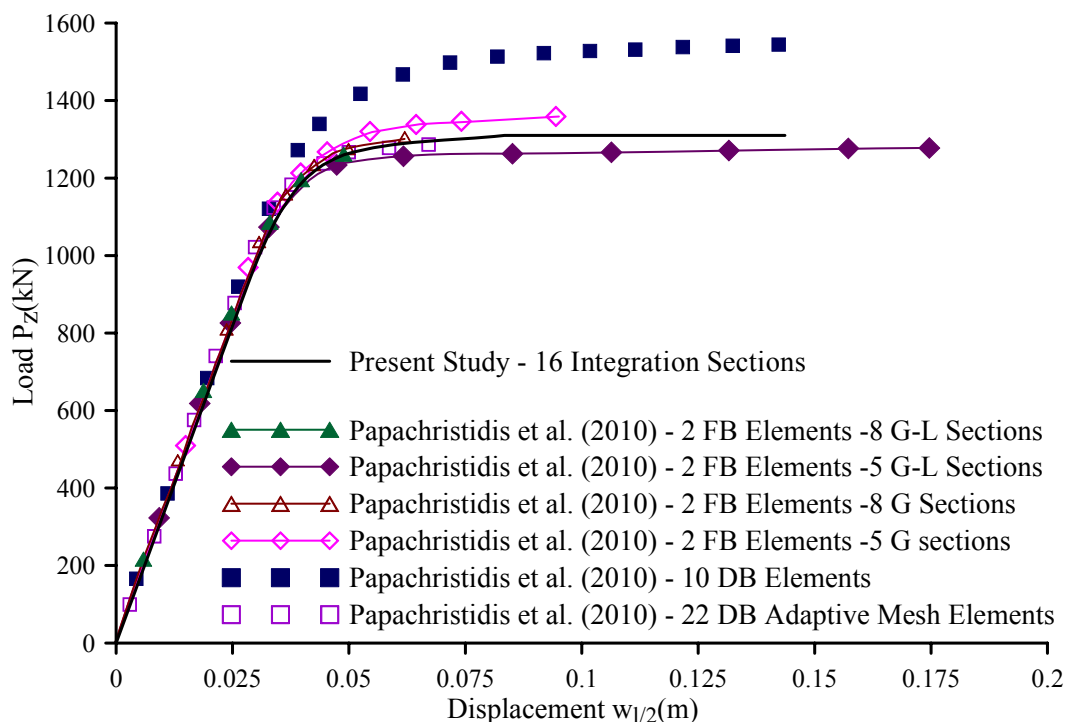


Fig. 4.34. Load–displacement curve at the midpoint of the beam of example 9, performing geometrically linear analysis.

In Fig. 4.35 the load–displacement curves are presented, performing either geometrically nonlinear or linear inelastic analysis for different types of material properties ignoring the foundation reaction. From this figure, it is concluded that large displacements, influence significantly the behaviour of the beam since the developed restoring force does not allow the evolvment of the plastic hinges and thus the plastic collapse. This can also be evident from the contrast observed between the von Mises stress distribution contour diagram as presented in Figs. 4.36a,b performing either geometrically nonlinear or linear inelastic analysis for perfectly plastic and strain hardening material, respectively.

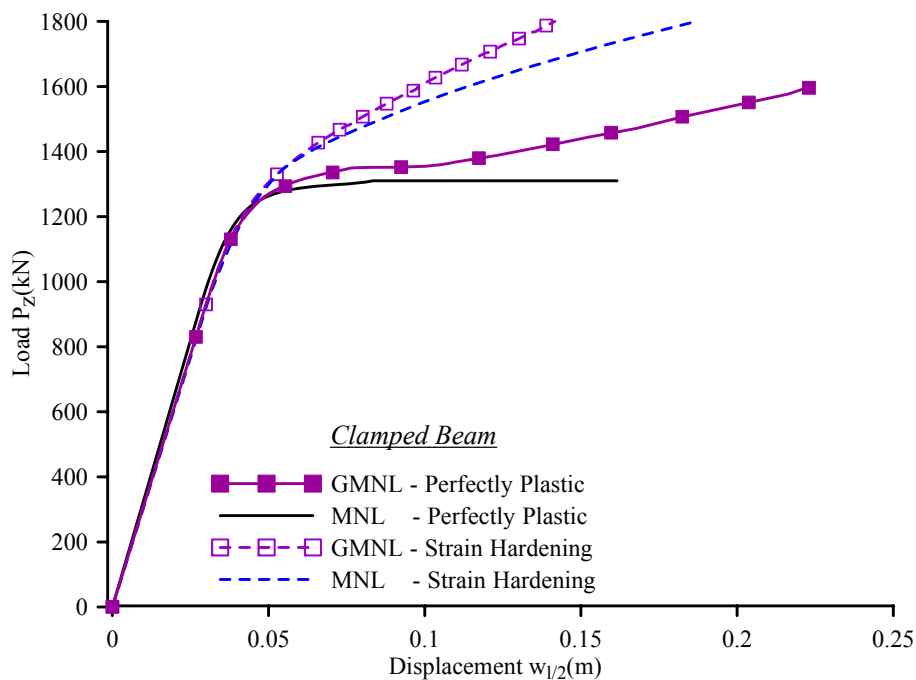


Fig. 4.35. Load–displacement curve at the midpoint of the beam of example 9.

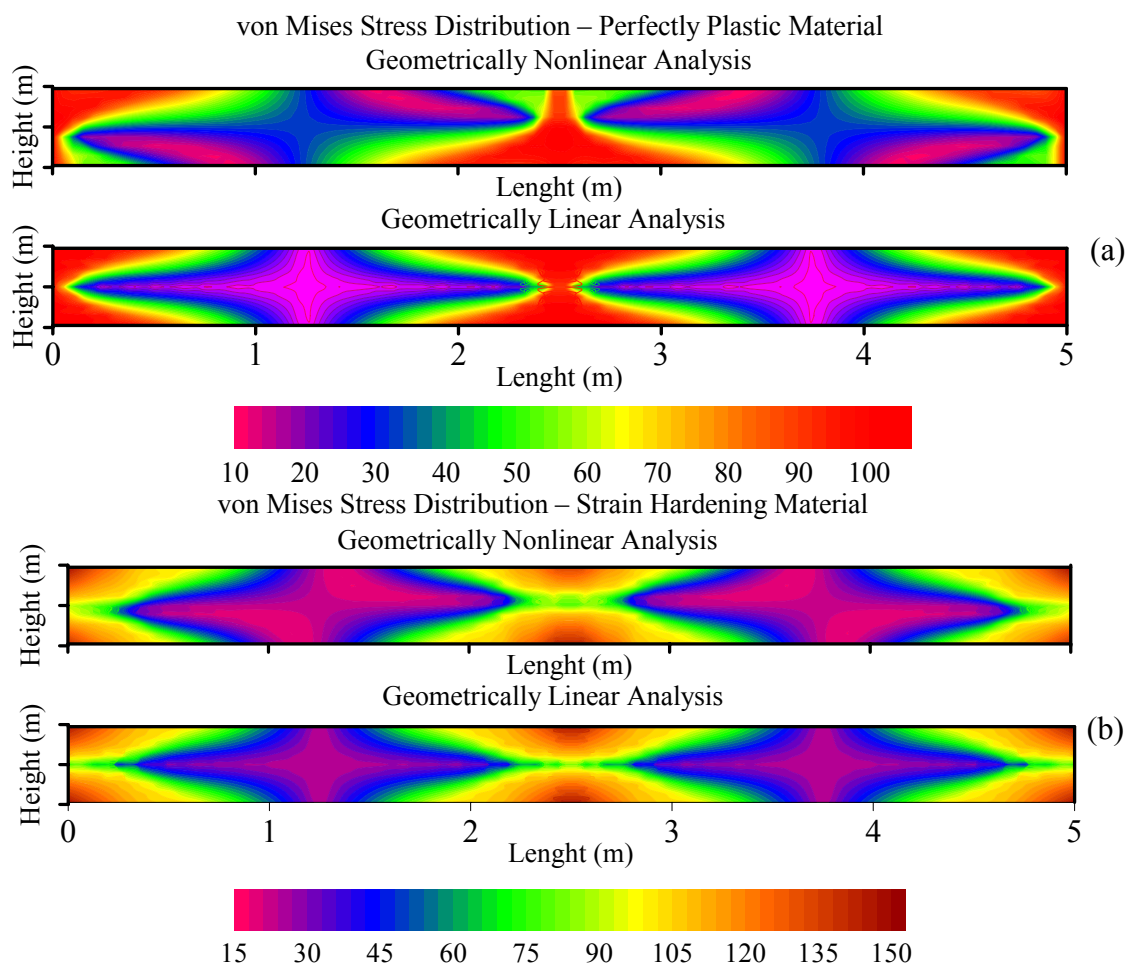


Fig. 4.36. Von Mises stress (MPa) distribution along the beam length, of example 10.

Finally, in Fig. 4.37 the load–displacement curves of the beam–foundation system are presented, performing either geometrically nonlinear or linear inelastic analysis for different types of material properties, while in Table 4.10 the extreme values of the von Mises stresses for the all the conducted analyses are shown illustrating once again the paramount importance of both geometrical and material nonlinearity in the beam–foundation system analysis.

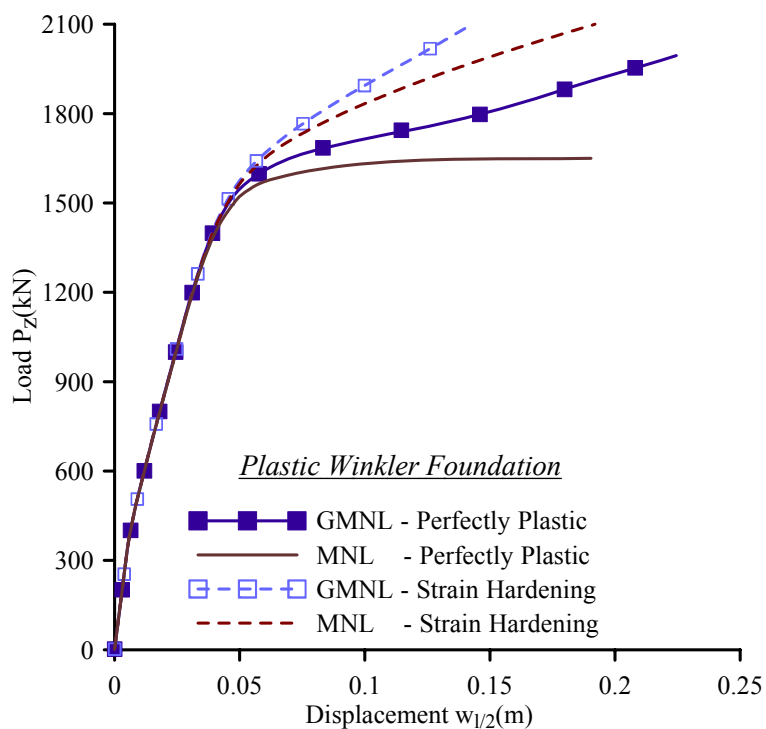


Fig. 4.37. Load–displacement curve at the midpoint of the beam of example 10, resting on nonlinear foundation.

4.4.11 Case Study – Pile–Foundation System: Numerical and Experimental Validation

The main purpose of this final example is to validate the developed beam model against a series of Laboratory Pushover tests on vertical single piles embedded in dry sand under different load paths to failure in M – Q space, conducted in the Laboratory of Soil Mechanics/Dynamics in NTUA by Gerolymos (2012) and Giannakos (2013). The obtained results are further compared to those from a fully 3D Nonlinear Finite Element simulation (Giannakos 2013) implemented in the finite element code ABAQUS (Dassault 2009).

Table 4.10. Extreme values of the von Mises stress of the beam-foundation system of example 10.

Clamped Beam				
Analysis	Perfectly Plastic		Strain Hardening	
	Linear	Nonlinear	Linear	Nonlinear
$Max S_{vM} (MPa)$	100	100	157.089	149.5203
$Min S_{vM} (MPa)$	9.236	12.104	12.179	17.81618
Beam-Foundation System				
Analysis	Perfectly Plastic		Strain Hardening	
	Linear	Nonlinear	Linear	Nonlinear
$Max S_{vM} (MPa)$	100	100	141.389	134.994
$Min S_{vM} (MPa)$	9.420	9.025	12.998	16.726

To this end, the proposed beam formulation is utilized for the simulation of a vertical pile placed in a sand mass of uniform density. The model pile is a hollow aluminium 6063–F25 cylinder of 3cm external diameter, 2.8cm internal diameter, and 60cm length. The elasticity modulus of the pile is $E_0 = 70GPa$ and the yield stress of the aluminium is 215MPa. The geometrical, material and model properties of the examined pile are summarized in Table 4.11. The stiffness coefficients of the soil independent springs are calculated according to Makris and Gazetas (1992). In order to simplify the complicated physics of the examined problem, an equivalent constant friction angle of $\varphi = 64^\circ$ was found for the sand through back analysis of Test 1, based on Brom's expression for cohesionless soils (Broms 1964b):

$$p_u = 3 K_p \gamma z d \quad (4.41)$$

where K_p is the passive earth pressure coefficient, γ the unit weight of soil, z the depth from ground surface and d the pile diameter. The pile is fixed at the base of the sandbox to ensure verticality during the sand raining process; however, its length is sufficiently large for the bending failure (plastic hinge) not to be affected by the tip boundary conditions. The load is applied to the pile at a distance e from ground surface, while the aboveground height of the pile is f . The experimental setup is portrayed in

Fig 4.38. For more details on the laboratory testing process the reader is referred to the studies of Gerolymos (2012) and Giannakos (2013).

Table 4.11. Pile properties for the proposed beam model.

Model Properties	Symbol	Values
Length	l	0.6 m
Area / Moment of Inertia	Ω / I_y	$9.11 \times 10^{-5}\text{ m}^2 / 9.6 \times 10^{-9}\text{ m}^4$
Young's modulus	E_0	$7.0 \times 10^4\text{ MPa}$
Shear modulus	G	$26.9 \times 10^3\text{ MPa}$
Yield Stress	σ_{Y0}	215 MPa
Number of elements	150 (120 embedded length – 30 free length)	
Cross-sectional Discretization	100 quadrilateral cells and 3×3 Gauss integration scheme for each cell	

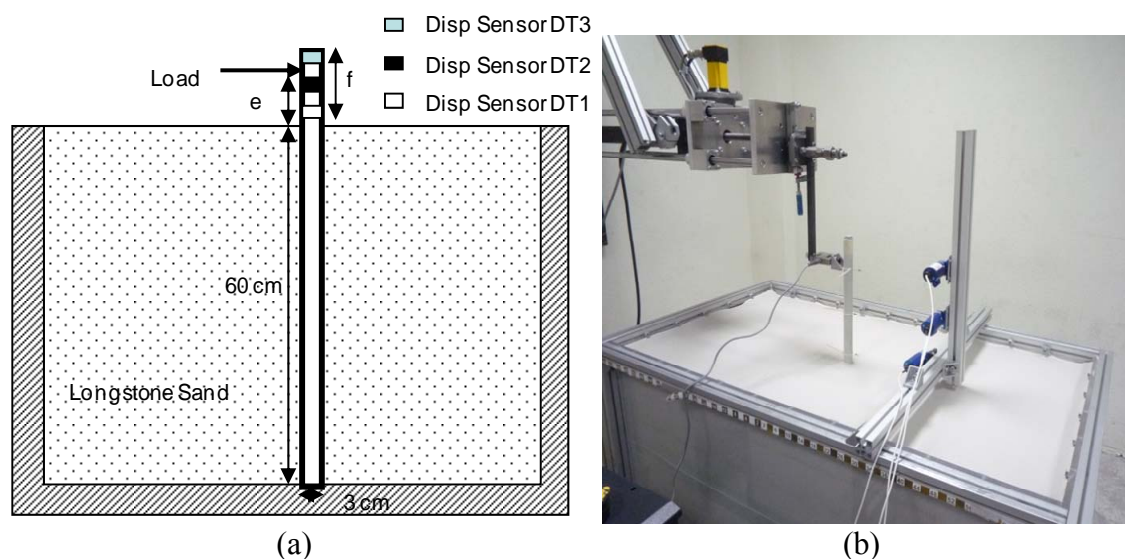


Fig. 4.38. Pushover model setup; geometry (a) and instrumentation (b).

The piles studied were subjected to displacement control lateral loading. Monotonic loading was imposed either at the pile head considered to be at the ground surface or at a specified distance from ground surface in order to produce a moment acting at the pile head. A total number of 8 experiments were examined; namely:

- Test 1. Lateral load at the ground surface level in order to determine the plastic yield shear force of the pile-soil system ($Q_Y = 97.15\text{kg}$; Point 1, 0 in $M/M_Y - Q/Q_Y$ space)
- Test 2. Pure moment conditions in order to validate the plastic yield moment of the pile-soil system ($M_Y = 18.19\text{kgm}$; Point 0, 1)
- Test 3. Lateral load applied at 32cm above the ground surface (Point 0.47, 0.80)
- Test 4. Lateral load applied at 20cm above the ground surface (Point 0.59, 0.63)
- Test 5. Retest of the pile under lateral load applied at 32cm above the ground surface in order to check the repeatability of the experiments (Point 0.46, 0.79)
- Test 6. Lateral load applied at 10cm above the ground surface (Point 0.75, 0.40)
- Test 7. Lateral load applied at 6cm above the ground surface (Point 0.88, 0.28)
- Test 8. Lateral load applied at 56cm above the ground surface (Point 0.28, 0.84)

For the first experiment, only lateral load was applied at the pile head in order to determine the ultimate lateral load capacity Q_Y of the pile-soil system. Similarly, for the second experiment only overturning moment was applied for the determination of the ultimate moment capacity M_Y . Subsequently, different combinations of moment and horizontal force at the ground surface were produced by changing the above ground height e of application of the horizontal load Q (hence $M = Qe$). Aiming to ensure the validity and repeatability of the testing procedure and gain confidence in the presented data, the lateral pushover test for the pile subjected to lateral load at 32cm above the ground surface (Test 3) was repeated (Test 5).

These pushover tests are also modelled numerically with a fully 3D Finite Element model taking into account material nonlinearities for static analysis using the finite element code ABAQUS (Dassault 2009), as presented in Giannakos (2013) and Kampitsis et al. (2014). The pile and soil are analyzed at model scale, assuming model parameters appropriate for very small confining pressures. The view of the three dimensional Finite Element mesh used for the simulation of the pile and the sandbox is depicted in Fig. 4.39. Approximately 45000 elements are used for each analysis. The soil is modelled with 8-node brick elements while the pile is modelled as elastic-perfectly plastic with 3D beam elements placed at its centre and connected with appropriate kinematic constraints, namely Multi-Point Constrains (MPC) boundaries,

with the nodes at the perimeter of the pile in order to model the complete geometry of the pile. Hence, the nodes of the 8-node brick elements at the perimeter of the pile at a specific elevation follow the displacement of the node of the 3D Beam element at that elevation (Giannakos et al. 2012). The solid elements inside the perimeter of the pile have no stiffness, thus each pile section behaves as a rigid disc. The sophisticated procedure of calibrating the 3D FE Model parameters (i.e. beam and soil constitutive models, hardening law, plastic flow rule, etc.) to capture the soil-pile system behaviour is presented in Giannakos (2013) and Kampitsis et al. (2014).

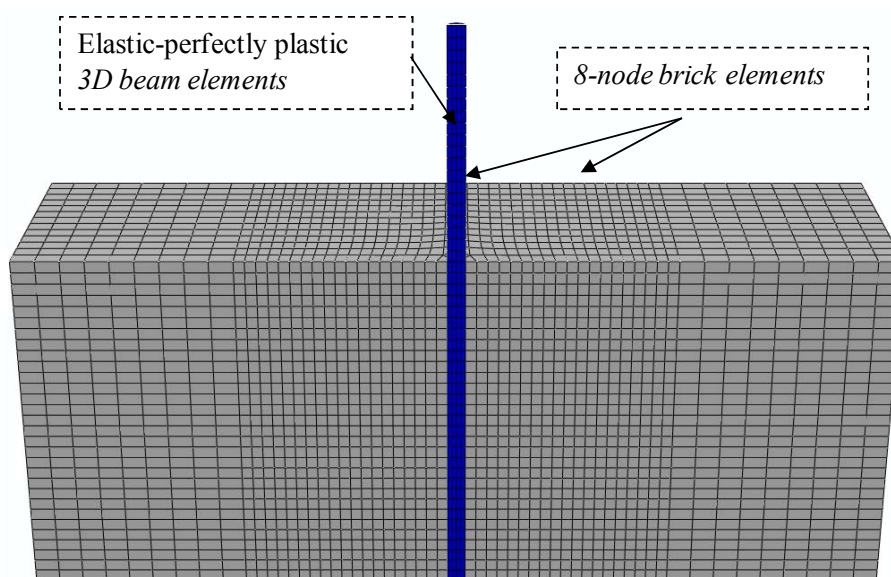


Fig. 4.39. Mesh discretization of the 3D Finite Element Model for Pushover Tests.

In Fig. 4.40, the force–displacement curves at the pile head derived from the proposed beam model for Test 1 is presented as compared with the experimental results and those from the calibrated 3D FE model. It is observed that both the stiffness and the maximum lateral capacity of the pile of the calibrated 3D model match the experimental values. On the contrary, the beam model matches well the maximum lateral capacity of the pile, but has a stiffer response than the experiment and the 3D numerical analysis. Moreover, in Table 4.12 the ultimate lateral Q_Y (Test 1) and moment M_Y (Test 2) capacities of the pile-soil system obtained from both numerical models are compared with those measured from the laboratory tests. The calculated results indicate that the numerical models are calibrated to capture accurately the response of the system in case of Tests 1 and 2.

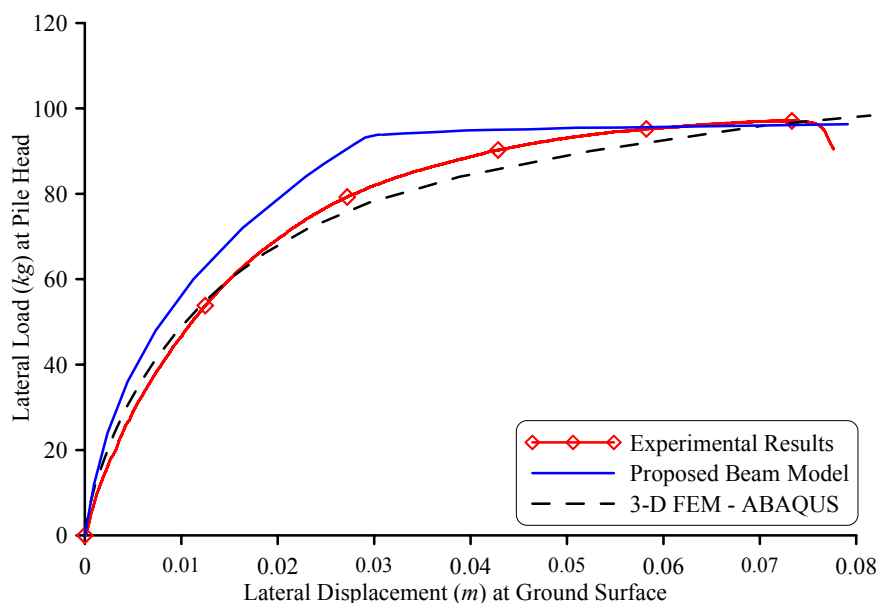


Fig. 4.40. Experimental and calibrated (Proposed Beam and 3D FE models) force–displacement curves at pile head for Test 1 (lateral loading acting at the ground surface).

Table 4.12. Ultimate load capacity of the pile-soil system.

Plastic Yield Components	Proposed Beam Model	Experimental Measurements	3D FE Model
Q_Y (kg)	96.80	97.15	102
M_Y (kgm)	18.22	18.19	18.16

Subsequently, the validation of the proposed beam formulation is performed through the examinations of the response of each individual test (Tests 3 to 8). In Figs 4.41 to 4.45 the calculated lateral force acting at various heights on the pile with the corresponding displacement at the ground surface obtained from the proposed beam model are presented and compared with the measured values from the experiment and the calculated results from the 3D FE analysis. Both the stiffness and the maximum force values from the two numerical models compare well with the measured results from the experiments. More specifically, it is observed that the beam model exhibits a stiffer behaviour compared to the 3D FE model, as expected since it does not capture the strain softening behaviour of the soil, but it captures accurately the ultimate capacity of the system. In general, from the conducted investigation, it is deduced that the proposed beam model can be employed providing minimum calculation effort while

retaining good precision in the obtained results for the soil–pile inelastic systems instead of executing complicated 3D analyses.

Similar trend is observed in Fig. 4.41, where the lateral force–horizontal displacement curves at the pile head from Tests 3 and 5 are compared with the calculated response from both numerical methods. The measured experimental results show quite satisfactory agreement between the original and repeated test, indicating that the experimental conditions are repeated with good accuracy in every experiment.

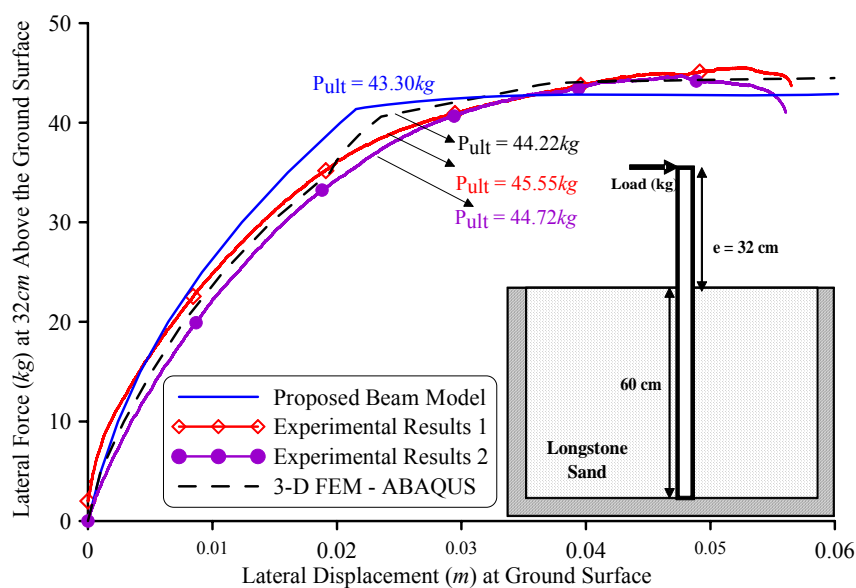


Fig. 4.41. Experimental and computed force–displacement curves at pile head for Tests 3 & 5 (lateral force at 32cm above the ground level).

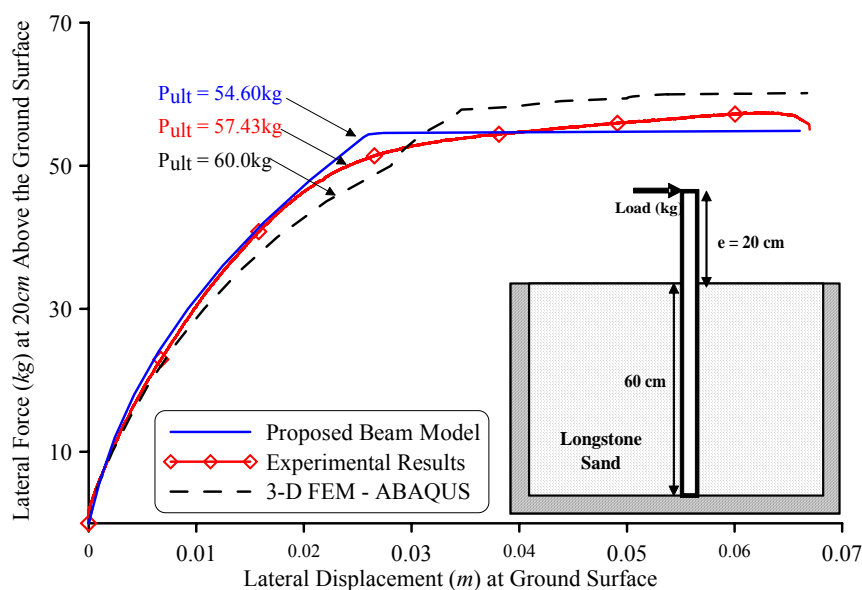


Fig. 4.42. Experimental and computed force–displacement curves at pile head for Test 4 (lateral force at 20cm above the ground level).

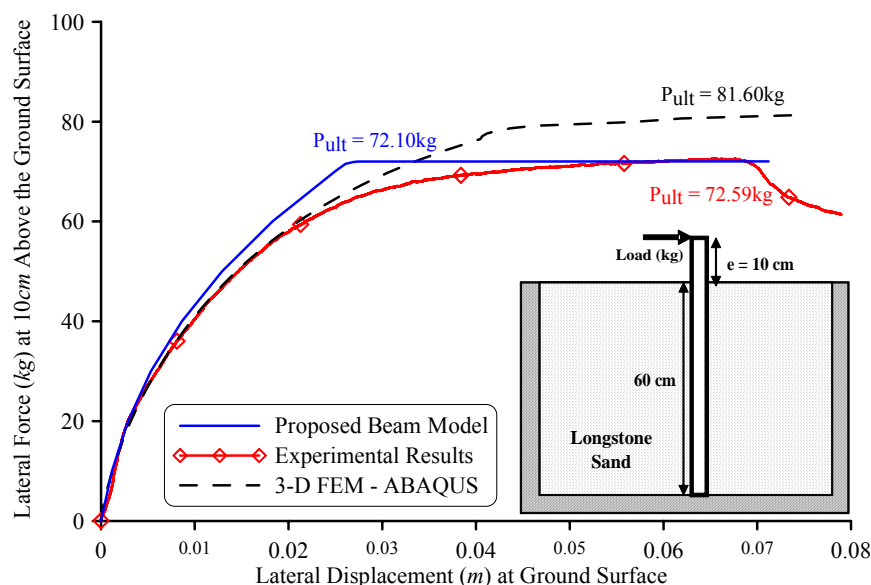


Fig. 4.43. Experimental and computed force–displacement curves at pile head for Test 6 (lateral force at 10cm above the ground level).

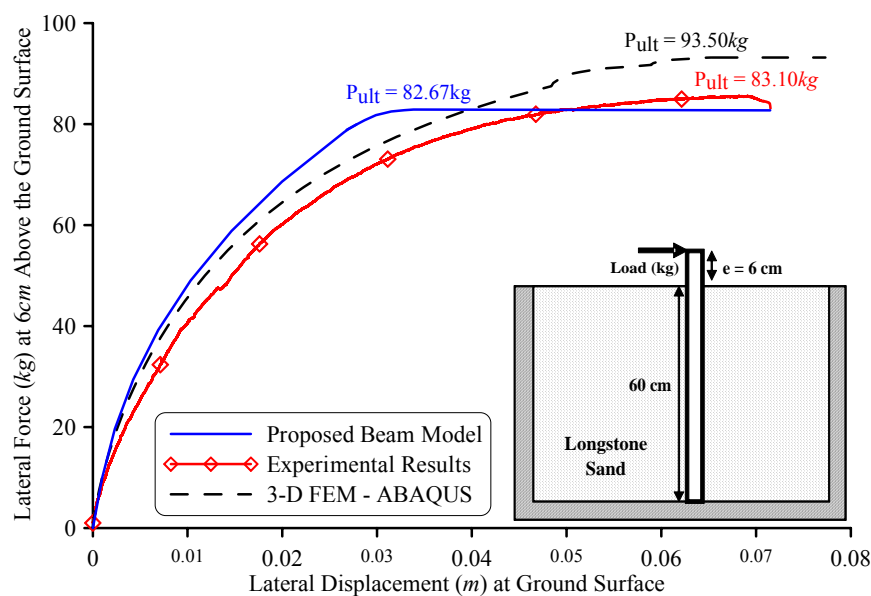


Fig. 4.44. Experimental and computed force–displacement curves at pile head for Test 7 (lateral force at 6cm above the ground level).

Furthermore, Fig. 4.46 depicts a) the failure envelope of the analytical expression of eqns.(4.42), presented by Gerolymos (2012) and Giannakos (2013) for pile embedded in cohesionless soil for the case when the lateral force and the bending moment at the pile head act towards the same direction as compared with the points of overturning moment and lateral force ($M - Q$) at failure, normalized with the values of pure

moment M_Y and pure lateral loading Q_Y capacities respectively as derived from b) the laboratory experiments, c) the proposed beam model and d) the 3D FE model.

$$f = \left| \operatorname{sgn}(Q) \left| \frac{Q}{Q_Y} \right|^{3/2} + \left| \frac{M}{M_Y} \right| \operatorname{sgn}(M) \right| - I = 0 \quad \text{for} \quad \left| \frac{M}{M_Y} \right| < I \quad (4.42a)$$

and

$$f = \left| \frac{M}{M_Y} \right| - I = 0 \quad \text{for} \quad \left| \frac{M}{M_Y} \right| = I \quad (4.42b)$$

It is observed that both the measured points from the experiments and the calculated points from the two numerical analyses almost coincide with the proposed failure envelope. The green triangular symbol on the figure corresponds to the repeated Test 5, performed in order to check the repeatability of the experiments for pile under lateral load applied at 32cm above the ground surface (Test 3).

In Table 4.13, the measured depths of the formation of the plastic hinge from the experiments are presented in comparison to the calculated ones from the proposed and the solid models. It is observed that both numerical methods predict well the decrease of the depth of the plastic hinge with the increase of the bending moment acting at the pile head. Hence, the maximum depth of plastic hinge is measured at 24cm (Test1) from the ground surface while the minimum one is located at the pile head (0cm) when only bending moment acts at the pile head. Since this is a mesh-dependent problem, and the mesh in the simplified beam model is denser (0.5cm in the vertical direction) than the 3D FE model (2cm), the simplified beam model presents a slightly better accuracy for the depth of the plastic hinge

Additionally, in Fig. 4.47 the cross-sectional distributions of *von Mises* stresses σ_{VM} accounting for (a-c) or ignoring (d-f) shear deformation effect, at the depth of the plastic hinge are presented for three load levels as calculated from the proposed beam model with respect to Test 4. The first load level (a, d) corresponds to an elastic behaviour, while the remaining ones refer to inelastic response. By comparing the results, it is concluded that accounting the shear deformation effect leads to slight increase of the developed stresses and consequently to more rapid spread of plasticity leading to the formation of the plastic hinge (collapse) for lower values of the applied load.

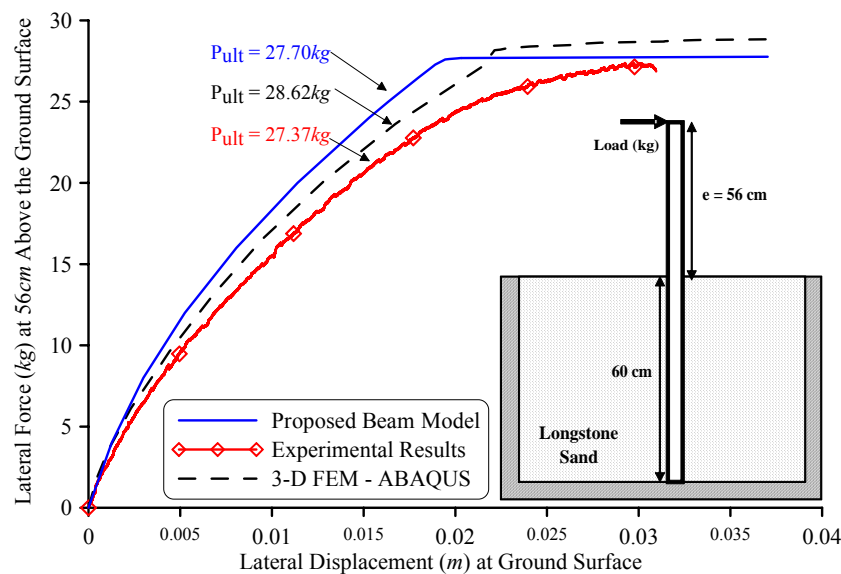


Fig. 4.45. Experimental and computed force–displacement curves at pile head for Test 8 (lateral force at 56cm above the ground level).

Table 4.13. Depth (cm) of plastic hinge from the ground surface

Experiment	Measured Depth Experiment	Calculated Depth Proposed Beam Model	Calculated Depth 3D FE Model
Test 1	24	22.5	22
Tests 3& 5	15	12	10
Test 4	18	14	14
Test 6	21	19	18
Test 7	22	20.5	20
Test 8	11	8.5	8

4.5 Concluding Remarks

In this chapter a Boundary Element Method is developed for the geometrically nonlinear inelastic analysis of Timoshenko beams resting on inelastic tensionless two-parameter foundation. To account for shear deformations, the concept of shear deformation coefficients is used. A displacement based formulation is developed and inelastic redistribution is modelled through a distributed plasticity (fibre) approach. Two alternative incremental–iterative solution strategies are developed. The main conclusions that can be drawn from this investigation are

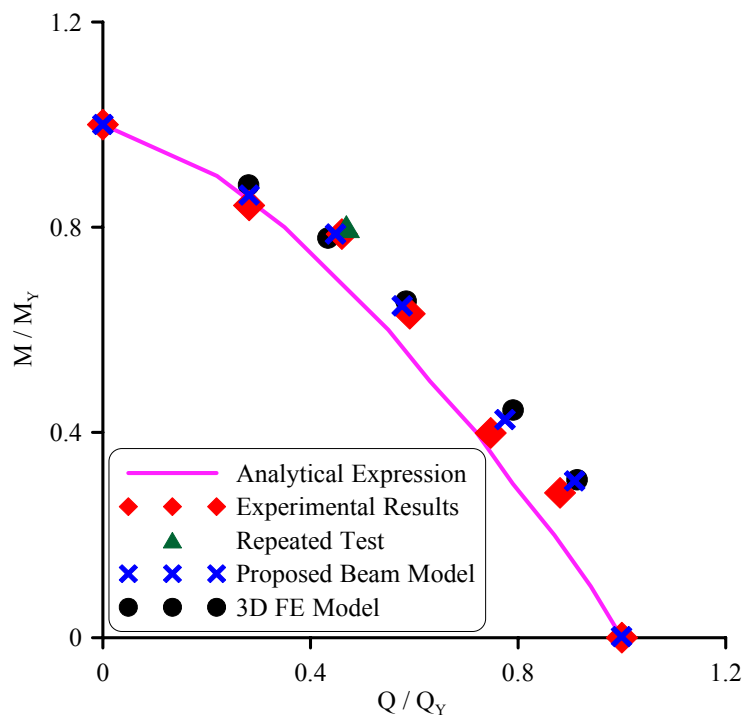


Fig. 4.46. Comparison of the failure envelope from the analytical expression Gerolymos (2012) and Giannakos (2013) for piles embedded in cohesionless soil with the results from a) the LSMD experiments, b) the proposed beam model and c) the 3D FE analysis.

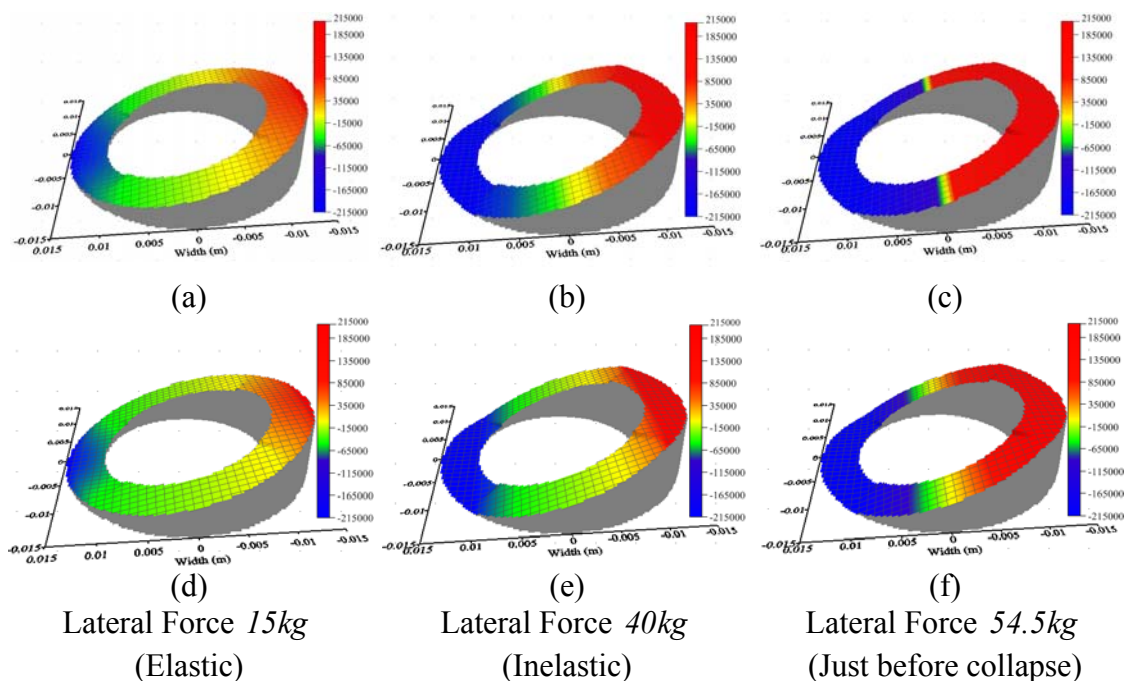


Fig. 4.47. Cross-sectional distribution of von Mises stresses (kPa) at the hinge point of Test 4, accounting for (a-c) or ignoring (d-f) shear deformation effect.

- i. The proposed beam formulation is capable of yielding results of high accuracy, as verified by comparing with analytical, experimental and FEM results, with minimum computational cost, providing a simple and efficient computational tool for the geometrically nonlinear inelastic analysis of beam-foundation systems.
- ii. The proposed model accurately captures both, the initial yielding and the ultimate (collapse) load, as well as the stress distribution and the region of the plastic hinge.
- iii. The influence of geometrical nonlinearity is illustrated through the significant discrepancy between the results of the linear and the nonlinear analyses.
- iv. The proposed model takes into account coupling effects of bending, shear and axial deformations, illustrating the paramount importance of this interaction in the inelastic analysis either under small or large displacement formulation.
- v. The significant influence of the inelastic character of the foundation is also demonstrated.
- vi. A small number of cells (fibres) is required in order to achieve satisfactory convergence.
- vii. The beam character of the developed formulation confers advantages over more refined approaches in the sense of modelling effort, model handling, results interpretation and isolation of structural phenomena.
- viii. The developed procedure retains most of the advantages of a BEM solution while requiring a small number of nodal points to achieve high accuracy.
- ix. The use of BEM enables the accurate calculation of the stress resultants which are very important during both the analysis and the design of beam-foundation systems.

Geometrically Nonlinear Dynamic Inelastic Analysis of Beam-Soil Interaction Systems

5.1. Introduction

The dynamic analysis of beam-soil interaction systems is an area of extensive research activity in both structural and geotechnical engineering. The dynamic analysis of such systems is often mandatory in design of significant civil engineering structures as for instance bridges, offshore piles and wind-turbine foundations.

Currently, the design procedure is based on a set of simplifying assumptions while the nonlinear static pushover analysis is preferred over the dynamic time domain procedures. This is attributed to the intricate dynamic methodologies as well as to the increased computational cost. Nevertheless, modern design codes are based on concepts such as the displacement based design and the performance based design for the estimation of structural integrity (Priestley et al. 2007, Fardis 2010). That implies that in order to evaluate the necessary design quantities, a vast amount of nonlinear dynamic analyses are required. Thus, an efficient computational tool capable of performing nonlinear dynamic analysis is essential, conferring several advantages over the pushover procedure (Bozorgnia & Bertero 2004) and providing insight into complicated phenomena attributed to the inertia and the dynamic motion of the structure.

In order to fully comprehend the beam-soil mechanism as well as to accurately estimate the response of the structure, all possible causes of nonlinearities should be taken into account. The nonlinearities with the most profound influence on the response of a structure originate from the inherent nonlinear stress-strain behaviour of the materials (material nonlinearity) as well as from the significant variations of the geometrical configuration during dynamic loading (geometrical nonlinearity). On the contrary, in engineering practice the foundation elements are designed to behave elastically for every type of loading. Modern design codes and the existing regulations indicate that the beam-soil interaction systems, such as piles and deep embedded foundations, are designed in order to prohibit the occurrence of any kind of nonlinearity,

neither of material nor of geometrical nature. More specifically, Eurocode-8 (EN 1998, EC-8, Part 2, § 5.8) explicitly states that “...*foundations shall not be intentionally used as sources of hysteretic energy dissipation and therefore shall, as far as practicable, be designed to remain undamaged under the design seismic action.*” This restriction, however, is most likely to be extremely conservative leading to financially or even physically unfeasible structures. In recent years, significant research efforts (Paolucci 1997, Gazetas et al. 2003, Gajan et al. 2005, Gerolymos et al. 2008, Harden & Hutchinson 2009, Gerolymos et al. 2009, Anastasopoulos et al. 2010, Gelagoti et al. 2012, Chiou et al. 2012, Figini et al. 2012) have investigated the beneficial character of permitting nonlinearities and inelasticity to occur at the beam-soil interaction system.

Furthermore, in order to conduct precise analysis and design cost-effective structures the realistic estimation of the structural member transient response is essential. Towards this direction, the material nonlinearity is incorporated in the analysis either by a refined distributed plasticity (fibre) formulation or by the simplified concentrated plasticity (plastic-hinge) approach. Although time efficient, the cross-sectional stress resultant approaches (Attalla et al. 1994) or lumped plasticity idealizations (Orbison et al. 1982, Ngo-Huu et al. 2007) come at the cost of accuracy. On the contrary, the fibre models are proved capable of accurately capturing the inelastic response (Teh & Clarke 1999, Nukala & White 2004, Saritas & Filippou 2009), while their main drawback is the increased computational cost due to the numerical integrations at the cross-sectional level. Various beam element models accounting for the nonlinear stress-strain behaviour of the materials, have been proposed following either the displacement-based (Bathe 2007) or force-based formulations (Sivaselvan & Reinhorn 2003, Saritas & Filippou 2004, Papachristidis et al. 2010). Moreover, dissipation phenomena have to be explicitly taken into account in the dynamic analysis of nonlinear systems. To this end, several hysteretic modes have been proposed (Dahl 1978, Visintin 2003, Papoulia et al. 2007) with the most commonly used the Bouc-Wen family of hysteric models (Bouc 1967, Wen 1976, Sivaselvan & Reinhorn 2003, Charalampakis & Koumoussis 2008, 2009). The hysteric Bouc-Wen model has been successfully introduced into the inelastic analysis of structural members (Symeonov et al. 2000, Guggenberger & Grundmann 2005, Triantafyllou & Koumoussis 2011, 2012a-c). Lately, Gkimoussis and Koumoussis (2013) presented distributed plasticity fibre beam formulations for both displacement and force based approach, while Kottari et al. (2014) presented a consistent smooth Bouc–Wen type degrading hysteretic model, incorporating stiffness degradation, strength deterioration, pinching,

asymmetric hysteresis and strain hardening characteristics. On the contrary, little has been done in case of soil-structure interaction systems (Gerolymos & Gazetas 2006, 2007).

So far, considerable effort has been made into investigating the dynamic response of beam-soil interaction systems employing the *Beam-on-Nonlinear-Winkler-Foundation* (BNWF) method. Within this framework, several researches have proposed various formulations assuming nonlinear laws ($p-y$) for the foundation load-displacement relation while the beam remains elastic throughout the analysis. Trochanis et al. (1991a) were the first to utilize a phenomenological hysteresis model for the simulation of the load-displacement relation of the nonlinear soil springs. More specifically, their study aim in developing a simplified model that incorporates the main nonlinear features of the behaviour of single piles as well as the interaction between a pair of piles. Taking advantage of the acquired knowledge gained from the three-dimensional parametric study (Trochanis et al. 1991b), a model consisting of coupled inelastically supported piles was developed taking into account the slippage and the separation between the piles and the soil, as well as the overall inelastic soil behaviour including degradation. In this work the degrading hysteretic model developed by Wen (1976) for the analysis of single and multi-degree oscillators was employed in order to describe the soil springs' constitutive law. The proposed model was verified by an extensive comparison with numerical results from the refined three-dimensional study, as well as with results from experimental field tests. Nogami et al (1992) presented a rational dynamic soil-pile interaction model adopting Winkler's hypothesis with a special attention to the conditions in which the strong nonlinearity is induced in the vicinity of the pile shaft under dynamic loading. The soil medium was approximated by a simple configuration of frequency independent mass, springs, and dashpots that consists a near-field and a far-field element. The far-field element, describes the elastic behaviour of the soil outside the plastification region while the near-field element reproduces the strongly nonlinear soil behaviour in the vicinity of the pile shaft. Therefore, the model enables the time-domain nonlinear analysis in a relatively simple manner. The nonlinear condition and the dynamic condition were coupled forming a complex soil action to the pile shaft motion while special consideration of the gap formation at the soil-pile interface was taken. Badoni and Makris (1996) developed a macroscopic model that consists of distributed hysteretic springs and frequency dependent dashpots. A one-dimensional finite element formulation was proposed for the evaluation of the nonlinear response of single piles under dynamic lateral loads. The

Bouc-Wen model (Bouc 1971, Wen 1976) was combined with a distributed viscous dashpot placed in parallel, in order to simulate the nonlinear behaviour of the springs. The model is physically motivated, adequate for cohesive and cohesionless soils and involves standard geotechnical parameters. Only two parameters have to be calibrated by fitting experimental data, while hysteretic damping was taken into account using the Bouc-Wen model and the radiation damping through a realistic frequency dependent expression. The model was calibrated and validated against five well instrumented full-scale experiments. Boulanger et al. (1999) developed a dynamic beam on nonlinear Winkler foundation analysis method for analyzing seismic soil–pile–structure interaction and evaluated it against the results of a series of dynamic centrifuge model tests. Sensitivity of the results to dynamic p - y model parameters and site response calculations were also examined. Nikolaou et al. (2001) implemented a beam on dynamic Winkler foundation model for piles in homogeneous and layered soils illustrating that the magnitude of kinematic moments depends mainly on the stiffness contrast between the soil layers, the pile-soil stiffness contrast, the excitation frequency, and the number of excitation cycles.

Although the soil inelasticity has been extensively investigated (Brown & Shie 1991, Laman et al. 1999, Kim & Jeong 2011) only few studies have encountered the inelastic behaviour of both the beam and the foundation elements in dynamic analysis. According to this context, the beam stress-strain and the foundation load-displacement relations are assumed to follow nonlinear inelastic constitutive laws. To start with, Budek et al (2000) presented a Winkler beam model formulation to represent the lateral force response of a reinforced concrete pile in cohesionless soil. An inelastic finite-element analysis was performed on the structure, using as the pile constitutive model the section moment-curvature relationship based on confined stress-strain relationships for the concrete. The influence of various parameters, such as the pile head boundary conditions, the height of pile head above grade level and the soil stiffness were investigated. The soil models were assumed linear, bilinear and hyperbolic. The analysis revealed that shear could be significantly underestimated by an elastic analysis, as inelastic behaviour moved the point of maximum moment in the pile shaft closer to the surface, thus reducing the shear span. Moreover, it was proved that the plastic hinge lengths as well as the maximum moment depth in the pile shaft are strongly influenced by the soil stiffness. Hutchinson et al. (2004) used nonlinear static and dynamic analyses to evaluate the inelastic seismic response of bridge and viaduct structures supported on extended pile shafts. For the nonlinear dynamic soil–pile interaction

analyses the beam on nonlinear Winkler foundation model was employed. Nonlinear fibre beam-column elements were used to model the reinforced concrete sections, and one-dimensional site response analyses for the free-field soil profile response. Several parameters have been taken into consideration such as the ground motion characteristics, the site response, the geometric second order effects and performance measures. The results focused on the influence of the ground motion characteristics and the variations in structural configurations on the performance measures which evaluated the inelastic seismic response of the structures examined. Later on, Gerolymos and Gazetas (2005) studied the inelastic response of soil-pile interaction systems employing a phenomenological model. The nonlinear response of the soil was treated as a Winkler spring-dashpot model utilizing the BWGG model. The separation of the pile from the soil, the radiation damping and the loss of strength due to pore-water pressure were also taken under consideration. The pile inelasticity was treated macroscopically at a cross-sectional level through a plastic-hinge approach utilizing the BWGG mode. An explicit finite differences method was used to solve the system of differential equations while this formulation was applied to piles subjected to laterally monotonic and cyclic loading. The developed model was then applied to conduct a parametric study of pile-column supported bridge structures, in order to investigate the consequences of pile yielding behaviour and soil-structure interaction on structure ductility demand (Gerolymos et al. 2009). Allotey and El Naggar (2008) developed a generalized dynamic normal force–displacement BNWF model capable of accounting for various soil–structure interaction effects. The backbone curve of the model comprises a four-segment adaptable multi-linear curve that can represent both monotonic and post-peak behaviour. The cyclic degradation was modelled as a modified version of the rainflow-counting technique of Anthes (1997). The proposed model was verified by comparing the results with those from centrifuge tests of piles in weakening and partially weakening soil showing good agreement. Lately, Mullapudi and Ayoub (2010b) studied the cyclic performance of an inelastic beam resting on a nonlinear soil bed. The material nonlinearity was handled through a fibre beam element model and the discretization of the cross-section was introduced in order to derive the nonlinear terms of the governing equation regarding the uniaxial stress-strain relations. The soil was handled as a semi-infinite element consisting of a single layer Winkler springs in conjunction with a Vlasov's parameter that can provide moment resistance. The tensionless character of the soil was also taken into account, while the foundation parameters were based on a plane strain assumption. This investigation was then extended to the study of the seismic

behaviour of the inelastic beam resting on a nonlinear foundation (Mullapudi & Ayoub 2010c). In both studies the models were implemented in the finite element program FEAP (Taylor 2005).

In this chapter, a Boundary Element Method (BEM) is developed for the geometrically nonlinear inelastic analysis of Euler-Bernoulli beams of arbitrary doubly symmetric simply or multiply connected constant cross-section, resting on inelastic Winkler foundation. The beam is subjected to the combined action of arbitrarily distributed or concentrated transverse dynamic loading and bending moments in both directions as well as to axial loading, while its edges are subjected to the most general boundary conditions. A hysteretic Bouc-Wen force-displacement model is employed in order to describe the inelastic behaviour of the Winkler springs. A displacement based formulation is developed and inelastic redistribution is modelled through a distributed plasticity (fibre) approach. A uniaxial hysteretic law is considered for the evolution of the plastic part of the normal stress following the Sivaselvan and Reinhorn (2003) phenomenological hysteresis model. Numerical integration over the cross sections is performed in order to resolve the hysteric parts of the stress resultants. Three boundary value problems are formulated with respect to the transverse and axial displacements and solved using the Analog Equation Method (Katsikadelis 2002), a BE based method. Application of the boundary element technique yields a system of nonlinear Differential-Algebraic Equations (DAE), which are written in state-space form and together with the hysteretic evolution equations are solved iteratively using the Petzold-Gear backward differentiation formula (Brenan et al. 1989), a linear multistep method for differential equations coupled to algebraic equations.

Numerical examples are worked out confirming the accuracy and the computational efficiency of the proposed beam formulation through comparison with literature and FEM results. In these examples, the significant influence of material and geometrical nonlinearity in the response of a beam-foundations system are illustrated. The essential features and novel aspects of the present formulation compared with previous ones are summarized as follows.

- i. To the author's knowledge, the geometrically nonlinear dynamic response of beam-foundation systems where both the beam and the foundation are assumed to be inelastic is investigated for the first time in literature through the beam-on-nonlinear Winkler-foundation approach.

- ii. The proposed beam model accounts for the geometrical nonlinearity by retaining the square of the slope in the strain–displacement relations, avoiding in this way the inaccuracies arising from a linearized second-order analysis. For that purpose the total Lagrange formulation (intermediate non-linear theory) has been adopted.
- iii. A distributed plasticity (fibre) approach has been employed.
- iv. The formulation is a displacement based one taking into account inelastic redistribution along the beam axis.
- v. A uniaxial hysteretic law is considered for the evolution of the plastic part of the normal stress following the Sivaselvan and Reinhorn (2003) model.
- vi. The inelasticity of the soil medium is taken into account, employing a hysteretic Bouc-Wen force-displacement model.
- vii. The dynamic equilibrium equations are stated in state-space form and a predictor-corrector solution strategy is adopted for the numerical implementation.
- viii. The beam is supported by the most general time dependent boundary conditions.
- ix. The use of BEM permits the effective computation of derivatives of the field functions (e.g. stresses, stress resultants) which is very important during the dynamic inelastic response of beam-foundation systems.
- x. To the author’s knowledge, a BEM approach has not yet been used for the solution of the aforementioned problem, while the developed procedure retains most of the advantages of a BEM solution even though domain discretization is required.

Finally, it is worth mentioning that the outcome of the conducted research activity presented in this chapter of the doctoral dissertation has been published in national and international conferences (Kampitsis & Sapountzakis 2014a,b).

5.2 Statement of the Problem

Let us consider a prismatic beam of length l (Fig. 5.1) with an arbitrarily shaped doubly symmetric constant cross section, occupying the two dimensional multiply connected region Ω of the y, z plane bounded by the Γ_j ($j = 1, 2, \dots, K$) boundary curves, which are piecewise smooth, i.e. they may have a finite number of corners. In Fig. 5.1, C_{yz} is the principal bending coordinate system through the cross section’s centroid. The

normal stress-strain relationship for the material is assumed to be elastic-plastic-strain hardening with initial modulus of elasticity E , shear modulus G , post-yield modulus of elasticity E_t , yield stress σ_{Y0} , and yield strain ε_{Y0} . The beam is partially supported on inelastic Winkler foundation. According to the Winkler hypothesis, the foundation reaction is expressed as

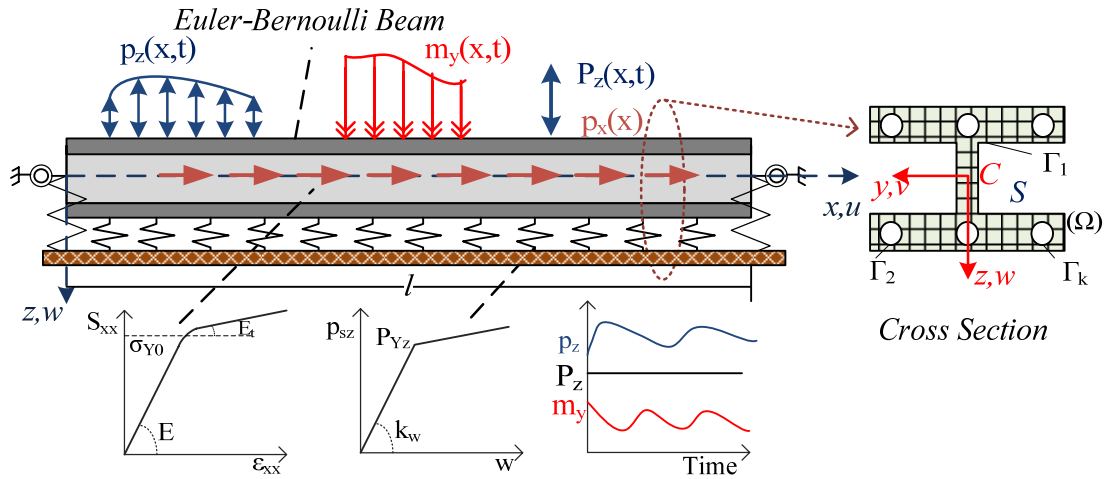


Fig. 5.1. x - z plane of prismatic beam resting on inelastic foundation under axial-flexural dynamic loading.

$$p_{sy}(x,t) = k_y v(x,t) \quad \text{and} \quad p_{sz}(x,t) = k_z w(x,t) \quad (5.1a,b)$$

while in order to take into consideration the nonlinear inelastic behaviour of the Winkler springs the hysteretic Bouc-Wen force-displacement relations are employed

$$p_{sy} = a_{sy} k_y v + (1 - a_{sy}) k_y z_{sy}^h \quad \text{and} \quad p_{sz} = a_{sz} k_z w + (1 - a_{sz}) k_z z_{sz}^h \quad (5.2a,b)$$

where p_{sy}, p_{sz} are the spring forces, k_y, k_z are the initial stiffnesses, v, w are the actual displacements, a_{sy}, a_{sz} are the inelastic to elastic stiffness ratio and z_{sy}^h, z_{sz}^h are the hysteretic parts of the actual displacements acting in the y, z directions, respectively and defined by the following Bouc-Wen evolution equations

$$\dot{z}_{sy}^h(z_{sy}^h, \dot{v}) = \left(1 - \left| \frac{z_{sy}^h}{z_{sy_Yield}^h} \right|^n \left(\beta + \gamma \text{sign}(z_{sy}^h \dot{v}) \right) \right) \dot{v} \quad (5.3a)$$

$$\dot{z}_{sz}^h(z_{sz}^h, \dot{w}) = \left(1 - \left| \frac{z_{sz}^h}{z_{sz_Yield}^h} \right|^n \left(\beta + \gamma \text{sign}(z_{sz}^h \dot{w}) \right) \right) \dot{w} \quad (5.3b)$$

In the above eqns. (5.3), the first term of the right hand side can be regarded as the uniaxial flow rule while the second terms as the corresponding cyclic loading rate, while the symbol $(\dot{})$ denotes differentiation with respect to time t . The dimensionless parameter n controls the smoothness of the transition from the elastic to the inelastic regime while β, γ are shape factors that define the shape of the loading and unloading branches of the hysteretic loop (Sivaselvan & Reinhorn, 2000).

The beam is subjected to the combined action of the arbitrarily distributed or concentrated time dependent axial loading $p_x = p_x(x, t)$, transverse loading $p_y = p_y(x, t)$, $p_z = p_z(x, t)$ acting in the y, z directions, respectively and bending moments $m_y = m_y(x, t)$, $m_z = m_z(x, t)$ along y, z axes, respectively (Fig. 1a).

5.2.1 Displacements, Strains & Stresses

Under the action of the aforementioned loading, the displacement field of the beam is given as (Ramm & Hofmann 1995)

$$\bar{u}(x, y, z, t) = u(x, t) - y\theta_z(x, t) + z\theta_y(x, t) \quad (5.4a)$$

$$\bar{v}(x, t) = v(x, t) \quad \bar{w}(x, t) = w(x, t) \quad (5.4b,c)$$

where \bar{u} , \bar{v} , \bar{w} are the axial and transverse beam displacement components with respect to the Cyz system of axes; $u(x, t)$, $v(x, t)$, $w(x, t)$ are the corresponding components of the centroid C and $\theta_y(x, t)$, $\theta_z(x, t)$ are the angles of rotation due to bending of the cross-section with respect to its centroid. By means of the well known Euler-Bernoulli beam theory, the additional angle of rotation of the cross-section due to

shear deformations are neglected therefore the angles of rotation due to bending are equal to the derivative of the displacement and are given by the following relations

$$\theta_z = \frac{dv}{dx} \quad \theta_y = -\frac{dw}{dx} \quad (5.5a,b)$$

Employing the strain-displacement relations of the three-dimensional elasticity the components of the Green-Lagrange strain are defined as

$$\varepsilon_{xx} = \frac{\partial \bar{u}}{\partial x} + \frac{1}{2} \left[\left(\frac{\partial \bar{u}}{\partial x} \right)^2 + \left(\frac{\partial \bar{v}}{\partial x} \right)^2 + \left(\frac{\partial \bar{w}}{\partial x} \right)^2 \right] \quad (5.6a)$$

$$\varepsilon_{yy} = \frac{\partial \bar{v}}{\partial y} + \frac{1}{2} \left[\left(\frac{\partial \bar{u}}{\partial y} \right)^2 + \left(\frac{\partial \bar{v}}{\partial y} \right)^2 + \left(\frac{\partial \bar{w}}{\partial y} \right)^2 \right] \quad (5.6b)$$

$$\varepsilon_{zz} = \frac{\partial \bar{u}}{\partial z} + \frac{1}{2} \left[\left(\frac{\partial \bar{u}}{\partial z} \right)^2 + \left(\frac{\partial \bar{v}}{\partial z} \right)^2 + \left(\frac{\partial \bar{w}}{\partial z} \right)^2 \right] \quad (5.6c)$$

$$\gamma_{xy} = \left(\frac{\partial \bar{v}}{\partial x} + \frac{\partial \bar{u}}{\partial y} \right) + \left(\frac{\partial \bar{u}}{\partial x} \frac{\partial \bar{u}}{\partial y} + \frac{\partial \bar{v}}{\partial x} \frac{\partial \bar{v}}{\partial y} + \frac{\partial \bar{w}}{\partial x} \frac{\partial \bar{w}}{\partial y} \right) \quad (5.6d)$$

$$\gamma_{xz} = \left(\frac{\partial \bar{w}}{\partial x} + \frac{\partial \bar{u}}{\partial z} \right) + \left(\frac{\partial \bar{u}}{\partial x} \frac{\partial \bar{u}}{\partial z} + \frac{\partial \bar{v}}{\partial x} \frac{\partial \bar{v}}{\partial z} + \frac{\partial \bar{w}}{\partial x} \frac{\partial \bar{w}}{\partial z} \right) \quad (5.6e)$$

$$\gamma_{yz} = \left(\frac{\partial \bar{w}}{\partial y} + \frac{\partial \bar{v}}{\partial z} \right) + \left(\frac{\partial \bar{u}}{\partial y} \frac{\partial \bar{u}}{\partial z} + \frac{\partial \bar{v}}{\partial y} \frac{\partial \bar{v}}{\partial z} + \frac{\partial \bar{w}}{\partial y} \frac{\partial \bar{w}}{\partial z} \right) \quad (5.6f)$$

Moreover, assuming relatively small centroidal axial displacement and moderate large transverse displacements (Ramm & Hofmann 1995, Rothert & Gensichen 1987, Brush & Almroth 1975) while strains remain small, the following strain components can be easily obtained

$$\varepsilon_{xx} = \frac{\partial \bar{u}}{\partial x} + \frac{1}{2} \left[\left(\frac{\partial \bar{v}}{\partial x} \right)^2 + \left(\frac{\partial \bar{w}}{\partial x} \right)^2 \right] \quad (5.7a)$$

$$\gamma_{xz} = \frac{\partial \bar{w}}{\partial x} + \frac{\partial \bar{u}}{\partial z} + \left(\frac{\partial \bar{v}}{\partial x} \frac{\partial \bar{v}}{\partial z} + \frac{\partial \bar{w}}{\partial x} \frac{\partial \bar{w}}{\partial z} \right) \quad (5.7b)$$

$$\gamma_{xy} = \frac{\partial \bar{v}}{\partial x} + \frac{\partial \bar{u}}{\partial y} + \left(\frac{\partial \bar{v}}{\partial x} \frac{\partial \bar{v}}{\partial y} + \frac{\partial \bar{w}}{\partial x} \frac{\partial \bar{w}}{\partial y} \right) \quad (5.7c)$$

$$\varepsilon_{yy} = \varepsilon_{zz} = \gamma_{yz} = 0 \quad (5.7d,e,f)$$

where it has been assumed that for moderate displacements $\left(\frac{\partial \bar{u}}{\partial x}\right)^2 \ll \frac{\partial \bar{u}}{\partial x}$, $\left(\frac{\partial \bar{u}}{\partial x}\right)\left(\frac{\partial \bar{u}}{\partial z}\right) \ll \left(\frac{\partial \bar{w}}{\partial x}\right) + \left(\frac{\partial \bar{u}}{\partial z}\right)$, $\left(\frac{\partial \bar{u}}{\partial x}\right)\left(\frac{\partial \bar{u}}{\partial y}\right) \ll \left(\frac{\partial \bar{v}}{\partial x}\right) + \left(\frac{\partial \bar{u}}{\partial y}\right)$. Exploiting the Euler-Bernoulli assumption and substituting the displacement components (5.4) to the strain-displacement relations (5.7), the normal strain component can be written as

$$\varepsilon_{xx}(x, y, z, t) = \frac{\partial u}{\partial x} - z \frac{\partial^2 w}{\partial x^2} - y \frac{\partial^2 v}{\partial x^2} + \frac{I}{2} \left(\frac{\partial v^2}{\partial x} + \frac{\partial w^2}{\partial x} \right) \quad (5.8)$$

Considering strains to be small, employing the work conjugate second Piola–Kirchhoff stress tensor (Crisfield 1991), assuming an isotropic and homogeneous material without exhibiting any damage during its plastification and neglecting the vanishing components, the normal stress is defined in terms of the strain one as

$$S_{xx} = E^* \varepsilon_{xx}^{el} \quad (5.9)$$

where the superscript *el* denotes the elastic part of the strain component and $E^* = E(1-\nu)/[(1+\nu)(1-2\nu)]$. If the plane stress hypothesis is undertaken then $E^* = E/(1-\nu^2)$ holds, while E is frequently considered instead of E^* ($E^* \approx E$) in beam formulations (Vlasov 1963, Armenakas 2006). This last consideration has been followed throughout the paper, while any other reasonable expression of E^* could also be used without any difficulty in many beam formulations.

As long as the material remains elastic the total strain is assumed to occupying the Hooke's law (i.e. $\varepsilon_{xx} = \varepsilon_{xx}^{el}$) while when plastic flow occurs the additive decomposition of the total strain rate into an elastic and a plastic component (Nemat-Nasser 1982) holds

$$\dot{\varepsilon}_{xx} = \dot{\varepsilon}_{xx}^{el} + \dot{\varepsilon}_{xx}^{pl} \quad (5.10)$$

where ε_{xx} the total normal strain, ε_{xx}^{el} the elastic part of the normal strain and ε_{xx}^{pl} the plastic part of the normal strain.

A uniaxial hysteretic law is considered herein for the evolution of the plastic part of the normal stress. Following the Sivaselvan and Reinhorn (2003) model, the normal stress can be decomposed into a reduced elastic and a hysteretic part as follows

$$S_{xx} = aS_{xx}^{el} + (1-a)S^h = aE\varepsilon_{xx} + (1-a)Ez^h \quad (5.11)$$

where S_{xx}^{el} , S^h are considered the elastic and hysteretic parts of the stress, respectively, a is the post yield stiffness to elastic stiffness ratio and z^h is a hysteretic deformation parameter which serves as an internal variable. The hysteretic part S^h evolves in time according to a nonlinear differential equation following the Bouc-Wen hysteretic rule as proposed by Casciati (1995) (Fig. 5.2)

$$\dot{S}^h(z^h, \dot{\varepsilon}_{xx}) = E\dot{z}^h = E(1-h_1h_2)\dot{\varepsilon}_{xx} \quad (5.12)$$

where h_1, h_2 are smooth Heaviside functions given as

$$h_1 = \left\| \Phi(S^h) + I \right\|^n \quad (5.13a)$$

$$h_2 = \beta + \gamma \operatorname{sign}(S^h \dot{\varepsilon}_{xx}) \quad (5.13b)$$

where Φ is the adopted yield criterion, sign is the signum function and n, β, γ are model's dimensionless parameters. More specifically, n controls the smoothness of the transition from the elastic to the inelastic regime while β, γ are shape factors that define the shape of the loading and unloading branches of the hysteretic loop. Furthermore, it has been proved by Erlicher and Bursi (2004, 2009) that the identified parameters β, γ should comply with the restriction $-\beta \leq \gamma \leq \beta$ in order to be an admissible

thermodynamic model, while in the special case where $\beta = \gamma = 0.5$ the unloading stiffness is equal to the elastic one. In general, eqns. (5.13) can be perceived as control functions of the hysteretic behaviour. In particular, the first Heaviside function describes the flow rule while, the second one controls loading-unloading phases during the dynamic loading.

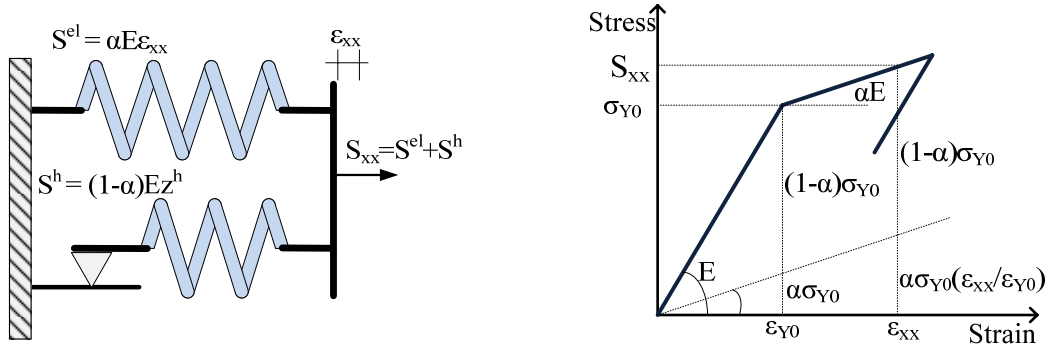


Fig. 5.2. Bouc-Wen hysteretic model (a) and stress-strain relation (b).

In the case where von Mises yield criterion, an associated flow rule and an isotropic hardening rule for the material are utilized (Crisfield 1991), the expression of the yield condition is described with the expression

$$\Phi = \Phi_{vM} = \frac{S_{xx}^2}{\sigma_Y^2 \left(\varepsilon_{eq}^{pl} \right)} - 1 \leq 0 \quad (5.14)$$

where σ_Y is the yield stress of the material and ε_{eq}^{pl} is the equivalent plastic strain (Fig. 5.3), the rate of which is defined in (Crisfield 1991) and is equal to $\dot{\varepsilon}_{eq}^{pl} = \dot{\lambda}$ with $\dot{\lambda}$ being the proportionality factor. Moreover, the plastic modulus h is defined as $h = \dot{\sigma}_Y / \dot{\varepsilon}_{eq}^{pl}$ or $\dot{\sigma}_Y = h \dot{\lambda}$ and can be estimated from a tension test as $h = E_t E / (E - E_t)$ (Fig. 5.3).

5.2.2 Stress Resultants, Equations of Equilibrium and Boundary Conditions

In order to establish the global equilibrium equations and the boundary conditions of the beam-foundation system, the principle of virtual work under a Total Lagrangian formulation neglecting body forces is employed as

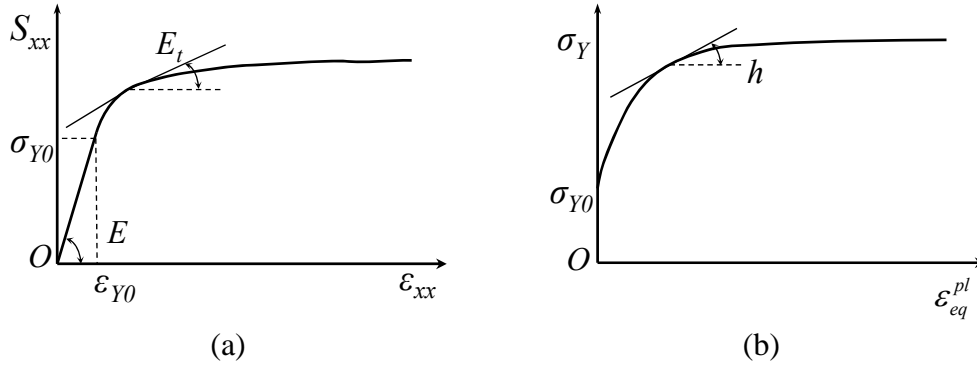


Fig. 5.3. Normal stress–strain (a) and yield stress – equivalent plastic strain (b) relationships.

$$\delta W_{int} + \delta W_{mass} = \delta W_{ext} \quad (5.15)$$

where $\delta(\cdot)$ denotes virtual quantities, W_{int} is the strain energy of the beam due to normal stress, W_{mass} is the kinetic energy and W_{ext} is the external load work, defined as

$$\delta W_{int} = \int_V (S_{xx} \delta \epsilon_{xx}) dV \quad \delta W_{mass} = \int_V \rho (\ddot{u} \delta \bar{u} + \ddot{v} \delta \bar{v} + \ddot{w} \delta \bar{w}) dV \quad (5.16a,b)$$

$$\begin{aligned} \delta W_{mass} = & \int_l (p_x \delta u + p_y \delta v + m_y \delta \theta_y + p_z \delta w + m_y \delta \theta_z) dx - \int_l (p_{sy} \delta v + p_{sz} \delta w) dx \\ & + \sum_b^{0,1} (N_b \delta u + V_{by} \delta v + V_{bz} \delta w + M_{bz} \delta \theta_z + M_{by} \delta \theta_y) \end{aligned} \quad (5.16c)$$

where V is the volume and l is the length of the beam in the undeformed configuration, p_{sy} , p_{sz} are the foundation reaction according to y and z axes, respectively while N_b , V_{by} , V_{bz} , M_{by} and M_{bz} are the externally applied forces and moments at the beam boundaries. The variations of strains are expressed in terms of displacements as

$$\begin{aligned} \delta \epsilon_{xx} = & \delta \left(\frac{\partial u}{\partial x} \right) - z \delta \left(\frac{\partial^2 w}{\partial x^2} \right) - y \delta \left(\frac{\partial^2 v}{\partial x^2} \right) + \frac{I}{2} \delta \left(\frac{\partial v^2}{\partial x} + \frac{\partial w^2}{\partial x} \right) = \\ = & \delta(u') - z \delta(w'') - y \delta(v'') + v' \delta(v') + w' \delta(w') \end{aligned} \quad (5.17)$$

where (') denotes differentiation with respect to x . Within this framework, the stress resultants of the beam are defined as

$$N = \int_{\Omega} S_{xx} d\Omega \quad (5.18)$$

$$M_y = \int_{\Omega} S_{xx} z d\Omega \quad M_z = -\int_{\Omega} S_{xx} y d\Omega \quad (5.18b,c)$$

where N correspond to the axial force and M_y , M_z correspond to the bending moments according to y and z axes, respectively. Subsequently, substituting the expressions of the stress component given from eqn. (5.11) and exploiting the strain-displacement relations (5.8), the stress resultants are obtained as

$$N = aEA \left[u' + \frac{1}{2} (v'^2 + w'^2) \right] + (1-\alpha) \int_{\Omega} S^h d\Omega = \alpha N^{el} + (1-\alpha) N^h \quad (5.19a)$$

$$M_y = -aEI_y w'' + (1-\alpha) \int_{\Omega} S^h z d\Omega = \alpha M_y^{el} + (1-\alpha) M_y^h \quad (5.19b)$$

$$M_z = aEI_z v'' - (1-\alpha) \int_{\Omega} S^h y d\Omega = \alpha M_z^{el} - (1-\alpha) M_z^h \quad (5.19c)$$

where N^h , M_z^h and M_y^h are area integrals consisting the hysteretic parts of the corresponding stress resultants, A is the cross section area, I_y , I_z the moments of inertia with respect to the principle bending axes given as

$$A = \int_{\Omega} d\Omega \quad (5.20a)$$

$$I_y = \int_{\Omega} z^2 d\Omega \quad I_z = \int_{\Omega} y^2 d\Omega \quad (5.20b,c)$$

It is worth noting that these stress resultants refer to the directions of the infinitesimal elements of the cross section at its deformed configuration, since they have been defined with respect to the second Piola-Kirchhoff stress tensor.

After substituting eqns. (5.8) and (5.19) into eqn. (5.15) and conducting some algebraic manipulations, the differential equations of motion of the beam-foundation system are obtained as

$$\rho A \ddot{u} - \alpha EA (u'' + v'v'' + w'w'') - \frac{(1-a)\partial N^h}{\partial x} = p_x(x, t) \quad (5.21a)$$

$$\begin{aligned} \rho A \ddot{v} + aEI_z v'''' - (1-a) \frac{\partial^2 M_z^h}{\partial x^2} - aEA \left[\left(u'v' + \frac{1}{2}v'^3 + \frac{1}{2}w'^2v' \right)' \right] - \\ - (1-a) \frac{\partial(N^h v')}{\partial x} + p_{sy}(x, t) = p_y(x, t) - m'_z(x, t) \end{aligned} \quad (5.21b)$$

$$\begin{aligned} \rho A \ddot{w} + aEI_y w'''' - (1-a) \frac{\partial^2 M_y^h}{\partial x^2} - aEA \left[\left(u'w' + \frac{1}{2}w'^3 + \frac{1}{2}v'^2w' \right)' \right] - \\ - (1-a) \frac{\partial(N^h w')}{\partial x} + p_{sz}(x, t) = p_z(x, t) + m'_y(x, t) \end{aligned} \quad (5.21c)$$

or in a more compact form these equations are written as

$$\rho A \ddot{u} - \left[\alpha \frac{\partial N^{el}}{\partial x} + (1-a) \frac{\partial N^h}{\partial x} \right] = p_x \quad (5.22a)$$

$$\rho A \ddot{v} + aEI_z v'''' - (1-a) \frac{\partial^2 M_z^h}{\partial x^2} - a \frac{\partial(N^{el} v')}{\partial x} - (1-a) \frac{\partial(N^h v')}{\partial x} + p_{sy} = p_y - m'_z \quad (5.22b)$$

$$\rho A \ddot{w} + aEI_y w'''' - (1-a) \frac{\partial^2 M_y^h}{\partial x^2} - a \frac{\partial(N^{el} w')}{\partial x} - (1-a) \frac{\partial(N^h w')}{\partial x} + p_{sz} = p_z + m'_y \quad (5.22c)$$

The differential equations of motion can also be written in terms of the total stress resultants as

$$\rho A \ddot{u} - \frac{\partial N}{\partial x} = p_x \quad (5.23a)$$

$$\rho A \ddot{v} + \frac{\partial^2 M_z}{\partial x^2} - \frac{\partial(Nv')}{\partial x} + p_{sy} = p_y - m'_z \quad (5.23b)$$

$$\rho A \ddot{w} - \frac{\partial^2 M_y}{\partial x^2} - \frac{\partial(Nw')}{\partial x} + p_{sz} = p_z + m'_y \quad (5.23c)$$

The above equations are easily simplified by crossing out the nonlinear terms regarding the hysteretic behaviour, leading to the well known differential equations governing the motion of an elastic beam assuming geometrical nonlinearity. It is noted that these equations are of the second order with respect to the axial and the fourth order with respect to the transverse directions.

The governing equations of motion are also subjected to the time dependent boundary conditions derived also from the principle of virtual work as

$$\left[\left[aEA \left(u' + \frac{1}{2}(v' + w') \right) + (1-a)N^h \right] \right]_0 + N_x^0 \delta u(0) = 0 \xrightarrow{\text{eqn.(5.19a)}} \quad (5.24a)$$

$$\left[\left[\alpha N^{el} + (1-\alpha)N^h \right] \right]_0 + N_x^0 \delta u(0) = 0 \longrightarrow \left[N(0) + N_x^0 \right] \delta u(0) = 0$$

$$\left[\left[aEA \left(u' + \frac{1}{2}(v' + w') \right) + (1-a)N^h \right] \right]_l + N_x^l \delta u(l) = 0 \xrightarrow{\text{eqn.(5.19a)}} \quad (5.24b)$$

$$\left[\left[\alpha N^{el} + (1-\alpha)N^h \right] \right]_l + N_x^l \delta u(l) = 0 \longrightarrow \left[N(l) + N_x^l \right] \delta u(l) = 0$$

$$\left[\left[aEA \left(u'v' + \frac{1}{2}v'^3 + \frac{1}{2}v'w'^2 \right) + (1-a)N^h v' \right] \right]_0 - \left[aEI_z v''' - (1-a) \frac{\partial M_z^h}{\partial x} \right] \right]_0 + \quad (5.24c)$$

$$+ V_y^0 \delta v(0) = 0 \xrightarrow{\text{eqns.(5.19a,b)}} \left[Nv' - \frac{\partial M_z}{\partial x} + V_y^0 \right] \delta v(0) = 0$$

$$\left[\left[aEA \left(u'v' + \frac{1}{2}v'^3 + \frac{1}{2}v'w'^2 \right) + (1-a)N^h v' \right] \right]_l - \left[aEI_z v''' - (1-a) \frac{\partial M_z^h}{\partial x} \right] \right]_l + \quad (5.24d)$$

$$+ V_y^l \delta v(l) = 0 \xrightarrow{\text{eqns.(5.19a,b)}} \left[Nv' - \frac{\partial M_z}{\partial x} + V_y^l \right] \delta v(l) = 0$$

$$\left[\left[aEA \left(u'w' + \frac{1}{2}w'^3 + \frac{1}{2}v'^2 w' \right) + (1-a)N^h w' \right] \right]_0 - \left[aEI_z w''' - (1-a) \frac{\partial M_y^h}{\partial x} \right] \right]_0 + \quad (5.24e)$$

$$+ V_z^0 \delta w(0) = 0 \xrightarrow{\text{eqns.(5.17a,c)}} \left[Nw' - \frac{\partial M_y}{\partial x} + V_z^0 \right] \delta w(0) = 0$$

$$\left[\left[aEA \left(u'w' + \frac{I}{2} w'^3 + \frac{I}{2} v'^2 w' \right) + (I-a) N^h w' \right] \right]_l - \left[aEI_z w''' - (I-a) \frac{\partial M_y^h}{\partial x} \right]_l + \quad (5.24f)$$

$$+ V_z^l \delta w(l) = 0 \xrightarrow{\text{eqns.(5.19a,c)}} \left[Nw' - \frac{\partial M_y}{\partial x} + V_z^l \right]_l \delta w(l) = 0$$

$$\left[\left(aEI_z v'' - (I-a) M_z^h \right) \right]_0 + M_z^0 \delta v'(0) \xrightarrow{\text{eqn.(5.19c)}} \left[M_z(0) + M_z^0 \right] \delta v'(0) = 0 \quad (5.24g)$$

$$\left[\left(aEI_z v'' - (I-a) M_z^h \right) \right]_l + M_z^l \delta v'(l) \xrightarrow{\text{eqn.(5.19c)}} \left[M_z(l) + M_z^l \right] \delta v'(l) = 0 \quad (5.24h)$$

$$\left[\left(aEI_y v'' - (I-a) M_y^h \right) \right]_0 + M_y^0 \delta w'(0) \xrightarrow{\text{eqn.(5.19b)}} \left[M_y(0) + M_y^0 \right] \delta w'(0) = 0 \quad (5.24i)$$

$$\left[\left(aEI_y v'' - (I-a) M_y^h \right) \right]_l + M_y^l \delta w'(l) \xrightarrow{\text{eqn.(5.19b)}} \left[M_y(l) + M_y^l \right] \delta w'(l) = 0 \quad (5.24j)$$

which can be written in a more convenient form as

$$\alpha_1 u(x,t) + \alpha_2 N_b(x,t) = \alpha_3 \quad (5.25a)$$

$$\beta_1 v(x,t) + \beta_2 V_{by}(x,t) = \beta_3 \quad \bar{\beta}_1 \frac{\partial v}{\partial x}(x,t) + \bar{\beta}_2 M_{bz}(x,t) = \bar{\beta}_3 \quad (5.25b,c)$$

$$\gamma_1 w(x,t) + \gamma_2 V_{bz}(x,t) = \gamma_3 \quad \bar{\gamma}_1 \frac{\partial w}{\partial x}(x,t) + \bar{\gamma}_2 M_{by}(x,t) = \bar{\gamma}_3 \quad (5.25d,e)$$

at the beam ends $x = 0, l$, together with the initial conditions

$$u(x,0) = \bar{u}_0(x) \quad \dot{u}(x,0) = \dot{\bar{u}}_0(x) \quad (5.26a,b)$$

$$v(x,0) = \bar{v}_0(x) \quad \dot{v}(x,0) = \dot{\bar{v}}_0(x) \quad (5.26c,d)$$

$$w(x,0) = \bar{w}_0(x) \quad \dot{w}(x,0) = \dot{\bar{w}}_0(x) \quad (5.26e,f)$$

where $\bar{u}_0(x)$, $\bar{v}_0(x)$, $\bar{w}_0(x)$, $\dot{\bar{u}}_0(x)$, $\dot{\bar{v}}_0(x)$ and $\dot{\bar{w}}_0(x)$ are prescribed functions. In the boundary eqns. (5.25b-e) V_{by} , V_{bz} and M_{bz} , M_{by} are the reactions and bending moments with respect to y , z , respectively given by the following relations

$$V_{by} = aEA \left[u' + \frac{I}{2}(v'^2 + w'^2) \right] v' + (1-a) N^h v' - aEI_z v''' + (1-a) \frac{\partial M_z^h}{\partial x} \quad (5.27a)$$

$$V_{bz} = aEA \left[u' + \frac{I}{2}(v'^2 + w'^2) \right] w' + (1-a) N^h w' - aEI_y w''' + (1-a) \frac{\partial M_y^h}{\partial x} \quad (5.27b)$$

$$M_{by} = -aEI_y w'' + (1-a) M_y^h \quad (5.27c)$$

$$M_{bz} = EI_z v'' - (1-a) M_z^h \quad (5.27d)$$

Finally, $\alpha_j, \beta_j, \bar{\beta}_j, \gamma_j, \bar{\gamma}_j$ ($j=1,2,3$) are functions specified at the beam ends $x=0,l$. Eqns. (5.25) describe the most general nonlinear boundary conditions associated with the problem at hand and can include elastic support or restraint. It is apparent that all types of the conventional boundary conditions (clamped, simply supported, free or guided edge) can be derived from these equations by specifying appropriately these functions (e.g. for a clamped edge it is $\alpha_1 = \beta_1 = \gamma_1 = 1$, $\bar{\beta}_1 = \bar{\gamma}_1 = 1$, $\alpha_2 = \alpha_3 = \beta_2 = \beta_3 = \gamma_2 = \gamma_3 = \bar{\beta}_2 = \bar{\beta}_3 = \bar{\gamma}_2 = \bar{\gamma}_3 = 0$).

The above equations of equilibrium and boundary conditions are easily simplified by crossing out the nonlinear terms corresponding to material nonlinearity, leading to the well known elastic formulation while, by crossing out the nonlinear terms corresponding to the geometrical nonlinearity leads to the well known second order with respect to the axial and the forth order with respect to the transverse directions.

5.3 Numerical Solution

According to the precedent analysis, the geometrically nonlinear inelastic problem of Euler-Bernoulli beams supported on nonlinear inelastic soil, reduces in establishing the displacement components $u(x,t)$ and $v(x,t)$, $w(x,t)$ having continuous derivatives up to the second order and up to the fourth order with respect to x , respectively and also having derivatives up to the second order with respect to t . These displacement

components must satisfy the coupled governing differential equations (5.23) inside the beam, the boundary conditions (5.25) at the beam ends $x = 0, l$ and the initial conditions (5.26). Eqns. (5.21) are solved using the Analog Equation Method (Katsikadelis 1994, 2002) as it is described in Appendix A1.

5.3.1 Axial $u(x, t)$ and Transverse Displacements $v(x, t), w(x, t)$

According to this method, let $u(x, t)$, $v(x, t)$ and $w(x, t)$ be the sought solution of the aforementioned initial value problem. Setting as $u_1(x, t) = u(x, t)$, $u_2(x, t) = v(x, t)$, $u_3(x, t) = w(x, t)$ and differentiating with respect to x these functions two and four times, respectively yields

$$\frac{\partial^2 u_i}{\partial x^2} = q_i(x, t) \quad \frac{\partial^4 u_i}{\partial x^4} = q_i(x, t) \quad (i = 2, 3) \quad (5.28)$$

Eqns. (5.28) are quasi-static that is the time variable appears as a parameter. They indicate that the solution of eqns. (5.23) can be established by solving eqns. (5.28) under the same boundary conditions (5.25), provided that the fictitious load distributions $q_i(x, t)$ ($i = 1, 2, 3$) are first established. Following the procedure as described in Appendix A1, the integral representations of the displacement components u_i ($i = 1, 2, 3$) obtained by eqn. (A1.8, A1.36) and their first derivatives with respect to x obtained by eqn. (A1.22, A1.43), when applied to the beam ends $(0, l)$, together with the boundary conditions (5.25) are employed to express the unknown boundary quantities $u_i(\zeta, t)$, $u_{i,x}(\zeta, t)$, $u_{i,xx}(\zeta, t)$ and $u_{i,xxx}(\zeta, t)$ ($\zeta = 0, l$) in terms of the fictitious loads q_i ($i = 1, 2, 3$). In order to accomplish this numerical formulation, the interval $(0, l)$ is divided into L elements, on which $q_i(x, t)$ is assumed to vary according to certain law (constant, linear, parabolic etc). The constant element assumption is employed here as the numerical implementation becomes very simple and the obtained results are of high accuracy.

Employing the aforementioned procedure, the following set of 20 nonlinear algebraic equations is obtained

$$\begin{bmatrix} \mathbf{T}_{11} & \mathbf{0} & \mathbf{0} \\ \mathbf{0} & \mathbf{T}_{22} & \mathbf{0} \\ \mathbf{0} & \mathbf{0} & \mathbf{T}_{33} \end{bmatrix} \begin{Bmatrix} \mathbf{d}_1 \\ \mathbf{d}_2 \\ \mathbf{d}_3 \end{Bmatrix} + \begin{Bmatrix} \mathbf{D}_1^h \\ \mathbf{D}_2^h \\ \mathbf{D}_3^h \end{Bmatrix} = \begin{Bmatrix} \mathbf{a}_3 \\ \mathbf{b}_3 \\ \mathbf{c}_3 \end{Bmatrix} \quad (5.29)$$

with

$$\mathbf{T}_{11} = \begin{bmatrix} \mathbf{F}_1^u & \mathbf{E}_{11}^u & \mathbf{E}_{12}^u \\ \mathbf{0} & \mathbf{D}_{12}^u & \mathbf{D}_{22}^u \end{bmatrix} \quad (5.30a)$$

$$\mathbf{T}_{22} = \begin{bmatrix} \mathbf{F}_1 & \mathbf{E}_{11} & \mathbf{E}_{12} & \mathbf{E}_{13} & \mathbf{E}_{14} \\ \mathbf{F}_2 & \mathbf{0} & \mathbf{E}_{22} & \mathbf{E}_{23} & \mathbf{E}_{24} \\ \mathbf{0} & \mathbf{D}_{11} & \mathbf{D}_{12} & \mathbf{0} & \mathbf{D}_{14} \\ \mathbf{0} & \mathbf{0} & \mathbf{D}_{22} & \mathbf{D}_{23} & \mathbf{D}_{24} \end{bmatrix} \quad \mathbf{T}_{33} = \begin{bmatrix} \mathbf{F}_1 & \mathbf{E}_{11} & \mathbf{E}_{12} & \mathbf{E}_{13} & \mathbf{E}_{14} \\ \mathbf{F}_2 & \mathbf{0} & \mathbf{E}_{22} & \mathbf{E}_{23} & \mathbf{E}_{24} \\ \mathbf{0} & \mathbf{G}_{11} & \mathbf{G}_{12} & \mathbf{0} & \mathbf{G}_{14} \\ \mathbf{0} & \mathbf{0} & \mathbf{G}_{22} & \mathbf{G}_{23} & \mathbf{G}_{24} \end{bmatrix} \quad (5.30b,c)$$

where $\mathbf{E}_{11}^u, \mathbf{E}_{12}^u, \mathbf{E}_{11} - \mathbf{E}_{48}$ are rectangular 2×2 known coefficient matrices resulting from the values of the kernels $A_j(r)$ ($j = 1, 2, 3, 4$) at the beam ends and $\mathbf{F}_1^u, \mathbf{F}_1, \mathbf{F}_2$ are $2 \times L$ rectangular known matrices originating from the integration of the kernels along the axis of the beam, as defined in Appendix A1. Moreover, $\mathbf{D}_{11} - \mathbf{D}_{24}$ and $\mathbf{G}_{11} - \mathbf{G}_{24}$ are 2×2 known square, time dependent matrices including the values of the functions $a_j, \beta_j, \bar{\beta}_j, \gamma_j, \bar{\gamma}_j$ ($j = 1, 2$) of eqns.(5.25), while $\mathbf{D}_1^h, \mathbf{a}_3$ and $\mathbf{D}_2^h, \mathbf{D}_3^h, \mathbf{b}_3, \mathbf{c}_3$ are 4×1 and 8×1 , respectively known, in general time dependent, column matrices including the boundary values of the functions $a_3, \beta_3, \bar{\beta}_3, \gamma_3, \bar{\gamma}_3$ of eqns. (5.25). Furthermore, $\mathbf{d}_1 - \mathbf{d}_3$ are the generalized unknown vectors including the L unknown time dependent nodal values of the fictitious loads $q_i = \{q_1^i, q_2^i, \dots, q_L^i\}^T$ ($i = 1, 2, 3$) and the vectors including the unknown time dependent boundary values of the respective boundary quantities. More specifically, the expressions of the matrices of eqn. (5.30) are given as

$$\mathbf{D}_{12}^u = \begin{bmatrix} \alpha_1^0 & 0 \\ 0 & \alpha_1^l \end{bmatrix} \quad \mathbf{D}_{22}^u = a \begin{bmatrix} \alpha_2^0 EA & 0 \\ 0 & \alpha_2^l EA \end{bmatrix} \quad (5.31a,b)$$

$$\mathbf{D}_1^h = \frac{aEA}{2} \begin{Bmatrix} [\emptyset] \\ \alpha_2^0 [\hat{u}_{2,x}(0) + \hat{u}_{3,x}(0)]^2 \\ \alpha_2^l [\hat{u}_{2,x}(l) + \hat{u}_{3,x}(l)]^2 \end{Bmatrix} + (1-a) \begin{Bmatrix} [\emptyset] \\ \alpha_2^0 [N^h(0)]^2 \\ \alpha_2^l [N^h(l)]^2 \end{Bmatrix} \quad \mathbf{a}_3 = \begin{Bmatrix} [\emptyset] \\ \alpha_3^0 \\ \alpha_3^l \end{Bmatrix} \quad (5.31c,d)$$

$$\mathbf{D}_{11} = \begin{bmatrix} \beta_1^0 & 0 \\ 0 & \beta_1^l \end{bmatrix} \quad \mathbf{D}_{12} = a \begin{bmatrix} \beta_2^0 N^{el}(0) & 0 \\ 0 & \beta_2^l N^{el}(l) \end{bmatrix} \quad \mathbf{D}_{14} = -aEI_z \begin{bmatrix} \beta_2^0 & 0 \\ 0 & \beta_2^l \end{bmatrix} \quad (5.32a-c)$$

$$\mathbf{D}_{22} = \begin{bmatrix} \bar{\beta}_1^0 & 0 \\ 0 & \bar{\beta}_1^l \end{bmatrix} \quad \mathbf{D}_{23} = aEI_z \begin{bmatrix} \bar{\beta}_2^0 & 0 \\ 0 & \bar{\beta}_2^l \end{bmatrix} \quad (5.32d,e)$$

$$\mathbf{D}_2^h = (1-a) \begin{Bmatrix} [\emptyset] \\ \beta_2^0 N^h \hat{u}_{2,x}(0) - \beta_2^0 \frac{\partial M_z^h(0)}{\partial x} \\ \beta_2^l N^h \hat{u}_{2,x}(l) - \beta_2^l \frac{\partial M_z^h(l)}{\partial x} \\ [\emptyset] \\ -\bar{\beta}_2^0 M_z^h(0) \\ -\bar{\beta}_2^l M_z^h(l) \end{Bmatrix} \quad \mathbf{b}_3 = \begin{Bmatrix} [\emptyset] \\ \beta_3^0 \\ \beta_3^l \\ [\emptyset] \\ \bar{\beta}_3^0 \\ \bar{\beta}_3^l \end{Bmatrix} \quad (5.32f,g)$$

$$\mathbf{G}_{11} = \begin{bmatrix} \gamma_1^0 & 0 \\ 0 & \gamma_1^l \end{bmatrix} \quad \mathbf{G}_{12} = a \begin{bmatrix} \gamma_2^0 N^{el}(0) & 0 \\ 0 & \gamma_2^l N^{el}(l) \end{bmatrix} \quad \mathbf{G}_{14} = -aEI_y \begin{bmatrix} \gamma_2^0 & 0 \\ 0 & \gamma_2^l \end{bmatrix} \quad (5.33a-c)$$

$$\mathbf{G}_{22} = - \begin{bmatrix} \bar{\gamma}_1^0 & 0 \\ 0 & \bar{\gamma}_1^l \end{bmatrix} \quad \mathbf{G}_{23} = aEI_y \begin{bmatrix} \bar{\gamma}_2^0 & 0 \\ 0 & \bar{\gamma}_2^l \end{bmatrix} \quad (5.33d,e)$$

$$\mathbf{D}_3^h = (I-a) \begin{Bmatrix} [\emptyset] \\ \gamma_2^0 N^h \hat{u}_{3,x}(0) - \gamma_2^0 \frac{\partial M_y^h(0)}{\partial x} \\ \gamma_2^l N^h \hat{u}_{3,x}(l) - \gamma_2^l \frac{\partial M_y^h(l)}{\partial x} \\ [\emptyset] \\ -\bar{\gamma}_i^0 M_y^h(0) \\ -\bar{\gamma}_i^l M_y^h(l) \end{Bmatrix} \quad \mathbf{b}_3 = \begin{Bmatrix} [\emptyset] \\ \gamma_3^0 \\ \gamma_3^l \\ [\emptyset] \\ \bar{\gamma}_3^0 \\ \bar{\gamma}_3^l \end{Bmatrix} \quad (5.33f,g)$$

$$\mathbf{d}_1 = \begin{Bmatrix} \mathbf{q}_1 \\ \hat{\mathbf{u}}_1 \\ \hat{\mathbf{u}}_{1,x} \end{Bmatrix} \quad \mathbf{d}_2 = \begin{Bmatrix} \mathbf{q}_2 \\ \hat{\mathbf{u}}_2 \\ \hat{\mathbf{u}}_{2,x} \\ \hat{\mathbf{u}}_{2,xx} \\ \hat{\mathbf{u}}_{2,xxx} \end{Bmatrix} \quad \mathbf{d}_3 = \begin{Bmatrix} \mathbf{q}_3 \\ \hat{\mathbf{u}}_3 \\ \hat{\mathbf{u}}_{3,x} \\ \hat{\mathbf{u}}_{3,xx} \\ \hat{\mathbf{u}}_{3,xxx} \end{Bmatrix} \quad (5.34)$$

where the boundary values of the displacement components u_i ($i=1,2,3$) and their derivatives with respect to x are written in matrix form as

$$\hat{\mathbf{u}}_i = \{u_i(0,t) \quad u_i(l,t)\}^T \quad (i=1,2,3) \quad (5.35a)$$

$$\hat{\mathbf{u}}_{i,x} = \left\{ \frac{\partial u_i(0,t)}{\partial x} \quad \frac{\partial u_i(l,t)}{\partial x} \right\}^T \quad (i=1,2,3) \quad (5.35b)$$

$$\hat{\mathbf{u}}_{i,xx} = \left\{ \frac{\partial^2 u_i(0,t)}{\partial x^2} \quad \frac{\partial^2 u_i(l,t)}{\partial x^2} \right\}^T \quad (i=2,3) \quad (5.35c)$$

$$\hat{\mathbf{u}}_{i,xxx} = \left\{ \frac{\partial^3 u_i(0,t)}{\partial x^3} \quad \frac{\partial^3 u_i(l,t)}{\partial x^3} \right\}^T \quad (i=2,3) \quad (5.35d)$$

Thereafter, the discretization of the integral representations of the displacement components u_i ($i=1,2,3$) and their derivatives with respect to x , and the application to the L collocation nodal points yields

$$\mathbf{u}_1 = \mathbf{A}_1^0 \mathbf{q}_1 + \mathbf{C}_0 \hat{\mathbf{u}}_1 + \mathbf{C}_1 \hat{\mathbf{u}}_{1,x} \quad (5.36a)$$

$$\mathbf{u}_{1,x} = \mathbf{A}_1^1 \mathbf{q}_1 + \mathbf{C}_0 \hat{\mathbf{u}}_{1,x} \quad \mathbf{u}_{1,xx} = \mathbf{q}_1 \quad (5.36b,c)$$

$$\mathbf{u}_2 = \mathbf{A}_2^0 \mathbf{q}_2 + \mathbf{C}_0 \hat{\mathbf{u}}_2 + \mathbf{C}'_1 \hat{\mathbf{u}}_{2,x} + \mathbf{C}_2 \hat{\mathbf{u}}_{2,xx} + \mathbf{C}_3 \hat{\mathbf{u}}_{2,xxx} \quad (5.37a)$$

$$\mathbf{u}_{2,x} = \mathbf{A}_2^1 \mathbf{q}_2 + \mathbf{C}_0 \hat{\mathbf{u}}_{2,x} + \mathbf{C}'_1 \hat{\mathbf{u}}_{2,xx} + \mathbf{C}_2 \hat{\mathbf{u}}_{2,xxx} \quad (5.37b)$$

$$\mathbf{u}_{2,xx} = \mathbf{A}_2^2 \mathbf{q}_2 + \mathbf{C}_0 \hat{\mathbf{u}}_{2,xx} + \mathbf{C}'_1 \hat{\mathbf{u}}_{2,xxx} \quad (5.37c)$$

$$\mathbf{u}_{2,xxx} = \mathbf{A}_2^3 \mathbf{q}_2 + \mathbf{C}_0 \hat{\mathbf{u}}_{2,xxx} \quad \mathbf{u}_{2,xxxx} = \mathbf{q}_2 \quad (5.37d,e)$$

$$\mathbf{u}_3 = \mathbf{A}_3^0 \mathbf{q}_3 + \mathbf{C}_0 \hat{\mathbf{u}}_3 + \mathbf{C}'_1 \hat{\mathbf{u}}_{3,x} + \mathbf{C}_2 \hat{\mathbf{u}}_{3,xx} + \mathbf{C}_3 \hat{\mathbf{u}}_{3,xxx} \quad (5.38a)$$

$$\mathbf{u}_{3,x} = \mathbf{A}_3^1 \mathbf{q}_3 + \mathbf{C}_0 \hat{\mathbf{u}}_{3,x} + \mathbf{C}'_1 \hat{\mathbf{u}}_{3,xx} + \mathbf{C}_2 \hat{\mathbf{u}}_{3,xxx} \quad (5.38b)$$

$$\mathbf{u}_{3,xx} = \mathbf{A}_3^2 \mathbf{q}_3 + \mathbf{C}_0 \hat{\mathbf{u}}_{3,xx} + \mathbf{C}'_1 \hat{\mathbf{u}}_{3,xxx} \quad (5.38c)$$

$$\mathbf{u}_{3,xxx} = \mathbf{A}_3^3 \mathbf{q}_3 + \mathbf{C}_0 \hat{\mathbf{u}}_{3,xxx} \quad \mathbf{u}_{3,xxxx} = \mathbf{q}_3 \quad (5.38d,e)$$

where \mathbf{A}_1^i , \mathbf{A}_2^j , \mathbf{A}_3^j ($i=0,1$), ($j=0,1,2,3$) are $L \times L$ known matrices; \mathbf{C}_0 , \mathbf{C}_1 , \mathbf{C}'_1 , \mathbf{C}_2 , \mathbf{C}_3 are $L \times 2$ known matrices and \mathbf{u}_i , $\mathbf{u}_{i,x}$, $\mathbf{u}_{i,xx}$, $\mathbf{u}_{i,xxx}$, $\mathbf{u}_{i,xxxx}$ are time dependent vectors including the values of $u_i(x,t)$ and their derivatives at the L nodal points. These equations can be assembled in a more convenient matrix form as

$$\mathbf{u}_1 = \mathbf{B}^u \mathbf{d}_1 \quad \mathbf{u}_{1,x} = \mathbf{B}^u_{,x} \mathbf{d}_1 \quad (5.39a,b)$$

$$\mathbf{u}_2 = \mathbf{B} \mathbf{d}_2 \quad \mathbf{u}_{2,x} = \mathbf{B}_{,x} \mathbf{d}_2 \quad \mathbf{u}_{2,xx} = \mathbf{B}_{,xx} \mathbf{d}_2 \quad \mathbf{u}_{2,xxx} = \mathbf{B}_{,xxx} \mathbf{d}_2 \quad (5.40a-d)$$

$$\mathbf{u}_3 = \mathbf{B} \mathbf{d}_3 \quad \mathbf{u}_{3,x} = \mathbf{B}_{,x} \mathbf{d}_3 \quad \mathbf{u}_{3,xx} = \mathbf{B}_{,xx} \mathbf{d}_3 \quad \mathbf{u}_{3,xxx} = \mathbf{B}_{,xxx} \mathbf{d}_3 \quad (5.41a-d)$$

where \mathbf{B}^u , \mathbf{B} and their derivatives are $L \times (L+4)$ and $L \times (L+8)$ known matrices, respectively arising from \mathbf{A}^u , \mathbf{A} , \mathbf{C}^u , \mathbf{C} and their derivatives as presented in Appendix A1.

In conventional BEM, the load vectors \mathbf{q}_i are known and eqns. (3.40-3.41) are used to evaluate $u_i(x,t)$ and their derivatives at the L nodal points. This, however, cannot

be applied here since \mathbf{q}_i are unknown. Thus, $3L$ additional equations are required in order to permit the establishment of \mathbf{q}_i . Therefore, the final step of AEM is implemented by applying the governing equations of motion (5.23) to the L collocation points and employing eqns. (3.39-3.41) leads to the formulation of the following set of $3 \times L$ semi-discretized nonlinear equations of motion

$$\mathbf{M}\ddot{\mathbf{d}} + \mathbf{K}\mathbf{d} + \mathbf{P}^h = \mathbf{f} \Rightarrow \mathbf{M} \begin{Bmatrix} \ddot{\mathbf{d}}_1 \\ \ddot{\mathbf{d}}_2 \\ \ddot{\mathbf{d}}_3 \end{Bmatrix} + \mathbf{K} \begin{Bmatrix} \mathbf{d}_1 \\ \mathbf{d}_2 \\ \mathbf{d}_3 \end{Bmatrix} + \mathbf{P}^h = \mathbf{f} \quad (5.42)$$

where \mathbf{P}^h is a generalized vector including the nonlinear terms due to geometrical and material nonlinearities and $\mathbf{M}, \mathbf{K}, \mathbf{f}$ are generalized mass, stiffness matrices and force vector respectively, defined as

$$\mathbf{M}_1 = \rho AB^u \quad \mathbf{K}_1 = -a[\mathbf{EA}]_{dg,L} \quad \mathbf{f}_1 = \mathbf{p}_x \quad (5.43a-c)$$

$$\mathbf{P}_1^h = aEA \left[[\mathbf{B}_{,xx}\mathbf{d}_2]_{dg} [\mathbf{B}_{,x}\mathbf{d}_2] + [\mathbf{B}_{,xx}\mathbf{d}_3]_{dg} [\mathbf{B}_{,x}\mathbf{d}_3] \right] + (1-a)\mathbf{N}_{,x}^h \quad (5.43d)$$

$$\mathbf{M}_2 = \rho AB \quad \mathbf{K}_2 = a \left([\mathbf{EI}_z]_{dg,L} - \mathbf{N}_x^{el} \mathbf{B}_{,x} - \mathbf{N}^{el} \mathbf{B}_{,xx} \right) + a_{sy} \mathbf{K}_y^{dg} \mathbf{B} \quad (5.44a-c)$$

$$\mathbf{P}_2^h = (1-a) \left[\mathbf{M}_{z,xx}^h - \left(\mathbf{N}_{,x}^h \mathbf{B}_{,x} - \mathbf{N}^h \mathbf{B}_{,xx} \right) \right] + (1-a_{sy}) k_y \left\{ z_{sy}^h \right\} \quad \mathbf{f}_2 = \mathbf{p}_y - \mathbf{m}_{z,x} \quad (5.44d)$$

$$\mathbf{M}_3 = \rho AB \quad \mathbf{K}_3 = a \left([\mathbf{EI}_y]_{dg,L} - \mathbf{N}_x^{el} \mathbf{B}_{,x} - \mathbf{N}^{el} \mathbf{B}_{,xx} \right) + a_{sz} \mathbf{K}_z^{dg} \mathbf{B} \quad (5.45a-c)$$

$$\mathbf{P}_3^h = (1-a) \left[\mathbf{M}_{y,xx}^h - \left(\mathbf{N}_{,x}^h \mathbf{B}_{,x} - \mathbf{N}^h \mathbf{B}_{,xx} \right) \right] + (1-a_{sz}) k_z \left\{ z_{sz}^h \right\} \quad \mathbf{f}_3 = \mathbf{p}_z + \mathbf{m}_{y,x} \quad (5.45d)$$

where \mathbf{N}^{el} , $\mathbf{N}_{,x}^{el}$ are $L \times L$ diagonal matrices containing the values of the elastic axial force and its derivatives with respect to x at the L nodal points, \mathbf{p}_y , \mathbf{p}_z , $\mathbf{m}_{y,x}$ and

$\mathbf{m}_{z,x}$ are $L \times I$ vectors containing the values of the external loading and its derivatives at these points, while \mathbf{P}_i^h , ($i = 1, 2, 3$) are hysteretic vector. Moreover, substituting eqns. (5.36) in eqn. (3.18a), the discretized counterpart of the elastic axial force at the neutral axis of the beam is given as

$$\mathbf{N}^{el} = EA(\mathbf{B}_{,x}^u \mathbf{d}_1) + \frac{I}{2} EA \left[\left[\mathbf{B}_{,xx} \mathbf{d}_2 \right]_{dg.} \left[\mathbf{B}_{,x} \mathbf{d}_2 \right] + \left[\mathbf{B}_{,xx} \mathbf{d}_3 \right]_{dg.} \left[\mathbf{B}_{,x} \mathbf{d}_3 \right] \right] \quad (5.46)$$

Subsequently, the initial conditions of the problem are formulated in discretized form by substituting eqns. (5.39) in eqns. (5.26) yielding the following $3L$ linear equations with respect to the generalized displacements \mathbf{d}_1 , \mathbf{d}_2 , \mathbf{d}_3 and the generalized velocities $\dot{\mathbf{d}}_1$, $\dot{\mathbf{d}}_2$, $\dot{\mathbf{d}}_3$ for $t = 0$ as

$$\mathbf{B}^u \mathbf{d}_1(0) = \bar{\mathbf{u}}_0 \quad \mathbf{B}^u \dot{\mathbf{d}}_1(0) = \dot{\bar{\mathbf{u}}}_0 \quad (5.47a,b)$$

$$\mathbf{B} \mathbf{d}_2(0) = \bar{\mathbf{v}}_0 \quad \mathbf{B} \dot{\mathbf{d}}_2(0) = \dot{\bar{\mathbf{v}}}_0 \quad (5.47c,d)$$

$$\mathbf{B} \mathbf{d}_3(0) = \bar{\mathbf{w}}_0 \quad \mathbf{B} \dot{\mathbf{d}}_3(0) = \dot{\bar{\mathbf{w}}}_0 \quad (5.47e,f)$$

The above equations (5.47a,c,e), together with eqns. (5.29) written for $t = 0$, form a set of $3L + 20$ nonlinear algebraic equations which are solved to establish the initial conditions $\mathbf{d}_1(0)$, $\mathbf{d}_2(0)$, $\mathbf{d}_3(0)$ while similarly equations (5.47b,d,f) together with 12 equations resulting after differentiating eqns. (5.29) with respect to time and writing them for $t = 0$, form a set of $3L + 20$ linear algebraic equations from which the initial conditions $\dot{\mathbf{d}}_1(0)$, $\dot{\mathbf{d}}_2(0)$, $\dot{\mathbf{d}}_3(0)$ are established.

The aforementioned initial conditions along with eqns. (5.29), (5.42) and the evolution eqns. (5.3), (5.12) form an initial value problem of Differential-Algebraic Equations (DAE), which can be solved using any efficient solver. Within the framework of this doctoral dissertation the Petzold Gear Method was used (Brenan et al. 1989) after introducing new variables to reduce the order of the system (Bazant & Cedolin 1991) and after differentiating (5.27) with respect to time to obtain an equivalent system with a value of system index $\text{ind} = 1$.

5.3.2. Dynamic Incremental–Iterative Solution Algorithm

In the framework of this doctoral thesis, a dynamic incremental–iterative solution algorithm has been implemented based on the fibre approach. The governing equations of motion are written in state-space form and a predictor-corrector differential solver based on the Petzold Gear method (Brenan et al. 1989) is adopted. It is worth noting that the standard second order representation of eqn. (5.40) could also be implemented incorporating any Newmark method in conjunction with an incremental–iterative Newton Raphson method for the integration of the equations of motion and the Bouc-Wen evolution equations governing the inelastic behaviour of the beam-foundation system.

5.3.2.1 State-Space Formulation / Fibre Approach

The developed beam formulation follows the displacement-based theory, thus load control (Crisfield 1991) over the time steps is used and load stations are chosen according to load history and convergence requirements. Having evaluated the load vector, the initial conditions as well as all the necessary numerical coefficients the standard second order representation of eqn. (5.40) can be brought into a state-space form, by introducing an auxiliary unknown vector. More specifically,

- i. A number of monitoring cross sections is defined. It is assumed that the monitoring sections coincide with the L nodal points of the beam interval as well as the beams boundaries.
- ii. Since the distribution of the normal stress within the cross section plane is not known in advance, the fibre approach is to be followed (Fig. 5.4) for the integration of the section internal axial force and moments. Therefore, each section is divided into a number of triangular or quadrilateral cells and standard two-dimensional Gauss quadrature rules are employed in each cell to resolve the hysteric parts of the stress resultants N^h , M_y^h , M_z^h . If the same number of Gauss points is employed in every cell, then $N_{dof} = N_{cells} \times N_{Gauss}$ holds. Thus, the monitoring stations of each cross section coincide with the Gauss points of its cells, while exact patch between adjacent cells is not required.
- iii. For a specific dynamic loading and known initial conditions (5.47), at each time step the dynamic differential equation of motion (5.42) and the evolution eqns.

(5.3), (5.12) are written in a system form of first order differential-algebraic equations as follows

$$G(t, Y, \dot{Y}) = 0 \quad (5.48)$$

where the generalized vectors are defined as

$$\{Y\} = \left\{ \underbrace{\mathbf{d}_1}_{L+4} \quad \underbrace{\mathbf{d}_2}_{L+8} \quad \underbrace{\mathbf{d}_3}_{L+8} \quad \underbrace{\dot{\mathbf{d}}_1}_{L+4} \quad \underbrace{\dot{\mathbf{d}}_2}_{L+8} \quad \underbrace{\dot{\mathbf{d}}_3}_{L+8} \quad \underbrace{\mathbf{z}^h}_{N_{dof}} \quad \underbrace{\mathbf{z}_{sy}^h}_L \quad \underbrace{\mathbf{z}_{sz}^h}_L \right\}^T \quad (5.49a)$$

$$\{\dot{Y}\} = \left\{ \underbrace{\dot{\mathbf{d}}_1}_{L+4} \quad \underbrace{\dot{\mathbf{d}}_2}_{L+8} \quad \underbrace{\dot{\mathbf{d}}_3}_{L+8} \quad \underbrace{\ddot{\mathbf{d}}_1}_{L+4} \quad \underbrace{\ddot{\mathbf{d}}_2}_{L+8} \quad \underbrace{\ddot{\mathbf{d}}_3}_{L+8} \quad \underbrace{\dot{\mathbf{z}}^h}_{N_{dof}} \quad \underbrace{\dot{\mathbf{z}}_{sy}^h}_L \quad \underbrace{\dot{\mathbf{z}}_{sz}^h}_L \right\}^T \quad (5.49b)$$

The above system of first order DAEs, is numerically integrated using a predictor-corrector differential solver base on the Petzold Gear method (Brenan et al. 1989). The iteration steps of the algorithm are executed until the dynamic load increment is fully undertaken from the beam-foundation inelastic system or convergence cannot be achieved.

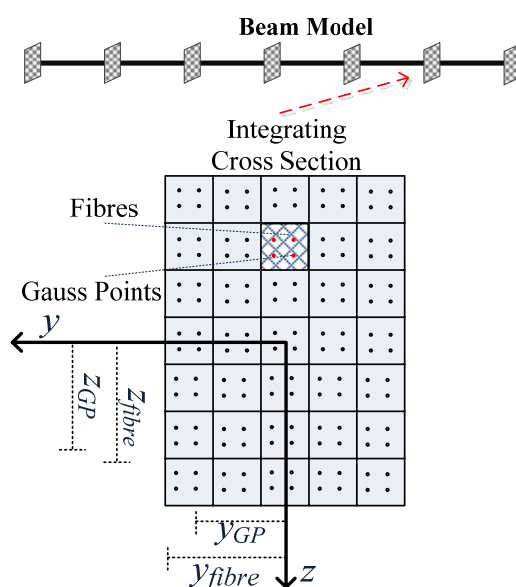


Fig.5.4. Discretization of the beam interval into integration cross sections and discretization of the cross sections into fibres.

- iv. Since convergence is achieved for the specific dynamic load step, then the total stress resultants are evaluated and the displacement and stress components are stored.
- v. The parameters of the problem are updated and the process described by steps (ii)-(iv) is repeated until the total load time history is examined or convergence cannot be achieved which means that the load cannot be fully undertaken (plastic collapse).

A step-by-step algorithmic approach of the nonlinear solution is presented in a flowchart form in Fig. 5.5.

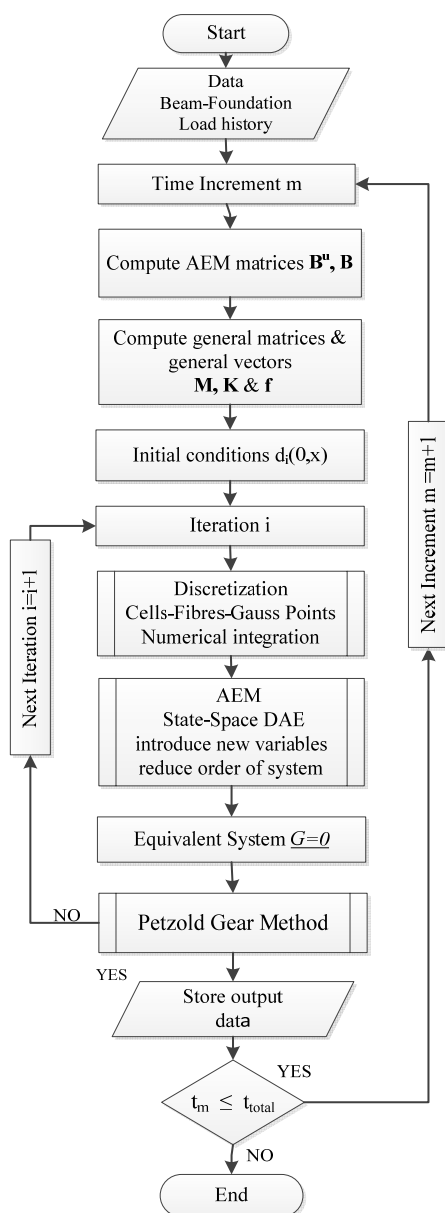


Fig. 5.5. Flowchart of the numerical implementation.

5.4 Numerical Examples

On the basis of the analytical and numerical procedures presented in the previous sections concerning the geometrically nonlinear inelastic analysis of Euler-Bernoulli beams on inelastic foundation, a computer program has been written using High Level 3G Fortran 90/95. Representative examples have been studied to demonstrate the efficiency, wherever possible the accuracy and the range of applications of the developed method.

5.4.1 Example 1 – Dynamic Inelastic Analysis of Cantilever Beam

For comparison purposes, in the first example a cantilever beam of length $l = 1m$ under concentrated tip force P_z , as depicted in Fig. 5.6a has been studied. The beam is made out of structural steel with modulus of elasticity $E = 210 GPa$, hardening ratio $\alpha = 0.002$, yielding stress $\sigma_{y0} = 240 MPa$ and mass density $\rho = 7.85 tn / m^3$. The cross section is assumed rectangular of width $b = 0.05m$ and height $h = 0.1m$, while the hysteretic parameters are considered $\beta = \gamma = 0.5$. For the longitudinal discretization 21 integration sections have been employed, while the cross-section has been discretized into 15 quadrilateral cells with a 2×2 Gauss integration scheme for each cell. The present example was first studied by Triantafyllou and Koumouisis (2012) who presented a hysteretic triangular plane stress element incorporating the Bouc-Wen model.

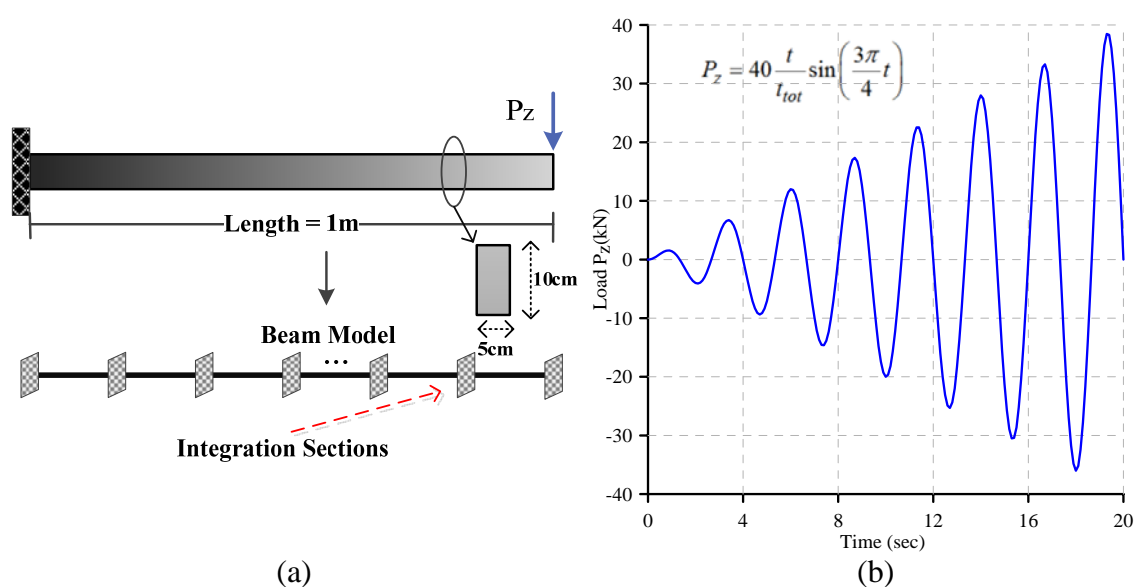


Fig. 5.6. Cantilever beam with tip load (a) applied sinusoidal load time history (b)

At first, the static response of the cantilever is investigated by assuming a monotonically increasing concentrated tip load. In Fig.5.7, the load-displacement curves at the cantilever's tip are presented considering both an elastic-perfectly plastic and a elastoplastic-strain hardening material. In the first case the results are compared with those obtained from Triantafyllou and Koumousis (2012) implementing a sparse mesh of 62 and a dense mesh of 328 hysteretic triangular plane stress element. Additionally, the FEM solution (NX Nastran 2007) obtained by employing 60 nonlinear beam elements and the 3-D FEM solution (NX Nastran 2007) obtained by employing 2560 solid (brick) are also presented. Furthermore, the theoretical values of the initial yield load and the lower bound for the ultimate load evaluated by the following analytical expressions (Lubliner 2008) are also depicted in this figure.

$$P_{yield} = \frac{\sigma_{Y0}bh^2}{6l} = 20kN \quad \text{and} \quad P_{ultimate} = \frac{\sigma_{Y0}bh^2}{4l} = 30kN \quad (5.50)$$

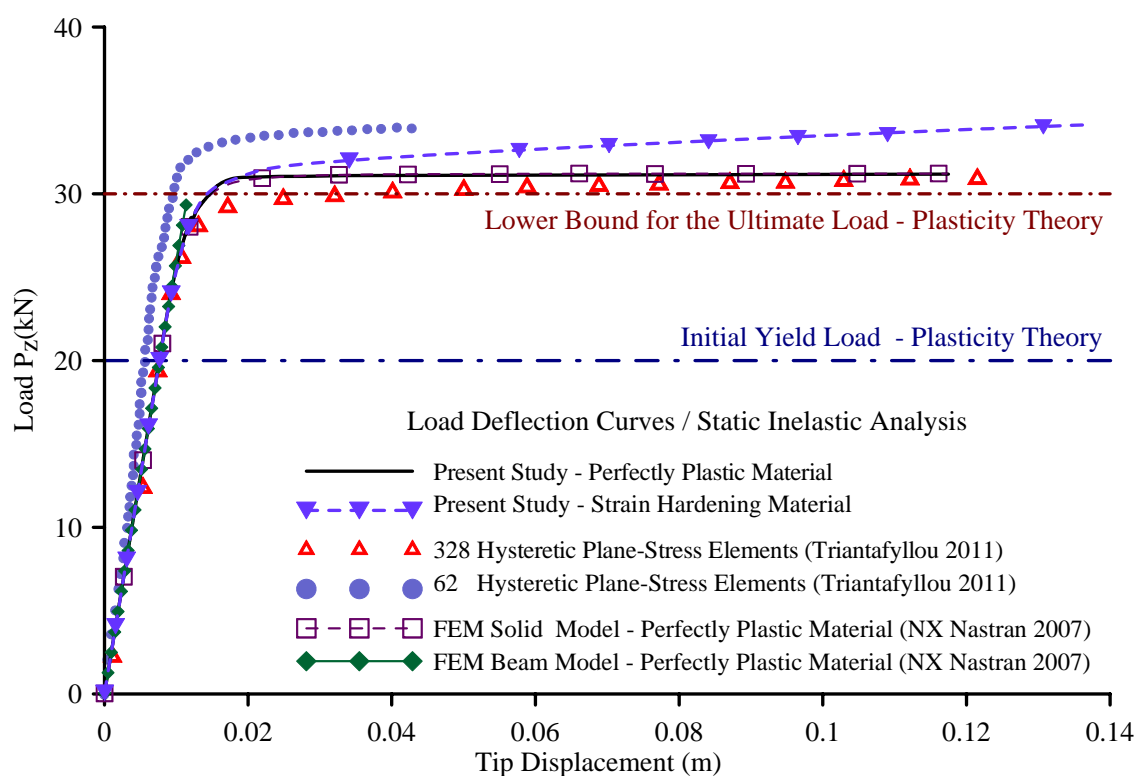


Fig. 5.7. Load–displacement curve at tip of the cantilever beam, of example 1.

Moreover, in Fig. 5.8, the normal stress distribution contour diagram along the beam length is plotted for the stage when the imposed load reaches the theoretically

derived collapse load ($P_z = 30\text{kN}$), as compared with the one obtained from the solid 3-D FEM model. At this stage, the plastic hinge mechanism predicted by plasticity theory is fully formed, as illustrated in this figure.

From the above, it is evident that the proposed beam formulation predicts accurately the nonlinear response of the cantilever in case of a statically imposed load. More specifically, the obtained results are almost identical with those of the solid FEM solution and demonstrate a very good agreement with the hysteric plane stress formulation. It is also worth noting that the implemented finite beam element model fails to capture accurately the nonlinear response and underestimates the collapse load.

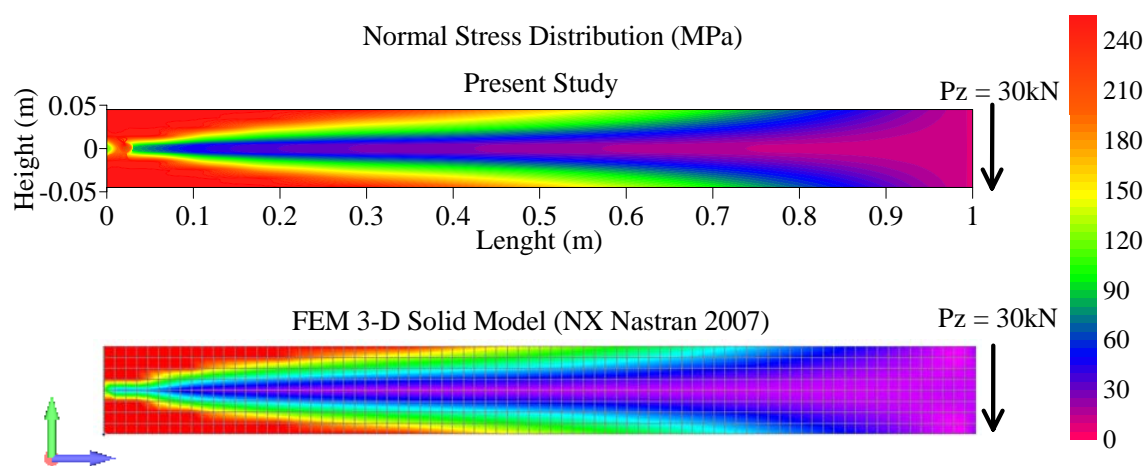


Fig 5.8. Normal stress distribution along the beam length for the theoretically derived collapse load stage, of the cantilever of example 1.

Thereinafter, the dynamic response of the cantilever beam is investigated. Two different load cases are considered namely a sinusoidal excitation of increasing amplitude (*case-a*, Fig. 5.6b) and a constant amplitude impact load (*case-b*) subjected at the tip of the beam. The analytical expressions of the applied time histories are as follow

$$(case-a) \quad P_z(l,t) = 40 \frac{t}{T_{tot}} \sin\left(\frac{3\pi}{4}t\right) \quad \text{for } t \in [0, T_{tot}] \quad (5.51a)$$

$$(case-b) \quad P_z(l,t) = 27\text{kN} \quad \text{for } t \in [0, T_{tot}] \quad (5.51b)$$

In Fig. 5.9 the response of the cantilever is plotted in terms of applied load versus tip displacement for load *case-a*, as compared with the one presented by Triantafyllou and Koumouisis (2012) illustrating excellent agreement. Finally, in Fig. 5.10 the time history of the tip displacement of the cantilever beam is presented for load *case-b*, assuming either elastic or inelastic material behaviour. From the contacted analysis, the accuracy of the proposed formulation is verified and the significant influence of the material nonlinearity is demonstrated.

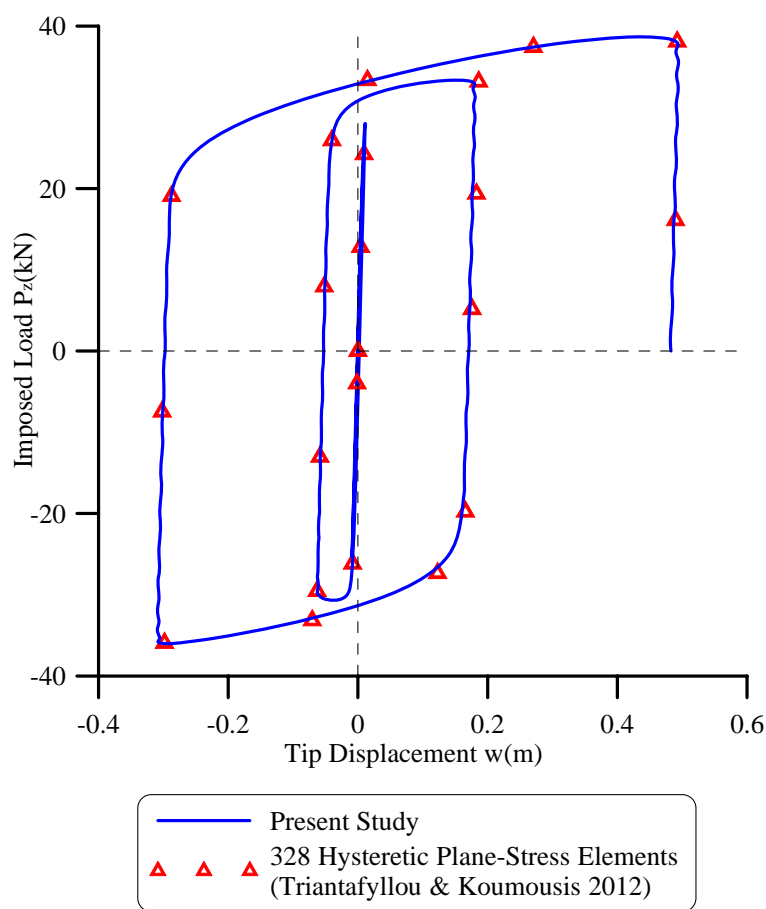


Fig. 5.9. Imposed load vs. tip displacement for sinusoidal excitation of increasing amplitude.

5.4.2 Example 2 – Dynamic Inelastic Analysis of Clamped Beam on Foundation

In order to illustrate the importance of material nonlinearity in the dynamic response of a beam-foundation systems, a rectangular cross-section ($h = 0.60\text{m}$, $b = 0.30\text{m}$) clamped beam of length $l = 6\text{m}$, as shown in Fig. 5.11, has been studied. An elastoplastic-strain

hardening material is considered, with $E = 32318.4MPa$, hardening ratio $\alpha = 0.02$, yielding stress $\sigma_{Y0} = 20MPa$ and mass density $\rho = 2.5tn/m^3$. The beam is supported on perfectly plastic Winkler foundation with initial stiffness $k_z = 20MPa$ and yielding force $P_{zY} = 60kN/m$. For the longitudinal discretization 21 integration sections have been employed, while the cross-section has been discretized into 15 quadrilateral cells with a 2×2 Gauss integration scheme for each cell.

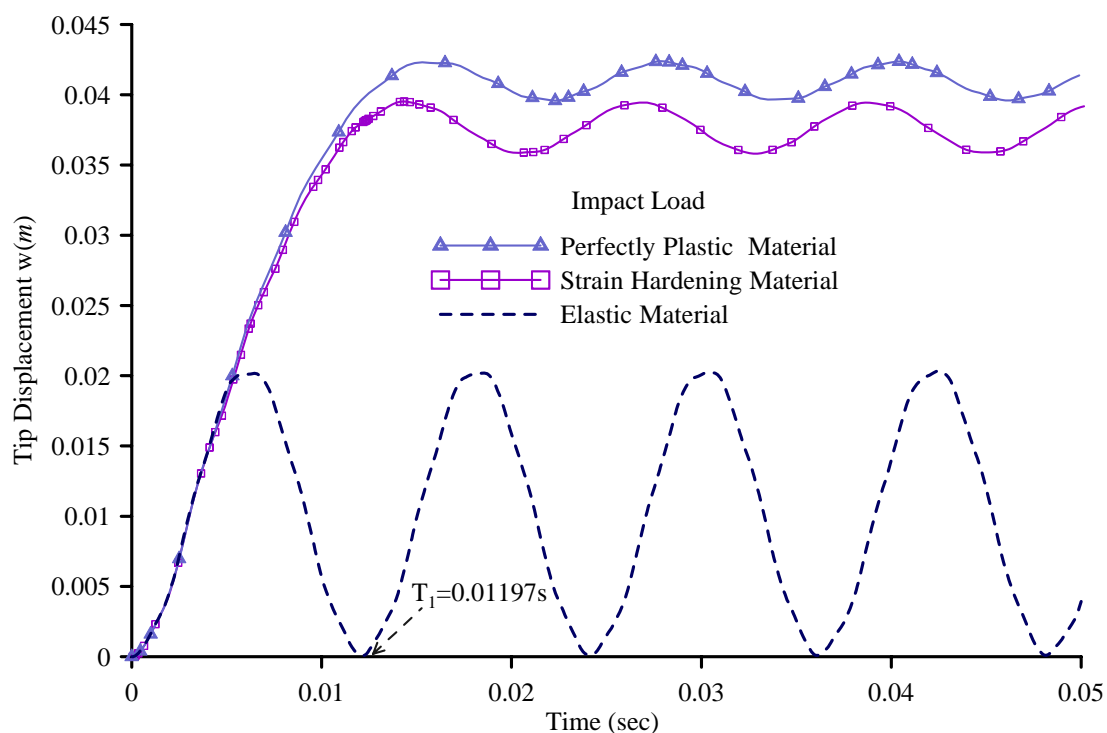


Fig. 5.10. Time history of the cantilever tip of example 1, for impact load.

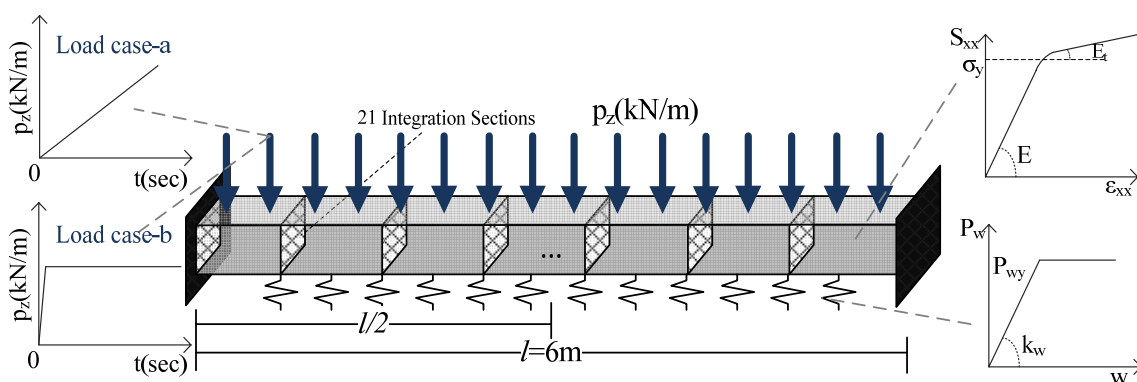


Fig. 5.11. Clamped beam on nonlinear foundation, subjected to uniformly distributed impact load.

Two load cases have been examined. More specifically, the beam is subjected to a “quasi-static” uniformly distributed load $p_z(x,t) = p_{z0}(t/T_{tot})$ for $0 \leq t \leq T_{tot}$ (*case-a*) and subsequently to an impact load $p_z(x,t) = p_{z0}$ for $t \geq T_{tot}$ with $T_{tot} = 0.05$ sec (*case-b*), as depicted in Fig. 5.11.

In Fig. 5.12 the load–displacement curves for load *case-a* are presented for different types of material properties ignoring the foundation reaction, performing either geometric and material nonlinear (GMNL) analysis or material nonlinear (MNL), as compared with those obtained by a 3-D FE model (NX Nastran 2007) employing 8640 solid (brick) elements. From this figure, the accuracy of the proposed formulation is confirmed through the excellent agreement between the compared results. Furthermore, the predominant character of the material nonlinearity is verified while the geometrical nonlinearity is of secondary importance, in this case.

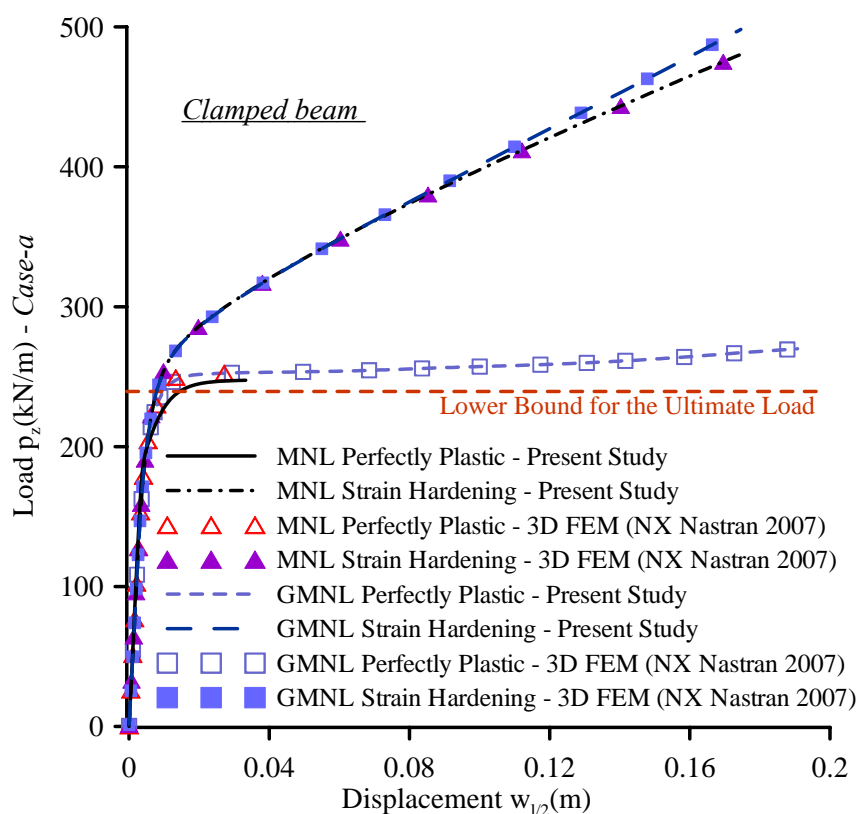


Fig. 5.12. Load–displacement curve at the midpoint of the clamped beam of example 2.

In Figs. 5.13, 5.14 the normal stress distribution along the beam’s length is presented, performing geometrically nonlinear inelastic analysis in case of either perfectly plastic or stain hardening material, respectively. The obtained contour maps

are presented in conjunction with the corresponding deformed 3-D FEM contour configurations, for different load stages (*case-a*). From these figures a very good agreement between the results is observed verifying that the proposed formulation accurately captures the spread of plasticity, while any minor divergence is attributed to the inherent difference between the models. Finally in Fig. 5.15 the number of Gauss points that have excided the yielding limit at the integration sections are presented for perfectly plastic or stain hardening material. From these figures, it is easily concluded that the spread of plasticity is more intense in the strain hardening case.

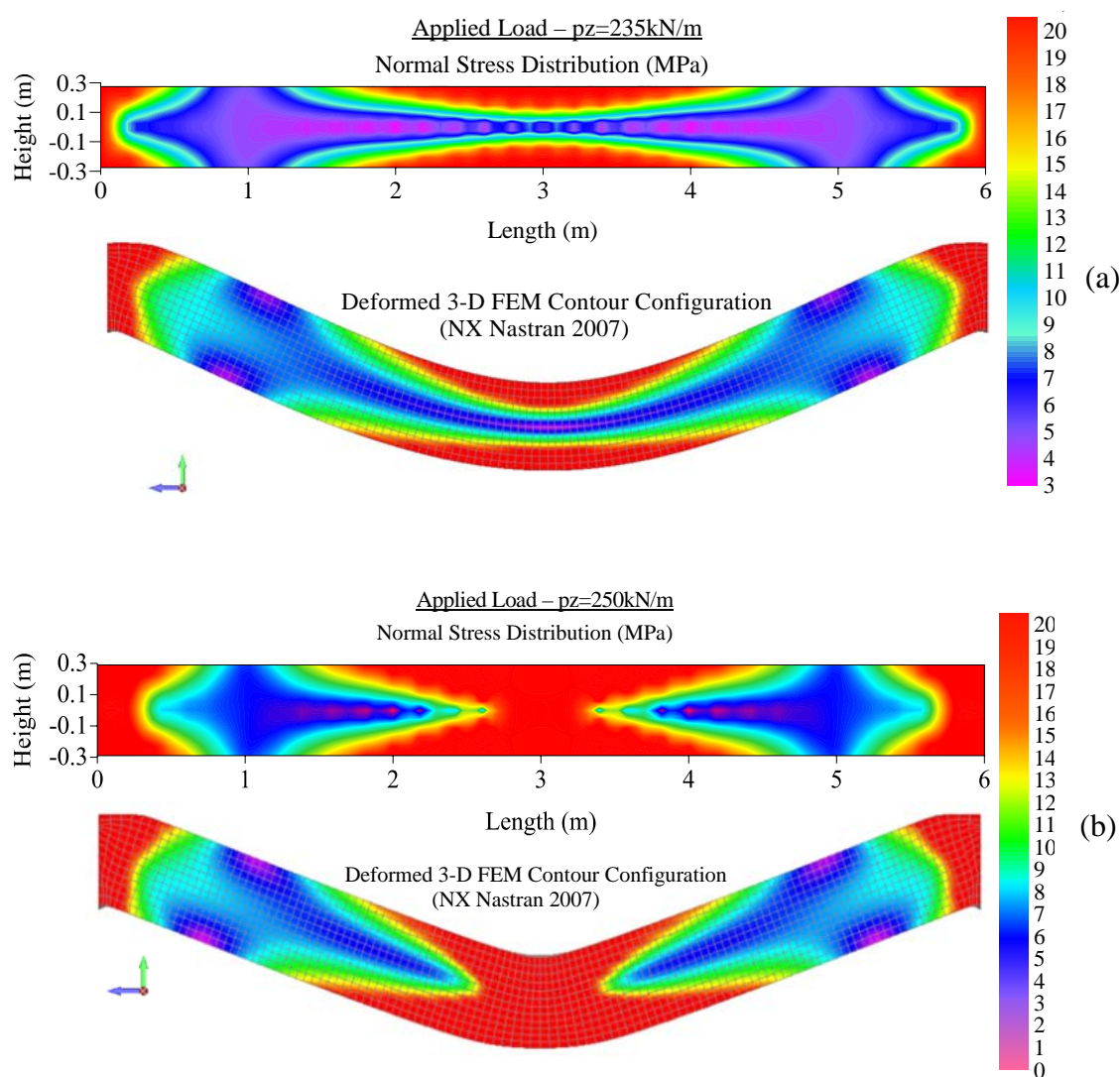


Fig. 5.13. Normal stress distributions along the beam's length, for perfectly plastic material for different load stages compared to the corresponding deformed 3-D FEM contour representations.

Moreover, in Fig. 5.16 the load–displacement curves at the midpoint $w(l/2)$ of the beam on Winkler foundation are depicted, for different types of beam and soil material properties in case of monotonically increasing load (*case-a*). The significant influence of the material nonlinearity to the beam–foundation system response is verified and the importance of the subgrade modelling to the overall behaviour is illustrated. Once again, it is observed that, in this case the geometrical nonlinearity has minor importance compared to the major influence of the material nonlinearity.

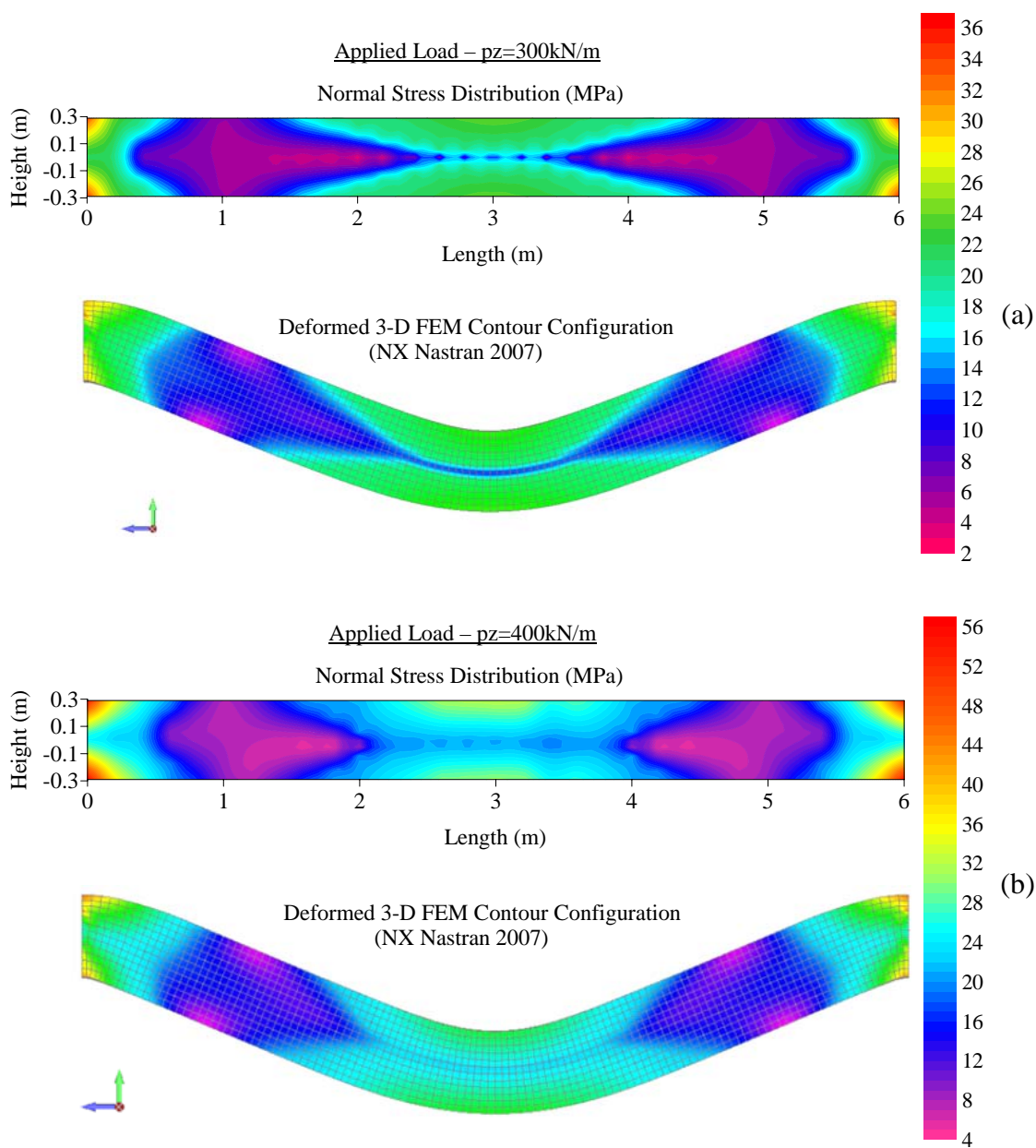


Fig. 5.14. Normal stress distributions along the beam's length, for strain hardening material for different load stages compared to the corresponding deformed 3-D FEM contour representations.

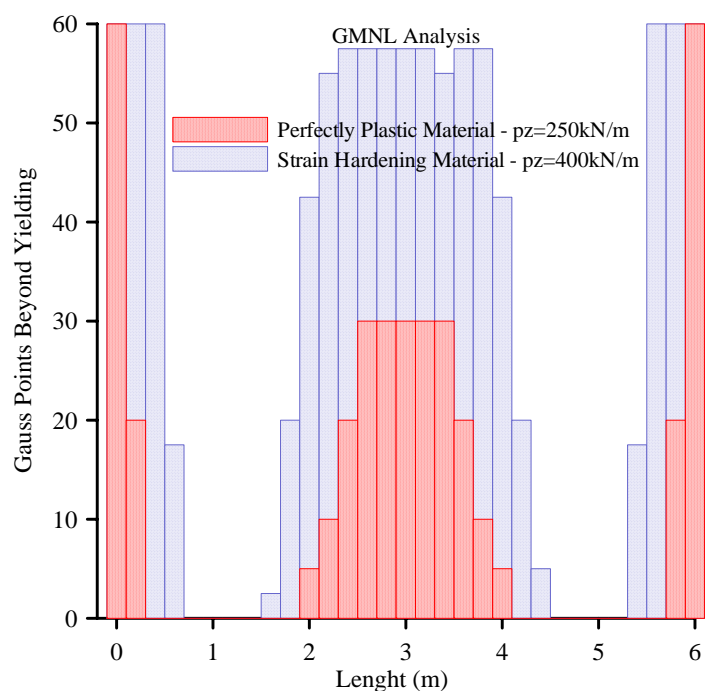


Fig. 5.15. Number of plastified Gauss points at integration sections along the beam of example 2.

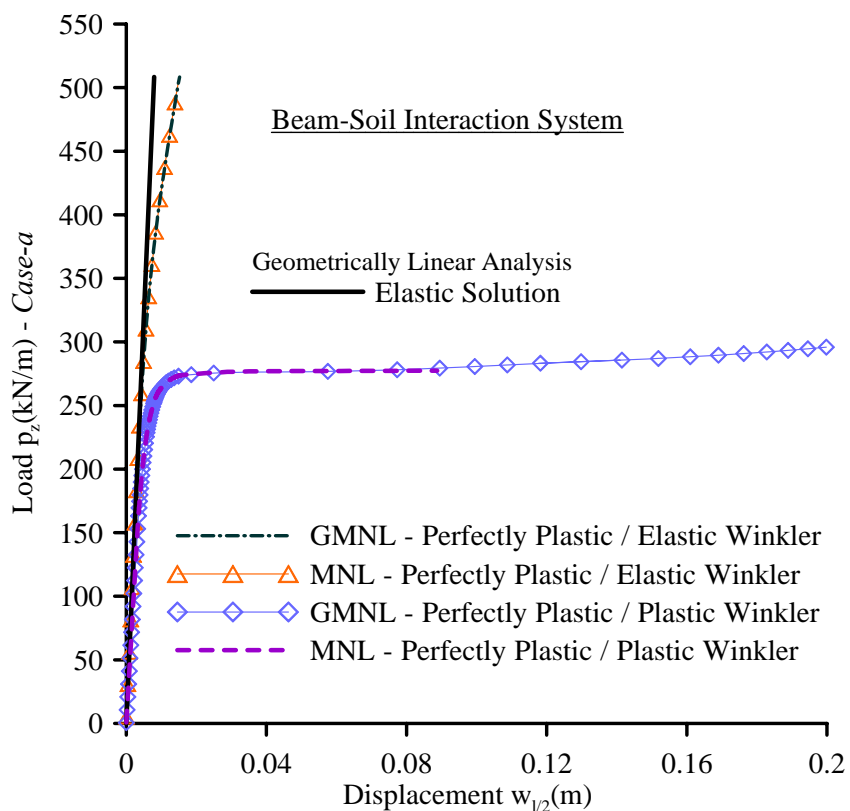


Fig. 5.16. Load–displacement curve at the midpoint of the clamped beam of example 2, resting on nonlinear foundation, for monotonically increasing uniformly distributed load.

Thereafter, validity of the proposed model is further assessed in the case of dynamic response of the beam-foundation system. In Fig. 5.17 the time history of the beam's midpoint displacement $w(t, l/2)$ free of foundation support performing either geometrically linear or nonlinear analysis, is presented for different types of material properties. In this figure the corresponding 3-D FEM solutions are also presented, highlighting the accuracy of the proposed model as well as the profound influence of both material and geometrical nonlinearity in the dynamic response of the system. These effects are also illustrated in Table 5.1, where the maximum values of displacements and normal stresses are presented for three time instants ($t_1 = 0.012$, $t_2 = 0.02$, $t_3 = 0.05 \text{ sec}$) in case of either perfectly plastic or strain hardening material. The importance of geometrical nonlinearity is also depicted in Fig. 5.18 where the time histories of the midpoint $w(t, l/2)$ of the beam are presented performing either geometrically linear or nonlinear analysis, assuming elastic-plastic strain hardening material behaviour. In Figs. 5.19 the normal stress distributions along the beam's length are presented, for three time instants (t_1, t_2, t_3) for the same case of analysis, as compared with the corresponding deformed 3-D FEM contour configurations. From this figure a very good agreement between the results is observed verifying that the proposed formulation accurately captures the spread of plasticity, also in the dynamic analysis.

Table 5.1. Maximum displacement w and normal stress S_{xx} of the beam of example 2, for different time instants (case-b).

Analysis	Geometrically Linear		Geometrically Nonlinear	
	$Max S_{xx} (kPa)$	$w(l/2) (cm)$	$Max S_{xx} (kPa)$	$w(l/2) (cm)$
Strain Hardening				
Time t_1	23542.1	1.1062	23546.7	1.08
Time t_2	15587.5	0.8276	16624.9	0.756
Time t_3	18487.1	1.0936	21178.5	0.909
Perfectly Plastic				
Time t_1	20000	1.0984	20000	1.1596
Time t_2	16328.2	1.0752	17426.9	1.0601
Time t_3	17005.9	1.155	19803.6	1.1176

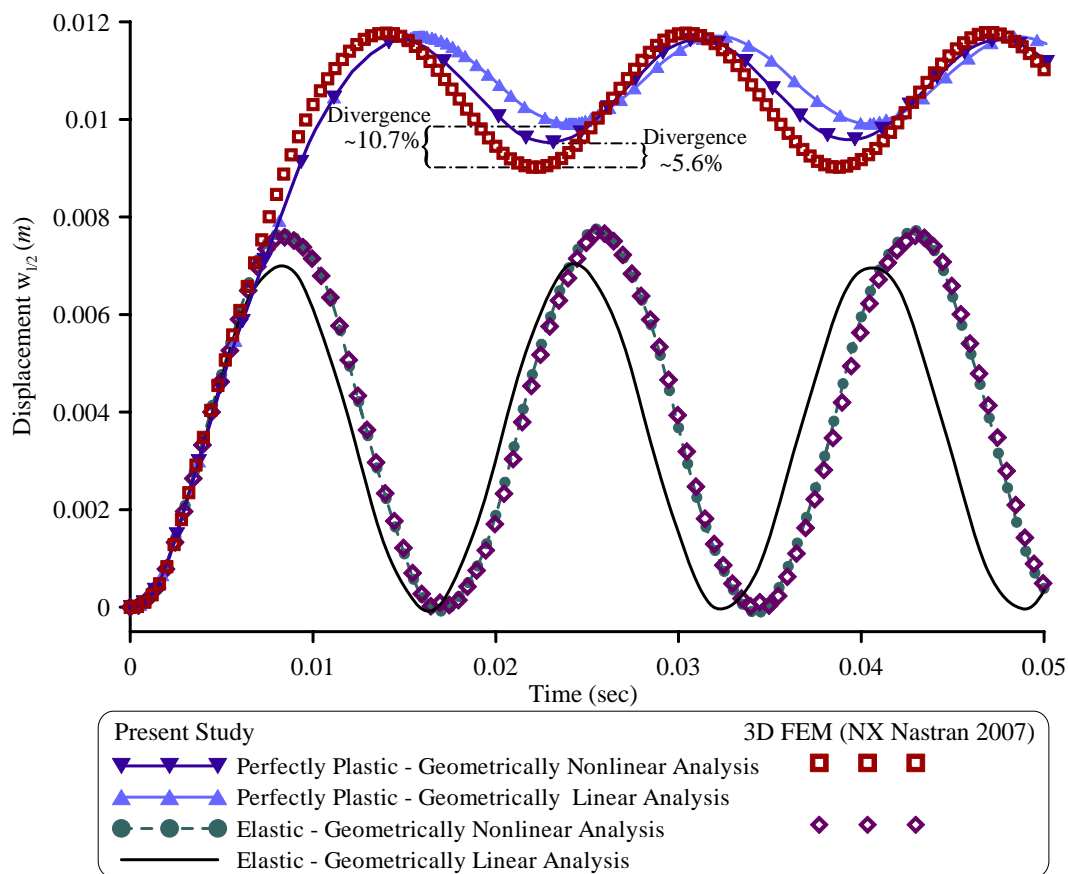


Fig. 5.17. Midpoint time history of the beam of example 2, for impact load (case-b).

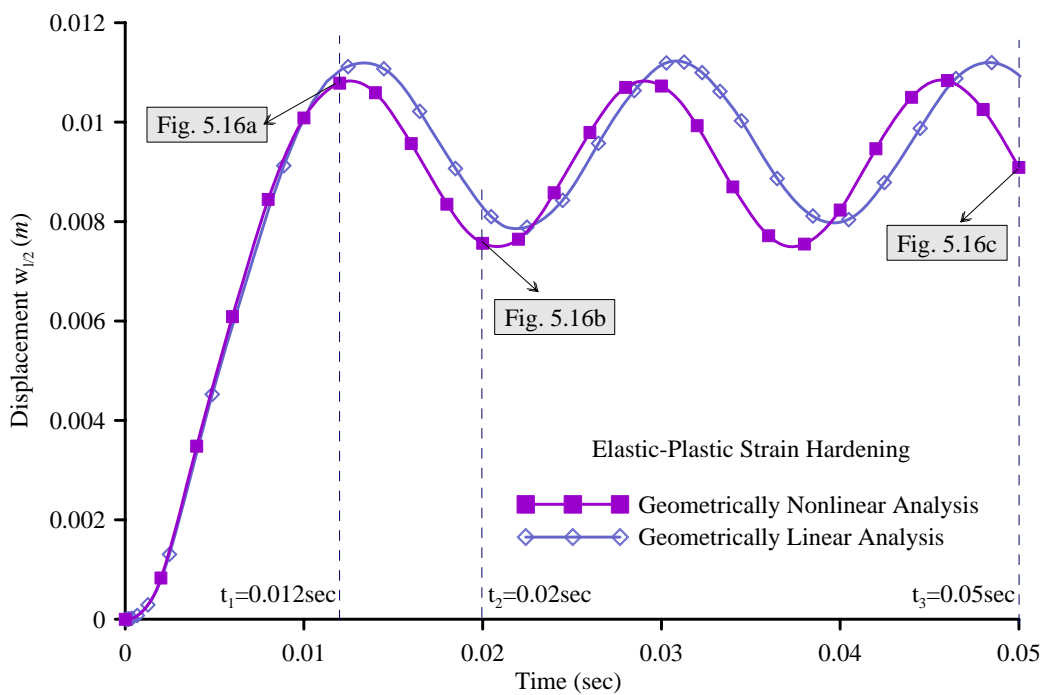


Fig. 5.18. Midpoint time history of the beam of example 2, for impact load (case-b) assuming elastic-plastic strain hardening material.

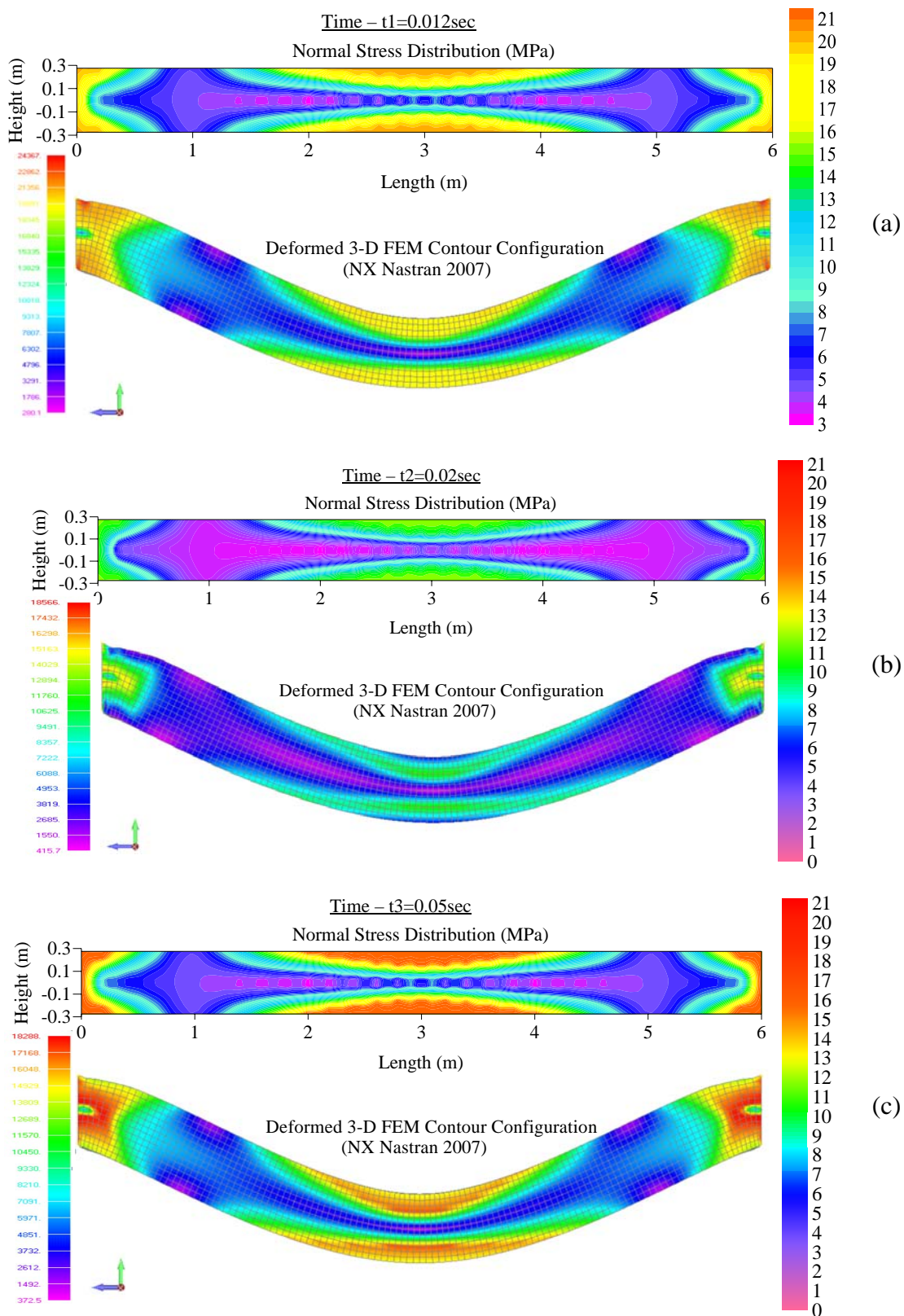


Fig. 5.19. Normal stress distributions along the beam's length, for strain hardening material for different time instants compared to the corresponding deformed 3-D FEM contour representations.

Finally, in Fig. 5.20 the time history at the midpoint $w(t, l/2)$ of the beam on Winkler foundation is presented, for different types of beam and soil material properties in case of impact load (*case-b*). The profound influence of material nonlinearity in the geometrically nonlinear dynamic response of the system is once again verified, as well as importance of the subgrade modelling to the overall dynamic behaviour of the system.

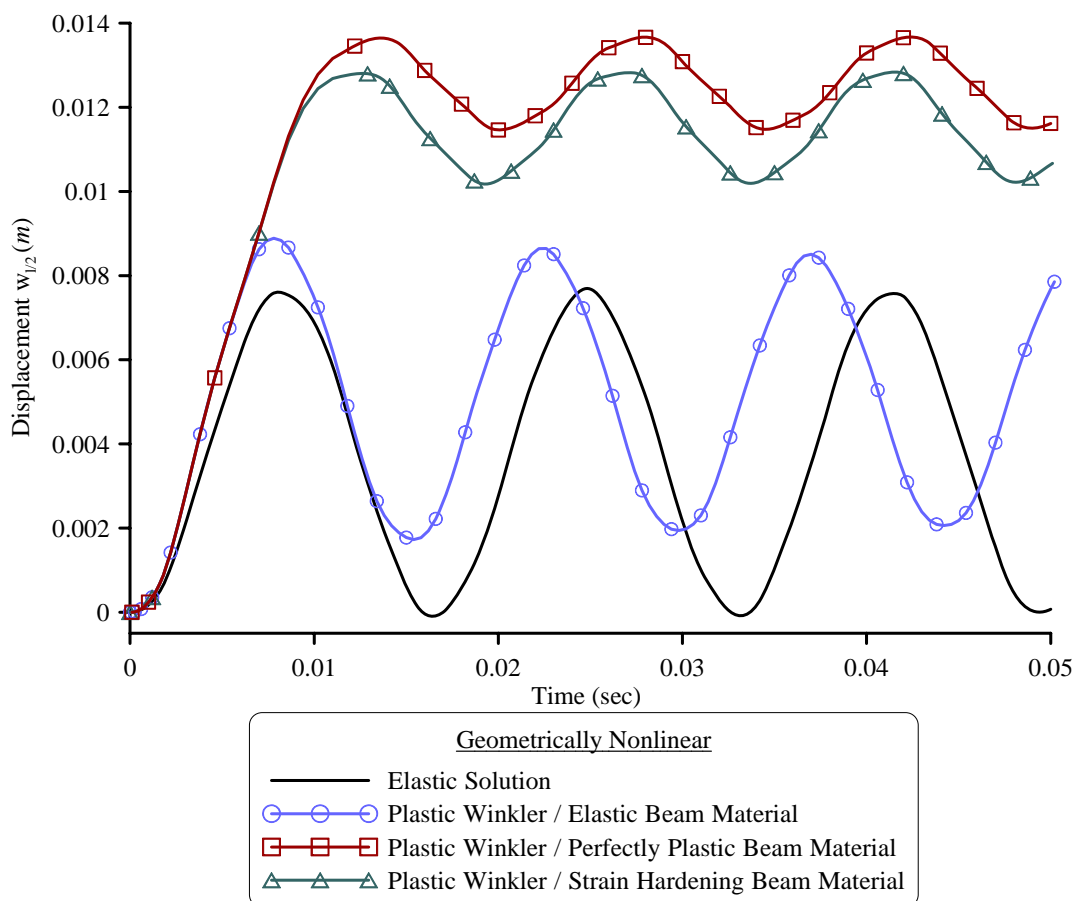


Fig. 5.20. Midpoint time history of the beam example 2, resting on nonlinear foundation for impact load (*case-b*).

5.4.3 Example 3 – I-Beam on Nonlinear Foundation

In this final numerical application, an I-shaped cross section (total height $h = 0.3m$, total width $b = 0.3m$, flange width $t_f = 0.02m$, web width $t_w = 0.01m$) fixed-pinned beam ($E = 213.4GPa$, $\sigma_{Y0} = 285MPa$) of length $l = 8m$ resting on an elastic-plastic Winkler foundation ($k_z = 25MPa$, $P_{zY} = 100kN/m$, $a_{sz} = 0.05$) has been studied,

employing 20 integration sections, 43 quadrilateral cells (15 fibres) and a 3×3 Gauss integration scheme for each cell (cross sectional discretization). The computational model implemented in the proposed formulation is presented in Fig. 5.21a. The beam is subjected to a uniformly distributed impact load $p_z(x,t) = p_{z0}$ for $t \geq T_{tot}$ with $T_{tot} = 0.2 \text{ sec}$.

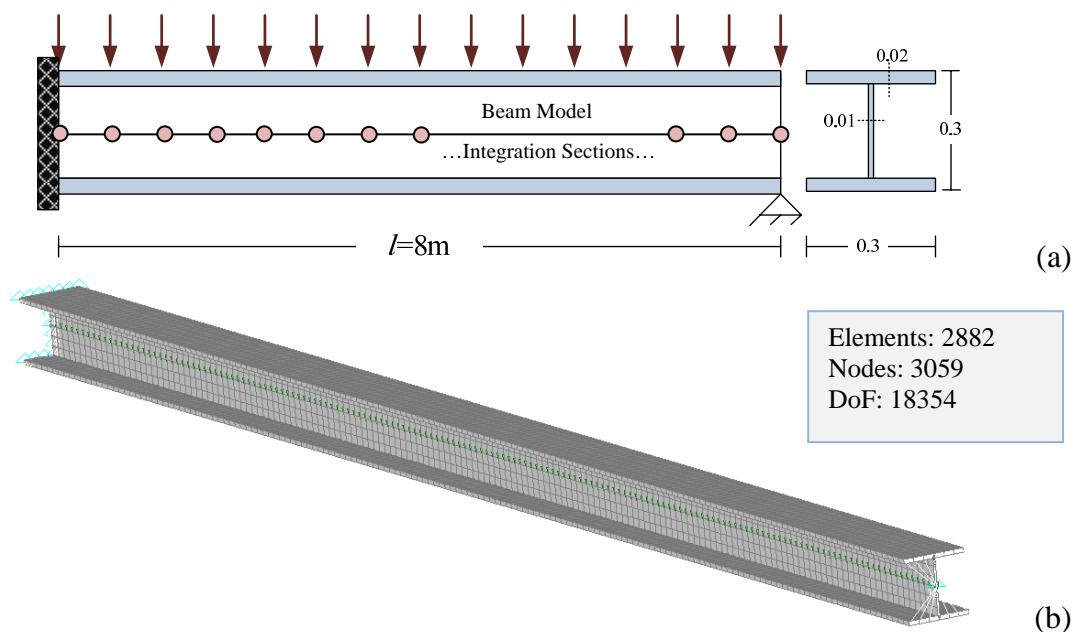


Fig. 5.21. Fixed pinned beam subjected to a uniformly distributed loading (a) and shell model implemented in NX Nastran (2007) (b).

At first, the static response of the beam-foundation system is investigated by assuming a monotonically increasing uniformly distributed load. In Figs. 5.22 the load-displacement curves are presented for different types of beam material properties ignoring the foundation reaction, as compared with a FEM solution (NX Nastran 2007) obtained by employing 2882 quadrilateral shell elements (Fig. 5.21b). Excellent agreement between the results is observed, verifying once again the accuracy and efficiency of the proposed formulation. More specifically, the initial yielding load and the ultimate load are accurately captured, as well as the load path in cases of hardening and large displacements analysis. Moreover, in Figs. 5.23 the load-displacement curves are presented for different types of beam and soil material properties. From these figures, the profound influence of both the geometrical and the material nonlinearity to the response of the beam-soil interaction systems is illustrated.

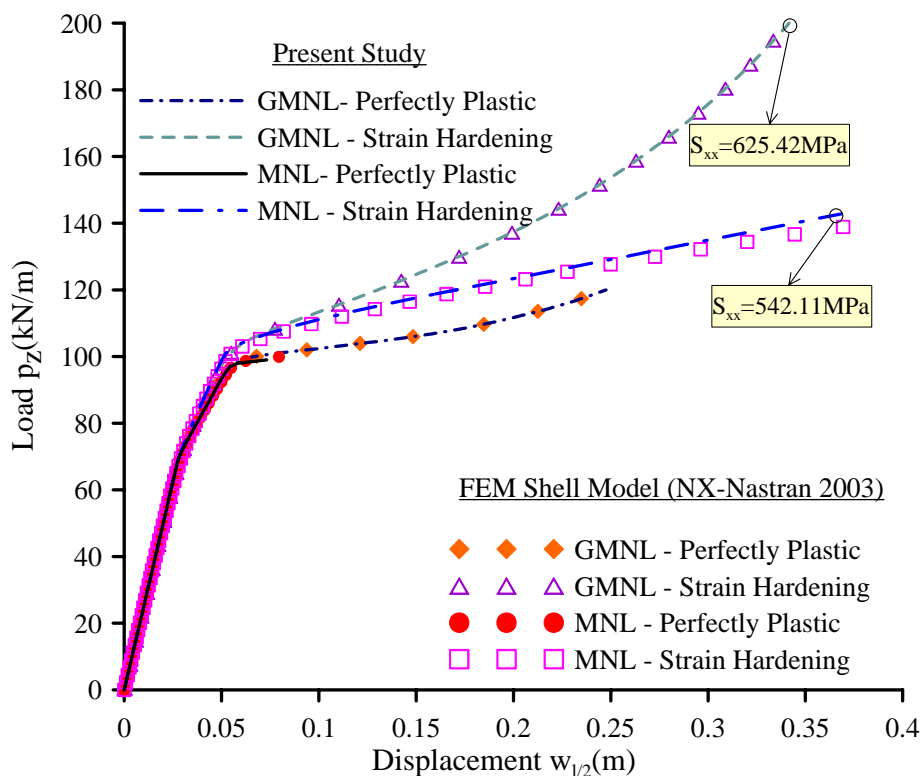


Fig. 5.22. Load–displacement curve of the beam of example 3, for monotonically increasing uniformly distributed load.

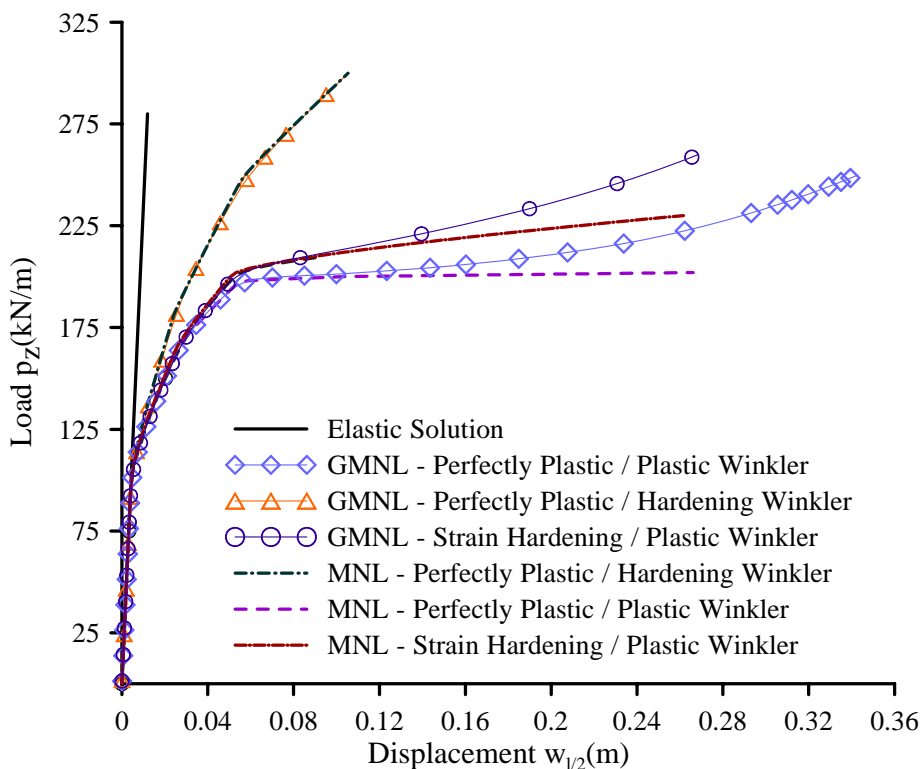


Fig. 5.23. Load–displacement curve of the beam of example 5 resting on nonlinear foundation, for monotonically increasing uniformly distributed load.

Thereinafter, the dynamic response of the system is investigated. In Fig. 5.24 the time history of the beam's midpoint displacement $w(t, l/2)$ free of foundation support performing either geometrically linear or nonlinear analysis, is presented for different types of material properties. In this figure the corresponding shell FEM solutions are also presented, highlighting the accuracy of the proposed model as well as the profound influence of both material and geometrical nonlinearity in the dynamic response of the beam. These effects are also illustrated in Table 5.2, where the maximum values of displacements and normal stresses are presented for three time instants ($t_1 = 0.05$, $t_2 = 0.1$, $t_3 = 0.2 \text{ sec}$) in the cases of elastic, perfectly plastic and strain hardening material. Moreover, in Fig. 5.25 the time history at the midpoint $w(t, l/2)$ of the beam on Winkler foundation is presented, for different types of beam and soil material properties. From this figure it is concluded that the dynamic response of the system is mainly affected by the inelasticity of the foundation elements. That implies that the subgrade modelling is of great importance to the overall dynamic behaviour of the system.

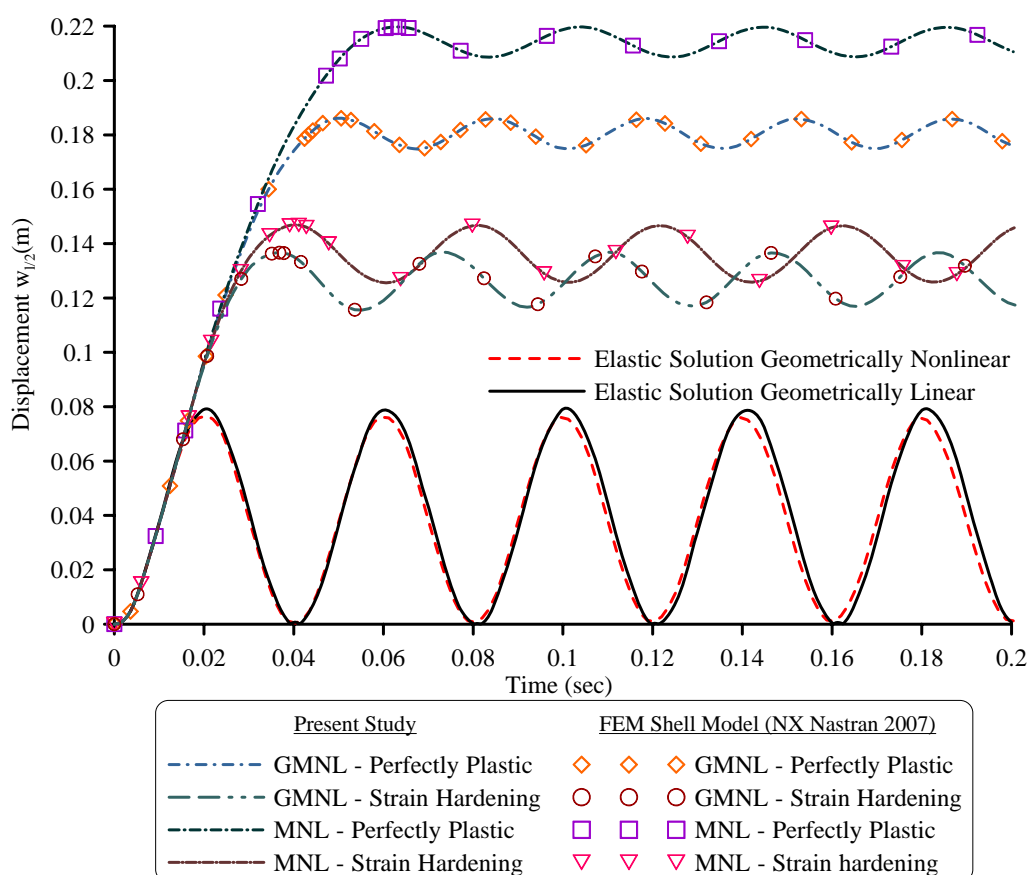


Fig. 5.24. Midpoint time history of the beam example 3, for impact load.

Table 5.2. Maximum displacement w and normal stress S_{xx} of the beam of example 3, for different time instants (case-b).

Analysis	Geometrically Linear		Geometrically Nonlinear	
	$Max S_{xx}$ (kPa)	$w(l/2)$ (cm)	$Max S_{xx}$ (kPa)	$w(l/2)$ (cm)
Elastic				
Time t_1	–	3.79	–	3.86
Time t_2	–	8.17	–	7.82
Time t_3	–	0.11	–	0.18
Perfectly Plastic				
Time t_1	285000	22.32	285000	19.75
Time t_2	284571	23.40	285000	18.61
Time t_3	281326	22.53	280148	18.77
Strain Hardening				
Time t_1	285987	14.24	253276	1242
Time t_2	258174	13.27	298977	1326
Time t_3	401548	15.43	255073	12.31

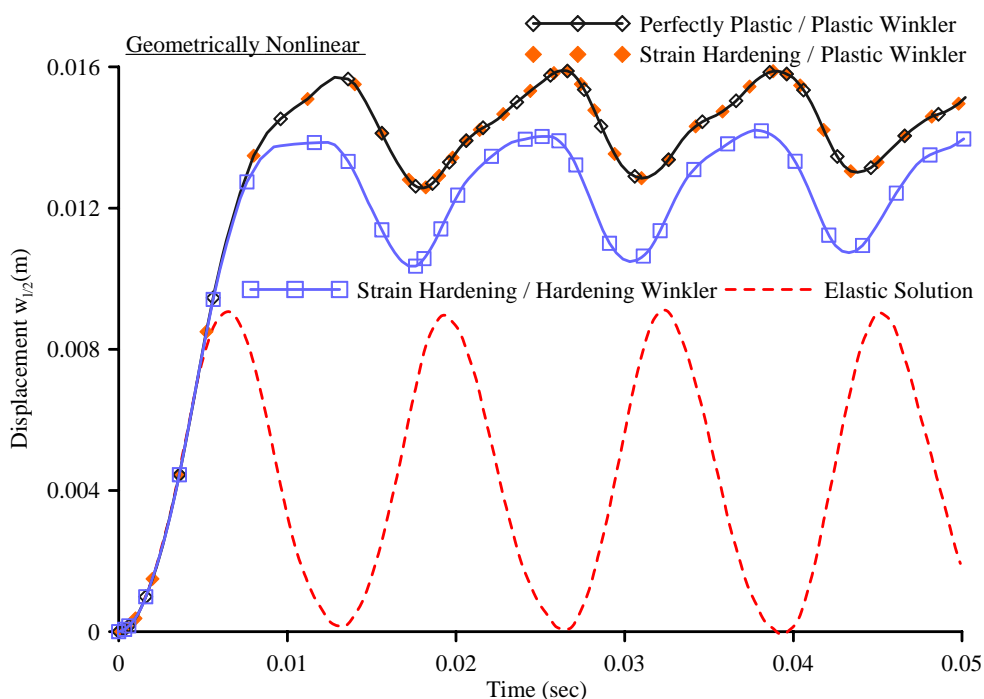


Fig. 5.25. Midpoint time history of the beam of example 3 resting on nonlinear foundation, for impact load.

5.5 Concluding Remarks

In this chapter, a Boundary Element Method is developed for the geometrically nonlinear inelastic analysis of Euler-Bernoulli beams of arbitrary doubly symmetric simply or multiply connected constant cross-section, resting on inelastic Winkler foundation. A hysteretic Bouc-Wen force-displacement model is employed in order to describe the inelastic behaviour of the Winkler springs. A displacement based formulation is developed and inelastic redistribution is modelled through a distributed plasticity (fibre) approach. A uniaxial hysteretic law is considered for the evolution of the plastic part of the normal stress following the Sivaselvan and Reinhorn (2003) model. Numerical integration over the cross sections is performed in order to resolve the hysteric parts of the stress resultants. Application of the boundary element technique yields a system of nonlinear Differential-Algebraic Equations which are written in state-space form and solved together with the hysteretic evolution equations. The main conclusions that can be drawn from this investigation are

- i. The proposed beam formulation is capable of yielding results of high accuracy, as verified by comparing with analytical and FEM results, with minimum computational cost, providing a simple and efficient computational tool for the geometrically nonlinear dynamic inelastic analysis of beam-foundation systems.
- ii. The significant influence of material nonlinearity in the dynamic response of the system is demonstrated through the significant discrepancy between the results of the elastic and inelastic analyses.
- iii. The proposed model accurately captures both, the initial yielding and the ultimate (collapse) load in cases of statically imposed loading.
- iv. The normal stress distribution and the regions of the developed plastic hinges are precisely described throughout the dynamic response.
- v. The influence of geometrical nonlinearity is illustrated through the significant discrepancy between the results of the linear and the nonlinear analyses.
- vi. The significant influence of the inelastic character of the foundation is also demonstrated.
- vii. A small number of cells (fibres) is required in order to achieve satisfactory convergence.

- viii. The developed procedure retains most of the advantages of a BEM solution while requiring a small number of nodal points to achieve high accuracy.
- ix. The use of BEM enables the accurate calculation of the stress resultants which are very important during both the analysis and the design of beam-foundation systems.

Conclusions and Future Research

6.1 Concluding Remarks

In this dissertation, a series of problems concerning the geometric and material nonlinear analysis of beam-soil interaction systems have been studied and solved. The main issues investigated are the following:

- The geometrically nonlinear static analysis of shear deformable beams on nonlinear foundation
- The geometrically nonlinear dynamic analysis of shear deformable beams on nonlinear foundation
- The geometrically nonlinear inelastic analysis of shear deformable beams on inelastic foundation
- The geometrically nonlinear dynamic inelastic analysis of beam-soil interaction systems

For the solution of the examined issues, innovative methods have been formulated and novel beam element models have been developed. These models are based on the Boundary Element Method (BEM) while the respective boundary-value and the initial-value problems are solved numerically employing the Analog Equation Method (AEM) as well as the Domain Boundary Element Method (D-BEM). The main conclusions that can be drawn from this doctoral dissertation are

- i. The proposed beam formulation is verified in terms of accuracy through comparison with various analytical, semi-analytical, FEM and experimental results.
- ii. The efficiency of the presented computational tool is also assessed via comparisons with refined shell and solid models implemented in commercial FE codes. The obtained results were in excellent agreement with those from the

sophisticate models, indicating the advantageous character of the beam approach in terms of computational cost, reliability and modelling.

- iii. The development of plastic deformations reduces the flexural rigidity of the beam and eventually leads to plastic collapse in case of geometrically linear analysis.
- iv. The fibre based beam element formulation is proved suitable for the capacity assessment of frame members, overcoming the well documented restrictions of the concentrated plasticity formulations.
- v. The proposed distributed plasticity model accurately captures both, the initial yielding and the ultimate (collapse) load in cases of statically imposed, cycling and dynamic loading., while the significant influence of material nonlinearity in the response of the beam-soil interaction system is demonstrated through the significant discrepancy between the results of the elastic and inelastic analyses.
- vi. The normal stress distribution and the regions of the developed plastic hinges are precisely described, while a small number of fibres is required in order to achieve satisfactory convergence.
- vii. The influence of geometrical nonlinearity is illustrated through the significant discrepancy between the results of small and large displacement assumptions, in almost all cases of analysis.
- viii. The kinematical components of an elastic beam under primary resonance are bounded due to the developed axial force resulting from the large displacement assumption (i.e. retaining the square of the slope in the strain–displacement relations). The response of both the kinematical components and the stress resultants is characterized by the beating phenomenon. It is worth noting that such phenomena cannot be described by the linearized second-order analysis.
- ix. The geometrical nonlinearity increases the flexural rigidity of the beam. Especially in case of inelastic analysis the arising axial force, either from the imposed axial loading or from the axially restraining boundary conditions, prevents the plastic collapse of the beam.
- x. The geometrical nonlinearity influences significantly the natural frequencies of an elastic beam, while the coupling effects of bending and shear deformations along the member as well as the shear forces along the span induced by the applied axial loading influences the response system.

- xi. The axial-shear-flexure interaction is proved to have paramount importance in the inelastic static analysis (J2 three-dimensional plasticity) either under small or large displacement assumption.
- xii. The shear deformation effect reduces the flexural stiffness of the beam, while results in larger transverse displacements and lower predicted eigen-frequencies for a given set of boundary conditions.
- xiii. The superiority of the Timoshenko beam formulation over the Euler-Bernoulli is verified, especially for low beam slenderness, by yielding results closer to those of refined shell and three-dimensional FE models.
- xiv. Shear-locking has been successfully eliminated, while the added shear mechanism alters significantly the dynamic characteristics of the elastic beam-soil interaction system.
- xv. The significant influence of the inelastic character of the foundation to the response of the beam-soil interaction system is demonstrated.
- xvi. The lift up of the beam caused by the tensionless (unilateral) character of the foundation is observed, leading to significantly different response compared to the bilateral one. This influence is magnified under dynamical excitations.
- xvii. In the elastic analysis, the response of the beam is strongly influenced by the linear and nonlinear parameters of the foundation reaction, while the damping coefficient is of paramount importance as it bounds the vibration amplitude.
- xviii. The versatility of the proposed formulation is also verified since several phenomena can be easily incorporated into the analysis (i.e. kinematic and inertial interaction), while the soil nonlinearity can be taken under consideration by means of several hybrid spring configurations (i.e. Winkler, Pasternak, three-Parameter, p - y spring in series to Kelvin–Voigt element, phenomenological springs, etc.)
- xix. The developed procedure retains most of the advantages of a BEM solution while requiring a small number of nodal points to achieve high accuracy.
- xx. The use of BEM enables the accurate computation of the derivatives of the field functions (e.g. stresses, stress resultants) which is very important during the analysis and the design of beam-foundation systems.

6.2 Future Research

This doctoral dissertation consist a contribution to the geometric and material nonlinear analysis of beam-soil interaction systems. The following are research directions that will further improve the presented work and will provide even better understanding of the influence of nonlinear phenomena to the beam-soil systems behaviour.

- i. The geometrically nonlinear inelastic analysis of beam-soil interaction systems presented in this work can be extended in order to take explicitly into account the axial-shear-flexural (J2 plasticity) interaction.
- ii. Incorporation of shear warping functions for the accurate shear stress distribution along the cross-section into the proposed computational tool.
- iii. The fibre beam formulation for the inelastic analysis can be further improved by incorporating kinematic hardening though the adopted hysteretic model.
- iv. As the fibre beam formulation is suitable for multi-phenomena analysis, the developed model can de further improved by embodying torsion and distortional warping in the large displacement regime.
- v. The springs' configuration describing the inelastic behaviour of the soil medium can be enriched by utilizing more sophisticated spring-dashpot formulations (i.e. BWGG) where the separation of the beam from the soil, the radiation damping and the degradation phenomena are taken under consideration.
- vi. The formulation presented in this dissertation can be extended to beams of composite cross-section.
- vii. Formulation of a finite beam-element for the study of structures, which will incorporate the phenomena, investigated in this dissertation as well as the future research directions.

Appendix A1

AEM for Ordinary Differential Equations of the 2nd and 4th Order

A1.1 Introduction

Several boundary value problems, formulated in this doctoral thesis, have been solved employing the Analog Equation Method (AEM). This method has been developed by Katsikadelis (1994, 2002b) and is based on the well known Boundary Element Method (BEM). AEM is capable of dealing with either linear or nonlinear, static or dynamic boundary value problems with constant or variable coefficients, subjected to either linear or nonlinear boundary conditions, overcoming the drawbacks of BEM.

Contrary to the numerical methods based on domain discretization like the Finite Element Method (FEM) or the Finite Difference Method (FDM), the BEM requires only boundary discretization, thereby reducing the dimensionality of the problem by one order. Thus, the discretization procedure is simplified while the number of unknowns is significantly reduced. Yet another important advantage of this method is its efficiency in determining accurately the derivatives of the field functions, which are the unknowns of the problem, as it does not require the use of shape functions, while it allows evaluation of the solution and its derivatives at any point of the domain of the problem and at any time instant (Hartmann 1989, Hartmann & Katz 2007, Katsikadelis 2002b).

Nevertheless, BEM is not free from drawbacks. At its current stage of development, this numerical method requires the determination of the *fundamental solution* (or Green's function), thereby it cannot be used to problems for which Green's functions are either unknown or cannot be calculated. Thus, it is not applicable to non-linear static or dynamic problems for which the principle of superposition is not valid. A further disadvantage is that typically boundary element formulations give rise to fully populated and non-symmetric matrices. This means that the storage requirements and computational time tend to grow, especially in large scale problems.

During the last years, intense research has been conducted in an effort to overcome these disadvantages (Yu et al. 2010). Most of the new developments in BEM aim at

dealing with complicated nonlinear time-dependent problems or linear problems for which the fundamental solution is not known; thereby the resulting integral solution involves domain integrals (Brebbia 2010). The most efficient techniques that successfully overcome most of the difficulties and at the same time preserve the pure boundary character of BEM are the Dual Reciprocity Method (DRM) (Kontoni et al 1991, Partridge et al 1992), which is a general technique for converting domain integrals to the boundary, and the Analog Equation Method (Katsikadelis 1994, Katsikadelis 2002b). The latter is a generally applicable boundary method for solving nonlinear static and dynamic problems in continuum mechanics; alleviated from the restrictions characterizing the DRM.

AEM (Katsikadelis 1994) is based on a simple concept, according to which the linear or nonlinear problem is replaced by an equivalent simple linear one under a fictitious source with the same boundary and initial conditions. The substitute problem is chosen so that the integral representation of the solution is known and it is solved using BEM. The numerical implementation of AEM involves domain discretization, altering the pure boundary character of the method. However, it is noted that domain discretization is employed only for the calculation of the domain integrals rather than the discretization of the continuum, as in the Finite Element Method. Thus, contrary to other domain methods, neither the concurrence of the internal nodes nor the continuity conditions between the elements are required. Lately, important developments have been achieved regarding AEM. Katsikadelis and Tsiatas (2003) presented a boundary-only method, in the sense that the discretization and integration are limited only to the boundary, in which the fictitious loads are represented by Radial Basis Function (RBF) series. Even though the method maintains all the advantages of the pure BEM, additional parameters are imposed due to the RBFs, which are not easily evaluated (Katsikadelis 2008, Babouskos 2011). Finally, a new purely meshless method for solving elliptic partial differential equations based on the analog equation principle (MAEM) is presented by Katsikadelis (2009).

In this appendix, the main principles of AEM in its general form are presented, in case of one-dimensional boundary value problems described by ordinary differential equations of the 2nd and 4th order, under the most general boundary conditions. It is noted that the governing equations as well as the boundary conditions of the problem can be either linear or nonlinear.

A1.2 Main Concepts of the Analog Equation Method

The main concept of the Analog Equation Method can be mathematically represented as follows: Consider the boundary value problem

$$N(u) = g(\mathbf{x}), \quad \mathbf{x} \in \Omega \quad (\text{A1.1a})$$

$$B(u) = \bar{g}(\mathbf{x}), \quad \mathbf{x} \in \Gamma \quad (\text{A1.1b})$$

where $N(\cdot)$, $B(\cdot)$ are in general nonlinear differential operators with constant or variable coefficients, $g(\mathbf{x})$ is a source or an external loading function of known distribution and $u = u(\mathbf{x})$ is the sought solution of the problem. Consider $N^*(\cdot)$ being a linear or nonlinear differential operator of the same order with N . By applying this operator to the solution of the problem $u(\mathbf{x})$, yields

$$N^*(u) = q(\mathbf{x}), \quad \mathbf{x} \in \Omega \quad (\text{A1.2})$$

where $q(\mathbf{x})$ is an unknown source density function. Eqn. (A1.2) is called *analog equation* of the initial problem and in combination with the boundary conditions (A1.1b) indicates that the solution of the original problem could be obtained, provided that the source density function $q(\mathbf{x})$ will be first determined. The establishment of this function, which hereinafter will be called fictitious source density function or *fictitious load*, is one of the essential ingredients of AEM. Implementation of the method leads to the numerical establishment of the fictitious load $q(\mathbf{x})$ in the domain Ω , through the solution of a system of linear or nonlinear algebraic equations. The boundary value problem defined in eqns. (A1.2) and (A1.1b) is called equivalent or substitute problem. It is noted that the analog equation is defined by a differential operator of the same order with that of the initial problem, while the same number of boundary conditions are obtained and continuity of the solution and its derivatives up to the order of the initial operator N is ensured.

Moreover, eqn. (A1.2) can be also employed for the solution of the boundary value problem defined in eqns. (A1.1), in case where $u = u(\mathbf{x}, \mathbf{y})$ and $g = g(\mathbf{x}, \mathbf{y})$ (where $\mathbf{y} \in \Omega$), $\bar{g} = \bar{g}(\mathbf{x}, \mathbf{y})$ (with $\mathbf{y} \in \Gamma$). Subsequently, the numerical implementation of

AEM leads to a system of differential equations the differential operator and boundary conditions of which depend only on y . Finally, it is noted that the AEM can be easily employed for the solution of boundary value problems with more than one unknown functions u by implementing eqn. (A1.2) for each one of the unknowns.

A1.3 AEM for Ordinary Differential Equations of the 2nd Order

A1.3.1 Integral Representation – Numerical Solution

Consider the one-dimensional boundary value problem

$$N\left(u, \frac{du}{dx}, \frac{d^2u}{dx^2}\right) = g(x), \quad x \in (0, l) \quad (\text{A1.3a})$$

$$a_1 B\left(u, \frac{du}{dx}\right) + a_2 u = a_3, \quad x = 0, l \quad (\text{A1.3b})$$

where $N(\cdot)$, $B(\cdot)$ are linear or nonlinear one-dimensional operators of the second and first order, respectively, a_i ($i = 1, 2, 3$) are functions specified at $x = 0, l$, $g(x)$ is the known source function defined at $(0, l)$ and $u = u(x)$ is the sought solution of the problem, having continuous derivatives up to the second order in $(0, l)$. According to the concept of AEM, the substitute problem is also of the second order, thus the following equation can be applied

$$\frac{d^2u}{dx^2} = q''(x) \quad (\text{A1.4})$$

In terms of mechanics of materials, eqn. (A1.4) describes the axial response of a beam with axial stiffness $EA = 1$, under the action of a fictitious loading $q''(x)$. According to section A1.2, eqn. (A1.4) indicates that the solution of the original problem (A1.3a,b) could be obtained as the solution of this equation subjected to the same boundary condition (A1.3b), provided that the fictitious loading $q''(x)$ will be first determined.

This can be accomplished as follows: The weak form of the analog equation is written as

$$\int_0^l [u''(x) - q''(x)] u^*(x, \xi) dx = 0 \Rightarrow \int_0^l u''(x) u^*(x, \xi) dx - \int_0^l q''(x) u^*(x, \xi) dx = 0 \quad (\text{A1.5})$$

where $(\cdot)'$ denotes differentiation with respect to x . The fundamental solution of the one-dimensional Laplace operator is adopted as the u^* function, which is a particular solution of the differential equation

$$\frac{d^2 u^*(x, \xi)}{dx^2} = \delta(x - \xi) \quad (\text{A1.6})$$

where $\delta(x - \xi)$ is the one-dimensional Dirac (δ) function. The fundamental solution u^* is obtained as

$$u^*(x, \xi) = \frac{1}{2} |r| \quad (\text{A1.7})$$

with $r = x - \xi$ being the distance between any two points x and ξ , where ξ is a constant collocation point while x runs through the interval $(0, l)$. By applying sequential integrations by parts in the first integral equation (A1.5), substituting eqns. (A1.4) and (A1.7) and exploiting the property of the Dirac function, yields

$$u(\xi) = \int_0^l A_2^u(x, \xi) q''(x) dx - \left[-A_1^u(x, \xi) u(x) + A_2^u(x, \xi) u'(x) \right]_{x=0}^{x=l} \quad (\text{A1.8})$$

where $A_i^u(r)$ ($i = 1, 2$) are the kernels, defined as

$$A_1^u(r) = \frac{1}{2} \operatorname{sgn} r \quad A_2^u(r) = \frac{1}{2} |r| \quad (\text{A1.9a,b})$$

with sgn being the *signum* function, defined as

$$sgn r = \begin{cases} +1, & r > 0 \\ -1, & r < 0 \end{cases} \quad (\text{A1.10})$$

for $r = 0$ the *signum* function is not defined. The relation (A1.8) constitutes the integral representation of the solution as a function of the fictitious load and the boundary quantities. In order to relate the boundary quantities with the fictitious load, the integral representation (A1.8) is applied to the interval edges $0, l$. In that case,

$$\xi \rightarrow \xi_0 = 0^+ \quad (\text{A1.11a})$$

$$\xi \rightarrow \xi_l = l^- \quad (\text{A1.11b})$$

Consequently, two boundary integral equations are obtained as

$$u(0) = \int_0^l A_2^u(x, \xi_0) q^u(x) dx - \left[-A_1^u(x, \xi_0) u(x) + A_2^u(x, \xi_0) u'(x) \right]_{x=0}^{x=l} \quad (\text{A1.12a})$$

$$u(l) = \int_0^l A_2^u(x, \xi_l) q^u(x) dx - \left[-A_1^u(x, \xi_l) u(x) + A_2^u(x, \xi_l) u'(x) \right]_{x=0}^{x=l} \quad (\text{A1.12b})$$

These integral equations can be written in a matrix form as

$$\begin{bmatrix} \mathbf{E}_1^u & \mathbf{E}_2^u \end{bmatrix} \begin{Bmatrix} \hat{\mathbf{u}} \\ \hat{\mathbf{u}}_{,x} \end{Bmatrix} = \mathbf{T}^u \quad (\text{A1.13})$$

where

$$\hat{\mathbf{u}}^T = [u(0) \quad u(l)] \quad \hat{\mathbf{u}}_{,x}^T = [u'(0) \quad u'(l)] \quad (\text{A1.14a,b})$$

$$\mathbf{E}_1^u = \begin{bmatrix} A_1^u(0, \xi_0) + 1 & -A_1^u(l, \xi_0) \\ A_1^u(0, \xi_l) & -A_1^u(l, \xi_l) + 1 \end{bmatrix} \quad \mathbf{E}_2^u = \begin{bmatrix} -A_2^u(0, \xi_0) & A_2^u(l, \xi_0) \\ -A_2^u(0, \xi_l) & A_2^u(l, \xi_l) \end{bmatrix} \quad (\text{A1.14c,d})$$

$$\mathbf{T}^u = \begin{Bmatrix} \int_0^l A_2^u(x, \xi_0) q^u(x) dx \\ \int_0^l A_2^u(x, \xi_l) q^u(x) dx \end{Bmatrix} \tag{A1.14e}$$

Substituting eqns. (A1.9) into the expressions of arrays (A1.14c,d), yields

$$\mathbf{E}_1^u = \begin{bmatrix} 1/2 & -1/2 \\ -1/2 & 1/2 \end{bmatrix} \quad \mathbf{E}_2^u = \begin{bmatrix} 0 & 1/2 \\ -1/2 & 0 \end{bmatrix} \tag{A1.15a,b}$$

The boundary integral equations (A1.13) together with the boundary conditions (A1.3b) permit the establishment of the boundary quantities $\hat{\mathbf{u}}, \hat{\mathbf{u}}_{,x}$ in terms of the fictitious load.

Thereafter, the discretization of the interval $(0, l)$ is performed and the approximation of the fictitious load is established. For this purpose, the interval is discretized into L elements employing the constant element assumption for the fictitious load distribution. More specifically, it is assumed that the fictitious function $q^u(x)$ maintains constant in each element, equal to its mid-point value (Fig. A1.1).

According to the above assumption, the column matrix \mathbf{T}^u is approximated as

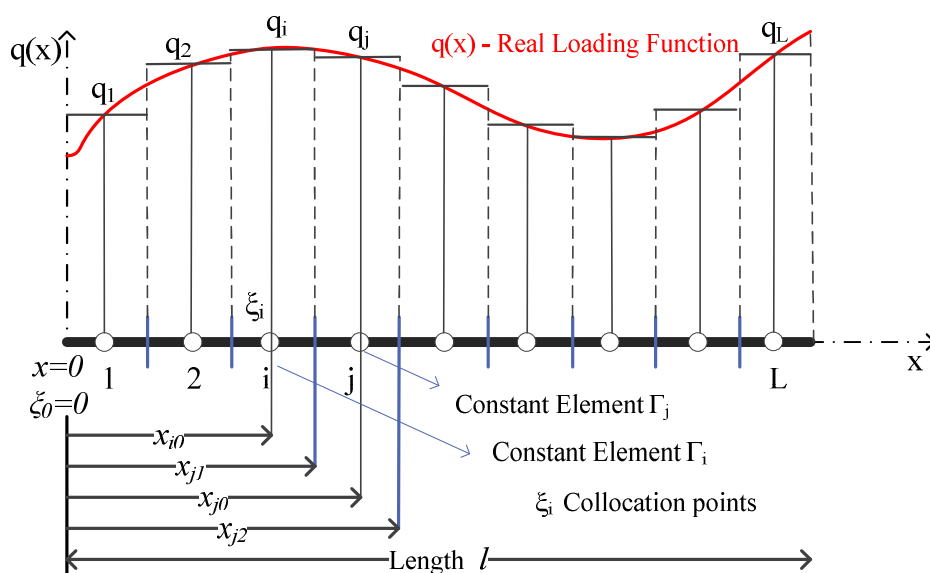


Fig. A1.1. Discretization of the interval $(0, l)$ with constant elements.

$$\mathbf{T}^u \approx \left\{ \begin{array}{l} \sum_{j=1}^L q_j^u \int_{\Gamma_j} A_2^u(x, \xi_0) dx \\ \sum_{j=1}^L q_j^u \int_{\Gamma_j} A_2^u(x, \xi_l) dx \end{array} \right\} \Rightarrow \mathbf{T}^u = \begin{bmatrix} \hat{F}_{11}^u & \hat{F}_{12}^u & \cdots & \hat{F}_{1L}^u \\ \hat{F}_{21}^u & \hat{F}_{22}^u & \cdots & \hat{F}_{2L}^u \end{bmatrix} \begin{Bmatrix} q_1^u \\ q_2^u \\ \vdots \\ q_L^u \end{Bmatrix} = \hat{\mathbf{F}}^u \mathbf{q}^u \quad (\text{A1.16})$$

where the coefficients \hat{F}_{ij}^u ($i = 1, 2$, $j = 1, 2, \dots, L$) are defined as

$$\hat{F}_{1j}^u = \int_{\Gamma_j} A_2^u(x, \xi_0) dx \quad \hat{F}_{2j}^u = \int_{\Gamma_j} A_2^u(x, \xi_l) dx \quad (\text{A1.17a,b})$$

Subsequently, the boundary conditions (A1.3b) can be written in a matrix form as

$$\begin{bmatrix} \mathbf{D}_1^u & \mathbf{D}_2^u \end{bmatrix} \begin{Bmatrix} \hat{\mathbf{u}} \\ \hat{\mathbf{u}}_{,x} \end{Bmatrix} + \hat{\mathbf{D}}_{1,nl}^u(\hat{\mathbf{u}}, \hat{\mathbf{u}}_{,x}) = \boldsymbol{\alpha}_3^u \quad (\text{A1.18})$$

where \mathbf{D}_1^u , \mathbf{D}_2^u are 2×2 known square matrices including the values of the functions a_i ($i = 1, 2$) of eqn. (A1.3b), $\hat{\mathbf{D}}_{1,nl}^u = \hat{\mathbf{D}}_{1,nl}^u(\hat{\mathbf{u}}, \hat{\mathbf{u}}_{,x})$ are 2×1 column matrices including the nonlinear terms of the same functions and $\boldsymbol{\alpha}_3^u$ are 2×1 known column matrix including the boundary values a_3 of eqn. (A1.3b). Relations (A1.13) and (A1.18) can be written in a more convenient form as

$$\begin{bmatrix} \mathbf{E}_1^u & \mathbf{E}_2^u \\ \mathbf{D}_1^u & \mathbf{D}_2^u \end{bmatrix} \begin{Bmatrix} \hat{\mathbf{u}} \\ \hat{\mathbf{u}}_{,x} \end{Bmatrix} + \begin{Bmatrix} \mathbf{0} \\ \hat{\mathbf{D}}_{1,nl}^u \end{Bmatrix} = \begin{Bmatrix} \hat{\mathbf{F}}^u \mathbf{q}^u \\ \boldsymbol{\alpha}_3^u \end{Bmatrix} \quad (\text{A1.19})$$

Alternatively,

$$\begin{bmatrix} \mathbf{F}^u & \mathbf{E}_1^u & \mathbf{E}_1^u \\ \mathbf{0} & \mathbf{D}_1^u & \mathbf{D}_2^u \end{bmatrix} \begin{Bmatrix} \mathbf{q}^u \\ \hat{\mathbf{u}} \\ \hat{\mathbf{u}}_{,x} \end{Bmatrix} + \hat{\mathbf{D}}_{nl}^u = \begin{Bmatrix} \mathbf{0} \\ \boldsymbol{\alpha}_3^u \end{Bmatrix} \Rightarrow \mathbf{E}^u \mathbf{d}^u + \hat{\mathbf{D}}_{nl}^u = \begin{Bmatrix} \mathbf{0} \\ \boldsymbol{\alpha}_3^u \end{Bmatrix} \quad (\text{A1.20})$$

where $\mathbf{F}^u = -\hat{\mathbf{F}}^u$, $(\hat{\mathbf{D}}_{nl}^u)^T = [\mathbf{0} \quad \hat{\mathbf{D}}_{l,nl}^u]$, while $(\mathbf{d}^u)^T = [\mathbf{q}^u \quad \hat{\mathbf{u}} \quad \hat{\mathbf{u}}_{,x}]$ is a $(L+4) \times 1$ generalized unknown vector including the values of the fictitious load and the boundary values of the respective boundary quantities. Eqns. (A1.20) constitute a nonlinear system of 4 algebraic equations with $L+4$ unknowns. In order to solve this system, L additional equations are required.

Exploiting the aforementioned discretization of the interval $(0, l)$ and the approximation of the fictitious load with constant elements (Fig A1.1), the integral representation of the solution (A1.8) for the ξ_i position of the i element ($\xi_i \neq 0, l$) can be written as

$$u(\xi_i) = \sum_{j=1}^L q_j^u \int_{\Gamma_j} A_2^u(x, \xi_i) dx - \left[-A_1^u(x, \xi_i)u(x) + A_2^u(x, \xi_i)u'(x) \right]_{x=0}^{x=l} \quad (\text{A1.21})$$

In order to solve the problem, the derivative of the solution is required. Thus, differentiating the above equation with respect to ξ , the discretized form of the derivative of the solution is obtained as

$$\frac{du(\xi_i)}{d\xi} = \sum_{j=1}^L q_j^u \int_{\Gamma_j} \frac{\partial A_2^u(x, \xi_i)}{\partial \xi} dx - \left[-\frac{\partial A_1^u(x, \xi_i)}{\partial \xi} u(x) + \frac{\partial A_2^u(x, \xi_i)}{\partial \xi} u'(x) \right]_{x=0}^{x=l} \quad (\text{A1.22})$$

where

$$\frac{\partial A_1^u(x, \xi)}{\partial \xi} = 0 \quad \text{for} \quad x = 0, l \quad (\text{A1.23a})$$

$$\frac{\partial A_2^u(x, \xi)}{\partial \xi} = -A_1^u(x, \xi) \quad \text{for} \quad \forall x \in [0, l] \quad (\text{A1.23b})$$

Finally, applying eqns. (A1.21) and (A1.22) to the L collocation points yield

$$\mathbf{u} = \mathbf{A}^u \mathbf{q}^u + \mathbf{C}^u \begin{Bmatrix} \hat{\mathbf{u}} \\ \hat{\mathbf{u}}_{,x} \end{Bmatrix} = \mathbf{B}^u \mathbf{d}^u \quad (\text{A1.24a})$$

$$\mathbf{u}_{,x} = \mathbf{A}_{,x}^u \mathbf{q}^u + \mathbf{C}_{,x}^u \begin{Bmatrix} \hat{\mathbf{u}} \\ \hat{\mathbf{u}}_{,x} \end{Bmatrix} = \mathbf{B}_{,x}^u \mathbf{d}^u \quad (\text{A1.24b})$$

where

$$\mathbf{u}^T = [(u)_1 \quad (u)_2 \quad \cdots \quad (u)_L] \quad \mathbf{u}_{,x}^T = [(u')_1 \quad (u')_2 \quad \cdots \quad (u')_L] \quad (\text{A1.25a,b})$$

are $L \times 1$ vectors including the unknown values of u and its derivative with respect to x , at the L nodal points of the interval, while \mathbf{A}^u , $\mathbf{A}_{,x}^u$ are $L \times L$ square matrices with coefficients defined as

$$A_{ij}^u = \int_{\Gamma_j} A_2^u(x, \xi_i) dx \quad A_{ij,x}^u = -\int_{\Gamma_j} A_1^u(x, \xi_i) dx \quad (\text{A1.26a,b})$$

where $i = 1, 2, \dots, L$, $j = 1, 2, \dots, L$. Moreover, \mathbf{C}^u , $\mathbf{C}_{,x}^u$ are $L \times 4$ matrices defined as (Mokos 2007)

$$\mathbf{C}^u = \left[\begin{array}{cc|cc} A_2^u(0, \xi_1) & -A_1^u(0, \xi_1) & -A_2^u(l, \xi_1) & A_1^u(l, \xi_1) \\ A_2^u(0, \xi_2) & -A_1^u(0, \xi_2) & -A_2^u(l, \xi_2) & A_1^u(l, \xi_2) \\ \vdots & \vdots & \vdots & \vdots \\ A_2^u(0, \xi_L) & -A_1^u(0, \xi_L) & -A_2^u(l, \xi_L) & A_1^u(l, \xi_L) \end{array} \right] \quad (\text{A1.27a})$$

$$\mathbf{C}_{,x}^u = \left[\begin{array}{cc|cc} -A_1^u(0, \xi_1) & 0 & A_1^u(l, \xi_1) & 0 \\ -A_1^u(0, \xi_2) & 0 & A_1^u(l, \xi_2) & 0 \\ \vdots & \vdots & \vdots & \vdots \\ -A_1^u(0, \xi_L) & 0 & A_1^u(l, \xi_L) & 0 \end{array} \right] \quad (\text{A1.27b})$$

while exploiting eqns. (A1.9) result in

$$A_1^u(0, \xi_i) = -\frac{l}{2} \quad A_2^u(0, \xi_i) = \frac{l}{2} \xi_i \quad (\text{A1.28a,b})$$

$$A_1^u(l, \xi_i) = \frac{l}{2} \quad A_2^u(l, \xi_i) = \frac{l}{2}(l - \xi_i) \quad (\text{A1.28c,d})$$

where $\xi_i = x_{i0}$ is the coordinate of the mid-point of the element Γ_i (Fig.A1.1) and \mathbf{B}^u , $\mathbf{B}_{,x}^u$ are $L \times (L+4)$ matrices defined as $\mathbf{B}^u = \begin{bmatrix} \mathbf{A}^u & \mathbf{C}^u \end{bmatrix}$, $\mathbf{B}_{,x}^u = \begin{bmatrix} \mathbf{A}_{,x}^u & \mathbf{C}_{,x}^u \end{bmatrix}$.

The final step of AEM is the application of the governing equation of the initial problem (A1.3) at the L internal nodal points and subsequently the substitution of the values of the field function u and its derivative u' at the L internal nodal points according to eqns. (A1.24). From the definition of the analog equation (A1.4) it is apparent that the values of the second derivative u'' at the nodal points are equal to the corresponding values of the fictitious load vector \mathbf{q}^u . Thus, L additional algebraic equations are derived with respect to the generalized unknown vector \mathbf{d}^u . These equations in combination with eqns. (A1.20) constitute a system of $L+4$ algebraic equations with $L+4$ unknowns. The solution of this system provides the values of the fictitious load at the L internal nodal points as well as the values of the field function u and its derivative u' at the edges of the examined interval. Thereafter, exploiting eqn. (A1.24) the vectors including the values of the solution and its derivative at the L internal nodal points are obtained. Finally, it is noted that the values of u and u' at any point of the interval $\xi \in (0, l)$ can be easily calculated by applying the integral representations (A1.21-22) substituting the value ξ_i with ξ .

A1.3.2 Evaluation of Integrals

In order to determine the coefficients of the matrices \mathbf{F}^u , \mathbf{A}^u and $\mathbf{A}_{,x}^u$ (relations (A1.20), (A1.24)) the integrals defined in eqns. (A1.17) and (A1.26) have first to be evaluated. This calculation can be easily performed employing any numerical integration scheme (e.g. Gauss, Gauss-Lobatto). Nevertheless, due to the closed form of the kernels, the analytic integration along the element's Γ_j length is indicated, thus avoiding any computational error and the increase of the computational time. Exploiting eqns. (A1.9), the analytic expressions of the integrals of the coefficients \hat{F}_{ij}^u ($i = 1, 2$, $j = 1, 2, \dots, L$) defined in eqns. (A1.17) are obtained as

$$\hat{F}_{1j}^u = \frac{l}{4} \left[x^2 \right]_{x=x_{j1}}^{x=x_{j2}} \quad \hat{F}_{2j}^u = -\frac{l}{4} \left[(l-x)^2 \right]_{x=x_{j1}}^{x=x_{j2}} \quad (\text{A1.29a,b})$$

where x_{j1} , x_{j2} are the coordinates of the element's Γ_j edges (Fig.A1.1). Moreover, from eqn. (A1.9), the analytic expressions of the coefficients A_{ij}^u ($i = 1, 2, \dots, L$, $j = 1, 2, \dots, L$) defined in eqn. (A1.26) are obtained as

$$A_{ij}^u = -\frac{I}{4} \left[(x_{i0} - x)^2 \right]_{x=x_{j1}}^{x=x_{j2}}, \quad i > j \quad (\text{A1.30a})$$

$$A_{ij}^u = \frac{I}{4} \left[(x_{i0} - x)^2 \right]_{x=x_{j1}}^{x=x_{j2}}, \quad i < j \quad (\text{A1.30b})$$

$$A_{ij}^u = -\frac{I}{4} \left[(x_{i0} - x)^2 \right]_{x=x_{j1}}^{x=x_{j0}} + \frac{I}{4} \left[(x_{i0} - x)^2 \right]_{x=x_{j0}}^{x=x_{j2}}, \quad i = j \quad (\text{A1.30c})$$

$$A_{ij,x}^u = \frac{I}{2} \left[x \right]_{x=x_{j1}}^{x=x_{j2}}, \quad i > j \quad A_{ij,x}^u = -\frac{I}{2} \left[x \right]_{x=x_{j1}}^{x=x_{j2}}, \quad i < j \quad A_{ij,x}^u = 0 \quad (\text{A1.30d,e,f})$$

where x_{j1} , x_{j2} and x_{j0} are the coordinates of the element's Γ_j edges and mid-point, respectively, while x_{i0} are the coordinates of mid-point of the element Γ_i (Fig.A1.1)

A1.4 AEM for Ordinary Differential Equations of the 4th Order

A1.4.1 Integral Representation – Numerical Solution

Consider the one-dimensional boundary value problem

$$N \left(\theta, \frac{d\theta}{dx}, \frac{d^2\theta}{dx^2}, \frac{d^3\theta}{dx^3}, \frac{d^4\theta}{dx^4} \right) = g(x), \quad x \in (0, l) \quad (\text{A1.31a})$$

$$a_1 B_1 \left(\theta, \frac{d\theta}{dx}, \frac{d^2\theta}{dx^2}, \frac{d^3\theta}{dx^3} \right) + a_2 \theta = a_3, \quad x = 0, l \quad (\text{A1.31b})$$

$$\beta_1 B_2 \left(\theta, \frac{d\theta}{dx}, \frac{d^2\theta}{dx^2} \right) + \beta_2 \frac{d\theta}{dx} = \beta_3, \quad x = 0, l \quad (\text{A1.31c})$$

where $N(\cdot)$ is a linear or nonlinear one-dimensional differential operator of the fourth order, $B_1(\cdot)$, $B_2(\cdot)$ are linear or nonlinear one-dimensional operators of third and

second order, respectively, a_i, β_i ($i = 1, 2, 3$) are functions specified at $x = 0, l$, $g(x)$ is the known source function defined at $(0, l)$ and $\theta = \theta(x)$ is the sought solution of the problem, having continuous derivatives up to the forth order in $(0, l)$. According to the concept of AEM, the substitute problem is also of the fourth order, thus the following equation can be applied

$$\frac{d^4 \theta}{dx^4} = q(x) \quad (\text{A1.32})$$

In terms of mechanics of materials, eqn. (II2.4.2) describes the flexural response of a beam with flexural stiffness $EI = I$, under the action of a fictitious loading $q(x)$. According to section A1.2, eqn. (A1.32) indicates that the solution of the original problem (A1.31a,b) could be obtained as the solution of this equation subjected to the same boundary condition (A1.31b,c), provided that the fictitious loading $q(x)$ will be first determined. This can be accomplished as follows: The weak form of the analog equation is written as

$$\begin{aligned} \int_0^l [\theta'''(x) - q(x)] \theta^*(x, \xi) dx &= 0 \Rightarrow \\ \int_0^l \theta'''(x) \theta^*(x, \xi) dx - \int_0^l q(x) \theta^*(x, \xi) dx &= 0 \end{aligned} \quad (\text{A1.33})$$

where $(\cdot)'$ denotes differentiation with respect to x . The fundamental solution of the one-dimensional Laplace operator is adopted as the θ^* function, which is a particular solution of the differential equation

$$\frac{d^4 \theta^*(x, \xi)}{dx^4} = \delta(x - \xi) \quad (\text{A1.34})$$

where $\delta(x - \xi)$ is the one-dimensional Dirac (δ) function. The fundamental solution θ^* is obtained as

$$\theta^*(x, \xi) = \frac{I}{12} (|r|^3 - 3l|r|^2 + 2l^3) \quad (\text{A1.35})$$

with $r = x - \xi$ being the distance between any two points x and ξ , where ξ is a constant collocation point while x runs through the interval $(0, l)$. By applying sequential integrations by parts in the first integral equation (A1.33), substituting eqns. (A1.32) and (A1.35) and exploiting the property of the Dirac function, yields

$$\begin{aligned} \theta(\xi) = & \int_0^l A_4(x, \xi) q(x) dx - \\ & - \left[-A_1(x, \xi) \theta(x) + A_2(x, \xi) \theta'(x) - A_3(x, \xi) \theta''(x) + A_4(x, \xi) \theta'''(x) \right]_{x=0}^{x=l} \end{aligned} \quad (\text{A1.36})$$

where $A_i(r)$ ($i = 1, 2, 3, 4$) are the kernels, defined as

$$A_1(x, \xi) = \frac{I}{2} \operatorname{sgn} r \quad A_2(x, \xi) = \frac{I}{2} (|r| - l) \quad (\text{A1.37a,b})$$

$$A_3(x, \xi) = \frac{I}{4} |r| (|r| - 2l) \operatorname{sgn} r \quad A_4(x, \xi) = \frac{I}{12} (|r|^3 - 3l|r|^2 + 2l^3) \quad (\text{A1.37c,d})$$

with sgn being the *signum* function, defined in relation (A1.10). The relation (A1.36) constitutes the integral representation of the solution as a function of the fictitious load and the boundary quantities. In order to relate the boundary quantities with the fictitious load, the integral representation (A1.36) is applied to the interval edges $0, l$. In that case,

$$\xi \rightarrow \xi_0 = 0^+ \quad (\text{A1.38a})$$

$$\xi \rightarrow \xi_l = l^- \quad (\text{A1.38b})$$

Consequently, two boundary integral equations are obtained as

$$\begin{aligned} \theta(0) = & \int_0^l A_4(x, \xi_0) q(x) dx - \\ & - \left[-A_1(x, \xi_0) \theta(x) + A_2(x, \xi_0) \theta'(x) - A_3(x, \xi_0) \theta''(x) + A_4(x, \xi_0) \theta'''(x) \right]_{x=0}^{x=l} \end{aligned} \quad (\text{A1.39a})$$

$$\theta(l) = \int_0^l \mathcal{A}_4(x, \xi_l) q(x) dx - \left[-\mathcal{A}_1(x, \xi_l) \theta(x) + \mathcal{A}_2(x, \xi_l) \theta'(x) - \mathcal{A}_3(x, \xi_l) \theta''(x) + \mathcal{A}_4(x, \xi_l) \theta'''(x) \right]_{x=0}^{x=l} \quad (\text{A1.39b})$$

These integral equations can be written in a matrix form as

$$\left[\mathbf{E}_{11} \quad \mathbf{E}_{12} \quad \mathbf{E}_{13} \quad \mathbf{E}_{14} \right] \begin{Bmatrix} \hat{\boldsymbol{\theta}} \\ \hat{\boldsymbol{\theta}}_{,x} \\ \hat{\boldsymbol{\theta}}_{,xx} \\ \hat{\boldsymbol{\theta}}_{,xxx} \end{Bmatrix} = \mathbf{T}_l \quad (\text{A1.40})$$

where

$$\hat{\boldsymbol{\theta}}^T = [\theta(0) \quad \theta(l)] \quad \hat{\boldsymbol{\theta}}_{,x}^T = [\theta'(0) \quad \theta'(l)] \quad (\text{A1.41a,b})$$

$$\hat{\boldsymbol{\theta}}_{,xx}^T = [\theta''(0) \quad \theta''(l)] \quad \hat{\boldsymbol{\theta}}_{,xxx}^T = [\theta'''(0) \quad \theta'''(l)] \quad (\text{A1.41c,d})$$

$$\mathbf{E}_{11} = \begin{bmatrix} \mathcal{A}_1(0, \xi_0) + I & -\mathcal{A}_1(l, \xi_0) \\ \mathcal{A}_1(0, \xi_l) & -\mathcal{A}_1(l, \xi_l) + I \end{bmatrix} \quad \mathbf{E}_{12} = \begin{bmatrix} -\mathcal{A}_2(0, \xi_0) & \mathcal{A}_2(l, \xi_0) \\ -\mathcal{A}_2(0, \xi_l) & \mathcal{A}_2(l, \xi_l) \end{bmatrix} \quad (\text{A1.41e,f})$$

$$\mathbf{E}_{13} = \begin{bmatrix} \mathcal{A}_3(0, \xi_0) & -\mathcal{A}_3(l, \xi_0) \\ \mathcal{A}_3(0, \xi_l) & -\mathcal{A}_3(l, \xi_l) \end{bmatrix} \quad \mathbf{E}_{14} = \begin{bmatrix} -\mathcal{A}_4(0, \xi_0) & \mathcal{A}_4(l, \xi_0) \\ -\mathcal{A}_4(0, \xi_l) & \mathcal{A}_4(l, \xi_l) \end{bmatrix} \quad (\text{A1.41g,h})$$

$$\mathbf{T}_l = \begin{Bmatrix} \int_0^l \mathcal{A}_4(x, \xi_0) q(x) dx \\ \int_0^l \mathcal{A}_4(x, \xi_l) q(x) dx \end{Bmatrix} \quad (\text{A1.41i})$$

Substituting eqns. (A1.37) into the expressions of arrays (A1.41e-h), yields

$$\mathbf{E}_{11} = \begin{bmatrix} l/2 & -l/2 \\ -l/2 & l/2 \end{bmatrix} \quad \mathbf{E}_{12} = \begin{bmatrix} l/2 & 0 \\ 0 & -l/2 \end{bmatrix} \quad (\text{A1.42a,b})$$

$$\mathbf{E}_{13} = \begin{bmatrix} 0 & l^2/4 \\ l^2/4 & 0 \end{bmatrix} \quad \mathbf{E}_{14} = \begin{bmatrix} -l^3/6 & 0 \\ 0 & l^3/6 \end{bmatrix} \quad (\text{A1.42c,d})$$

Differentiating integral representation of the solution eqn. (A1.36) with respect to ξ , the integral representation of its derivative is obtained

$$\frac{d\theta(\xi)}{d\xi} = \int_0^l \frac{\partial A_4(x, \xi)}{\partial \xi} q(x) dx - \left[-\frac{\partial A_1(x, \xi)}{\partial \xi} \theta(x) + \frac{\partial A_2(x, \xi)}{\partial \xi} \theta'(x) - \frac{\partial A_3(x, \xi)}{\partial \xi} \theta''(x) + \frac{\partial A_4(x, \xi)}{\partial \xi} \theta'''(x) \right]_{x=0}^{x=l} \quad (\text{A1.43})$$

where

$$\frac{\partial A_1(x, \xi)}{\partial \xi} = 0 \quad \text{for } x = 0, l \quad (\text{A1.44a})$$

$$\frac{\partial A_2(x, \xi)}{\partial \xi} = -A_1(x, \xi) \quad \text{for } x = 0, l \quad (\text{A1.44b})$$

$$\frac{\partial A_3(x, \xi)}{\partial \xi} = -A_2(x, \xi) \quad \text{for } x = 0, l \quad (\text{A1.44c})$$

$$\frac{\partial A_4(x, \xi)}{\partial \xi} = -A_3(x, \xi) \quad \text{for } \forall x \in [0, l] \quad (\text{A1.44d})$$

Exploiting eqns. (A1.44) and applying the integral representation at the intervals edges $0, l$ ($\xi \rightarrow \xi_0 = 0^+, \xi \rightarrow \xi_l = l^-$) the following boundary conditions are obtained

$$\frac{d\theta(0)}{d\xi} = -\int_0^l A_3(x, \xi_0) q(x) dx - \left[-A_1(x, \xi_0) \theta'(x) + A_2(x, \xi_0) \theta''(x) - A_3(x, \xi_0) \theta'''(x) \right]_{x=0}^{x=l} \quad (\text{A1.45a})$$

$$\frac{d\theta(l)}{d\xi} = -\int_0^l A_3(x, \xi_l) q(x) dx - \left[-A_1(x, \xi_l) \theta'(x) + A_2(x, \xi_l) \theta''(x) - A_3(x, \xi_l) \theta'''(x) \right]_{x=0}^{x=l} \quad (\text{A1.45b})$$

These integral equations (A1.45) can be written in a matrix form as

$$\begin{bmatrix} \mathbf{0} & \mathbf{E}_{21} & \mathbf{E}_{22} & \mathbf{E}_{23} \end{bmatrix} \begin{Bmatrix} \hat{\boldsymbol{\theta}} \\ \hat{\boldsymbol{\theta}}_{,x} \\ \hat{\boldsymbol{\theta}}_{,xx} \\ \hat{\boldsymbol{\theta}}_{,xxx} \end{Bmatrix} = \mathbf{T}_2 \quad (\text{A1.46})$$

where

$$\mathbf{E}_{21} = \begin{bmatrix} A_1(0, \xi_0) + 1 & -A_1(l, \xi_0) \\ A_1(0, \xi_l) & -A_1(l, \xi_l) + 1 \end{bmatrix} \quad \mathbf{E}_{22} = \begin{bmatrix} -A_2(0, \xi_0) & A_2(l, \xi_0) \\ -A_2(0, \xi_l) & A_2(l, \xi_l) \end{bmatrix} \quad (\text{A1.47a,b})$$

$$\mathbf{E}_{23} = \begin{bmatrix} A_3(0, \xi_0) & -A_3(l, \xi_0) \\ A_3(0, \xi_l) & -A_3(l, \xi_l) \end{bmatrix} \quad \mathbf{T}_2 = \begin{Bmatrix} -\int_0^l A_3(x, \xi_0) q(x) dx \\ -\int_0^l A_3(x, \xi_l) q(x) dx \end{Bmatrix} \quad (\text{A1.47c,d})$$

Substituting eqns. (A1.37) into eqns. (A1.47a-c), yield

$$\mathbf{E}_{21} = \begin{bmatrix} 1/2 & -1/2 \\ -1/2 & 1/2 \end{bmatrix} \quad \mathbf{E}_{22} = \begin{bmatrix} l/2 & 0 \\ 0 & -l/2 \end{bmatrix} \quad \mathbf{E}_{23} = \begin{bmatrix} 0 & l^2/4 \\ l^2/4 & 0 \end{bmatrix} \quad (\text{A1.48a,b,c})$$

Eqns. (A1.40) and (A1.46) can be written in a more compact form as

$$\begin{bmatrix} \mathbf{E}_{11} & \mathbf{E}_{12} & \mathbf{E}_{13} & \mathbf{E}_{14} \\ \mathbf{0} & \mathbf{E}_{21} & \mathbf{E}_{22} & \mathbf{E}_{23} \end{bmatrix} \begin{Bmatrix} \hat{\boldsymbol{\theta}} \\ \hat{\boldsymbol{\theta}}_{,x} \\ \hat{\boldsymbol{\theta}}_{,xx} \\ \hat{\boldsymbol{\theta}}_{,xxx} \end{Bmatrix} = \begin{Bmatrix} \mathbf{T}_1 \\ \mathbf{T}_2 \end{Bmatrix} \quad (\text{A1.49})$$

The boundary integral equations (A1.49) together with the boundary conditions (A1.31b) permit the establishment of the boundary quantities $\hat{\boldsymbol{\theta}}$, $\hat{\boldsymbol{\theta}}_{,x}$, $\hat{\boldsymbol{\theta}}_{,xx}$, $\hat{\boldsymbol{\theta}}_{,xxx}$ in terms of the fictitious load.

Thereafter, the discretization of the interval $(0, l)$ is performed and the approximation of the fictitious load is established. For this purpose, the interval is discretized into L elements employing the constant element assumption for the fictitious load $q(x)$. More specifically, it is assumed that the fictitious function $q(x)$

maintains constant in each element, equal to its mid-point value (Fig. A1.1). According to the above assumption, the column matrix $\mathbf{T}^T = [\mathbf{T}_1 \quad \mathbf{T}_2]$ is approximated as

$$\mathbf{T} = \begin{Bmatrix} \mathbf{T}_1 \\ \mathbf{T}_2 \end{Bmatrix} \approx \begin{Bmatrix} \sum_{j=1}^L q_j \int_{\Gamma_j} \Lambda_4(x, \xi_0) dx \\ \sum_{j=1}^L q_j \int_{\Gamma_j} \Lambda_4(x, \xi_l) dx \\ \hline -\sum_{j=1}^L q_j \int_{\Gamma_j} \Lambda_3(x, \xi_0) dx \\ -\sum_{j=1}^L q_j \int_{\Gamma_j} \Lambda_3(x, \xi_l) dx \end{Bmatrix} = \begin{bmatrix} \hat{F}_{11} & \hat{F}_{12} & \cdots & \hat{F}_{1L} \\ \hat{F}_{21} & \hat{F}_{22} & \cdots & \hat{F}_{2L} \\ \hline \hat{F}_{31} & \hat{F}_{32} & \cdots & \hat{F}_{3L} \\ \hat{F}_{41} & \hat{F}_{42} & \cdots & \hat{F}_{4L} \end{bmatrix} \begin{Bmatrix} q_1 \\ q_2 \\ \vdots \\ q_L \end{Bmatrix} \Rightarrow \mathbf{T} = \begin{bmatrix} \hat{\mathbf{F}}_1 \\ \hat{\mathbf{F}}_2 \end{bmatrix} \mathbf{q} \quad (\text{A1.50})$$

where the coefficients \hat{F}_{ij} ($i = 1, 2, 3, 4$, $j = 1, 2, \dots, L$) are defined as

$$\hat{F}_{1j} = \int_{\Gamma_j} \Lambda_4(x, \xi_0) dx \quad \hat{F}_{2j} = \int_{\Gamma_j} \Lambda_4(x, \xi_l) dx \quad (\text{A1.51a,b})$$

$$\hat{F}_{3j} = -\int_{\Gamma_j} \Lambda_3(x, \xi_0) dx \quad \hat{F}_{4j} = -\int_{\Gamma_j} \Lambda_3(x, \xi_l) dx \quad (\text{A1.51c,d})$$

Subsequently, the boundary conditions (A1.31b) can be written in a matrix form as

$$\begin{bmatrix} \mathbf{D}_{11} & \mathbf{D}_{12} & \mathbf{D}_{13} & \mathbf{D}_{14} \\ \mathbf{D}_{21} & \mathbf{D}_{22} & \mathbf{D}_{23} & \mathbf{D}_{24} \end{bmatrix} \begin{Bmatrix} \hat{\boldsymbol{\theta}} \\ \hat{\boldsymbol{\theta}}_{,x} \\ \hat{\boldsymbol{\theta}}_{,xx} \\ \hat{\boldsymbol{\theta}}_{,xxx} \end{Bmatrix} + \begin{Bmatrix} \hat{\mathbf{D}}_{1,nl}(\hat{\boldsymbol{\theta}}, \hat{\boldsymbol{\theta}}_{,x}, \hat{\boldsymbol{\theta}}_{,xx}, \hat{\boldsymbol{\theta}}_{,xxx}) \\ \hat{\mathbf{D}}_{2,nl}(\hat{\boldsymbol{\theta}}, \hat{\boldsymbol{\theta}}_{,x}, \hat{\boldsymbol{\theta}}_{,xx}) \end{Bmatrix} = \begin{Bmatrix} \boldsymbol{\alpha}_3 \\ \boldsymbol{\beta}_3 \end{Bmatrix} \quad (\text{A1.52})$$

where \mathbf{D}_{11} , \mathbf{D}_{12} , \mathbf{D}_{13} , \mathbf{D}_{14} , \mathbf{D}_{21} , \mathbf{D}_{22} , \mathbf{D}_{23} and \mathbf{D}_{24} are 2×2 known square matrices including the values of the functions a_i , β_i ($i = 1, 2$), as presented in eqns. (A1.31b,c), $\hat{\mathbf{D}}_{1,nl} = \hat{\mathbf{D}}_{1,nl}(\hat{\boldsymbol{\theta}}, \hat{\boldsymbol{\theta}}_{,x}, \hat{\boldsymbol{\theta}}_{,xx}, \hat{\boldsymbol{\theta}}_{,xxx})$, $\hat{\mathbf{D}}_{2,nl} = \hat{\mathbf{D}}_{2,nl}(\hat{\boldsymbol{\theta}}, \hat{\boldsymbol{\theta}}_{,x}, \hat{\boldsymbol{\theta}}_{,xx})$ are 2×1 column matrices including the nonlinear terms of the same functions and $\boldsymbol{\alpha}_3$, $\boldsymbol{\beta}_3$ are 2×1 known column matrix including the boundary values a_3 , β_3 of eqn. (A1.31b,c). Relations (A1.49) and (A1.52) can be written in a more convenient form as

$$\begin{bmatrix} \mathbf{E}_{11} & \mathbf{E}_{12} & \mathbf{E}_{13} & \mathbf{E}_{14} \\ \mathbf{0} & \mathbf{E}_{21} & \mathbf{E}_{22} & \mathbf{E}_{23} \\ \mathbf{D}_{11} & \mathbf{D}_{12} & \mathbf{D}_{13} & \mathbf{D}_{14} \\ \mathbf{D}_{21} & \mathbf{D}_{22} & \mathbf{D}_{23} & \mathbf{D}_{24} \end{bmatrix} \begin{Bmatrix} \hat{\boldsymbol{\theta}} \\ \hat{\boldsymbol{\theta}}_{,x} \\ \hat{\boldsymbol{\theta}}_{,xx} \\ \hat{\boldsymbol{\theta}}_{,xxx} \end{Bmatrix} + \begin{Bmatrix} \mathbf{0} \\ \mathbf{0} \\ \hat{\mathbf{D}}_{1,nl} \\ \hat{\mathbf{D}}_{2,nl} \end{Bmatrix} = \begin{Bmatrix} \hat{\mathbf{F}}_1 \mathbf{q} \\ \hat{\mathbf{F}}_2 \mathbf{q} \\ \boldsymbol{\alpha}_3 \\ \boldsymbol{\beta}_3 \end{Bmatrix} \quad (\text{A1.53})$$

Alternatively,

$$\begin{bmatrix} \mathbf{F}_1 & \mathbf{E}_{11} & \mathbf{E}_{12} & \mathbf{E}_{13} & \mathbf{E}_{14} \\ \mathbf{F}_2 & \mathbf{0} & \mathbf{E}_{21} & \mathbf{E}_{22} & \mathbf{E}_{23} \\ \mathbf{0} & \mathbf{D}_{11} & \mathbf{D}_{12} & \mathbf{D}_{13} & \mathbf{D}_{14} \\ \mathbf{0} & \mathbf{D}_{21} & \mathbf{D}_{22} & \mathbf{D}_{23} & \mathbf{D}_{24} \end{bmatrix} \begin{Bmatrix} \mathbf{q} \\ \hat{\boldsymbol{\theta}} \\ \hat{\boldsymbol{\theta}}_{,x} \\ \hat{\boldsymbol{\theta}}_{,xx} \\ \hat{\boldsymbol{\theta}}_{,xxx} \end{Bmatrix} + \hat{\mathbf{D}}_{nl} = \begin{Bmatrix} \mathbf{0} \\ \mathbf{0} \\ \boldsymbol{\alpha}_3 \\ \boldsymbol{\beta}_3 \end{Bmatrix} \Rightarrow \mathbf{E} \mathbf{d} + \hat{\mathbf{D}}_{nl} = \begin{Bmatrix} \mathbf{0} \\ \mathbf{0} \\ \boldsymbol{\alpha}_3 \\ \boldsymbol{\beta}_3 \end{Bmatrix} \quad (\text{A1.54})$$

where $\mathbf{F}_1 = -\hat{\mathbf{F}}_1$, $\mathbf{F}_2 = -\hat{\mathbf{F}}_2$, $(\hat{\mathbf{D}}_{nl})^T = [\mathbf{0} \ \mathbf{0} \ \hat{\mathbf{D}}_{1,nl} \ \hat{\mathbf{D}}_{2,nl}]$, while

$\mathbf{d}^T = [\mathbf{q} \ \hat{\boldsymbol{\theta}} \ \hat{\boldsymbol{\theta}}_{,x} \ \hat{\boldsymbol{\theta}}_{,xx} \ \hat{\boldsymbol{\theta}}_{,xxx}]$ is a $(L + \delta) \times l$ generalized unknown vector including the values of the fictitious load and the boundary values of the respective boundary quantities. Eqns. (A1.54) constitute a nonlinear system of δ algebraic equations with $L + \delta$ unknowns. In order to solve this system, L additional equations are required.

Exploiting the aforementioned discretization of the interval $(0, l)$ and the approximation of the fictitious load with constant elements (Fig.A1.1), the integral representation of the solution (A1.36) for the ξ_i position of the i element ($\xi_i \neq 0, l$) can be written as

$$\theta(\xi_i) = \sum_{j=1}^L q_j \int_{\Gamma_j} \mathcal{A}_4(x, \xi_i) dx - \left[-\mathcal{A}_1(x, \xi_i) \theta(x) + \mathcal{A}_2(x, \xi_i) \theta'(x) - \mathcal{A}_3(x, \xi_i) \theta''(x) + \mathcal{A}_4(x, \xi_i) \theta'''(x) \right]_{x=0}^{x=l} \quad (\text{A1.55})$$

In order to solve the problem, the derivatives of the solution are required. The integral representation of the first derivative has already been presented in eqn. (A1.43). Thus, differentiating this equation with respect to ξ , the discretized forms of the derivatives of the solution are obtained as

$$\frac{d\theta(\xi_i)}{d\xi} = -\sum_{j=1}^L q_j \int_{\Gamma_j} A_3(x, \xi_i) dx - \left[-A_1(x, \xi_i)\theta'(x) + A_2(x, \xi_i)\theta''(x) - A_3(x, \xi_i)\theta'''(x) \right]_{x=0}^{x=l} \quad (\text{A1.56a})$$

$$\frac{d^2\theta(\xi_i)}{d\xi^2} = \sum_{j=1}^L q_j \int_{\Gamma_j} A_2(x, \xi_i) dx - \left[-A_1(x, \xi_i)\theta''(x) + A_2(x, \xi_i)\theta'''(x) \right]_{x=0}^{x=l} \quad (\text{A1.56b})$$

$$\frac{d^3\theta(\xi_i)}{d\xi^3} = -\sum_{j=1}^L q_j \int_{\Gamma_j} A_1(x, \xi_i) dx - \left[-A_1(x, \xi_i)\theta'''(x) \right]_{x=0}^{x=l} \quad (\text{A1.56c})$$

Finally, applying eqns. (A1.55) and (A1.56) to the L collocation points yield

$$\boldsymbol{\theta} = \mathbf{A}\mathbf{q} + \mathbf{C} \begin{Bmatrix} \hat{\boldsymbol{\theta}} \\ \hat{\boldsymbol{\theta}}_{,x} \\ \hat{\boldsymbol{\theta}}_{,xx} \\ \hat{\boldsymbol{\theta}}_{,xxx} \end{Bmatrix} = \mathbf{B}\mathbf{d} \quad \boldsymbol{\theta}_{,x} = \mathbf{A}_{,x}\mathbf{q} + \mathbf{C}_{,x} \begin{Bmatrix} \hat{\boldsymbol{\theta}} \\ \hat{\boldsymbol{\theta}}_{,x} \\ \hat{\boldsymbol{\theta}}_{,xx} \\ \hat{\boldsymbol{\theta}}_{,xxx} \end{Bmatrix} = \mathbf{B}_{,x}\mathbf{d} \quad (\text{A1.57a,b})$$

$$\boldsymbol{\theta}_{,xx} = \mathbf{A}_{,xx}\mathbf{q} + \mathbf{C}_{,xx} \begin{Bmatrix} \hat{\boldsymbol{\theta}} \\ \hat{\boldsymbol{\theta}}_{,x} \\ \hat{\boldsymbol{\theta}}_{,xx} \\ \hat{\boldsymbol{\theta}}_{,xxx} \end{Bmatrix} = \mathbf{B}_{,xx}\mathbf{d} \quad \boldsymbol{\theta}_{,xxx} = \mathbf{A}_{,xxx}\mathbf{q} + \mathbf{C}_{,xxx} \begin{Bmatrix} \hat{\boldsymbol{\theta}} \\ \hat{\boldsymbol{\theta}}_{,x} \\ \hat{\boldsymbol{\theta}}_{,xx} \\ \hat{\boldsymbol{\theta}}_{,xxx} \end{Bmatrix} = \mathbf{B}_{,xxx}\mathbf{d} \quad (\text{A1.57c,d})$$

where

$$\boldsymbol{\theta}^T = [(\theta)_1 \quad (\theta)_2 \quad \cdots \quad (\theta)_L] \quad \boldsymbol{\theta}_{,x}^T = [(\theta')_1 \quad (\theta')_2 \quad \cdots \quad (\theta')_L] \quad (\text{A1.58a,b})$$

$$\boldsymbol{\theta}_{,xx}^T = [(\theta'')_1 \quad (\theta'')_2 \quad \cdots \quad (\theta'')_L] \quad \boldsymbol{\theta}_{,xxx}^T = [(\theta''')_1 \quad (\theta''')_2 \quad \cdots \quad (\theta''')_L] \quad (\text{A1.58c,d})$$

are $L \times 1$ vector including the unknown values of u and its derivative with respect to x , at the L nodal points of the interval, while \mathbf{A} , $\mathbf{A}_{,x}$, $\mathbf{A}_{,xx}$, $\mathbf{A}_{,xxx}$ are $L \times L$ square matrices with coefficients defined as

$$A_{ij} = \int_{\Gamma_j} A_4(x, \xi_i) dx \quad A_{ij,x} = -\int_{\Gamma_j} A_3(x, \xi_i) dx \quad (\text{A1.59a,b})$$

$$A_{ij,xx} = \int_{\Gamma_j} A_2(x, \xi_i) dx \quad A_{ij,xxx} = -\int_{\Gamma_j} A_1(x, \xi_i) dx \quad (\text{A1.59c,d})$$

where $i = 1, 2, \dots, L$, $j = 1, 2, \dots, L$. Moreover, \mathbf{C} , $\mathbf{C}_{,x}$, $\mathbf{C}_{,xx}$, $\mathbf{C}_{,xxx}$ are $L \times 8$ matrices defined as (Mokos 2007)

$$\mathbf{C} = \begin{bmatrix} \Lambda_4(0, \xi_1) & -\Lambda_3(0, \xi_1) & \Lambda_2(0, \xi_1) & -\Lambda_1(0, \xi_1) & | & -\Lambda_4(l, \xi_1) & \Lambda_3(l, \xi_1) & -\Lambda_2(l, \xi_1) & \Lambda_1(l, \xi_1) \\ \Lambda_4(0, \xi_2) & -\Lambda_3(0, \xi_2) & \Lambda_2(0, \xi_2) & -\Lambda_1(0, \xi_2) & | & -\Lambda_4(l, \xi_2) & \Lambda_3(l, \xi_2) & -\Lambda_2(l, \xi_2) & \Lambda_1(l, \xi_2) \\ \vdots & \vdots & \vdots & \vdots & | & \vdots & \vdots & \vdots & \vdots \\ \Lambda_4(0, \xi_L) & -\Lambda_3(0, \xi_L) & \Lambda_2(0, \xi_L) & -\Lambda_1(0, \xi_L) & | & -\Lambda_4(l, \xi_L) & \Lambda_3(l, \xi_L) & -\Lambda_2(l, \xi_L) & \Lambda_1(l, \xi_L) \end{bmatrix} \quad (\text{A1.60a})$$

$$\mathbf{C}_{,x} = \begin{bmatrix} -\Lambda_3(0, \xi_1) & \Lambda_2(0, \xi_1) & -\Lambda_1(0, \xi_1) & 0 & | & \Lambda_3(l, \xi_1) & -\Lambda_2(l, \xi_1) & \Lambda_1(l, \xi_1) & 0 \\ -\Lambda_3(0, \xi_2) & \Lambda_2(0, \xi_2) & -\Lambda_1(0, \xi_2) & 0 & | & \Lambda_3(l, \xi_2) & -\Lambda_2(l, \xi_2) & \Lambda_1(l, \xi_2) & 0 \\ \vdots & \vdots & \vdots & \vdots & | & \vdots & \vdots & \vdots & \vdots \\ -\Lambda_3(0, \xi_L) & \Lambda_2(0, \xi_L) & -\Lambda_1(0, \xi_L) & 0 & | & \Lambda_3(l, \xi_L) & -\Lambda_2(l, \xi_L) & \Lambda_1(l, \xi_L) & 0 \end{bmatrix} \quad (\text{A1.60b})$$

$$\mathbf{C}_{,xx} = \begin{bmatrix} \Lambda_2(0, \xi_1) & -\Lambda_1(0, \xi_1) & 0 & 0 & | & -\Lambda_2(l, \xi_1) & \Lambda_1(l, \xi_1) & 0 & 0 \\ \Lambda_2(0, \xi_2) & -\Lambda_1(0, \xi_2) & 0 & 0 & | & -\Lambda_2(l, \xi_2) & \Lambda_1(l, \xi_2) & 0 & 0 \\ \vdots & \vdots & \vdots & \vdots & | & \vdots & \vdots & \vdots & \vdots \\ \Lambda_2(0, \xi_L) & -\Lambda_1(0, \xi_L) & 0 & 0 & | & -\Lambda_2(l, \xi_L) & \Lambda_1(l, \xi_L) & 0 & 0 \end{bmatrix} \quad (\text{A1.60c})$$

$$\mathbf{C}_{,xxx} = \begin{bmatrix} -\Lambda_1(0, \xi_1) & 0 & 0 & 0 & | & \Lambda_1(l, \xi_1) & 0 & 0 & 0 \\ -\Lambda_1(0, \xi_2) & 0 & 0 & 0 & | & \Lambda_1(l, \xi_2) & 0 & 0 & 0 \\ \vdots & \vdots & \vdots & \vdots & | & \vdots & \vdots & \vdots & \vdots \\ -\Lambda_1(0, \xi_L) & 0 & 0 & 0 & | & \Lambda_1(l, \xi_L) & 0 & 0 & 0 \end{bmatrix} \quad (\text{A1.60d})$$

while exploiting eqns. (A1.37) result in

$$\Lambda_1(0, \xi_i) = -\frac{l}{2} \quad \Lambda_2(0, \xi_i) = \frac{l}{2}(\xi_i - l) \quad (\text{A1.61a,b})$$

$$\Lambda_3(0, \xi_i) = -\frac{l}{4}\xi_i(\xi_i - 2l) \quad \Lambda_4(0, \xi_i) = \frac{l}{12}(\xi_i^3 - 3l\xi_i^2 + 2l^3) \quad (\text{A1.61c,d})$$

$$\Lambda_1(l, \xi_i) = \frac{l}{2} \quad \Lambda_2(l, \xi_i) = -\frac{l}{2}\xi_i \quad (\text{A1.61e,f})$$

$$\Lambda_3(l, \xi_i) = -\frac{l}{4}(l^2 - \xi_i^2) \quad \Lambda_4(l, \xi_i) = \frac{l}{12}((l - \xi_i)^3 - 3l(l - \xi_i)^2 + 2l^3) \quad (\text{A1.61g,h})$$

where $\xi_i = x_{i0}$ is the coordinate of the mid-point of the element Γ_i (Fig.A1.1) and \mathbf{B} , $\mathbf{B}_{,x}$, $\mathbf{B}_{,xx}$, $\mathbf{B}_{,xxx}$ are $L \times (L+8)$ matrices defined as $\mathbf{B} = [\mathbf{A} \quad \mathbf{C}]$, $\mathbf{B}_{,x} = [\mathbf{A}_{,x} \quad \mathbf{C}_{,x}]$, $\mathbf{B}_{,xx} = [\mathbf{A}_{,xx} \quad \mathbf{C}_{,xx}]$, $\mathbf{B}_{,xxx} = [\mathbf{A}_{,xxx} \quad \mathbf{C}_{,xxx}]$.

The final step of the AEM is the application of the governing equation of the initial problem (A1.31) at the L internal nodal points and subsequently the substitution of the values of the field function θ and its derivative at the L internal nodal points according to eqns. (A1.57). From the definition of the analog equation (A1.32) it is apparent that the values of fourth derivative θ'''' at the nodal points are equal to the corresponding values of the fictitious load vector \mathbf{q} . Thus, L additional algebraic equations are derived with respect to the generalized unknown vector \mathbf{d} . These equations in combination with eqns. (A1.54) constitute a system of $L+8$ algebraic equations with $L+8$ unknowns. The solution of this system provides the values of the fictitious load at the L internal nodal points as well as the values of the field function θ and its derivatives θ' , θ'' , θ''' at the edges of the examined interval. Thereafter, exploiting eqn. (A1.57) the vectors including the values of the solution and its derivative at the L internal nodal points are obtained. Finally, it is noted that the values of θ , θ' , θ'' , θ''' at any point of the interval $\xi \in (0, l)$ can be easily calculated, by applying the integral representations (A1.55-56) substituting the value ξ_i with ξ .

A1.4.2 Evaluation of Integrals

In order to determine the coefficients of the matrices \mathbf{F}_1 , \mathbf{F}_2 , \mathbf{A} , $\mathbf{A}_{,x}$, $\mathbf{A}_{,xx}$ and $\mathbf{A}_{,xxx}$ (relations (A1.54), (A1.57)) the integrals defined in eqns. (A1.51) and (A1.59) have first to be evaluated. This calculation can be easily performed employing any numerical integration scheme (e.g. Gauss, Gauss-Lobatto). Nevertheless, due to the closed form of the kernels, the analytic integration along the element's Γ_j length is indicated, thus avoiding any computational error and the increase of the computational time. Exploiting eqns. (A1.37), the analytic expressions of the integrals of the coefficients \hat{F}_{ij} ($i = 1, 2, 3, 4$, $j = 1, 2, \dots, L$) defined in eqns. (A1.4.21) are obtained as

$$\hat{F}_{1j} = \frac{l}{12} \left[2l^3 x + \frac{l}{4} x^4 - lx^3 \right]_{x=x_{j1}}^{x=x_{j2}} \quad (\text{A1.62a})$$

$$\hat{F}_{2j} = \frac{l}{12} \left[2l^3 x - \frac{l}{4}(l-x)^4 + l(l-x)^3 \right]_{x=x_{j1}}^{x=x_{j2}} \quad (\text{A1.62b})$$

$$\hat{F}_{3j} = -\frac{l}{4} \left[\frac{l}{3} x^3 - lx^2 \right]_{x=x_{j1}}^{x=x_{j2}} \quad \hat{F}_{4j} = -\frac{l}{4} \left[\frac{l}{3}(l-x)^3 - l(l-x)^2 \right]_{x=x_{j1}}^{x=x_{j2}} \quad (\text{A1.62c,d})$$

where x_{j1} , x_{j2} are the coordinates of the element's Γ_j edges (Fig.A1.1). Moreover, from eqns. (A1.37), the analytic expressions of the coefficients A_{ij} , $A_{ij,x}$, $A_{ij,xx}$ and $A_{ij,xxx}$ ($i = 1, 2, \dots, L$, $j = 1, 2, \dots, L$) defined in eqns. (A1.59) are obtained as

$$A_{ij} = \frac{l}{12} \left[2l^3 x - \frac{l}{4}(x_{i0} - x)^4 + l(x_{i0} - x)^3 \right]_{x=x_{j1}}^{x=x_{j2}}, \quad i > j \quad (\text{A1.63a})$$

$$A_{ij} = \frac{l}{12} \left[2l^3 x + \frac{l}{4}(x - x_{i0})^4 - l(x - x_{i0})^3 \right]_{x=x_{j1}}^{x=x_{j2}}, \quad i < j \quad (\text{A1.63b})$$

$$A_{ij} = \frac{l}{12} \left[2l^3 x - \frac{l}{4}(x_{i0} - x)^4 + l(x_{i0} - x)^3 \right]_{x=x_{j1}}^{x=x_{j0}} + \frac{l}{12} \left[2l^3 x + \frac{l}{4}(x - x_{i0})^4 - l(x - x_{i0})^3 \right]_{x=x_{j0}}^{x=x_{j2}}, \quad i = j \quad (\text{A1.63c})$$

$$A_{ij,x} = -\frac{l}{4} \left[\frac{l}{3}(x_{i0} - x)^3 - l(x_{i0} - x)^2 \right]_{x=x_{j1}}^{x=x_{j2}}, \quad i > j \quad (\text{A1.64a})$$

$$A_{ij,x} = -\frac{l}{4} \left[\frac{l}{3}(x - x_{i0})^3 - l(x - x_{i0})^2 \right]_{x=x_{j1}}^{x=x_{j2}}, \quad i < j \quad (\text{A1.64b})$$

$$A_{ij,x} = -\frac{l}{4} \left[\frac{l}{3}(x_{i0} - x)^3 - l(x_{i0} - x)^2 \right]_{x=x_{j1}}^{x=x_{j0}} - \frac{l}{4} \left[\frac{l}{3}(x - x_{i0})^3 - l(x - x_{i0})^2 \right]_{x=x_{j0}}^{x=x_{j2}}, \quad i = j \quad (\text{A1.64c})$$

$$A_{ij,xx} = -\frac{I}{2} \left[\frac{I}{2} (x_{i0} - x)^2 + lx \right]_{x=x_{j1}}^{x=x_{j2}}, \quad i > j \quad (\text{A1.65a})$$

$$A_{ij,xx} = \frac{I}{2} \left[\frac{I}{2} (x - x_{i0})^2 - lx \right]_{x=x_{j1}}^{x=x_{j2}}, \quad i < j \quad (\text{A1.65b})$$

$$A_{ij,xx} = -\frac{I}{2} \left[\frac{I}{2} (x_{i0} - x)^2 + lx \right]_{x=x_{j1}}^{x=x_{j0}} + \frac{I}{2} \left[\frac{I}{2} (x - x_{i0})^2 - lx \right]_{x=x_{j0}}^{x=x_{j2}}, \quad i = j \quad (\text{A1.65c})$$

$$A_{ij,xxx} = \frac{I}{2} [x]_{x=x_{j1}}^{x=x_{j2}}, \quad i > j \quad (\text{A1.4.36a})$$

$$A_{ij,xxx} = -\frac{I}{2} [x]_{x=x_{j1}}^{x=x_{j2}}, \quad i < j \quad (\text{A1.4.36b})$$

$$A_{ij,xxx} = 0, \quad i = j \quad (\text{A1.4.36c})$$

where x_{j1}, x_{j2} and x_{j0} are the coordinates of the element's Γ_j edges and mid-point, respectively, while x_{i0} are the coordinates of mid-point of the element Γ_i (Fig. A1.1).

Appendix A2

Domain BEM for Ordinary Differential Equations of the 2nd Order

A2.1 Introduction

Several boundary value problems, formulated in this doctoral thesis, have been solved employing the Domain Boundary Element Method (D-BEM). In numerical analysis, D-BEM belongs to the family of Boundary Element Methods (BEM) and is applicable to either linear or nonlinear, static or dynamic boundary value problems with constant or variable coefficients, subjected to either linear or nonlinear boundary conditions. Even though, pure BEM requires the calculation of the *fundamental solution* (or Green's function), placing considerable restrictions on the range and applicability of the method, the D-BEM is capable of dealing with problems at which the fundamental solution is unknown. According to this method, the boundary integral representation is supplemented with domain integrals. That is, both boundary and domain discretization are required. Typical approaches for evaluating the domain integrals involving discretization of the interior of the domain (Lagrangian Interpolants, Numerical Quadrature) could be incorporated in BEMs. Nevertheless, this additional discretization devaluates one of the main attractions of using a boundary element technique.

Over the years, several approaches for either evaluating or eliminating domain integrals have been developed, in order to maintain the pure boundary character of the method. Nardini and Brebbia (1982) proposed a generalization of the concept of particular integrals, known as Dual Reciprocity Method (DRM) (Kontoni et al 1991, Partridge et al 1992), while Ahmad and Banerjee (1986) used a closed form representation of a Particular Solution. Both methods require approximation of the field function in the interior of the domain with the use of Radial Basis Functions (RBF). Korsmeyer et al (1993) used the Fast Multipole Method (FMM) to study three dimensional potential problems, while a vast amount of applications have been presented by Katsikadelis and Sapountzakis (1988, 1991), Katsikadelis et al. (1990) and Sapountzakis and Katsikadelis (1991, 1992) in which the Classical Domain Integration

is implemented. In general, this approach is employed in cases where the values of the field function at the interior points are unknown. This domain integration technique requires the subdivision of the interior of the domain into triangular or quadrilateral interior elements. These elements contain the unknown quantities of the field function at the interior points and can be evaluated by either *iterative processes* or by *collocation techniques* (Ingber et al. 2001). In the first, the domain integral can be evaluated with an initial guess for the unknowns allowing an approximate boundary solution to be found. Based on this approximate solution new values for the unknowns can be found, leading to an improved estimation of the solution. The iteration is repeated until convergence is succeeded within the required level of accuracy. Even though, this procedure is versatile the convergence is not guaranteed. However, according to the collocation technique, the field function's values at the interior element nodes are introduced as additional unknowns. A system of equations is formulated by applying the boundary integral equations of the problem into these nodes and the solution of the system yields the unknown quantities of the field function.

In this appendix, the main principles of D-BEM are presented, in case of one-dimensional boundary value problems described by ordinary differential equations of the 2nd order. It is noted that the differential operator of the problem can be either linear or nonlinear, while similar procedure could be followed for the 4th order differential equations.

A2.2 Main Concepts of the Domain – Boundary Element Method

Consider the one-dimensional boundary value problem

$$\frac{d^2u}{dx^2} - \frac{dN(x,u,u')}{dx} = g(x), \quad x \in (0,l) \quad (\text{A2.1a})$$

$$a_1 \left(\frac{du}{dx} - N(x,u,u') \right) + a_2 u = a_3, \quad x = 0,l \quad (\text{A2.1b})$$

where $(\cdot)'$ denotes differentiation with respect to x , $N(\cdot)$ is linear or nonlinear one-dimensional operator of first order, a_i ($i=1,2,3$) are functions specified at $x=0,l$, $g(x)$ is the known source function defined at $(0,l)$ and $u=u(x)$ is the sought solution

of the problem, having continuous derivatives up to the second order in $(0, l)$. According to BEM and employing eqns. (A1.4), (A1.3a) the integral representation of the solution (A1.8) can be written as

$$u(\xi) = \int_0^l A_2^u(x, \xi) [N'(x, u, u') + g(x)] dx - \left[-A_1^u(x, \xi)u(x) + A_2^u(x, \xi)u'(x) \right]_{x=0}^{x=l} \quad (\text{A2.2})$$

where A_1^u , A_2^u are the kernels as defined in eqns. (A1.9). By applying integration by parts the above equation can be written as

$$u(\xi) = \int_0^l A_2^u(x, \xi) g(x) dx - \int_0^l A_1^u(x, \xi) N(x, u, u') dx + \left[A_2^u(x, \xi) N(x, u, u') \right]_{x=0}^{x=l} - \left[-A_1^u(x, \xi)u(x) + A_2^u(x, \xi)u'(x) \right]_{x=0}^{x=l} \quad (\text{A2.3})$$

while differentiating with respect to ξ , yields

$$u'(\xi) = -\int_0^l A_1^u(x, \xi) g(x) dx + N(\xi, u, u') + \left[A_1^u(x, \xi) [u'(x) - N(x, u, u')] \right]_{x=0}^{x=l} \quad (\text{A2.4})$$

Thereafter, the interval $(0, l)$ is discretized into L elements. The integral representation of the field function (A2.3) and its derivative (A2.4) can be written as follows

$$u(\xi) = \int_0^l A_2^u(x, \xi) g(x) dx - \sum_{j=1}^L \int_{\Gamma_j} A_1^u(x, \xi) N(x, u, u') dx - \left[-A_1^u(x, \xi)u(x) + A_2^u(x, \xi)(u'(x) - N(x, u, u')) \right]_{x=0}^{x=l} \quad (\text{A2.5})$$

$$u'(\xi) = -\int_0^l A_1^u(x, \xi) g(x) dx + N(\xi, u, u') + \left[A_1^u(x, \xi) [u'(x) - N(x, u, u')] \right]_{x=0}^{x=l} \quad (\text{A2.6})$$

A2.3 Classical Domain Integration

As it is mentioned above, the classical domain integration is implemented in cases where the values of the field function at the interior points are unknown. The integral

$\int_{\Gamma_j} A_I^u(x, \xi) N(x, u, u') dx$ ($j = 1, 2, \dots, L$), as defined in eqn. (A2.5), is approximated as a weighted sum of the integrand at a finite set of points called integration points. The integration points and weights depend on the specific rule employed and the required accuracy. Herein, the Gauss rule has been adopted and K integration points are assumed in each element. Thus the above integral can be written as

$$\int_{\Gamma_j} A_I^u(x, \xi) N(x, u, u') dx = \sum_{k=1}^K A_I^u(x_{jk}, \xi) N(x_{jk}, u_{jk}, u'_{jk}) w_k \quad (\text{A2.7})$$

where w_k ($k = 1, 2, \dots, K$) are known weights, while x_{jk} ($k = 1, 2, \dots, K$) are predetermined Gauss points located within the element j ($j = 1, 2, \dots, L$). Substituting the above equation into eqn. (A2.5), yields

$$\begin{aligned} u(\xi) = & \int_0^l A_2^u(x, \xi) g(x) dx - \sum_{j=1}^L \sum_{k=1}^K A_I^u(x_{jk}, \xi) N(x_{jk}, u_{jk}, u'_{jk}) w_k - \\ & - \left[-A_I^u(x, \xi) u(x) + A_2^u(x, \xi) (u'(x) - N(x, u, u')) \right]_{x=0}^{x=l} \end{aligned} \quad (\text{A2.8})$$

By applying the integral representations (A2.6) and (A2.8) to the $L \times K$ collocation points ($\xi_i = x_{jk}$ $i = 1, 2, \dots, L \times K$, $j = 1, 2, \dots, L$, $k = 1, 2, \dots, K$) together with the integral representation (A2.8) to the interval's edges ($\xi = \xi_0 = 0$, $\xi = \xi_{L \times K + 1} = l$), a system of $2L \times K + 2$ algebraic equations with $2L \times K + 4$ unknowns is formulated. This system in combination with the boundary conditions constitutes a system of $2L \times K + 4$ algebraic equation with $2L \times K + 4$ unknowns; namely, the internal u_i, u'_i ($i = 1, 2, \dots, L \times K$) and the boundary quantities $u_j, u'_j - N(x_j, u_j, u'_j)$ ($j = 1, L + 1$) at $\xi = \xi_0 = 0$, $\xi = \xi_{L \times K + 1} = l$. The solution of this system provides the values of u, u' at $L \times K$ internal nodal points as well as the values of u and $u' - N(x, u, u')$ at the edges of the examined interval. It is noted that the values of u and u' at any point of the interval $\xi \in (0, l)$ can be easily calculated from the integral representations (A2.6) and (A2.8) for the examined value of ξ . Furthermore, in order to avoid singularities in case

the collocation point ξ_i is located within the element j , the integral presented in eqn. (A2.7) is normalized according to Katsikadelis and Sapountzakis (1988) as follows

$$\int_{\Gamma_j} A_I^u(x, \xi_i) N(x, u, u') dx = \int_{\Gamma_j} A_I^u(x, \xi_i) (N(x, u, u') - N(\xi_i, u_i, u_i')) dx + N(\xi_i, u_i, u_i') \int_{\Gamma_j} A_I^u(x, \xi_i) dx \quad (\text{A2.9})$$

Since the quantity $A_I^u(x, \xi_i) (N(x, u, u') - N(\xi_i, u_i, u_i'))$ of the above equation has a finite value, the first integral of the right hand side can be evaluated performing any domain integration rule, while the second one can be evaluated analytically. Finally, it is worth mentioning that the integrals $\int_0^l A_I^u(x, \xi) g(x) dx$ and $\int_0^l A_2^u(x, \xi) g(x) dx$ of eqns. (A2.5) and (A2.6), respectively, can also be analytically evaluated provided that $g(x)$ is a known function.

A2.4 Approximation of the Field Function

The approximation of the field function technique is usually adopted in case the field function is known at any point of the domain. It requires approximation of the unknown field function in the interior of the domain with simple shape functions, leading to the formulation of integrals which can be evaluated either analytically or numerically (Sapountzakis 2000). More specifically, it is assumed that the unknown function u varies within the element j , according to a specific distribution rule (i.e. constant, linear, quadratic, cubic etc). Thus, the distribution of the function's derivative u' can be easily obtained. The explicit definition of the boundary value problem with respect to the unknown quantities u, u' at any point of the interval, permits the analytical determination of the integral $\int_{\Gamma_j} A_I^u(x, \xi) N(x, u, u') dx$ ($j = 1, 2, \dots, L$) of eqn. (A2.5).

By applying the integral representations (A2.5,6) to the L collocation points ξ_i ($i = 1, 2, \dots, L$) together with the integral representation (A2.5) to the interval's edges ($\xi = \xi_0 = 0, \xi = \xi_{L+1} = l$), a system of $2L + 2$ algebraic equations with $2L + 4$ unknowns is formulated. This system in combination with the boundary conditions constitutes a system of $2L + 4$ algebraic equation with $2L + 4$ unknowns. The solution

of this system provides the values of the distribution rule quantities of u at the L nodal points and the boundary quantities $u_j, u'_j - N(x_j, u_j, u'_j)$ ($j = 1, L + 1$) at the intervals edges $\xi = \xi_0 = 0, \xi = \xi_{L+1} = l$. It is noted that the values of u and u' at any point of the interval $\xi \in (0, l)$ can be easily calculated from the integral representations (A2.5) and (A2.6) for the examined value of ξ . Finally, it is worth mentioning that the integrals $\int_0^l A_1^u(x, \xi) g(x) dx$ and $\int_0^l A_2^u(x, \xi) g(x) dx$ of eqns. (A2.5) and (A2.6), respectively, can be also analytically evaluated provided that $g(x)$ is a known function, while in the special case where the operator N is only a function of u' only one of the integral representations has to be employed for the solution of the problem.

Appendix A3

Shear Centre – Shear Deformation Coefficients

A3.1 Introduction

In engineering practice the analysis of beam members is frequently encountered. In the vast majority of these cases the assumptions of the well established Euler-Bernoulli theory plays a dominant role on the structural analysis. Nevertheless, in cases where shear deformation is not negligible, this theory fails to give acceptable results.

To this end, Stephen Timoshenko (1921, 1922) developed and established a beam model that takes into account the shear deformation effect making it suitable for describing the behaviour of short beams or beam under significant transverse loading. Under a physical perspective, the Timoshenko beam theory accounts for the displacement w_s of the beam axis due to shear deformation in addition to the one due to bending w_b (Fig. A3.1a). Thus, the total angles of rotation is not equal to the derivative of the transverse displacement but equals to the sum of this derivative and the corresponding shear strain component (Fig. A3.1b). Under this consideration, the key assumption of the Euler-Bernoulli theory, stated as “*plane sections initially perpendicular to the centroidal axis, remain plane and perpendicular to the axis after deformation*” is relaxed to “*plane sections initially perpendicular to the centroidal axis, remain plane to the axis after deformation*” implying that the cross-sections are allowed to develop shear strain.

From a practical point of view, the added shear deformation mechanisms reduces the stiffness of the beam, resulting in larger displacements and lower predicted eigenfrequencies for a specific set of boundary conditions. Moreover, it is worth noting that for relatively large ratio of length over thickness of the beam or if the shear stiffness is relatively high (compared to the flexural one), the Timoshenko beam theory converges to the Euler-Bernoulli one.

In general, shear stresses due to shear loading develop in a non-uniform way within the cross section. Thus, the distribution of shear strains will be non-uniform

resulting in warping of the cross section. Consequently, the Euler-Bernoulli assumption is not valid (Fig.A3.2). In case of a beam under constant shear force along the length and unrestrained longitudinal displacements, the applied shear load is undertaken only by shear stresses that are maximized on the boundary. This is called *Uniform Shear* (Timoshenko & Goodier 1951, Love 1952, Sokolnikoff 1956). On the contrary, if the shear load varies along the length or/and warping is restrained due to loading or support conditions, shear stresses develop. Theories regarding *Non-uniform Shear* of homogenous beams have been stated by Fatmi (2007a, 2007b).

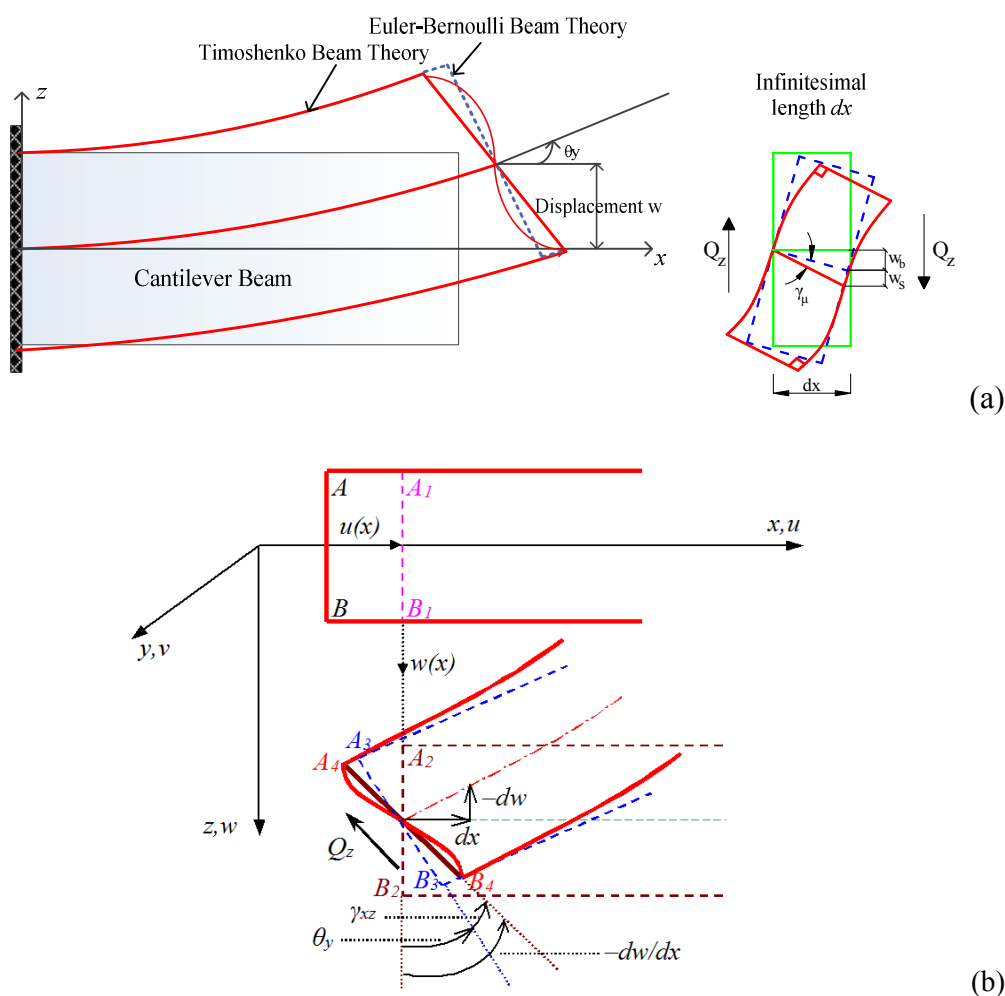


Fig. A3.1 Cantilever beam under transversal load and an infinitesimal segment (a) displacement field of shear deformable Timoshenko beam (b).

Warping due to shear is considered in general to be small. Thus, stresses due to shear loading are usually determined considering uniform shear, while the effect of warping is taken implicitly into account with the use of appropriate shear deformation

coefficients. Timoshenko (1921, 1922) was the first who considered the influence of shear deformation using correction factors (k) and altering appropriately the equilibrium equations of the beam. More specifically, similarly to the ordinary beam theory, the Timoshenko one yields a differential equation of the fourth order to describe the equilibrium of the beam. The difference lies in the additional second order spatial derivative, which is multiplied by a shear deformation coefficient in order to correct the value of the calculated shear force. The inaccuracy of the originally obtained shear force is attributed to the assumption of constant shear stress distribution along the cross-section. As a result, the beam theory which takes into account these coefficients is known as *Timoshenko Beam Theory*.

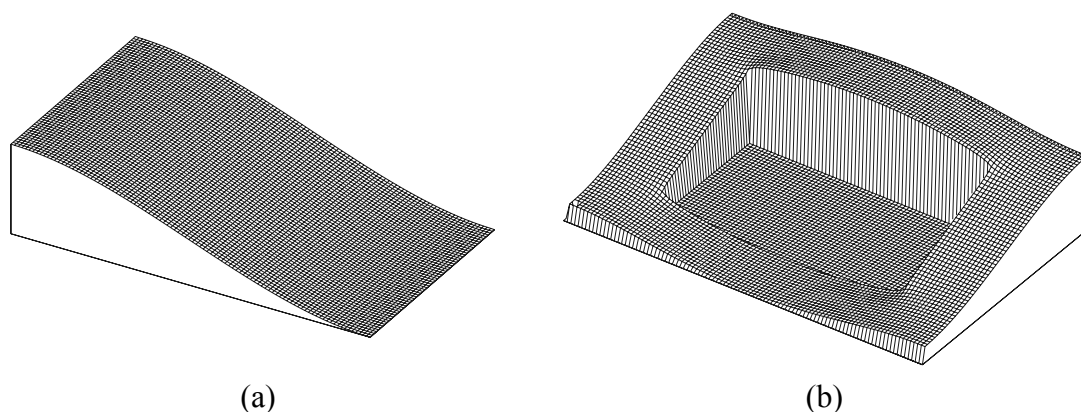


Fig. A3.2. Warping due to shear for rectangular (a) and hollow rectangular (b) cross section.

Furthermore, in beams under transverse loading, shear stresses are developed and usually occur in conjunction with bending, while in case this externally imposed loading is not applied through the shear centre of the cross section, except for shear, torsional stresses are also developed due to eccentricity. Thus, in order to avoid torsional effects the shear centre S is defined as “the point in the cross sectional plane where a shear force can be applied without introducing any torsional moment due to shear stresses, that is,

$$Q_z \cdot Y^S - Q_y \cdot Z^S = \int_{\Omega} (\tau_{xz} \cdot Y - \tau_{xy} \cdot Z) d\Omega \quad (\text{A3.1})$$

where Q_y, Q_z are the shear forces along y and z axes respectively, C_{xyz} is the centroidal system of axes, y^S, z^S are the shear centre S coordinates with respect to the cross section centroid C and τ_{xy}, τ_{xz} are the shear stresses developed over the cross section (Fig. A3.3). The left hand side of eqn. (A3.1) expresses the external moment while the right hand side expresses the internal moment due to shear stresses. If the centroid C coincides with the shear centre S , the twisting moment due to the shear stresses becomes equal to zero. If the shear stresses due to shear loading are known, the position of the shear centre can be determined. In case the shear stresses are computed for a Poisson's ratio equal to zero ($\nu=0$), the position of the shear centre is independent of the type and the size of the external loading and depends only on the shape of the beam's cross section (Weber 1924, Trefftz 1935).

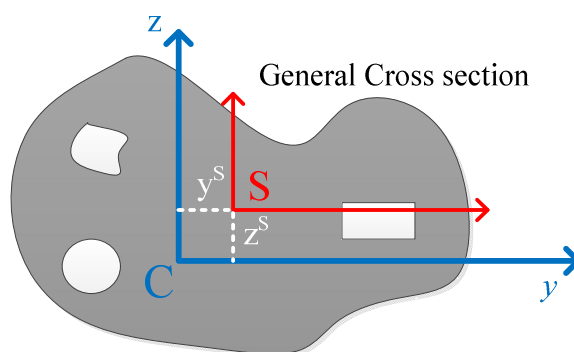


Fig. A3.3. Shear centre S with respect to the centroid C .

Thus, considering the above, the solution of uniform shear problem can be obtained by the determination of shear stresses over the interior of the cross section, the position of the shear centre S and the shear deformation coefficients a of the beam's cross section.

The “accurate” statement of uniform shear problem is described by a boundary value problem, avoiding in this way the approximations arising from the shear engineering beam theory (Sauer 1980, Hartmann & Katz 2007) and the thin-walled theory (Vlasov, 1964, 1965). The formulation of this problem can be obtained either with respect to the displacement or to the stress field (Mokos & Sapountzakis 2005), with the aid of the theory of elasticity.

Over the years, the calculation of the shear deformation coefficients has been a subject of extensive research activity (Kaneko 1975, Renton 1991, 1997, Hutchinson

2001). According to Timoshenko (1921, 1922), this coefficient is evaluated as the ratio of the average value of the developed shear stresses over the cross section divided by the value of the shear stress at the centroid of the cross section. Apparently, the previously mentioned definition has difficulties during implementation when the centroid is placed out of the domain of the cross section. Later, Cowper (1966) suggested a new shear deformation coefficient formulating the equilibrium equations of the beam by integrating the equilibrium equations of the three-dimensional elasticity, which take more into account the influence of warping (compared with Timoshenko coefficient) mainly in dynamic analysis of high frequency beams. The suggested coefficients by Timoshenko and Cowper for a variety of simple cross sections are the same for a Poisson's ratio $\nu = 0$. The Cowper coefficient concerns only symmetric cross sections with an orientation about the principal axis bending system which results in the existence of two shear deformation coefficients a_{yy} and a_{zz} . Mason and Herrmann (1968) tried to extend Cowper's method in asymmetric cross sections with an arbitrary system of axis resulting in having instead of a_{yy} and a_{zz} , two new unequal coefficients, the a_{yz} and a_{zy} . Apparently, the use of the two unequal coefficients a_{yz} and a_{zy} in analysis is not appropriate since it leads to non-symmetric stiffness matrices. The aforementioned shear deformation coefficients do not take into account the width b to depth h ratio of the cross section yielding inaccurate results with the decrement of the depth. To this end, Stephen (1980) based on Cowper's theory suggested a new expression for shear deformation coefficients which takes into account the ratio b/h . Hutchinson (2001) using a different methodology derived the same expression as Stephen. Puchegger et al. (2003) verified experimentally the accuracy of Stephen–Hutchinson coefficient for a rectangular cross section of a b/h ratio between 1 and 4. However, Stephen–Hutchinson coefficient, which is valid for symmetric cross sections, as the b/h ratio is increasing exhibits a discontinuity and then takes negative values with the result of not taking realistically into account the influence of warping for some b/h ratios.

A different formulation of shear deformation coefficients can be achieved with the aid of the energy method (Bach & Baumann 1924, Gruttmann and Wagner 2001) according to which the exact strain energy of the beam, owing to the shear stresses calculated according to elasticity theory, is equal to the approximate strain energy of the beam, owing to the shear stresses according to Timoshenko theory. For an arbitrary

cross section with an arbitrary system of axis the energy method allows the determination of the four shear deformation coefficients a_{yy} , a_{zz} , a_{yz} , a_{zy} with a_{yz} and a_{zy} being symmetric ($a_{yz} = a_{zy}$), which take into account Poisson's ratio ν and width to depth ratio b/h of the cross section (Schramm et al. 1994, Pilkey 2002). It should be noted that the coefficients obtained by the energy method (taking into account the b/h ratio) proved to be very effective in dealing with the shear–locking computational problem (Pilkey 2002, Wunderlich & Pilkey 2003). In addition to this, the reliability of shear deformation coefficients based on the energy method is verified with the aid of solid finite elements (Fatmi & Zenzri 2004). Thus, according to the above mentioned, the most appropriate method for the formulation of shear deformation coefficients is the energy method.

Coefficients a_{ij} , ($i, j = y, z$) are the components of a plane (2×2) symmetric second-order tensor while they abide with the transformation law of second-order tensors (Schramm et al. 1997). Thus, corresponding to the plane tensor of bending moments of inertia, the diagonalization of the tensor a_{ij} , ($i, j = y, z$) (Pilkey 2002) will lead to a principal system which is called principal shear system and for asymmetric cross sections does not coincide with the principal bending one. The result of this difference between the two principal systems of axes is the coupling of the displacement components of the beam in y and z directions, even if the cross section system of axes coincides with the principal bending one (Schramm et al. 1997, Pilkey 2002). In case of a symmetric cross section, the principal shear system coincides with the corresponding principal bending one and the deflection components on the principal axes are not coupled ($a_{yz} = a_{zy} = 0$ and $I_{yz} = I_{zy} = 0$).

Reviewing the international literature it is observed that the problem of a prismatic beam subjected in shear torsionless loading has been widely studied from both analytical and numerical point of view. Theoretical discussions concerning flexural shear stresses (Weber 1924, Trefftz 1935, Goodier 1944) or the problem of the centre of shear (Osgood 1943, Goodier 1944, Weinstein 1947, Reissner & Tsai 1972) and text books giving detailed representations of these topics (Love 1952, Sokolnikoff 1956, Muskhelishvili 1963, Timoshenko & Goodier 1984) are mentioned among the extended analytical studies. In all these studies a stress function formulation is presented. This formulation is based on either splitting the stress function into a primary part

independent of the beam material describing the beam equilibrium and a secondary one dependent on the Poisson's ratio satisfying compatibility equations or on splitting the governing differential equation into two parts representing shear and torsion problems. Moreover, these studies are limited in the analysis based on the principal cross section system of axes.

Numerical methods have also been used for the analysis of the aforementioned problem. Among these methods the majority of researchers have employed the *Finite Element Method* (FEM). Mason and Herrmann (1968) based on assumptions for the displacement field and exploiting the principle of minimum potential energy developed triangular finite elements for a beam of arbitrary cross section and isotropic material subjected to bending. This method using triangular or quadrilateral finite elements has also been used for beams with orthotropic (Tolf 1985) and anisotropic material (Haberl & Och 1974, Kosmatka 1993). Later, a finite element solution for the evaluation of the shear stresses (Gruttmann et. al. 1998, 1999) and the shear deformation coefficients (Gruttmann & Wagner 2001) was developed formulating all basic equations to an arbitrary coordinate system, using isoparametric element functions and introducing a stress function which fulfils the equilibrium equations.

Moreover, boundary integral methods seem to be an alternative powerful tool for the solution of the aforementioned problem, having in mind that finite element methods require the whole cross section to be discretized into area (triangular or quadrilateral) elements and are also limited with respect to the shape (distortion) of the elements. *Boundary Element Method* (BEM) solutions require only boundary discretization resulting in line or parabolic elements instead of area elements of FEM solutions, while a small number of line elements are required to achieve high accuracy. Boundary element procedure was first employed by Sauer (1980) for the shear stresses calculation based on Weber analysis (1924) and neglecting Poisson's ratio. BEM was also used for the calculation of the shear centre location in an arbitrary cross section by Chou (1993) and for the presentation of a solution to the general flexure problem in an isotropic only simply connected arbitrary cross section beam by Friedman and Kosmatka (2000). In this research effort the analysis is accomplished with respect only to the principal bending axes of the cross section restricting in this way its generality. Finally, Sapountzakis and Mokos (2005) and Mokos and Sapountzakis(2005) presented a stress function solution employing BEM for the general transverse shear loading problem of homogeneous and composite beams of arbitrary constant cross section, respectively,

while the same authors (Sapountzakis & Mokos 2009) presented a displacement based solution for the same problem of composite beams.

Within this appendix, the solution for the general transverse shear loading problem in beams of arbitrary simply or multiply connected constant cross section is briefly presented. The formulation follows the displacement field adopted in Wagner and Gruttmann (2002) and Sapountzakis and Mokos (2009). The shear deformation coefficients are obtained from the solution of two boundary value problems with respect to warping functions, using pure BEM. The shear deformation coefficients are evaluated using an energy approach (Pilkey 2002) instead of Timoshenko's (1984) and Cowper's (1966) definitions, for which several authors (Schramm et al. 1994, 1997) have pointed out that lead to unsatisfactory results or definitions given by other researchers (Stephen 1980, Hutchinson 2001) for which these factors take negative values.

A3.2 Statement of the problem

Consider a prismatic beam of length L , of arbitrarily shaped cross section, occupying the two dimensional multiply connected region Ω of the y, z plane bounded by Γ_j ($j = 1, 2, \dots, K$) boundary curves, as shown in Fig. A3.4a. Let also denote as Γ the union of the boundaries of the region Ω . These boundary curves are piecewise smooth, i.e. they may have a finite number of corners. The material of the beam (Fig. A3.4b) is assumed homogeneous, isotropic and linearly elastic with modulus of elasticity E , shear modulus G and Poisson ratio ν . Without loss of generality, it may be assumed that the beam end with centroid at point C is fixed, while the x – axis of the coordinate system is the line joining the centroids of the cross sections.

The beam is subjected to concentrated load Q , having components Q_y , Q_z along y, z axes, respectively, applied at the shear centre S of its free end cross section. Under the action of the aforementioned loading, the displacement field of the beam is given as

$$\bar{u}(x, y, z) = \theta_y(x)z - \theta_z(x)y + \tilde{\varphi}_c(y, z) \quad (\text{A3.2a})$$

$$\bar{v}(x, y, z) = v(x) \quad \bar{w}(x, y, z) = w(x) \quad (\text{A3.2b,c})$$

where \bar{u} , \bar{v} , \bar{w} are the axial and transverse beam displacement components with respect to the $Cxyz$ system; $\theta_y(x), \theta_z(x)$ are the angles of rotation about the centroidal y and z axes; $v(x), w(x)$ describe the deflections of a reference point in y and z directions, respectively.

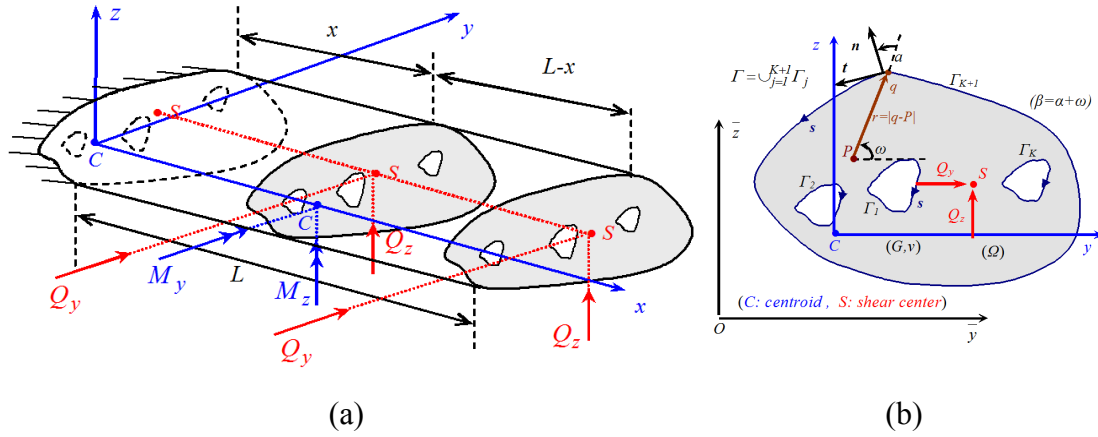


Fig. A3.4. Prismatic beam subjected to torsionless bending (a) with a cross-section of arbitrary shape occupying the two dimensional region Ω (b)

Moreover, $\tilde{\phi}_c(y, z)$ is the warping function due to shear, according to the centroid. The warping function $\tilde{\phi}_c(y, z)$ depends only on the geometry of the cross section, i.e. is a parameter of the cross section and is independent from x coordinate. From a physical point of view, the warping function expresses the displacement of the points on a cross section in the longitudinal direction. However, in a more refined model the influence of this coordinate may also be considered (Dikaros & Sapountzakis 2014a,b).

Employing the strain–displacement equations of the three-dimensional elasticity (Love 1952, Armenakas 2006), the following strain components are obtained

$$\varepsilon_{xx} = \frac{\partial \theta_y}{\partial x} z - \frac{\partial \theta_z}{\partial x} y \quad (\text{A3.3a})$$

$$\gamma_{xy} = \frac{\partial v}{\partial x} - \theta_z + \frac{\partial \tilde{\phi}_c(y, z)}{\partial y} \quad (\text{A3.3b})$$

$$\gamma_{xz} = \frac{\partial w}{\partial x} + \theta_y + \frac{\partial \tilde{\phi}_c(y, z)}{\partial z} \quad (\text{A3.3c})$$

$$\varepsilon_{yy} = \varepsilon_{zz} = \gamma_{yz} = 0 \quad (\text{A3.3d-f})$$

Moreover, the stress-stain relation for isotropic material is given from the following relation

$$\begin{bmatrix} \sigma_{xx} \\ \sigma_{yy} \\ \sigma_{zz} \\ \tau_{xy} \\ \tau_{yz} \\ \tau_{xz} \end{bmatrix} = \begin{bmatrix} \lambda + 2G & \lambda & \lambda & 0 & 0 & 0 \\ \lambda & \lambda + 2G & \lambda & 0 & 0 & 0 \\ \lambda & \lambda & \lambda + 2G & 0 & 0 & 0 \\ 0 & 0 & 0 & G & 0 & 0 \\ 0 & 0 & 0 & 0 & G & 0 \\ 0 & 0 & 0 & 0 & 0 & G \end{bmatrix} \cdot \begin{bmatrix} \varepsilon_{xx} \\ \varepsilon_{yy} \\ \varepsilon_{zz} \\ \gamma_{xy} \\ \gamma_{yz} \\ \gamma_{xz} \end{bmatrix} \quad (\text{A3.4})$$

where $\lambda = \nu E / [(1 + \nu)(1 - 2\nu)]$ is Lamé's constant and $G = E / [2(1 + \nu)]$ is the shear modulus. Substituting eqns. (A3.3a-f) into the above relation and having in mind that in engineering beam theory the Poisson ratio vanishes ($\nu = 0$), the stress components are given as

$$\sigma_{xx} = E \left(\frac{\partial \theta_y}{\partial x} z - \frac{\partial \theta_z}{\partial x} y \right) \quad (\text{A3.5a})$$

$$\tau_{xy} = G \left(\frac{\partial v}{\partial x} - \theta_z + \frac{\partial \tilde{\phi}_c(y, z)}{\partial y} \right) \quad (\text{A3.5b})$$

$$\tau_{xz} = G \left(\frac{\partial w}{\partial x} + \theta_y + \frac{\partial \tilde{\phi}_c(y, z)}{\partial z} \right) \quad (\text{A3.5c})$$

$$\sigma_{yy} = \sigma_{zz} = \tau_{yz} = 0 \quad (\text{A3.5d-f})$$

Introducing the unit warping function $\phi_c(y, z)$ due to shear as

$$\phi_c(y, z) = \left(\frac{\partial v}{\partial x} - \theta_z \right) y + \left(\frac{\partial w}{\partial x} + \theta_y \right) z + \tilde{\phi}_c(y, z) \quad (\text{A3.6})$$

and applying the stress components (A3.5a-c) incorporating eqn.(A3.6) in the first elasticity equation of equilibrium neglecting the body forces (Love 1952, Armenakas 2006)

$$\frac{\partial \sigma_{xx}}{\partial x} + \frac{\partial \tau_{yx}}{\partial y} + \frac{\partial \tau_{zx}}{\partial z} = 0 \quad (\text{A3.7})$$

results in

$$G \left(\frac{\partial^2 \phi_c}{\partial y^2} + \frac{\partial^2 \phi_c}{\partial z^2} \right) = E \left(\frac{\partial^2 \theta_y}{\partial x^2} z - \frac{\partial^2 \theta_z}{\partial x^2} y \right) \quad (\text{A3.8})$$

while the last two elasticity equations of equilibrium are identically satisfied. From eqn. (A3.8) a particular differential equation can be obtained in which the only unknown quantity is the warping function ϕ_c , thus the right hand side term has to be determined.

Exploiting eqn. (A3.5a) the bending moments can be written as

$$M_y = \int_{\Omega} \sigma_{xx} z \, d\Omega = E \left(\frac{\partial \theta_y}{\partial x} \int_{\Omega} z^2 \, d\Omega - \frac{\partial \theta_z}{\partial x} \int_{\Omega} yz \, d\Omega \right) = E \left(\frac{\partial \theta_y}{\partial x} I_{yy} - \frac{\partial \theta_z}{\partial x} I_{yz} \right) \quad (\text{A3.9a})$$

$$M_z = \int_{\Omega} \sigma_{yy} z \, d\Omega = E \left(\frac{\partial \theta_y}{\partial x} \int_{\Omega} z^2 \, d\Omega - \frac{\partial \theta_z}{\partial x} \int_{\Omega} yz \, d\Omega \right) = E \left(\frac{\partial \theta_y}{\partial x} I_{yy} - \frac{\partial \theta_z}{\partial x} I_{yz} \right) \quad (\text{A3.9b})$$

while using eqns. (A3.5b,c) in combination with eqn.(A3.6) the shear forces can be written as

$$Q_y = \int_{\Omega} \tau_{xy} \, d\Omega = G \int_{\Omega} \frac{\partial \phi_c}{\partial y} \, d\Omega \quad (\text{A3.10a})$$

$$Q_z = \int_{\Omega} \tau_{xz} \, d\Omega = G \int_{\Omega} \frac{\partial \phi_c}{\partial z} \, d\Omega \quad (\text{A3.10b})$$

where

$$I_{yy} = \int_{\Omega} z^2 \, d\Omega \quad I_{zz} = \int_{\Omega} y^2 \, d\Omega \quad I_{yz} = \int_{\Omega} yz \, d\Omega \quad (\text{A3.11a-c})$$

are the moments and the product of inertia of the cross section, respectively. Alternatively, by differentiating relations (A3.9) the shear forces can also be obtained as

$$Q_y = -\frac{\partial M_z}{\partial x} = E \left(\frac{\partial^2 \theta_y}{\partial x^2} I_{yz} - \frac{\partial^2 \theta_z}{\partial x^2} I_{zz} \right) \quad (\text{A3.12a})$$

$$Q_z = \frac{\partial M_y}{\partial x} = E \left(\frac{\partial^2 \theta_y}{\partial x^2} I_{yy} - \frac{\partial^2 \theta_z}{\partial x^2} I_{yz} \right) \quad (\text{A3.12b})$$

Performing algebraic manipulations the following relations are obtained

$$\frac{\partial^2 \theta_y}{\partial x^2} = \frac{1}{E} \frac{Q_z I_{zz} - Q_y I_{yz}}{\Delta} \quad (\text{A3.13a})$$

$$\frac{\partial^2 \theta_z}{\partial x^2} = \frac{1}{E} \frac{Q_z I_{yz} - Q_y I_{zz}}{\Delta} \quad (\text{A3.13b})$$

where Δ is defined as $\Delta = (I_{yy} I_{zz} - I_{yz}^2)$. Substituting the above relations in eqn. (A3.8) the following differential equation is obtained

$$G \left(\frac{\partial^2 \phi_c}{\partial y^2} + \frac{\partial^2 \phi_c}{\partial z^2} \right) = \frac{1}{\Delta} \left[(Q_z I_{zz} - Q_y I_{yz}) z - (Q_z I_{yz} - Q_y I_{zz}) y \right] \quad (\text{A3.14})$$

while setting as $g(y, z)$ the right hand side of the above equation, the partial Poisson type differential equation governing the unit warping function is obtained as

$$\nabla^2 \phi_c(y, z) = \frac{\partial^2 \phi_c}{\partial y^2} + \frac{\partial^2 \phi_c}{\partial z^2} = -\frac{1}{G} g(y, z) \quad (\text{A3.15})$$

where $\nabla^2 \equiv \partial^2 / \partial y^2 + \partial^2 / \partial z^2$ is the Laplace operator.

Moreover, the boundary condition of the aforementioned warping function with respect to the cross section's centroid C is derived from the physical consideration that the traction vector in the direction of the normal vector n vanishes on the free prismatic surface of the beam (Fig. A3.4), that is

$$\tau_{xn} = \tau_{xy}n_y + \tau_{xz}n_z = 0 \xrightarrow{\text{eqns. (A3.4d,c)}} \frac{\partial \phi_c}{\partial n} = 0 \quad (\text{A3.16})$$

where $n_y = \cos(y, n)$ and $n_z = \sin(y, n)$ are the direction cosines of the normal vector n to the boundary Γ , while this vector is positive when points outward of the domain Ω , as shown in Fig. A3.5.

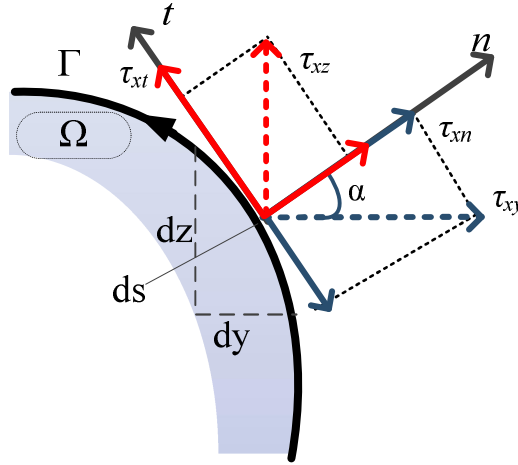


Fig. A3.5. Shear stresses at the cross section boundary.

According to the above, the warping function due to shear can be obtained from the solution of the following Neumann type problem of the Poisson differential equation

$$\nabla^2 \phi_c(y, z) = \frac{\partial^2 \phi_c}{\partial y^2} + \frac{\partial^2 \phi_c}{\partial z^2} = f(y, z) \quad \text{in } \Omega \quad (\text{A3.17a})$$

$$\frac{\partial \phi_c(y, z)}{\partial n} = 0 \quad \text{on } \Gamma \quad (\text{A3.17b})$$

where $f(y, z) = -1/G \cdot g(y, z)$. In order to solve the Neumann problem defined in eqns. (A3.17), the following must apply (Hsiao and Wendland 2008)

$$\int_{\Gamma} \frac{\partial (\phi_c - \phi_c^p)}{\partial n} ds = 0 \quad (\text{A3.18})$$

where ϕ_c^p is a partial solution of the Poisson equation (A3.17a). It can be proved that this condition applies. Moreover, the Neumann problem solution is a function of an arbitrary constant (rigid body motion along x) which cannot be determined from the boundary conditions. However, quantities involving derivatives of the solution (i.e. stresses) are independent from this constant. Thus, setting as c the arbitrary constant of the rigid body motion (integration constant), the warping function due to shear can be written as

$$\bar{\phi}_c(y, z) = \phi_c(y, z) + c \quad (\text{A3.19})$$

The above relation verifies the Poisson eqn. (A3.17a) and the boundary condition (A3.17b), while the constant c can be determined by the requirement of

$$\int_{\Omega} \phi_c(y, z) d\Omega = 0 \quad (\text{A3.20})$$

After substituting eqn. (A3.19) in the above integral, relation (A3.19) can be written as

$$\phi_c(y, z) = \bar{\phi}_c(y, z) - \frac{1}{A} \int_{\Omega} \bar{\phi}_c(y, z) d\Omega \quad (\text{A3.21})$$

where $A = \int_{\Omega} d\Omega$ is the area of the cross section.

Having in mind that the shear centre S is defined as the point of the cross section at which the torsional moment arising from the transverse shear stress distribution vanishes, the coordinates $\{y_S, z_S\}$ of this point with respect to the $Cxyz$ system of axes can be derived from the condition

$$y_S Q_z - z_S Q_y = M_x \Leftrightarrow y_S Q_z - z_S Q_y = \int_{\Omega} (\tau_{xz} y - \tau_{xy} z) d\Omega \quad (\text{A3.22})$$

For $\{Q_y = 0, Q_z = I\}$ and after substituting eqns. (A3.3b,c) in eqn. (A3.22), the y_S coordinate of the shear centre S can be obtained as

$$y_S = G \int_{\Omega} \left(y \frac{\partial \phi_{cy}}{\partial z} - z \frac{\partial \phi_{cy}}{\partial y} \right) d\Omega \quad (\text{A3.23})$$

Similarly, for $\{Q_y = I, Q_z = 0\}$ the z_S coordinate is given as

$$z_S = G \int_{\Omega} \left(y \frac{\partial \phi_{cz}}{\partial z} - z \frac{\partial \phi_{cz}}{\partial y} \right) d\Omega \quad (\text{A3.24})$$

Eqns. (A3.23) and (A3.24) declare that the coordinates of the shear centre S are independent from shear loading. Moreover, it can be shown that the coordinates of the shear centre S , coincide with the coordinates of the centre of twist M as given in Sapountzakis (2000). This coincidence of these centres was first recognized by Weber (1924) applying the Betty-Maxwell reciprocal relations and Trefftz (1935) using an energy approach.

Furthermore, the shear deformation coefficients α_y, α_z and $\alpha_{yz} = \alpha_{zy}$ which are introduced from the approximate formula for the evaluation of the shear strain energy per unit length (Schramm et al. 1997) given as

$$U_{appr} = \frac{\alpha_y Q_y^2}{2AG} + \frac{\alpha_z Q_z^2}{2AG} + \frac{\alpha_{yz} Q_y Q_z}{AG} \quad (\text{A3.25})$$

are evaluated equating this approximate energy with the exact one given from

$$U_{exact} = \int_{\Omega} \frac{\tau_{xy}^2 + \tau_{xz}^2}{2G} d\Omega \quad (\text{A3.26})$$

For $\{Q_y \neq 0, Q_z = 0\}$ setting as $\phi_{cy}(y, z)$ the resulting warping function and substituting relations (A3.5b-c) incorporating eqn. (A3.6), the coefficient α_y is obtained as

$$\alpha_y = \frac{I}{\kappa_y} = \frac{AG^2}{Q_y^2} \int_{\Omega} \left[\left(\frac{\partial \phi_{cy}}{\partial y} \right)^2 + \left(\frac{\partial \phi_{cy}}{\partial z} \right)^2 \right] d\Omega \quad (\text{A3.27})$$

For $\{Q_y = 0, Q_z \neq 0\}$ setting as $\phi_{cz}(y, z)$ the resulting warping function and substituting relations (A3.5b-c) incorporating eqn. (A3.6), the coefficient α_z is obtained as

$$a_z = \frac{I}{\kappa_z} = \frac{AG^2}{Q_z^2} \int_{\Omega} \left[\left(\frac{\partial \phi_{cz}}{\partial y} \right)^2 + \left(\frac{\partial \phi_{cz}}{\partial z} \right)^2 \right] d\Omega \quad (\text{A3.28})$$

Similarly, for $\{Q_y \neq 0, Q_z \neq 0\}$ setting as $\phi_{cyz}(y, z)$ the resulting warping function and substituting relations (A3.5b-c) incorporating eqn. (A3.6) together with eqns. (A3.27), (A3.28) the coefficient α_{yz} is obtained as

$$a_{yz} = \frac{I}{\kappa_{yz}} = \frac{AG^2}{Q_y Q_z} \int_{\Omega} \left[\left(\frac{\partial \phi_{cyz}}{\partial y} \right)^2 + \left(\frac{\partial \phi_{cyz}}{\partial z} \right)^2 \right] d\Omega - \frac{AG^2}{Q_y Q_z} \int_{\Omega} \left[\left(\frac{\partial \phi_{cz}}{\partial y} \right)^2 + \left(\frac{\partial \phi_{cz}}{\partial z} \right)^2 \right] d\Omega - \frac{AG^2}{Q_y Q_z} \int_{\Omega} \left[\left(\frac{\partial \phi_{cy}}{\partial y} \right)^2 + \left(\frac{\partial \phi_{cy}}{\partial z} \right)^2 \right] d\Omega \quad (\text{A3.29})$$

where $\kappa_y, \kappa_z, \kappa_{yz}$ are called shear correction factors or shear stiffness factors (Pilkey 2002). It is worth noting that the warping function $\phi_{cy}(y, z)$ of eqns. (A3.22), (A3.26) and (A3.28), results from the solution of the Neumann boundary value problem

$$\nabla^2 \phi_{cy}(y, z) = \frac{I_{yz}y - I_{zz}z}{G(I_{yy}I_{zz} - I_{yz}^2)} \quad \text{in } \Omega \quad (\text{A3.30a})$$

$$\frac{\partial \phi_{cy}(y, z)}{\partial n} = 0 \quad \text{on } \Gamma = \bigcup_{j=1}^{K+1} \Gamma_j \quad (\text{A3.30b})$$

and the warping function $\phi_{cz}(y, z)$ of eqns. (A3.24), (A3.28) and (A3.29), results from the solution of the Neumann boundary value problem

$$\nabla^2 \phi_{cz}(y, z) = \frac{I_{yy}y - I_{yz}z}{G(I_{yy}I_{zz} - I_{yz}^2)} \quad \text{in } \Omega \quad (\text{A3.31a})$$

$$\frac{\partial \phi_{cz}(y,z)}{\partial n} = 0 \quad \text{on} \quad \Gamma = \bigcup_{j=1}^{K+1} \Gamma_j \quad (\text{A3.31b})$$

Employing the shear deformation coefficients α_y, α_z and α_{yz} the cross section shear rigidities of the Timoshenko's beam theory are defined as

$$GA_{sy} = \frac{GA}{\alpha_y} \quad GA_{sz} = \frac{GA}{\alpha_z} \quad GA_{syz} = \frac{GA}{\alpha_{yz}} \quad (\text{A3.32a-c})$$

The numerical evaluation of the shear deformation coefficients implies the estimation of the warping functions. This is accomplished employing BEM (Katsikadelis 2002a) as this is presented in Mokos (2007) and Sapountzakis and Mokos (2009).

References

Ahmad, S., Banerjee, P.K., 1986. Free Vibration Analysis of BEM Using Particular Integrals. *Journal of Engineering Mechanics*, Volume 112, p. 682–695.

Allotey, N., El Naggar, M.H., 2008. Generalized Dynamic Winkler Model for Nonlinear Soil Structure Interaction Analysis. *Canadian Geotechnical Journal*, Volume 45, pp. 560-573.

Anastasopoulos, I., Gazetas, G., Loli, M., Apostolou, M., Gerolymos, N., 2010. Soil Failure can be used for Seismic Protection of Structures. *Bull of Earthquake Eng.*, Volume 8, pp. 309-326.

Anoyatis, G., Di Laora, R., Mandolini, A., Mylonakis, G., 2013. Kinematic Response of Single Piles for Different Boundary Conditions: Analytical Solutions and Normalization Schemes. *Soil Dynamics and Earthquake Engineering*, Volume 44, p. 183–195.

Ansari, M., Esmailzadeh, E., Younesian, D., 2010. Internal/External Resonance of Beams on Non-Linear Viscoelastic Foundation Traversed by Moving Load. *Nonlinear Dynamics*, Volume 61, p. 163–182.

ANSYS, Swanson, J.A., n.d. *Analysis System*, Houston USA: Inc. 201 Johnson Road PA 15342-1300.

Antes, H., Schanz, M., Alvermann, S., 2004. Dynamic Analyses of Plane Frames by Integral Equations for Bars and Timoshenko Beams. *Journal of Sound and Vibration*, Volume 276, p. 807–836.

- Anthes, R., 1997. Modified Rainflow Counting Keeping the Load Sequence. *International Journal of Fatigue*, Volume 19, pp. 529-535.
- Arboleda-Monsalve, L.G., Zapata-Medina, D.G., Aristizabal-Ochoa, J.D., 2008. Timoshenko Beam-Column with Generalized End Conditions on Elastic Foundation: Dynamic-Stiffness Matrix and Load Vector. *Journal of Sound and Vibration*, Volume 310, p. 1057–1079.
- Armenakas, A., 2006. *Advanced Mechanics of Materials and Applied Elasticity*. New York: Taylor & Francis Group.
- Ashour, M., Norris, G., 2000. Modeling Lateral Soil-Pile Response Based on Soil-Pile Interaction. *Journal of Geotechnical and Geoenvironmental Engineering*, 126(5), pp. 420-428.
- Attalla, M.R., Deierlein, G.G., McGuire, W., 1994. Spread of Plasticity: Quasi-Plastic-Hinge Approach. *Journal of Structural Engineering*, Volume 120, pp. 2451-2473.
- Avramidis, I.E., Morfidis, K., 2006. Bending of Beams on Three-Parameter Elastic Foundation. *Int. Journal of Solids and Structures*, Volume 43, pp. 357-375.
- Ayoub, A., 2003. Mixed Formulation of Nonlinear Beam on Foundation Elements. *Computers and Structures*, Volume 81, p. 411–421.
- Baba, S., Kajita, T., 1982. Plastic Analysis of Torsion of a Prismatic Beam. *International Journal for Numerical Methods in Engineering*, Volume 18, pp. 927-944.
- Babouskos, N., 2011. *Analysis and Optimization of Elastic and Viscoelastic Plates Using the Boundary Element Method*. Athens : National Technical University of Athens, DOI 10.12681/eadd/24943.
- Bach, C., Baumann, R., 1924. *Elastizität und Festigkeit*. Berlin: Springer Verlag.
- Badoni, D., Makris, N., 1996. Nonlinear Response of Single Piles under Lateral Inertial and Seismic Loads. *Soil Dynamics and Earthquake Engineering*, Volume 15, pp. 29-43.

- Bathe, K., 2007. *Finite Element Procedures*. New York: Prentice Hall Engineering, Science, Mathematics.
- Bazant, Z.P., Cedolin, L., 1991. *Stability of Structures: Elastic, Inelastic, Fracture and Damage Theories*. New York: Oxford University Press.
- Beaufait, F.W., Hoadley, P.W., 1980. Analysis of Elastic Beams on Non-Linear Foundations. *Computer and Structures*, Volume 12, pp. 669-676.
- Blaney, G.W., O'neill, M.W., 1989. Dynamic Lateral Response of Pile Groups in Clay. *Geotechnical Testing Journal*, Volume 10, p. 22-24.
- Bouc, R., 1967. *Forced Vibration of Mechanical Systems with Hysteresis*. Prague, Czechoslovakia, Proceedings of the Fourth Conference on Non-linear oscillation.
- Boulanger, R.W., Curras, C.J., Kutter, B.L., Wilson, D.W., Abghari, A., 1999. Seismic Soil-Pile-Structure Interaction Experiments and Analyses. *Journal Geotechnical and Geoenvironmental Engineering*, Volume 125, pp. 750-759.
- Bozorgnia, Y., Bertero, V., 2004. *Earthquake Engineering from Engineering Seismology to Performance-Based Engineering*. New York: CRC Press.
- Brebbia, C., 2010. *In Praise of John Katsikadelis - A Well Deserved Eulogy, Recent Developments in Boundary Element Methods A volume to honour John T. Katsikadelis, 1-15*. E.J. Sapountzakis ed. s.l.:WIT PRESS.
- Brenan, K.E., Campbell, S.L., Petzold, L.R., 1989. *Numerical Solution of Initial-value Problems in Differential-Algebraic Equations*. Amsterdam: North-Holland.
- Broms, B., 1964a. Lateral Resistance of Piles in Cohesive Soils. *Journal of Soil Mechanics and Foundation Division, ASCE*, 90(2), pp. 27-63.
- Broms, B., 1964b. Lateral Resistance of Piles in Cohesionless Soils. *Journal of Soil Mechanics and Foundation Division, ASCE*, 90(3), pp. 123-156.
- Broms, B., 1965. Design of Laterally Loaded Piles. *Journal of Soil Mechanics and Foundation Division, ASCE*, 91(3), pp. 77-99.

Brown, D.A., Shie, C., 1990. Three Dimensional Finite Element Model of Laterally Loaded Piles. *Computers and Geotechnics*, Volume 10, pp. 59-79.

Brown, D.A., Shie, C.F., 1991. Some Numerical Experiments with a Three Dimensional Finite Element Model of a Laterally Loaded Pile. *Computers and Geotechnics*, Volume 12, pp. 149-162.

Brush, D.O., Almroth, B.O., 1975. *Buckling of Bars, Plates and Shells*. New York, USA: McGraw - Hill Book Co.

Budek, A.M., Priestley, M.J.N., Benzoni, G., 2000. Inelastic Seismic Response of Bridge Drilled-shaft RC Pile/Columns. *Journal of Structural Engineering*, 126(4), pp. 510-517.

Burr, J.P., Pender, M.J., Larkin, T.J., 1997. Dynamic Response of Laterally Excited Pile Groups. *Journal Geotechnical Engineering*, Volume 123, pp. 1-8.

Calim, F., 2009. Dynamic Analysis of Beams on Viscoelastic Foundation. *European Journal of Mechanics A/Solids*, Volume 28, pp. 469-476.

Casciati, F., 2006. Stochastic Dynamics of Hysteretic Media. *Probabilistic Methods in Applied Physics*, Springer Berlin / Heidelberg, pp. 270-283.

Castelli, F., Maugeri, M., 2009. Simplified Approach for the Seismic Response of a Pile Foundation. *Journal Geotechnical and Geoenvironmental Engineering*, Volume 135, pp. 1440-1451.

CEN, 2005. *Eurocode 8: Design of Structures for Earthquake Resistance Part 3: Strengthening and Repair of Buildings*. Brussels, Belgium: Final Draft prEN 1998-2, European Committee for Standardization.

CEN, 2005. *Eurocode 8: Design of Structures for Earthquake Resistance. Part 2: Bridges*. Brussels, Belgium: Final Draft prEN 1998-2, European Committee for Standardization.

- Chang, T.P., Liu, Y.N., 1996. Dynamic Finite Element Analysis of a Nonlinear Beam Subjected to a Moving Load. *Int. Journal of Solids and Structures*, 33(12), pp. 1673-1688.
- Chang, S., 2004. Studies of Newmark Method for Solving Nonlinear Systems: (I) Basic Analysis. *Journal of the Chinese Institute of Engineers*, 27(5), pp. 651-662.
- Charalampakis, A.E., Koumousis, V.K., 2008a. Identification of Bouc–Wen Hysteretic Systems by a Hybrid Evolutionary Algorithm. *Journal of Sound and Vibration*, 314(3-5), pp. 571-585.
- Charalampakis, A.E., Koumousis, V.K., 2008b. Ultimate Strength Analysis of Composite Sections under Biaxial Bending and Axial Load. *Advances in Engineering Software*, 39(11), pp. 923-936.
- Charalampakis, A.E., Koumousis, V.K., 2009. A Bouc Wen Model Compatible with Plasticity Postulates. *Journal of Sound and Vibration*, 322(4-5), pp. 954-968.
- Chau, K.T., Shen, C.Y., Guo, X., 2009. Non Linear Seismic Soil–Pile–Structure Interactions: Shaking Table Tests And Fem Analyses. *Soil Dynamics and Earthquake Engineering*, Volume 29, pp. 300-310.
- Chen, G., Trahair, N.S., 1992. Inelastic Nonuniform Torsion of Steel I-Beams. *Journal of Constructional Steel Research*, Volume 23, pp. 189-207.
- Chen, J.S., Chen, Y.K., 2011. Steady State and Stability of a Beam on a Damped Tensionless Foundation Under a Moving Load. *International Journal of Non-Linear Mechanics*, Volume 46, pp. 180-185.
- Chen, J.T., Chen, P.Y., 2007. A Semi-Analytical Approach for Stress Concentration of Cantilever Beams with Holes under Bending. *Journal of Mechanics*, 23(3), pp. 211-221.
- Chen, W.Q., Lu, C.F., Bian, Z.G., 2004. A Mixed Method for Bending and Free Vibration of Beams Resting on a Pasternak Elastic Foundation. *Applied Mathematical Modeling*, Volume 28, p. 877–890.

- Chen, Y.H., Huang, Y.H., Shih, C.T., 2001. Response of an Infinite Timoshenko Beam on a Viscoelastic Foundation to a Harmonic Moving Load. *Journal of Sound and Vibration*, 241(5), pp. 809-824.
- Chen, C., 2002. DQEM Vibration Analyses of Non-Prismatic Shear Deformable Beams Resting on Elastic Foundations. *Journal of Sound and Vibration*, 255(5), pp. 989-999.
- Chiou, J.S., Tsai, Y.C., Chen, C.H., 2012. Investigating Influencing Factors on the Ductility Capacity of a Fixed-Head Reinforced Concrete Pile in Homogeneous Clay. *Journal of Mechanics*, 28(3), pp. 489-49.
- Choros, J., Adams, G.G., 1979. A Steadily Moving Load on an Elastic Beam Resting on a Tensionless Winkler Subgrade. *Journal of Applied Mechanics ASME*, 46(1), pp. 175-180.
- Chou, S., 1993. Determination of Centers of Flexure Using the Boundary Element Method. *Engineering Analysis with Boundary Elements*, Volume 12, pp. 321-324.
- Coskun, I., 2000. Non-Linear Vibrations of a Beam Resting on a tensionless Winkler Foundation. *Journal of Sound and Vibration*, 236(3), pp. 401-411.
- Coskun, I., 2003. The Response of a Finite Beam on a Tensionless Pasternak Foundation Subjected to a Harmonic Load. *European Journal of Mechanics A/Solids*, 22(1), p. 151-161.
- Cowper, G., 1966. The Shear Coefficient in Timoshenko's Beam Theory. *Journal of Applied Mechanics, ASME*, 33(2), pp. 335-340.
- Crisfield, M., 1991. *Non-linear Finite Element Analysis of Solids and Structures, Vol. 1: Essentials*. New York USA: John Wiley and Sons.
- Dahlberg, T., 2002. *Dynamic Interaction Between Train and Nonlinear Railway Model*. Munich, Proc. of Fifth Int. Conf. on Structural Dynamics.
- Dahl, P., 1976. Solid Friction Damping of Mechanical Vibrations. *AIAA Journal*, 14(12), p. 1675.

- Dassault Systemes Simulia Corp, 2009. *Abaqus User's Manual*. Ri, USA: Providence.
- De Rosa, M., 1995. Free Vibrations of Timoshenko Beams on Two-Parameter Elastic Foundation. *Computers & Structures*, 57(1), pp. 151-156.
- Dezi, F., Carbonari, S., Leoni, G., 2010. Kinematic Bending Moments in Pile Foundations. *Soil Dynamics and Earthquake Engineering*, Volume 30, p. 119–132.
- Di Laora, R., Mandolini, A., Mylonakis, G., 2012. Insight on Kinematic Bending of Flexible Piles in Layered Soil. *Soil Dynamics and Earthquake Engineering*, Volume 43, p. 309–322.
- Dikaros, I.C., Sapountzakis, E.J., 2014. Generalized Warping Analysis of Composite Beams of Arbitrary Cross Section by BEM. Part I: Theoretical Considerations and Numerical Implementation. *Journal of Engineering Mechanics, ASCE*, DOI: 10.1061/(ASCE)EM.1943-7889.0000775, 140(9).
- Dikaros, I.C., Sapountzakis, E.J., 2014. Generalized Warping Analysis of Composite Beams of Arbitrary Cross Section by BEM. Part II: Numerical Applications. *Journal of Engineering Mechanics, ASCE*, DOI: 10.1061/(ASCE)EM.1943-7889.0000776, 140(9).
- Dimitrovova, Z., 2010. A General Procedure for the Dynamic Analysis of Finite and Infinite Beams on Piece-Wise Homogeneous Foundation under Moving Loads. *Journal of Sound and Vibration*, Volume 329, pp. 2635-2653.
- El Naggar, M.H., Novak, M., 1996. Nonlinear Analysis for Dynamic Lateral Pile Response. *Journal of Soil Dynamics and Earthquake Engineering*, 14(3), pp. 141-157.
- El-Marsafawi, H., Han, Y.C., Novak, M., 1992. Dynamic Experiments on Two Pile Groups. *Journal Geotechnical Engineering*, Volume 118, p. 576–592.
- El-Mously, M., 1999. Fundamental Frequencies of Timoshenko Beams Mounted on Pasternak Foundation. *Journal of Sound and Vibration*, 228(2), pp. 452-457.

- Erlicher, S., Bursi, O.S., 2009. Bouc–Wen-Type Models with Stiffness Degradation: Thermodynamic Analysis and Applications. *Journal of Engineering Mechanics*, Volume 134, pp. 843-855.
- Erlicher, S., Point, N., 2004. Thermodynamic Admissibility of Bouc Wen Type Hysteresis Models. *C. R. Mecanique*, Volume 332, pp. 51-57.
- Fardis, M., 2010. *Advances in Performance-Based Earthquake Engineering*. Berlin: Springer.
- Fatmi, R.E., Zenzri, H., 2004. Numerical Method for the Exact Elastic Beam Theory Applications to Homogeneous and Composite Beams. *International Journal of Solids and Structures*, Volume 41, p. 2521–2537.
- Fatmi, R., 2007a. Non-Uniform Warping Including the Effects of Torsion and Shear Forces. Part I: A General Beam Theory. *International Journal of Solids and Structures*, Volume 44, pp. 5912-5929.
- Fatmi, R., 2007b. Non-Uniform Warping Including the Effects of Torsion and Shear Forces. Part II: Analytical and Numerical Applications. *International Journal of Solids and Structures*, Volume 44, pp. 5930-5952.
- Ferro, N.C.P., Venturini, W.S., 1992. *BEM–FEM Coupling for Building Structure Analysis*. Southampton, In: Brebbia CA, editor. *Boundary elements XIV: stress analysis and computational aspects*, 2. p. 451–465..
- Figini, R., Paolucci, R., Chatzigogos, C.T., 2012. A Macro-Element Model for Non-linear Soil–Shallow Foundation–Structure Interaction under Seismic Loads: Theoretical Development and Experimental Validation on Large Scale Tests. *Earthquake Engineering & Structural Dynamics*, 41(3), pp. 475-493.
- Filho M.R., Mendonca A.V, Paiva J.B., 2005. Static Boundary Element Analysis of Piles Subjected To Horizontal and Vertical Loads. *Engineering Analysis with Boundary Elements*, Volume 29, p. 195–203.

- Filonenko-Borodich, M., 1940. *Some Approximate Theories of Elastic Foundation*. Moscow: Universiteta Mekhanika: Uchenyie Zapiski Moskovskogo Gosudarstvennogo, 46, 3–18.
- Friedman, Z., Kosmatka, J.B., 2000. Torsion and Flexure of a Prismatic Isotropic Beam Using the Boundary Element Method. *Computers and Structures*, Volume 74, pp. 479-494.
- Friswell, M.I., Adhikari, S., Lei, Y., 2007. Vibration Analysis of Beams With Non-Local Foundations using the Finite Element Method. *International Journal for Numerical Methods in Engineering*, 71(11), p. 1365–1386.
- Fryba, L., 1999. *Vibration of Solids and Structures under Moving Loads*. Londo: Thomas Telford.
- Gajan, S., Phalen, J.D., Kutter, B.L., Hutchinson, T.C., Martin, G., 2005. Centrifuge Modeling of Load Deformation Behavior of Rocking Shallow Foundations. *Soil Dynamics and Earthquake Engineering*, 25(7-10), p. 773–783.
- Gazetas, G., Apostolou, M., Anastasopoulos, I., 2003. Seismic Uplifting of Foundations on Soft Soil, with Examples from Adapazari (Izmit 1999, Earthquake). Foundations: Innovations, Observations, Design & Practice. *British Geotechnical Association*, p. 37–50.
- Gazetas, G., Mylonakis, G., 1998. *Seismic Soil-Structure Interaction: New Evidence and Emerging Issues*. Proceedings of The 3rd Conference on Geotechnical Earthquake Engineering and Soil Dynamics, ASCE p. 1119-1174.
- Gelagoti, F., Kourkoulis, R., Anastasopoulos, I., Gazetas, G., 2012. Rocking Isolation of Low-Rise Frame Structures Founded on Isolated Footings. *Earthquake Engineering & Structural Dynamics*, 41(7), pp. 1177-1197.
- Georgiadis, M., 1983. *Development of p-y Curves for Layered Soils*. ASCE, Proceedings of the Geotechnical Practice in Offshore Engineering, pp 536-545.

Gerolymos, N., Drosos, V., Gazetas, G., 2009. Seismic Response of Single-Column Bent on Pile: Evidence of Beneficial Role of Pile and Soil Inelasticity. *BEE*, 7(2), pp. 547-573.

Gerolymos, N., Gazetas, G., 2005. Phenomenological Model Applied to Inelastic Response of Soil-Pile Interaction Systems. *Soils and Foundations*, 45(4), pp. 119-132.

Gerolymos, N., Gazetas, G., 2006. Development of Winkler Model for Static and Dynamic Response of Caisson Foundations with Soil and Interface Nonlinearities. *Soil Dynamics and Earthquake Engineering*, 26(5), p. 363–376.

Gerolymos, N., Gazetas, G., 2007. A Model for Grain-Crushing-Induced Landslides—Application to Nikawa, Kobe 1995. *Soil Dynamics and Earthquake Engineering*, 27(9), pp. 803-819.

Gerolymos, N., Giannakou, A., Anastasopoulos, I., Gazetas, G., 2008. Evidence of Beneficial Role of Inclined Piles: Observations and Summary of Numerical Analyses. *Bull of Earthquake Eng*, 6(4), pp. 705-722.

Gerolymos, N., Papakyriakopoulos, O., Brinkgreve, R., 2014. *Macroelement Modeling of Piles in Cohesive Soil Subjected to Combined Lateral and Axial Loading*. Delft, 18-20 June, Proceedings of the 8th European Conference on Numerical Methods in Geotechnical Engineering, Rotterdam: Balkema.

Gerolymos, N., 2012. *A Macro-Element Model for Nonlinear Static and Dynamic Response of Piles*, Laboratory of Soil Mechanics, NTUA: Technical Report for PEVE 2008 research project (Contract number 65/1694).

Giannakos, S., Gerolymos, N., Gazetas, G., 2012. Cyclic Lateral Response of Piles in Dry Sand: Finite Element Modelling and Validation. *Computers and Geotechnics*, Volume 14, pp. 116-131.

Giannakos, S., 2013. *Contribution to the Static and Dynamic Lateral Response of Piles*, National Technical University of Athens: Doctoral Dissertation.

- Gkimousis, I.A., Koumousis, V.K., 2013. *Distributed Plasticity Analysis of Frame Structures in Rate Form*. Barcelona, Spain , COMPLAS XII, International Conference on Computational Plasticity. Fundamentals and Applications.
- Goodier, J., 1944. A Theorem on the Shearing Stress in Beams with Applications to Multicellular Sections. *Journal of Aeronautical Sciences*, Volume 11, pp. 272-280.
- Gruttmann, F., Sauer, R., Wagner, W., 1999. Shear Stresses in Prismatic Beams with Arbitrary Cross-Sections. *International Journal for Numerical Methods in Engineering*, Volume 45, pp. 865-889.
- Gruttmann, F., Wagner, W., Sauer, R., 1998. Zur Berechnung der Schubspannungen aus Querkräften in Querschnitten Prismatischer Stäbe mit der Methode der Finiten Elemente. *Bauingenieur*, 73(11), pp. 485-490.
- Gruttmann, F., Wagner, W., 2001. Shear Correction Factors in Timoshenko's Beam Theory for Arbitrary Shaped Cross-Sections. *Computational Mechanics*, Volume 27, pp. 199-207.
- Guggenberger, J., Grundmann, H., 2005. Stochastic Response of Large FEM Models with Hysteretic Behaviour in Beam Elements. *Computer Methods in Applied Mechanics and Engineering*, 194(12-16), pp. 1739-1756.
- Haberl, G., Och, F., 1974. A Finite Element Solution for the Torsional Rigidity and the Shear Center of Arbitrary Cross Section. *Z. Flugwiss*, 22(4), pp. 115-119.
- Han, Y.C., Novak, M., 1988. Dynamic Behavior of Single Piles Under Strong Harmonic Excitation. *Can. Geotech. Journal*, Volume 25, p. 523-534.
- Han, Y., 1989. Coupled Vibration of Embedded Foundation. *Journal Geotechnical Engineering*, Volume 115, p. 1227-1238.
- Harden, C.W., Hutchinson, T.C., 2009. Beam-on-Nonlinear-Winkler-Foundation Modeling of Shallow, Rocking-Dominated Footings. *Earthquake Spectra*, 25(2), p. 277-300.

Hartmann, F., Katz, C., 2007. *Structural Analysis with Finite Elements*. Berlin Heidelberg: Springer-Verlag.

Hartmann, F., Katz, C., 2007. *Structural Analysis with Finite Elements*. Berlin Heidelberg: Springer-Verlag .

Hartmann, F., 1989. *Introduction to Boundary Elements- Theory and Applications*. Berlin Heidelberg: Springer-Verlag.

Heteneyi, M., 1946. *Beams on Elastic Foundation*. Ann Arbor: The University of Michigan Press.

Hetenyi, M., 1966. Beams and Plates on Elastic Foundations and Related Problems. *Applied Mechanics Reviews*, Volume 19, pp. 95-102.

Hsiao, G.C., Wendland, W.L., 2008. *Boundary Integral Equations*. Berlin: Springer-Verlag.

Huang, W., Zou, Y. , 1994. The dynamic response of a Viscoelastic Winkler Foundation-Supported Elastic Beam Impacted by a Low Velocity Projectile. *Computers & Structures*, 52(3), pp. 431-436.

Hutchinson, T.C., Chai, Y.H., BoulangerR, R.W., Idriss, I.M., 2004. Inelastic Seismic Response Of Extended Pile-Shaft-Supported Bridge Structures. *Earthquake Spectra*, Volume 20, pp. 1057-1080.

Hutchinson, J., 2001. Shear Coefficients for Timoshenko Beam Theory. *Journal of Applied Mechanics ASME*, Volume 68, pp. 87-92.

Idriss, I.M., Sun, J.I., 1991. *Shake91: A Computer Program for Conducting Equivalent Linear Seismic Response Analyses of Horizontally Layered Soil Deposits*. University Of California, Davis: Center For Geotechnical Modeling Report. Department Of Civil And Environmental Engineering.

- Ingber, M.S., Mammoli, A.A., Brown, M.J., 2001. A Comparison of Domain Integral Evaluation Techniques for Boundary Element Methods. *International Journal for Numerical Methods in Engineering*, Volume 52, pp. 417-432.
- Inglis, C., 1934. *A Mathematical Treatise on Vibration in Railway Bridges*. Cambridge: The Cambridge University Press.
- Isaacson, E., Keller, H.B., 1966. *Analysis of Numerical Methods*. New York: John Wiley and Sons.
- Ishibashi, I., Zhang, X., 1993. Unified Dynamic Shear Moduli and Damping Ratios of Sand and Clay. *Soils and Foundations*, Volume 33, pp. 182-191.
- Iwnicky, S., 2007. *Handbook of Railway Vehicle Dynamics*. New York: Taylor and Francis.
- Kaliszky, S., Logo, J., 1994. *Analysis of Nonlinear Beams on Nonlinear Foundation by the use of Mixed Extremum Principles*. National Technical University of Athens, Collection of Papers Dedicated to Prof. P.S. Theocaris, A.N. Kounadis p. 65-80..
- Kampitsis, A.E., Giannakos, S., Gerolymos, N., Sapountzakis, E.J., 2014. Inelastic Analysis of Pile-Foundation Systems:Numerical Analysis and Experimental Validation. *Under Review*.
- Kampitsis, A.E., Sapountzakis, E.J., Giannakos, S., Gerolymos, N., 2013a. Seismic Soil–Pile–Structure Kinematic and Inertia Interaction - A New Beam Approach. *Soil Dynamics and Earthquake Engineering*, Volume 55, p. 211–224.
- Kampitsis, A.E., Sapountzakis, E.J., Giannakos, S., Gerolymos, N., 2013b. *Seismic Soil-Pile Kinematic and Inertia Interaction—3D versus Beam Modeling*. Kos, Greece, 4th International Conference on Computational Methods in Structural Dynamics and Earthquake Engineering –COMDYN.
- Kampitsis, A.E., Sapountzakis, E.J., 2014a. *Boundary Element Formulation for the Inelastic Dynamic Analysis of Beams*. Barcelona, Spain, Word Congress of Computational Mechanic. WCCM XI-ECCM V-ECFD VI.

Kampitsis, A.E., Sapountzakis, E.J., 2014b. *A New Computational Tool for the Inelastic Analysis of Steel Structures*. Tripoli Greece, 8th Hellenic National Conference of Steel Structures.

Kaneko, T., 1975. On Timoshenko's Correction for Shear in Vibrating Beams. *Journal of Physics*, Volume 8, pp. 1927-1936.

Karamanlidis, D., Prakash, V., 1988. Buckling and Vibration Analysis of Flexible Beams Resting on an Elastic Half-Space. *Earthquake Engineering and Structural Dynamics*, Volume 16, pp. 1103-1114.

Kargarnovin, M.H., Younesian, D., Thompson, D.J., Jones, C.J.C., 2005. Response of Beams on Nonlinear Viscoelastic Foundations to Harmonic Moving Loads. *Computers & Structures*, Volume 83, pp. 1865-1877.

Kargarnovin, M.H., Younesian, D., 2004. Dynamics of Timoshenko Beams on Pasternak Foundation Under Moving Load. *Mechanics Research Communications*, Volume 31, p. 713-723.

Kaschiev, S., Mikhajlov, K., 1995. A Beam Resting on a Tensionless Winkler Foundation. *Computers & Structures*, 55(2), pp. 261-264.

Katsikadelis, J.T., Sapountzakis, E.J., Zorba, E.G., 1990. A BEM Approach to Static and Dynamic Analysis of Plates with Internal Supports. *Computational Mechanics*, Volume 7, pp. 31-40.

Katsikadelis, J.T., Sapountzakis, E.J., 1988. An Approach to the Vibration Problem of Homogeneous, Non-Homogeneous and Composite Membranes Based on the Boundary Element Method. *International Journal for Numerical Methods in Engineering*, Volume 26, pp. 2439-2455.

Katsikadelis, J.T., Sapountzakis, E.J., 1991. A BEM Solution to Dynamic Analysis of Plates with Variable Thickness. *Computational Mechanics*, Volume 7, pp. 369-379.

- Katsikadelis, J.T., Tsiatas, G.C., 2003. Nonlinear Dynamic Analysis of Heterogeneous Orthotropic Membranes by the Analog Equation Method. *Engineering Analysis with Boundary Elements*, Volume 27, pp. 115-124.
- Katsikadelis, J., 1994. *The Analog Equation Method: A Powerful BEM-Based Solution Technique for Solving Linear and Non-linear Engineering Problems*. Boundary Element Method , XVI.
- Katsikadelis, J., 2002. *Boundary Elements: Theory and Applications*. Oxford, UK: Elsevier.
- Katsikadelis, J., 2002. The Analog Equation Method. A Boundary-Only Integral Equation Method for Nonlinear Static and Dynamic Problems in General Bodies. *Theoretical and Applied Mechanics*, Volume 27, pp. 13-38.
- Katsikadelis, J., 2008. A generalized Ritz Method for Partial Differential Equations in Domains of Arbitrary Geometry Using Global Shape Functions. *Engineering Analysis with Boundary Elements*, Volume 32, pp. 353-367.
- Katsikadelis, J., 2009. The Meshless Analog Equation Method: I. Solution of Elliptic Partial Differential Equations. *Archive of Applied Mechanics*, Volume 79, pp. 557-578.
- Kavvadas, M., Gazetas, G., 1993. Kinematic Seismic Response and Bending of Free-Head Piles in Layered Soil. *Geotechnique*, Volume 43, p. 207–222.
- Kerisel, J., Adam, M., 1967. Calcul Des Forces Horizontales Applicables Aux Fondations Profondes Dans Les Argiles Et Limons. *Annales d'Institut Technique Du Batiment Et Des Travaux Publics, Paris*, Volume 239, pp. 1653-1694.
- Kim, S.M., Cho, Y.H., 2006. Vibration and Dynamic Buckling of Shear Beam-Columns on Elastic Foundation Under Moving Harmonic Loads. *Int. Journal of Solids and Structures*, Volume 43, p. 393–412.
- Kim, Y., Jeong, S., 2011. Analysis of Soil Resistance on Laterally Loaded Piles Based on 3D Soil–Pile Interaction. *Computers and Geotechnics*, Volume 38, p. 248–257.

Kolousek, V., 1973. *Dynamics of Civil Engineering Structures-partI: General Problems*. 2nd-partII ed. Prague, Butterworth, London: Continuous Beams and Frame Systems, second ed.-partIII: Selected Topics, SNTL, Prague, (1967, 1956, 1961), (inCzech). Dynamics in Engineering Structures, Academia.

Kontoni, D.P.N., Partridge, P.W., Brebbia, C.A., 1991. The Dual Reciprocity Boundary Element Method for the Eigenvalue Analysis of Helmholtz Problems. *Advances in Engineering Software and Workstations*, Volume 13, pp. 2-16.

Korsmeyer, F.T., Yue, D.K.P., Nabors, K., White J., 1993. *Multipole-Accelerated Preconditioned Iterative Methods for Threedimensional Potential Problems*. Southampton, In Boundary Elements, vol. XV, Brebbia CA, Rencis JJ (eds), Computational Mechanics Publications, 517–527.

Kosmatka, J., 1993. Flexure-Torsion Behavior of Prismatic Beams, Part I: Section Properties via Power Series. *AIAA Journal*, 31(1), pp. 170-179.

Kottari, A.K., Charalampakis, A.E., Koumouisis, V.K., 2014. A Consistent Degrading Bouc–Wen Model. *Engineering Structures*, Volume 60, p. 235–240.

Krylov, A., 1905. Über die Erzwungenen Schwingungen von Gleichformigen Elastischen Staben (About Forced Vibrations of Prismatic Elastic Beams). *Mathematische Annalen*, Volume 61, p. 211–234.

Kuczma, M.S., Switka, R. , 1990. Bending of Elastic Beams on Winkler-type Viscoelastic Foundations with Unilateral Constraints. *Computers & Structures*, 34(1), pp. 125-136.

Lai, Y.C., Ting, B.Y., Lee, W.S., Becker, W.R., 1992. Dynamic Response of Beams on Elastic Foundation. *International Journal for Structural Engineering ASCE*, Volume 118, pp. 853-858.

Laman, M., King, G.J.W., Dickin, E.A., 1999. Three-dimensional finite element Studies of the Moment-carrying Capacity of Short Pier Foundations in Cohesionless Soil. *Computers and Geotechnics*, Volume 25, pp. 141-155.

- Lewandowski, R., 1989. Nonlinear Free Vibrations of Multispan Beams on Elastic Supports. *Computers & Structures*, 32(2), pp. 305-312.
- Love, A., 1952. *A Treatise on the Mathematical Theory of Elasticity*. New York: Dover Publications.
- Lowan, A., 1935. On Transverse Oscillations of Beams under The Action of Moving Variable Loads. *Philosophical Magazine, Series 7*, 19(127), p. 708–715.
- Ma X., Butterworth, J.W., Clifton, G.C., 2009b. Static Analysis of an Infinite Beam Resting on a Tensionless Pasternak Foundation. *European Journal of Mechanics A/Solids*, Volume 28, pp. 697-703.
- Ma, X., Butterworth, J.W., Clifton, G.C., 2009a. Response of an Infinite Beam Resting on a Tensionless Elastic Foundation Subjected to Arbitrarily Complex Transverse Loads. *Mechanics Research Communications*, Volume 36, pp. 818-825.
- Maheshwari, P., 2007. Analysis of Beams on Tensionless Reinforced Granular Fill-Soil System. *Int. Journal for Numerical and Analytical Methods in Geomechanics*, Volume 32, pp. 1479-1494.
- Maiorano, R.M.S., De Sanctis, L., Aversa, S., Mandolini, A., 2009. Kinematic Response Analysis of Piled Foundations under Seismic Excitation. *Can. Geotech. Journal*, Volume 46, pp. 571-584.
- Makris, M., Gazetas, G., Delis, E., 1996. Dynamic Soil-Pile Foundation-Structure Interaction: Records and Predictions. *Geotechnique*, Volume 46, pp. 33-50.
- Makris, N., Gazetas, G., 1992. Dynamic Pile-Soil-Pile Interaction. Part II: Lateral And Seismic Response. *Earthquake Engineering and Structural Dynamics*, Volume 21, pp. 145-162.
- Manna, B., Baidya, D.K., 2010. Dynamic Nonlinear Response of Pile Foundations Under Vertical Vibration—Theory vs Experiment. *Soil Dynamics and Earthquake Engineering*, Volume 30, pp. 456-469.

- Mason, W.E., Herrmann, L.R., 1968. Elastic Shear Analysis of General Prismatic Beams. *Journal of Engineering Mechanics Division, ASCE*, 94(4), pp. 965-983.
- Matlock, H., 1970. *Correlations for Design of Laterally Loaded Piles in Soft Clay*. Houston, Texas: Proceedings Of The 11 Annual Offshore Technology Conference.
- Matsui, T., Oda, K. , 1996. Foundation Damage Of Structures. *Special Issue Soils Foundation*, p. 189–200.
- Matsunaga, H., 1999. Vibration and Buckling of Deep Beam-Columns on Two-Parameters Elastic Foundation. *Journal of Sound and Vibration*, 228(2), pp. 359-376.
- Mazzoni, S., McKenna, F., Fenves, G.L., 2005. *OpenSees Command Language Manual*. USA: The Regents Of The University Of California.
- Millan, M.A., Dominguez, J., 2009. Simplified BEM/FEM model for Dynamic Analysis of Structures on Piles and Pile Groups in Viscoelastic and Poroelastic Soils. *Engineering Analysis with Boundary Elements*, Volume 33, pp. 25-34.
- Mizuno, H., 1987. Pile Damage During Earthquake In Japan (1923–1983). In: Dynamic Response of Pile Foundations Experiment, Analysis and Observations. *Geotechnical Special Publication ASCE*, Volume 11, p. 53–78.
- Mokos, V., 2007. *Contribution to the Generalised Theory of Composite Beams by the Boundary Element Method*. Athens : National Technical University of Athens.
- More, Jorge, Garbow, B., Hillstom, K., 1980. *User guide for MINPACK-1*, Argonne, Illinois: Argonne National Labs Report ANL-80-74.
- Morgan, M.R., Sinha, S.C., 1983. Influence of a Viscoelastic Foundation on the Stability of Beck's Column: An Exact Analysis. *Journal of Sound and Vibration*, 91(1), pp. 85-101.
- Mullapudi, R., Ayoub, A., 2010a. Nonlinear Finite Element Modeling of Beams on Two-Parameter Foundations. *Computers and Geotechnics*, Volume 37, p. 334–342.

- Mullapudi, R., Ayoub, A., 2010b. Nonlinear Vlasov Foundation Model for Performance Assessment of Cyclically Loaded Structures. *Engineering, Science, Construction and Operations in Challenging Environments, ASCE*, pp. 2907-2916.
- Mullapudi, R., Ayoub, A., 2010c. *Seismic Analysis of Beams on Two-Parameter Foundations*. s.l., 19th Analysis & Computation Specialty Conference, ASCE.
- Muscolino, G., Palmeri, A., 2007. Response of Beams Resting on Viscoelastically Damped Foundation to Moving Oscillators. *Int. Journal of Solids and Structures*, Volume 44, p. 1317–1336.
- Muskhelishvili, N., 1963. *Some Basic Problems of the Mathematical Theory of Elasticity*. s.l.:P. Noordhoff Ltd.
- Mylonakis, G., Nikolaou, A., Gazetas, G., 1997. Soil–Pile–Bridge Seismic Interaction: Kinematic and Inertial Effects. Part I: Soft Soil. *Earthquake Engineering and Structural Dynamics*, Volume 26, p. 337–359.
- Mylonakis, G., 2001. Simplified Model for Seismic Pile Bending at Soil Layer Interfaces. *Soils and Foundations*, Volume 41, p. 47–58.
- Nardini, D, Brebbia, C.A., 1982. *A New Approach to Free Vibration Analysis Using Boundary Elements*. Berlin, In Boundary Elements, vol. IV, Brebbia CA (ed), Springer-Verlag, 312–348.
- Nemat-Nasser, S., 1982. On Finite Deformation Elasto-Plasticity. *International Journal of Solids and Structures*, 18(10), p. 857–872.
- Ngo-Huu, C., Kim, S., Oh, J., 2007. Nonlinear Analysis of Space Steel Frames using Fiber Plastic Hinge Concept. *Engineering Structures*, Volume 29, pp. 649-657.
- Nikolaou, S., Mylonakis, G., Gazetas, G., Tazoh, T., 2001. Kinematic Pile Bending During Earthquakes: Analysis and Field Measurements. *Geotechnique*, Volume 51, pp. 425-440.

- Nogami, T., Otani, J., Konagai, K., Chen, H., 1992. Nonlinear Soil-Pile Interaction Model for Dynamic Lateral Motion. *Journal of Geotechnical Engineering*, 118(1), pp. 89-106.
- Novak, M., Grigg, R.F., 1976. Dynamic Experiments with Small Pile Foundations. *Can. Geotech.*, Volume 13, p. 372–385.
- Nukala, P., White, D., 2004. A Mixed Finite Element for Three-Dimensional Nonlinear Analysis of Steel Frames. *Computer Methods in Applied Mechanics and Engineering*, Volume 193, pp. 2507-2545.
- NX Nastran, 2007. *User's Guide*. s.l.:Siemens PLM Software Inc.
- O'Neil, M.W., Murchison, J.M., 1983. *An Evaluation of p-y Relationships in Sands*, Texas: A report to the American Petroleum Institute, PRAC 82-41-1, University of Houston.
- Orbison, J.G., McGuire, W., Abel, J.F. , 1982. Yield Surface Applications in Nonlinear Steel Frame Analysis. *Computer Methods in Applied Mechanics and Engineering*, Volume 33, pp. 557-573.
- Ortiz, M., Simo, J., 1986. Analysis of a New Class of Integration Algorithms for Elastoplastic Constitutive Relations. *International Journal for Numerical Methods in Engineering*, Volume 23, pp. 353-366.
- Osgood, W., 1943. The Centre of Shear Again. *Journal of Applied Mechanics*, 10(2), pp. A62-A64.
- Paolucci, R., 1997. Simplified Evaluation of Earthquake Induced Permanent Displacements of Shallow Foundations. *Journal of Earthquake Engineering*, Volume 1, p. 563–579.
- Papachristidis, A., Fragiadakis, M., Papadrakakis, M., 2010. A 3D Fibre Beam-Column Element with Shear Modelling for the Inelastic Analysis of Steel Structures. *Computational Mechanics*, Volume 45, pp. 553-572.

- Papoulia, K.D., Panoskaltsis, V.P., Bahuguma, S., Korovajchuk, I., 2007. The Generalized Kuhn Model of Linear Viscoelasticity. *Mechanics of Time-Dependent Materials*, 11(3-4), pp. 217-230.
- Partridge, P.W., Brebbia, C.A., Wrobel, L.C., 1992. *The Dual Reciprocity Method*. Southampton: Computational Mechanics Publications.
- Pasternak, P., 1954. *Fundamentals of a New Method of Analyzing Structures on an Elastic Foundation by Means of Two Foundation Moduli*. Moscow: Gosudarstvennoe Izdatelstro Liberaturi po Stroitelstvui Arkhitekture (in Russian).
- Pecker, A., 1998. Capacity Design Principles for Shallow Foundations in Seismic Areas. *Proceedings of the 11th European Conference on Earthquake Engineering*, pp. 303-316.
- Pecker, A., 2003. *A Seismic Foundation Design Process, Lessons Learned from two Major Projects : the Vasco de Gama and the Rion Antirion bridges*. La Jolla, USA, ACI International Conference on Seismic Bridge Design and Retrofit, University of California at San Diego.
- Pereira, W., 2003. *Numerical Formulation for Analysis of Beams In Contact With Elastic Bases-M.Sc. Thesis*. Brazil: Feeral University Of Ouro Preto.
- Pilkey, W., 2002. *Analysis and Design of Elastic Beams: Computational Methods*. New York: Wiley.
- Powell, M., 1977a. Restart Procedures for the Conjugate Gradient Method. *Mathematical Programming*, Volume 12, pp. 241-254.
- Powell, M., 1977b. Quadratic Termination Properties of Davidon's NEw Variable Metric Algorithm. *Mathematical Programming*, Volume 12, pp. 141-147.
- Powell, M., 1977. Restart Procedures for the Conjugate Gradient Method. *Mathematical Programming*, Volume 12, pp. 241-254.

- Powell, M., 1985. On the Quadratic Programming Algorithm of Goldfarb and Idnani. *Mathematical Programming Study*, Volume 25, pp. 46-61.
- Priestley, M.J.N., Calvi, G.M., Kowalsky, M.J., 2007. *Displacement Based Seismic Design of Structures*. Pavia, Italy, IUSS.
- Puchegger, S., Bauer, S., Loidl, D., Kromp, K., Peterlik, H., 2003. Experimental Validation of the Shear Correction Factor. *Journal of Sound and Vibration*, Volume 261, pp. 177-184.
- Rades, M., 1972. Dynamic Analysis of an Inertial Foundation Model. *Int. Journal of Solids and Structures*, Volume 8, pp. 1353-1372.
- Ramm E., H. T., 1995. *Stabtragwerke: Der Ingenieurbau. Mehlhorn, Band Baustatik/Baudynamik*. G ed. Berlin: Ernst & Sohn.
- Reddy, J., 1997. On Locking-Free Shear Deformable Beam Finite Elements. *Comput Methods Appl Mech Eng (Containing papers presented at the Symposium on Advances in Computational Mechanics)*, 149(1-4), p. 113-132.
- Reese, L.C., Van Impe, W.F., 2001. *Single Piles and Pile Groups under Lateral Loading*. Rotterdam: A.A.Balkema.
- Reese, L.C., Cox, W.R., Koop, F.D., 1975. *Field Testing and Analysis of Laterally Loaded Piles in Stiff Clay*. Houston, Texas: Proceedings Of The Vii Annual Offshore Technology Conference.
- Reissner, E., Tsai, W.T., 1972. On the Determination of the Centers of Twist and of Shear for Cylindrical Shell Beams. *Journal of Applied Mechanics*, Volume 39, pp. 1098-1102.
- Renton, J., 1991. Generalized Beam Theory Applied to Shear Stiffness. *International Journal of Solids and Structures*, Volume 27, p. 1955-1967.
- Renton, J., 1997. A Note on the Form of the Shear Coefficient. *International Journal of Solids and Structures*, Volume 34, p. 1681-1685.

- Rothert H., Gensichen V., 1987. *Nichtlineare Stabstatik*. Berlin: Springer Verlag.
- Saitoh, M., 2012. On the Performance of Lumped Parameter Models With Gyro-Mass Elements for the Impedance Function of a Pile-Group Supporting a Single-Degree-of-Freedom System. *Earthquake Engineering and Structural Dynamics*, Volume 41, pp. 623-641.
- Sapountzakis, E.J., Katsikadelis, J.T., 2000. Elastic Deformation of Ribbed Plates Under Static, Transverse and Inplane Loading. *Computers and Structures*, Volume 74, pp. 571-581.
- Sapountzakis, E.J., Dikaros, I.C., Kampitsis, A.E., Koroneou, A.D., 2014. Nonlinear Response of Wind Turbines under Wind and Seismic Excitations with Soil–Structure Interaction. *Journal of Computational and Nonlinear Dynamics-ASME*, doi:10.1115/1.4027697.
- Sapountzakis, E.J., Dikaros, I.C., Kampitsis, A.E., Panagiotakopoulos, G.D., 2013. *Nonlinear Response of Wind Turbine Towers under Wind and Seismic Excitations*. Crete, Greece, 10th HSTAM International Congress of Mechanics.
- Sapountzakis, E.J., Kampitsis, A.E., Koroneou, A.D., 2010. *Nonlinear Dynamic Analysis of Pile – Columns of Bridge Piers – Application in Valleybridges of Metsovo and in Metsovitikos River Bridge* Interdisciplinary Interuniversity Conference of NTUA, September, Metsovo, Greece. Metsovo, Greece, 6th Interdisciplinary Interuniversity Conference of NTUA.
- Sapountzakis, E.J., Kampitsis, A.E., 2009a. *Nonlinear Dynamic Analysis of Timoshenko Beam-Columns Partially Supported on Elastic Foundation*. Slovakia, Proc. of the CMAS Computational Modeling and Advanced Simulations, Slovak University of Technology.
- Sapountzakis, E.J., Kampitsis, A.E., 2009b. *Nonlinear Dynamic Analysis of Timoshenko Beam-Columns Partially Supported on Nonlinear Elastic Foundation Including Shear Deformation Effect*. Greece., Proc. of the 3rd Greece – Japan Workshop on Seismic Design, Observation and Retrofit of Foundations.

Sapountzakis, E.J., Kampitsis, A.E., 2010a. Nonlinear Analysis of Shear Deformable Beam-Columns Partially Supported on Tensionless Winkler Foundation. *International Journal of Engineering, Science and Technology (IJEST)*, 2(4), pp. 31-53.

Sapountzakis, E.J., Kampitsis, A.E., 2010b. Nonlinear Dynamic Analysis of Timoshenko Beam-Columns Partially Supported on Tensionless Winkler Foundation. *Computers & Structures*, 88(21-22), pp. 1206-1219.

Sapountzakis, E.J., Kampitsis, A.E., 2010c. *Nonlinear Dynamic Analysis of Shear Deformable Beam-Columns on Nonlinear 3-Parameter Viscoelastic Foundation*. Paris France, Proc. of the ECCM IV European Conference on Computational Mechanics.

Sapountzakis, E.J., Kampitsis, A.E., 2010d. *Nonlinear Analysis of Shear Deformable Beam-Columns Partially Supported on Tensionless Three-Parameter Foundation*. Valencia Spain, Proc. of the CST - Tenth International Conference on Computational Structures Technology.

Sapountzakis, E.J., Kampitsis, A.E., 2010e. *Nonlinear Analysis of Shear Deformable Beam-Columns Partially Supported on Tensionless Winkler Foundation*. Berlin, Germany, Proc. of the BeTeq10 International Conference on Boundary Element Techniques.

Sapountzakis, E.J., Kampitsis, A.E., 2010f. *Nonlinear Dynamic Analysis of Partially Supported Beam-Columns on Nonlinear Elastic Foundation Including Shear Deformation Effect*. Chapter 1: Computational Modelling and Advanced Simulations, Springer.

Sapountzakis, E.J., Kampitsis, A.E., 2011a. Nonlinear Analysis of Shear Deformable Beam-Columns Partially Supported on Tensionless Three-Parameter Foundation. *Archive of Applied Mechanics*, 81(12), pp. 1833-1851.

Sapountzakis, E.J., Kampitsis, A.E., 2011b. Nonlinear Response of Shear Deformable Beams on Tensionless Nonlinear Viscoelastic Foundation under Moving Loads. *Journal of Sound and Vibration*, 330(22), p. 5410–5426.

- Sapountzakis, E.J., Kampitsis, A.E., 2011c. *Shear Deformable Beams on Nonlinear Viscoelastic Foundation under Moving Loading*. Kos, Greece, Proc. of the IV International Conference on Computational Methods for Coupled Problems in Science and Engineering - COUPLED PROBLEMS.
- Sapountzakis, E.J., Kampitsis, A.E., 2011d. *Nonlinear Vibrations of Piles in Viscoelastic Foundation*. Chianciano Terme, Italy, Proc. of the 8 Int. Conf. on Earthquake Resistant Engineering Structures-ERES.
- Sapountzakis, E.J., Kampitsis, A.E., 2011e. *Nonlinear Inelastic Analysis of Beams on Nonlinear Foundation*. Crete, Greece, Proc. of the Second Int. Conf. on Soft Computing Technology in Civil, Structural and Environmental Engineering-CSC.
- Sapountzakis, E.J., Kampitsis, A.E., 2012a. A BEM Approach for Inelastic Analysis of Beam-Foundation Systems under Cyclic Loading. *Computer Modeling in Engineering & Science-CMES*, 87(2), pp. 97-124.
- Sapountzakis, E.J., Kampitsis, A.E., 2012b. *Inelastic Analysis of Beams on Two Parameter Elastoplastic Foundation*. Prague, Czech Republic, Proc. of the BeTeq12 International Conference on Boundary Element Techniques.
- Sapountzakis, E.J., Kampitsis, A.E., 2012c. *Nonlinear Seismic Response Analysis of Piles in Nonlinear Viscoelastic Foundation*. Vienna, Austria, Proc. of the 6th European congress on computational methods in applied sciences and engineering (ECCOMAS).
- Sapountzakis, E.J., Kampitsis, A.E., 2013a. Nonlinear Dynamic Analysis of Shear Deformable Beam-Columns on Nonlinear 3-Parameter Viscoelastic Foundation Part I: Theory and Numerical Implementation. *Journal of Engineering Mechanics ASCE*, 139(7), pp. 886-896.
- Sapountzakis, E.J., Kampitsis, A.E., 2013b. Nonlinear Dynamic Analysis of Shear Deformable Beam-Columns on Nonlinear 3-Parameter Viscoelastic Foundation Part II: Applications and Validation. *Journal of Engineering Mechanics ASCE*, 139(7), pp. 897-902.

Sapountzakis, E.J., Kampitsis, A.E., 2013c. Inelastic Analysis of Beams on Two-Parameter Tensionless Elastoplastic Foundation. *Engineering Structures*, Volume 48, p. 389–401.

Sapountzakis, E.J., Kampitsis, A.E., 2013d. *Cyclic Inelastic Response of Beam-Foundation Systems by BEM*. Cagliari, Sardinia, Italy, Fourteenth International Conference on Civil, Structural and Environmental Engineering Computing.

Sapountzakis, E.J., Kampitsis, A.E., 2013e. *Nonlinear Vibrations of Soil-Pile System under Seismic Ground Motion*. Seismic Ground Motion and Interaction with Foundation: Wessex Institute of Technology.

Sapountzakis, E.J., Katsikadelis, J.T., 1991. Boundary Element Solution for Plates of Variable Thickness. *Journal of Engineering Mechanics*, Volume 117, pp. 1241-1256.

Sapountzakis, E.J., Katsikadelis, J.T., 1992. Unilaterally Supported Plates on Elastic Foundations by the Boundary Element Method. *Journal of Applied Mechanics Transactions ASME*, Volume 59, pp. 580-586.

Sapountzakis, E.J., Mokos, V.G., 2005. A BEM Solution to Transverse Shear Loading of Beams. *Computational Mechanics*, Volume 36, pp. 384-397.

Sapountzakis, E.J., Mokos, V.G., 2007. Analysis of Plates Stiffened by Parallel Beams. *International Journal for Numerical Methods in Engineering*, Volume 70, pp. 1209-1240.

Sapountzakis, E.J., Mokos, V.G., 2009. A Displacement Solution to Transverse Shear Loading of Composite Beams by BEM. *CMC-Computers, Materials, & Continua*, 10(1), pp. 1-39.

Sapountzakis, E., 2000. Solution of Non-Uniform Torsion of Bars By an Integral Equation Method. *Computers & Structures*, Volume 77, pp. 659-667.

Saritas, A., Filippou, F.C., 2009. Frame Element for Metallic Shear-Yielding Members under Cyclic Loading. *Journal of Structural Engineering*, Volume 135, pp. 1115-1123.

- Saritas, A., Filippou, F.C., 2009. Inelastic Axial-Flexure–Shear Coupling in a Mixed Formulation Beam Finite Element. *International Journal of Non-Linear Mechanics*, 44(8), pp. 913-922.
- Sauer, E., 1980. *Schub und Torsion bei Elastischen Prismatischen Balken*. Berlin: Mitteilungen aus dem Institut für Massivbau der Technischen Hochschule Darmstadt, Verlag Wilhelm Ernst & Sohn.
- Schramm, U., Kitis, L., Kang, W., Pilkey, W.D., 1994. On the Shear Deformation Coefficient in Beam Theory. *Finite Elements in Analysis and Design*, Volume 16, pp. 141-162.
- Schramm, U., Rubenchik, V., Pilkey, W.D. , 1997. Beam Stiffness Matrix Based on the Elasticity Equations. *International Journal for Numerical Methods in Engineering*, Volume 40, pp. 211-232.
- Seed, H.B., Idriss, I.M., 1970. *Soil Moduli and Damping Factors for Dynamic Response Analysis*. Berkeley: Report No. Eerc 70-10 University Of California,.
- Sharma, S., DasGupta, S., 1975. The Bending Problem of Axially Constrained Beams on Elastic Foundations. *Int. Journal of Solids and Structures*, Volume 11, pp. 853-858.
- Shirma, L.M., Giger, M.W., 1990. Timoshenko Beam Element Resting on Two-Parameter Elastic Foundation. *Journal of Engineering Mechanics*, 118(2), p. 280–295.
- Sica, S., Mylonakis, G., Simonelli, A.L., 2011. Transient Kinematic Pile Bending In Two-Layer Soil. *Soil Dynamics and Earthquake Engineering*, Volume 31, p. 891–905.
- Silveira, R.A.M., Pereira, W.L.A., Goncalves, P.B., 2008. Nonlinear Analysis of Structural Elements under Unilateral Contact Constraints by a Ritz Type Approach. *International Journal of Solids and Structures*, Volume 45, p. 2629–2650.
- Simo, J.C., Hjelmstad, K.D., Taylor, R.L., 1984. Numerical Formulations of Elasto-Viscoplastic Response of Beams Accounting for the Effect of Shear. *Computer Methods in Applied Mechanics and Engineering*, 42(3), p. 301–330.

- Simo, J.C., Hughes, T.J.R., 1998. *Computational Inelasticity*. New York: Springer-Verlag.
- Sivaselvan, M.V., Reinhorn, A.M., 2000. Hysteretic Models for Deteriorating Inelastic Structures. *Journal of Engineering Mechanics*, 126(6), pp. 633-640.
- Sivaselvan, M.V., Reinhorn, A.M., 2003. *Nonlinear Analysis Towards Collapse Simulation – A dynamic Systems Approach*, s.l.: MCEER Technical Report.
- Sokolnikoff, I., 1956. *Mathematical Theory of Elasticity*. New York: McGraw-Hill.
- Stephen, N., 1980. Timoshenko's Shear Coefficient from a Beam Subjected to Gravity Loading. *Journal of Applied Mechanics ASME*, Volume 47, pp. 121-127.
- Sun, L., 2001a. A ClosedForm Solution of a Bernoulli-Euler Beam on a Viscoelastic Foundation under Harmonic Line Loads. *Journal of Sound and Vibration*, 242(4), pp. 619-627.
- Sun, L., 2001b. Dynamic Displacement Response of Beam Type Structures to Moving Line Loads. *International Journal of Solids and Structures*, Volume 38, pp. 8869-8878.
- Sun, L., 2002. A Closed-Form Solution of Beam on Viscoelastic Subgrade Subjected to Moving Loads. *Computers and Structures*, Volume 80, pp. 1-8.
- Symeonov, V.K., Sivaselvan, M.V., Reinhorn, A.M., 2000. Nonlinear Analysis of Structural Frame Systems by the State Space Approach. *Computer Aided Civil and Infrastructure Engineering*, Volume 15, pp. 76-89.
- Taylor, R., 2005. *FEAP pv: A Finite Element Analysis Program. User Manual*. 2nd ed. Berkeley, Calif: Department of Civil and Environmental Engineering, University of California at.
- Teh, L., Clarke, M., 1999. Plastic-Zone Analysis of 3D Steel Frames Using Beam Elements. *Journal of Structural Engineering*, Volume 125, pp. 1328-1337.

- Thambiratnam, D., Zhuge, Y., 1996. Dynamic Analysis of Beams on an Elastic Foundation Subjected to Moving Loads. *Journal of Sound and Vibration*, 198(2), pp. 149-169.
- Thambiratnam, D., Zhuge, Y., 1996. Free Vibration Analysis of Beams on Elastic Foundation. *Computer & Structures*, 60(6), pp. 971-980.
- Thavaraj, T., Finn, W.D.L., Wu, G., 2010. Seismic Response Analysis of Pile Foundation. *Geotech. Geol. Eng*, Volume 28, p. 275–286.
- Thomson, W., 1981. *Theory of Vibration with Applications*. EnglewoodCliffs: Prentice Hall.
- Timoshenko, S., Young, D.H., Weaver, W., 1974. *Vibration problems in Engineering*. 4th ed. New York: Wiley.
- Timoshenko, S.P., Goodier, J.N., 1951. *Theory of Elasticity*. New York, Toronto, London: McGraw-Hill Book Comp.
- Timoshenko, S.P., Goodier, J.N., 1984. *Theory of Elasticity*. 3rd ed. New York: McGraw-Hill.
- Timoshenko, S., 1911. Erzwungene Schwingungen prismatischer Stäbe (Forced Vibrations of Prismatic Beams). *Zeitschrift für Mathematik und Physik*, 59(2), p. 163–203.
- Timoshenko, S., 1921. On the Correction for Shear of the Differential Equation for Transverse Vibrations of Prismatic Bars. *Philosophical Magazine*, Volume 41, pp. 744-746.
- Timoshenko, S., 1922. On the Transverse Vibrations of Bars of Uniform Cross Section. *Philosophical Magazine*, Volume 43, pp. 125-131.
- Tokimatsu, K., Mizuno, H., Kakurai, M., 1996. Building Damage Associated to Geotechnical Problems. *Special Issue Soils Foundation*, pp. 189-200.

- Tolf, G., 1985. St. Venant Bending of an Orthotropic Beam. *Composite Structures*, Volume 4, pp. 1-14.
- Trefftz, E., 1935. Über den Schubmittelpunkt in einem durch eine Einzellast gebogenen Balken. *ZAMM*, Volume 15, pp. 220-225.
- Triantafyllou, S.P., Koumouisis, V.K., 2011. An Inelastic Timoshenko Beam Element with Axial–Shear–Flexural Interaction. *Computational Mechanics*, Volume 48, p. 713–727.
- Triantafyllou, S.P., Koumouisis, V.K., 2012a. Small and Large Displacement Dynamic Analysis of Frame Structures Based on Hysteretic Beam Elements. *Journal of Engineering Mechanics ASCE*, 138(1), pp. 36-49.
- Triantafyllou, S.P., Koumouisis, V.K., 2012b. Bouc-Wen Type Hysteretic Plane Stress Element. *Journal of Engineering Mechanics ASCE*, 138(3), pp. 235-246.
- Triantafyllou, S.P., Koumouisis, V.K., 2012c. An Hysteretic Quadrilateral Plane Stress Element. *Archive of Applied Mechanics*, Volume 82, p. 1675–1687.
- Trochanis, A., Bielak, J., Christiano, P., 1991a. Simplified Model for Analysis of One or Two Piles. *Journal of Geotechnical Engineering*, 117(3), p. 448–466.
- Trochanis, A., Bielak, J., Christiano, P., 1991b. Three-Dimensional Nonlinear Study of Piles. *Journal of Geotechnical Engineering*, 117(3), p. 429–447.
- Tsiatas, G., 2010. Nonlinear Analysis of Non-Uniform Beams on Nonlinear Elastic Foundation. *Acta Mech.*, Volume 209, pp. 141-152.
- Tullin, N., Tralli, A., 2010. Static Analysis of Timoshenko Beam Resting on Elastic Half-Plane Based on The Coupling of Locking-Free Finite Elements and Boundary Integral. *Computational Mechanics*, Volume 45, p. 211–225.
- Vallabhan, C.V.G., Sivakumar, J., 1986. *Coupling of BEM and FEM for 3D Problems in Geotechnical Engineering*. Southampton, In: Brebbia CA Connor JJ et al. editors. BETECH 86. p.675–686.

- Veletsos, A.S., Verbic, B., 1973. Vibration of Viscoelastic Foundations. *Earthquake Engineering and Structural Dynamic*, Volume 2, pp. 87-102.
- Veletsos, A.S., Wei, Y.T., 1971. Lateral and Rocking Vibration of Footings. *Journal of the Soil Mechanics and Foundations Division, ASCE*, 97(9), pp. 1227-1248.
- Visintin, A., 2003. *Differential Models of Hysterisis*. New York: Springer.
- Vlasov, L., 1966. *Beams, Plates, and Shells on Elastic Foundation*. Jerusalem: Israel Program for Scientific Translations.
- Vlasov, V., 1963. *Thin-walled Elastic Beams*, Jerusalem: Israel Program for Scientific Translations.
- Vlassov, W., 1964. *Dünnwandige elastische Stäbe, Band 2*. Berlin: VEB Verlag für Bauwesen.
- Vlassov, W., 1965. *Dünnwandige elastische Stäbe, Band 2*. Berlin: VEB Verlag für Bauwesen.
- Wagner, W., Gruttmann, F., 2002. A Displacement Method for the Analysis of Flexural Shear Stresses in Thin-Walled Isotropic Composite Beams. *Computers and Structures*, Volume 80, pp. 1843-1851.
- Wang, S., Kutter, B.L., Chacko, J.M., Wilson, D.W., Boulanger, R.W., Abghari A., 1998. Nonlinear Seismic Soil-Pile-Superstructure Interaction. *Earthquake Spectra*, 14(2), pp. 377-396.
- Wang, T.M., Stephens, J.E., 1977. Natural Frequencies of Timoshenko Beams on Pasternak Foundation. *Journal of Sound and Vibration*, 51(2), pp. 149-155.
- Weber, C., 1924. Biegung und Schub in Geraden Balken. *ZAMM*, Volume 4, pp. 334-348.
- Weinstein, A., 1947. The Centre of Shear and the Centre of Twist. *Quarterly of Applied Mathematics*, 5(1), pp. 97-99.

- Weitsman, Y., 1971. Onset of Separation Between a Beam and a Tensionless Elastic Foundation under a Moving Load. *Int. Journal of Mechanical Sciences*, Volume 13, pp. 707-711.
- Wen, Y., 1976. Method of Random Vibration of Hysteretic Systems. *Journal of Engineering Mechanics Division ASCE*, 102(2), pp. 249-263.
- Whitaker, T., Cooke, R.W., 1966. *An Investigation of the Shaft and Base Resistance of Large Bored Piles in London Clay*. s.l., Proc Symp Large Bored Piles, p. 7-49.
- Winkler, E., 1867. *Theory of Elasticity and Strength*. Dominicus Prague: Czechoslovakia.
- Wolf, P. J., 1985. *Dynamic Soil-Structure Interaction*. William J. Hall ed. New Jersey: Prentice-Hall, Inc., Englewood Cliffs.
- Worndle, R., 1982. Calculation of the Cross-Section Properties and the Shear Stresses of Composite Rotor Blades. *Vertica*, Volume 6, pp. 111-29.
- Wu, T.X., Thompson, D.J., 2004. *The Effects of Track Non-Linearity on Wheel/Rail Impact*. Proc. Inst. Mech. Eng. Part F, J Rail Rapid Transit, 218 1-15.
- Wunderlich, W., Pilkey, W.D., 2003. *Mechanics of Structures: Variational and Computational Methods*. 2nd ed. Washington D.C: CRC Press LLC.
- Yankelevsky, D.Z., Eisenberger, M., Adin, M.A., 1989. Analysis of Beams on Nonlinear Winkler Foundation. *Computer and Structures*, 31(2), pp. 287-292.
- Ying, J., Lu, C.F., Chen, W.Q., 2008. Two-dimensional Elasticity Solution for Functionally Graded Beams resting on Elastic Foundations. *Computers & Structures*, Volume 84, pp. 209-219.
- Yokoyama, T., 1988. Parametric Instability of Timoshenko Beams Resting on an Elastic Foundation. *Computers & Structures*, 28(2), pp. 207-216.

- Younesianand, D., Kargarnovin, M.H., 2009. Response of the Beams on Random Pasternak Foundations Subjected to Harmonic Moving Loads. *Journal of Mechanical Science and Technology*, Volume 23, pp. 3013-3023.
- Yu, K.H., Kadarman, A.H., Djojodihardjo, H., 2010. Development and Implementation of Some BEM Variants - A Critical Review. *Engineering Analysis with Boundary Elements*, Volume 34, pp. 884-899.
- Zehsaz, M., Sadeghi, M.H., Ziaei Asl, A., 2009. Dynamic Response of Railway Under a Moving Load. *Journal of Applied Sciences*, 9(8), pp. 1474-1481.
- Zhang, K., Murphy, D., 2004. Response of a Finite Beam in Contact with a Tensionless Foundation Under Symmetric and Asymmetric Loading. *Int. Journal of Solids and Structures*, Volume 41, p. 6745–6758.
- Zhang, Y.Q., Lu, Y., Wang, S.L., Liu, X., 2008. Vibration and Buckling of a Double-Beam System under Compressive Axial Loading. *Journal of Sound and Vibration*, Volume 318, p. 341–352.
- Zhang, Y., 2008. Tensionless Contact of a Finite Beam Resting on Reissner Foundation. *International Journal of Mechanical Sciences*, Volume 50, pp. 1035-1041.
- Zhaohua, F., Cook, R.D., 1983. Beam Elements on Two Parameter Elastic Foundations. *Journal of Engineering Mechanics ASCE*, 109(6), p. 1390–1402.
- Zienkiewicz, O.C., Taylor, R.L., 2005. *The Finite Element Method for Solid and Structural Mechanics*. Amsterdam, Netherlands: Elsevier.